이학박사 학위논문

Morphology and Interface Control of Conducting Materials

전도성 물질의 형태와 경계면 제어

2016 년 2 월

서울대학교 대학원

화학부 유기화학전공

멘크 플로리안

Abstract

Morphology and Interface Control of Conduction Materials

Florian Menk
Organic Chemistry, Department of Chemistry
The Graduate School
Seoul National University

The dissertation at hand focusses on two different subjects. On the one hand, approaches which allow controlling the morphology of conducting materials were developed. On the other hand, new approaches for the incorporation of anchor groups into conjugated polymers were investigated. To compete with inorganic devices, improved efficiencies of organic and hybrid optoelectronic devices are required. The morphology of the films assembling an optoelectronic device has been identified as an important factor influencing the device performance. Therefore, approaches which enable the manipulation of the conducting materials' morphology were developed. The first approach in the context of morphology control deals with organic/inorganic nanocomposites. A semiconducting polymer was synthesized via RAFT polymerization and a reactive ester end group was incorporated using a functional CTA. Exploiting the reactive ester, the polymer was equipped with a photocleavable anchor group. The anchor group's affinity towards TiO_2 nanorods enabled the fabrication of stable nanocomposites composed of individually dispersed nanorods as observed via TEM. Finally, upon irradiation with UV light, self-assembly of the nanorods into spherical aggregates was achieved. In the second approach which focuses on a manipulation of the morphology, amphiphilic block

copolymers exhibiting one conjugated and one non-conjugated block were synthesized. In contrast to previous reports of the synthesis of such polymers, the block copolymers were synthesized in a facile one-pot procedure. Using the obtained polymers, micelles were fabricated with differing sizes and optical properties depending on the block copolymer composition and the micellization procedure. In the second part of this dissertation, approaches which permit the incorporation of various anchor groups into conjugated polymers were developed. Therefore, a combination of Siegrist polycondensation and RAFT polymerization was used for the synthesis of block copolymers composed of a conjugated DEH-PPV block and a reactive ester block. Consequently, the reactive ester block was exploited for the incorporation of different anchor groups. The resulting polymers were then applied for the functionalization of CdSe nanoplatelets and the influence of the anchor groups on the optical and material properties were investigated. Furthermore, two approaches enabling the incorporation of anchoring end groups into P3HT were investigated. Both, via copper catalyzed azide-alkyne Huisgen cycloaddition and via Vilsmeier reaction, P3HT was equipped with various anchor groups. As demonstrated, stable nanocomposites composed of P3HT and either TiO_2 or CdSe@ZnS nanocrystals could be obtained. In addition, electron transfer from the polymer to the TiO_2 nanocrystals under irradiation was observed via KPFM.

Keywords : block copolymers, conjugated polymers, living polymerization, morphology, optoelectronics, ROMP

Student Number : 2015-30737

Zusammenfassung

Im Rahmen der vorliegenden Dissertation wurden zwei verschiedenen Themen bearbeitet. Einerseits wurden Strategien entwickelt, die eine Morphologiekontrolle bei leitenden Materialien ermöglichen. Andererseits wurden Synthesewege erforscht, die die Einführung von Ankergruppen in konjugierte Polymere ermöglichen.

Die Effizienz ist der ausschlaggebende Faktor bei optoelektronischen Anwendungen. Generell geringe Effizienzen bedingen, dass organische und hybride Bauteile ihren rein anorganischen Gegenstücken bisher unterlegen sind. Daher ist eine Effizienzsteigerung im Falle der organischen und hybriden Systeme erforderlich, um eine Konkurrenzfähigkeit gegenüber anorganischen Systemen zu erzielen. Die Morphologie eines Bauteils spielt eine zentrale Rolle für dessen Effizienz. Daher wurden im Rahmen dieser Dissertation Ansätze entwickelt, um die Morphologie von leitenden Materialien zu beeinflussen. Der erste Ansatz befasste sich dabei mit der Morphologiekontrolle von organisch/anorganischen Hybridmaterialien. Zunächst wurde dazu ein halbleitendes Polymer per RAFT (reversibler Additions-Fragmentierungs Kettenübertragungs) Polymerisation hergestellt. Dieses Polymer wurde durch die zur Polymerisation verwenden Kettenübertragungsreagenz (CTA) mit einer Reaktivester-Endgruppe ausgestattet. Im Weiteren wurde diese Endgruppe mit einem Amin umgesetzt, um eine photospaltbare Ankergruppe einzuführen. Danach konnten TiO_2 Nanostäbchen per Ligandenaustausch mit dem Polymer beschichtet werden. Die so erhaltenen organisch/anorganischen Komposite bildeten Dispersionen mit einzeln verteilten Nanostäbchen wie durch Transmissionselektronen-mikroskopie (TEM) belegt werden konnte. Anschließend gelang es die Polymere von den Nanostäbchen durch Bestrahlung mit UV-Licht abzuspalten. Daraufhin aggregierten die Nanostäbchen und lagerten sich zu kugelförmigen Aggregaten zusammen. In einem zweiten Ansatz wurden amphiphile Blockcopolymere hergestellt, welche sich aus einem konjugierten und einen nicht konjugierten Block zusammensetzten. Dabei wurden diese Blockcopolymere, im Gegensatz zu bisherigen Berichten, in einer simplen Eintopfreaktion synthetisiert. Die so erhaltenen amphiphilen Blockcopolymere wurden später zur Herstellung von Mizellen verwendet. Diese Mizellen konnten, in Abhängigkeit der Polymerzusammensetzung und des Mizellierungsprotokolls, in ihrer Größe und ihren optischen Eigenschaften variiert werden.

Der zweite Teil der Dissertation widmet sich Methoden zur Einführung diverser Ankergruppen in konjugierte Polymere. In ersten Ansatz wurden Blockcopolymere bestehend aus einem konjugierten 2,5-Di(2'-ethylhexyloxy)poly-p-phenylene vinylene (DEH-PPV) Block und einem Reaktivesterblock über eine Kombination von Siegrist Polykondensation und RAFT Polymerisation hergestellt. Der Reaktivesterblock wurde dann zur Einführung diverser Ankergruppen ausgenutzt. Mit den resultierenden Polymere und Nanoplättchen wurden Hybridmaterialien hergestellt, wodurch der Einfluss der verschiedenen Ankergruppen auf die optischen Eigenschaften und die Materialeigenschaften untersucht werden konnte. Des Weiteren wurden zwei Strategien zum Einbau von Ankergruppen am Kettenende von Poly(3-alkylthiophen) (P3HT) entwickelt. Dazu wurde einerseits kupferkatalysierte 1,3-dipolare Cycloaddition und andererseits eine Kombination aus Vilsmeier-Reaktion und anschließender Umsetzung des entstandenen Aldehyds mit dem entsprechenden Aminen genutzt. Diese Polymere wurden abschließend verwendet, um Hybridmaterialien mit TiO_2 oder CdSe@ZnS Nanokristallen herzustellen. Darüber hinaus konnte, unter Bestrahlung der Probe, Elektronentransfer vom Polymer zu den TiO_2 Nanokristallen per Kelvinsonden-kraftmikroskopie (KPFM) nachgewiesen werden.

Abstract (in Korean)

전도성 물질의 형태와 경계면 제어

멘크 플로리안
화학부 유기화학 전공
서울대학교 대학원

본 박사학위논문은 두 가지 주제에 중점을 두고 있다. 한 가지는 전도성 물질의 형태를 제어하는 방법의 개발에 대한 것 이고, 다른 한 가지는 공액고분자에 앵커기(anchor group)를 도입하는 새로운 접근법의 개발에 대한 것이다.

무기물 기반 소자에 경쟁하기 위해서는 유기물 혹은 하이브리드 광전자 소자의 효율 향상이 필수적이다. 광전자 소자를 구성하는 박막의 형태는 소자의 성능에 영향을 주는 중요한 요소로 밝혀져 왔다. 그에 따라 전도성 물질의 형태를 조절 가능하게 하는 접근법들이 개발되었다. 형태 조절을 위한 첫 번째 접근법은 유기/무기 나노복합재 (nanocomposites)를 이용하는 것이다. 반도체 성질을 갖는 고분자를 가역적 첨가-분절 연쇄이동 (reversible addition-fragmentation chain transfer; RAFT) 중합법으로 합성하고 반응성을 갖는 에스테르 말단기(reactive ester group)를 연쇄 이동제 (chain-transfer agent; CTA)를 이용하여 도입하였다. 이 에스테르 말단기를 이용함으로써 고분자에 광 절단이 가능한(photocleavable) 앵커기를 달았다. TiO_2 나노막대에 친화성을 가지는 앵커기를 이용해 각각 잘 분산되는 안정한 나노 복합재를 제작하는 것이 가능했고 이를 TEM으로 관찰하였다. 마지막으로, 자외선을 조사하여 나노막대를 구형 집합체로 자기조립 하였다. 형태조절을 위한 두 번째 접근법은 한 블록이 공액고분자로 이루어진 양친성 로드-코일 블록공중합체의 합성이다. 이런 고분자들의 합성에 대한 기존의 발표들과는 반대로, 손쉬운 원-포트(one-pot) 과정으로 고분자를 합성하였다. 이렇게

합성한 고분자로, 고분자 구성 비율과 마이셀 제작 과정에 따라 다양한 크기와 광성질을 갖는 마이셀을 제작하였다.
본 학위논문의 두 번째 부분에서는 공액고분자에 다양한 앵커기를 도입하는 것을 가능하게 하는 접근법을 개발하였다. Siegrist 축합중합과 RAFT 중합법의 조합이 공액고분자인 DEH-PPV 블록과 반응성을 가진 에스테르 블록으로 구성된 블록공중합체의 합성에 사용되었다. 따라서, 반응성을 갖는 에스테르 블록이 서로 다른 앵커기의 도입을 위해 이용되었다. 만들어진 고분자는 CdSe 나노판의 기능화에 응용되었고, 이 앵커기가 광성질 및 물성에 미치는 영향이 연구되었다. 또한 앵커 말단기를 P3HT 고분자에 도입하는 두 가지 접근법 또한 연구되었다. 구리촉매를 이용한 아자이드-알카인 Huisgen 고리화 첨가 반응(azide-alkyne Huisgen cycloaddition)과 Vilsmeier 반응을 이용해 P3HT 고분자에 다양한 앵커기를 달았다. 앞서 증명한 것처럼, P3HT와 TiO_2 혹은 CdSe@ZnS나노결정으로 구성된 안정한 나노복합재를 만들 수 있었다. 또한 빛 조사에 의한 고분자에서 TiO_2 나노결정으로의 전자 이동이 KPFM을 통해 관찰되었다.

주요어: 블록공중합체, 공액성 고분자, 리빙 중합, 형태학, 광전자학, 고리개환복분해중합
학번: 2015-30737

Table of Contents

1. Abstracts

1.1 Abstract

The dissertation at hand focusses on two different subjects. On the one hand, approaches which allow controlling the morphology of conducting materials were developed. On the other hand, new approaches for the incorporation of anchor groups into conjugated polymers were investigated.

To compete with inorganic devices, improved efficiencies of organic and hybrid optoelectronic devices are required. The morphology of the films assembling an optoelectronic device has been identified as an important factor influencing the device performance. Therefore, approaches which enable the manipulation of the conducting materials' morphology were developed. The first approach in the context of morphology control deals with organic/inorganic nanocomposites. A semiconducting polymer was synthesized via RAFT polymerization and a reactive ester end group was incorporated using a functional CTA. Exploiting the reactive ester, the polymer was equipped with a photocleavable anchor group. The anchor group's affinity towards TiO_2 nanorods enabled the fabrication of stable nanocomposites composed of individually dispersed nanorods as observed via TEM. Finally, upon irradiation with UV light, self-assembly of the nanorods into spherical aggregates was achieved. In the second approach which focuses on a manipulation of the morphology, amphiphilic block copolymers exhibiting one conjugated and one non-conjugated block were synthesized. In contrast to previous reports of the synthesis of such polymers, the block copolymers were synthesized in a facile one-pot procedure. Using the obtained polymers, micelles were fabricated with differing sizes and optical properties depending on the block copolymer composition and the micellization procedure.

In the second part of this dissertation, approaches which permit the incorporation of various anchor groups into conjugated polymers were developed. Therefore, a combination of Siegrist polycondensation and RAFT polymerization was used for the synthesis of block copolymers composed of a conjugated DEH-PPV block and a reactive ester block. Consequently, the reactive ester block was exploited for the incorporation of different anchor groups. The resulting polymers were then applied for the functionalization of CdSe nanoplatelets and the influence of the anchor groups on the optical and material properties were investigated. Furthermore, two approaches enabling the incorporation of anchoring end groups into P3HT

were investigated. Both, via copper catalyzed azide-alkyne Huisgen cycloaddition and via Vilsmeier reaction, P3HT was equipped with various anchor groups. As demonstrated, stable nanocomposites composed of P3HT and either TiO_2 or CdSe@ZnS nanocrystals could be obtained. In addition, electron transfer from the polymer to the TiO_2 nanocrystals under irradiation was observed via KPFM.

1.2 Inhalt der vorliegenden wissenschaftlichen Arbeit

Im Rahmen der vorliegenden Dissertation wurden zwei verschiedenen Themen bearbeitet. Einerseits wurden Strategien entwickelt, die eine Morphologiekontrolle bei leitenden Materialien ermöglichen. Andererseits wurden Synthesewege erforscht, die die Einführung von Ankergruppen in konjugierte Polymere ermöglichen.

Die Effizienz ist der ausschlaggebende Faktor bei optoelektronischen Anwendungen. Generell geringe Effizienzen bedingen, dass organische und hybride Bauteile ihren rein anorganischen Gegenstücken bisher unterlegen sind. Daher ist eine Effizienzsteigerung im Falle der organischen und hybriden Systeme erforderlich, um eine Konkurrenzfähigkeit gegenüber anorganischen Systemen zu erzielen. Die Morphologie eines Bauteils spielt eine zentrale Rolle für dessen Effizienz. Daher wurden im Rahmen dieser Dissertation Ansätze entwickelt, um die Morphologie von leitenden Materialien zu beeinflussen. Der erste Ansatz befasste sich dabei mit der Morphologiekontrolle von organisch/anorganischen Hybridmaterialien. Zunächst wurde dazu ein halbleitendes Polymer per RAFT (reversibler Additions-Fragmentierungs Kettenübertragungs) Polymerisation hergestellt. Dieses Polymer wurde durch die zur Polymerisation verwenden Kettenübertragungsreagenz (CTA) mit einer Reaktivester-Endgruppe ausgestattet. Im Weiteren wurde diese Endgruppe mit einem Amin umgesetzt, um eine photospaltbare Ankergruppe einzuführen. Danach konnten TiO_2 Nanostäbchen per Ligandenaustausch mit dem Polymer beschichtet werden. Die so erhaltenen organisch/anorganischen Komposite bildeten Dispersionen mit einzeln verteilten Nanostäbchen wie durch Transmissionselektronen-mikroskopie (TEM) belegt werden konnte. Anschließend gelang es die Polymere von den Nanostäbchen durch Bestrahlung mit UV-Licht abzuspalten. Daraufhin aggregierten die Nanostäbchen und lagerten sich zu kugelförmigen Aggregaten zusammen. In einem zweiten Ansatz wurden amphiphile Blockcopolymere hergestellt, welche sich aus einem konjugierten und einen nicht konjugierten Block zusammensetzten. Dabei wurden diese Blockcopolymere, im Gegensatz zu bisherigen Berichten, in einer simplen Eintopfreaktion synthetisiert. Die so erhaltenen amphiphilen Blockcopolymere wurden später zur Herstellung von Mizellen verwendet. Diese Mizellen konnten, in Abhängigkeit der Polymerzusammensetzung und des Mizellierungsprotokolls, in ihrer Größe und ihren optischen Eigenschaften variiert werden.

Der zweite Teil der Dissertation widmet sich Methoden zur Einführung diverser Ankergruppen in konjugierte Polymere. In ersten Ansatz wurden Blockcopolymere bestehend aus einem konjugierten 2,5-Di(2'-ethylhexyloxy)poly-p-phenylene vinylene (DEH-PPV) Block und einem Reaktivesterblock über eine Kombination von Siegrist Polykondensation und RAFT Polymerisation hergestellt. Der Reaktivesterblock wurde dann zur Einführung diverser Ankergruppen ausgenutzt. Mit den resultierenden Polymere und Nanoplättchen wurden Hybridmaterialien hergestellt, wodurch der Einfluss der verschiedenen Ankergruppen auf die optischen Eigenschaften und die Materialeigenschaften untersucht werden konnte. Des Weiteren wurden zwei Strategien zum Einbau von Ankergruppen am Kettenende von Poly(3-alkylthiophen) (P3HT) entwickelt. Dazu wurde einerseits kupferkatalysierte 1,3-dipolare Cycloaddition und andererseits eine Kombination aus Vilsmeier-Reaktion und anschließender Umsetzung des entstandenen Aldehyds mit dem entsprechenden Aminen genutzt. Diese Polymere wurden abschließend verwendet, um Hybridmaterialien mit TiO_2 oder CdSe@ZnS Nanokristallen herzustellen. Darüber hinaus konnte, unter Bestrahlung der Probe, Elektronentransfer vom Polymer zu den TiO_2 Nanokristallen per Kelvinsonden-kraftmikroskopie (KPFM) nachgewiesen werden.

1.3 초록

본 박사학위논문은 두 가지 주제에 중점을 두고 있다. 한 가지는 전도성 물질의 형태를 제어하는 방법의 개발에 대한 것 이고, 다른 한 가지는 공액고분자에 앵커기(anchor group)를 도입하는 새로운 접근법의 개발에 대한 것이다.

무기물 기반 소자에 경쟁하기 위해서는 유기물 혹은 하이브리드 광전자 소자의 효율 향상이 필수적이다. 광전자 소자를 구성하는 박막의 형태는 소자의 성능에 영향을 주는 중요한 요소로 밝혀져 왔다. 그에 따라 전도성 물질의 형태를 조절 가능하게 하는 접근법들이 개발되었다. 형태 조절을 위한 첫 번째 접근법은 유기/무기 나노복합재(nanocomposites)를 이용하는 것이다. 반도체 성질을 갖는 고분자를 가역적 첨가-분절 연쇄이동 (reversible addition-fragmentation chain transfer; RAFT) 중합법으로 합성하고 반응성을 갖는 에스테르 말단기(reactive ester group)를 연쇄 이동제 (chain-transfer agent; CTA)를 이용하여 도입하였다. 이 에스테르 말단기를 이용함으로써 고분자에 광절단이 가능한(photocleavable) 앵커기를 달았다. TiO_2 나노막대에 친화성을 가지는 앵커기를 이용해 각각 잘 분산되는 안정한 나노 복합재를 제작하는 것이 가능했고 이를 TEM으로 관찰하였다. 마지막으로, 자외선을 조사하여 나노막대를 구형 집합체로 자기조립 하였다. 형태조절을 위한 두 번째 접근법은 한 블록이 공액고분자로 이루어진 양친성 로드-코일 블록공중합체의 합성이다. 이런 고분자들의 합성에 대한 기존의 발표들과는 반대로, 손쉬운 원-포트(one-pot) 과정으로 고분자를 합성하였다. 이렇게 합성한 고분자로, 고분자 구성 비율과 마이셀 제작 과정에 따라 다양한 크기와 광성질을 갖는 마이셀을 제작하였다.

본 학위논문의 두 번째 부분에서는 공액고분자에 다양한 앵커기를 도입하는 것을 가능하게 하는 접근법을 개발하였다. Siegrist 축합중합과 RAFT 중합법의 조합이 공액고분자인 DEH-PPV 블록과 반응성을 가진 에스테르 블록으로 구성된 블록공중합체의 합성에 사용되었다. 따라서, 반응성을 갖는 에스테르 블록이 서로 다른 앵커기의 도입을 위해 이용되었다. 만들어진 고분자는 CdSe 나노판의 기능화에 응용되었고, 이 앵커기가 광성질 및 물성에 미치는 영향이 연구되었다. 또한 앵커 말단기를 P3HT 고분자에 도입하는 두 가지 접근법 또한 연구되었다. 구리촉매를 이용한 아자이드-알카인 Huisgen 고리화 첨가 반응(azide-alkyne Huisgen cycloaddition)과 Vilsmeier 반응을 이용해 P3HT 고분자에 다양한 앵커기를 달았다. 앞서 증명한 것처럼, P3HT와 TiO_2 혹은 CdSe@ZnS나노결정으로 구성된 안정한 나노복합재를 만들 수 있었다. 또한 빛 조사에 의한 고분자에서 TiO_2 나노결정으로의 전자 이동이 KPFM을 통해 관찰되었다.

2. Introduction

The research on renewable energy sources such as solar power is one of the main topics of the recent decades. Its impact is increasing due to the limited deposits of fossil energy sources (e.g. ore and oil). The problem of limited fossil energy sources is particularly intensified by the growing demand of energy for developing and emerging countries. Unfortunately, the efficiencies of renewable energy sources are still relatively low compared to the production costs. Therefore, aspects increasing the efficiencies and lowering the production costs have to be developed.

Organic and hybrid optoelectronic devices are very promising candidates for lower cost production. Due to the high optical absorption coefficients of organic molecules (small molecules or polymers), large amounts of light can be absorbed by a small amount of material. Therefore, large amounts of energy can be harvested in thin film devices. Such thin film devices are very attractive as only small amounts of the usually relatively expensive active materials are needed which significantly reduce the costs per device.

There are several factors strongly influencing the performance of optoelectronic devices. One of the most important factors is the active material. In organic optoelectronics the active materials are usually composed of conjugated small molecules or polymers. A delocalized conjugated system is important to achieve the desired optical and electronical properties. Due to the conjugated system, the materials exhibit high absorption coefficients which enable sufficient light harvesting in thin film devices.
Another key aspect to achieving high performance is an optimized morphology of the active layer. Typically the active layer is composed of two materials, one electron donor (hole conducting material) and one electron acceptor (electron conducting material). Through the absorption of light, electrons can be excited from the HOMO (highest occupied molecular orbital) or valence band of the active materials to the LUMO (lowest unoccupied molecular orbital) or conduction band, respectively, and create electron-hole pairs (or excitons). These electron-hole pairs, however, have to be separated and the charge carriers have to be transported to the electrodes. The separation of the electron-hole pair takes place only at the interface of electron donor and acceptor. The driving force for the charge separation results from different HOMO/LUMO levels of donor and acceptor. In order to enable the transportation of electrons the LUMO of the acceptor should have a lower energy than the LUMO of the donor. In addition, the HOMO of the acceptor should exhibit a lower energy

than the HOMO of the donor to support the transportation of holes. Furthermore, due to an average exciton diffusion length of approximately 10 to 30 nm, solely electron-hole pairs which are generated close to the interface can be separated.[I1] Therefore, on the one hand the interface between both materials should be as high as possible to enable an effective charge separation. On the other hand, once separated, charge carriers need a percolated pathway for the electrons to enable effective charge transport. Consequently, an optimized morphology displays percolated pathways for the charge carriers and a sufficiently large interface between acceptor and donor to allow sufficient charge separation.

An improvement of the morphology of the active layer can often be achieved by involving an annealing step which increases the grain size and the crystallinity of the active materials and, therefore, results in higher charge carrier mobilities.[I2] The impact of an optimized morphology was studied by Padinger *et al*. who showed that during the annealing process a first increase of the device's performance is followed by a drastic decrease once the annealing process is continued for an extended period of time.[I3]

In the case of hybrid optoelectronic devices, an additional factor strongly influencing the device performance has to be taken into account. To prevent the inorganic nanoparticles from aggregating, they are usually covered with so-called surfactants. These surfactants interact with unsaturated metal centers at the nanoparticles surface and, thereby, complete their coordination sphere. Additionally, repulsive forces of the surfactant coating prevent the nanoparticles to approach one another. Surfactants can be either small molecules or polymers. For polymer surfactants, anchor groups enabling an effective binding of the polymer to the inorganic nanoparticles have to be incorporated into the polymer. Such polymeric surfactants mediate an effective mixing of the inorganic nanoparticles with an appropriate polymer matrix and avoid phase separation. Therefore, such polymer surfactants enable the fabrication of homogeneous films. The group interacting with the inorganic surface (small molecule surfactant or anchor group incorporated into a polymer), however, strongly influences the device performance which will be further discussed in Section 2.3.

In the following subsections we will therefore, first, provide a short introduction into conducting polymers with the focus on synthetic methods enabling advanced polymer architectures. Second, we will outline approaches which enable a control over the morphology of conducting materials and, third, discuss the role of interface control regarding surfactants.

2.1 Conducting Polymers

There are many different synthetic approaches for the synthesis of conducting polymers. For the synthesis of low band gap polymers mostly polycondensations are used such as Suzuki-Miyaura coupling or Stille coupling. Unfortunately, these polycondensation reactions are no living polymerization techniques and, therefore, suffer from relatively large molecular weight distributions. Even more severe, these polymerization techniques do not enable an advanced control of the polymer architecture such as the incorporation of functional end groups and the simple synthesis of block copolymers (without involving multiple end group reactions). Such a control, however, is very important with regards to the introduction of anchor groups for the effective binding to inorganic nanoparticles and the synthesis of rod-coil block copolymers which enable directional self-assembly.

By contrast, polymerization techniques such as reversible addition-fragmentation chain transfer (RAFT) polymerization, Grignard metathesis (GRIM) polymerization and ring-opening metathesis polymerization (ROMP) allow for both, the synthesis of conducting polymers with the desired optoelectronic properties and, in addition, exhibit a living nature which allows for the introduction of functional end groups and the simple synthesis of block copolymers. For that reason, we will describe these polymerization techniques in greater detail in the following subsections. Moreover, the Siegrist polycondensation which is another approach for the synthesis of conjugated polymers will be described. Though it is not a living polymerization and, hence, is not capable of synthesizing block copolymers, polymers obtained via Siegrist polycondensation exhibit a defined functional end group. This functional end group was used to modify the obtained polymer and achieve the desired properties.

2.1.1 Reversible Addition-Fragmentation Chain Transfer (RAFT) polymerization

The basic concept of RAFT polymerization was already investigated by Tatemoto in 1992 and Wang and Matyjaszewski in 1995 who reported an “iodine transfer polymerization”.[I4] The approach which is understood as RAFT polymerization today, however, was first described by Rizzardo, Moad and Thang in 1998.[I5]

The mechanism of RAFT polymerization is shown in **Figure 1**. During the polymerization process only a small amount of free radicals exist in the reaction mixture due to the addition-fragmentation equilibrium. While a polymer chain is attached to the CTA it cannot react with monomers and is, therefore, called dormant species. The equilibrium between the dormant species and the active, free radicals in the reaction mixture lies on the side of the dormant species. Thus, much more growing polymer chains exit in solution compared to the free radicals causing the quasi living nature of RAFT polymerization. RAFT polymerization is a suitable technique for various applications due to its tolerance of many functional groups which can be introduced into the monomer (R_1 and R_2). Therefore, semiconducting polymers are accessible via RAFT polymerization, for example by the incorporation of triphenylamine side groups. Caused by the quasi living nature RAFT polymerization is suitable for the simple synthesis of block copolymers. Furthermore, it offers the possibility to introduce a variety of functional end groups via the chain transfer agent (CTA). The side group R is incorporated as the polymer end group and can be equipped with functional groups such as reactive esters or azides.[I6]

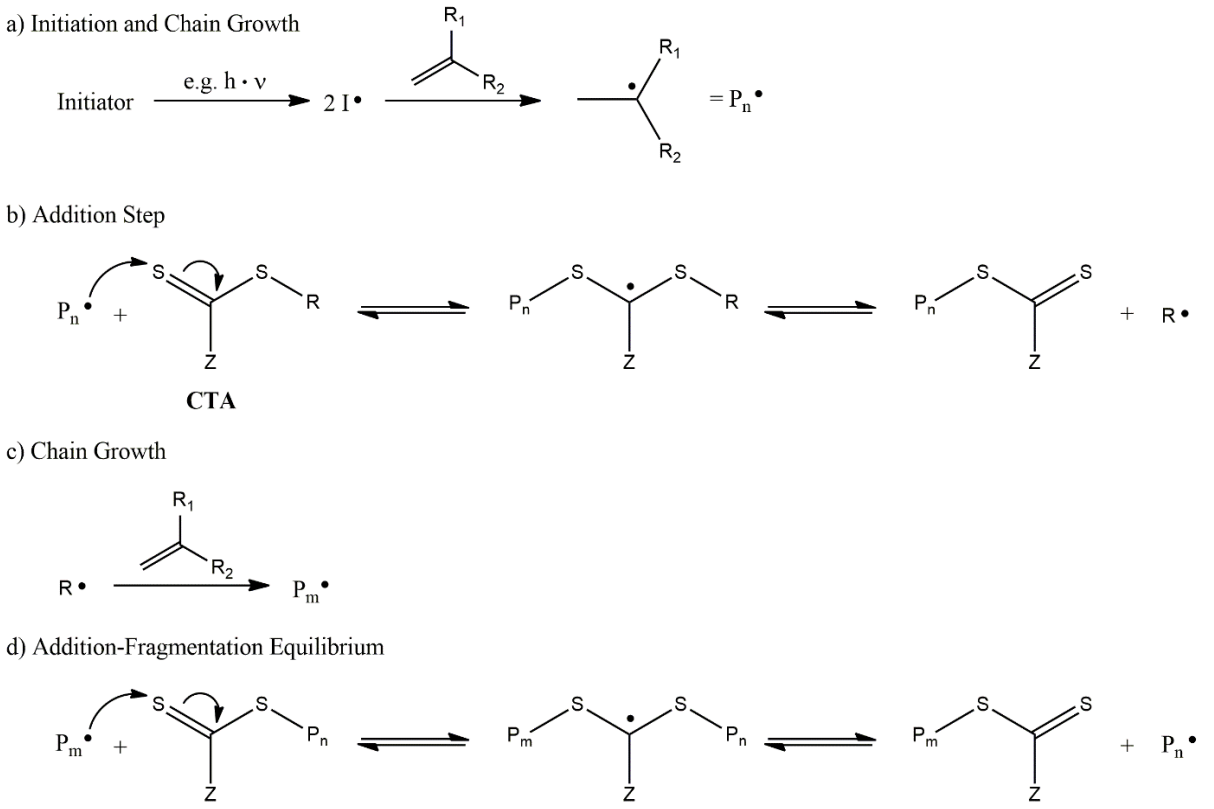

Figure 1. Mechanism of RAFT polymerization.

RAFT polymerization was exploited in this work for the synthesis of a semiconducting polymer and the incorporation of a photocleavable anchor group which was realized via a functional end group introduced by the CTA. The project involving RAFT polymerization will be discussed in Section 4.1.1.

2.1.2 Siegrist Polycondensation

The Siegrist polycondensation is based on the "Anil-Synthese" reported by Siegrist in 1967.[I7,I8] As it is a polycondensation, controlling the molecular weight is quite difficult and high molecular weights are rarely achieved. As the reaction starts upon the addition of the solvent (dimethylformamide – DMF), the upscaling process is especially problematic and often leads to a broad molecular weight distribution. The DMF is of great importance as it is involved in the reaction mechanism. By contrast, other amides with similar permittivities need higher temperatures and result in much lower yields already in the case of a single, low molecular weight coupling reaction. As base usually potassium *tert*-butoxide is used due to the improved solvation of the potassium cation compared with sodium or lithium.

However, the selectivity of the polymerization is quite remarkable as solely *trans* double bonds are formed.[I7,I9] Furthermore, the Siegrist polycondensation offers the possibility to introduce a defined functional end group via the quenching with water.[I9,I10] Thus, an aldehyde end group is incorporated at the chain end and can be used for further modifications.

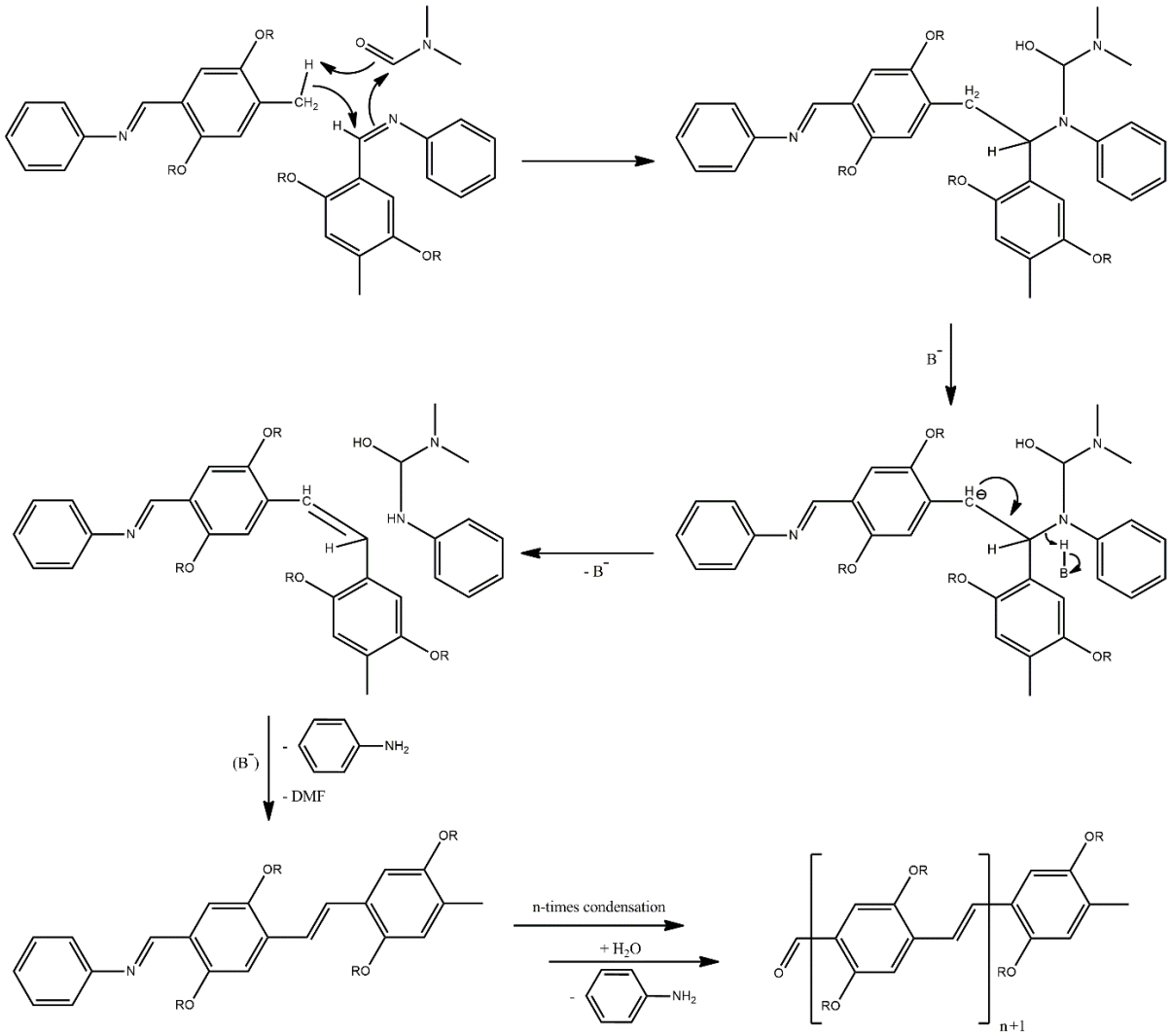

Figure 2. Mechanism of the Siegrist polycondensation for the synthesis of PPVs and incorporation of an aldehyde end group via quenching with water.

The Siegrist polycondensation was used in this work because of its last named advantage. The aldehyde was used for the incorporation of a CTA by multiple end group reactions. The CTA enabled the incorporation of a reactive ester via RAFT polymerization which was employed to introduce various anchor groups. This project will be discussed in Section 4.2.1.

2.1.3 Grignard Metathesis (GRIM) Polymerization

The GRIM polymerization based on the Kumada coupling was first described in 1992 by McCullough *et al*.[I11] Contrasting RAFT polymerization, GRIM polymerization is not a radical polymerization. Very advantageous for optoelectronic applications, polymers obtained via the GRIM polymerization exhibit a conjugated backbone. Furthermore, the polymers are highly regioregular. Thus, polymers obtained via GRIM polymerization have generally a long average conjugation length which leads to excellent optoelectronic properties.

The suggested mechanism explaining the regioregularity and additional characteristics of the GRIM polymerization can be found in **Figure 3**. The mechanism is explained on the example of the most common class of polymers synthesized via GRIM polymerization, poly(3-alkythiophenes) (P3ATs).

In the first step of the approach a Grignard metathesis takes place and the monomer precursor is converted into monomers **1** and **1'**. Using a sterically demanding Girgnard reagent for the metathesis such as *tert*-butylmagnesium chloride the metathesis becomes quite selective and compound **1** can be obtained in great excess (85 %).[I12] This is desired as only compound **1** is polymerized due to the sterical hinderance in proximity to the aryl-magnesium chloride of compound **1'**.[I13] In the next step, monomer **1** reacts with the nickel catalyst (most often Ni(dppp)Cl_2 – dichloro(1,3-bis(diphenylphosphino)propane)nickel(II)). After reductive elimination, an associated pair composed of a catalyst and a dimer which possesses tail-to-tail configuration is built. The nickel catalyst which enables the Kumada coupling sticks to the polymer and moves along the conjugated polymer backbone (so-called "ring-walking").[I14] The catalyst is never detached from the polymer which causes the living nature of GRIM polymerization. As shown in **Figure 3**, the polymer develops following a chain growth mechanism and the monomer repeating units are regioregularly incorporated exhibiting a head-to-tail (HT) configuration. Thus, the polymer backbone displays an almost complete HT configuration leading to an increased average conjugation length and improved electronic conductivity compared with regioirregular P3ATs.

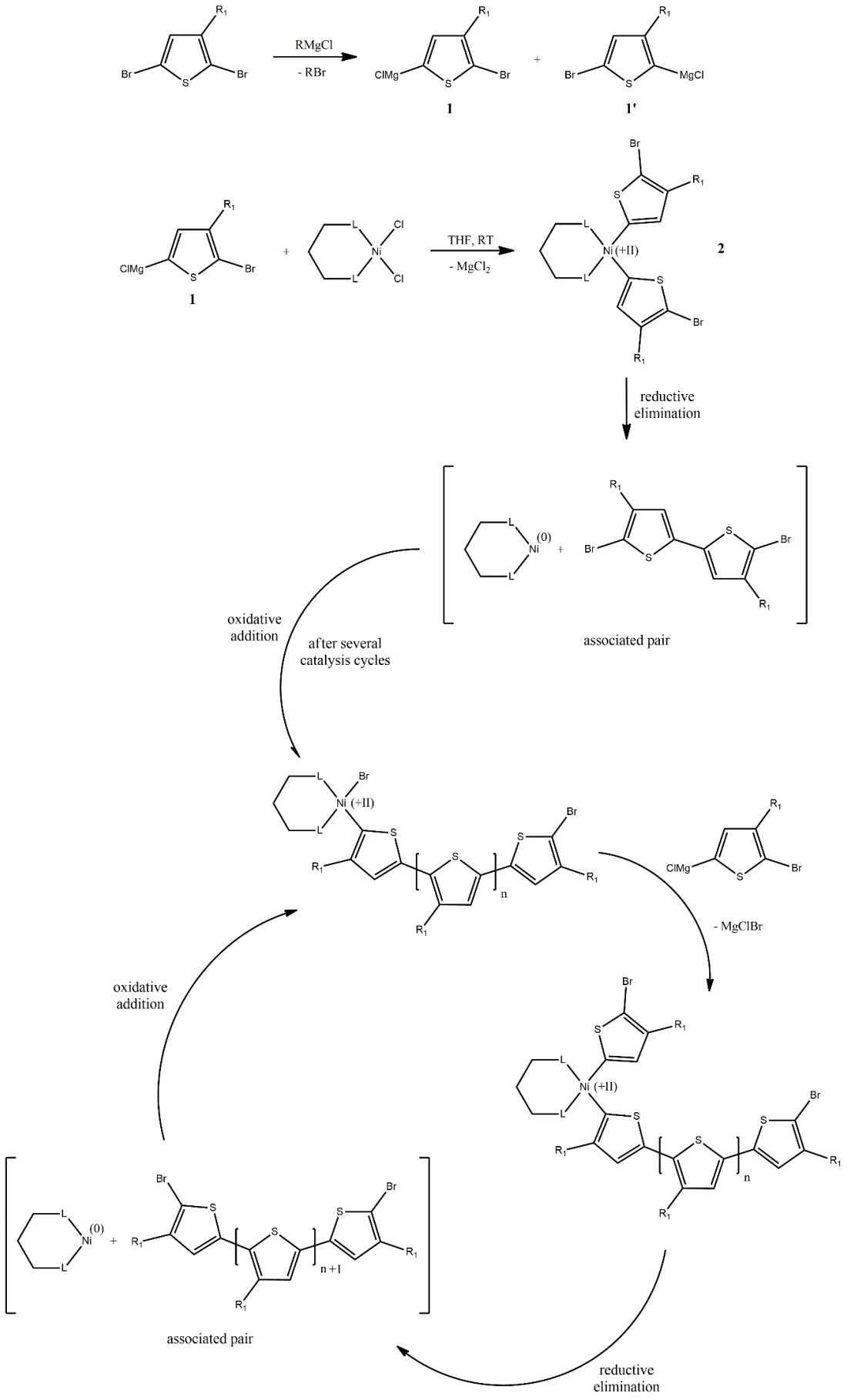

Figure 3. Proposed mechanism of the GRIM polymerization.

The living nature of GRIM polymerization enables the synthesis of block copolymers and the incorporation of defined, functional end groups via several approaches.[I13,I15,I16] The approach which will be exploited in the study at hand is shown in **Figure 4**. As displayed in the mechanism, the quenching with a Grignard reagent leads, depending on the Grignard reagent, to a mono- or difunctionalized polymer.[I15,I17]

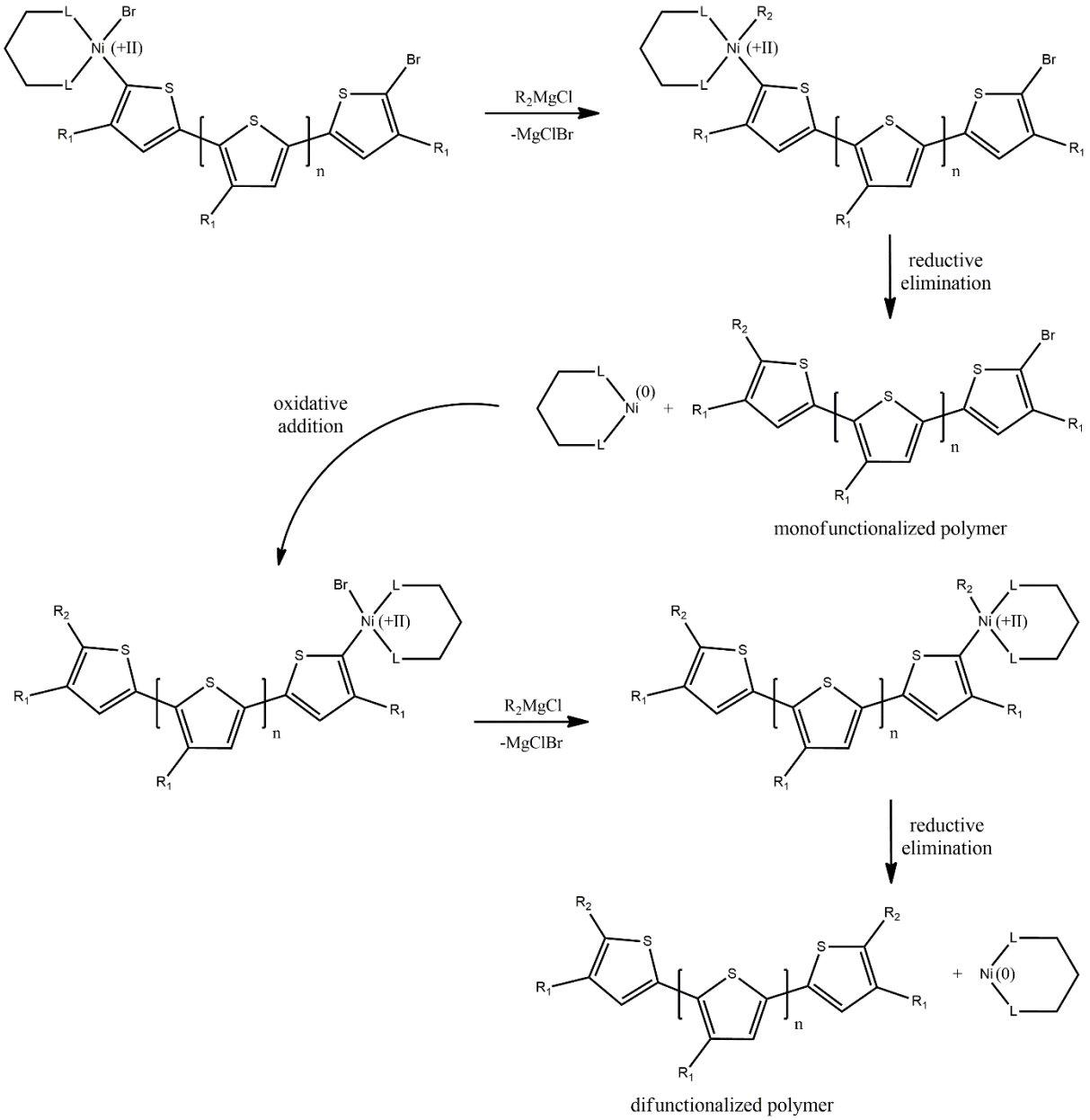

Figure 4. Mechanism of end group modification via Grignard quenching.

The GRIM polymerization was used in this work for the incorporation of an alkyne as polymer end group. Various functional groups were then incorporated by azide-alkyne Huisgen cycloaddition. This project will be discussed in Section 4.2.2.

2.1.4 Ring-Opening Metathesis Polymerization (ROMP)

The ring-opening metathesis polymerization (ROMP) is a chain-growth polymerization based on olefin metathesis. The driving force of ROMP is the release of ring strain energy of strained, cyclic olefins. Usually, transition metal carbene complexes such as Grubbs' and Schrock catalysts (see **Figure 5**) are used for the polymerization.

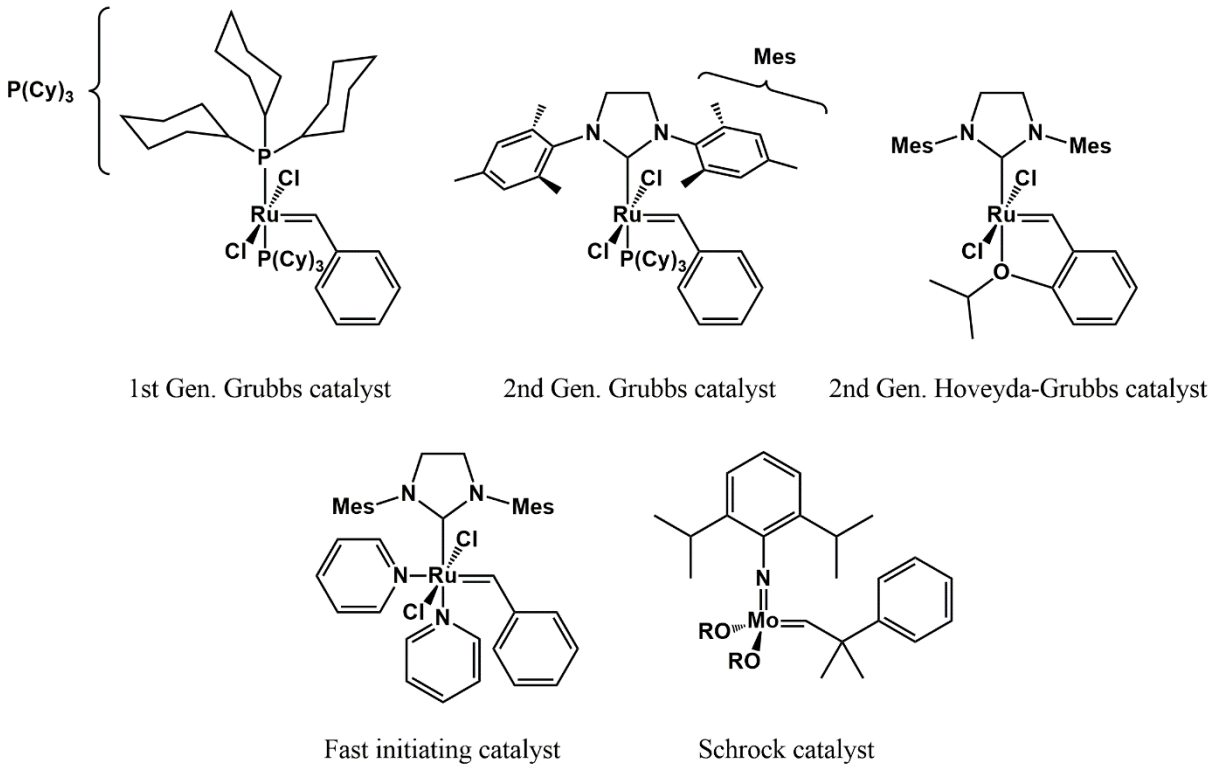

Figure 5. Transition metal carbene complexes used in ROMP.

The mechanism of ROMP, although intensively studied, is not yet completely understood and still topic of ongoing research. The mechanism seems to depend on various factors such as catalyst, solvent and monomer. In most cases, however, a dissociative mechanism seems to be the major pathway. For example Romero *et al*. carried out NMR studies and observed a bottom-bound metallacyclobutane (MCB) as an intermediate.[118] The bottom-bound MCB suggests a dissociative pathway. Unfortunately, only in the case of catalysts bearing a SiMes

ligand (1,3-Bis(2,4,6-trimethylphenyl)-4,5-dihydroimidazol-2-ylidene) the MCB was stable enough to be detected. MCBs formed from catalysts bearing the $P(Cy)_3$ ligand (tricyclohexylphosphine) were not observable which, however, is consistent with DFT calculations.[I19] Therefore, the dissociative pathway is shown in **Figure 6** to demonstrate ROMP by the example of a norbornene monomer polymerized using 2nd generation Grubbs catalyst.

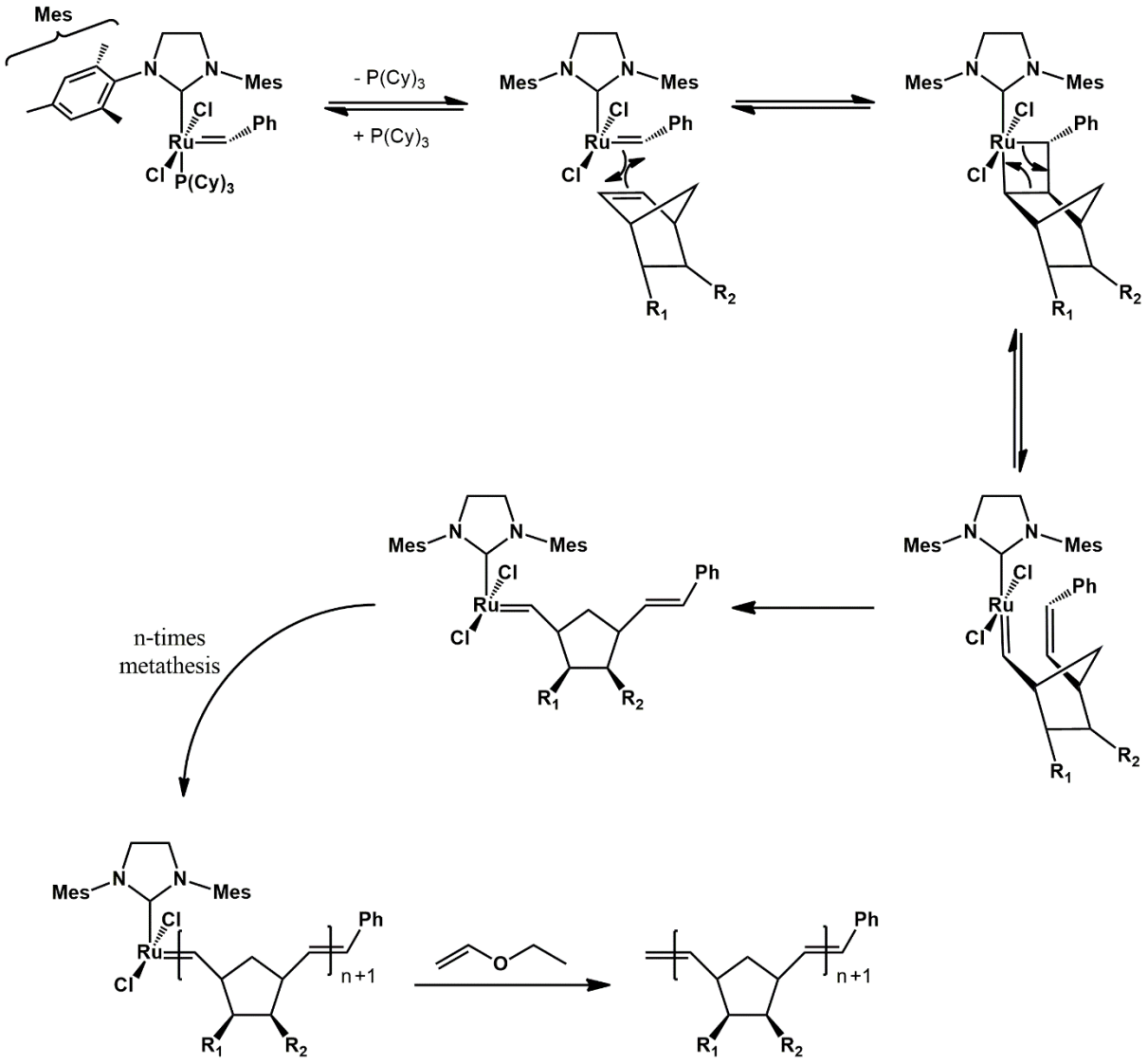

Figure 6. ROMP of a norbornene monomer using 2nd generation Grubbs catalyst. The mechanism shown involves a dissociation of the phosphine ligand prior to the addition of the olefin. Therefore, a bottom-bound metallacyclobutane is formed. The reaction is stopped by the addition of ethyl vinyl ether (EVE).

Despite the undissolved questions regarding the mechanism, ROMP is a widely used polymerization technique because of its various advantages. Under careful treatment and without contamination of the reaction mixture with impurities which would decompose the catalyst, no termination reactions occur. Furthermore, in many cases the initiation rate is much faster than the propagation rate which is an important aspect for the synthesis of block copolymers. As ROMP usually creates a low number of side products while quantitative conversion is often reached, block copolymers can be synthesized in simple one-pot procedures. The possibility of simple block copolymerization enables the incorporation of different functionalities in a single polymer backbone. In addition, functional end groups can be incorporated via modified catalysts or quenching agents carrying functional groups.[I20]

ROMP was used in this work to synthesize block copolymers composed of a conjugated and a non-conjugated block via a simple one-pot procedure (Section 4.1.2). The benefit of this procedure was to avoid multiple end group reactions which usually lead to a contamination of the final product with polymeric impurities. Such polymeric impurities (precursor polymers) are in the majority of cases difficult to remove and can, therefore, affect the desired properties of the final product. Given that finding the optimized conditions was quite difficult, we conducted a detailed kinetic study of the monomer (four different isomers of dimethoxy-(2-ethylhexyloxy)-[2.2]paracyclophane-1,9-diene) for the conjugated block. Thereby, we revealed several interesting aspects of the system which will be discussed in Section 4.1.2.

2.2 Morphology Control

In the study at hand we focused on the morphology control of (semi)conducting materials. To achieve control over the morphology, an advanced polymer architecture is usually needed. Therefore, polymerization techniques permitting a modification of the polymer according to the desired properties, such as the polymerization techniques discussed in the previous section 2.1, are needed. In this section 0, an introduction into the morphology control of biphasic hybrid systems will be provided. First, several synthetic approaches to achieve stable nanocomposites will be discussed. Second, we will present routes which support the controlled fabrication of percolated morphologies. Third, an overview of applications integrating nanocomposites which are affected by the morphology of the biphasic system will be provided. Fourth, a short outline regarding the fabrication of nanoparticles (e.g. micelles) composed of amphiphilic block copolymers will be presented. The first three subjects were discussed in a review article published by the author and his colleagues in 2015. Therefore, this review article is inserted in the following Section 2.2.1. The fourth subject will be discussed thereafter, in Section 2.2.2.

The main parts of the following review article were written by myself and Ms. Ana Fokina who was mainly involved preparing most of the drawings, both supervised by Prof. Dr. R. Zentel. Prof. Dr. F. Schmid contributed the discussion regarding simulations of the morphology. All other authors contributed with supervision and council.

2.2.1 Publication in Macromolecular Rapid Communications, 2015, 36, 959–983

Morphology Control in Biphasic Hybrid Systems of Semiconducting Materials

Florian Mathias, Ana Fokina, Katharina Landfester, Wolfgang Tremel, Friederike Schmid, Kookheon Char, Rudolf Zentel*

Abstract

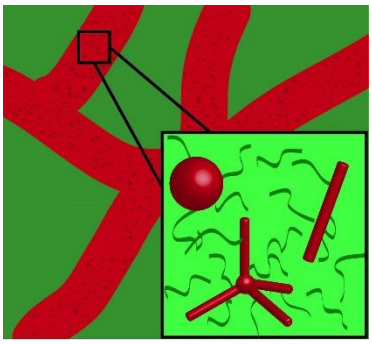

Simple blends of inorganic nanocrystals and organic (semiconducting) polymers usually lead to macroscopic segregation. Thus, such blends typically exhibit inferior properties than expected. To overcome the problem of segregation, polymer coated nanocrystals (nanocomposites) have been developed. Such nanocomposites are highly miscible within the polymer matrix. In this review we present a summary of synthetic approaches to achieve stable nanocomposites in a semiconducting polymer matrix. Furthermore, we provide a theoretical background as well as an overview concerning morphology control of the inorganic NCs in the polymer matrix. In addition, the morphologic behavior of highly anisotropic nanoparticles (i.e. liquid crystalline phase formation of nanorod-composites) and branched nanoparticles (spatial orientation of tetrapods) is described. Moreover, we discuss the morphology requirements for the application of inorganic/organic hybrid systems in light emitting diodes and solar cells as well as provide potential solutions to achieve the required morphologies.

1. Introduction

The topic of this review/feature article is dispersion control of the semiconducting particles in semiconducting polymer matrices. Thereby it combines two aspects: First, the application of semiconducting materials in light emitting diodes – LEDs or organic LEDs (OLEDs), logic elements or photovoltaics – and second, the more basic aspect of placing inorganic nanoparticles in a matrix of polymer chains (for this aspect the semiconductivity of the matrix is, however, primarily irrelevant).

While polymers (mostly conjugated polymers) and nanoparticles with semiconducting properties have been investigated in parallel for some time, it recently turned out that a combination of both may lead to nanocomposites whose properties are much superior than that of their constituents.[1] Since then, several applications of these new hybrid materials have been developed, especially in light emitting diodes and photovoltaic cells. Recent reviews on the topic can be found in ref. 2 - 6.[2–6] Generally, semiconducting hybrid systems combine the beneficial properties associated with semiconducting polymers such as light weight, flexibility, ink jet printing, roll-to-roll production, low cost and solvent processability over a large area[2, 7] with the advantages of inorganic nanocrystals (NCs) such as high electron mobility, tunable optical properties, and optical stability.[1, 4] During the last decade, remarkable progress has been made in colloidal synthesis[8, 9] and the self-assembly[10] of NCs with well controlled shapes reaching from simple dots[11] to rods[12] and to more complicated structures such as tetrapods,[13, 14] hyperbranched structures,[15, 16] and wires[17] among other structures. A large variety of semiconductor materials, e.g. metal sulfides,[18, 19] metal selenides,[20, 21] metal tellurides,[22, 23] and metal oxides[24] have been investigated in relation to this topic. The possibility to precisely tune the optical band gap of NCs from the ultraviolet to the near-infrared range allows for the preparation of either very bright quantum dot light emitting diodes (QLEDs) or solar cells composed of *p-type* donor polymers and *n-type* acceptor inorganic nanoparticles which absorb a significant range of the solar spectrum.

In optoelectronic applications controlling the morphology is a crucial aspect regarding performance. For QLEDs a homogenously dispersed structure is most desirable. Therefore, intimate contact between NCs and polymers (no demixing) is essential. Although solar cells benefit from improved dispersion (short exciton diffusion lengths), they require for the most part a percolated structure to facilitate the macroscopic transport of electrons and holes to the respective electrodes. Requirements for homogeneous dispersion as well as percolated structures make it necessary to control the organic-inorganic interface. While for a specific

application the correct choice of dispersed semiconducting component and surrounding matrix with the correct band gap is essential[25] this is not important for general studies with regard to structure formation. To conclude, the control over the NCs' dispersability in a polymer matrix is essential for applications as it directly influences the film morphology. Therefore, it will be discussed in the first part of this review.

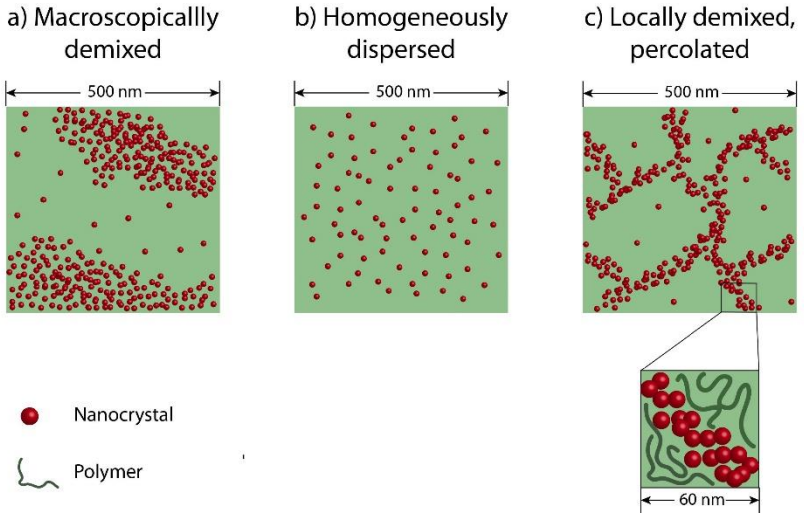

Figure 1. Schematic illustration of a macroscopically demixed (a), homogeneously distributed (b) and locally demixed, a percolated network forming (c) film composed of a mixture of NCs and polymer.

Creating a well-defined and on the nanoscale percolated morphology in a system consisting of two components is challenging. This applies especially to the dispersion of hard (impermeable) particles in a polymer matrix where both components are highly incompatible due to strong aggregation forces of the inorganic nanoparticles in combination with the depletion forces exerted by the polymers.[26, 27] Nevertheless, polymer nanocomposites have attracted substantial academic and industrial interest for more than twenty years.[28] Nanocomposites have been investigated in detail for example concerning "molecular reinforcement" (the distribution of fibers in flexible polymers)[29, 30] or the placement of inorganic nanoparticles in block copolymer structures.[31] Numerous investigations in the field of nanocomposites have been carried out motivated by promising observations such as significant property changes at very low volume fractions of added nanoparticles and the possibility to incorporate new functions through the integration of nanoparticles providing specific properties.[32]

One of the main drawbacks of organic/inorganic mixed systems is the strong tendency of NCs to segregate macroscopically (**Figure 1a and 2a**).[2, 33] For an application, however, either a homogeneous distribution of the NCs or a finely dispersed bicontinuous structure is needed (see **Figure 1**). For the preparation of such a percolated structure a controlled demixing is suitable which is stopped (further coarsening is prevented) before the demixed structures get larger than several hundred nm (see **Figure 1c**). Preparation techniques such as kinetic

entrapment [34] and in situ polymerization[35] have been successfully applied to achieve highly dispersed states in nanocomposites. However, regarding the generalization of the production of nanocomposites, a thermodynamic compatibilization of both components is necessary to provide miscibility of nanoparticles within a polymer matrix. A general and versatile route to obtain fully miscible nanocomposites can be achieved by coating nanoparticles with a brush-like polymer layer (**Figure 2b**). This approach prevents nanoparticle aggregation over a large range of nanoparticle volume fractions.[36–39] This approach requires that the size of the grafted chains is comparable to the chains of the polymer matrix. As a result ligands from the NC synthesis, such as, long chain acids and phosphonates only provide solubility in low molar mass solvents but not dispersibility in a polymer matrix. In addition, the grafting shall not be too dense because highly stretched polymer chains are not efficient for achieving compatibility.[40, 41] This approach allows the production of homogeneous nanocomposites whose morphology is independent of the preparation procedure and simultaneously achieves long-term thermodynamic stability.[40]

Generally the preparation of locally demixed but macroscopically homogeneous mixtures (middle of **Figure 3**) is possible in two ways. On the one hand there is the controlled demixing starting from a homogeneous solution. This approach implies aspects of thermodynamic equilibrium and non-equilibrium. There are methods to induce thermodynamic compatibility by grafting polymers to the surface of nanoparticles. Percolated structures, however, are usually the results of non-equilibrium processes (e.g. kinetically frozen structures resulting from spinodal demixing) which start from a homogenously dispersed system (**Figure 3a**). Thus, it is not enough to create compatibility also a controlled variation of the compatibility is desirable to induce demixing at a later stage of processing.[42–44]

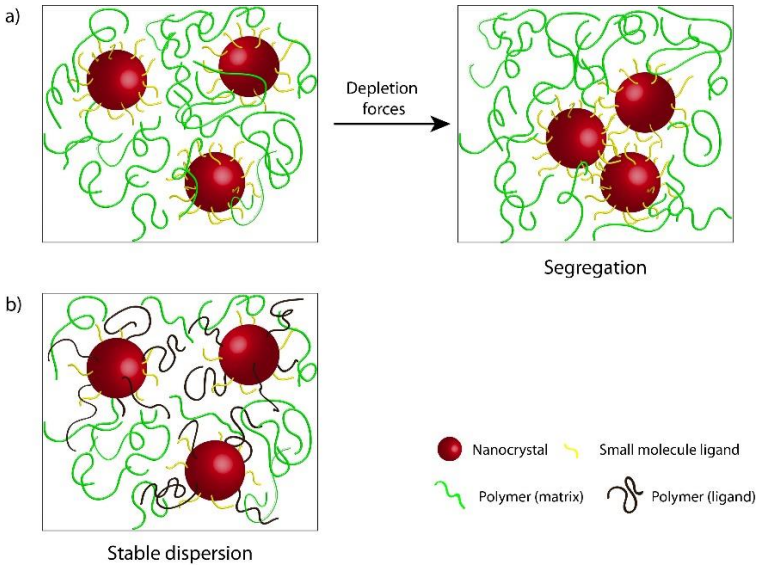

Figure 2. Blend of NCs and non-adsorbing polymers leading to aggregation of the NCs due to depletion forces (a). NCs functionalized with a matrix miscible polymer ligand leading to a stable dispersion (b).

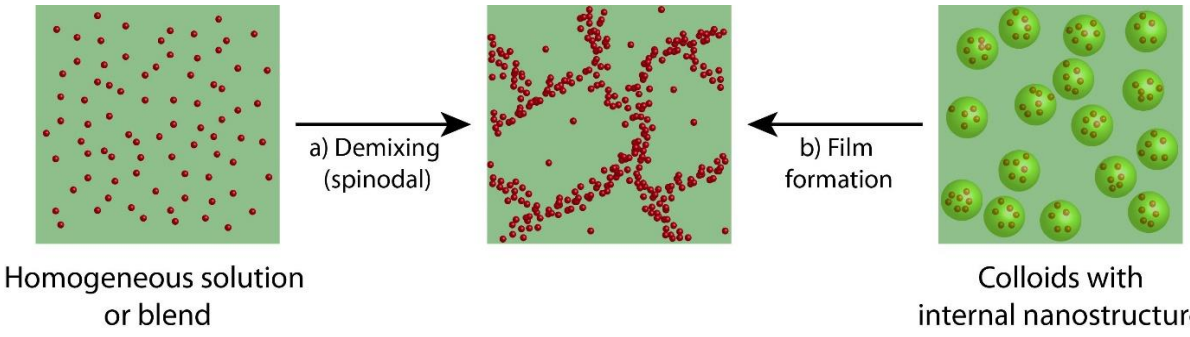

Figure 3. Locally demixed and macroscopically homogeneously distributed morphology can be achieved either from an initially homogeneous dispersed system as a result of spinodal demixing (a) or from pre-structured colloids during the film formation process (b).

On the other hand it is possible to observe structure formation during film formation of internally structured colloids. This kind of structure formation represents a type of "bottom-up" approach compared to demixing.[45–47]

Summing up, in this review we will first discuss equilibrium aspects to improve the compatibility of inorganic nanoparticles in a polymer matrix making it possible to homogeneously disperse the nanoparticles in the matrix. These concepts are useful to disperse fluorescent quantum dots (QDs) in a semiconducting matrix, as needed for the preparation of quantum dot LEDs (QLEDs).[48–50] Furthermore, it is elucidated what impact the NCs' shape (spheres, rods as well as more complex structures like tetrapods) has on their dispersion in polymer matrix. An insight on the formation of liquid crystalline phases which can be observed using rod like NCs is provided.[38, 39] We will also illustrate structure formation in dispersions of particles with a branched shape, like tetrapods.[51] In addition, we will discuss formation of aggregated structures. Two methods will be elucidated, stimulated demixing of inorganic nanoparticles from a homogeneous nanocomposite as well as a "bottom-up" approach.[42, 43] This approach involves the structural evolution during the film formation starting from internally prestructured colloids.[52, 46, 47] Finally, we will present examples of organic/inorganic hybrid-based light emitting diodes and solar cells.

2. Compatibilization of Nanoparticles and Polymers

The dispersion of inorganic nanocrystals (NCs) in polymer matrices offers the possibility to synthesize materials with improved properties over the property characteristics of the constituent materials.[53] As a consequence, the possibility to combine a great variety of organic and inorganic materials into stable nanocomposites is highly desirable.

In general, it is, unfortunately, not trivial to obtain a homogeneously dispersed film of nanoparticles and a semiconducting polymer. Casting a film from a solution composed of nanoparticles and non-adsorbed polymers leads to macroscopic aggregation of the nanoparticles and formation of phase separated structures on the micrometer scale.[54] Nevertheless, several attempts have been described in the literature where improved casting procedures to prevent macroscopic phase separation by various types of kinetic entrapment were used. This is usually achieved by inducing very strong interactions between organic and inorganic components or by adsorption of the nanoparticles onto preformed polymer structures.

A uniform distribution of TOPO-capped CdSe NCs in poly(3-hexylthiophene-2,5-diyl) (P3HT) can be achieved by self-assembly of these NCs on preformed regioregular P3HT (rr-P3HT) nanowires for example. Such nanowires can be obtained through slow precipitation from solvents such as *p*-xylene or cyclohexane which are poor solvents for P3HT at room temperature but good solvents at elevated temperatures.[55] Another very prominent approach first reported by Greenham *et al.* uses ligand exchange of the initially strongly bound surfactants (e.g. TOPO) by pyridine. The pyridine substitutes the initial ligands to some extent and is only loosely bound to the NC surface. During the casting process the pyridine ligands are claimed to be partially removed from the NC surface resulting in “bare” NCs. The NCs can then directly interact with the conductive polymer matrix as there is no insulating ligand shell located between both compounds. This has a positive influence on both the film morphology and their performance in hybrid solar cells.[56] These examples, yet, as well as other process-based approaches suffer from two main drawbacks. First, the production process is strongly dependent on the different components and hardly adaptable to new systems. Second, a homogeneous dispersion is not the thermodynamically favorable state in blend systems. This leads to aging effects (such as aggregation over long periods of time) of the active layer in optoelectronic devices.

Of special interest is to consider semicrystalline polymers (e.g. P3HT) as a matrix. Generally, crystallinity reduces the compatibility of polymers and NCs strongly as the NCs disturb the crystalline packing of the polymers in their vicinity. Thus, the nanoparticles will be concentrated at the grain boundaries of the partially crystalline structure during crystallization of the matrix (see **Figure 4**). The resulting structures may, however, be interesting as macroscopically dispersed but at the same time nanoscopically percolated systems of electron donor and acceptor materials in solar cells. The exact structure will depend strongly on the crystallization conditions. In addition, it should be considered that the crystallization in these systems requires time. Therefore, directly after spin coating the NCs may still be compatible with the amorphous (not yet crystallized) polymer matrix and the biphasic structure may only develop after prolonged annealing. In this respect the morphology of systems consisting of NCs compatibilized with an amorphous polymer are much easier to predict. To overcome these barriers and enable the preparation of a large variety of stable organic/inorganic hybrid materials it is necessary to achieve full thermodynamic compatibilization. Therefore, for the above mentioned reasons NC aggregation has to be eliminated or at least minimized.

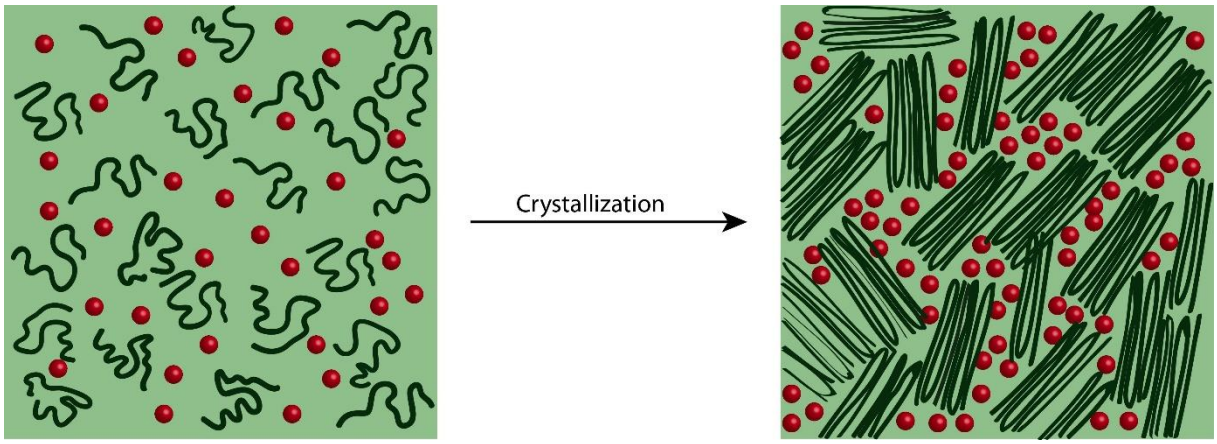

Figure 4. Schematic presentation of NCs‘ assembly on the grain boundaries due to the crystallization of the polymer matrix.

2.1. Examples of Individually Dispersed and Completely Miscible Nanocomposites

Generally grafting of polymer chains to a nanoparticle (i.e. the fixation of polymer brushes at the interface) reduces depletion forces organic/inorganic mixture. For planar substrates it is, however, known that even polymer coatings in the dimension of the surrounding matrix may be insufficient to provide complete miscibility if the coating is too dense. The reason for this is the loss of conformational entropy of the matrix polymers close to the nanoparticle surface

in a too densely packed brush layer.[57] This problem can easily be overcome by reducing the segment density of the polymer brush to provide sufficient conformational freedom for the matrix polymers. There are two ways to achieve such a lower segment density. From a synthetic side it may result from imperfect grafting. In addition, it is achieved as a consequence of using short anchor blocks to bind the semiconducting polymers to the NC (**Figure 5a and b**).[36, 38]

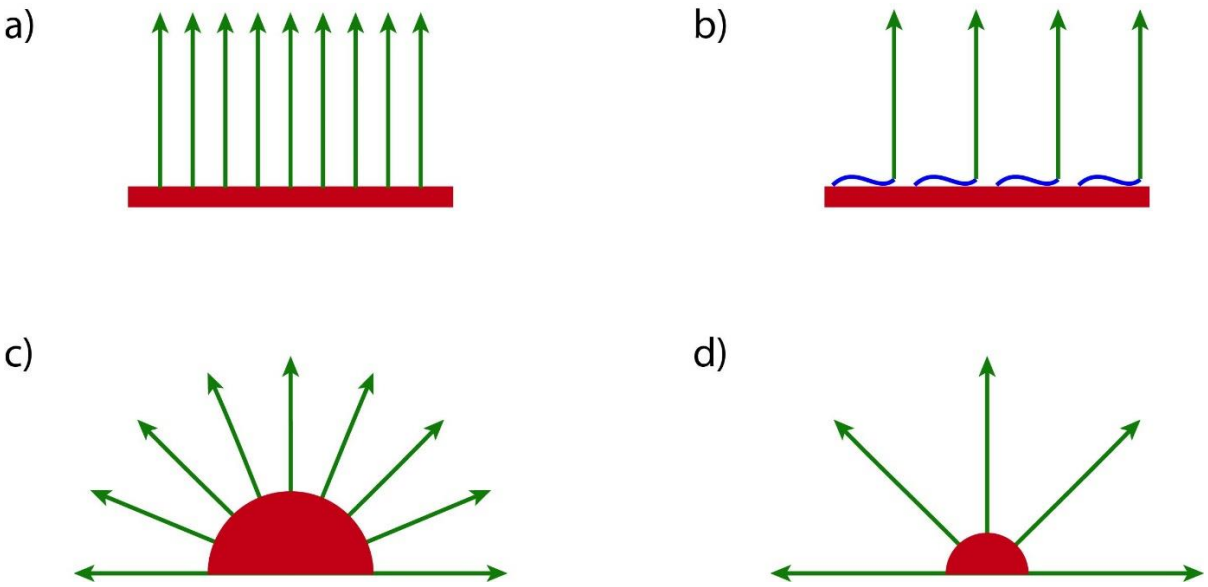

Figure 5. Simplified model illustrating the decrease on the grafting density coming from end functionalized polymer ligands (a) to block copolymers containing an anchor block (b). In addition, the influence of the curvature is shown. Comparing samples with the same interpolymer distance (m), decreasing the radius from $r = \infty$ (a), to $r = 8m/\pi$ (c) and $r = 4m/\pi$ (d) visualizes the increase of free space available at the periphery.

The use of short anchor blocks here also offers the advantage of strong and reproducible binding due to multivalency. Besides, there is a geometrical aspect which influences the interligand distance. In case of spherical NCs the segment density of the covering polymer brush decreases at its periphery solely due to its topology. Logically, this effect is increased with decreasing radius (**Figure 5a**, **c** and **d**).[40].[58] The above mentioned geometrical effect happens naturally and cannot be prevented. It has recently been discussed by Förster *et al.* in great detail.[40, 41]

A simplified model illustrating the increase in free volume per polymer depending on whether an end functionalized polymer or an anchor block containing polymer is used as well as the effect of curvature is shown in **Figure 5**. For sufficiently small spherical NCs, calculations

predict that a stable dispersion can even be achieved when the polymers used as ligands exhibit a lower DP than the chains of the polymer matrix.[59] These calculations are supported by a recent study on polymer-brush coated nanoparticles in dilute solutions.[60] This study indicated that spherical polymer brushes can suppress aggregation in cases of appropriate grafting density.[61, 40] This prediction has also been applied to partially crystalline polymers.[62]

Förster's group reported nanocomposites exhibiting individually dispersed spherical NCs over a large area. By deploying end functionalized polymers with a very small PDI synthesized by anionic polymerization they were able to obtain nanocomposites combining different organic and inorganic compounds. These composites showed well defined interparticle distances and complete miscibility which means no aggregation occurred in diluted mixtures, a polymer matrix or in films composed of the pure nanocomposite.

In addition to the curvature control, the use of copolymers with a short anchor block offers a facile approach for a reduction of the segment density of the grafted polymer brush.[36, 39] The density reduction can be explained by the ability of the anchor block to cover a certain surface area of the NC. Thus, it limits the least possible distance between two polymer chains (**Figure 5a** and **b**). Therefore, with an increasing size of the anchor block the distance between two adsorbed polymers can be increased leading to a reduced segment density of the polymer chains interacting with the polymer matrix.[38]

This approach was successfully applied to spherical,[50, 63, 49, 25] rodlike[64, 39] and tetrapod shaped nanoparticles[51] using different side chain conjugated semiconducting block copolymers as ligands. Dynamic light scattering (DLS) in dilute solutions revealed that the NCs were individually dispersed and not aggregated.[39]

Such block copolymers with a small PDI are accessible via RAFT polymerization. These polymers consist of a solubilizing unit in the first block (which may carry semiconducting moieties) and a reactive ester repeating unit in the second block. By postpolymerization modification various anchor groups (e.g. catechol, thiol or disulfide) can be introduced into the reactive ester block (**Figure 6**). Thus, the anchor can easily be adjusted to allow for effective binding to NCs of different compositions.[65] Therefore well dispersed nanocomposites composed of different types of QDs such as TiO_2, ZnO, CdSe/ZnS have become accessible.[39, 66, 49] Nanocomposites obtained following the approach shown in **Figure 6** were studied as potential systems for various applications. For example in systems consisting of semiconducting polymers and ZnO NCs fluorescence quenching of the QDs' emission was observed. It is assumed that the quenching originated from an effective charge

transfer between polymer corona and QDs due to their intimate contact. In addition, photoinduced charge separation was confirmed by Kelvin probe force microscopy (KPFM) experiments. Upon illumination potential changes on the order of tens of millivolts were observed for individual structures.[64] Positive charges were observed in the hole conducting polymer even at a distance of around 300 nm away from the inorganic NCs in self-assembled fiber of those nanocomposites. Thus, charge transport along the polymer fibers can be assumed and is reported.[67]

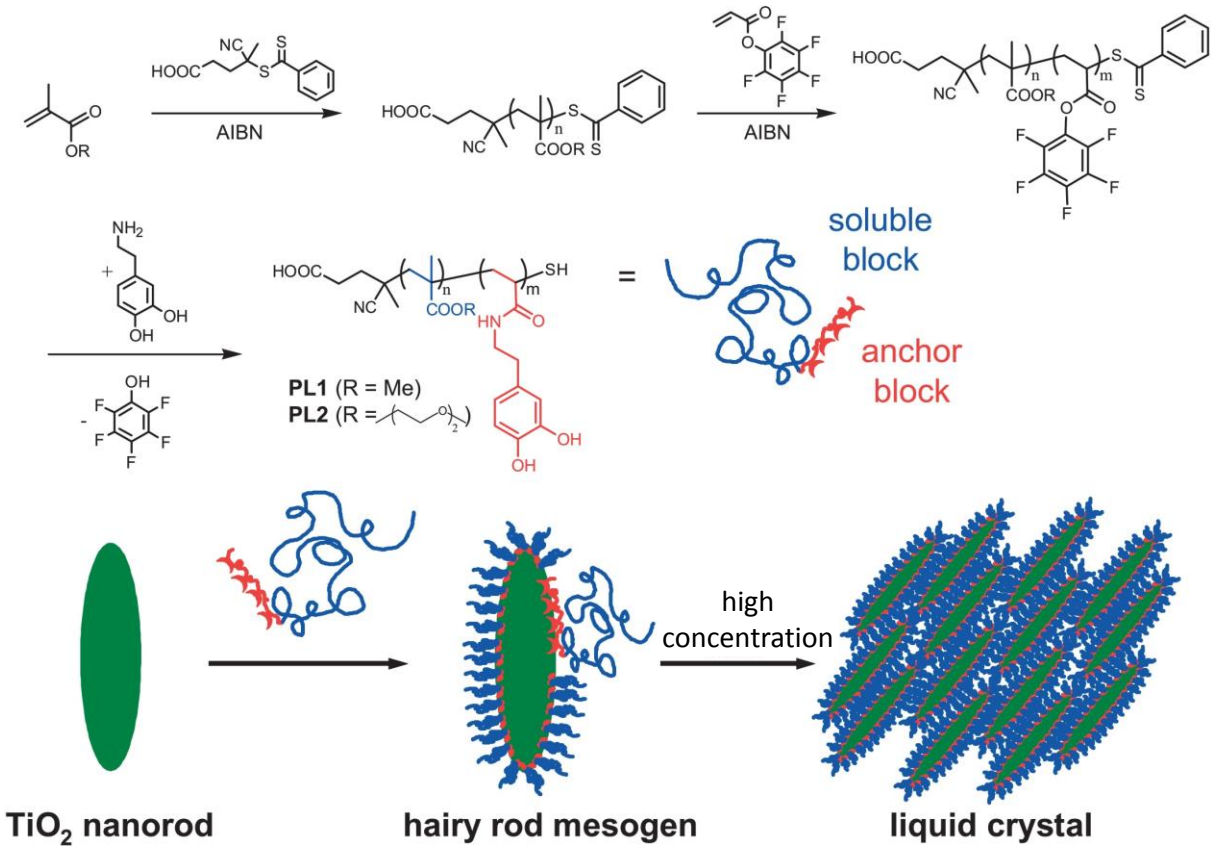

Figure 6. First, synthesis scheme of a block copolymer via RAFT polymerization and introduction of anchor units using postpolymerization modification. Second, functionalization of inorganic nanorods and their LC self-organization. Adapted with permission.[36] Copyright 2007, Wiley-VCH Verlag GmbH.

Implementation of semiconducting polymer/CdSe nanocomposites in QLEDs led to devices with improved properties such as a 3-fold increase in the external quantum efficiency compared to devices composed of unfunctionalized QDs.[49] Ligand exchange of the initial insulating ligands (e.g. oleic acid) with the semiconducting polymer ligands facilitates charge injection into the QDs and in turn resulted in a significant improvement of the device performance.[50] Devices composed of CdSe@ZnS-QDs/poly(TPD-*b*-SSMe) nanocomposite

layers showed a homogeneous distribution of the QDs which led to stable device operation in a current density range of 1-200 mA/cm^2. This reduced efficiency roll-off could be explained by the suppression of exciton quenching, as well as an improved charge balance within the active layer. This resulted in devices with stable external quantum efficiencies of EQE = 1.38 % and a standard deviation of SD(σ) = ±0.03 % (compared to EQE = 1.20 % and SD(σ) = ±0.11 % in case of unfunctionalized QDs which showed a drastic efficiency roll-off at current densities above 50 mA/cm^2).[63]

Furthermore, following the above mentioned block copolymer approach energy storage devices were fabricated using carbon coated anatase TiO_2 nanorods (NRs) and nanotubes (NTs) as an alternative anode material. For that purpose a block copolymer consisting of a poly(acrylonitrile) block and a dopamine-based anchor block was used to achieve a stable polymer coating at the NRs' surface. Subsequent, thermal treatment of the material at 700 °C transformed the acrylonitrile block into partially graphitic structures.[68] The resulting NRs showed improved electrochemical properties with respect to long-term cycling stability and specific capacities.[69]

2.2. Chemical Approaches to Achieve Stable Nanocomposites of Nanocrystals in a Semiconducting Matrix

For the preparation of nanoparticles which are miscible within a polymer matrix and form thermodynamically stable composites it is necessary to cover the nanoparticle surfaces with a layer of a matrix-miscible polymer whose dimensions are comparable to that of the matrix polymer.[70] There are three main synthetic approaches to obtaining such a polymer brush coating reported in the literature. By name, these are the grafting-from (section 2.2.1), the grafting-to approach (section 2.2.2) and the ligand exchange procedure (section 2.2.3) as depicted in **Figure 7**. In the following sections the three above mentioned chemical approaches as well as their consequences for device applications will be elucidated in detail. Care has to be taken in this regard, as often the very local effect of improved intimate contact between polymers and nanoparticles due to chemical binding (on the scale of some nm or below) is not clearly separated from the improved morphology (on the scale of hundreds of nm).

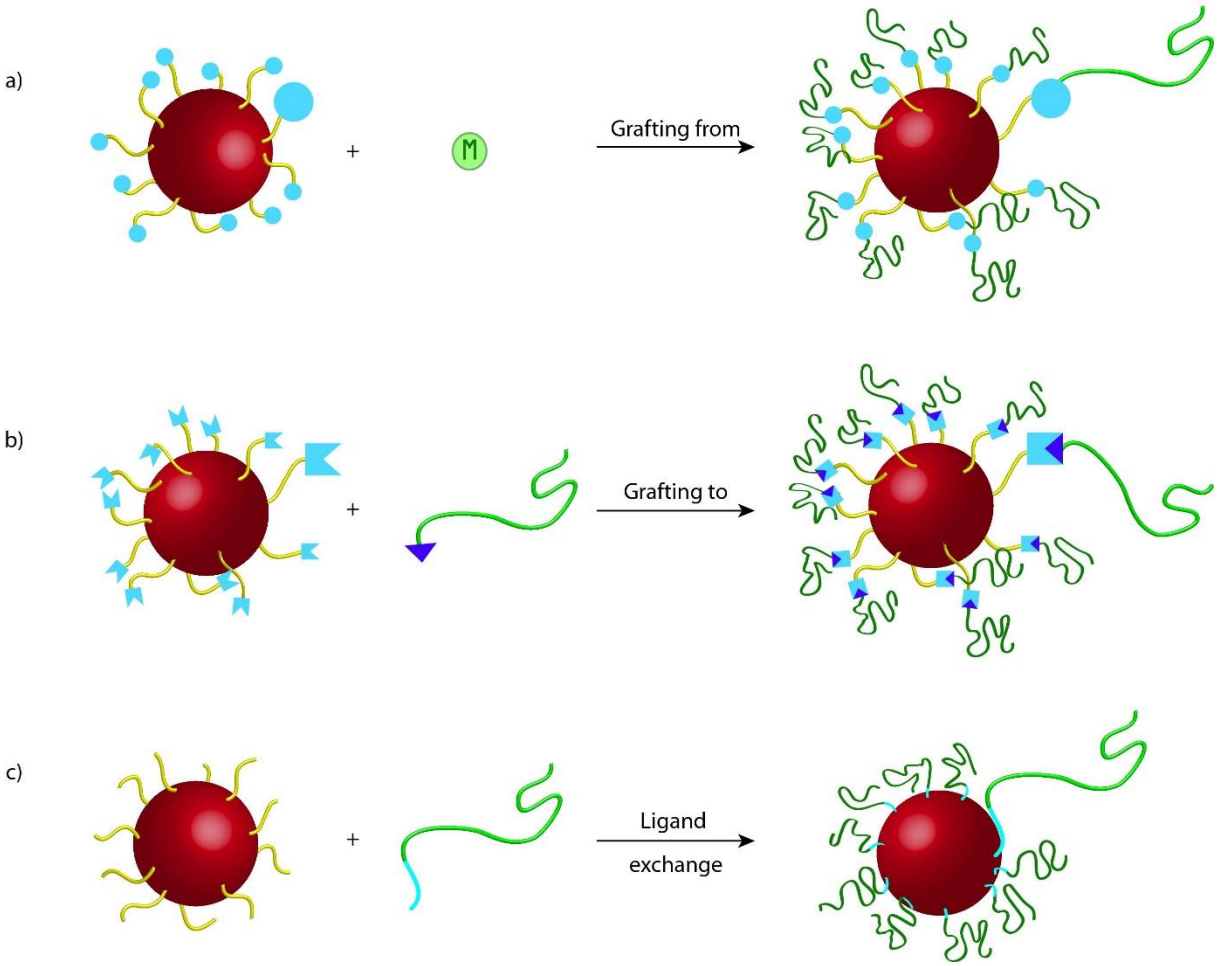

Figure 7. Schematic presentation of the main synthetic approaches to achieve polymer brush coated NCs: Grafting-from (a), grafting-to (b) and ligand exchange (c). In a) "M" represents the monomer used for polymerization.

2.2.1. Grafting a Polymer Brush from the Nanocrystal Surface

The grafting-from approach starts with functionalizing the NC's surface with ligands which act as initiators or monomers during the polymerization process. During polymerization the semiconducting polymer shell is formed. It is claimed that this approach enables control of the grafting density. However, it is more complicated to control the polymerization procedure once the NC surface gets involved.[3] In addition, the ligand must be able to act as a surfactant during the NC synthesis. Otherwise the ligand must be introduced via an additional ligand exchange step.[71]

The grafting-from approach has been most commonly used in combination with polymerization techniques such as atom transfer radical polymerization (ATRP),[72] nitroxide-mediated radical polymerization (NMP),[73] reversible addition-fragmentation chain transfer

polymerization (RAFT polymerization)[74], ring-opening metathesis polymerization (ROMP)[75] as well as oxyanionic vinyl polymerization.[76] Nevertheless there are just a few examples in the literature using the grafting-from approach for the synthesis of all-semiconducting nanocomposites. The first implementation of grafting a semiconducting polymer from an inorganic nanoparticle was reported by Emrick's group. They used *p*-bromobenzyl-di-*n*-octyl phosphine oxide (DOPO-Br) as a surfactant during the synthesis of CdSe quantum dots. This surfactant was then used as an initiator for the copolymerization of 1,4-divinylbenzene and 1,4-dibromobenzene derivatives using a palladium-catalyzed Heck-type polycondensation to obtain the corresponding Poly(*p*-phenylene vinylene)s (PPVs). The resulting PPV-CdSe nanocomposites showed improved dispersibility in a PPV matrix (**Figure 8**).[77] However, this approach resulted in oligomers of different sizes (mostly trimers and tetramers), which is unfavorable for many applications as their energy levels vary significantly with the number of repeating units. The difference in energy levels leads to trap-assisted recombination. It occurs once an electron (hole) is located in a LUMO (HOMO) with energy lower (higher) than the surrounding ones. Thus, deviations of HOMO and LUMO levels may lower the device performance.[2, 78]

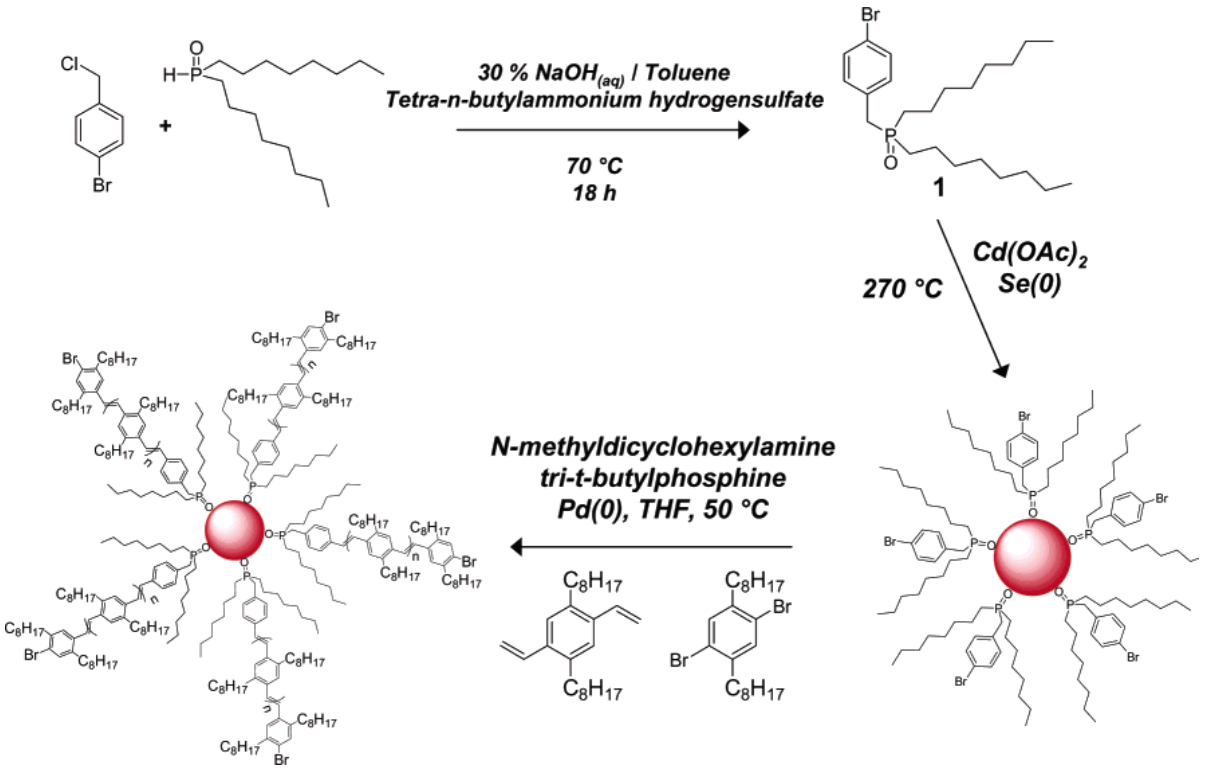

Figure 8. Synthetic scheme of DOPO-Br, growth of DOPO-Br-covered CdSe NCs and grafting a PPV derivative from the NCs via Heck-type polymerization. Reprinted with permission.[77] Copyright 2004, American Chemical Society.

Kanelidis *et al.* reported a facile synthetic route grafting oligo- and poly(fluorene) derivatives from CdSe QDs. Using the amino-functional fluorene 6,6′-(2,7-dibromo-9H-fluorene-9,9-diyl)dihexan-1-amine as a surfactant during the NC synthesis they were able to graft oligo(fluorene) from the nanoparticle surface by a *bis*(1,5-cyclooctadiene)nickel(0) mediated Yamamoto polycondensation. In the same manner the NCs were functionalized with the statistical copolymer using 2,7-dibromo-9,9-dioctyl-9H-fluorene as a second monomer.[79]
Besides the grafting-from approach, grafting-to is another common strategy to achieve polymer coated NCs as will be pointed out in the following section.

2.2.2. Grafting a Polymer Brush to the Nanocrystal Surface

In the grafting-to approach the NC's surface is covered with bifunctional ligands. The first functional group enables the ligand's coordination to the NC, while the second group facilitates the coupling reaction with functionalized polymer chains. NCs with bifunctional ligands can be obtained via direct synthesis or ligand exchange procedure similar to the grafting-from approach.
In 2007, Xu *et al*. reported the synthesis of poly(3-hexylthiophene) (P3HT) functionalized CdSe QDs via Pd-catalyzed Heck coupling of vinyl-terminated P3HT with [(4-bromophenyl)methyl]dioctylphosphine oxide (DOPO-Br) capped CdSe QDs.[80] The initial QDs were prepared by direct synthesis using $Cd(OAc)_2$ and Se as precursors to avoid a ligand exchange step. The vinyl-terminated P3HT was synthesized via quasi-living Grignard metathesis (GRIM) polymerization leading to a regioregular polymer which is essential for good device performance. The success of the coupling was monitored by the disappearance of the vinyl end group signals in ^{1}H-NMR spectroscopy and a shift of the DOPO-Br signal in ^{31}P-NMR spectroscopy. Moreover, the nanocomposites synthesized via grafting-to approach were compared to a physically blended mixture of P3HT and CdSe QDs. A significant difference was noticeable from transmission electron microscopy (TEM) images which showed aggregation behavior in the physically blended case and well distributed QDs in the nanocomposite case.
In 2011, Zhao *et al*. introduced the direct synthesis of CdSe nanorods (NRs) capped with bromobenzylphosphonic acid (BBPA). In this case the phosphine oxide anchoring group was replaced with phosphonic acid to enable the anisotropic growth of the nanoparticles. The CdSe NRs were thereafter functionalized with rr-P3HT via Pd-catalyzed Heck coupling.[81] In the same year Lin and coworkers converted the BBPA functionalized CdSe NRs into azide-

benzylphosphonic acid (N_3-BPA) capped NRs and thus making them eligible for the catalyst-free click reaction.[82] N_3-BPA capped NRs reacted with ethynyl-functionalized P3HT resulting in the 1,2,3-triazole ring formation (see **Figure 9**). It should be noted that the catalyst free click reaction was performed to eliminate the possibility of remaining trace metals in the composite which may later diminish device performance.

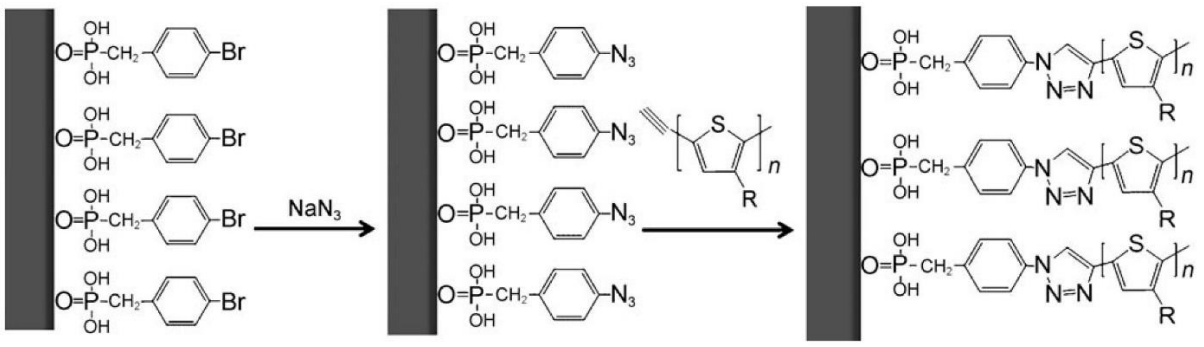

Figure 9. Grafting P3HT (R = C_6H_{13}) to a N_3-BPA coated CdSe nanorods using catalyst-free click reaction. Reprinted with permission.[82] Copyright 2011, Wiley-VCH Verlag GmbH.

Once in the device, moving from QDs to NRs and to tetrapods should increase the efficiency of the electron transport in conducting polymer/inorganic NC composites. In 2013, Lin and coworker were able to prepare N_3-BPA capped CdTe tetrapods and subsequently functionalized them with P3HT via the previously mentioned catalyst-free click reaction.[83]

The ligand exchange procedure presents an alternative way to produce NCs capped with bifunctional ligands. Zhang *et al*. synthesized P3HT capped CdSe NRs via Heck reaction of vinyl functionalized P3HT with DOPO-Br or 2-(4-bromo-2,5-di-n-octyl-phely) ethanethiol (BP-SH) functionalized NRs.[84] To prepare DOPO-Br and BP-SH capped NRs tri-n-octylphosphine oxide (TOPO) functionalized NRs were first refluxed in pyridine in order to replace TOPO with loosely bound pyridine ligands and later treated with a solution of a bifunctional ligand. It was found that the P3HT surface coverage of the NRs was higher using the thiol anchoring group compared to the phosphine oxide group. A nearly complete quenching of P3HT photoluminescence was observed in P3HT-NRs nanocomposites indicating an efficient charge transport process while in the physically blended mixtures only a slight decrease of the photoluminescence was observed.

Whereas the grafting-from as well as the grafting-to approach must be adjusted very carefully to every combination of organic and inorganic compound, the ligand exchange procedure can be applied to a variety of combinations with only slight modifications as will be shown in the following section. In addition, this is also the basis for the adsorption of the block copolymers presented in **Figure 6**.

2.2.3. Brush Formation via the Ligand Exchange Procedure

Polymers containing groups which can interact with the NC surface, so-called anchor groups, enables the substitution of the initial surfactants (attached to the NC surface as stabilizing ligands during their synthesis) for the polymers. This facile approach defines the ligand exchange procedure. It allows a larger diversity in the choice of both the organic and the inorganic compound.

The ligand exchange procedure, unfortunately, comes with a disadvantage of difficulties to control the coating density often resulting in undesirably low functionalization values.[3] To solve this problem it is important to understand the factors which influence the ligand exchange efficiency. Therefore, some theoretical considerations will be described below. Finally, synthetic examples from the literature will be presented and discussed.

Looking at the theoretical background, the dynamics of the ligand exchange process can be explained by the adsorption/desorption process.[85] The arguments in the literature are based on a system comprised of only one type of ligands and neglect interactions of any other molecule with the NC surface. It is, however, still a helpful tool to understand the ligand exchange procedure. The processes of adsorption and desorption and their rates can be described with the following equations:

Adsorption: $M + L \rightarrow ML$

$$(d[ML]/dt)_a = k_a[M][L] \quad (1)$$

Desorption: $ML \rightarrow M + L$

$$(d[ML]/dt)_d = - k_d[ML] \quad (2)$$

where M, L and ML refer to free binding sites on the NC surface, free ligands in solution and ligands bound respectively. The reaction constants which are strongly dependent on the binding strength of the ligand are given as k_a and k_d, for adsorption and desorption respectively.

Therefore, the average surface ligand coverage of the NCs can be calculated as follows:

$$\theta = [ML]/([M] + [ML]) \quad (3)$$

Given that the total number of bonding states is constant ([M] + [ML]), Equation (1) and (2) can be rearranged to:

Adsorption: $(d\theta/dt)_a = k_a(1 - \theta)[L]$ (4)

Desorption: $(d\theta/dt)_d = - k_d\theta$ (5)

The two most important results from the adsorption/desorption process are first that NC coating is a dynamic process which enables ligand exchange and second that the adsorption only depends on the concentration of free ligands in solution. Thus, the NCs can be coated even with loosely bound ligands if the ligands are added in great excess.

Using thermodynamic considerations the ligand exchange can be described with the reaction equation $NC\text{-}L_1 + L_2 \rightleftarrows NC\text{-}L_2 + L_1$. From the reaction equation results the law of mass action (Equation 6):

$$[NC\text{-}L_2] = K \frac{[NC\text{-}L_1][L_2]}{[L_1]} \quad (6)$$

In Equation 6 L_1 is the initial ligand and L_2 the new ligand, while $NC\text{-}L_1$ and $NC\text{-}L_2$ are the nanocrystals covered with the initial ligand and the new ligand, respectively. *K* is the equilibrium binding constant which is strongly affected by the binding strength of both ligands. According to Equation 6 a significantly higher binding strength of L_2 or its excess will lead to the newly functionalized nanocomposite $NC\text{-}L_2$.[41]

With these considerations in mind, it becomes clear that a low coating density can be caused by either weak binding strength of the desired ligand (or a too strong binding strength of the initial ligand) and/or by an insufficient excess of the desired ligand. One aspect which is not accounted for in theory is that in case of polymer ligands steric repulsion plays an important role. Thus, bound ligands hinder adsorption of additional ligands.[86, 38] In summary, short polymers (or oligomers) which exhibit strong-binding anchor-groups in large excess produce a densely packed polymer coating.

With the theoretic knowledge in mind we will continue with experimental studies. Examples of semiconducting oligomers and polymers introduced to NCs via ligand exchange are shown in **Figure 10**.

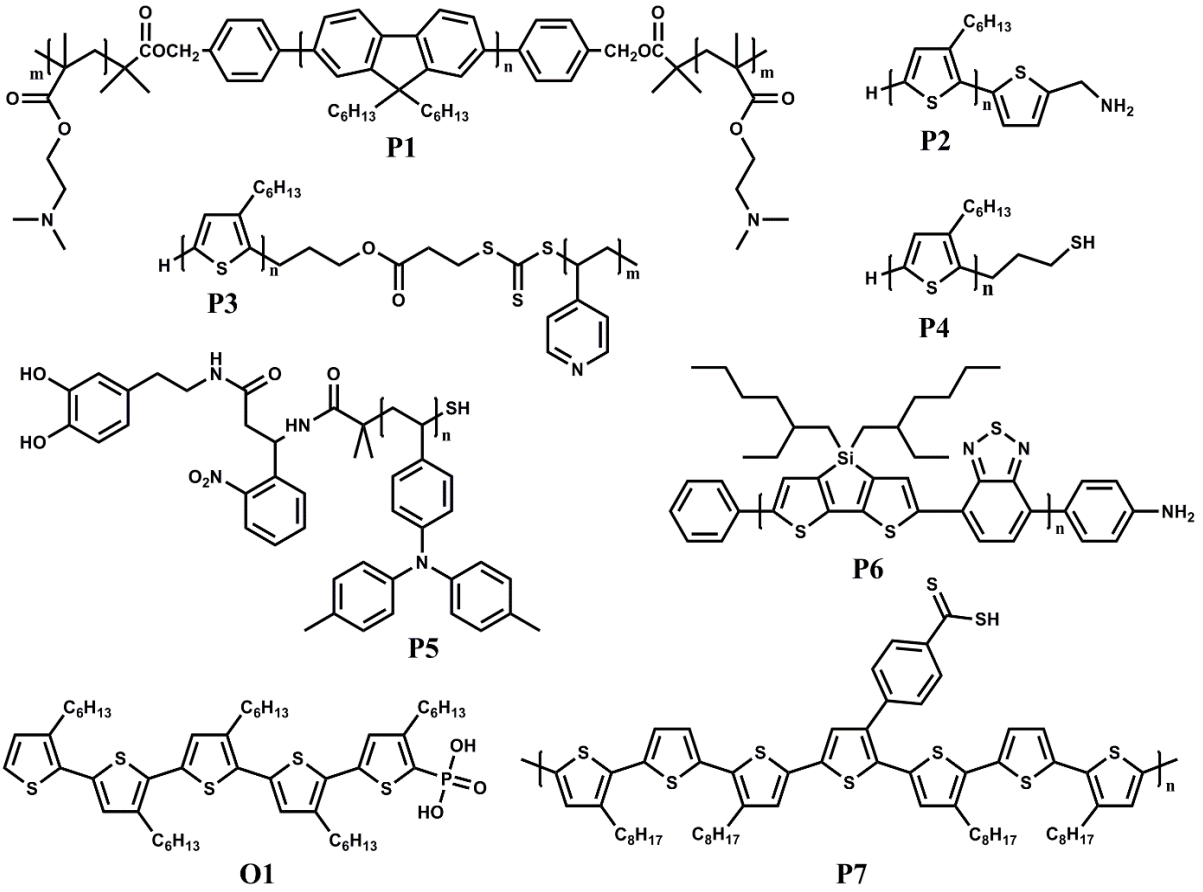

Figure 10. Semiconducting oligomers and polymers used to functionalize NCs via ligand exchange.

For example Milliron *et al.* synthesized penta(3-hexylthiophene) carrying a phosphonic acid end group (**O1**) in a multi-step reaction. Using this oligo(thiophene) they successfully carried out ligand exchange with TOPO coated CdSe QDs. The resulting QDs exhibited fluorescence quenching of the ligand indicating a photoinduced charge transfer due to the intimate contact of both materials.[87] Similar approaches were carried out using several anchor-groups such as thiols, phosphine oxides and dibenzylthio functionalities as well as various conjugated oligomers like oligo-*p*-(phenylene vinylene)s and oligo(phenylene ethynylene)s and different NCs (e.g. TiO_2 NRs). These studies showed likewise results.[88, 89]

Oligomers are less desirable for NC coatings than polymers due to the fact that charge carrier mobility increases with increasing molecular weight. In general, increasing molecular weight (M_n) by one order of magnitude increases the charge carrier mobility by 4-5 orders of magnitude.[90] In addition, oligomers are less effective for compatibilization.

Using a single functional end group for the inorganic NCs' functionalization is increasingly difficult as the chain length is increased moving from oligomers to polymers. This effect comes from the fact that with an increasing molecular weight the ratio of end groups to the number of repeating units is decreased and therefore the odds of the anchor group being in a position to interact with the NC decreases.[2]

A solution to this problem is the introduction of anchoring units as polymer side chains. In 2006, Querner *et al.* synthesized olgio- and poly(thiophene)s using oxidative polymerization with $FeCl_3$. These polymers are unique in the fact that they contain carbodithioate side groups which are strongly binding anchor groups for various semiconducting and metal NCs (**P7**). Due to the strong binding ability of these ligands the exchange with TOPO coated CdSe QDs occurred almost completely under mild conditions.[91] The nanocomposite exhibited photoinduced charge transfer at the organic/inorganic interface and showed an improved resistance against photooxidation due to the strong chelating effect of the bidentate anchor group.[92] Due to the fact that the introduction of anchoring functionalities on poly(thiophene)s or PPVs as side chains is a versatile and relatively simple methodology to obtain multidentate ligands it has been exploited.[93, 48]

Though, the bulkiness of anchor-groups which are introduced as polymer side chains often disturb the polymers' regioregularity or decrease polymer planarity which are critical issues in terms of electronic properties. As reported for P3HT the polymers' regioregularity controls the HOMO/LUMO levels, as well as, the band gap.[2] Moreover, the charge carrier mobility exhibited by non-regioregular and less planar polymers is several orders of magnitude lower than regioregular polymers.[94] Finally, irregularities in the polymer structure hinder the formation of supramolecular structures, such as fibers which can strongly improve the device performance.[95, 19] Consequently, regioregular conducting polymers with a small PDI and a high DP are desirable for optoelectronic devices.

Although it is quite difficult to effectively functionalize NCs with an end functionalized polymer (not oligomer) via a ligand exchange approach it has been successfully carried out in the literature via two approaches.

First, it is possible to achieve an effective ligand exchange using polymers terminated with one or multiple relatively strong anchor groups. This approach was recently demonstrated for the ligand exchange of a side chain conjugated polymer which is based on triphenylamine. The polymer was synthesized via RAFT polymerization and a catechol anchor group was introduced at terminal position by post polymerization modification (**P5**). Due to the fact that catechol is a strong anchor group for metal oxides, ligand exchange could be successfully performed with TiO_2 NCs which was subsequently verified by TEM and FT-IR spectroscopy.[42]

As another example Zhang *et al.* synthesized a low band-gap polymer containing a thiol end group. This polymer was used to carry out ligand exchange with PbS NCs leading to nanocomposites which absorbed light in the near-infrared region.[96] The chelating effect can be further taken advantage of with the use of block copolymers. This was first demonstrated by Fang *et al.* who synthesized an ABA-type triblock copolymer that consisted of a central poly(fluorene) block and two poly(2-(dimethylamino)-ethylmethacrylate) blocks (**P1**). Ligand exchange of the polymer **P1** was carried out using TOPO functionalized CdSe NCs without the previous introduction of intermediate pyridine ligands. This is possible due to the strong chelating effect provided by both anchor blocks.[97] This multidentate binding is also the basis for the successful application of the block copolymers presented in **Figure 6**.[36]

In 2011 Palaniappan *et al.* synthesized a poly(3-hexylthiophene)-*b*-poly(4-vinylpyridine) diblock copolymer via a combination of GRIM and RAFT polymerization (**P3**). Comparing the block copolymer with the initial P3HT precursor they observed improved dispersibility of the CdSe QDs in the block copolymers as shown in TMAFM (tapping mode atomic force microscopy) images.[98]

Besides polythiophenes, PPV derivatives are another prominent class of conjugated polymers. Zur Borg *et al*. recently synthesized a block copolymer consisting of a PPV block and an anchor block using a combination of Siegrist polycondensation and RAFT polymerization (**Figure 11**). A catechol functionality introduced in the second block allowed successful ligand exchange with TiO_2 NCs. The resulting nanocomposites were used for the formation of organogels and self-assembled in fibers in the size of several micrometers to achieve percolated structures.[67]

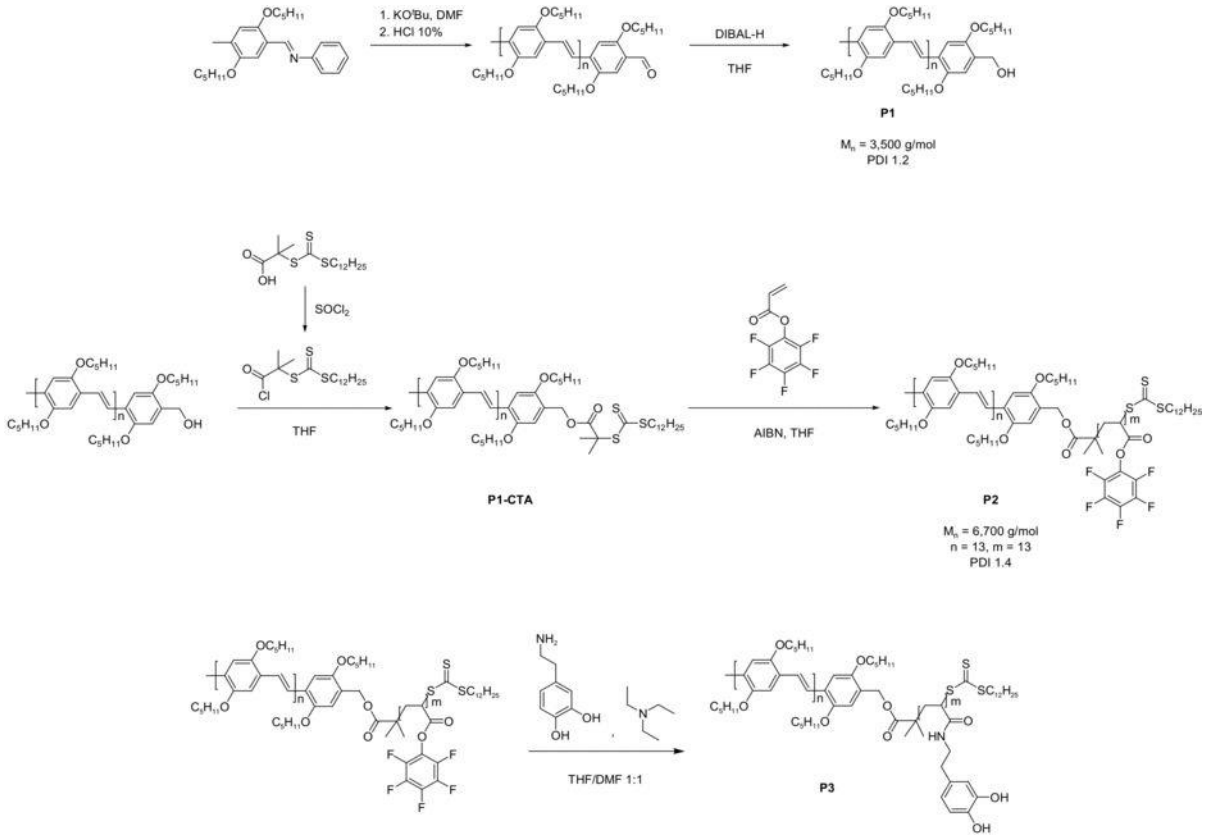

Figure 11. Synthesis of a PPV derivative via Siegrist polycondensation and end group functionalization leading to a CTA carrying polymer. Introduction of a reactive ester block using RAFT polymerization and postpolymerization modification with dopamine. Reproduced with permission.[67] Copyright 2013, Wiley-VCH Verlag GmbH.

However, in some cases it may be difficult to introduce such anchor groups as strong as catechol into semiconducting polymers due to synthetic constraints. An alternative approach relies on the introduction of loosely bound intermediate ligands such as pyridine prior to the ligand exchange with polymer. This methodology was first shown by Greenham *et al.*[56] It exploits that a huge excess of pyridine ligands shifts the action of mass law to the side of the pyridine coated NCs even though the ligand's binding constant is relatively small (see Equation (6)). Thereafter, the exchange of the desired end functionalized polymer is possible since the anchor group of the polymer has a stronger binding ability than pyridine. This approach was successfully exploited by Fréchet's group who synthesized regioregular P3HT (rr-P3HT) (using the GRIM method) which contained a primary amine at the chain end and was then used to coat CdSe NRs (**P2**). Carrying out, firstly, the exchange against pyridine and then against the desired P3HT ligand improved the device performance from a power conversion efficiency (PCE) of 0.5 % using bromine end functionalized P3HT to 1.4 % using

the amino functionalized polymer. Two effects were taken into account to explain this behavior. First, TEM images of the bromine terminated P3HT/CdSe blend showed significant phase separation whereas the amino terminated P3HT/CdSe hybrid exhibited a high degree of homogeneity. This led to a larger organic/inorganic interfacial area which improved charge separation. Second, more intimate contact between both materials in the case of the amino functionalized polymer also facilitates the charge separation.[99]

In a very similar approach Palaniappan *et al.* investigated CdSe QDs mixed with Br/H-, Br/allyl- or H/thiol-terminated P3HT (**P4**). It was determined that the best PCE of 0.9 % was achieved using allyl terminated polymer as the donor material. This was attributed to grain size closer to the optimum value in the case of an allyl terminated P3HT/CdSe QD mixture whose importance was already reported.[100–103] The imperfect grain sizes exceeds the benefits from the more intimate contact in the case of thiol terminated P3HT/CdSe QD nanocomposites.[104]

Chen *et al*. synthesized mono aniline terminated poly[(4,4′-bis(2-ethylhexyl)-dithieno[3,2-b:2′,3′-d]silole)-2,6-diyl-alt-(2,1,3-benzothiadiazole)-4,7-diyl] (PSBTBT-NH_2) using a Suzuki polycondensation reaction terminated by the addition of phenylboronic acid and *p*-bromaniline (**P6**). They carried out ligand exchange with CdTe nanorods and tetrapods coated with a combination of different surfactants. Using the tetrapod nanocomposite they assembled organic photovoltaic devices which showed improved efficiencies (PCE of 3.2 %) compared to solar cells using PSBTBT without anchoring end group.[22]

Additionally, nickel catalysts were used to introduce anchor-groups like pyridine, thiol and phosphonic ester-moieties.[105, 106] Those polymers were used for the functionalization of CdSe@ZnS, Au or Fe_3O_4 NCs. It should be noted that Monnaie *et al.* did not carry out pyridine treatment prior to the ligand exchange with functional P3HT. This led to low P3HT content of the nanocomposites with exception of the gold NCs as estimated from FT-IR spectra. The Au NCs were treated with thiol terminated polymers and as thiol has a very strong affinity to gold it enables a stable functionalization even without pyridine treatment.[106]

Using the ligand exchange procedure the large initial surfactants which are coated onto the inorganic NC surface (usually carrying large alkyl groups) can be removed by smaller ligands with poorer anchor ability (e.g. pyridine, butylamine) or by semiconducting polymer ligands. Mixing the resulted QDs and semiconducting polymer leads to a close contact between donor (polymer) and acceptor (QDs) components in the solar cell active layer. The close contact is advantageous for charge separation and contributes to the improved device performance. QD

solar cells composed of blends of small molecule functionalized QDs and unfunctionalized polymers, however, usually exhibit better performances compared to the devices using polymer functionalized QDs. The enhanced performance exhibited by solar cells composed of blends can be explained by domain sizes of the individual materials in the active layer. The domain sizes in blends are closer to the ideal values resulting in long percolated QD paths which consequentially lead to improved charge transport.[100–103] To achieve better device performance it is essential to control the film morphology as well as phase separation during or after the film formation process, which we will discuss in chapter 3. In addition, film morphology can be influenced once the nanocomposite shows liquid crystalline behavior as it will be discussed in the following.

2.3. Liquid Crystalline Phases from Semiconducting Nanoparticles

Another interesting propertability of nanocomposites is the formation of liquid crystalline phases (LC phases), if the inorganic particles are highly shape anisotropic (e.g. rod-like). Most liquid crystalline phases are composed of organic compounds. Yet, liquid crystals made of inorganic anisotropic materials nanoparticles have already be known since 1925.[107] In those inorganic compounds the liquid crystalline phases are formed by ionically stabilized, natural nanorods. The formation of these kinds of LC phases has also been observed using dispersions in polymer matrices. For example, the naturally occurring imogolite ($Al_2SiO_3(OH)_4$) which possesses a rigid, rod like shape and exhibits hydroxyl groups on its surface, was successfully dispersed in a solution of hydroxypropyl cellulose (HPC) or polyvinyl alcohol (PVA).[108] Mesophase formation of those and other mixtures like vanadium(V) oxide (V_2O_5) or boehmite (γ-AlO(OH)) were intensively studied during the past years.[109, 110] Finally, artificial nanorods like semiconducting CdSe nanorods with aspect ratio up to 15 which were coated with long aliphatic chains, were investigated and showed nematic LC phases.[111, 110]

For many applications, such as optoelectronics, LC phases of semiconducting inorganic NCs in a semiconducting polymer matrix are very desirable. Therefore, two key aspects have to be taken into account. First, the inorganic NCs have to be anisotropic (e.g. rodlike) and exhibit a high aspect ratio (> 4).[112] Second, the concentration of the inorganic NCs should be sufficiently high to enable the formation of mesophases. Additionally, to facilitate a stable dispersion in high concentrations, a robust coating of the NCs with a matrix miscible polymer is necessary e.g. by applying ligand exchange procedure as described in section 2.2.3.

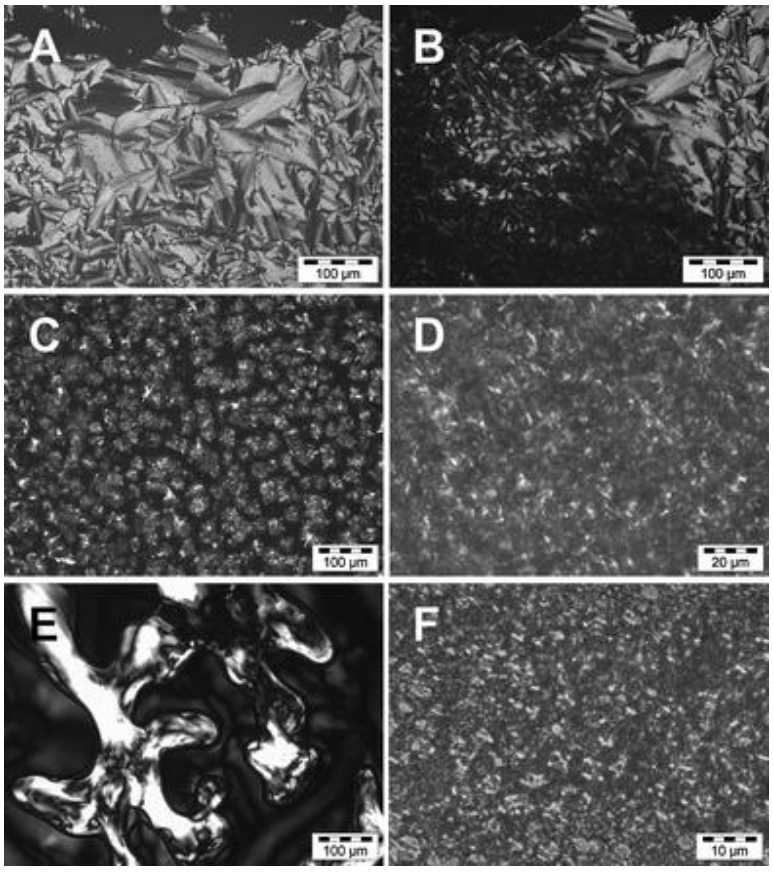

Figure 12. POM images of: PMMA/dopamine 70/30 functionalized TiO_2 nanorods (50 wt%), at 45 °C exhibiting a smectic phase (A) and at the smectic-nematic phase transition around 55 °C (B). Poly(diethylene glycol monomethyl ether) methacrylate (PDEGMEMA)/ dopamine 40/30 functionalized TiO_2 nanorods (50 wt%) in excess polymer at RT (C). SnO_2 (D) and ZnO (E) nanorods (70 wt%) functionalized with PS/dopamine 90/10 in a oligostyrene matrix at RT. PS/cysteamine 90/10 functionalized CdTe nanorods (70 wt%) in a oligostyrene matrix at RT. Reproduced with permission.[38] Copyright 2008, The Royal Society of Chemistry.

In adaption of classic liquid crystalline materials, in such a hybrid system the inorganic nanorods act as mesogenes and the flexible polymer chains promote solubility and prevent aggregation.[113]

This idea was successfully realized using block copolymers prepared by RAFT polymerization (**Figure 6**). Individually dispersed nanorods were obtained in dilute solutions as evidenced by light scattering measurements.[39] Using these nanocomposites LC phases could be observed in high NC concentrations as observed by polarized optical microscopy (POM) and differential scanning calorimetry (DSC).[36, 39] This approach was used for several semiconducting nanorods like TiO_2, CdTe, ZnO and SnO_2 (see **Figure 12**).[38] In high boiling point solvents such as oligomeric PEG (M_n = 400 g mol^{-1}) and oligomeric PS (M_n = 580 g mol^{-1}) thermotropic behavior was observed for PMMA and PS coated nanorods, respectively. Thus, clearing and restoration of the liquid crystalline phases was detected in a certain temperature range.[36] Morphology could be controlled in the way that an orientation parallel to the surface with a relatively high nematic order (S = 0.7) could be obtained in thin nanocomposite films upon solvent evaporation once a structured surface was used. This was

caused by convective forces at the meniscus.[114] Another approach to induce an orientation into the nanorods is to dry a sample of the nanocomposite between two electrodes to which an AC electric field is applied. Due to the interactions with the surface a "Fredericks" transition can be observed (**Figure 13**). Therefrom, an orientation of rods perpendicular to the surface in the bulk and parallel to the surface near the electrodes can be achieved.[66] This approach was successfully applied to a semiconducting triphenylamine-based polymer which allowed the oriented self-assembly of semiconducting nanorods in a semiconducting matrix.[115] This might be very interesting for optoelectronic applications due to the possibility to obtain percolated pathways while preserving a large interfacial area between donor and acceptor. In addition to metal or metal oxide NCs, the same approach was successfully applied to carbon nanotubes (CNTs) and in analogy LC phases were observed using POM.[37, 116]

In the following section we will proceed with more complex structures than nanorods and discuss systems made of polymers and inorganic tetrapods.

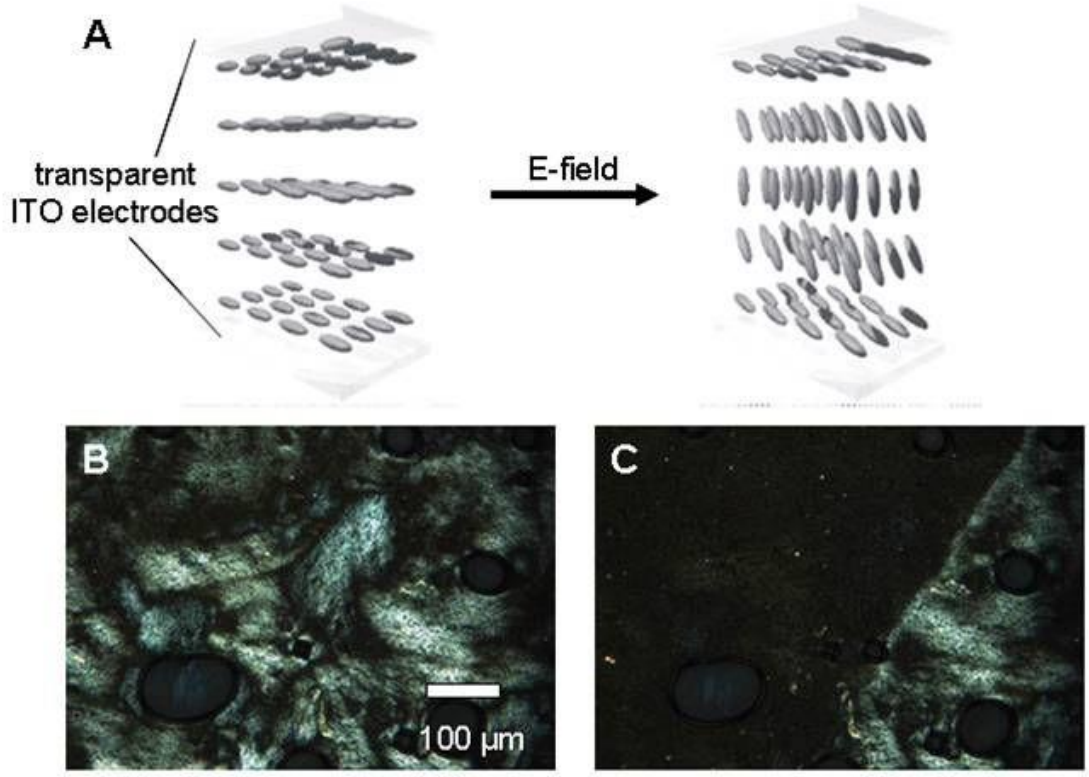

Figure 13. Schematic presentation of the Fredericks transition before and after applying an electric field (A). POM images of a film of PS functionalized ZnO nanorods 60 wt% in 40 wt% of oligostyrene in a liquid crystal test cell. Depicted is the area at the border of the electrode before (B) and after (C) the AC electric field was switched on. After applying the AC field, in the area of the electrode (left) the texture is vanished due to the homotropic alignment of the nanorods. Adapted with permission.[66] Copyright 2010, Wiley-VCH Verlag GmbH.

2.4 Influence of Branching on the NCs' Dispersibility in Polymer Matrices: Tetrapod/Polymer Mixtures

Apart from pre-structuring nanoparticles, varying their shape is another possible way to design nanoparticle dispersions with improved properties. In this respect, branched nanostructures are particularly promising. A recent review from Li *et al*. discusses this topic.[16] In this paper we will focus on the simplest space-filling geometry, branched tetrapods (TPs). These nanoparticles have originally been suggested for use as filler particles for mechanical reinforcement of flexible polymers,[29, 30] and they have also been applied in solar cells.[117, 20] In the context of semiconducting materials, TPs are interesting because they can promote charge transport in all three spatial directions, regardless of the orientation of the TPs.[118] Based on simple Flory-type calculations, Wendorff and coworkers argued that rigid TPs should be more compatible with flexible polymers than rigid rods.[30] Nevertheless, dispersibility remains an issue.

Tetrapods consist of a small core with four arms under tetrahedral angles. Their branched shape prevents dense packing and flat alignment in a plane. This makes it difficult for them to self-assemble into globally ordered structures. According to theoretical predictions by Blaak *et al.* based on the Onsager theory,[119] systems of hard, purely repulsive TPs should develop a cubatic order at high densities. However, this has not yet been observed experimentally. In real systems, TPs are embedded in a medium and cannot be considered as ideal hard particles. They have complicated effective interactions that result from the interplay of direct van der Waals attractions, direct excluded volume effects, and indirect interactions mediated by the medium such as entropic depletion interactions. Hasegawa *et al.* studied ordered diblock copolymer phases with tetrapod-shaped structural elements. They found that only three types of ordered three-dimensional continuous structures are possible for TPs: The Wurtzite, the single-diamond, and the double-diamond.[120] Zanella *et al.* studied the self-assembly of ZnTe/CdTe TPs in solutions containing polymeric additives which induce attractive depletion interactions.[121] Depending on the additive, the authors observed disordered clusters or loosely ordered structures where the TPs form honeycomb-like networks.

However, TPs form ordered networks solely under very special circumstances. In the majority of cases, they assemble into disordered clusters. Preventing this aggregation in order to stabilize homogeneous dispersions remains a challenge. One possible strategy to overcome this problem was recently suggested by Lim *et al.*[51] They proposed to coat the TPs with polymer brushes and showed that the aggregation of such polymer-TP nanocomposites in

polymer matrices is greatly reduced compared to uncoated TPs. The researchers demonstrated the effect experimentally and in numerical simulations. In the experiments, poly-TPDF (poly(vinyltriphenylamine dimer) with two trifluomethyl groups) of a narrow molecular weight distribution was synthesized via RAFT polymerization and highly uniform CdSe TPs were synthesized via the "continuous precursor injection" approach (CPI). This approach allows for a simple, controllable and scalable synthesis of CdSe TPs.[14] Hence, both the arm's length and the diameter of the TPs could be varied separately over a range of about 40 to 100 nm and 3 to 10 nm, respectively (**Figure 14**).

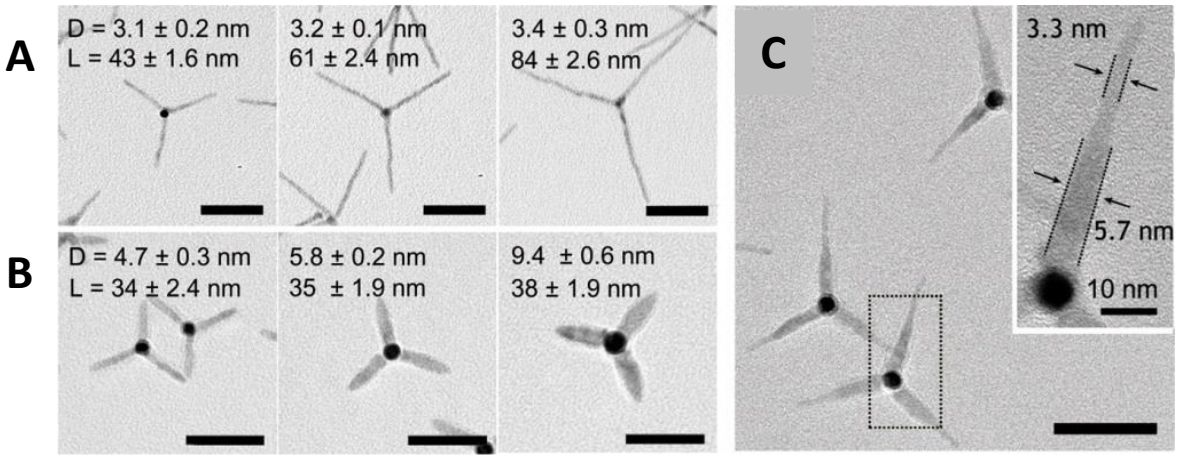

Figure 14. TEM images: Controlled variation of CdSe-TP arm's length (A), variation of arm's diameter (B) and stepwise variation of arm's diameter (C). Adapted with permission.[14] Copyright 2012, American Chemical Society.

The controlled synthesize of these TPs is an important issue regarding morphology control as the geometry strongly influences the TPs packing and aggregation behavior which is demonstrated in **Figure 15**.

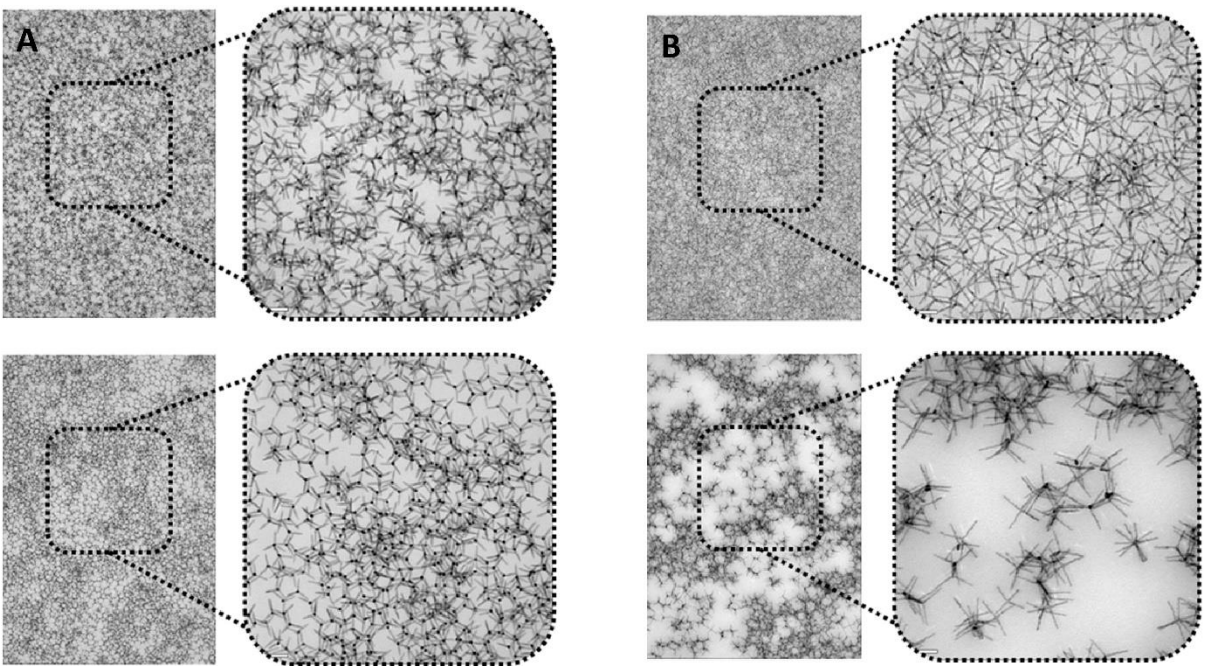

Figure 15. TEM images of 40 nm (A) and 70 nm (B) arm's length TPs mixed with polymers in polymer/tetrapod ratio (wt%) 50/50. Top: nanocomposite samples, bottom: blend samples. Scale bars in insets: 100 nm. Adapted with permission.[51] Copyright 2014, Wiley-VCH Verlag GmbH.

Finally, the TPs were coated with poly-TPDF using a ligand exchange procedure. The morphologies of thin films made of blends containing poly-TPDF and poly-TPDF/TP nanocomposites were compared with those of poly-TPDF and uncoated TPs. Exemplary results are shown in **Figure 15**. While the uncoated TPs have a strong tendency to cluster, the TP nanocomposites remain homogeneously dispersed in the polymer matrix.[122] This result could be rationalized by numerical simulations. In the theoretical model, it was assumed that a depletion interaction mediated by the polymer matrix competes with a repulsive interaction generated by the polymer coating. The effect of the polymer matrix was described in a coarse-grained manner by the Asakura-Oosawa model,[123] and the free energy penalty associated with brush compression was calculated within the Alexander-de Gennes model.[124] The resulting effective potential between two TPs with minimum distance D is obtained by minimizing the total free energy with respect to the brush thickness h and takes the form

$$V_{eff}(D) \propto \begin{cases} \infty & \text{for} \quad D < 0 \\ \rho_p D + 2h_0\sigma^{3/2}\left(\left(\frac{2h_0}{D}\right)^2 - 1\right) & \text{for} \quad D < 2h_0 \\ \rho_p D & \text{for} \quad 2h_0 < D < 2h_0 + 2R_g{}' \\ 2\rho_p(h_0 + R_g) & \text{for} \quad D > 2h_0 + 2R_g \end{cases}$$

Where the quantities σ (grafting density) and h_0 (uncompressed brush height) characterize the polymer brush coating, while ρ_p (number density) and R_g (radius of gyration) characterize the polymer matrix of free polymers. The effective potential for uncoated TPs is obtained by setting $h_0 = 0$.

These potentials were used to study the aggregation of systems of TPs in MC simulations in the NVT ensemble (periodic boundary conditions), starting from an initially aligned configuration. Exemplary results are shown in **Figure 16**. In accordance with the experiments we find that coating suppresses aggregation.

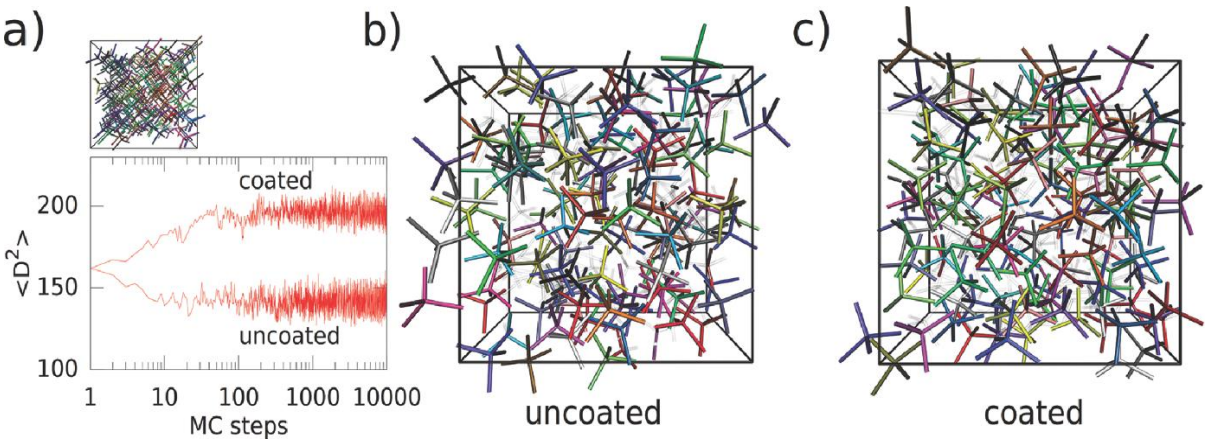

Figure 16. Evolution of the average squared minimum distance between coated (nanocomposite) and uncoated TPs in Monte Carlo simulations, starting from an initially aligned configuration (a). Final configuration after 1 million Monte Carlo steps for uncoated TPs (b) and nanocomposite TPs (c). The parameters of the simulation were adjusted to the experimental system shown in Figure 15 with an arm's length of 40 nm. Reprinted with permission.[51] Copyright 2014, Wiley-VCH Verlag GmbH.

Summing up, experiments by us and other groups as well as simulations show that, contrary to expectations raised by the pioneering papers in this field,[29, 30] uncoated TP structures are not compatible with melts of flexible polymers. However, they can be made compatible by

grafting suitable polymers onto them. The compatibilization is, however, not the only aspect which should be taken into account. Another key issue for future applications is the morphology control of hybrid films which shall be elucidated in the following chapter.

3. Routes to Percolated Morphologies

Once applied to solar cells polymer/NCs films should exhibit a certain degree of aggregation to obtain percolated pathways for a sufficient charge transport. The film morphology can be influenced using an external stimulus to obtain controlled aggregation of NCs. Two methodologies to achieve a controlled aggregation will be further presented.

3.1. Controlled Demixing from Previously Homogeneous Composites

Self-assembly of monodisperse inorganic NCs into superlattices or superparticles has been studied increasingly during the last few years. The self-assembly is a spontaneous process and leads to different types of structures depending on the NC shape and the applied technique. Two main strategies are used for the formation of superparticles or superlattices. The first approach deploys solvophobic interactions (due to the addition of a poor solvent for the NCs) to induce the self-assembly.[125] The second common approach uses interactions between the particles (or a template-based assembly) which lead to aggregation during the film formation process.[126, 43] Those approaches were applied to spherical NCs as well as anisotropic NCs such as rods, cubes, plates or prisms.[9, 127] Anisotropic NCs usually exhibit anisotropic superparticles (e.g. rods usually form cylindrical disks), whereas the use of spherical NCs result in spherical aggregates.[128] However, it should be mentioned that also anisotropic structures can be obtained using isotropic, spherical NCs.[61]

Several reviews have been published concerning the topic of aggregates/superparticles or superlattices from nanoparticles which can be found in the following literature.[129, 26, 9, 127] Anyhow, for many applications it would be desirable to separate film formation and controlled aggregation. For example for hybrid solar cells, on the one hand the possibility to create a smooth film without defects has a large impact on the device performance. On the other hand percolated pathways for charge carriers also play an important role. Thus, the formation of aggregates from previously stable, homogeneous nanocomposites induced by an external stimulus which is applicable in films (beside the addition of a poor solvent) such as light and temperature shall be discussed in this section.

Among those approaches the most common way is to use a thermal stimulus. Functionalization of NCs with polymers exhibiting a lower critical solution temperature (LCST) such as Poly(*N*-isopropylacrylamide) (PNIPAAm) leads to nanocomposites which show temperature dependent collapse of the polymer corona.[130] Above the LCST the polymer corona can no longer stabilize the NC and aggregates are formed which was detected using TEM and DLS (see **Figure 17**). Large aggregates lead to strong scattering of the solution (loss of transmittance), whereas measurements in dilute solution show a slow increase of the particle size due to slow aggregation.

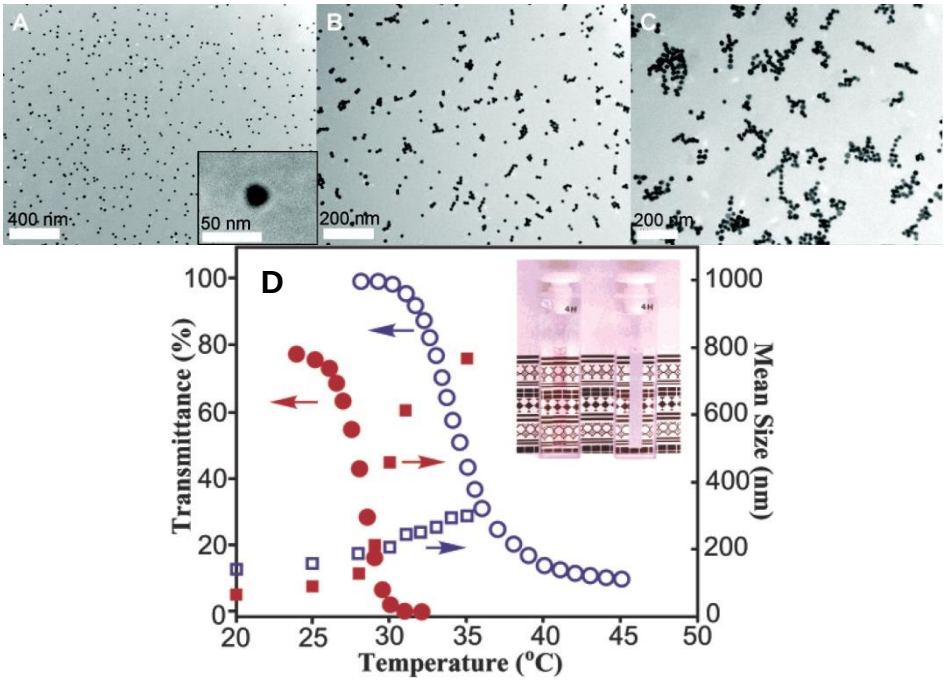

Figure 17. TEM images of gold NCs functionalized with poly(oligoethylene glycol acrylate-co-di(ethylene glycol) ethyl ether acrylate) (poly(OEGA-co-DEGA)) at 25 °C (A), 30 °C (B) and 35 °C (C). Inset: Phosphotungsten acid stained sample showing the polymer shell as a white halo. Thermoresponsive changes in transmittance (dots) and mean diameter (from DLS) (squares) of PPA-functionalized gold NCs (red) and pure PPA (blue) of 0.59 nM solutions (D). The size of the NCs increases more dramatically than the pure polymer. Adapted with permission.[148] Copyright 2009 and 2004, respectively, American Chemical Society.

Another stimulus, which can be applied to a nanocomposite film is electromagnetic radiation. The first ones to report such an approach were Klajn *et al*. who functionalized spherical gold NCs with a mixture of dodecylamine, didodecyldimethylammonium bromide and different amounts of the photoactive surfactant (4,4’ bis(11-mercaptoundecanoxy) azobenzene (ADT).

The last ligand, a *trans*-azobenzene, easily performed *trans*-*cis*-isomerization upon UV-irradiation which induced a molecular dipole. As a consequence of the *cis*-ADT dipoles aggregation of the NCs occurred and superparticle formation was observed. Moreover, the self-assembly of the NCs was reversible as irradiation with visible light led back to *trans*-ADT and hence, to disassembly of the aggregates. In addition, with varying the amount of ADT ligands it was possible to control the superparticle size.[43, 44]
In these studies, small ligands were used, similar to approaches which were published recently.[131]

Yet, for the application in hybrid solar cells a polymer ligand coating which acts as an active material would be very desirable. Such an approach leading to end functionalized polymers containing a photocleavable group was recently reported.[42] In this study, a side chain conjugated triphenylamine-based polymer was introduced as polymer coating on TiO_2 nanorods. This polymer contained a catechol unit at its chain end which enabled a strong interaction with the NCs. In addition, a photocleavable group was introduced between the anchor and the semiconducting polymer (**Figure 18A)**. Upon irradiation with UV light, the polymers were cleaved off the NCs and attractive interactions between the small moieties remaining on the NC surfaces were assumed to direct aggregation into superparticles (see **Figure 18B** and **C**).[42]
However, it should be mentioned that none of those studies reported stimuli-triggered aggregation of NCs in a film yet. Therefore, further studies are required to proof the applicability of the approaches described in this section in nanocomposite-based films and their incorporation in the field of optoelectronic applications.
In the next section we will discuss an alternative method to control the morphology of hybrid films via internally pre-structured colloids.

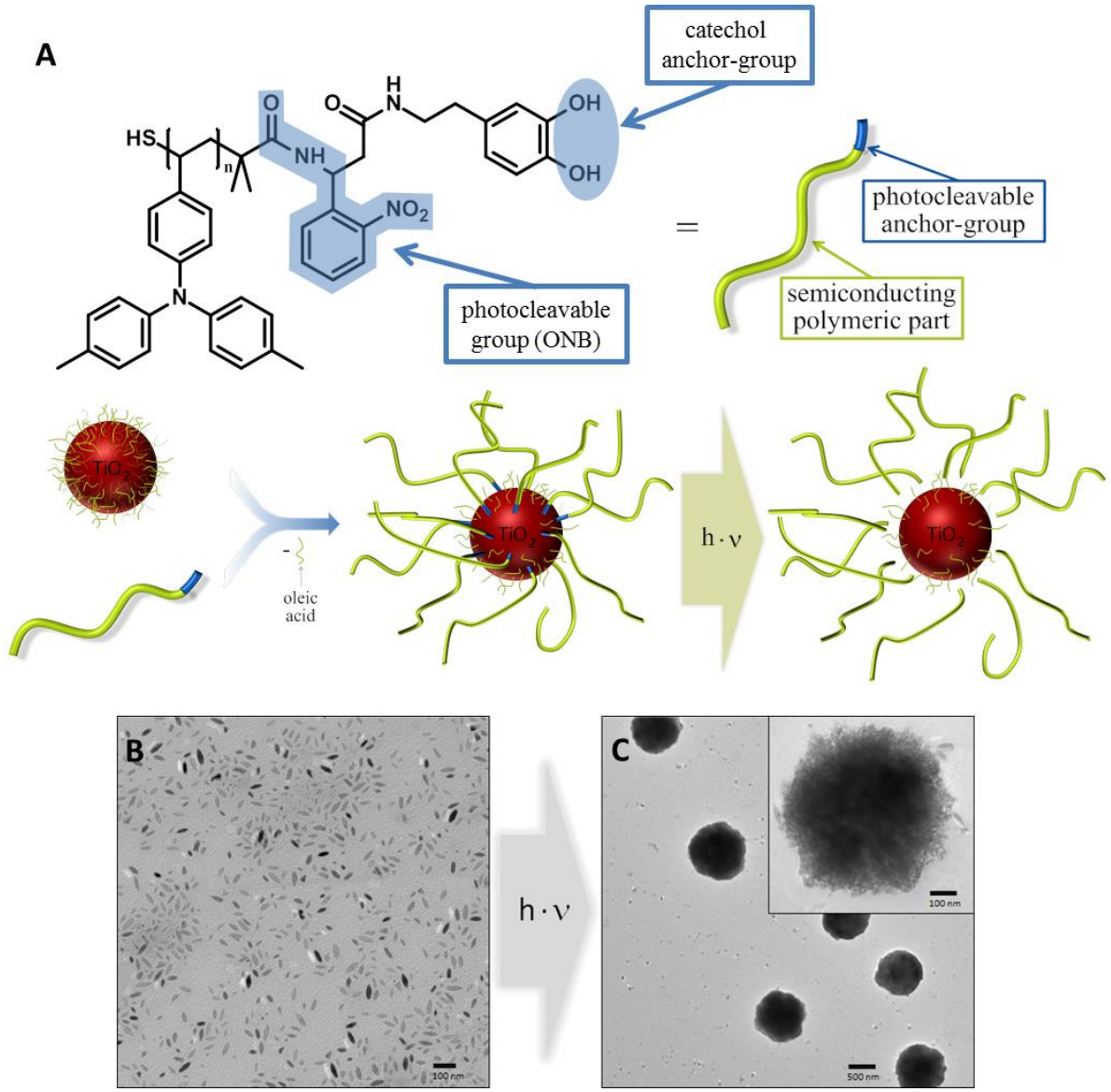

Figure 18. Schematic presentation of the functionalization of TiO_2 NCs with a semiconducting triphenylamine-based polymer containing an anchor and a photocleavable group (A). TEM images of the nanocomposite before (B) and after irradiation induced aggregation into superparticles (C). Adapted with permission.[42] Copyright 2014, Wiley-VCH Verlag GmbH.

3.2 Finely Dispersed Blends Starting from Internally Structured Colloids

The fabrication of structured films on the base of colloids is well established and can be achieved using different techniques such as horizontal deposition, vertical deposition, spin-casting and surface pattern-assisted deposition. In addition, those methods were successfully applied to produce nanocomposites of polymer colloids and inorganic nanoparticles. Grunlan *et al*. were the first to demonstrate this approach in 2006. Deposition of a finely dispersed

solution of both, CNTs and polymer colloids, led to an ordered film upon water evaporation. While the colloids self-assembled in a close-packed configuration, CNTs were placed in the interstices. Finally, annealing above the minimum film formation temperature (MFFT) enables coalescence and a segregated network was obtained.[132] Furthermore, other approaches were developed attaching the NCs directly on the colloid surface exploiting hetero-flocculation or Pickering polymerization.[133]

Yet, all approaches have in common nanostructures that are governed by the polymer colloid particle size as the NCs cannot interpenetrate the colloid spheres. To achieve an interpenetrated network from colloids, the colloidal particles themselves must exhibit such an intermingled structure. In addition, regarding optoelectronics, semiconducting compounds are needed.

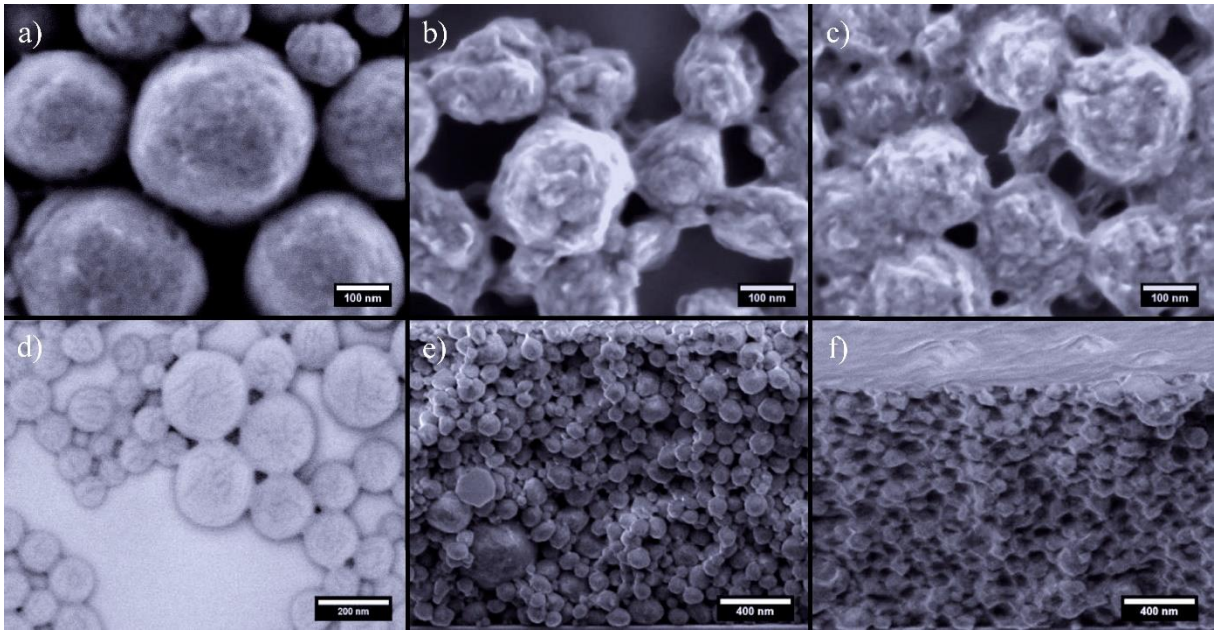

Figure 19. SEM images of P3HT/PCBM composites. Particles prepared at 50 °C: a) no further treatment applied, b) with ethanol or c) hexane treatment applied. Detection of backscattered electrons investigating an OsO_4 stained sample d). Cross section SEM images of drop-casted films before e) and after annealing to 95 °C for 12.5 min f).[45]

Recently, Landfester's group investigated P3HT/PCBM composite particles which exhibited an intermixed structure.[45] The mixing could be visualized through detection of the backscattered electrons via scanning electron microscopy (SEM) using OsO_4 stained samples. As OsO_4 reacts solely with PCBM, dark areas could be assigned to P3HT while bright areas would indicate PCBM (**Figure 19d**). Applying either an ethanol or a hexane treatment during

solvent evaporation at elevated temperatures makes it possible to create semi-fused particles (see **Figure 19a - c**).[45] Once implemented into a device, such a semi-fused system should improve charge transport to the electrodes since it would diminish the number of particle boundaries.

Furthermore, drop- or spin-casting a solution of those pre-structured composite particles enabled the fabrication of homogeneous films. In combination with the before-mentioned treatments and an additional annealing step films composed of partially fused particles were obtained as can be seen in **Figure 19 e** and **f**, respectively. Solar cells fabricated with those films as an active layer exhibited PCEs of about 0.53 %.[45]

It has been shown that two component particles are superior for the application in solar cells to a mixture of single component particles.[134] An external quantum efficiency of ca. 4 % was measured for devices made from polymer blend nanoparticles containing PFB:F8BT [poly(9,9-dioctylfluorene-2,7-diyl-*co*-bis-*N*,*N*'-(4-butylphenyl)-bis-*N*,*N*'-phenyl-1,4-phenylenediamine):poly(9,9-dioctylfluorene-2,7-diyl-*co*-benzothiadiazole)] at a weight ratio of 1:2 in each individual nanosphere.[135] Since the solar cell efficiency was almost not affected by the choice of solvent used in the nanoparticle fabrication process, it was concluded that the dimension of phase separation in these layers is indeed determined by the particle diameter.

In addition, such an approach was also applied to an organic/inorganic nanocomposite. Bannwarth *et al*. created well-defined nanofibers from spherical colloids composed of poly(styrene-*ran*-sodium 4-styrenesulfonate) and magnetic iron oxide NCs.[47] Those colloids exhibited a homogeneous distribution of the NCs in the polymer particles. This was achieved using miniemulsion droplets with dispersed magnetic nanoparticles as seeds for the emulsion polymerization of styrene. In a flow setup combined with an external magnetic field the colloids assembled linearly and annealing above the glass transition temperature led to fusion of the particles. Since the fusion was strongly temperature dependent the degree of fusion and thus the topology of the fibers were controlled from necklace like structures to uniform fibers. Additionally, Janus particles were synthesized and applied to the same setup affording zigzag fibers.[47] In summary, a combination of the above-mentioned techniques might lead to an interpenetrating morphology in a film composed of a semiconducting organic/inorganic composite.

A short insight into the optoelectronic applications in which organic/inorganic composites are used shall be given in the following chapter.

4. Applications of Semiconducting Nanocomposites

Previously in this review we devoted our attention to the synthesis of the nanocrystals/semiconducting polymer nanocomposites as well as the methods to control morphology of the nanocomposite-based films. Here we will briefly summarize the work done in the fields of solar cells and light emitting diodes. The nanocomposites used for the fabrication of optoelectronic devices are summarized in **Table 1**.

4.1. Hybrid Solar Cells

There are numerous studies about semiconducting polymer/nanocrystals nanocomposite-based hybrid solar cells. As the presentation of hybrid solar cells is not the main purpose of this review we only will highlight some examples. More detailed overviews can be found in the following reviews.[54, 3, 6, 136] Already in 2004, Liu *et al*. showed that higher power conversion efficiencies could be achieved using P3HT/CdSe QD nanocomposites with amino end functionalized P3HT instead of a polymer/QDs blend.[99] It is believed that an intimate contact between polymer and QDs is accountable for the improved device performance. Therefore, in order to improve the intimate contact between polymer and QDs rod-coil block copolymers with multiple anchor functionalities were synthesized and investigated in devices.[137] The improved charge separation of the systems with the close contact is, however, in some cases not enough to obtain devices with enhanced performance.[104] This result leads to the assumption that a perfect dispersion of NCs in polymer matrix prevents the formation of percolated NCs channels which are necessary for an efficient electron transport. Moreover, the improved device performance can be achieved by adjusting energy levels between polymer and nanocrystals. The open circuit voltage (V_{oc}), hence the efficiency of the solar cell can be increased by increasing the energy gap between the LUMO level of the acceptor (QD) and the HOMO level of the donor (polymer). The larger energy gap can be reached by utilizing QDs with higher LUMO energies and polymers with lower HOMO energies. A possible alternative to P3HT and PPV could be low band gap polymers such as Poly[2,6-(4,4-bis-(2-ethylhexyl)-4H-cyclopenta [2,1-b;3,4-b′]dithiophene)-alt-4,7(2,1,3-benzothiadiazole)] (PCPDTBT) or Poly[N-9′-heptadecanyl-2,7-carbazole-alt-5,5-(4′,7′-di-2-thienyl-2′,1′,3′-benzothiadiazole)] (PCDTBT) which exhibit lower HOMO levels.[138] Besides, the use of low band gap polymers would lead to absorption of more photons. CdTe or CdS QDs could serve as alternative acceptors to CdSe QDs with higher LUMO energy.[139] Chen *et al*. has presented a hybrid solar cell with the 3,2 % using low band gap polymer PSBTBT

and CdTe tetrapods.[22] However, it should be taken into account that the difference between LUMOs of QD and polymer as well as the difference between their HOMOs should be kept large enough to assure the charge separation. To conclude, over the time solar cells with polymer/QDs, polymer/nanorods as well as polymer/tetrapods have been investigated. The improved electron transport moving from QDs to tetrapods led to an enhanced device performance. The observed change in the electron transport is assumed to originate from expanded geometries of nanorods and tetrapods.[140]

4.2. Light Emitting Diodes

The possibility to exploit the joint advantages of QDs and polymers motivated researchers to fabricate lighting devices containing QD/polymer blends. Insulating as well as semiconducting polymers have been used in the active layers of such LEDs. Once the QDs are mixed with semiconducting polymers, the blend can be used as an active media of light emitting diodes. There are multiple studies about generating white light from such blends by tuning the emission intensities of the components. The tuning can be realized via changing the components ratios or varying the applied bias.[141, 142] Most studies use poly(N-vinylcarbazole) (PVK) as the semiconducting polymer matrix and the combined simultaneous emission of organic and inorganic components is investigated.[141, 143] However, there are examples where QDs imbedded in the MEH-PPV matrix do not contribute to the electroluminescent profile but are responsible for the improved electroluminescence efficiency compared to the device fabricated using pure MEH-PPV as the active layer.[144] Moreover, it was shown that once polymer/QD nanocomposites with polymers chemically grafted to the QDs are used the device performance is even further improved compared to physically mixed blends.[48] Utilizing chemical grafting instead of physical blending it is also possible to increase the QDs ratio within the polymer matrix while retaining the homogeneous distribution of the QDs within polymer.[145] The increased ratio of QDs enables to produce LEDs with the pure QDs electroluminescence without contribution of the polymer signal.[146, 50] In addition, it is possible to fabricate LEDs with an inverted structure. In these devices the polymer is responsible for the hole transport to the QDs. In this context, devices employing polymers with various HOMO levels were prepared and the role of the polymer HOMO level in the device performance was investigated.[25] Additionally, devices with active layers of polymer/QD nanocomposites were shown to have improved charge carrier balance as well as the necessary charge carrier distribution.[63]

Table 1. Nanocomposites used for the fabrication of optoelectronic devices.[a)]

Nanocomposite	Preparation Method	HOMO/LUMO [eV]		Performance	Device
		QDs[b)]	Polymer		
CdSe@ZnS QDs/ poly(TPA-*b*-CAA)[49]	Ligand exchange	- 6.8/ - 4.4	- 5.7/	EQE ≈ 0.25 %	QLED
CdSe@ZnS QDs/ poly(TPD-*b*-SSMe)[63]	Ligand exchange	- 6.5/ - 4.2	- 5.6/ -2.6	EQE = 1.38 ±0.03 %	QLED
CdSe@ZnS QDs/ poly(TPA-*b*-CAA)[50]	Ligand exchange	- 6.8/ - 4.4	- 6.0/ - 2.8	EQE = 1.5 %	QLED
CdSe/CdS/CdZnS QDs/ poly(TPDF-b-SSMe)[25]	Ligand exchange	-	- 5.9/ - 2.9	EQE = 3.37 %	QLED
CdSe@ZnS QDs/ S3-PPV[48]	Ligand exchange	-	- 5.28/ - 2.98	Current efficiency = 2.25 cd/A	OLED
CdS QDs/ poly(HEA-*co*-NVK)[145]	Grafting-to	-	-	-	QLED
CdSe@ZnS QDs/ PFH-NH 2 F-39-1[146]	Ligand exchange	-	- 5.45/ - 2.50	Current efficiency = 0.36 cd/A	QLED
P3HT/ TiO_2 NRs/ oligo-3HT-(Br)COOH[89]	Ligand exchange	- 7.54/ - 4.11	- 3.03/ - 4.93 - 3.05/ - 4.97	PCE = 1.19 %	Solar cell
PbS NCs/ P3[96]	Ligand exchange	-	-	PCE = 0.02 %	Solar cell
CdSe NCs/ rr-P3HT-thiophene-CH_2NH_2[99]	Ligand exchange	-	-	PCE ≈ 1.4 %	Solar cell
CdSe QDs/ rr-P3HT-thiol[104]	Ligand exchange	-	-	PCE = 0.60 %	Solar cell
CdTe QDs/ PSBTBT-NH_2[22]	Ligand exchange	- 5.78/ - 4.07	- 5.10/ - 3.65	PCE = 3.20 %	Solar cell
CdSe NRs/ rr-P3HT-PS[137]	Ligand exchange	-/ - 3.67	- 5.10/ - 2.51	PCE = 0.170%	Solar cell

[a)] For further information (e.g. device composition or active areas) and polymer structures the reader should refer to the corresponding reference; [b)] For NCs HOMO and LUMO refers to conductive band and valence band, respectively.

5. Conclusions and Perspectives

In this review we showed that hybrid materials can offer unique properties as they combine properties of organic and inorganic compounds. Experimental results so far, however, strongly differ from theoretical predictions.

One critical aspect is to provide miscibility of nanoparticles within a polymer matrix. Since a simple mixing of both compounds leads to macroscopic segregation in the micrometer scale due to depletion forces, a thermodynamic compatibilization of both components is necessary to mediate miscibility of the nanoparticles within the polymer matrix. Therefore, with special focus on semiconducting materials, we reviewed various approaches to achieve polymer coated nanoparticles as well as to control morphology in hybrid films.

Starting with approaches concerning the functionalization of NCs with a polymer shell using grafting-from, grafting-to or ligand exchange, we proceeded with discussion of controlled demixing from previously homogeneous composites. In addition, we elaborated on the fact that the film morphology can be controlled starting from internally pre-structured colloids. Furthermore, (anisotropic) NCs can be oriented as they may assemble into liquid crystalline phases or align themselves to an applied electric field between two electrodes when the conditions are adjusted carefully. Finally, we discussed the influence of the NCs' shape – ranging from spherical to rod like and tetrapod shaped NCs – on the film morphology.

The most prominent applications of hybrid materials are light emitting diodes and solar cells. Alongside with interface engineering and morphology control other factors such as energy level alignment have an important influence on solar cell performance A recent breakthrough addressing band alignment led to QD solar cells exhibiting certified efficiencies of 8.6 %. These cells were fabricated from solution and remained stable under air without encapsulation over 150 days.[147] The energy level alignment is also of crucial importance for hybrid solar cells. Varying the band energies of QDs as well as the HOMO and LUMO levels of polymers could lead to increased V_{oc} and thus to an enhanced device performance. Research which combines the advancements of multiple areas may lead to further breakthroughs thus resulting in hybrid based devices which can compete with the state of the art solar cells.

In addition, nanocomposites may find use in numerous applications such as energy storage, thermoelectrics, nanoelectrics, catalysis, (bio)sensors and more. Thus, continuative research in this field involving researchers of different disciplines might lead to new insights, materials and devices with currently unexcelled properties.

Acknowledgements: The authors thank Christopher C. Brown and Kerstin Menk for discussions. The work was funded by the Deutsche Forschungsgemeinschaft (DFG): International Research Training Group (IRTG) 1404 “Self-Organized Materials for Optoelectronics” as well as the Graduate School Materials Science in Mainz.

Received: December 1, 2014; Revised: January 23, 2015; Published online: March 3, 2015; DOI: 10.1002/marc.201400688

Keywords: compatibilization, conjugated polymers, morphology, nanocomposites, optoelectronics

References

[1] V. L. Colvin, M. C. Schlamp, A. P. Alivisatos. *Nature.* **1994**, *370*, 354–357.

[2] P. Reiss, E. Couderc, J. de Girolamo, A. Pron. *Nanoscale.* **2011**, *3*, 446.

[3] L. Zhao, Z. Lin. *Adv. Mater.* **2012**, *24*, 4353–4368.

[4] M. Wright, A. Uddin. *Solar Energy Materials and Solar Cells.* **2012**, *107*, 87–111.

[5] J. Chandrasekaran, D. Nithyaprakash, K. Ajjan, S. Maruthamuthu, D. Manoharan, S. Kumar. *Renewable and Sustainable Energy Reviews.* **2011**, *15*, 1228–1238.

[6] R. Liu. *Materials.* **2014**, *7*, 2747–2771.

[7] a) E. Arici, N. Sariciftci, D. Meissner. *Adv. Funct. Mater.* **2003**, *13*, 165–171. b) E. Tekin, P. J. Smith, S. Hoeppener, A. M. J. van den Berg, A. S. Susha, A. L. Rogach, J. Feldmann, U. S. Schubert. *Adv. Funct. Mater.* **2007**, *17*, 23–28. c) F. C. Krebs. *Solar Energy Materials and Solar Cells.* **2009**, *93*, 394–412. d) H.-G. Cheong, R. E. Triambulo, G.-H. Lee, I.-S. Yi, J.-W. Park. *ACS Appl. Mater. Interfaces.* **2014**, *6*, 7846–7855. e) D. C. Olson, J. Piris, R. T. Collins, S. E. Shaheen, D. S. Ginley. *Thin Solid Films.* **2006**, *496*, 26–29.

[8] a) L. Manna, E. Scher, A. Alivisatos. *Journal of Cluster Science.* **2002**, *13*, 521–532. b) T. Pellegrino, L. Manna, S. Kudera, T. Liedl, D. Koktysh, A. L. Rogach, S. Keller, J. Rädler, G. Natile, W. J. Parak. *Nano Lett.* **2004**, *4*, 703–707. c) X. Peng. *Adv. Mater.* **2003**, *15*, 459–463. d) H. Yu, J. Li, R. A. Loomis, P. C. Gibbons, Wang, W. E. Buhro. *J. Am. Chem. Soc.* **2003**, *125*, 16168–16169.

[9] Y. Yin, A. P. Alivisatos. *Nature.* **2005**, *437*, 664–670.

[10] a) L.-S. Li, A. Alivisatos. *Adv. Mater.* **2003**, *15*, 408–411. b) L. Carbone, C. Nobile, M. de Giorgi, F. Della Sala, G. Morello, P. Pompa, M. Hytch, E. Snoeck, A. Fiore, I. R. Franchini, M. Nadasan, A. F. Silvestre, L. Chiodo, S. Kudera, R. Cingolani, R. Krahne, L. Manna. *Nano Lett.* **2007**, *7*, 2942–2950. c) K. M. Ryan, A. Mastroianni, K. A. Stancil, H. Liu, A. P. Alivisatos. *Nano Lett.* **2006**, *6*, 1479–1482. d) A. Ghezelbash, B. Koo, B. A. Korgel. *Nano Lett.* **2006**, *6*, 1832–1836. e) C.-C. Kang, C.-W. Lai, H.-C. Peng, J.-J. Shyue, P.-T. Chou. *ACS Nano.* **2008**, *2*, 750–756. f) C. Querner, M. D. Fischbein, P. A. Heiney, M. Drndić. *Adv. Mater.* **2008**, *20*, 2308–2314.

[11] a) L. E. Brus. *J. Chem. Phys.* **1984**, *80*, 4403. b) A. P. Alivisatos. *Science.* **1996**, *271*, 933–937. c) P. V. Kamat. *J. Phys. Chem. C.* **2008**, *112*, 18737–18753. d) B. O. Dabbousi, J. Rodriguez-Viejo, F. V. Mikulec, J. R. Heine, H. Mattoussi, R. Ober, K. F. Jensen, M. G. Bawendi. *J. Phys. Chem. B.* **1997**, *101*, 9463–9475. e) D. A. Schwartz, N. S. Norberg, Q. P. Nguyen, J. M. Parker, D. R. Gamelin. *J. Am. Chem. Soc.* **2003**, *125*, 13205–13218.

[12] a) P. Yang, C. M. Lieber. *Science.* **1996**, *273*, 1836–1840. b) Y.-w. Jun, S.-M. Lee, N.-J. Kang, J. Cheon. *J. Am. Chem. Soc.* **2001**, *123*, 5150–5151. c) L. E. Greene, M. Law, D. H. Tan, M. Montano, J. Goldberger, G. Somorjai, P. Yang. *Nano Lett.* **2005**, *5*, 1231–1236. d) J. Perezjuste, I. Pastorizasantos, L. Lizmarzan, P. Mulvaney. *Coordination Chemistry Reviews.* **2005**, *249*, 1870–1901.

[13] a) L. Manna, E. C. Scher, A. P. Alivisatos. *J. Am. Chem. Soc.* **2000**, *122*, 12700–12706. b) L. Manna, D. J. Milliron, A. Meisel, E. C. Scher, A. P. Alivisatos. *Nat Mater.* **2003**, *2*, 382–385. c) A. Fiore, R. Mastria, M. G. Lupo, G. Lanzani, C. Giannini, E. Carlino, G. Morello, M. de Giorgi, Y. Li, R. Cingolani, L. Manna. *J. Am. Chem. Soc.* **2009**, *131*, 2274–2282.

[14] J. Lim, W. K. Bae, K. U. Park, L. Zur Borg, R. Zentel, S. Lee, K. Char. *Chem. Mater.* **2013**, *25*, 1443–1449.

[15] a) Y.-w. Jun, H.-W. Chung, J.-t. Jang, J. Cheon. *J. Mater. Chem.* **2011**, *21*, 10283. b) T. Yang, Z. D. Gordon, C. K. Chan. *Crystal Growth & Design.* **2013**, *13*, 3901–3907.

[16] H. Li, A. G. Kanaras, L. Manna. *Acc. Chem. Res.* **2013**, *46*, 1387–1396.

[17] a) D. J. Milliron, S. M. Hughes, Y. Cui, L. Manna, J. Li, L.-W. Wang, A. Paul Alivisatos. *Nature.* **2004**, *430*, 190–195. b) K.-S. Cho, D. V. Talapin, W. Gaschler, C. B. Murray. *J. Am. Chem. Soc.* **2005**, *127*, 7140–7147. c) L. J. Lauhon, M. S. Gudiksen, D. Wang, C. M. Lieber. *Nature.* **2002**, *420*, 57–61.

[18] a) M. Bredol, K. Matras, A. Szatkowski, J. Sanetra, A. Prodi-Schwab. *Solar Energy Materials and Solar Cells.* **2009**, *93*, 662–666. b) A. Guchhait, A. K. Rath, A. J. Pal. *Solar Energy Materials and Solar Cells.* **2011**, *95*, 651–656.

[19] S. Ren, L.-Y. Chang, S.-K. Lim, J. Zhao, M. Smith, N. Zhao, V. Bulović, M. Bawendi, S. Gradečak. *Nano Lett.* **2011**, *11*, 3998–4002.

[20] S. Dayal, N. Kopidakis, D. C. Olson, D. S. Ginley, G. Rumbles. *Nano Lett.* **2010**, *10*, 239–242.

[21] a) J.-S. Lee, M. V. Kovalenko, J. Huang, D. S. Chung, D. V. Talapin. *Nature Nanotech.* **2011**, *6*, 348–352. b) K. F. Jeltsch, M. Schädel, J.-B. Bonekamp, P. Niyamakom, F. Rauscher, H. W. A. Lademann, I. Dumsch, S. Allard, U. Scherf, K. Meerholz. *Adv. Funct. Mater.* **2012**, *22*, 397–404.

[22] H.-C. Chen, C.-W. Lai, I.-C. Wu, H.-R. Pan, I.-W. P. Chen, Y.-K. Peng, C.-L. Liu, C.-h. Chen, P.-T. Chou. *Adv. Mater.* **2011**, *23*, 5451–5455.

[23] Y. Kang, N.-G. Park, D. Kim. *Appl. Phys. Lett.* **2005**, *86*, 113101.

[24] a) Y.-Y. Lin, T.-H. Chu, S.-S. Li, C.-H. Chuang, C.-H. Chang, W.-F. Su, C.-P. Chang, M.-W. Chu, C.-W. Chen. *J. Am. Chem. Soc.* **2009**, *131*, 3644–3649. b) W. J. E. Beek, M. M. Wienk, M. Kemerink, X. Yang, R. A. J. Janssen. *J. Phys. Chem. B.* **2005**, *109*, 9505–9516. c) X. Wang, J. Zhuang, Q. Peng, Y. Li. *Nature.* **2005**, *437*, 121–124.

[25] L. Zur Borg, D. Lee, J. Lim, W. K. Bae, M. Park, S. Lee, C. Lee, K. Char, R. Zentel. *J. Mater. Chem. C.* **2013**, *1*, 1722.

[26] C. B. Murray, C. R. Kagan, M. G. Bawendi. *Annu. Rev. Mater. Sci.* **2000**, *30*, 545–610.

[27] R. Tuinier, J. Rieger, C. de Kruif. *Advances in Colloid and Interface Science.* **2003**, *103*, 1–31.

[28] a) R. A. Vaia, H. Ishii, E. P. Giannelis. *Chem. Mater.* **1993**, *5*, 1694–1696. b) A. Usuki, Y. Kojima, M. Kawasumi, A. Okada, Y. Fukushima, T. Kurauchi, O. Kamigaito. *J. Mater. Res.* **1993**, *8*, 1179–1184. c) T. Lan, T. J. Pinnavaia. *Chem. Mater.* **1994**, *6*, 2216–2219.

[29] W. Heitz, C. Meckel-Jonas, R. Neuhaus, M. D. Roth, V. Stümpflen, J. H. Wendorff. *Polym. Adv. Technol.* **1998**, *9*, 549–558.

[30] B. Schartel, J. H. Wendorff. *Polym. Eng. Sci.* **1999**, *39*, 128–151.

[31] a) W. A. Lopes, H. M. Jaeger. *Nature.* **2001**, *414*, 735–738. b) M. R. Bockstaller, Y. Lapetnikov, S. Margel, E. L. Thomas. *J. Am. Chem. Soc.* **2003**, *125*, 5276–5277. c) Y. Lin, A. Böker, J. He, K. Sill, H. Xiang, C. Abetz, X. Li, J. Wang, T. Emrick, S. Long, Q. Wang, A. Balazs, T. P. Russell. *Nature.* **2005**, *434*, 55–59.

[32] a) A. C. Balazs, T. Emrick, T. P. Russell. *Science.* **2006**, *314*, 1107–1110. b) D. Paul, L. Robeson. *Polymer.* **2008**, *49*, 3187–3204. c) S. K. Kumar, R. Krishnamoorti. *Annu. Rev. Chem. Biomol. Eng.* **2010**, *1*, 37–58. d) J. Kao, K. Thorkelsson, P. Bai, B. J. Rancatore, T. Xu. *Chem. Soc. Rev.* **2013**, *42*, 2654.

[33] R. A. Vaia, H. D. Wagner. *Materials Today.* **2004**, *7*, 32–37.

[34] S. M. Liff, N. Kumar, G. H. McKinley. *Nat Mater.* **2006**, *6*, 76–83.

[35] Y. Lu, Y. Yang, A. Sellinger, M. Lu, J. Huang, H. Fan, R. Haddad, G. Lopez, A. R. Burns, D. Y. Sasaki, J. Shelnutt, C. J. Brinker. *Nature.* **2001**, *410*, 913–917.

[36] S. Meuer, P. Oberle, P. Theato, W. Tremel, R. Zentel. *Adv. Mater.* **2007**, *19*, 2073–2078.

[37] S. Meuer, L. Braun, R. Zentel. *Chem. Commun.* **2008**, 3166.

[38] M. Zorn, S. Meuer, M. N. Tahir, Y. Khalavka, C. Sönnichsen, W. Tremel, R. Zentel. *J. Mater. Chem.* **2008**, *18*, 3050.

[39] S. Meuer, K. Fischer, I. Mey, A. Janshoff, M. Schmidt, R. Zentel. *Macromolecules.* **2008**, *41*, 7946–7952.

[40] S. Fischer, A. Salcher, A. Kornowski, H. Weller, S. Förster. *Angew. Chem. Int. Ed.* **2011**, *50*, 7811–7814.

[41] S. Ehlert, S. M. Taheri, D. Pirner, M. Drechsler, H.-W. Schmidt, S. Förster. *ACS Nano.* **2014**, *8*, 6114–6122.

[42] F. Mathias, M. N. Tahir, W. Tremel, R. Zentel. *Macromol. Chem. Phys.* **2014**, *215*, 604–613.

[43] R. Klajn, K. J. M. Bishop, M. Fialkowski, M. Paszewski, C. J. Campbell, T. P. Gray, B. A. Grzybowski. *Science.* **2007**, *316*, 261–264.

[44] R. Klajn, K. J. M. Bishop, B. A. Grzybowski. *Proceedings of the National Academy of Sciences.* **2007**, *104*, 10305–10309.

[45] B. Freisinger, *Investigation of P3HT/PCBM particle-based solar cells: Dissertation*, Johannes Gutenberg-University, Mainz, June, **2013**.

[46] T. Wang, J. L. Keddie. *Advances in Colloid and Interface Science.* **2009**, *147-148*, 319–332.

[47] M. B. Bannwarth, S. W. Kazer, S. Ulrich, G. Glasser, D. Crespy, K. Landfester. *Angew. Chem. Int. Ed.* **2013**, *52*, 10107–10111.

[48] K.-B. Chen, M.-H. Chen, S.-H. Yang, C.-H. Hsieh, C.-S. Hsu, C.-C. Chen, H.-J. Chien. *J. Polym. Sci. A Polym. Chem.* **2006**, *44*, 5378–5390.

[49] M. Zorn, W. K. Bae, J. Kwak, H. Lee, C. Lee, R. Zentel, K. Char. *ACS Nano.* **2009**, *3*, 1063–1068.

[50] J. Kwak, W. K. Bae, M. Zorn, H. Woo, H. Yoon, J. Lim, S. W. Kang, S. Weber, H.-J. Butt, R. Zentel, S. Lee, K. Char, C. Lee. *Adv. Mater.* **2009**, *21*, 5022–5026.

[51] J. Lim, L. Zur Borg, S. Dolezel, F. Schmid, K. Char, R. Zentel. *Macromol. Rapid Commun.* **2014**, *35*, 1685–1691.

[52] S.-J. Jeon, S.-M. Yang, B. J. Kim, J. D. Petrie, S. G. Jang, E. J. Kramer, D. J. Pine, G.-R. Yi. *Chem. Mater.* **2009**, *21*, 3739–3741.

[53] K. I. Winey, R. A. Vaia. *MRS Bull.* **2007**, *32*, 314–322.

[54] E. Holder, N. Tessler, A. L. Rogach. *J. Mater. Chem.* **2008**, *18*, 1064.

[55] J. Xu, J. Hu, X. Liu, X. Qiu, Z. Wei. *Macromol. Rapid Commun.* **2009**, *30*, 1419–1423.

[56] N. Greenham, X. Peng, A. Alivisatos. *Phys. Rev. B.* **1996**, *54*, 17628–17637.

[57] P.-G. d. Gennes, *Scaling concepts in polymer physics*, Ithaca, N.Y, Cornell University Press. **1979**.

[58] a) J. Xu, F. Qiu, H. Zhang, Y. Yang. *J. Polym. Sci. B Polym. Phys.* **2006**, *44*, 2811–2820. b) S. E. Harton, S. K. Kumar. *J. Polym. Sci. B Polym. Phys.* **2008**, *46*, 351–358.

[59] a) G. D. Smith, D. Bedrov. *Langmuir.* **2009**, *25*, 11239–11243. b) T. B. Martin, P. M. Dodd, A. Jayaraman. *Phys. Rev. Lett.* **2013**, *110*.

[60] M. S. Nikolic, C. Olsson, A. Salcher, A. Kornowski, A. Rank, R. Schubert, A. Frömsdorf, H. Weller, S. Förster. *Angew. Chem. Int. Ed.* **2009**, *48*, 2752–2754.

[61] P. Akcora, H. Liu, S. K. Kumar, J. Moll, Y. Li, B. C. Benicewicz, L. S. Schadler, D. Acehan, A. Z. Panagiotopoulos, V. Pryamitsyn, V. Ganesan, J. Ilavsky, P. Thiyagarajan, R. H. Colby, J. F. Douglas. *Nat Mater.* **2009**, *8*, 354–359.

[62] M. Bieligmeyer, S. M. Taheri, I. German, C. Boisson, C. Probst, W. Milius, V. Altstädt, J. Breu, H.-W. Schmidt, F. D'Agosto, S. Förster. *J. Am. Chem. Soc.* **2012**, *134*, 18157–18160.

[63] W. K. Bae, J. Lim, M. Zorn, J. Kwak, Y.-S. Park, D. Lee, S. Lee, K. Char, R. Zentel, C. Lee. *J. Mater. Chem. C.* **2014**, *2*, 4974.

[64] M. Zorn, S. A. L. Weber, M. N. Tahir, W. Tremel, H.-J. Butt, R. Berger, R. Zentel. *Nano Lett.* **2010**, *10*, 2812–2816.

[65] a) M. Eberhardt, R. Mruk, R. Zentel, P. Théato. *European Polymer Journal.* **2005**, *41*, 1569–1575. b) M. Eberhardt, P. Théato. *Macromol. Rapid Commun.* **2005**, *26*, 1488–1493.

[66] M. Zorn, M. N. Tahir, B. Bergmann, W. Tremel, C. Grigoriadis, G. Floudas, R. Zentel. *Macromol. Rapid Commun.* **2010**, *31*, 1101–1107.

[67] L. Zur Borg, A. L. Domanski, R. Berger, R. Zentel. *Macromol. Chem. Phys.* **2013**, *214*, 975–984.

[68] a) B. Oschmann, D. Bresser, M. N. Tahir, K. Fischer, W. Tremel, S. Passerini, R. Zentel. *Macromol. Rapid Commun.* **2013**, *34*, 1693–1700. b) D. Bresser, B. Oschmann, M. N. Tahir, F. Mueller, I. Lieberwirth, Tremel Wolfgang, R. Zentel, S. Passerini. *Journal of The Electrochemical Society.* **2015**, *162*, A3013-A3020.

[69] D. Bresser, B. Oschmann, M. N. Tahir, W. Tremel, R. Zentel, S. Passerini. *Journal of Power Sources.* **2014**, *248*, 852–860.

[70] a) I. Borukhov, L. Leibler. *Phys. Rev. E.* **2000**, *62*, R41. b) I. Borukhov, L. Leibler. *Macromolecules.* **2002**, *35*, 5171–5182. c) M. K. Corbierre, N. S. Cameron, M. Sutton, K. Laaziri, R. B. Lennox. *Langmuir.* **2005**, *21*, 6063–6072.

[71] N. Tomczak, R. Liu, J. G. Vancso. *Nanoscale.* **2013**, *5*, 12018.

[72] A. C. C. Esteves, L. Bombalski, T. Trindade, K. Matyjaszewski, A. Barros-Timmons. *Small.* **2007**, *3*, 1230–1236.

[73] K. Sill, T. Emrick. *Chem. Mater.* **2004**, *16*, 1240–1243.

[74] H. Skaff, T. Emrick. *Angew. Chem. Int. Ed.* **2004**, *43*, 5383–5386.

[75] H. Skaff, M. F. Ilker, E. B. Coughlin, T. Emrick. *J. Am. Chem. Soc.* **2002**, *124*, 5729–5733.

[76] L. Zhou, C. Gao, W. Xu. *J. Mater. Chem.* **2009**, *19*, 5655.

[77] H. Skaff, K. Sill, T. Emrick. *J. Am. Chem. Soc.* **2004**, *126*, 11322–11325.

[78] L.-G. Yang, F. Chen, H. Xu, M. Wang, H.-Z. Chen. *J. Appl. Phys.* **2009**, *106*, 73701.

[79] I. Kanelidis, A. Vaneski, D. Lenkeit, S. Pelz, V. Elsner, R. M. Stewart, J. Rodríguez-Fernández, A. A. Lutich, A. S. Susha, R. Theissmann, S. Adamczyk, A. L. Rogach, E. Holder. *J. Mater. Chem.* **2011**, *21*, 2656.

[80] J. Xu, J. Wang, M. Mitchell, P. Mukherjee, M. Jeffries-EL, J. W. Petrich, Z. Lin. *J. Am. Chem. Soc.* **2007**, *129*, 12828–12833.

[81] L. Zhao, X. Pang, R. Adhikary, J. W. Petrich, M. Jeffries-EL, Z. Lin. *Adv. Mater.* **2011**, *23*, 2844–2849.

[82] L. Zhao, X. Pang, R. Adhikary, J. W. Petrich, Z. Lin. *Angew. Chem. Int. Ed.* **2011**, *50*, 3958–3962.

[83] J. Jung, X. Pang, C. Feng, Z. Lin. *Langmuir.* **2013**, *29*, 8086–8092.

[84] Q. Zhang, T. P. Russell, T. Emrick. *Chem. Mater.* **2007**, *19*, 3712–3716.

[85] a) X. Ji, D. Copenhaver, C. Sichmeller, X. Peng. *J. Am. Chem. Soc.* **2008**, *130*, 5726–5735. b) A. J. Morris-Cohen, V. Vasilenko, V. A. Amin, M. G. Reuter, E. A. Weiss. *ACS Nano.* **2012**, *6*, 557–565.

[86] W. J. Brittain, S. Minko. *J. Polym. Sci. A Polym. Chem.* **2007**, *45*, 3505–3512.

[87] D. Milliron, A. Alivisatos, C. Pitois, C. Edder, J. Fréchet. *Adv. Mater.* **2003**, *15*, 58–61.

[88] a) A. Javier, C. S. Yun, J. Sorena, G. F. Strouse. *J. Phys. Chem. B.* **2003**, *107*, 435–442. b) B. C. Sih, M. O. Wolf. *J. Phys. Chem. C.* **2007**, *111*, 17184–17192. c) P. K. Sudeep, K. T. Early, K. D. McCarthy, M. Y. Odoi, M. D. Barnes, T. Emrick. *J. Am. Chem. Soc.* **2008**, *130*, 2384–2385. d) R. Stalder, D. Xie, R. Zhou, J. Xue, J. R. Reynolds, K. S. Schanze. *Chem. Mater.* **2012**, *24*, 3143–3152.

[89] Y.-C. Huang, J.-H. Hsu, Y.-C. Liao, W.-C. Yen, S.-S. Li, S.-T. Lin, C.-W. Chen, W.-F. Su. *J. Mater. Chem.* **2011**, *21*, 4450.

[90] a) R. Kline, M. McGehee, E. Kadnikova, J. Liu, J. Fréchet. *Adv. Mater.* **2003**, *15*, 1519–1522. b) R. J. Kline, M. D. McGehee, E. N. Kadnikova, J. Liu, J. M. J. Fréchet, M. F. Toney. *Macromolecules.* **2005**, *38*, 3312–3319. c) J.-M. Verilhac, G. LeBlevennec, D. Djurado, F. Rieutord, M. Chouiki, J.-P. Travers, A. Pron. *Synthetic Metals.* **2006**, *156*, 815–823.

[91] C. Querner, A. Benedetto, R. Demadrille, P. Rannou, P. Reiss. *Chem. Mater.* **2006**, *18*, 4817–4826.

[92] C. Querner, P. Reiss, J. Bleuse, A. Pron. *J. Am. Chem. Soc.* **2004**, *126*, 11574–11582.

[93] G. Zotti, B. Vercelli, A. Berlin, M. Pasini, T. Nelson, R. McCullough, T. Virgili. *Chem. Mater.* **2010**, *22*, 1521–1532.

[94] H. Sirringhaus, P. J. Brown, R. H. Friend, M. M. Nielsen, K. Bechgaard, B. M. W. Langeveld-Voss, A. J. H. Spiering, R. A. J. Janssen, E. W. Meijer, P. Herwig, D. M. de Leeuw. *Nature.* **1999**, *401*, 685–688.

[95] S. Berson, R. De Bettignies, S. Bailly, S. Guillerez. *Adv. Funct. Mater.* **2007**, *17*, 1377–1384.

[96] J. Zhang, L. Bahrig, A. Puetz, I. Kanelidis, D. Lenkeit, S. Pelz, S. G. Hickey, M. F. Klein, A. Colsmann, U. Lemmer, A. Eychmüller, E. Holder. *Polymer.* **2013**, *54*, 5525–5533.

[97] C. Fang, X.-Y. Qi, Q.-L. Fan, L.-H. Wang, W. Huang. *Nanotechnology.* **2007**, *18*, 35704.

[98] K. Palaniappan, N. Hundt, P. Sista, H. Nguyen, J. Hao, M. P. Bhatt, Y.-Y. Han, E. A. Schmiedel, E. E. Sheina, M. C. Biewer, M. C. Stefan. *J. Polym. Sci. A Polym. Chem.* **2011**, *49*, 1802–1808.

[99] J. Liu, T. Tanaka, K. Sivula, A. P. Alivisatos, J. M. J. Fréchet. *J. Am. Chem. Soc.* **2004**, *126*, 6550–6551.

[100] Y. Zhou, F. S. Riehle, Y. Yuan, H.-F. Schleiermacher, M. Niggemann, G. A. Urban, M. Krüger. *Appl. Phys. Lett.* **2010**, *96*, 13304.

[101] J. Olson, G. Gray, S. Carter. *Solar Energy Materials and Solar Cells.* **2009**, *93*, 519–523.

[102] B. C. Thompson, J. M. J. Fréchet. *Angew. Chem. Int. Ed.* **2008**, *47*, 58–77.

[103] L.-M. Chen, Z. Hong, G. Li, Y. Yang. *Adv. Mater.* **2009**, *21*, 1434–1449.

[104] K. Palaniappan, J. W. Murphy, N. Khanam, J. Horvath, H. Alshareef, M. Quevedo-Lopez, M. C. Biewer, S. Y. Park, M. J. Kim, B. E. Gnade, M. C. Stefan. *Macromolecules.* **2009**, *42*, 3845–3848.

[105] a) A. Smeets, K. van den Bergh, J. de Winter, P. Gerbaux, T. Verbiest, G. Koeckelberghs. *Macromolecules.* **2009**, *42*, 7638–7641. b) N. Doubina, S. A. Paniagua, A. V. Soldatova, A. K. Y. Jen, S. R. Marder, C. K. Luscombe. *Macromolecules.* **2011**, *44*, 512–520.

[106] F. Monnaie, W. Brullot, T. Verbiest, J. de Winter, P. Gerbaux, A. Smeets, G. Koeckelberghs. *Macromolecules.* **2013**, *46*, 8500–8508.

[107] H. Zocher. *Z. Anorg. Allg. Chem.* **1925**, *147*, 91–110.

[108] a) H. Hoshino, M. Yamaha, N. Donkai, V. Sinigersky, K. Kajiwara, T. Miyamoto, H. Inagaki. *Polymer Bulletin.* **1992**, *28*, 607–614. b) H. Hoshino, T. Ito, N. Donkai, H. Urakawa, K. Kajiwara. *Polymer Bulletin.* **1992**, *29*, 453–460.

[109] P. Davidson, P. Batail, J. Gabriel, J. Livage, C. Sanchez, C. Bourgaux. *Progress in Polymer Science.* **1997**, *22*, 913–936.

[110] P. Davidson, J.-C. P. Gabriel. *Current Opinion in Colloid & Interface Science.* **2005**, *9*, 377–383.

[111] L.-s. Li, J. Walda, L. Manna, A. P. Alivisatos. *Nano Lett.* **2002**, *2*, 557–560.

[112] R. Zentel, W. Pisula, M. Zorn, J. Y. Chang, K. Müllen, R. Zentel. *Macromol. Rapid Commun.* **2009**, *30*, 1179–1202.

[113] E.-K. Fleischmann, R. Zentel. *Angew. Chem. Int. Ed.* **2013**, *52*, 8810–8827.

[114] M. Zorn, S. Meuer, M. N. Tahir, W. Tremel, K. Char, R. Zentel. *J. Nanosci. Nanotech.* **2010**, *10*, 6845–6849.

[115] M. Zorn, R. Zentel. *Macromol. Rapid Commun.* **2008**, *29*, 922–927.

[116] S. Meuer, L. Braun, T. Schilling, R. Zentel. *Polymer.* **2009**, *50*, 154–160.

[117] a) B. Sun, E. Marx, N. C. Greenham. *Nano Lett.* **2003**, *3*, 961–963. b) Y. Zhou, Y. Li, H. Zhong, J. Hou, Y. Ding, C. Yang, Y. Li. *Nanotechnology.* **2006**, *17*, 4041–4047.

[118] I. R. Franchini, A. Cola, A. Rizzo, R. Mastria, A. Persano, R. Krahne, A. Genovese, A. Falqui, D. Baranov, G. Gigli, L. Manna. *Nanoscale.* **2010**, *2*, 2171.

[119] R. Blaak, B. M. Mulder, D. Frenkel. *J. Chem. Phys.* **2004**, *120*, 5486.

[120] H. Hasegawa, H. Tanaka, K. Yamasaki, T. Hashimoto. *Macromolecules.* **1987**, *20*, 1651–1662.

[121] M. Zanella, G. Bertoni, I. R. Franchini, R. Brescia, D. Baranov, L. Manna. *Chem. Commun.* **2010**, *47*, 203.

[122] B. Oschmann, M. N. Tahir, F. Mueller, D. Bresser, I. Lieberwirth, W. Tremel, S. Passerini, Zentel R. *Macromol. Rapid Commun.* **2015**, DOI: 10.1002/marc.201400647.

[123] S. Asakura, F. Oosawa. *J. Chem. Phys.* **1954**, *22*, 1255.

[124] a) S. Alexander. *J. Phys. France.* **1977**, *38*, 983–987. b) P. de Gennes. *J. Phys. France.* **1976**, *37*, 1445–1452.

[125] a) C. B. Murray, C. R. Kagan, M. G. Bawendi. *Science.* **1995**, *270*, 1335–1338. b) J. H. Masliyah, S. Bhattacharjee, *Electrokinetic and colloid transport phenomena*, Hoboken, N.J, Wiley-Interscience. **2006**.

[126] V. M. Rotello, A. K. Boal, F. Ilhan, J. E. DeRouchey, T. Thurn-Albrecht, T. P. Russell. *Nature.* **2000**, *404*, 746–748.

[127] B. L. Cushing, V. L. Kolesnichenko, C. J. O'Connor. *Chem. Rev.* **2004**, *104*, 3893–3946.

[128] a) J. Zhuang, H. Wu, Y. Yang, Y. C. Cao. *J. Am. Chem. Soc.* **2007**, *129*, 14166–14167. b) J. Zhuang, H. Wu, Y. Yang, Y. C. Cao. *Angew. Chem. Int. Ed.* **2008**, *47*, 2208–2212.

[129] T. Wang, D. LaMontagne, J. Lynch, J. Zhuang, Y. C. Cao. *Chem. Soc. Rev.* **2013**, *42*, 2804.

[130] a) I. Luzinov, S. Minko, V. V. Tsukruk. *Soft Matter.* **2008**, *4*, 714. b) M. I. Gibson, R. K. O'Reilly. *Chem. Soc. Rev.* **2013**, *42*, 7204.

[131] a) Y. Shiraishi, K. Tanaka, E. Shirakawa, Y. Sugano, S. Ichikawa, S. Tanaka, T. Hirai. *Angew. Chem. Int. Ed.* **2013**, *52*, 8304–8308. b) Y. Shiraishi, E. Shirakawa, K. Tanaka, H. Sakamoto, S. Ichikawa, T. Hirai. *ACS Appl. Mater. Interfaces.* **2014**, *6*, 7554–7562. c) J. A. Krings, B. Vonhören, P. Tegeder, V. Siozios, M. Peterlechner, B. J. Ravoo. *J. Mater. Chem. A.* **2014**, *2*, 9587.

[132] J. C. Grunlan, Y.-S. Kim, S. Ziaee, X. Wei, B. Abdel-Magid, K. Tao. *Macromol. Mater. Eng.* **2006**, *291*, 1035–1043.

[133] a) S. Harley, D. W. Thompson, B. Vincent. *Colloids and Surfaces.* **1992**, *62*, 163–176. b) S. Cauvin, P. J. Colver, S. A. F. Bon. *Macromolecules.* **2005**, *38*, 7887–7889.

[134] T. Kietzke, D. Neher, K. Landfester, R. Montenegro, R. Güntner, U. Scherf. *Nat Mater.* **2003**, *2*, 408–412.

[135] T. Kietzke, D. Neher, M. Kumke, R. Montenegro, K. Landfester, U. Scherf. *Macromolecules.* **2004**, *37*, 4882–4890.

[136] V. J. Babu, S. Vempati, S. Sundarrajan, M. Sireesha, S. Ramakrishna. *Solar Energy.* **2014**, *106*, 1–22.

[137] S. Li, Y. Li, C. A. Wisner, L. Jin, N. Leventis, Z. Peng. *RSC Adv.* **2014**, *4*, 35823.

[138] H. Dong, H. Zhu, Q. Meng, X. Gong, W. Hu. *Chem. Soc. Rev.* **2012**, *41*, 1754.

[139] C. M. de Donegá. *Chem. Soc. Rev.* **2011**, *40*, 1512.

[140] E. Martínez-Ferrero, J. Albero, E. Palomares. *J. Phys. Chem. Lett.* **2010**, *1*, 3039–3045.

[141] F. Li, T. Guo, T. Kim. *Appl. Phys. Lett.* **2010**, *97*, 62104.

[142] a) Y. Li, A. Rizzo, M. Mazzeo, L. Carbone, L. Manna, R. Cingolani, G. Gigli. *J. Appl. Phys.* **2005**, *97*, 113501. b) P. T. K. Chin, R. A. M. Hikmet, R. A. J. Janssen. *J. Appl. Phys.* **2008**, *104*, 13108. c) K. Kwak, K. Cho, S. Kim. *Appl. Phys. Lett.* **2014**, *104*, 103303.

[143] J. Y. Park, R. C. Advincula. *Phys. Chem. Chem. Phys.* **2014**, *16*, 8589.

[144] C.-W. Lee, C. Renaud, C.-S. Hsu, T.-P. Nguyen. *Nanotechnology.* **2008**, *19*, 455202.

[145] J. Zhou, W.-Q. Tang, C.-F. Wang, L. Chen, Q. Chen, S. Chen. *J. Polym. Sci. A Polym. Chem.* **2012**, *50*, 3736–3742.

[146] Z.-S. Guo, L. Zhao, J. Pei, Z.-L. Zhou, G. Gibson, J. Brug, S. Lam, S. S. Mao. *Macromolecules*. **2010**, *43*, 1860–1866.

[147] C.-H. M. Chuang, P. R. Brown, V. Bulović, M. G. Bawendi. *Nat Mater.* **2014**, *13*, 796–801.

[148] a) C. Boyer, M. R. Whittaker, M. Luzon, T. P. Davis. *Macromolecules.* **2009**, *42*, 6917–6926. b) M.-Q. Zhu, L.-Q. Wang, G. J. Exarhos, A. D. Q. Li. *J. Am. Chem. Soc.* **2004**, *126*, 2656–2657.

2.2.2 Nanoparticles Composed of Amphiphilic Block Copolymers

In this subsection 2.2.2 we will give a short introduction into the fabrication of nanosized aggregates composed of amphiphilic block copolymers. The most popular type of such nanoparticles are micelles. Micelles are spherelike aggregates in a liquid which form a stable colloidal suspension or dispersion.

The basic requirement for the formation of micelles is the amphiphilicity of the compound which should self-assemble into micelles. Therefore, most typically the compound exhibits a hydrophilic "head" and a hydrophobic "tail". In the case of micelles (or nanosized aggregates) composed of polymers, the polymer is usually a block copolymer exhibiting a hydrophilic block (e.g. PEG or acrylic acid) and a hydrophobic block (e.g. polystyrene or polybutadiene). A normal phase micelle is defined as a micelle in which the hydrophilic part is in contact with the surrounding liquid (typically water) and the hydrophobic part can be found at the center of the micelle. In the case of an inverse micelle the situation is reversed (hydrophobic part interacts with the surrounding liquid).[I21]

Beside spherelike micelles, there are various other shapes of nanosized aggregates such as compound micelles, vesicles or cylindrical aggregates (see **Figure 7**). The shape and size of the nanoparticles is depending on various factors, e.g. the amphiphile, micellization procedure, pH value or temperature.

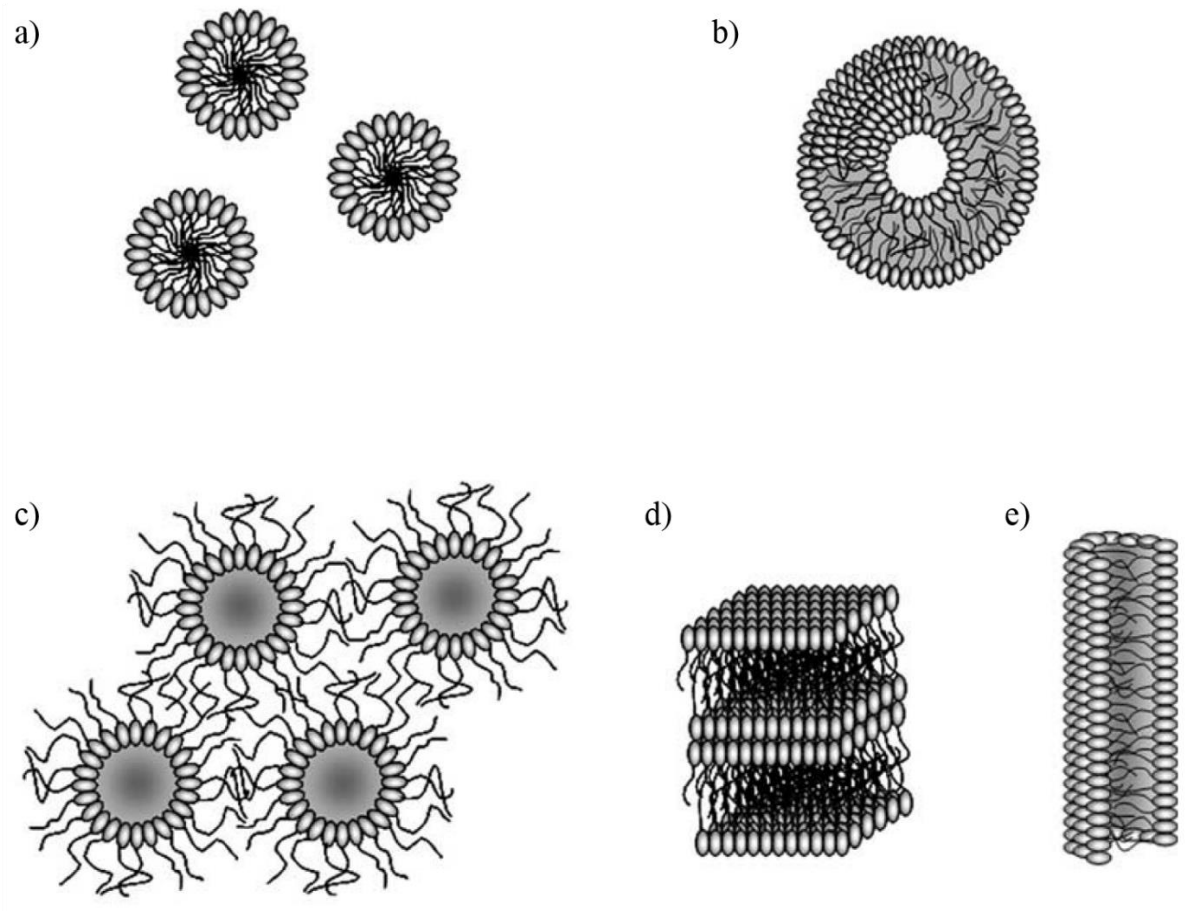

Figure 7. Differently shaped nanoparticles obtained from amphiphilic block copolymers: a) normal phase micelles, b) vesicles, c) inverse micelles, d) lamellar structures and e) cylindrical structures.[I21]

However, in all cases the nanoparticles will only form after a certain concentration is exceeded, the so-called critical micelle concentration (CMC). In addition, the temperature of the system has to be higher than the critical micelle temperature (CMT).[I21] The process of micelle formation is a thermodynamic phenomenon and a schematic is illustrated in **Figure 8**. The self-assembly into micelles takes place spontaneously (upon reaching the CMC), once the energy loss from the decrease in entropy due to the formation of micelles is exceeded by the energy gain caused through the release of solvent molecules interacting with the hydrophobic part (increase in entropy).

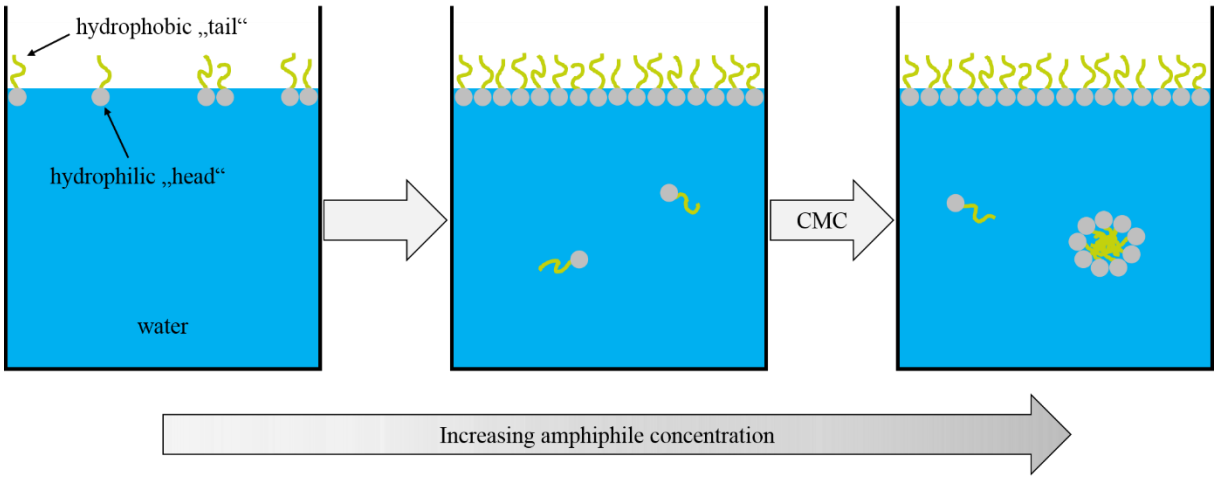

Figure 8. Schematic illustrating the self-assembly of amphiphiles into micelles once the concentration of the amphiphiles exceeds the critical micelle concentration (CMC).

The application of polymer micelles as drug delivery systems was first proposed by Ringsdorf and coworkers.[I22] The basic idea of this concept was to incorporate a drug, which is hydrophobic and, in turn, not well soluble in water (or blood), in the hydrophobic center of the polymer micelles. Therefore, it would be well soluble in aqueous systems. The approach was investigated in detail and the group of Prof. K. Kataoka was the first to bring polymer micelle drug delivery systems into clinical trials.[I23]

The process of micelle formation, however, is always an equilibrium between polymers incorporated in the micelle and free polymers (unimers) in solution. The CMC of polymer micelles is usually much lower compared to low molecular weight amphiphiles and the equilibrium is far more on the side of the amphiphiles incorporated into the micelle. Nevertheless, an exchange between polymers incorporated into the micelles and unimers in solution exists. Therefore, micelles are dynamic systems, yet, drugs which are simply absorbed into micelles suffer from an unspecific release during the circulation in the body. To overcome this problem and to achieve a controlled release of the drugs, approaches investigating a reversible covalent binding of the drug to the micelle core have been developed.[I24] Another interesting application of micelles is the incorporation of a fluorescent compound into the micelle core. Such micelles can be used as imaging tools for the visualization of tumors.[I25]

2.3 Interface Control and Engineering

In this section 2.3 we will focus on the role of surfactants interacting with the surface of inorganic nanoparticles. Such surfactants can be either low molecular weight compounds or polymers. Generally, they exhibit functional groups such as amines, thiols or carboxylic acids to allow for an effective binding to the nanoparticle surface. In this context the functional groups are often referred to as anchor groups. The stability of the interaction between nanoparticles and anchor groups, however, is strongly depending on the individual combination of nanoparticles and functional groups. Generally, carboxylic acids form very stable coatings on oxidic nanoparticles such as TiO_2 and ZnO. By contrast, the interaction of carboxylic acids with Au or CdSe nanoparticles is weak which results in a loosely bound coating. Thiols, in contrast, bind very effectively to CdSe and Au nanoparticles. This behavior can be explained taking the "hard soft acids and bases" (HSAB) theory into account. According to the HSAB theory Ti^{4+} and Zn^{2+} are hard acids and the carboxylate ($RCOO^-$) is a hard base. $Au^{(0)}$ and Cd^{2+} are soft acids and the thiolate (RS^-) is a soft base.[I26] The question whether a very stable interaction with the nanoparticles is desired or a loosely bound coating is preferred depends on the individual application. Furthermore, the functional groups can also affect processes taking place at the surface of the nanoparticles such as the exciton separation. In the following subsections we will, therefore, discuss different circumstances and the effect of different coatings on the desired properties.

2.3.1 Effects of the Coating Stability

The interaction of the surfactants with the nanoparticle surface is a dynamic process which means that an equilibrium between adsorption and desorption exists (see also subsection 2.2.3 in the publication inserted as subsection 2.2.1). To achieve a coating which is as stable as possible, it is, therefore, necessary to shift the equilibrium far to the side of adsorption. One single anchor group which provides a very strong binding to the nanoparticle surface can be used to achieve a stable coating. For example, when using a single, bidentate catechol group a very stable functionalization of TiO_2 nanoparticles can be achieved.[I27] Enediols (e.g. catechol) are, however, extraordinary anchor groups for oxidic materials. Interacting with unsaturated metal centers at the nanoparticle surface, enediols form a coordination complex with a perfect

five-membered ring geometry. Thus, the six-coordinated octahedral geometry of the surface titanium atoms is restored.[I28,I29] Once the interaction of the anchor group to the nanoparticle surface is less effective, a multidentate anchor group is needed to achieve a stable coating.

Block copolymers offer the possibility to incorporate a block exhibiting many anchor groups and are, therefore, multidentate surfactants. Block copolymer surfactants have been used in several approaches to achieve a stable functionalization of nanoparticles with the polymer surfactant. Therefore, the properties of the nanoparticles can be tailored and, for example, the solubility can be modified.[I30,I31] Furthermore, films fabricated from nanoparticles functionalized with a stable polymer coating exhibit a different morphology compared to simple mixtures of non-adsorbing polymers and nanoparticles (blend). While the functionalized nanoparticles are individually dispersed, the nanoparticles in the blend show a strong tendency to form aggregated structures (see subsection 2.2.1). Shape anisotropic nanoparticles with a stable polymer coating have been successfully applied to achieve liquid crystalline phases with thermotropic behavior.[I29,I32] Once a semiconducting polymer coating is used to functionalize appropriate nanoparticles, the hybrid can be applied for the fabrication of optoelectronic devices. In the case of light emitting diods (LEDs) such hybrids resulted in devices with improved performances as compared to devices fabricated using unfunctionalized nanoparticles. Devices assembled with hybrids showed respectable efficiencies of up to 3.4 % external quantum efficiency (EQE).[I30,I33]

Unfortunately, solar cells fabricated using nanoparticles with a stable coating generally exhibit worse efficiencies than the respective blend system. This is believed to be caused by the different requirements for both applications. In case of LEDs, the charges are forced to move through the hybrid film due to the applied voltage. As soon as an electron and a hole meet at the interface of an inorganic nanoparticle and the surrounding polymer coating, the charges can combine which causes the luminescence of the LED. Once an electron enters a nanoparticle, it might be even trapped in this nanoparticle as the nanoparticles are much better electron transporting materials compared to the polymer. However, in the case of LEDs, electrons which are trapped in the nanoparticles might even be beneficial as they will recombine with a hole as soon as it is in the surrounding polymer coating. Contrarily, in the case of solar cells, recombination of electrons and holes is not desired. The trapping of electrons in isolated nanoparticles, therefore, leads to a reduced device efficiency. For the application in solar cells percolated pathways which enable the charge transport to the respective electrodes are required.

The formation of such percolated pathways benefits from a less stable functionalization of the nanoparticles with loosely bound surfactants. The most popular approach to exchanging the initial ligands by loosely bound ligands was first reported by Geenham *et al*. in 1996. CdSe quantum dots (QDs) primarily coated with tri-*n*-octylphosphine oxide (TOPO) were treated with excess pyridine to substitute the strongly bound TOPO coating with loosely bound pyridine molecules. Thus, the insulating shell of TOPO ligands was removed and substituted by the aromatic pyridine. Pyridine ligands are assumed to be partially removed from the QD surface during the film casting process and leave "bare" nanoparticles.[I34] Electrons can, therefore, easily pass the QD/QD and QD/polymer interfaces. Furthermore, blends of MEH-PPV and the pyridine treated nanoparticles exhibited an improved morphology with percolated pathways compared to the TOPO coated QDs (see **Figure 9**). Both aspects led to an improved device performance.

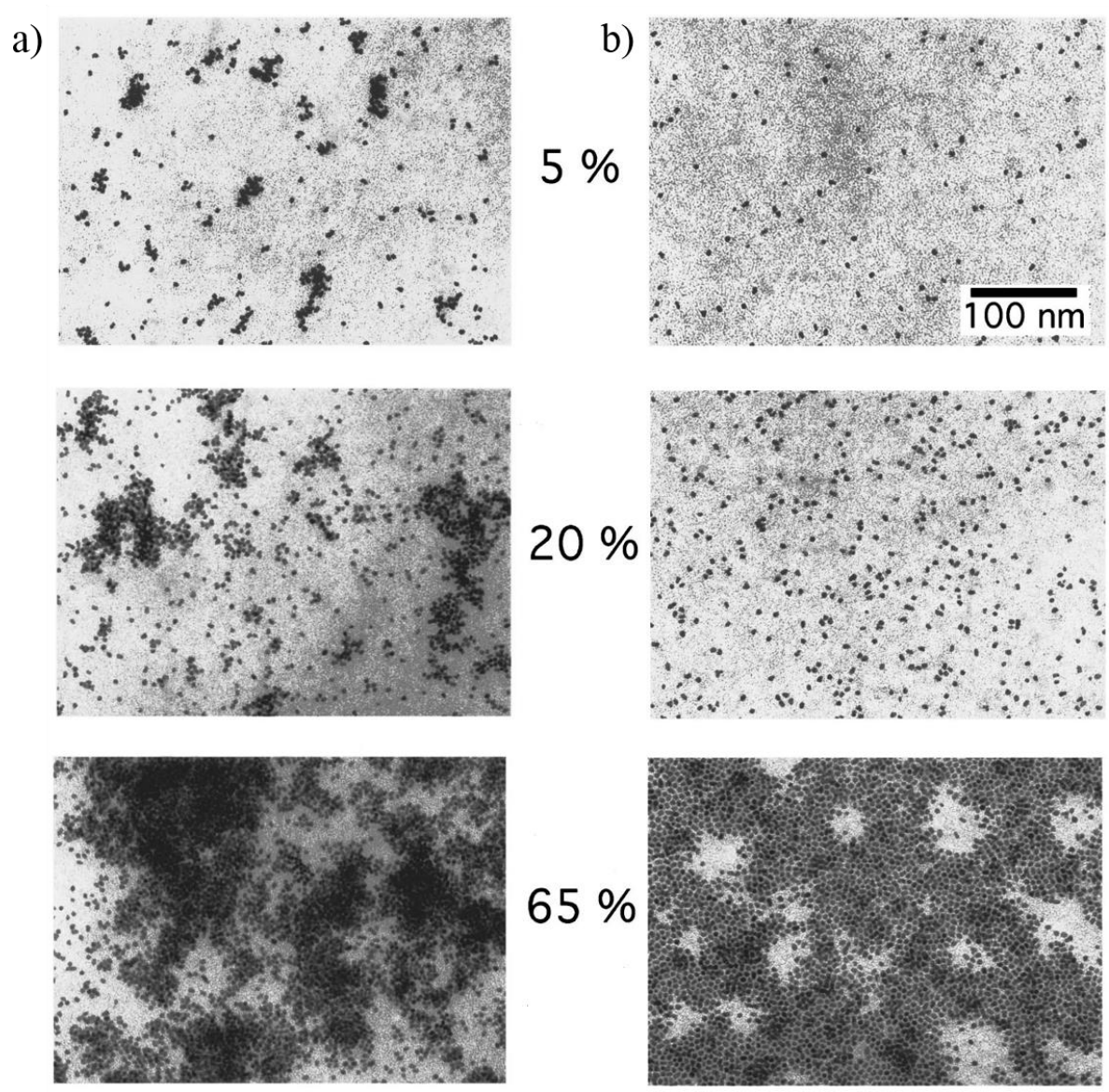

Figure 9. TEM-images of MEH-PPV/CdSe QDs blend with 5, 20 and 65 wt% QD content. a) Pyridine treated QDs and b) TOPO coated QDs. Percolated structures of the QDs can be clearly seen in the images obtained from pyridine treated QDs.[I34]

A more detailed investigation of the surfactants' role on performance was carried out by Olson *et al*. who investigated the varying degree of phase separation depending on several surfactants.[I35] Unfortunately, no consistent tendency throughout all the surfactants was found which suggests that in addition to the influence on the morphology further effects have to be taken into account.

2.3.2 Influence of the Length and Chemical Nature of the Anchor Groups

Lek *et al*. conducted a study on the role of size and chemical nature of anchor groups on the solar cell performance using several surfactants. The study revealed that the smallest ligand used (pyridine) showed the best performance while the largest surfactant (dodecylphosphonic acid) performed the worst. In case of the two surfactants 2-thiophenemethylamine and 2-thiopheneethylamine carrying the same anchor group, the shorter anchor group achieved better device performance (see **Figure 10**).[I36] Unfortunately, the functional groups were not kept the same over more than two surfactants and, hence, a confident argumentation regarding the influence of neither the chemical nature nor the length of the anchors can be made. In addition, characterizations were carried out using only casted films instead of e.g. photoluminescence quenching in a solution.

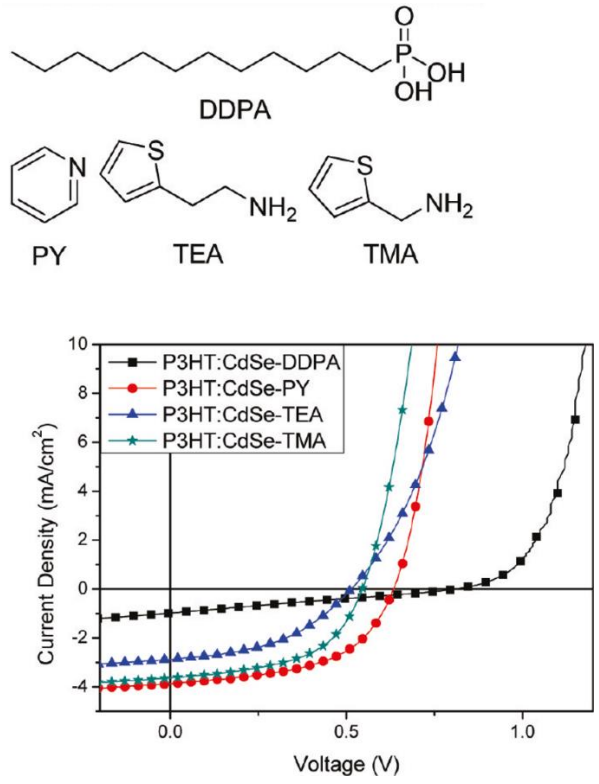

Figure 10. Structures of dodecylphosphonic acid (DDPA), pyridine (Py), 2-thiopheneethylamine (TEA), 2-thiophenemethylamine (TMA) and the corresponding current density-voltage (J-V) characteristics.[I36]

Studying small clusters of CdSe (Cd_6Se_6 and $Cd_{13}Se_{13}$), Yang *et al*. investigated the influence of various ligands on the clusters' band gap. Although the influence decreased with an increasing size of the cluster (from Cd_6Se_6 to $Cd_{13}Se_{13}$) the varying band gaps presumably create an effect of surfactants on the electronic structure of QDs.[I37] In addition, the influence of different ligands on the energy levels of InAs and CdSe QDs has been studied as well.[I38,I39] In the case of InAs nanocrystals no shift in the absorption spectrum was observed leading to the conclusion that the band gap was not influenced by the surfactants. A shift in the first reduction potential, however, suggests a shift of both the HOMO and LUMO energy levels in the same extend.[I38] Consequently, an enormous influence on the charge carrier separation at the QD/polymer interface can be presumed.

Several examples report the positive influence of ligand exchange procedures on the device performance. For example 1,2-ethanedithiol has been applied successfully in several examples to achieve highly efficient devices with power conversion efficiencies (PCEs) of up to 4.7 % under 1 sun AM1.5G conditions.[I40] However, a comparative study is yet to be carried out. This study should investigate the influence of surfactants on the optoelectronic properties of QDs in solution (to diminish the influence of the morphology) and in the film. In addition, the study should discuss the effect of the varied properties on device performance using a typical polymer such as regioregular poly(3-hexylthiophene-2,5-diyl) (rr-P3HT).

The lack of understanding becomes obvious considering that one of the best performing devices was fabricated using rarely investigated PbS_xSe_{1-x} QDs. The system composed of poly(2,6-(*N*-(1-octylnonyl)dithieno[3,2-*b*:20,30-d]pyrrole)-*alt*-4,7-(2,1,3-benzothiadiazole)) (PTDPBT) and PbS_xSe_{1-x} QDs reached a PCE of 5.5 % under 1 sun AM1.5G conditions.[I41]

However, a complete study investigating the influence of surfactants on the properties of QDs and the device performance would be very complex. Therefore, we will discuss the influence of different anchor groups incorporated into a poly(*p*-phenylene vinylene) on the optoelectronic properties and the film forming properties of CdSe nanoplatelets (see Section 4.2.1). Furthermore, we will demonstrate two different versatile synthetic approaches enabling the incorporation of various anchor groups into P3HT and MEH-PPV, respectively (see Section 4.2.2 and 4.1.2, respectively).

References

(I1) Wöhrle, D.; Hild, O. R. *Chemie in unserer Zeit* **2010**, *44*, 174–189.

(I2) Günes, S.; Neugebauer, H.; Sariciftci, N. S. *Chemical reviews* **2007**, *107*, 1324–1338.

(I3) Padinger, F.; Rittberger, R. S.; Sariciftci, N. S. *Adv. Funct. Mater.* **2003**, *13*, 85–88.

(I4) a) Tatemoto, M. *Kobunshi Ronbunshu* **1992**, *49*, 765–783; b) Wang, J.-S.; Matyjaszewski, K. *J. Am. Chem. Soc.* **1995**, *117*, 5614–5615.

(I5) Chiefari, J.; Chong, Y. K.; Ercole, F.; Krstina, J.; Jeffery, J.; Le, T. P. T.; Mayadunne, R. T. A.; Meijs, G. F.; Moad, C. L.; Moad, G.; Rizzardo, E.; Thang, S. H. *Macromolecules* **1998**, *31*, 5559–5562.

(I6) a) Roth, P. J.; Wiss, K. T.; Zentel, R.; Theato, P. *Macromolecules* **2008**, *41*, 8513–8519; b) Gondi, S. R.; Vogt, A. P.; Sumerlin, B. S. *Macromolecules* **2007**, *40*, 474–481.

(I7) Siegrist, A. E. *Helv. Chim. Acta* **1967**, *50*, 906–957.

(I8) Siegrist, A. E. *Helv. Chim. Acta* **1981**, *64*, 662–680.

(I9) Kretzschmann, H.; Meier, H. *Tetrahedron Letters* **1991**, *32*, 5059–5062.

(I10) Zur Borg, L.; Domanski, A. L.; Berger, R.; Zentel, R. *Macromol. Chem. Phys.* **2013**, *214*, 975–984.

(I11) McCullough, R. D.; Lowe, R. D.; Jayaraman, M.; Anderson, D. L. *J. Org. Chem.* **1993**, *58*, 904–912.

(I12) Loewe, R. S.; Ewbank, P. C.; Liu, J.; Zhai, L.; McCullough, R. D. *Macromolecules* **2001**, *34*, 4324–4333.

(I13) Iovu, M. C.; Sheina, E. E.; Gil, R. R.; McCullough, R. D. *Macromolecules* **2005**, *38*, 8649–8656.

(I14) Komber, H.; Senkovskyy, V.; Tkachov, R.; Johnson, K.; Kiriy, A.; Huck, W. T. S.; Sommer, M. *Macromolecules* **2011**, *44*, 9164–9172.

(I15) Jeffries-EL, M.; Sauvé, G.; McCullough, R. D. *Adv. Mater.* **2004**, *16*, 1017–1019.

(I16) a) Smeets, A.; van den Bergh, K.; Winter, J. de; Gerbaux, P.; Verbiest, T.; Koeckelberghs, G. *Macromolecules* **2009**, *42*, 7638–7641; b) Monnaie, F.; Brullot, W.; Verbiest, T.; Winter, J. de; Gerbaux, P.; Smeets, A.; Koeckelberghs, G. *Macromolecules* **2013**, *46*, 8500–8508.

(I17) Jeffries-EL, M.; Sauvé, G.; McCullough, R. D. *Macromolecules* **2005**, *38*, 10346–10352.

(I18) Romero, P. E.; Piers, W. E. *J. Am. Chem. Soc.* **2005**, *127*, 5032–5033.

(I19) a) Nelson, D. J.; Manzini, S.; Urbina-Blanco, C. A.; Nolan, S. P. *Chem. Commun. (Camb.)* **2014**, *50*, 10355–10375; b) Cavallo, L. *J. Am. Chem. Soc.* **2002**, *124*, 8965–8973.

(I20) Leitgeb, A.; Wappel, J.; Slugovc, C. *Polymer* **2010**, *51*, 2927–2946.

(I21) Rodriguez-Hernandez, J.; Checot, F.; Gnanou, Y.; Lecommandoux, S. *Progress in Polymer Science* **2005**, *30*, 691–724.

(I22) Pratten, M. K.; Lloyd, J. B.; Hörpel, G.; Ringsdorf, H. *Makromol. Chem.* **1985**, *186*, 725–733.

(I23) a) Kwon, G. S.; Kataoka, K. *Advanced Drug Delivery Reviews* **1995**, *16*, 295–309; b) Matsumura, Y.; Kataoka, K. *Cancer Science* **2009**, *100*, 572–579;

(I24) a) O'Reilly, R. K.; Hawker, C. J.; Wooley, K. L. *Chemical Society reviews* **2006**, *35*, 1068–1083; b) Cheng, R.; Meng, F.; Deng, C.; Klok, H.-A.; Zhong, Z. *Biomaterials* **2013**, *34*, 3647–3657.

(I25) a) Park, J.-H.; Maltzahn, G. von; Ruoslahti, E.; Bhatia, S. N.; Sailor, M. J. *Angew. Chem. Int. Ed.* **2008**, *47*, 7284–7288; b) Erogbogbo, F.; Yong, K.-T.; Roy, I.; Hu, R.; Law, W.-C.; Zhao, W.; Ding, H.; Wu, F.; Kumar, R.; Swihart, M. T.; Prasad, P. N. *ACS nano* **2011**, *5*, 413–423.

(I26) a) Pearson, R. G. *J. Am. Chem. Soc.* **1963**, *85*, 3533–3539; b) Pearson, R. G. *J. Chem. Educ.* **1968**, *45*, 581; c) Pearson, R. G. *J. Chem. Educ.* **1968**, *45*, 643.

(I27) Mathias, F.; Tahir, M. N.; Tremel, W.; Zentel, R. *Macromol. Chem. Phys.* **2014**, *215*, 604–613.

(I28) Rajh, T.; Chen, L. X.; Lukas, K.; Liu, T.; Thurnauer, M. C.; Tiede, D. M. *J. Phys. Chem. B* **2002**, *106*, 10543–10552.

(I29) Zorn, M.; Meuer, S.; Tahir, M. N.; Khalavka, Y.; Sönnichsen, C.; Tremel, W.; Zentel, R. *J. Mater. Chem.* **2008**, *18*, 3050.

(I30) Zorn, M.; Bae, W. K.; Kwak, J.; Lee, H.; Lee, C.; Zentel, R.; Char, K. *ACS nano* **2009**, *3*, 1063–1068.

(I31) Oschmann, B.; Bresser, D.; Tahir, M. N.; Fischer, K.; Tremel, W.; Passerini, S.; Zentel, R. *Macromol. Rapid Commun.* **2013**, *34*, 1693–1700.

(I32) Meuer, S.; Oberle, P.; Theato, P.; Tremel, W.; Zentel, R. *Adv. Mater.* **2007**, *19*, 2073–2078.

(I33) Zur Borg, L.; Lee, D.; Lim, J.; Bae, W. K.; Park, M.; Lee, S.; Lee, C.; Char, K.; Zentel, R. *J. Mater. Chem. C* **2013**, *1*, 1722.

(I34) Greenham, N. C.; Peng, X.; Alivisatos, A. P. *Phys. Rev. B* **1996**, *54*, 17628–17637.

(I35) Olson, J. D.; Gray, G. P.; Carter, S. A. *Solar Energy Materials and Solar Cells* **2009**, *93*, 519–523.

(I36) Lek, J. Y.; Xi, L.; Kardynal, B. E.; Wong, L. H.; Lam, Y. M. *ACS applied materials & interfaces* **2011**, *3*, 287–292.

(I37) Yang, P.; Tretiak, S.; Ivanov, S. *J Clust Sci* **2011**, *22*, 405–431.

(I38) Soreni-Harari, M.; Yaacobi-Gross, N.; Steiner, D.; Aharoni, A.; Banin, U.; Millo, O.; Tessler, N. *Nano letters* **2008**, *8*, 678–684.

(I39) Munro, A. M.; Zacher, B.; Graham, A.; Armstrong, N. R. *ACS applied materials & interfaces* **2010**, *2*, 863–869.

(I40) Zhou, R.; Stalder, R.; Xie, D.; Cao, W.; Zheng, Y.; Yang, Y.; Plaisant, M.; Holloway, P. H.; Schanze, K. S.; Reynolds, J. R.; Xue, J. *ACS nano* **2013**, *7*, 4846–4854.

(I41) Liu, Z.; Sun, Y.; Yuan, J.; Wei, H.; Huang, X.; Han, L.; Wang, W.; Wang, H.; Ma, W. *Adv. Mater.* **2013**, *25*, 5772–5778.

3. Objectives

Renewable energy sources such as solar power have increasingly attracted attention during the past decades due to the limited deposits of fossil energy sources such as ore and oil. Organic and hybrid optoelectronic devices have attracted great interest caused by advantages such as the potential fabrication of thin film devices. In addition, their solution processability enables production via low-cost printing and patterning techniques on arbitrary substrates in a large scale. Unfortunately, organic and hybrid optoelectronic devices are still not reaching the efficiencies of inorganic devices. From an economic point of view, the minor efficiencies of organic and hybrid devices compared to all inorganic devices cannot yet be compensated by their lower production costs. Therefore, research addressing improved efficiencies of organic and hybrid optoelectronic devices is essential to compete with inorganic devices.

The most crucial aspects in terms of device performances are the active material, the morphology of the individual films assembling the device and, regarding hybrid optoelectronics, the interface between the organic and inorganic materials. Thus, research on the before mentioned aspects is of tremendous importance to achieve optoelectronic devices with improved properties.

On the one hand, the aim of this dissertation is to develop new synthetic strategies controlling the morphology of conducting materials. On the other hand, this thesis focuses on approaches equipping conducting polymers with various anchor groups. That is because the modification of a single polymer precursor with different anchor groups permits investigations of the anchor groups' influence on the organic-inorganic interface without the interference of any other factors.

In the first part of this dissertation, the focus will be set on the development of new synthetic approaches which allow controlling the morphology of conducting materials. In the second part, approaches to incorporate various anchor groups into a conducting polymer will be presented.

In order to achieve control over the morphology of conducting materials, two approaches will be developed in the context of this dissertation. In the first project, a side chain conjugated polymer will be synthesized via RAFT polymerization. This polymer is supposed to carry a cleavable anchor group at the polymer chain end which in turn facilitates the functionalization of inorganic nanoparticles via ligand exchange procedure. Finally, upon exposure to an

external stimulus (i.e., UV light) the polymer will be detached from the nanoparticles inducing the aggregation of the nanoparticles (see **Figure 111**). The realization of this project will be described in section 4.1.1.

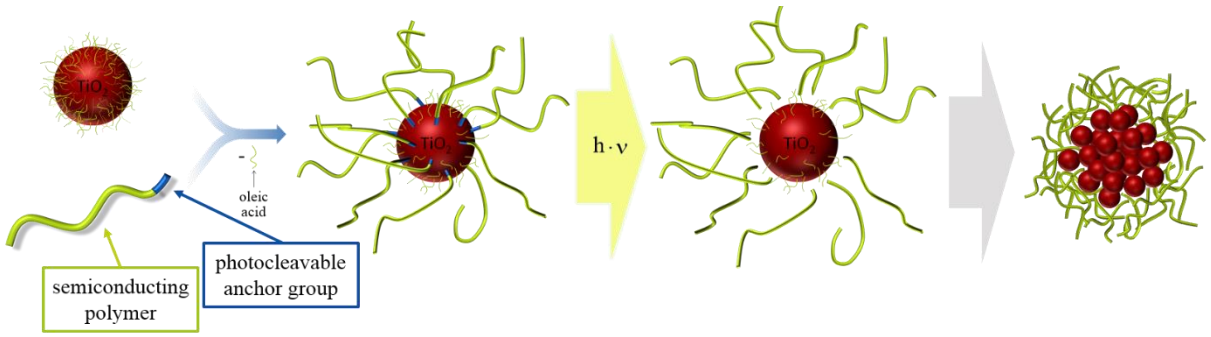

Figure 111. Schematic presentation illustrating the formation of aggregates induced upon detachment of the semiconducting polymer from the inorganic nanoparticles upon UV irradiation.

The second project presented in the dissertation at hand aims at synthesizing a backbone conjugated polymer with subsequent self-assembly into micelles. Therefore, amphiphilic block copolymers composed of a conjugated and a non-conjugated functional block will be synthesized. As these block copolymers usually cannot be synthesized applying a single polymerization technique, they are typically synthesized following complicated procedures involving multiple end group reactions. Multiple end group reactions, however, are prone to causing polymeric impurities which do not possess the desired properties and are difficult to remove. Therefore, block copolymers composed of a conjugated and a non-conjugated block will be synthesized here in a facile one-pot procedure. MEH-PPV which is, due to its favorable optoelectronic properties, one of the most studied conjugated polymers will be installed as the conjugated block. To enable the desired synthesis of block copolymers combining a conjugated and a non-conjugated block in a one-pot procedure, ROMP will be applied as this technique is capable of synthesizing both conjugated and non-conjugated polymers. Exploiting the living nature of ROMP, amphiphilic block copolymers carrying one conjugated and one non-conjugated block are expected to be accessible in a one-pot procedure and will enable the self-assembly into micelles exhibiting the conjugated block as the core of the micelles (see **Figure 112**).

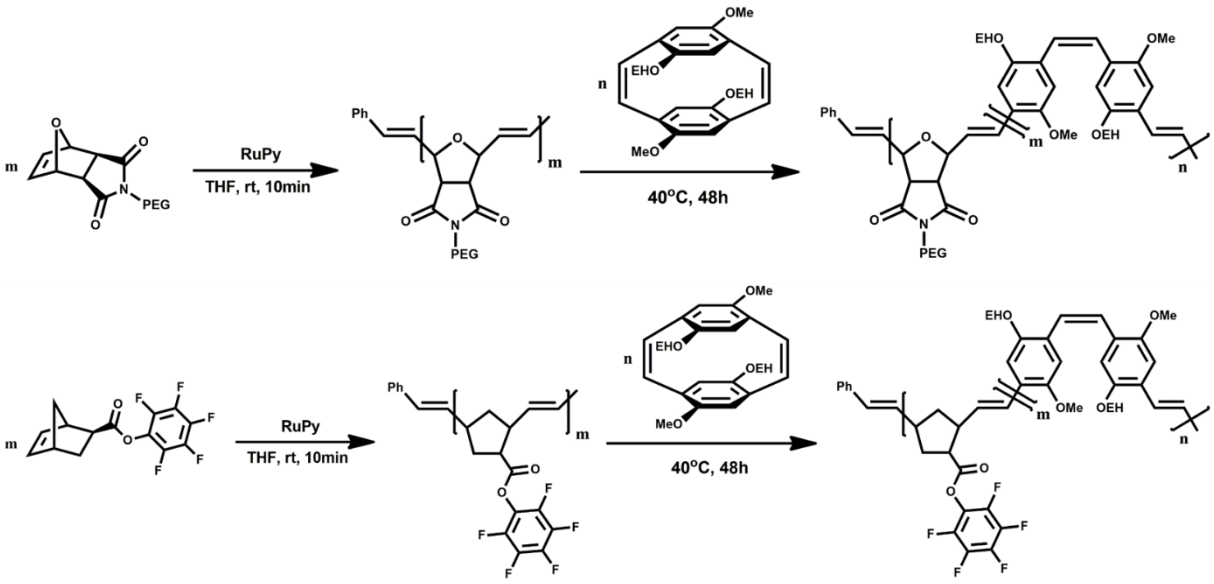

Figure 112. Reaction scheme illustrating the synthesis of block copolymers composed of a conjugated and a non-conjugated block via ROMP.

Connecting the first with the second topic of this dissertation, the synthesis of block copolymers via ROMP will further be exploited for the incorporation of a reactive ester block (see **Figure 112**). The reactive ester will permit reaction with various amines. Thereby, the block copolymers will be equipped with different anchor groups facilitating the functionalization of CdSe@ZnS QDs via ligand exchange and demonstrating potential applications in optoelectronics. This project will be discussed in section 4.1.2.

In a further project, the influence of different anchor groups on the organic inorganic interface in nanocomposites will be investigated. Therefore, a synthetic approach which would enable the incorporation of various anchor groups starting from a single precursor polymer is required. This approach will be accomplished by a combination of Siegrist polycondensation and RAFT polymerization. Via Siegrist polycondensation, poly(*p*-(2,5-di(2'-ethylhexyloxy)phenylene vinylene) (DEH-PPV) exhibiting a defined aldehyde end group will be synthesized. The aldehyde end group will, subsequently, be exploited for the incorporating of a trithiocarbonate converting the polymer into a macro-CTA. In a following RAFT polymerization a reactive ester block will be added enabling the incorporation of various amines (see **Figure 113**). The realization of this project along with a study concerning the influence of the anchor group on the organic inorganic interface will be described in section 4.2.1.

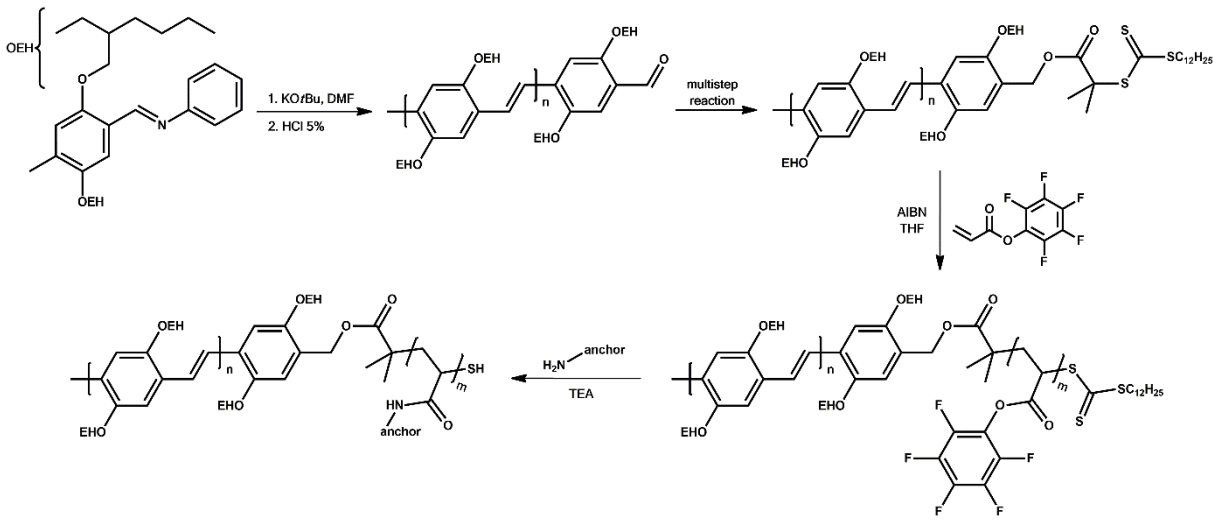

Figure 113. General reaction scheme illustrating the synthesis of block copolymers by a combination of Siegrist polycondensation and RAFT polymerization. The block copolymers exhibiting a conjugated and an anchor block are synthesized via a single reactive ester precursor.

Finally, a synthetic approach allowing to equip poly(3-alkylthiophene)s (P3ATs), a very frequently used class of conjugated polymers, with various end groups will be developed. Similar to the previous approach, the anchor groups are supposed to be incorporated starting from a single precursor polymer. Therefore, two approaches will be investigated.

In the first approach, an ethynyl-terminated P3AT will be synthesized as polymer precursor. Consequently, various azides carrying anchor groups will be incorporated via copper catalyzed azide-alkyne Huisgen cycloaddition as illustrated in **Figure 114**.

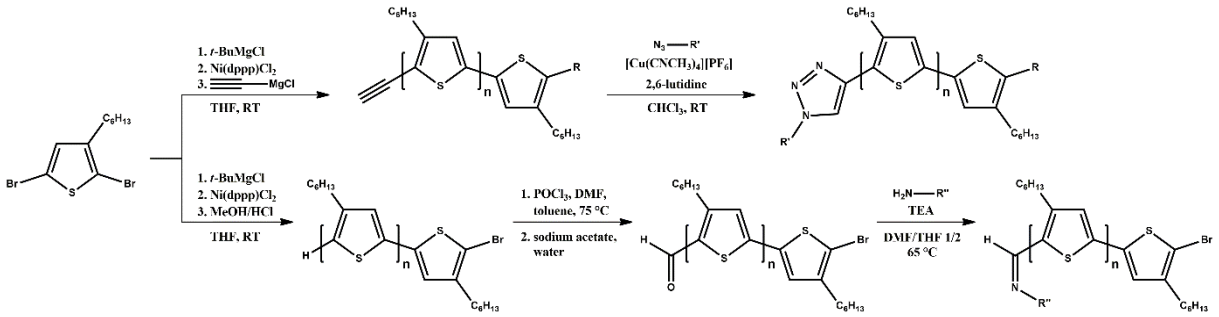

Figure 114. Reaction scheme elucidating the incorporation of anchor groups via copper catalyzed azide-alkyne Huisgen cycloaddition (top) and via aldehyde end functionalized P3HT (bottom).

In the second approach, α-bromo-ω-formyl P3HT will be synthesized via Vilsmeier reaction of α-bromo P3HT. A reaction of the obtained polymer with amines will enable the incorporation of different amines via formation of an imine as displayed in **Figure 114**. Both approaches will enable the incorporation of various anchor groups starting from a single polymer precursor. Therefore, the polymers will differ solely in the anchoring end group but exhibit the same conjugated backbone. An identical conjugated backbone is mandatory when aiming at studying the influence of different anchor groups as alterations of the conjugated backbone would interfere with the effects originating from the varying anchor groups. This project will be discussed in section 4.2.2.

4. Results and Discussion

In this chapter the realization of the projects outlined in the objectives will be presented and discussed. The chapter is composed of publications written by the author in the context of this dissertation. Prior to each publication, the topic and aim of the publication will briefly be described to introduce the reader to the subject.
The chapter will be divided into two main topics – 4.1 Morphology Control of Conducting Materials and 4.2 Approaches for the Incorporation of Anchor Groups into Conjugated Polymers – which will be discussed throughout the integrated publications in detail.

4.1 Morphology Control of Conducting Materials

Organic and hybrid optoelectronic devices have been the topic of intense research due to aspects such as the potential solution processability which permits the fabrication of devices via low-cost printing and patterning techniques at a large scale. Regarding solar cells, the high absorption coefficients of organic compounds allow for efficient absorption in thin films which reduces the amount of expensive active material needed per device. Although solution processability and thin film devices provide huge beneficial factors from an economic point of view, they cannot yet compensate the low efficiencies of organic and hybrid optoelectronic devices compared to inorganic devices.
Controlling the morphology of conducting materials is an important aspect regarding the fabrication of improved optoelectronic devices. The efficiency of optoelectronic devices strongly depends on the morphology of the films assembling the device. Therefore, the development of new approaches to enable control over the morphology of conducting materials is crucial with respect to an improved device performance.

In the following subsections, two new synthetic approaches will be presented enabling a control over the morphology. In the first approach, organic/inorganic nanocomposites which can be applied to hybrid optoelectronic devices were assembled in a controlled manner into spherical aggregates. In the second approach, amphiphilic block copolymers composed of a

conjugated and a non-conjugated block were synthesized in a facile one-pot procedure. The obtained polymers were assembled into micelles to demonstrate a potential processability from water.

4.1.1 Controlled Assembly of Organic/Inorganic Nanocomposites

In the following publication, a procedure to achieve a controlled assembly of organic/inorganic nanocomposites was developed. Therefore, a triphenyl amine derivative was polymerized via RAFT polymerization to yield a side chain conjugated polymer. The polymerization was conducted using a trithiocarbonate CTA equipped with a reactive ester. Thus, the reactive ester was incorporated at the polymer chain end which enabled further modification of the polymer end group. In order to exploit the unique properties of the reactive ester which are selective reaction with amines while being tolerant of alcohols, a catechol anchor group was installed at the polymer chain end. Moreover, the incorporated amine possessed a photocleavable group which permitted to separate the anchoring end group and the polymer upon UV irradiation. Consequently, the catechol anchor group was exploited to facilitate functionalization of TiO_2 nanorods via ligand exchange. While the resulting dispersions were composed of individually distributed nanorods, large spherical particles were obtained after applying UV irradiation to split-off the polymer chains as verified via TEM. Following this approach, large spherical aggregates were fabricated from previously stable dispersions of semiconducting polymer/inorganic nanocrystal composites upon an external stimulus (i.e., UV light).

In the context of this publication, Muhammad Nawaz Tahir provided the inorganic TiO_2 nanorods and recorded the TEM images. The synthesis of the semiconducting polymer which possessed a photocleavable end group as well as the functionalization of the inorganic nanorods via ligand exchange procedure and all characterizations with the exception of TEM were conducted by the author of this dissertation.

4.1.1.1 Publication in Macromolecular Chemistry and Physics, 2014, 215, 604–613

Functionalization of TiO_2-Nanoparticles with Semiconducting Polymers Containing a Photocleavable Anchor Group and Separation via Irradiation Afterwards

Florian Mathias, Muhammad Nawaz Tahir, Wolfgang Tremel, Rudolf Zentel*

Abstract

This paper describes the controlled radical polymerization (RAFT polymerization) of semiconducting polymers based on poly(4,4'-dimethyl-triphenyl-amine). These polymers are afterwards end-functionalized with a photocleavable group and an anchor unit (catechol) for oxidic nanoparticles. Serving as a reference, polystyrene oligomers with the same end groups are synthesized, too. Using these polymers allows functionalizing TiO_2 nanoparticles, leading to an improved solubility and miscibility in organic solvents or polymer matrices. Irradiation in the UV region is used to split the photocleavable group and remove the polymer chains from the nanoparticles, which leads to an aggregation of the nanoparticles.

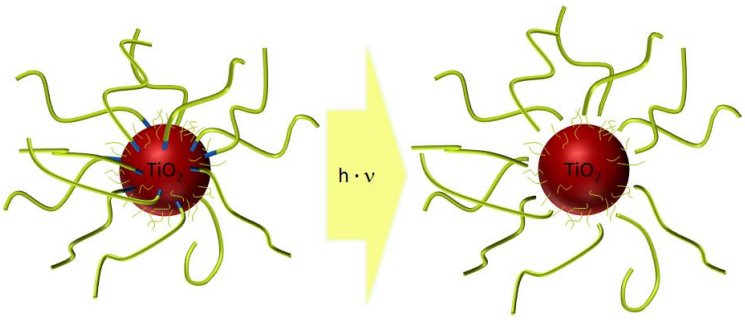

1. Introduction

Evolving out of research regarding the unique properties of hybrid materials, the interest in dispersing inorganic nanoparticles (NPs) in polymer matrices has been rising. This also includes quantum dots (QDs). The primarily unmodified nanoparticles demix, however, completely due to a strong incompatibility with the polymer coils. A successful approach to

overcome this incompatibility is the grafting of polymer chains to the nanoparticle or – in other words – the creation of polymer brushes on the nanoparticle surface.[1, 2] This can be achieved by either using a grafting-from[3, 4] or a grafting-to approach.[5, 6]

Recently we have developed a grafting-to approach based on block copolymers with a short anchor-block,[7, 8] which can be prepared by RAFT polymerization. The synthesis of these block copolymers via the intermediate step of a reactive ester polymer allows to introduce different anchor groups into the polymer.[9, 10, 8] This enables the functionalization of many types of NPs like metal oxides or sulfides with almost the same polymer.[8, 11, 12] Detailed investigations show that the NPs, functionalized using this method, can be individually dispersed (dissolved) in suitable solvents and polymers.[7, 13] By coating CdSe quantum dots with a suitable hole conducting polymer, which acts as a solubilizing block, it is possible to disperse QDs homogeneously in for example an excess hole conducting polymer matrix.[5, 14] This allows the preparation of QD-LEDs.[12, 15]

While several applications rely just on dispersion, others require a finely dispersed system, in which the inorganic NPs are percolated simultaneously; which is fulfilled by a bicontinuous structure of organic and inorganic materials. The reasons therefor are especially obvious for photovoltaic applications of hybrid systems. In that matter donor and acceptor material – usually the organic part is the donor and the inorganic material the acceptor – should be well dispersed to allow an effective exciton splitting.[16, 17] At the same time, however, a bicontinuous structure with "highways" for both negative and positive charges is required to allow an effective charge transport to the electrodes and thereby minimizes the chance of efficiency limiting processes like charge recombination.[18–20] Thus, it is essential to control dispersibility! In this context photochemically cleavable polymer brush systems are attractive.[21, 22] The control of film morphology and the solubility of a film triggered by photocleavable groups are a current field of research and very interesting for the application in optoelectronic devices.[23, 24] Here we use the potential of polymers containing a photocleavable anchor to make inorganic nanoparticles – at first – well dispersible in a polymer matrix and to induce separation (leading to percolation) at a later stage. This is a new approach to control the morphology of hybrid films.

Here we describe the chemical realization of such a system, which consists of a triarylamine based hole transporting polymer, an anchor group for oxidic semiconducting nanoparticles and a photocleavable group. Finely dispersed NPs can be obtained by functionalization with the polymer on the first hand and effective splitting of organic and inorganic materials by irradiation can be demonstrated afterwards.

2. Experimental Section

2.1. Materials

All commercial chemicals were purchased form Sigma-Aldrich, Acros Organics, Alfa Aesar or Fluka and used without further purification unless noted otherwise. The radical initiator 2,2'-azobisisobutyronitrile (AIBN, from Fluka) was recrystallized from ethanol prior to polymerization and was stored at -20 °C. Anhydrous THF was freshly distilled from sodium under a nitrogen atmosphere. *S*-1-Dodecyl-*S*'-(α,α'-dimethyl-α''-acetic acid)trithiocarbonate[25], pentafluorophenyl trifluoroacetate[26] and *S*-1-Dodecyl-*S*'-(α,α'-dimethyl-α''-pentafluorophenyl acetate)trithiocarbonate (PFP-CTA, **6**)[27] were synthesized according to the literature. Besides the first step (see below) 4,4'-dimethyl-4''-vinyl-triphenylamine (Vinyl-TPA, **5**) was synthesized according to the literature.[28] All solvents used for column chromatography were purified by distillation and THF for polymerization was dried over sodium and distilled before use.

2.2. Characterization

All NMR spectra were measured in $CDCl_3$ or DMSO-d_6 (both purchased from Deutero GmbH) at room temperature. ^{1}H-NMR spectra were acquired on a Bruker AC 300 at a Lamor frequency of 300 MHz or on a Bruker ARX 400 at a Lamor frequency of 400 MHz. ^{13}C-NMR spectra were also acquired on a Bruker AC 300 at a Lamor frequency of 75 MHz and ^{19}F-NMR spectra were recorded using a Bruker DRX 400 at a Lamor frequency of 400 MHz. FTIR spectra were measured on a Vector 22 ATR-FTIR-spectrometer made by Bruker. Molecular weights of all synthesized polymers were determined by gel permeation chromatography (GPC) in 1.2 mg · mL^{-1} THF with polystyrene as external and toluene as internal standard. Transmission electron microscopy (TEM) was obtained using a Philips EM420 instrument with an acceleration voltage of 120 kV. TEM samples were prepared by

dropping a dilute solution of the as-synthesized nanorods in chloroform on a carbon coated copper grid. Irradiation was carried out in a 40-80 mg · mL^{-1} dichloromethane solution in a quartz cuvette using an irradiation unit of LOT-Oriel GmbH & Co. KG containing a 500 W Hg arc lamp LSB 640 and a quartz condenser. UV/Vis spectra (see Supporting Information) were collected using a Jasco V-630 spectrophotometer (1 cm · 1 cm quartz cuvette).

2.3. Monomer Synthesis

2.3.1. 4,4'-dimethyltriphenylamine

4,4'-dimethyltriphenylamine was synthesized according a modified literature procedure.[28] In a Ullmann-type reaction 4-iodotoluene (25.0 g, 115 mmol), potassium carbonate (31.8 g, 230 mmol), which was dried at 120 °C for 4 h prior to use, copper(I) iodide (0.9 g, 5 mmol) and copper-zinc alloy containing 50 wt% copper (14.6 g, n(Cu) = 115 mmol) were suspended in dry 1,2-dichlorobenzene (300 mL) under argon. Freshly distilled aniline (4.3 g, 46 mmol) was added and the reaction was heated to reflux (179 °C) for 6 days. The hot reaction mixture was filtered and the solvent was removed under reduced pressure. Purification by column chromatography on silica using cyclohexane as eluent (R_f = 0.29) gave the product as a colorless solid (9.2 g, 34 mmol, 74 % yield).

^{1}H-NMR (300 MHz, $CDCl_3$, δ): 7.24-7.18 (m, 2H; *m*-Ar H), 7.09-6.92 (m, 11H; Ar H), 2.32 (s, 6H; CH_3)

^{13}C-NMR (75 MHz, $CDCl_3$, δ): 148.39 (N-**C** arom.), 145.58 (N-**C** Ar-Me), 132.41 (Me-**C** arom.), 129.95 (Me-**Ar**), 129.14 (**Ar**), 124.58 (Me-**Ar**), 123.07 (**Ar**), 121.82 (**Ar**), 20.94 (**C**H_3)

IR: ν = 3024 (w, =C-H), 2917 (w, -CH_3), 1593 (s), 1505 (s), 1486 (vs), 1318 (s), 1276 (vs), 814 (vs), 750 (vs), 697 cm^{-1} (vs)

2.3.2. 4,4'-dimethyl-4''-vinyl-triphenylamine (Vinyl-TPA, **5**)

4,4'-dimethyl-4''-vinyl-triphenylamine was synthesized as described in the literature[28] and isolated as a colorless solid (6.48 g, 21.6 mmol, 87 % yield).

^{1}H-NMR (300 MHz, $CDCl_3$, δ): 7.25 (d, $^3J_{HH}$ = 8.5 Hz, 2H; CH_2=CH-Ar H), 7.08 (d, $^3J_{HH}$ = 8.1 Hz, 4H; Me-Ar H), 7.02-6.88 (m, 6H; Ar H), 6.65 (dd, $^3J_{HH}$ = 17.6; 10.9 Hz, 1H; CHH=C**H**), 5.61 (dd, $^3J_{HH}$ = 17.6; 1.0 Hz, 1H; ArCH=C**H**H), 5.11 (dd, $^3J_{HH}$ = 10.9; 1.0 Hz, 1 H; ArCH=CH**H**), 2.30 (s, 6H; CH_3)

^{13}C-NMR (75 MHz, $CDCl_3$, δ): 148.04 (N-**C** arom.), 145.30 (N-**C** Ar-Me), 136.44 (Ar-**C**H), 132.71 (Me-**C** arom.), 131.09 (C_2H_3-**C** arom.), 130.01 (Me-**Ar**), 127.05 (C_2H_3-**Ar**), 124.78 (Me-**Ar**), 122.52 (C_2H_3-**Ar**), 111.73 (CH=**C**H_2), 20.97 (**C**H_3)
IR: ν = 3026 (w, =C-H), 2920 (w, -CH_3), 1600 (s), 1502 (vs), 1320 (s), 1272 (s), 814 cm^{-1} (s)

2.4. Synthesis of the Chain Transfer Agent

2.4.1. *S*-1-Dodecyl-*S*'-(α,α'-dimethyl-α''-pentafluorophenyl acetate)trithiocarbonate (PFP-CTA, **6**)

S-1-Dodecyl-*S*'-(α,α'-dimethyl-α''-pentafluorophenyl acetate)trithiocarbonate (PFP-CTA, **6**) was synthesized from *S*-1-Dodecyl-*S*''-(α,α'-dimethyl-α''-acetic acid)trithiocarbonate according to the literature.[27]
^{1}H-NMR (300 MHz, $CDCl_3$, δ): 3.31 (t, $^3J_{HH}$ = 7.5 Hz, 2H; *S-CH$_2$*), 1.86 (s, 6H; O=C-(CH_3)$_2$), 1.69 (p, $^3J_{HH}$ = 7.5 Hz, 2H; S-CH_2-CH_2), 1.42-1.18 (m, 18H), 0.88 (t, $^3J_{HH}$ = 6.5 Hz, 3H; CH_2-CH_3)
^{19}F-NMR (400 MHz, $CDCl_3$, δ): -152.69 (d, $^3J_{FF}$ = 17.7 Hz, 2F; *o*-Ar F), -158.92 (t, $^3J_{FF}$ = 21.7 Hz, 1F; *p*-Ar F), -163.51 (dd, $^3J_{FF}$ = 21.7; 17.7 Hz, 2F; *m*-Ar F)
^{13}C-NMR (75 MHz, $CDCl_3$, δ): 220.02 (S=**C**), 169.70 (O= **C**), 141.35 (md, $^1J_{CF}$ = 254 Hz, *o*-**C** PhF_5), 139.67 (td, $^1J_{CF}$ = 254 Hz, $^2J_{CF}$ = 13.0 Hz; *p*-**C** PhF_5), 137.96 (td, $^1J_{CF}$ = 255 Hz, $^2J_{CF}$ = 13.7 Hz; *m*-**C** PhF_5), 125.45 (t, $^2J_{CF}$ = 13.7 Hz; *i*-**C** PhF_5), 55.52 (S-**C**(Me)$_2$), 37.29 (S-**C**H_2), 32.06 (S-CH_2-**C**H_2), 29.77 (2 x **C**H_2), 29.70 (**C**H_2), 29.57 (**C**H_2), 29.49 (**C**H_2), 29.24 (**C**H_2), 29.05 (**C**H_2), 27.97 (**C**H_2), 25.54 (SC-**C**H_3), 22.84 (CH_3-**C**H_2), 14.24 (CH_2-**C**H_3)
IR: ν = 2924 (s, -CH_3), 2853 (m, -C-H), 1778 (s, C=O), 1466 (vs, PhF_5), 1080 (vs), 992 (vs), 815 cm^{-1} (s)

2.5. General Polymerization Procedure

In an exemplary polymerization reaction Vinyl-TPA **5** (1.500 g, 5.000 mmol), the PFP-CTA **6** (17.72 mg, 0.0334 mmol) and AIBN (0.55 mg, 0.0033 mmol) were dissolved in dry THF (5 mL) using a Schlenk-tube as reaction vessel. In three freeze-pump-thaw cycles all oxygen was exchanged by nitrogen before the polymerization was then carried out at 67 °C for 48 h. To purify the polymer it was repeatedly precipitated in methanol and *n*-hexane. The purified polymer **7** was isolated as a pale yellow solid (0.528 g, 35 % yield, M_n = 15.0 kg · mol^{-1}, PDI = 1.08).

Exemplary ^{1}H-NMR (400 MHz, $CDCl_3$, δ): 7.02-6.68 (br, 10H; Ar H repeating unit), 6.68-6.33 (br, 2H; CH-Ar H repeating unit), 3.33 (t, $^{3}J_{HH}$ = 7.42 Hz, 2H; $C_{11}H_{23}$-CH_2-S), 2.42-0.97 (br, 9H; CH_3 + CH_2 + CH repeating unit), 0.91 (t, $^{3}J_{HH}$ = 6.50 Hz, 3H; H_3C-$C_{11}H_{22}$-S)

2.6. Synthesis of Photocleavable Anchor Group

2.6.1. 3-(*tert*-butoxycarbonylamino)-3-(2-nitrophenyl)propionic acid (Boc-ANP, **1**)

In analogy to the *meta*-nitro-compound 3-amino-3-(2-nitrophenyl)propionic acid (ANP, 2.50 g, 11.9 mmol) was suspended in 1,4-dioxane (80 mL) and cooled to 0 °C.[29] Di-*tert*-butyl dicarbonate (3.89 g, 17.8 mmol) and 40 mL of 1 N NaOH-solution were added slowly at 0 °C and the reaction mixture was stirred for 30 minutes to perform a pale brown suspension. The reaction mixture was allowed to warm to room temperature and stirred for 22 h (TLC: $CHCl_3$/MeOH/AcOH 45/4/1, R_f = 0.72). Then dioxane was removed from the solution under reduced pressure to give a brown aqueous solution which was mixed with 150 mL dichloromethane. After that the mixture was washed with 160 mL of 0,5 N HCl-solution (pH < 3). The aqueous layer was extracted one more time with 150 mL dichloromethane. The united organic layers were then washed with saturated NaCl-solution (200 mL), dried over Mg_2SO_4 and the solvent was removed under reduced pressure to yield the product, a pale brown solid (0.58 g, 1.88 mmol, 16 % yield). The united aqueous layers were set to a pH of about 7.5 to precipitate the product. After filtration through a frit and drying in vacuum at 40 °C the product was isolated (1.72 g, 5.53 mmol, 48 % yield) to give an overall yield of 64 %.
^{1}H-NMR (300 MHz, DMSO-d_6, δ): 12.40 (bs, 1H; *O***H**), 7.90 (dd, $^{3}J_{HH}$ = 8.1, $^{4}J_{HH}$ = 1.1 Hz, 1H; Ar H), 7.77-7.67 (m, 3H; Ar H + NH), 7.50 (dt, $^{3}J_{HH}$ = 7.5, $^{4}J_{HH}$ = 1.1 Hz, 1H; Ar H), 5.38-5.13 (m, 1H; NH-CH), 2.72-2.57 (m, 2H; O=C-CH_2), 1.30 + 1.10 (2 · s, 9H; CH_3)
^{13}C-NMR (75 MHz, DMSO-d_6, δ): 171.27 (O=**C**-CH_2), 154.74 (O=**C**-O-), 147.91 (NO_2-**C** arom.), 138.36 (HC-**C** arom.), 133.67 (NO_2-**Ar**), 128.24 (2 x NO_2-**Ar**), 123.96 (NO_2-**Ar**), 78.20 ((CH_3)$_3$**C**), 46.96 (HN-**C**H), 40.07 (O=C-**C**H_2), 28.21 (**C**H_3)
IR: *v* = 3374 (m, N-H), 2992 (w, =C-H), 2937 (w, -C-H), 1702 (vs, C=O), 1674 (vs, C=O), 1515 (vs, NO_2), 1346 (s), 1149 cm^{-1} (s)

2.6.2. Pentafluorophenyl 3-(*tert*-butoxycarbonylamino)-3-(2-nitrophenyl)propionate (PFP-Boc-ANP, **2**)

In a round bottom flask 3-(*tert*-butoxy-carbonylamino)-3-(2-nitrophenyl)propionic acid **1** (1.62 g, 5.22 mmol) and triethylamine (1.02 g, 10.1 mmol) were dissolved in dry DMF (70 mL). Pentafluorophenyl trifluoroacetate (2.8 g, 10.0 mmol) was added slowly through a syringe before the reaction mixture was stirred at room temperature for 3 h. It was diluted with 70 mL dichloromethane and then washed three times with 75 mL of water. The aqueous layer was extracted with 75 mL dichloromethane once and the united organic layers were dried over Mg_2SO_4. The solvent was removed under reduced pressure followed by purification using column chromatography on silica using a mixture of cyclohexane and ethyl acetate (2:1) as an eluent, (R_f = 0.52) obtaining the product as a pale brown nearly colorless solid (2.23 g, 4.68 mmol, 90 % yield).

^{1}H-NMR (300 MHz, DMSO-d_6, δ): 8.06 (d, $^3J_{HH}$ = 8.4 Hz, 1H; Ar H), 8.00 (d, $^3J_{HH}$ = 7.9 Hz, 1H; Ar H), 7.84-7.77 (m, 2H; Ar H + NH), 7.57 (ddd, $^3J_{HH}$ = 8.5; 6.4, $^4J_{HH}$ = 2.3 Hz, 1H; Ar H), 5.67-5.33 (m, 1H; NH-CH), 3.29-3.11 (m, 2H; O=C-CH_2), 1.32 + 1.12 (2 · s, 9H; CH_3)

^{19}F-NMR (400 MHz, DMSO-d_6, δ): -153.67 (d, $^3J_{FF}$ = 19.5 Hz, 2F; *o*-Ar F), -158.14 (t, $^3J_{FF}$ = 23.2 Hz, 1F; *p*-Ar F), -162.96 (dd, $^3J_{FF}$ = 23.2; 19.5 Hz, 2F; *m*-Ar F)

^{13}C-NMR (75 MHz, DMSO-d_6, δ): 166.45 (O=**C**-CH_2), 154.65 (O=**C**-O-), 147.68 (NO_2-**C** arom.), 140.50 (md, $^1J_{CF}$ = 249 Hz, *o*-**C** PhF_5), 139.08 (td, $^1J_{CF}$ = 255 Hz, $^2J_{CF}$ = 13.0 Hz; *p*-**C** PhF_5), 137.53 (td, $^1J_{CF}$ = 250 Hz, $^2J_{CF}$ = 13.6 Hz; *m*-**C** PhF_5), 137.31 (HC-**C** arom.), 134.13 (NO_2-**Ar**), 128.88 (NO_2-**Ar**), 128.25 (NO_2-**Ar**), 124.33 (NO_2-**Ar**), 124.03 (t, $^2J_{CF}$ = 13.7 Hz; *i*-**C** PhF_5), 78.57 ($(CH_3)_3$**C**), 46.89 (HN-**C**H), ≈ 40 (O=C-**C**H_2 covered by DMSO-d_6), 28.02 (**C**H_3)

IR: ν = 3372 (m, N-H), 3006 (w, =C-H), 2942 (w, -C-H), 1791 (s, C=O), 1677 (s, C=O), 1518 (vs, NO_2), 1351 (s), 1094 (s), 993 cm^{-1} (vs)

2.6.3. 3,4-dihydroxyphenethyl 3-(*tert*-butoxycarbonylamino)-3-(2-nitrophenyl)propionamide (dopamine-Boc-ANP, **3**)

Dopamine hydrochloride (1.75 g, 9.24 mmol), triethylamine (0.94 g, 9.24 mmol) and PFP-Boc-ANP **2** (2.20 g, 4.62 mmol) were dissolved in DMF (40 mL). The reaction mixture was stirred at room temperature for 6 h and after control by TLC (ethyl acetate, R_f = 0.51) filtered to remove a precipitated solid. The DMF solution was then added dropwise to water to precipitate the product. After filtration through a frit and drying under vacuum at 30 °C, the product was isolated as a pale brown solid (1.98 g, 4.44 mmol, 96 % yield).

^{1}H-NMR (300 MHz, DMSO-d_6, δ): 8.84 (bs, 2H; Ar-OH), 7.88 (dd, $^{3}J_{HH}$ = 8.1, $^{4}J_{HH}$ = 1.3 Hz, 1H; NO_2-Ar H), 7.84 (t, $^{3}J_{HH}$ = 5.6 Hz, 1H; NO_2-Ar H), 7.76-7.56 (m, 3H; NO_2-Ar H + NH (x2)), 7.49 (t, $^{3}J_{HH}$ = 7.6 Hz, 1H; NO_2-Ar H), 6.62 (d, $^{3}J_{HH}$ = 8.0 Hz, 1H; $(HO)_2$-Ar H), 6.56 (d, $^{4}J_{HH}$ = 2.0 Hz, 1H; $(HO)_2$-Ar H), 6.39 (dd, $^{3}J_{HH}$ = 8.0, $^{4}J_{HH}$ = 2.0 Hz, 1H; $(HO)_2$-Ar H), 5.47-5.13 (m, 1H; NH-CH), 3.14 (m, 2H; NH-CH_2), 2.65-2.38 (m, 4H; $(HO)_2$-Ar-CH_2 + O=C-CH_2), 1.31 + 1.10 (2 · s, 9H; CH_3)

^{13}C-NMR (75 MHz, DMSO-d_6, δ): 168.78 (O=**C**-CH_2), 154.69 (O=**C**-O-), 148.17 (NO_2-**C** arom.), 145.20 (*m*-HO-**C** arom.), 143.66 (*p*-HO-**C** arom.), 138.52 (HC-**C** arom.), 133.48 (NO_2-**Ar**), 130.22 (H_2C-**C** arom.), 128.42 (NO_2-**Ar**), 128.21 (NO_2-**Ar**), 123.98 (NO_2-**Ar**), 119.26 ($(HO)_2$-**Ar**), 116.00 ($(HO)_2$-**Ar**), 115.63 ($(HO)_2$-**Ar**), 78.31 ($(CH_3)_3$**C**), 47.25 (HN-**C**H), 41.08 (O=C-**C**H_2), 40.81 (HN-**C**H_2), 34.77 (Ar-**C**H_2), 28.21 (**C**H_3)

IR: *v* = 3335 (m, N-H), 2981 (w, =C-H), 2932 (w, -C-H), 1678 (s, C=O), 1645 (vs, C=O), 1519 (vs, NO_2), 1361 (s), 1275 (s), 1249 (s), 1166 cm^{-1} (s)

2.6.4. *N*-(3,4-dihydroxyphenethyl)-3-amino-3-(2-nitrophenyl)propionamide (dopamine-ANP, **4**)

A round bottom flask was equipped with dopamine-Boc-ANP **3** (1.84 g, 4.13 mmol) before trifluoroacetic acid, which was cooled to -10 °C, was added to give a dark green solution. The reaction mixture was at first stirred at 0 °C for 15 minutes and then at room temperature for 45 minutes. Trifluoroacetic acid was removed from the mixture by codistillation with toluene (3 times). Purification by column chromatography on silica ($CHCl_3$/MeOH/DIPEA 5/1/0,05, R_f = 0.48) gave the product as a viscous orange oil (2.61 g, composed of 3.85 mmol dopamine-ANP and 9.90 mmol DIPEA, 93 % yield), which contained DIPEA (*N*,*N*-diisopropylethylamine) as an impurity (content of product ≈ 28 mol% calculated from ^{1}H-NMR). The DIPEA could not be removed from the product neither by drying under vacuum at 60 °C nor by column chromatography (CHCl3/MeOH 9/1 → 1/1).

^{1}H-NMR (300 MHz, DMSO-d_6, δ): 8.80 + 8,74 (2 · bs, 2H; Ar-OH), 8.17 (t, $^{3}J_{HH}$ = 5.5 Hz, 1H; NO_2-Ar H), 7.98 (dd, $^{3}J_{HH}$ = 8.2, $^{4}J_{HH}$ = 1.1 Hz, 1H; NO_2-Ar H), 7.91-7.74 (m, 2H; NO_2-Ar H + NH), 7.60 (ddd, $^{3}J_{HH}$ = 8.2; 7.0, $^{4}J_{HH}$ = 1.8 Hz, 1H; NO_2-Ar H), 6.60 (d, $^{3}J_{HH}$ = 8.6 Hz, 1H; $(HO)_2$-Ar H), 6.53 (d, $^{4}J_{HH}$ = 1.8 Hz, 1H; $(HO)_2$-Ar H), 6.33 (dd, $^{3}J_{HH}$ = 8.6, $^{4}J_{HH}$ = 1.8 Hz, 1H; $(HO)_2$-Ar H), 4.99 (t, $^{3}J_{HH}$ = 6.9 Hz, 1H; NH_2-CH), ≈3.09 (2H; NH-CH_2, covered by DIPEA), 2.75 (d, $^{3}J_{HH}$ = 6.9 Hz, 2H; O=C-CH_2), 2.41 (t, $^{3}J_{HH}$ =7.4 Hz, 2H; $(HO)_2$-Ar-CH_2)

^{13}C-NMR (75 MHz, DMSO-d_6, δ): 168.43 (O=**C**-CH_2), 148.71 (NO_2-**C** arom.), 145.17 (*m*-HO-**C** arom.), 143.66 (*p*-HO-**C** arom.), 133.99 (HC-**C** arom.), 133.72 (NO_2-**Ar**), 130.00

(H_2C-**C** arom.), 129.46 (NO_2-**Ar**), 128.66 (NO_2-**Ar**), 124.53 (NO_2-**Ar**), 119.13 ($(HO)_2$-**Ar**), 115.94 ($(HO)_2$-**Ar**), 115.52 ($(HO)_2$-**Ar**), 46.49 (H_2N-**C**H), 41.64 (O=C-**C**H_2), 40.19 (HN-**C**H_2), 34.52 (Ar-**C**H_2)
IR: ν = 3269 (m, N-H), 2991 (w, =C-H), 1670 (vs, C=O), 1527 (s, NO_2), 1198 (vs), 1176 (vs), 1127 cm^{-1} (vs)

2.7. End-group Functionalization

In an exemplary reaction poly(TPA) (319.8 mg, M_n = 15.0 kg · mol^{-1}, 0.0213 mmol), dopamine-ANP **4** (≈ 0.15 g, ≈ 0.43 mmol) and triethylamine (0.22 g, 2.2 mmol) were dissolved in dry THF (4 mL) under argon. The reaction mixture was then stirred at 65 °C for 6 days. After purification by repeated precipitation in *n*-hexane and methanol the polymer **8** was isolated as a pale yellow solid (289.9 mg, 0.0193 mmol, 91 % yield).
Exemplary ^{1}H-NMR (400 MHz, $CDCl_3$, δ): 7.87 (t, $^3J_{HH}$ = 7.80 Hz, 1H; NO_2-Ar H), 7.02-6.68 (br, 10H; Ar H repeating unit), 6.68-6.33 (br, 2H; CH-Ar H repeating unit), 6.30 (d, $^3J_{HH}$ = 10.0 Hz, 1H; $(HO)_2$-Ar H), 6.25 (s, 1H; $(HO)_2$-Ar H), 5,81 (s, 1H; $(HO)_2$-Ar H), 5.50 (s, 1H; NH-CH), 3.35 (t, $^3J_{HH}$ = 7.42 Hz, 2H; $C_{11}H_{23}$-CH_2-S), 3.16 (t, $^3J_{HH}$ = 6.50 Hz, 2H; NH-CH_2), 2.60 (s, 2H; O=C-CH_2), 2.44 (s, 2H; $(HO)_2$-Ar-CH_2), 2.42-0.97 (br, 9H; CH_3 + CH_2 + CH repeating unit), 0.92 (t, $^3J_{HH}$ = 6.50 Hz, 3H; H_3C-$C_{11}H_{22}$-S)

2.8. Functionalization of TiO_2-Nanoparticles with Polymer

In an exemplary reaction poly(TPA) carrying an anchor end-group **8** (50 mg, M_n = 15.0 kg · mol^{-1}, 0.0033 mmol) was dissolved in chloroform (5 mL) under argon. In a separate vessel 50 mg of TiO_2-nanorods (functionalized with oleic acid) were well dispersed in 15 mL of chloroform. During ultra sonification the polymer solution the dispersion were added through a syringe. The reaction mixture was heated to 40 °C and stirred for 17 h. The nanoparticles were then precipitated by addition of ethanol (15 mL), centrifuged, the solution decanted and the nanoparticles redispersed in chloroform. To remove unfunctionalized nanoparticles, which are soluble in *n*-hexane, the nanoparticles were precipitated in *n*-hexane and then redispersed in chloroform for two times.

2.9. Photocleavage

In a quartz cuvette a solution of the functionalized nanoparticles in dichloromethane (40-80 mg · mL^{-1}) was stirred under irradiation for 6-16 h. As a light source a Hg arc light was used and run at 500 W (no filter was used). The photocleavage was carried out at a wavelength of 245 nm, which is the first maximum of the light source. Then the nanoparticles were precipitated by the addition of ethanol, centrifuged, the overlaying solution was removed and the nanoparticles were redispersed in dichloromethane. For further purification the nanoparticles were precipitated in *n*-hexane and redispersed in dichloromethane twice.

3. Results and Discussion

To realize our task, a triarylamine based hole transporting polymer, poly(4,4'-dimethyl-triphenylamine) was synthesized by RAFT polymerization, which allowed introduction of a reactive end group via the CTA (**Scheme 2**). Then a photocleavable anchor group for oxidic semiconducting nanoparticles was incorporated and used to functionalize TiO_2-nanoparticles. The photocleavable anchor *N*-(3,4-dihydroxyphenethyl)-3-amino-3-(2-nitrophenyl)propion-amide (dopamine-ANP, **4**) was chosen because photocleavage of the central unit can be induced at a wavelength of about 200 to 260 nm and furthermore it carries an anchor for oxidic materials and an amino group for linking to the polymer. It was synthesized as shown in **Scheme 1**.

The commercially available compound 3-amino-3-(2-nitrophenyl)propionic acid (ANP) was protected with di-*tert*-butyl dicarbonate to give compound **1**, which was then reacted with pentafluorophenyl trifluoroacetate to yield the reactive ester **2**. By reacting the reactive ester with dopamine hydrochloride the catechol anchor group was attached (compound **3**). Deprotection with trifluoroacetic acid resulted in the photocleavable anchor group **4** (**Scheme 1**).

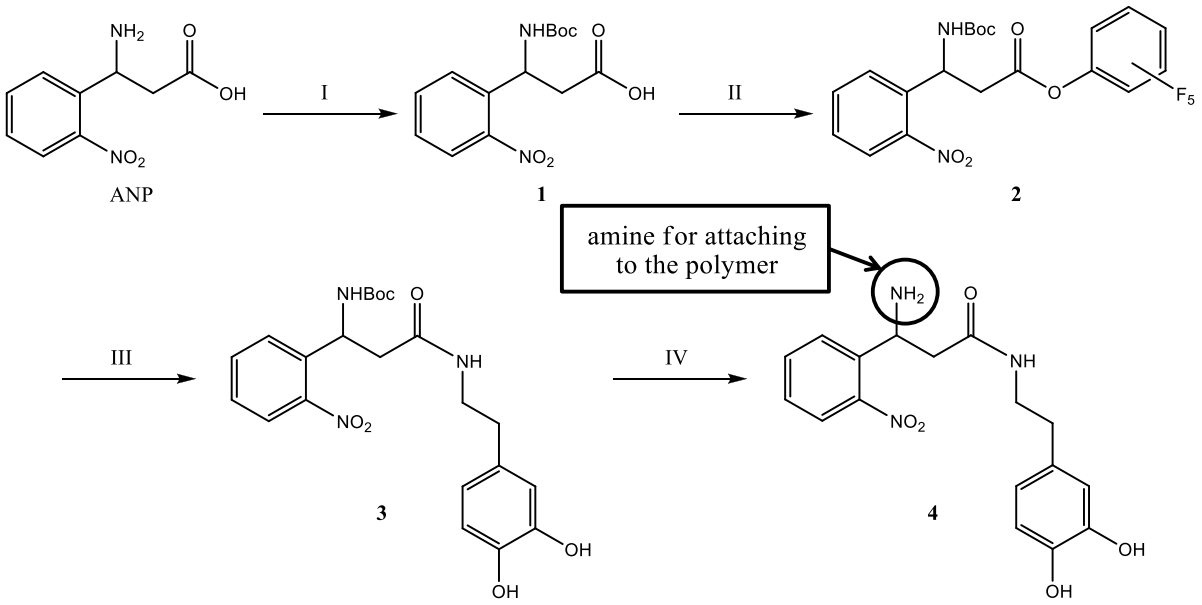

Scheme 1. Synthesis of the photocleavable anchor dopamine-ANP. Reagents and conditions were: I) 1. Boc_2O, NaOH, dioxane, H_2O, 0 °C 30 min, 22 h RT, 2. 80 mL 0,5 N HCl-sol.; II) PFP-O-TFA, TEA, Ar-atmosphere, DMF, 3 h, RT; III) dopamine hydrochloride, TEA, DMF, 6 h, RT; IV) TFA, 0-20 °C, 1 h.

The synthetic routes to polymer poly(4,4'-dimethyl-triphenylamine) (poly(TPA), **P1a-P4a**) which was synthesized by RAFT polymerization and then end-group modified (compound **P1b-P4b**) are shown in Scheme 2. On the basis of this synthetic route any (photocleavable) anchor group carrying an amine can be introduced to the polymer chain. The monomer with the 4,4'-dimethyl-triphenylamine unit was synthesized in a three-step reaction. 4,4'-dimethyl-triphenylamine was chosen because it acts – under illumination – as a donor with respect to TiO_2 nanoparticles.[30] In the first step aniline and 4-iodotoluene were reacted in an Ullmann-type reaction to yield 4,4'-dimethyltriphenylamine, which was then at first converted to the corresponding aldehyde via a Vilsmeier reaction and in a following Wittig reaction to the monomer, vinyl-TPA **5** as described in the literature.[28] This monomer was polymerized in a RAFT polymerization using *S*-1-Dodecyl-*S*'-(α,α'-dimethyl-α''-pentafluorophenyl acetate)tri-thiocarbonate (PFP-CTA, **6**) as chain transfer agent and AIBN as initiator to obtain poly(TPA) **P1a-P4a** as it is shown in **Scheme 2** and **Table 1**. This polymer is a semi-conducting polymer, which is applicable as a hole-conducting material in optoelectronic devices such as organic solar cells or organic light emitting diodes. The average molecular weights of polymers (M_n) determined by GPC against polystyrene standards reached from 8.8 to 17.7 kg · mol^{-1} and the polydispersity indices (PDI = M_n/M_w) were between 1.08 and 1.14. All poly(TPA) polymers are listed in **Table 1**.

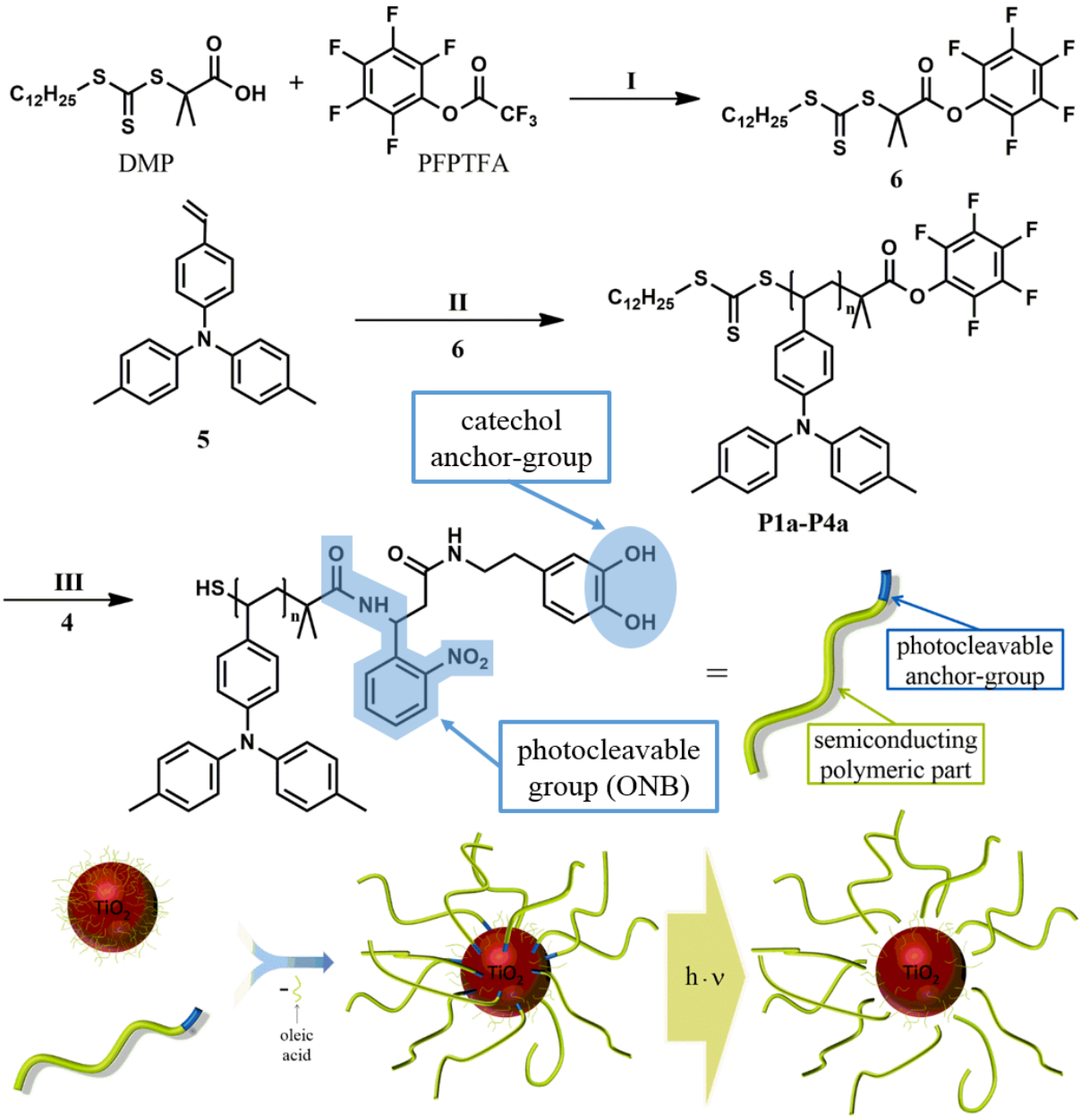

Scheme 2. Functionalization of TiO_2-nanoparticles with photocleavable anchor group containing poly(TPA) **P1b-P4b** and separation by irradiation afterwards. Reagents and conditions were: I) DIPEA, DMF (dry), 0 °C, 1 h; II) PFP-CTA 6, AIBN, THF, 65 °C, 48 h; III) dopamine-ANP 4, TEA, THF, 65 °C, 6 days; IV) $CHCl_3$, Ar-atmosphere, 40 °C, 17 h; V) DCM, 6 h, Hg arc light at 500 W.

These polymers carry a reactive ester at the α-end incorporated during the polymerization via the chain transfer agent (PFP-CTA, **6**). As depicted in **Scheme 2** this reactive ester end-group can be reacted with dopamine-ANP **4** to give poly(TPA) containing a photocleavable anchor group at the α-end (P1b-P4b in **Scheme 2** and **Table 1**). Proof that the reactive ester end-

group was quantitatively substituted is given by ^{19}F-NMR spectroscopy. Signals in the 400 MHz ^{1}H-NMR spectrum arising from the photocleavable anchor at 7.87 ppm (NO_2-Ar H) as well as at 6.25 and 5.81 ppm ($(HO)_2$-Ar H) verify successfully the incorporation of the photocleavable anchor group (see experimental section chapter 2.7).

Table 1. Properties of polymers **P1-4** (see **Scheme 2**)

Polymers	M_w[a)] **[kg · mol^{-1}]**	M_n[a)] **[kg · mol^{-1}]**	**PDI**[a)]	**End Group**
P1a	9.8	8.8	1.11	reactive ester
P1b	10.1	8.9	1.13	dopamine-ANP
P2a	12.2	11.2	1.09	reactive ester
P2b	12.3	11.2	1.10	dopamine-ANP
P2c	12.1	11.0	1.10	dopamine
P3a	16.2	15.0	1.08	reactive ester
P3b	16.1	14.8	1.09	dopamine-ANP
P4a	20.2	17.7	1.14	reactive ester
P4b	20.5	18.1	1.13	dopamine-ANP

[a)] Molecular weights (M_n and M_w) as well as polydispersity indices were measured by GPC using THF as the eluent and polystyrene standards for calibration.

Using a strong anchor group for oxidic materials like a catechol allows efficient functionalization of NPs even when only one anchor group is located at the chain end.[2] Enediols like the catechol group are known for being one of the best anchors for metal oxides such as TiO_2 and also worked well in the grafting-to experiments performed here.[8, 31] We chose TiO_2 as counterpart for the 4,4'-dimethyl-triphenylamine based polymer as the latter acts – under illumination – as an electron donor.[30] The NPs utilized in this work were synthesized according to a process described in the literature[32] and had an average length of around 45 nm with an average diameter of approximately 13 nm (a representative picture can be found in **Figure 1**). After functionalization with polymers **P1b–P4b** the TiO_2 nanoparticles became well dispersible in chloroform, dichloromethane or THF. Moreover the dispersions of the TiO_2-NPs functionalized with polymer showed an improved stability[5, 13] when compared to NPs functionalized with oleic acid as shown in **Figure 1**. The NPs functionalized with polymer remained well dispersed for several days (and even weeks) in contrast to NPs functionalized with oleic acids which started to sediment already after several hours (for pictures of the dispersions see Supporting Information). Transmission electron microscopy

(TEM) measurements showed that the NPs functionalized with poly(TPA) are individually dispersed whereas NPs stabilized with oleic acid tend to stick together (**Figure 1**), which proved the previously obtained results.

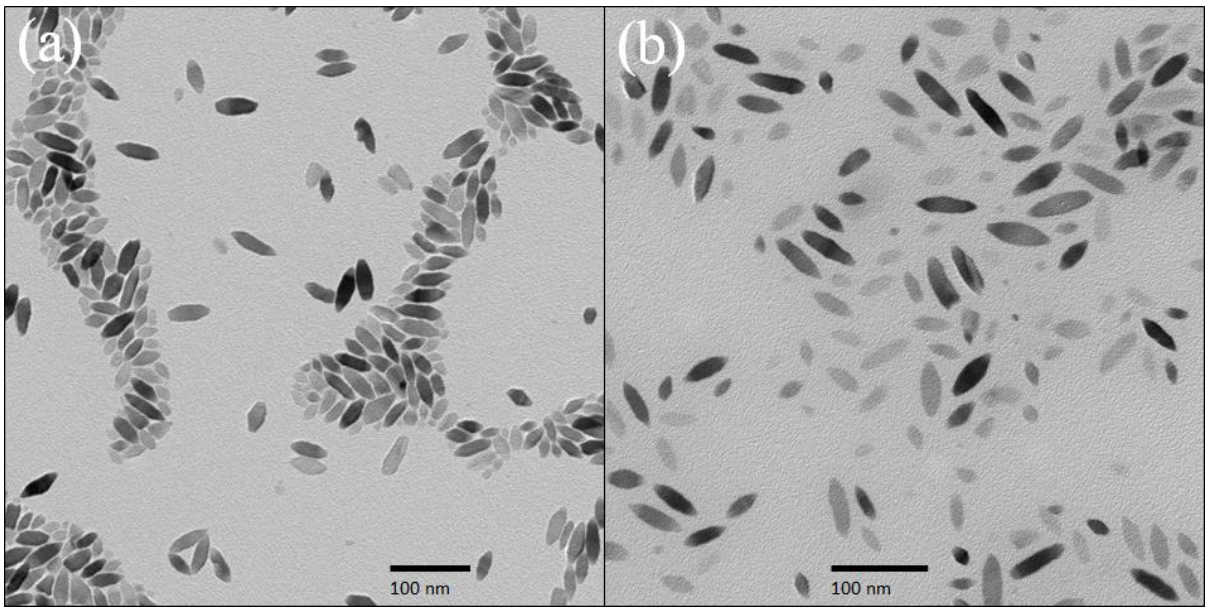

Figure 15. TEM-images of TiO_2-NPs (a) coated with oleic acid, (b) coated with polymer **P2b**.

The splitting of polymers and NPs was successfully achieved by irradiation with UV-light and proven by FTIR spectroscopy before and after irradiation (**Figure 2**). For this purpose a dispersion of NPs functionalized with polymer (40-80 mg · mL^{-1} in dichloromethane) was irradiated with UV-light (UV/Vis spectra of the photocleavable anchor group **4**, poly(TPA) **P3b** and TiO2-NPs are available in the Supporting Information). Thereafter NPs and polymers were separated by centrifugation and FTIR spectra were acquired (see **Figure 2a**). In the case of the NPs functionalized with polymer, signals of poly(TPA) can be observed in the FTIR spectrum at 1604 cm^{-1} and 1504 cm^{-1} arising from the aromatic rings of the triphenylamine repeating unit. Furthermore C-N bands are visible at 1318 cm^{-1} and 1272 cm^{-1}. As it is shown in **Figure 2** all these bands arising from poly(TPA) vanished after irradiation. Only few bands remain visible, e.g. the bands at 2922 cm^{-1} and 2852 cm^{-1}, which belong to the TiO_2-NPs or the bands in the region from 700 to 1800 cm^{-1} which probably arise from the small organic parts remaining on the NP surface after photocleavage.

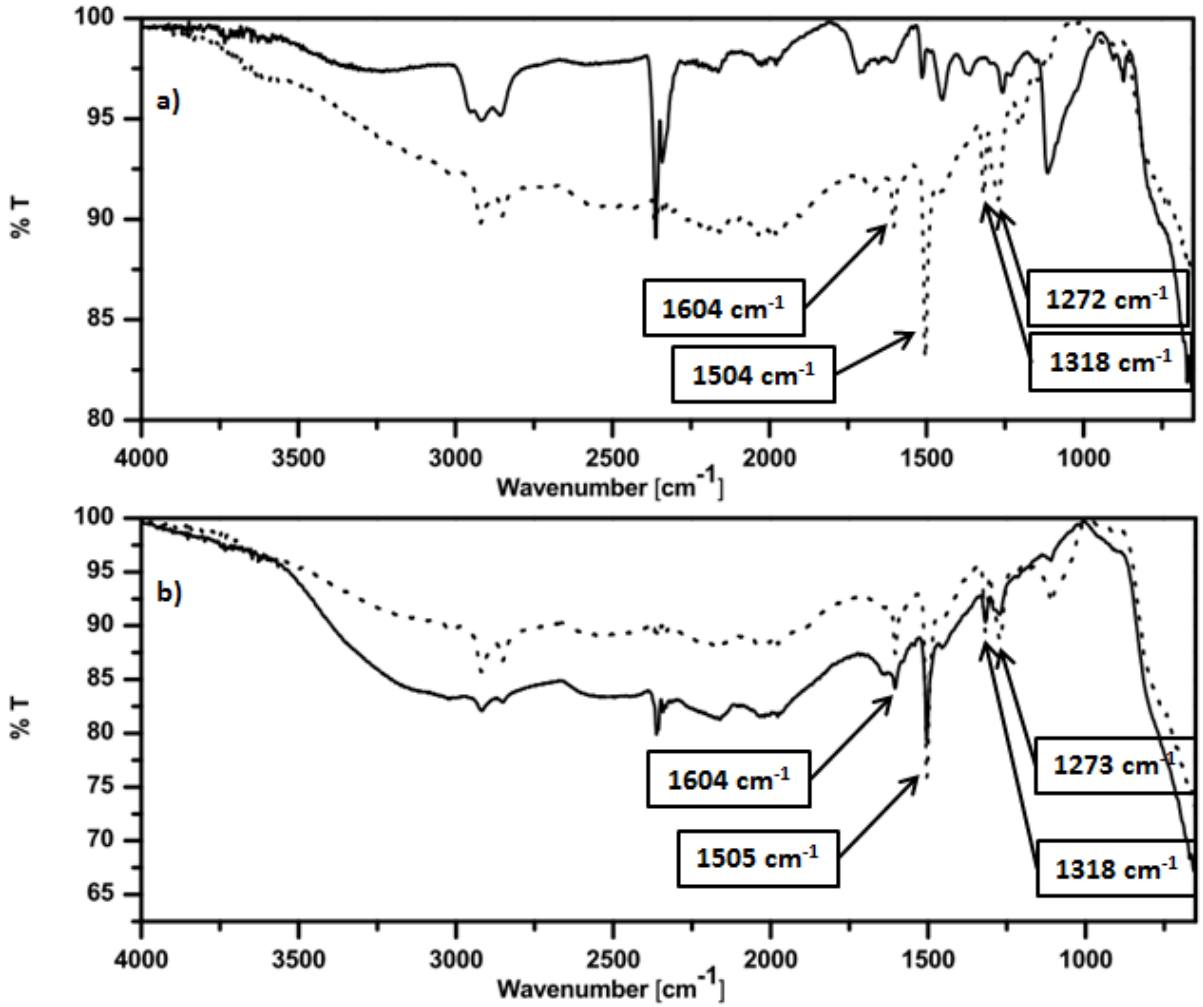

Figure 16. FTIR-spectra of a) TiO_2-NPs functionalized with poly(TPA) before (dotted line) and after (solid line) cleavage; b) poly(TPA) with dopamine end-group (reference system) before (dotted line) and after (solid line) irradiation.

To exclude that the splitting-off of the polymer is due to the action of titanium dioxide as photo-oxidant, we used a reference system.[33] In this reference dopamine hydrochloride was reacted with poly(TPA) carrying a reactive ester end-group **7** to obtain a polymer with an anchor group at the chain end but without a photocleavable group (**P2c** in **Table 1**). Thereupon TiO_2-NPs were functionalized with this polymer and a solution of the received nanoparticles was irradiated under the same conditions as NPs functionalized with polymer containing a photocleavable group. After irradiation the reaction mixture was worked up in the same manner as mentioned above and a FTIR spectrum was measured, which is shown in **Figure 2b**. The FTIR spectrum after irradiation in the absence of a photocleavable group still shows intensive, characteristic signals originating from the poly(TPA). The bands at 1604 cm^{-1} and 1505 cm^{-1} arise from the aromatic rings of the triphenylamine repeating unit and the C-N bands at 1318 cm^{-1} and 1273 cm^{-1} (**Figure 2b**). This indicates that the polymer was still

bound to the TiO_2-NPs, meaning no cleavage has happened. These results are consistent with literature reports about dopamine functionalized TiO_2 nanoparticles.[34] Thus it is proven that the cleavage is caused by the photocleavable ONB-group.

The consequence of the successful detachment of the polymers can also be verified by TEM. TEM-images recorded after irradiation show strongly aggregated structures (see **Fig. 3**, right), whereas the polymer coated NPs had been individually dispersed. After photocleavage mostly sphere-like aggregates are observed. In the corona of the aggregates, nanoparticles can be observed (see amplified aggregate in **Figure 3**). This indicates that the aggregates are made of TiO_2-NPs which carry no stabilizing polymers at their surface.

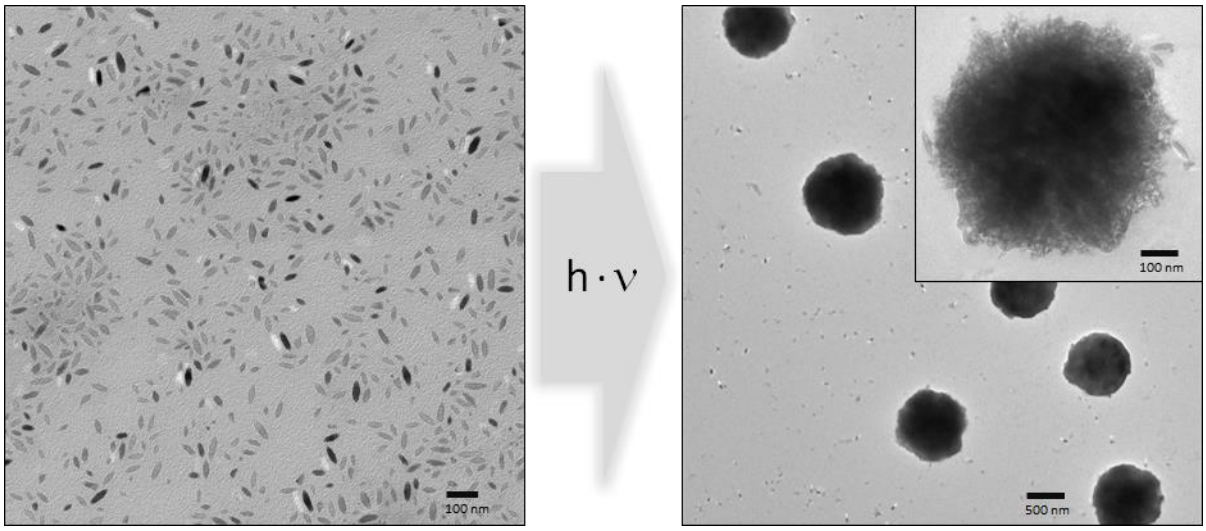

Figure 17. TEM-images of TiO_2-NPs functionalized with polymer before photocleavage (left, scale bar: 100 nm) and the same nanoparticles after photocleavage (right, scale bar: 500 nm; inset 100 nm). Once photocleaved, aggregated structures can be observed. In the amplified picture (upper right corner) nanoparticles are visible in the corona of the particle.

To verify photosplitting even further, a second reference system was used which was composed of oligomeric polystyrene.

The oligostyrenes used for this purpose were prepared by RAFT polymerization with the same CTA as polymers **P1a–P4a**. They are collected in **Tab. 2** as **P5–P6** and are three or seven repeating units long. Because of this fact the different end-group reactions were easily to be monitored by FTIR spectroscopy as shown in **Figure 4**. Concerning the molecular weight determination it is not surprising that the incorporation of the photocleavable end group caused a shift in molecular weights to higher weights whereas the molecular weights were not affected significantly for polymers **P1-P4** (see **Table 1**).

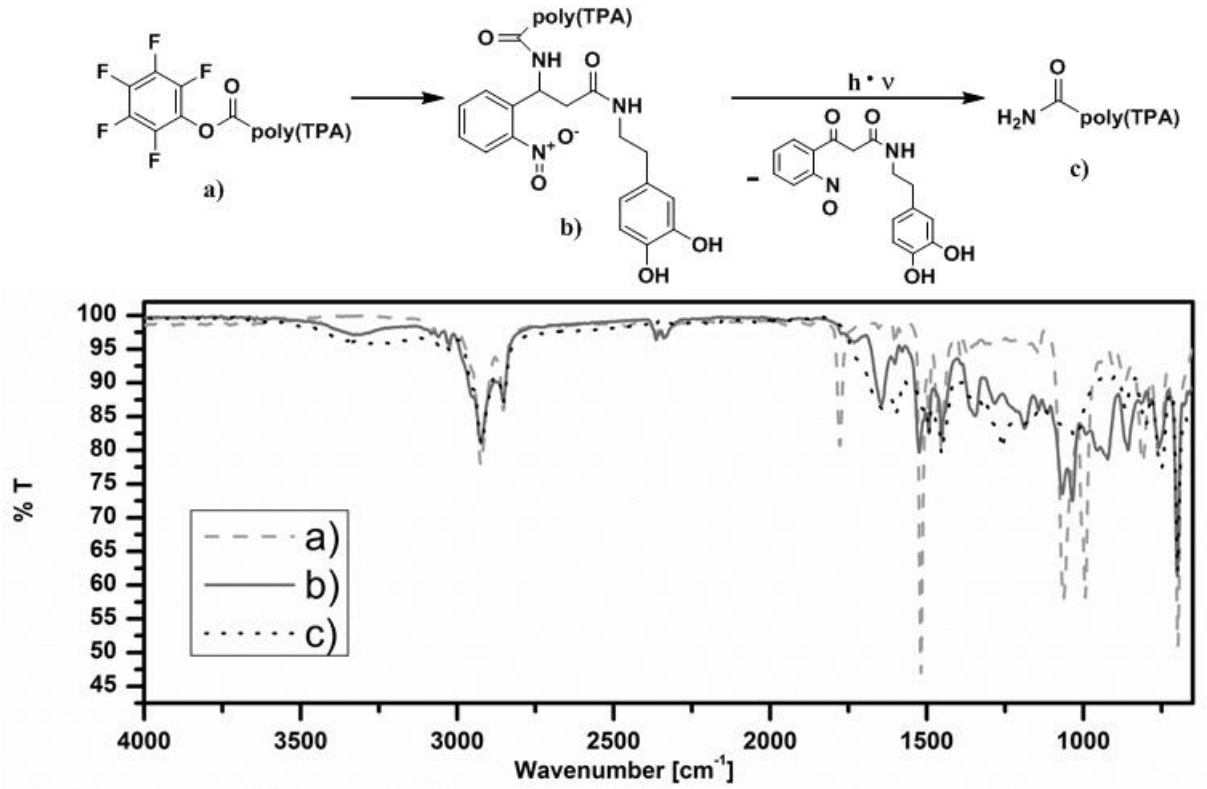

Figure 18. FTIR spectra of oligomeric polystyrene **P6** carrying a reactive ester (dashed line, a), the photocleavable anchor (solid line, b) and after photocleavage an amide (dotted line, c) as an end-group.

Regarding the oligomer **P6a** which carries a reactive ester end-group, a C=O band appears at 1777 cm^{-1}. A second strong band appears at 1519 cm^{-1} arising from the pentafluorophenyl ring.[35, 36] After attaching the photocleavable anchor group (**P6b**) these bands vanish completely and instead amide bands appear at 1645 cm^{-1} and 1525 cm^{-1} (see **Figure 4**, notice that the second band appearing in that region is a clear evidence for a secondary amide). In addition a broad band appears at 3329 cm^{-1} which is caused by the N-H- and O-H-groups. Detachment of the photocleavable anchor group via irradiation leads to an oligomer with a primary amide as an end group. An amide band at 1639 cm^{-1} plus the shift of the second band from 1525 cm^{-1} to 1600 cm^{-1} indicate a successful photocleavage leading to a primary amide.
In all spectra shown in **Figure 4**, signals of the styrene repeating unit at 3026 cm^{-1} (aromatic C-H band), 2924 cm^{-1} and 2852 cm^{-1} (aliphatic C-H bands) occur, indicating that the oligomeric backbone is not affected by the reactions taking place at the end-group.

Table 2. Properties of polymers **P5** and **P6**

Polymers	M_w[a)] [g · mol^{-1}]	M_n[a)] [g · mol^{-1}]	PDI[a)]	End Group
P5a	864	836	1.03	reactive ester
P5b	929	878	1.06	dopamine-ANP
P6a	1196	1136	1.05	reactive ester
P6b	1336	1211	1.10	dopamine-ANP

[a)] Molecular weights (M_n and M_w) as well as polydispersity indices were measured by GPC using THF as the eluent and polystyrene standards for calibration.

4. Conclusions

Inorganic TiO_2-nanoparticles were functionalized with a semiconducting poly(TPA) via a photocleavable anchor group, which allowed the splitting-off of the polymers by irradiation. In the same manner any oxidic nanoparticle could be reversibly functionalized with a polymer. This offers the potential to initially make inorganic nanoparticles well dispersible in a polymer matrix and to induce demixing, causing percolation later at a desired point of time. This concept is interesting for optoelectronic devices where control over film formation properties and morphology is desired. Using this approach, smooth and flat films may be prepared in which, through separation of polymers and NPs via irradiation, demixing can be induced at a later stage of time. This demixing process should be adjustable by controlling the mobility of the NPs in the film for example through solvent annealing and its time scale. Hence film morphology could be controlled and optimized.

Supporting Information

Supporting Information is available from the Wiley Online Library or from the author.

Appendix/Nomenclature/Abbreviations

Acknowledgements: We thank Janine Heimstadt for synthetic support and the International Research Training Group (IRTG) 1404: Self Organized Materials for Optoelectronics supported by the Deutsche Forschungsgemeinschaft (DFG) for financial support.

Received: December 4, 2013; Revised: January 13, 2014; Published online: February 22, 2014; DOI: 10.1002/macp.201300759

Keywords: morphology, optoelectronics, photocleavable polymers, RAFT, semiconducting polymer

References

[1] N. Tomczak, R. Liu, J. G. Vancso, *Nanoscale.* **2013**.

[2] N. Tomczak, D. Jańczewski, M. Han, G. J. Vancso, *Progress in Polymer Science.* **2009**, *34*, 393.

[3] A. C. C. Esteves, L. Bombalski, T. Trindade, K. Matyjaszewski, A. Barros-Timmons, *Small.* **2007**, *3*, 1230.

[4] P. J. Roth, P. Theato, *Chem. Mater.* **2008**, *20*, 1614.

[5] M. Zorn, W. K. Bae, J. Kwak, H. Lee, C. Lee, R. Zentel, K. Char, *ACS Nano.* **2009**, *3*, 1063.

[6] Q. Zhang, S. Gupta, T. Emrick, T. P. Russell, *J. Am. Chem. Soc.* **2006**, *128*, 3898.

[7] S. Meuer, P. Oberle, P. Theato, W. Tremel, R. Zentel, *Adv. Mater.* **2007**, *19*, 2073.

[8] M. Zorn, S. Meuer, M. N. Tahir, Y. Khalavka, C. Sönnichsen, W. Tremel, R. Zentel, *J. Mater. Chem.* **2008**, *18*, 3050.

[9] M. Eberhardt, R. Mruk, R. Zentel, P. Théato, *European Polymer Journal*. **2005**, *41*, 1569.

[10] M. Eberhardt, P. Théato, *Macromol. Rapid Commun.* **2005**, *26*, 1488.

[11] L. Zur Borg, A. L. Domanski, A. Breivogel, M. Bürger, R. Berger, K. Heinze, R. Zentel, *J. Mater. Chem. C.* **2013**, *1*, 1223.

[12] L. Zur Borg, D. Lee, J. Lim, W. K. Bae, M. Park, S. Lee, C. Lee, K. Char, R. Zentel, *J. Mater. Chem. C.* **2013**, *1*, 1722.

[13] S. Meuer, K. Fischer, I. Mey, A. Janshoff, M. Schmidt, R. Zentel, *Macromolecules.* **2008**, *41*, 7946.

[14] M. Zorn, R. Zentel, *Macromol. Rapid Commun.* **2008**, *29*, 922.

[15] J. Kwak, W. K. Bae, M. Zorn, H. Woo, H. Yoon, J. Lim, S. W. Kang, S. Weber, H.-J. Butt, R. Zentel, S. Lee, K. Char, C. Lee, *Adv. Mater.* **2009**, *21*, 5022.

[16] S. Ren, L.-Y. Chang, S.-K. Lim, J. Zhao, M. Smith, N. Zhao, V. Bulović, M. Bawendi, S. Gradečak, *Nano Lett.* **2011**, *11*, 3998.

[17] N. Radychev, D. Scheunemann, M. Kruszynska, K. Frevert, R. Miranti, J. Kolny-Olesiak, H. Borchert, J. Parisi, *Organic Electronics.* **2012**, *13*, 3154.

[18] A. C. Arias, J. D. MacKenzie, R. Stevenson, J. J. M. Halls, M. Inbasekaran, E. P. Woo, D. Richards, R. H. Friend, *Macromolecules.* **2001**, *34*, 6005.

[19] L.-M. Chen, Z. Hong, G. Li, Y. Yang, *Adv. Mater.* **2009**, *21*, 1434.

[20] M. C. Lechmann, S. A. L. Weber, J. Geserick, N. Hüsing, R. Berger, J. S. Gutmann, *J. Mater. Chem.* **2011**, *21*, 7765.

[21] M. Kang, B. Moon, *Macromolecules.* **2009**, *42*, 455.

[22] H. Zhao, E. S. Sterner, E. B. Coughlin, P. Theato, *Macromolecules.* **2012**, *45*, 1723.

[23] S. W. Thomas, *Macromol. Chem. Phys.* **2012**, *213*, 2443.

[24] W. Gu, H. Zhao, Q. Wei, E. B. Coughlin, P. Theato, T. P. Russell, *Adv. Mater.* **2013**, *25*, 4690.

[25] J. T. Lai, D. Filla, R. Shea, *Macromolecules.* **2002**, *35*, 6754.

[26] M. Green, J. Berman, *Tetrahedron Letters.* **1990**, *31*, 5851.

[27] K. Godula, D. Rabuka, K. T. Nam, C. R. Bertozzi, *Angew. Chem. Int. Ed.* **2009**, *48*, 4973.

[28] M. Behl, E. Hattemer, M. Brehmer, R. Zentel, *Macromol. Chem. Phys.* **2002**, *203*, 503.

[29] N. Brunner, C. Freiberg, T. Lampe, P. Nell, M. Otteneder, J. Pernerstorfer, J. Pohlmann, G. Schiffer, S. Mitsuyuki, N. Svenstrup, Bayer AG, 51373 Leverkusen, DE. 10236340.4 **2002**.

[30] M. Zorn, S. A. L. Weber, M. N. Tahir, W. Tremel, H.-J. Butt, R. Berger, R. Zentel, *Nano Lett.* **2010**, *10*, 2812.

[31] T. Rajh, L. X. Chen, K. Lukas, T. Liu, M. C. Thurnauer, D. M. Tiede, *J. Phys. Chem. B.* **2002**, *106*, 10543.

[32] B. Oschmann, D. Bresser, M. N. Tahir, K. Fischer, W. Tremel, S. Passerini, R. Zentel, *Macromol. Rapid Commun.* **2013**, *34*, 1693.

[33] A. Fujishima, X. Zhang, *Comptes Rendus Chimie.* **2006**, *9*, 750.

[34] N. M. Dimitrijevic, E. Rozhkova, T. Rajh, *J. Am. Chem. Soc.* **2009**, *131*, 2893.

[35] J. Choi, P. Schattling, F. D. Jochum, J. Pyun, K. Char, P. Theato, *J. Polym. Sci. A Polym. Chem.* **2012**, *50*, 4010.

[36] P. J. Roth, K. T. Wiss, R. Zentel, P. Theato, *Macromolecules.* **2008**, *41*, 8513.

Supporting Information

Functionalization of TiO_2-Nanoparticles with Semiconducting Polymers Containing a Photocleavable Anchor Group and Separation via Irradiation Afterwards

Florian Mathias, Muhammad Nawaz Tahir, Wolfgang Tremel, Rudolf Zentel*

zentel@uni-mainz.de (R. Zentel)

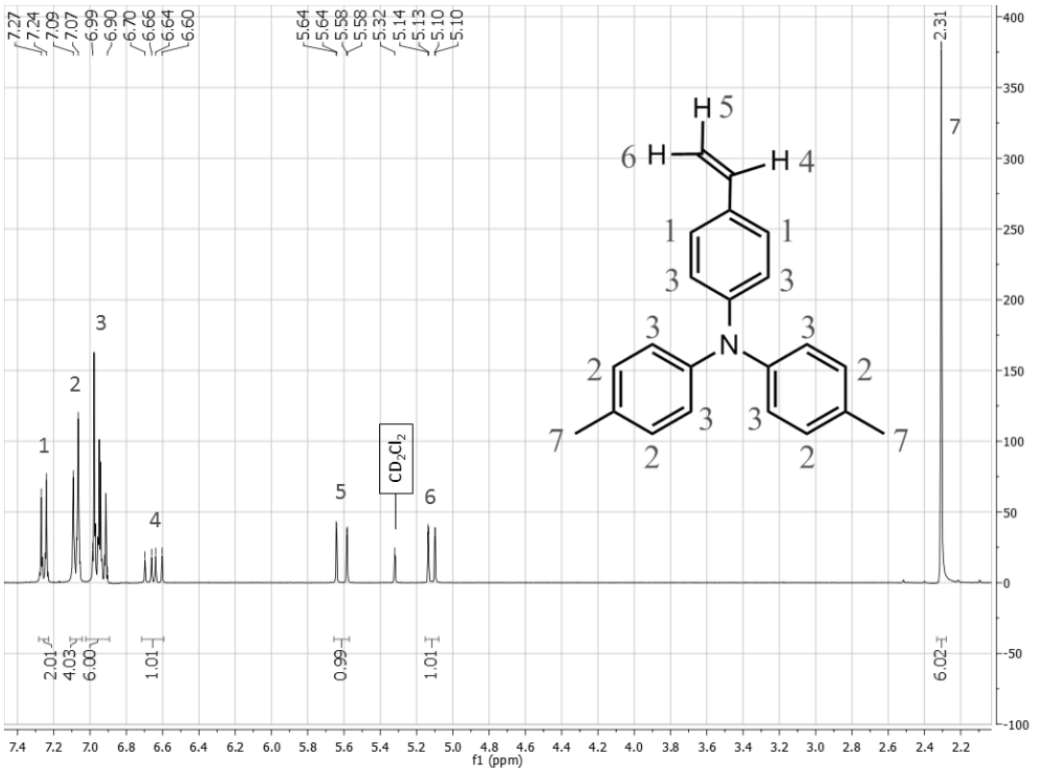

Figure S1. 300 MHz ^{1}H-NMR in CD_2Cl_2 of 4,4'-dimethyl-4''-vinyl-triphenylamine (Vinyl-TPA, **5**).

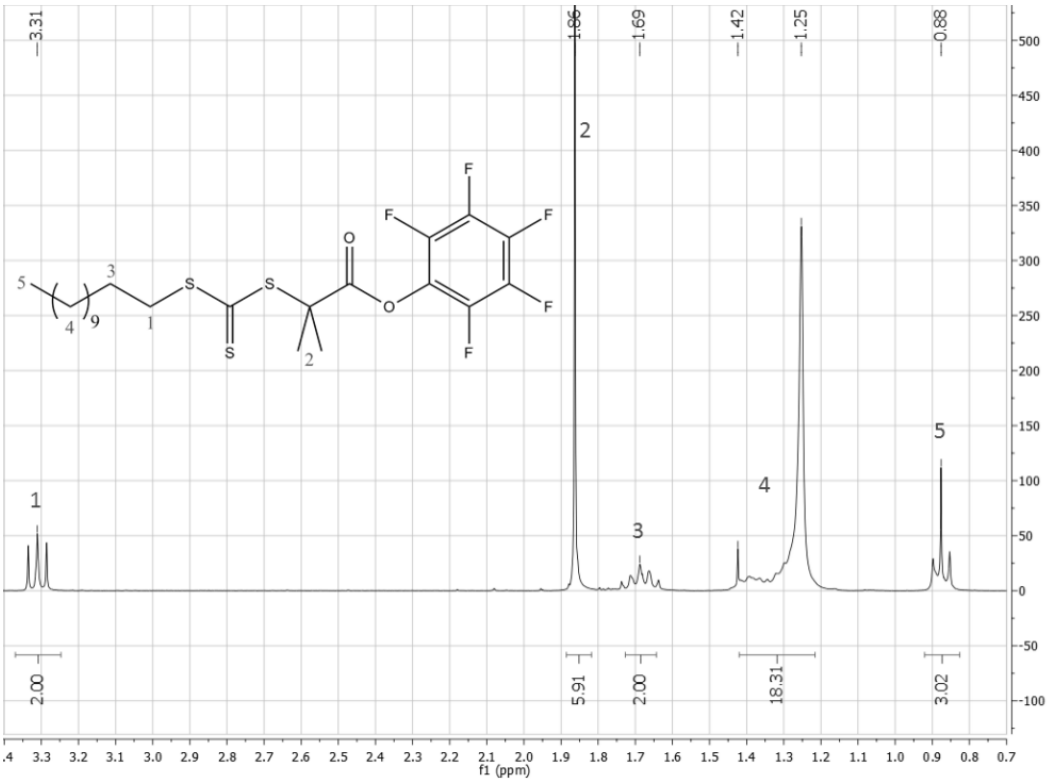

Figure S2. 300 MHz ^{1}H-NMR in $CDCl_3$ of S-1-Dodecyl-S'-(α,α'-dimethyl-α''-pentafluorophenyl acetate)trithiocarbonate (PFP-CTA, **6**).

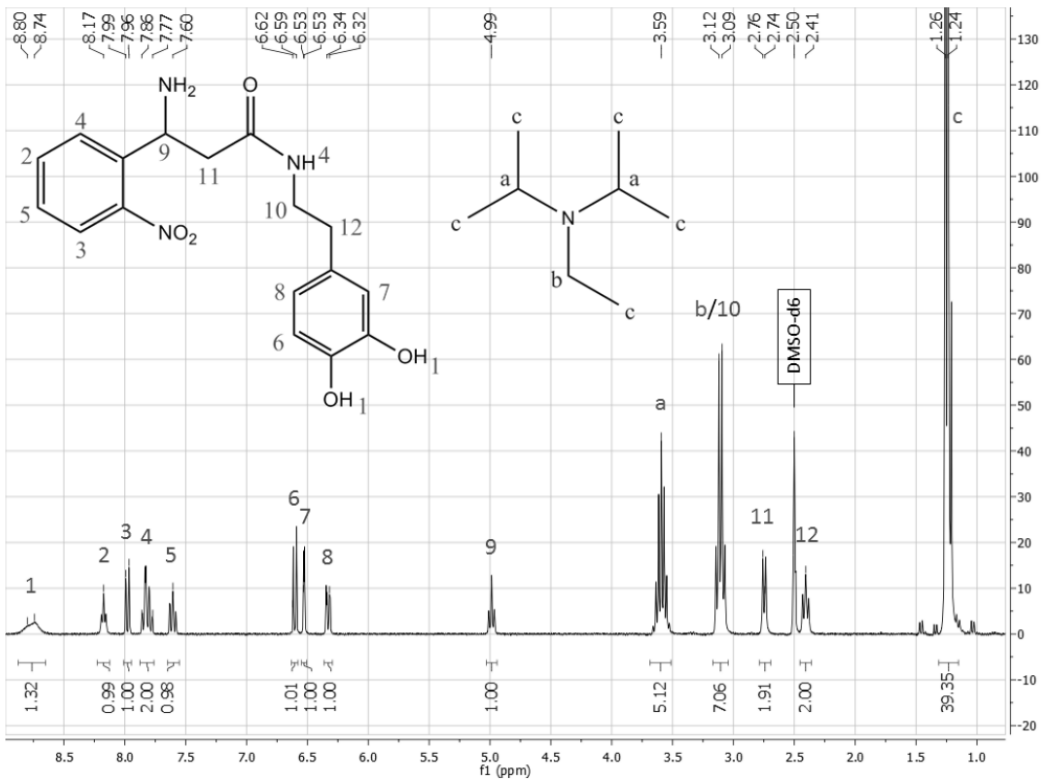

Figure S3. 300 MHz ^{1}H-NMR in DMSO-d_6 of N-(3,4-dihydroxyphenethyl)-3-amino-3-(2-nitrophenyl)propionamide (dopamine-ANP, **4**).

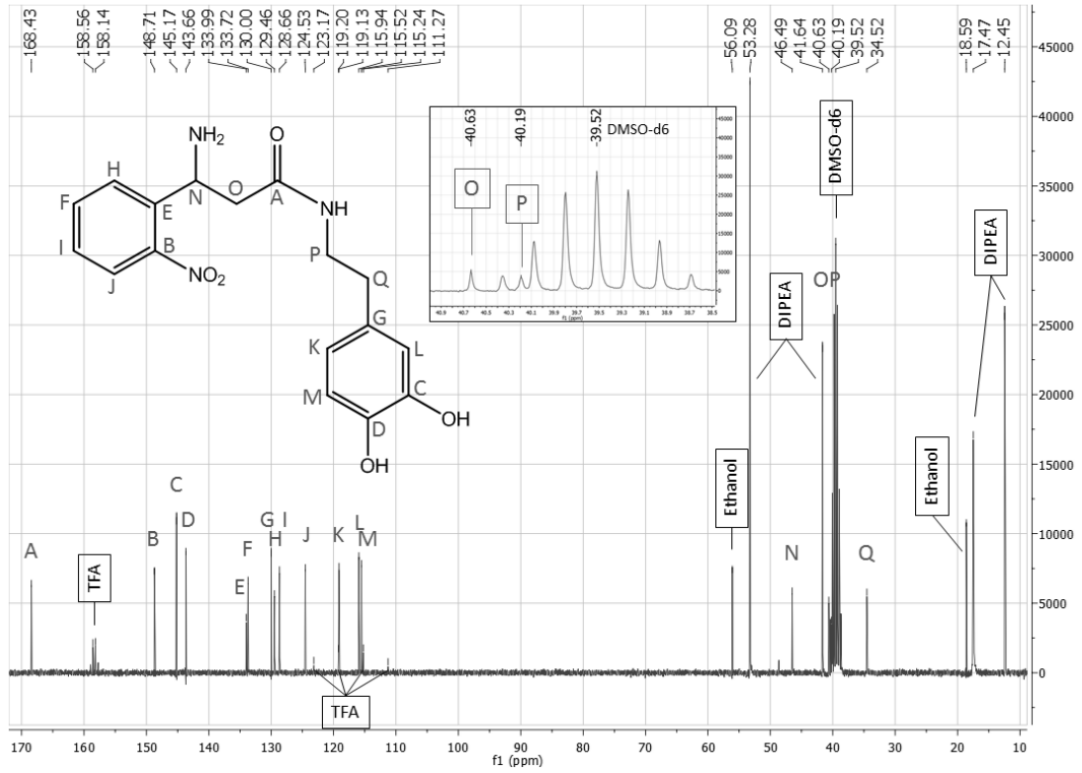

Figure S4. 75 MHz ^{13}C-NMR in DMSO-d_6 of N-(3,4-dihydroxyphenethyl)-3-amino-3-(2-nitrophenyl)propionamide (dopamine-ANP, **4**).

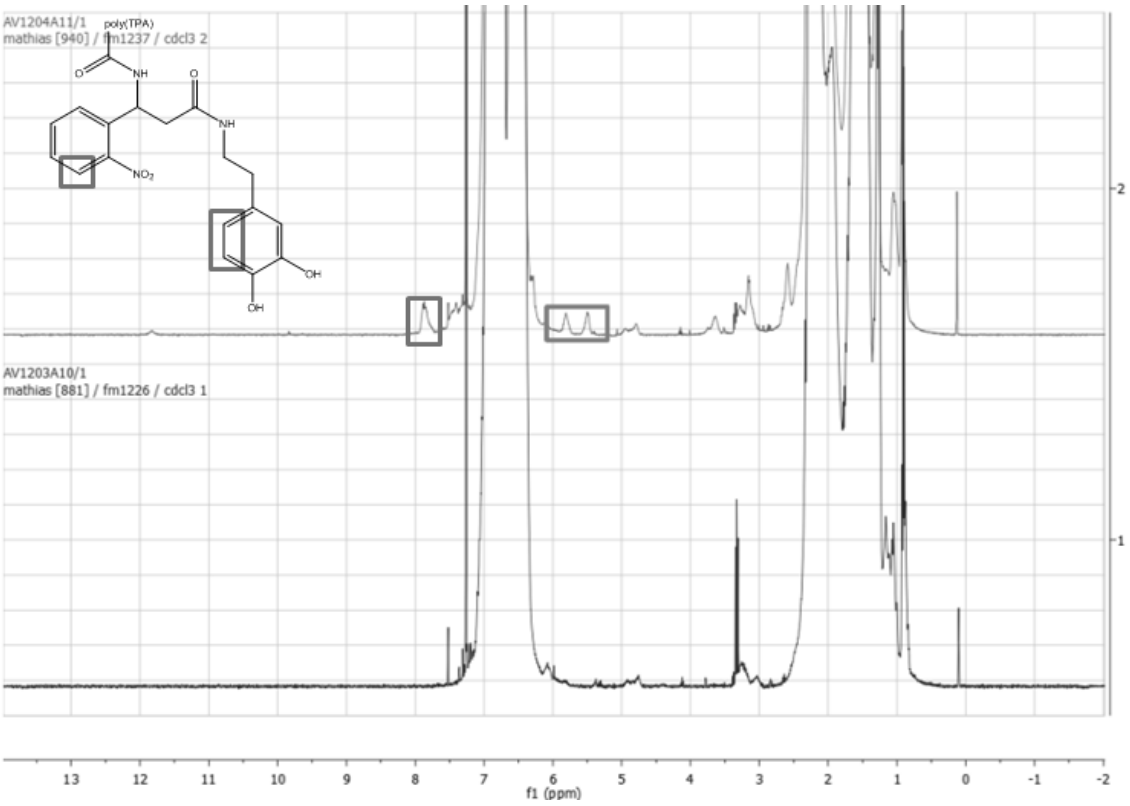

Figure S5. 400 MHz ^{1}H-NMR in $CDCl_3$ of poly(TPA) before introduction of the photocleavable anchor group (lower spectrum, **P2a**) and after introduction (upper spectrum, **P2b**).

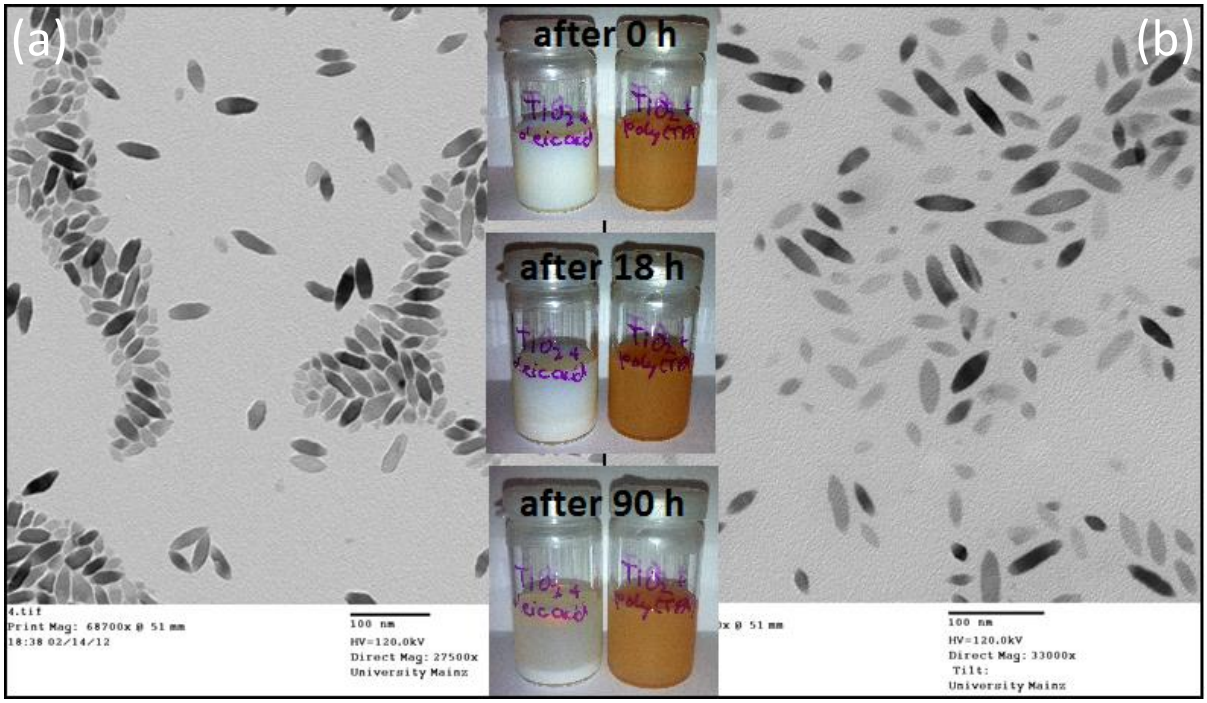

Figure S6. TEM-images of TiO_2-NPs (a) coated with oleic acid, (b) coated with poly(TPA) **P2b** and photography of dispersions of TiO_2-NPs with oleic acid (left) and poly(TPA) **P2b** (right), respectively (both with a concentration of 30 mg · mL TiO_2 in chloroform).

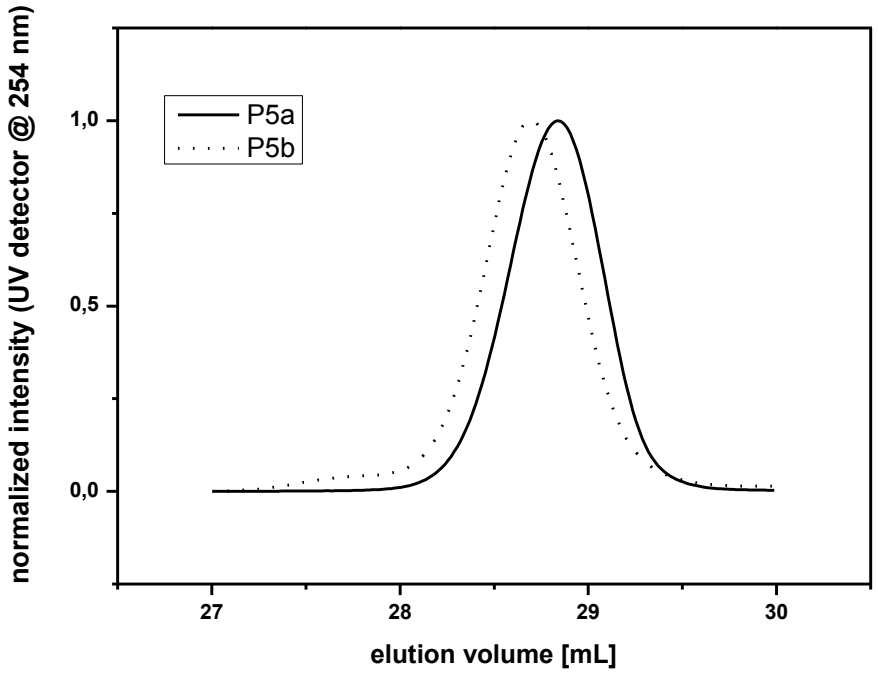

Figure S7. GPC curves of oligomeric polystyrene **P5a** (reactive ester end group) and **P5b** (dopamine-ANP and group).

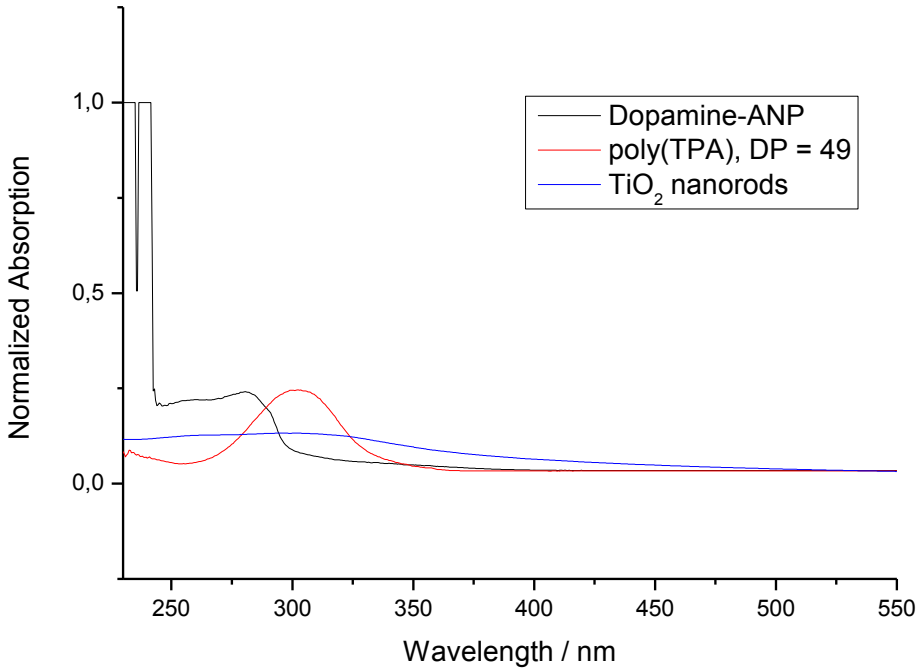

Figure S8. UV/Vis spectra of Dopamine-ANP **4**, poly(TPA) **P3b** and TiO_2 nanorods measured in THF (c=0,015 mg/mL).

4.1.2 Facile One-Pot Synthesis of Block Copolymers Composed a Conjugated and a Non-Conjugated Block

Block copolymers composed of a conjugated and a non-conjugated block possess interesting features such as their self-assembly properties. To date, unfortunately, such polymers have to be synthesized following complicated procedures. The synthetic approaches often involve multiple end group reactions or end group reactions between two polymers. Resulting from such synthetic procedures, the desired block copolymers are usually contaminated with unreacted polymeric byproducts which alter the properties of the desired block copolymer.

In the second project presented in this dissertation, a synthetic procedure to obtain block copolymers composed of a backbone conjugated block and a non-conjugated block was developed. Therefore, MEH-PPV which is, due to its favorable optoelectronic properties, one of the most studied conjugated polymers was selected. Moreover, PPVs can be synthesized via ROMP which, in addition, is a polymerization technique capable of synthesizing non-conjugated polymers. To achieve optimized polymerization conditions, however, a detailed study on the reactivity behavior of the four individual isomers of the monomer (dimethoxy-(2-ethylhexyloxy)-[2.2]paracyclophane-1,9-diene) was necessary. This study will be presented in the first publication included in this subsection.
Nevertheless, once conditions have been optimized, the living nature of ROMP enabled the synthesis of functional block copolymers combining a conjugated and a non-conjugated block in a facile one-pot procedure. Thus, amphiphilic block copolymers became accessible and enabled the formation of micelles. Size and optical properties of the micelles could be varied depending on the block copolymer composition and the micellization procedure. Furthermore, the synthesis of block copolymers exhibiting a reactive ester carrying polynorbornene block enabled the incorporation of various amines. Consequently, the block copolymers were equipped with anchor groups which facilitated the functionalization of CdSe@ZnS QDs.

Mihail Mondeshki contributed to the first publication with discussions regarding the assignment of the isomers and recorded the solid state NMR spectra. Dmytro Dudenko carried out the NMR calculations that helped to assign the four isomers. Suyong Shin supported with guidance concerning ROMP and provided catalyst **6**. Dieter Schollmeyer collected and interpreted single crystal X-ray crystallographic data and Oliver Ceyhun synthesized catalysts

3, **5** and **7** under the author's supervision. The monomer synthesis and the kinetic studies were carried out by the author of this dissertation. Furthermore, the author of this thesis developed the model of the catalyst coordinated chain end and interpreted the NMR data.

Concerning the second publication, Suyong Shin collected the TEM and AFM images. Kyung-Oh Kim provided the reactive ester carrying norbornene derivative and Martin Scherer collected and plotted the DLS data. The whole synthetic part, including the fabrication of the micelles as well as the collection of the NMR spectra and all optical measurements, was carried out by the author of this disseration.

4.1.2.1 Publication in Macromolecules, 2015, 48, 7435–7445

Reactivity Studies of Alkoxy Substituted [2.2]Paracyclophane-1,9-dienes and Specific Coordination of the Monomer Repeating Unit during ROMP

Florian Menk, Mihail Mondeshki, Dmytro Dudenko, Suyong Shin, Dieter Schollmeyer, Oliver Ceyhun, Tae-Lim Choi*, Rudolf Zentel*

Abstract

The polymerization of alkoxy substituted [2.2]paracyclophane-1,9-dienes via ring-opening metathesis polymerization (ROMP) to obtain soluble poly(*p*-phenylene vinylene)s

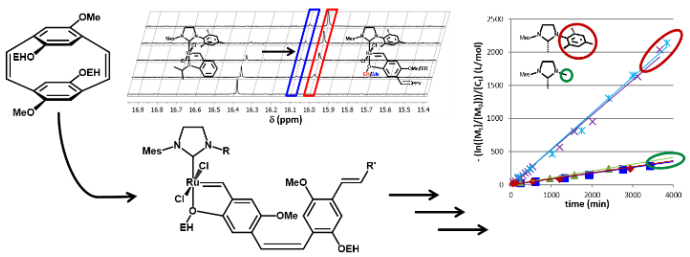

is a versatile method due to its living nature which enables the possibility of block copolymerization and end group modification. However, detailed studies on the reactivity behavior and the polymerization process of alkoxy substituted [2.2]paracyclophane-1,9-dienes have not been reported so far. Herein we present a detailed study on the varying tendencies of the four isomers of dimethoxy-(2-ethylhexyloxy)-[2.2]paracyclophane-1,9-diene to undergo ROMP. Therefore, we carried out polymerization combining all individual isomers with five different metathesis catalysts and collected initiation and propagation kinetics for various combinations. Furthermore, we revealed a specific coordination of the monomer repeating unit to the catalyst during the polymerization process and succeeded to polymerize not only the pseudo-geminal isomers but also one of the pseudo-*ortho* isomers.

1. Introduction

Since the first electroluminescence of a polymer was reported by Tang and Van Slyke in 1987, conjugated polymers have been the subject of intensive research.[1] Conjugated polymers are frequently used materials for organic and hybrid electronic devices such as light-emitting diodes, solar cells, field-effect transistors, optical waveguides and lasers.[2,3,4] Among many conjugated polymers, poly(*p*-phenylene vinylene) (PPV) derivatives are one of the most widely studied compounds. Although various synthetic approaches have been studied, most suffer from a broad molecular weight distribution and do not offer any control over a functional end group.[5] Even those few examples offering a precise end group control suffer from problems such as insufficient controllability, low molecular weights (M_n) and the incapability of direct block copolymerization.[6] In 2006, Turner and Yu published pioneering results which described the polymerization of tetraoctyloxy-[2.2]paracyclophane-1,9-diene via ring-opening metathesis polymerization (ROMP) to prepare soluble poly(dioctyloxy-*p*-phenylene vinylene). Their approach allowed for a control over M_n and exhibited low polydispersity indices (PDIs), thereby confirming the living nature of the polymerization. A scheme illustrating the most important steps of the synthetic route on the example of the monomers used in the study at hand is shown in **Figure 19**.[7] Furthermore, this first report about synthesis of soluble PPVs using a living polymerization technique enabled end group modification and simple block copolymerization.[8–10]

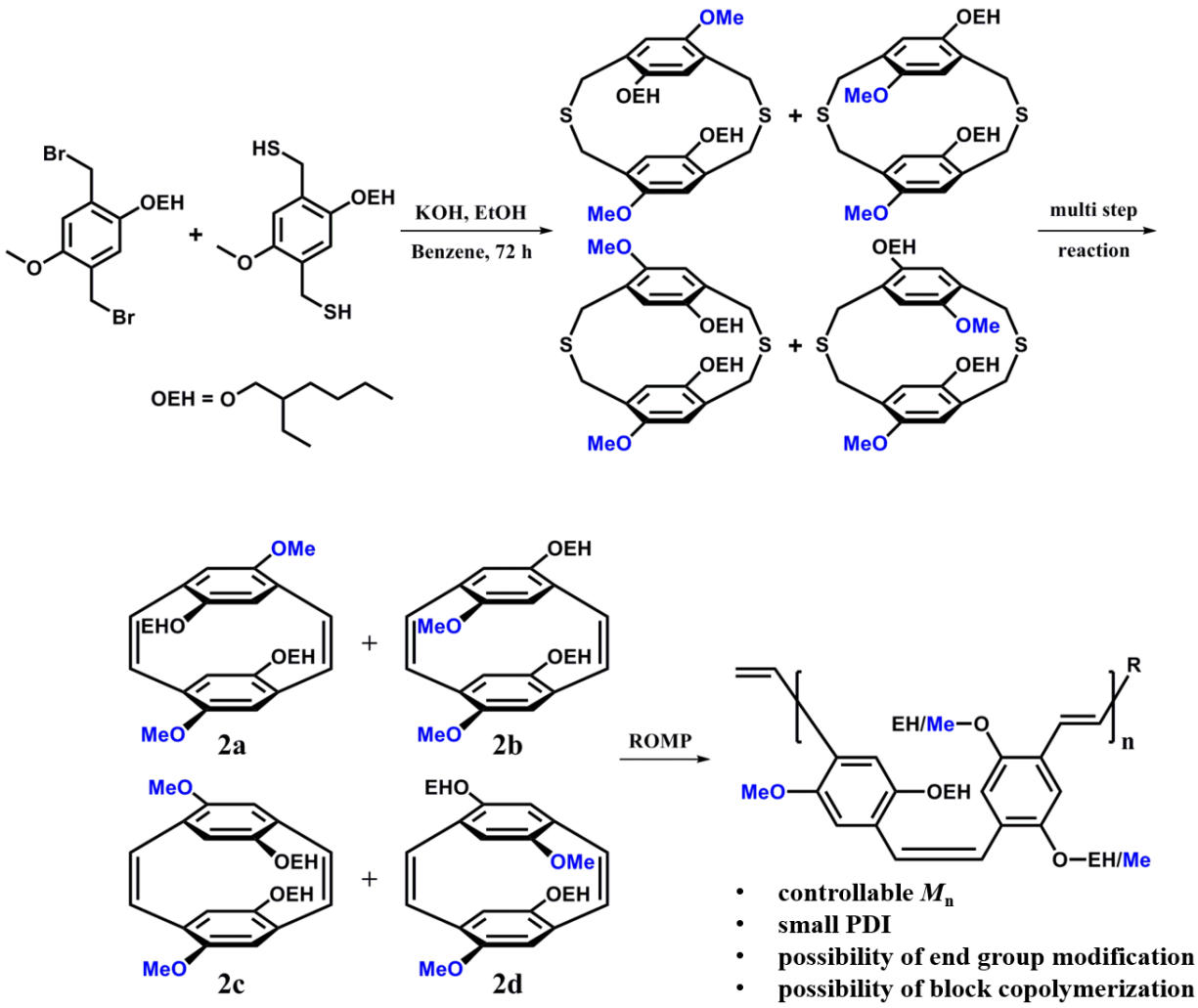

Figure 19. Reaction scheme depicting the monomer synthesis and ROMP polymerization of MEH-PPV following the route described by Turner and Yu.[11]

In addition to already known polymers such as the popular MEH-PPV, also structurally new PPVs and poly(thienylene vinylenes) (PTVs) became accessible.[10,12,13] The polymerization of asymmetrically substituted monomers – such as the monomer necessary for MEH-PPV – is especially challenging because four isomers result from the synthesis. These four isomers have to be separated due to their varying tendencies to undergo ROMP and the differences in the resulting configuration of the polymer backbone which will be discussed in relation to **Figure 25**. To avoid the complicated separation process, symmetrically substituted monomers or monomers which bear substituents only on one aromatic ring have been synthesized. Unfortunately, the asymmetric substituents are essential for the favorable optoelectronic properties of MEH-PPV or MDMO-PPV (poly[2-methoxy-5-(3′,7′-dimethyloctyloxy)-1,4-phenylene vinylene]) as they prevent the "side-chain crystallization effect".[14] Recently, the incorporation of functional end groups into PPVs via ROMP was exploited

either to enable a combination with atom transfer radical polymerization (ATRP) or to allow self-assembly into supramolecular block copolymers.[8,15] The living nature of ROMP makes this approach the most versatile method for the synthesis of PPVs as it enables many interesting features such as rod-coil block copolymers, polymerization induced self-assembly and the introduction of cleavable or anchor groups.[16]

However, the polymerization of tetraalkoxy-[2.2]paracyclophane-1,9-dienes via ROMP proceeds unexpectedly slow and is limited to the pseudo-geminal isomers which possess an eclipsed conformation of the substituents. In addition, no detailed reactivity studies regarding isomers and catalysts have been reported so far. In this study, we present a detailed investigation of the reactivity behavior for all four isomers of dimethoxy-(2-ethylhexyloxy)-[2.2]paracyclophane-1,9-diene (**2a-d**) in combination with several catalysts. On the basis of our results, we propose a unique polymerization model originating from the monomer structure. This model provides an explanation for the generally slow polymerization observed for alkoxy substituted [2.2]paracyclophane-1,9-diene derivatives. Furthermore, we achieved polymerization of pseudo-*ortho* isomer **2c** and synthesized MEH-PPV with head-to-head configuration of substituents obtained from polymerization of isomer **2b**.

2. Experimental Section

Materials and Characterization. All commercially available chemicals were purchased from Alfa Aesar, Acros Organics, Fluka, Sigma-Aldrich, or Tokyo Chemical Industry and used without further purification unless noted otherwise. Anhydrous THF was freshly distilled from sodium under a dry argon atmosphere. All reactions were carried out under dry argon atmospheres using standard Schlenkline techniques. All anhydrous deuterated solvents – d_8-THF (99.5%) and d_8-toluene (99.6%) – were purchased from Deutero GmbH or Euriso-Top and were degassed for 10 min prior to use. Molecular weights of all synthesized polymers were determined by gel permeation chromatography (GPC) with a concentration of 1.2 mg · mL^{-1} in THF with polystyrene as external and toluene as internal standard. Monomer precursors **1a-d** were synthesized by modifying literature procedures. Procedures are described in detail in the supporting information (see **Figures S1-3**).[11,17,18] Catalysts **3**, **5**, **6** and **7** were synthesized following the procedures described in literature.[19–21] ^{1}H-NMR and ^{13}C-NMR spectra were acquired on a Bruker ARX 400 at a Lamor frequency of 400 MHz and 101 MHz, respectively or by Varian/Oxford As-500 (500 MHz for ^{1}H/125 MHz for ^{13}C)

spectrometer. FTIR spectra were performed on a Vector 22 ATR-FTIR-spectrometer made by Bruker or a JASCO FT/IR-660 plus spectrometer. UV/Vis spectra were obtained by Jasco Inc. UV/vis-Spectrometer V-630. All solid state NMR experiments were recorded on a Bruker Avance 400 DSX spectrometer at ^{1}H frequency of 399.87 and ^{13}C frequency of 100.55 MHz. A two channel commercial Bruker 2.5 mm probe head at spinning speeds of 25 kHz was used for all measurements (for further information see the supporting information). Single crystal X-ray crystallographic data was collected using a Bruker Smart Apex II diffractometer. The entire crystallographic data of compound **2a** is deposited under CCDC-1419086 and can be obtained free of charge from The Cambridge Crystallographic Data Centre via www.ccdc.cam.ac.uk/data_request/cif.

Geometry optimization and NMR calculations. In this work we used the CASTEP version 6.1 package with ultrasoft pseudopotentials.[22] All calculations on structural optimization were carried out with the commonly used PBE density functional in conjunction with Tkatchenko-Scheffler (TS) dispersion correction (DC) scheme as this scheme has known in general higher accuracy comparing to the scheme of Grimme (G06).[23] As it was previously shown dispersion-correction to DFT (DFT-DC) is mandatory and is the crucial point for structural studies.[24] In all calculations we used a Monkhorst-Pack Brillouin zone sampling grid of spacing 2π x 0.1 Å and a plane-wave basis set cutoff of 800 eV. During structure optimization calculations, the settings of CASTEP were taken as follows: forces, stresses on the unit cells, energies and displacements were converged to better than 0.01 eV Å−1, 0.01 GPa, 0.00001 eV, and 0.001 Å, respectively.

The NMR chemical shift calculations (carried out on the geometry optimized structure) employed the GIPAW method to determine the shielding tensor for each nucleus in the crystal structure as well as in model conformers in the gas phase.[25] The NMR calculations used the same level of theory and accuracy as the geometry optimisation.

Synthesis of Isomers 2a-d. The four isomers of dimethoxy-(2-ethylhexyloxy)-[2.2]paracyclophane-1,9-diene were synthesized according to a modified literature procedure.[11] A mixture of the corresponding bis-sulfoxides **1a-d** (8.40 g, 10.87 mmol) was dissolved in 600 mL xylene (mixture of isomers). The solution was degased for 20 min and an argon atmosphere was established. The solution was then heated to reflux for 21 h. After cooling to room temperature the mixture was diluted with 300 mL of dichloromethane, extracted twice with 300 mL 1 N aqueous HCl and once with 300 mL of water. The organic layer was dried over $MgSO_4$, filtered and concentrated. The crude product was purified by

column chromatography using a gradient eluent system of DCM/*n*-hexane, 2/5 to 1/1 – R_f (**2a**) ≈ 0.40 (DCM/*n*-hexane 2/5), R_f (**2c**) ≈ 0.34 (DCM/*n*-hexane 1/2), R_f (**2d**) ≈ 0.27 (DCM/*n*-hexane 1/2), R_f (**2b**) ≈ 0.31 (DCM/*n*-hexane 1/1). Further purification of the individual isomers was achieved by column chromatography using eluent systems ranging from toluene/*n*-hexane 1/1 to 6/1. The individual isomers were obtained either as a light yellow solid (**2a**), semi-solid (**2b**) or oil (**2c** and **2d**) in an overall yield of 56 % (3.17 g, 6.08 mmol).

Isomer 2a. m.p. 63.6 °C; ^{1}H-NMR (400 MHz, $CDCl_3$, δ): 6.96 (d, J = 10 Hz, 2H, =CH-); 6.92 (d, J = 10 Hz, 2H, =CH-); 5.91 (s, 2H, Ar-H); 5.82 (s, 2H, Ar-H); 3.81 and 3.79 (2xdd, J_1 = 9, J_2 = 6 Hz, 2H, OCH_2-), 3.65 (s, 6H, OCH_3), 3.61 and 3.59 (2xdd, J_1 = 9, J_2 = 6 Hz, 2H, OCH_2-), 1.63 – 1.54 (m, 2H, OCH_2CH), 1.50 – 1.26 (m, 16H, -CH_2-), 0.93 – 0.87 (m, 12H, -CH_3); IR: ν = 1361 cm^{-1}; MS (FD): *m/z*: 520.5 (M^+).

Isomer 2b. ^{1}H-NMR (400 MHz, $CDCl_3$, δ): 6.98 (s, 2H, =CH-); 6.92 (s, 2H, =CH-); 5.86 (s, 4H, Ar-H); 2x3.73 (2xdd, J_1 = 9, J_2 = 7 Hz, 2H, OCH_2-), 3.68 (s, 6H, OCH_3), 3.61 and 3.59 (2xdd, J_1 = 9, J_2 = 7 Hz, 2H, OCH_2-), 1.67 – 1.58 (m, 2H, OCH_2CH), 1.48 – 1.21 (m, 16H, -CH_2-), 0.91 – 0.85 (m, 12H, -CH_3); IR: ν = 1362 cm^{-1}; MS (FD): *m/z*: 520.4 (M^+).

Isomer 2c. ^{1}H-NMR (400 MHz, $CDCl_3$, δ): 6.85 (s, 2H, =CH-); 6.82 (s, 2H, =CH-); 6.21 (s, 2H, Ar-H); 6.19 (s, 2H, Ar-H); 2x3.76 (2xdd, J_1 = 9, J_2 = 6 Hz, 2H, OCH_2-), 3.69 (s, 6H, OCH_3), 2x3.65 (2xdd, J_1 = 9, J_2 = 6 Hz, 2H, OCH_2-), 1.65 – 1.56 (m, 2H, OCH_2CH), 1.54 – 1.26 (m, 16H, -CH_2-), 0.95 – 0.89 (m, 12H, -CH_3); IR: ν = 1379, 1362, 1331 cm^{-1}; MS (FD): *m/z*: 520.5 (M^+).

Isomer 2d. ^{1}H-NMR (400 MHz, $CDCl_3$, δ): 6.87 (d, J = 10 Hz, 2H, =CH-); 6.82 (d, J = 10 Hz, 2H, =CH-); 5.91 (s, 2H, Ar-H); 6.20 (s, 2H, Ar-H); 3.76 – (m, 4H, OCH_2-), 3.68 (s, 6H, OCH_3), 1.64 – 1.54 (m, 2H, OCH_2CH), 1.54 – 1.26 (m, 16H, -CH_2-), 0.95 – 0.89 (m, 12H, -CH_3); IR: ν = 1379, 1362, 1331 cm^{-1}; MS (FD): *m/z*: 520.4 (M^+).

The solid-state ^{1}H-NMR and ^{13}C-NMR spectra of isomer **2a**, calculated spectra, ^{1}H-NMR, ^{13}C-NMR and HSQC solution spectra as well as magnified FTIR spectra of all individual isomers can be found in the supporting information.

Polymerization Kinetics. Before a kinetic measurement was started the NMR spectrometer was adjusted to the desired temperature. The monomer (8.33 mg, 0.016 mmol, 10 eq.) was dissolved in 400 µL of dry d_8-THF (or d_8-toluene) which was degassed for 10 min prior to use. The monomer solution was then transferred into a sealed (with a septum) and flame dried NMR tube. The catalyst (2.4 µmol) was then separately dissolved in 150 µL of dry and

degassed d_8-THF (or d_8-toluene). Then 100 µL of the catalyst's solution (1.6 µmol, 1 eq.) was added to the monomer solution. The NMR tube was quickly shaken and then the collection of the NMR spectra was started.

3. Results and Discussion

MEH-PPV is the most widely studied PPV derivative due to its favorable optoelectronic properties. Therefore, it was applied to various applications (e.g. light-emitting diodes, solar cells and lasers) making the research on improved synthetic strategies highly relevant.[3,4,26] In principle, MEH-PPV can be synthesized via ROMP from the four different isomers of dimethoxy-(2-ethylhexyloxy)-[2.2]paracyclophane-1,9-diene. However, previous studies using tetraalkoxy-[2.2]paracyclophane-1,9-diene derivatives for the synthesis of soluble poly(*p*-phenylene vinylene)s reported that solely the pseudo-geminal isomers (eclipsed conformation of substituents on the aromatic rings) were able to react in the context of ring-opening metathesis reaction.[11] This behavior was explained by the varying sterical hindrance in proximity to the double bonds (comparing both isomers). During the initiation process, the catalyst has to approach the double bond (from the front or the back side oriented to the double bond) to allow for the interaction of π-orbitals. In case of a staggered conformation of the substituents (pseudo-*ortho* isomers) the initiation is hindered on both sides.[11] However, all four individual isomers of dimethoxy-(2-ethylhexyloxy)-[2.2]paracyclophane-1,9-diene (see **Figure 21**) provide a different spatial freedom in proximity to the double bonds caused by the large difference in size of both substituents (methoxy and 2-ethylhexyloxy). Therefore, dimethoxy-(2-ethylhexyloxy)-[2.2]paracyclophane-1,9-diene serve as an ideal model compound to investigate the varying reactivities of structural isomers. To conduct a detailed reactivity study in the context of ROMP, however, the separation, assignment and consequently a complete characterization of all individual isomers is crucial. Following the synthetic route presented in the literature, we slightly modified the last step of the synthesis – thermal elimination of sulfenic acid from sulfoxides **1a-d** – by exchanging the solvent from DMF to xylenes (mixture of isomers).[11,17,18] This slight modification increased the yield from 25 % reported in the literature to 48 – 60 % (**Figure S4**).[11] A single crystal of compound **2a** was grown by slow evaporation from a concentrated solution in acetone to which small amounts of water were added. The X-ray crystal structure of compound **2a** (**Figure 20**) exhibits a deformation of the aromatic rings with C3 and C6 located 0.116 (3) Å out of the

rings' mean square planes. In addition, the angle between C7-C3···C6 is not 180 ° as it should be, but 150.7 (2) ° (see **Figure 20**). This deformation of the aromatic rings causes a high ring strain energy and makes this isomer an efficient monomer for ROMP.

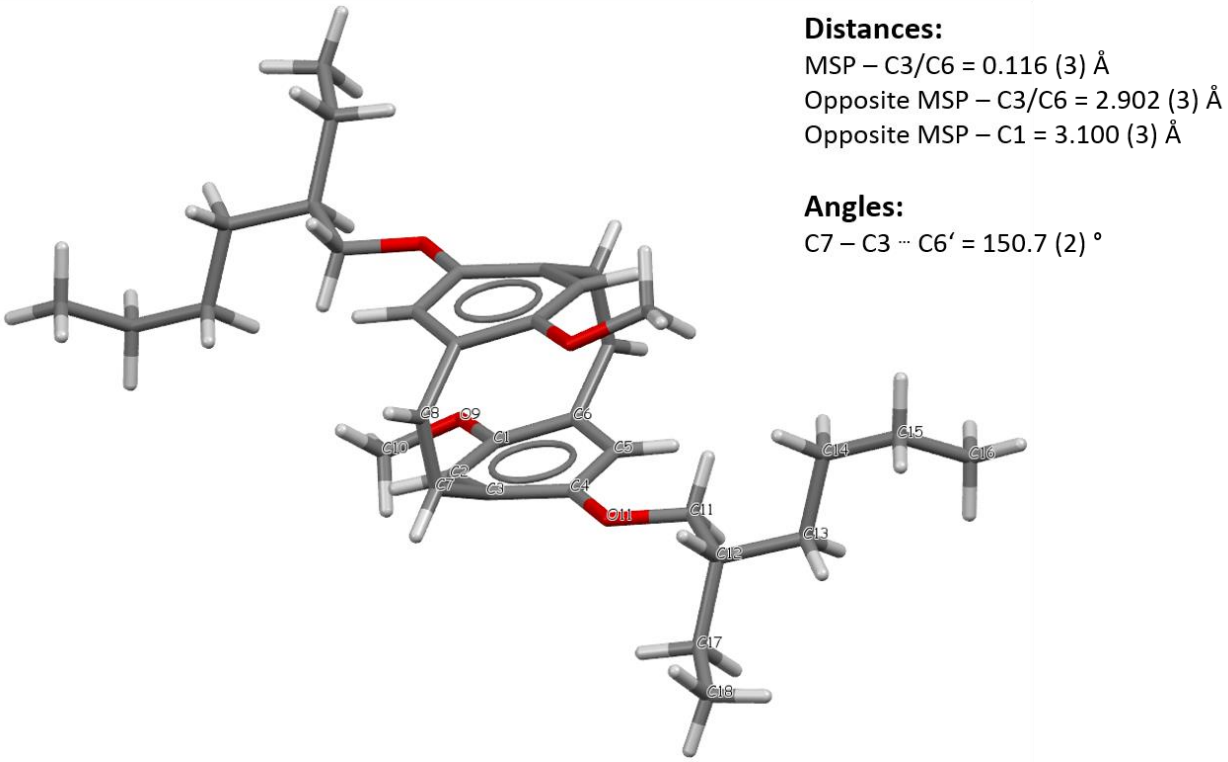

Figure 20. Solid-state structure of compound **2a** exhibiting free space between the double bond (C7-C8) and the alkoxy substituents. The symmetry of the molecule is Ci. The distances and angles shown in the picture elucidate the ring strain of the molecule.

Combining the crystal structure, theoretical calculations, solid state and solution NMR and FTIR spectroscopy allows for an unambiguous assignment of all isomers. The solution ^{1}H-NMR spectra vary in the pattern of signals as well as in their chemical shifts, both related to the conformation of the substituents on the aromatic rings. **Figure 21** depicts the aromatic region of the ^{1}H-NMR spectra of the isomers **2a-d** with the respective molecular structures assigned. The olefinic protons of all isomers resonate in the spectral region of 6.8 – 7.0 ppm. The general downfield shift of the olefinic signals compared to the protons of ethylene (5.4 ppm) originates from their location in proximity to the aromatic rings which causes a strong deshielding effect due to the aromatic ring currents as reported in literature.[27]

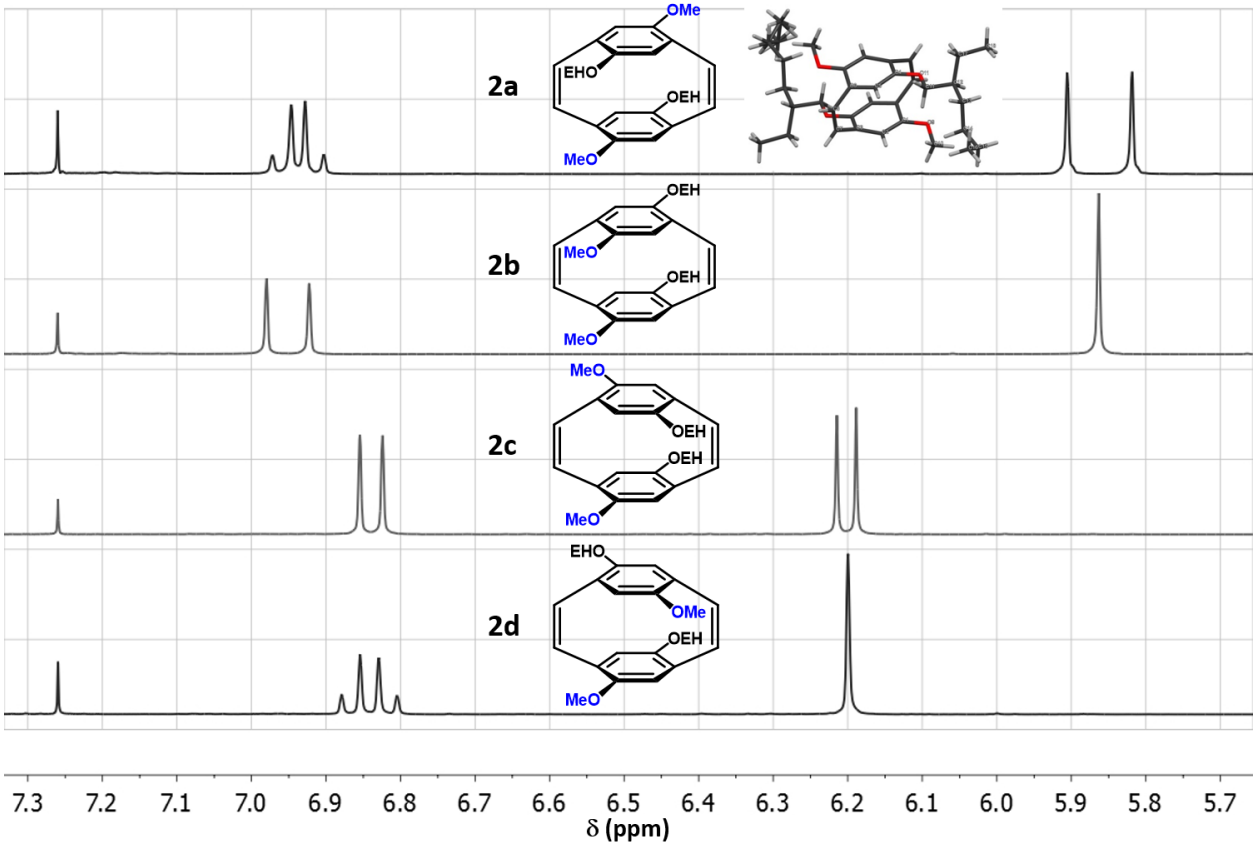

Figure 21. Magnified aromatic region of the ^{1}H-NMR spectra of isomers **2a-d** (measured in $CDCl_3$), corresponding molecular structures and the solid state structure of isomer **2a**.

In principle two patterns of the olefinic signals can be observed in the ^{1}H-NMR spectra. In isomers **2a** and **2d** the protons on a distinct double bond are inequivalent due to their different electronic environments (proximity to different substituents on the aromatic rings). Thus, the spectra of isomers **2a** and **2d** depict a pseudo-quartet which is composed of two doublets. In the spectrum of isomer **2a** these doublets resonate at 6.92 ppm and 6.96 ppm, while they resonate at 6.87 ppm and 6.82 ppm in case of isomer **2d**. The differences of the resonance frequencies are comparable to the strength of the ^{3}J couplings between the olefinic protons, with calculated values of $\Delta\nu/J = 1.76$ and 2.04 for isomers **2a** and **2d**, respectively. This leads to the observation of higher order effects for this AB system (i.e., pseudo-quartets). While in isomers **2a** and **2d** the hydrogens on one individual double bond have different chemical environments, the olefinic hydrogens in isomers **2b** and **2c** are chemically and magnetically equivalent. Thus, two distinct singlets with slightly different chemical shifts can be observed for isomers **2c** and **2d** as shown in **Figure 21**. For a further understanding of the spectra, one has to consider the electronic structures of the isomers. The electronic structures of the

isomers depend on the conformation of substituents on the aromatic rings. Therefore, for isomers with an eclipsed conformation of substituents (pseudo-geminal isomers, **2a** and **2b**), the olefinic signals are slightly shifted downfield (by ca. 0.1 ppm) while the aromatic signals are shifted upfield (by ca. 0.35 ppm) compared to the isomers with a staggered conformation (pseudo-*ortho* isomers). These findings are fully supported by DFT calculations reporting that the CS (chemical shift) mean value of olefinic protons is roughly by 0.2 ppm lower for the staggered isomers (**2c** and **2d**) and at the same time the CS mean value of aromatic protons is by 0.4 ppm higher than it is in the corresponding eclipsed conformers (**2a** and **2b**). In addition, the calculated values accord very well with the experimental values. The downfield shift of the aromatic protons in both pseudo-*ortho* isomers (**2c** and **2d**) compared to the pseudo-geminal isomers (**2a** and **2b**) can be attributed to the fact that the surrounding of those aromatic protons is of more electron-accepting nature (due to the oxygen atoms, which appear to be located directly on top of the respective aromatic protons and are, therefore, close enough to cause a small deshielding (by 0.3 - 0.4 ppm) of the aromatic protons.

For a relation of the crystal structure with NMR spectroscopy a solid state ^{1}H-NMR (ssNMR) spectrum of isomer **2a** was collected (see **Figures S14** and **S15**). In the ssNMR, the olefinic hydrogens are upfield shifted by ca. 0.37 ppm compared to the solution NMR spectrum and resonate at about 6.57 ppm. This upfield shift in the solid state can be understood by taking the packing in the solid state into account. The olefinic hydrogens are located above the adjacent aromatic ring in a distance of approximately 2.87 Å (see **Figure S19**). This causes the observed shielding effect of the olefinic protons in the ssNMR compared to the soluation NMR spectrum (further details concerning the ssNMR can be found in the supporting information).

Moreover, the FTIR spectra (see **Figure S20**) depict two pairs of patterns as well. While isomers **2c** and **2d** show two additional bands at 1379 cm^{-1} and 1331 cm^{-1}, these bands are absent in isomers **2a** and **2b**. Summarizing the experimental and calculated data leads to the assignment shown in **Figure 21**.

For the investigation of the varying tendencies to undergo ROMP, we carried out studies combining various metathesis catalysts with all four isomers. On the one hand we used the commercially available catalyst **4** (**Figure 22**), which is known to be stable even under harsh conditions such as high temperatures.[13,28] On the other hand we used catalyst **6** which is known to be fast initiating and, thus, enables living controlled polymerization. In addition, it can easily be synthesized from commercially available Grubbs 2nd Gen. catalyst.[20,29]

Furthermore, highly reactive catalysts **3**, **5** and **7** were synthesized and they were expected to show an improved ROMP activity for the sterically hindered isomers due to the sterically less demanding NHC-ligand.[19,21]

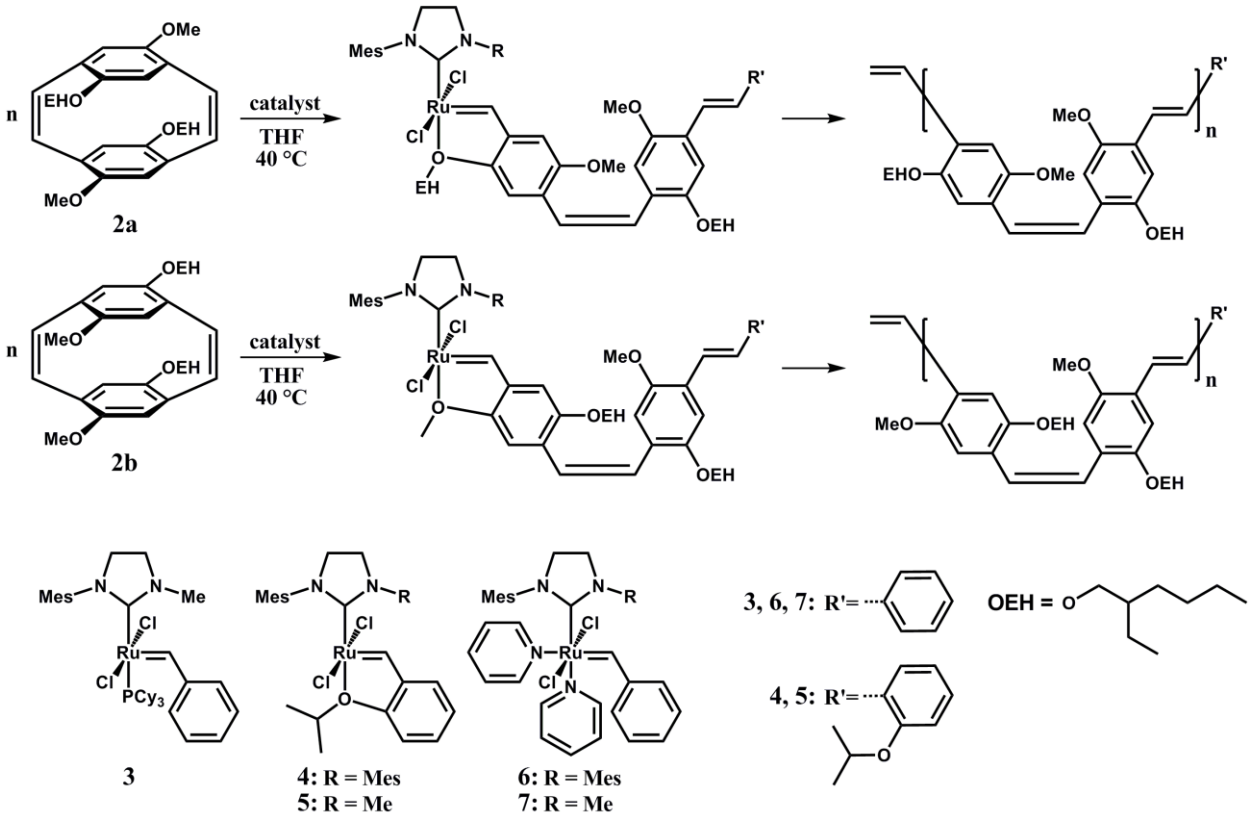

Figure 22. Polymerization of isomers **2a** and **2b** depicting coordination of the monomer's aromatic ether to ruthenium after the first ring-opening step with the most probable coordination (**2a** = 2-ethylhexyloxy substituent, **2b** = methoxy substituent), the complete polymer structure after quenching with EVE and the structures of catalysts **3** - **7**.

Using the following equations we calculated the initiation and propagation rates of various catalyst/isomer combinations:

Initiation: $$R_i = -\frac{d[C]}{dt} = k_i\,[C] \quad (1)$$

Propagation: $$R_p = -\frac{d[M]}{dt} = k_p\,[M][C] \quad (2)$$

where R_i is the rate of initiation, k_i the initiation rate constant, [C] the catalyst concentration, R_p the rate of propagation, k_p the propagation rate constant, [M] the monomer concentration and t the time. Generally we performed all polymerization, if possible, at 40 °C. For the investigation of the initiation process, however, it was in some cases necessary to work at lower temperatures to adjust for the time resolution of NMR spectroscopy.

By monitoring the shift of the hydrogens attached to the carbene using ^{1}H-NMR spectroscopy, we plotted the initiation rates and calculated the initiation rate constants. Screening the different catalysts using isomer **2a** as monomer showed a comparatively large initiation rate constant in case of catalyst **6** (k_i = 0.2240 min^{-1}) and an even larger constant for catalyst **7** (k_i = 0.3670 min^{-1}). Initiation rates using catalyst **6** and **7** were recorded at 25 °C as initiation at 40 °C proceeded too quickly. Initiation with catalyst **3** was carried out at 25 °C due to its low stability at elevated temperature giving an initiation rate constant of k_i = 0.0063 min^{-1}. Catalyst **4** exhibited a similar initiation rate with k_i = 0.0059 min^{-1} at 40 °C, while in case of catalyst **5** a surprisingly small initiation rate constant of k_i = 0.0022 min^{-1} (at 40 °C) was determined (see **Table 1**, entry 1 - 5). In conclusion, the initiation kinetics agree with the expectation that Grubbs 3rd Gen. type catalysts would show fast initiation, while Grubbs 2nd Gen. and Hoveyda-Grubbs 2nd Gen. type catalyst would exhibit much slower initiation (see **Figure 23**).

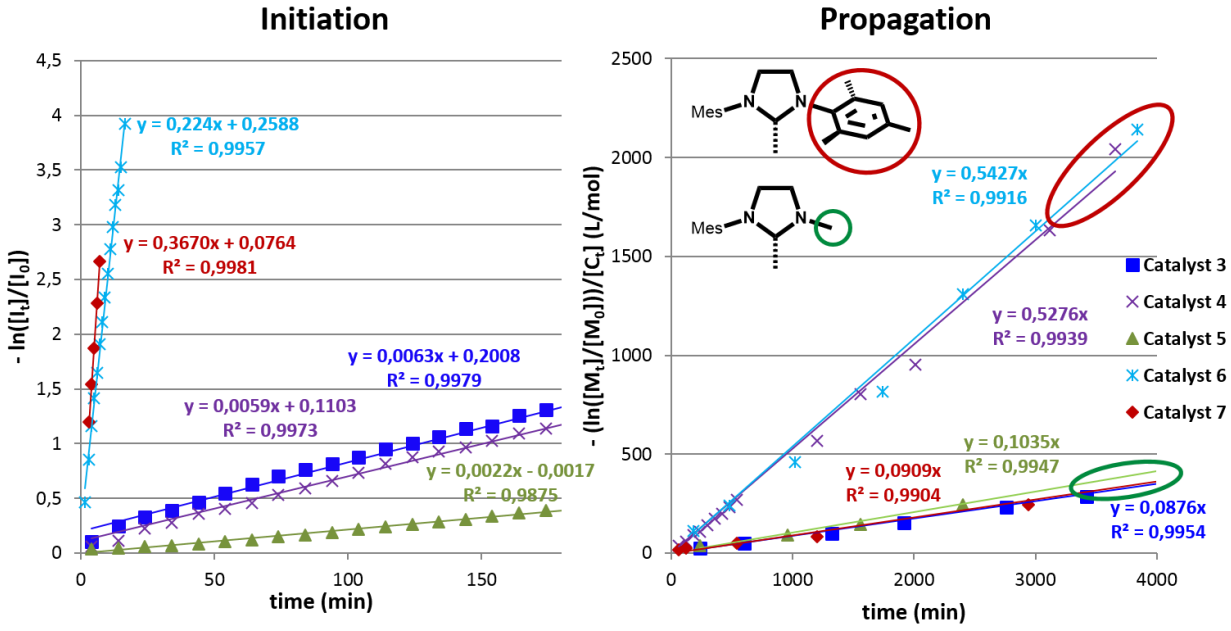

Figure 23. Initiation (left) and propagation (right) kinetics of isomer **2a** in combination with catalysts **3** - **7**. (propagation: **3** - **7** @ 40 °C; initiation: **3**, **6**, **7** @ 25 °C, **4**, **5** @ 40 °C). On the right graph the correlation of the propagation rate with the NHC-ligand is visualized.

While recording the initiation process, we observed that the carbene signals of initiated species could be divided into two groups. Catalysts bearing the sterically less demanding NHC ligand (catalysts **3**, **5** and **7**) exhibited carbene signals at around 15.64 and 15.72 ppm (in d_8-THF) with a ratio around 20:3, whereas catalysts **4** and **6** bearing SIMes ligand (1,3-bis(2,4,6-trimethylphenyl)dihydroimidazole) exhibited signals at 16.00 and 16.09 ppm (in d_8-THF) with a ratio around 20:5. The chemical shifts were observed in a typical range for Hoveyda-Grubbs (HG) type catalysts in d_8-THF (the small upfield shift compared to HG catalysts originates from the substituents on the aromatic ring).[30] Therefore, we assume a coordination of the oxygen of the aromatic ether on the monomer repeating unit to the ruthenium after initiation (see **Figure 24**).

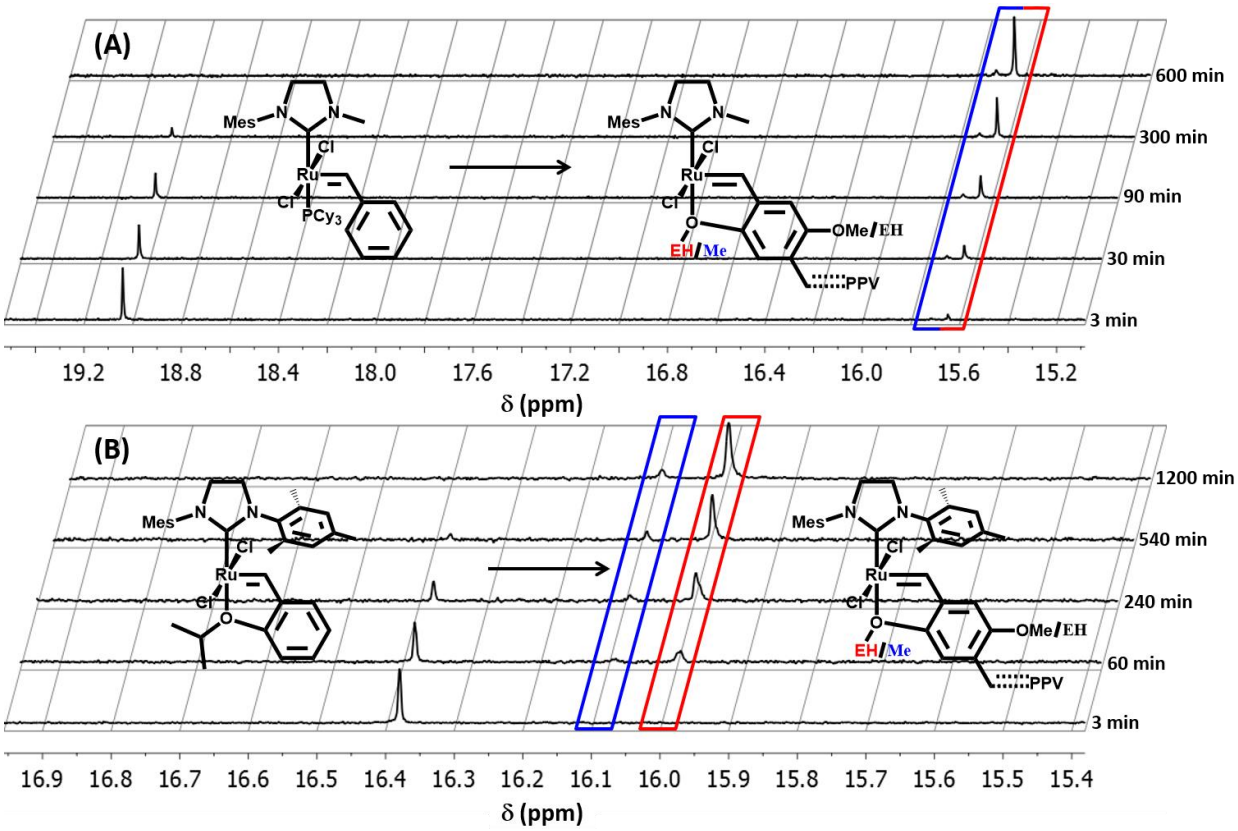

Figure 24. Representative ^{1}H-NMR spectra (in d_8-THF) monitoring the initation process via the carbene signals. The chemical shifts of the initiated species vary depending on the NHC ligand and the coordination of the aromatic ether (2-ethylhexyloxy or methoxy). (A) with catalyst **3** (bearing the sterically less demanding NHC ligand) and (B) with catalyst **4** (bearing SIMes ligand). (Spectra depicting the carbene signals for all initiated species using isomer **2a** are available in the supporting information **Figure S22**.)

Following the observations made for isomer **2b** (see below), the signal which is more downfield shifted can be assigned to a coordination of methoxy and the signal that is more upfield shifted can be understood as coordination of 2-ethylhexyloxy substituent's oxygen to ruthenium (see **Figure 24** and **S20**). This model of a coordinated monomer is supported by the propagation kinetics. Alongside with the unique ability of the monomer to coordinate to the ruthenium, comes the high stability which is typical for Hoveyda-Grubbs type catalysts and allows for the prolonged reaction times needed to collect the kinetic data. This becomes most obvious in case of catalyst **3** which is neither a fast initiating nor a very stable catalyst. Thus, during the first hour after addition of the catalyst's solution, 15.9 % of the catalyst decomposed while during the following six hours only 4.0 % decomposed. Most crucially, over a period of about two days after complete initiation only 3.0 % of further decomposition was observed.

For the determination of the propagation rate (k_p) we plotted - (ln([M_t]/[M_0]))/[C_t] vs time and calculated the catalyst's concentration for every data point to eliminate the effect of catalyst decomposition (results using the initial catalyst concentration to calculate k_p show similar trends and can be obtained from the supporting information **Figure S24**). All polymerizations using isomer **2a** were conducted at 40 °C. Propagation rates for catalyst **4** and **6** proved to be very similar with values of k_p = 0.5276 and 0.5427 L mol^{-1} min^{-1}, respectively. These values are almost equivalent within the experimental error (small deviations originate from slightly differing ratios between both coordinating substituents) and this result implies that the common propagating species as a result of the coordination of the aromatic ether to ruthenium (see **Figure 24**) prohibit a re-coordination of other ligands (such as pyridine or phosphine) until the dissociation of the ether. Same holds true for the catalysts **3**, **5** and **7** with k_p = 0.0876, 0.1035 and 0.0909 L mol^{-1} min^{-1}, respectively (see **Figure S22**). The coordination of the monomer repeating unit may be one reason for the generally slow polymerization of alkoxy substituted [2.2]paracyclophane-1,9-diene derivatives as Hoveyda-Grubbs type catalysts are known to exhibit relatively slow initiation. Notable are the significantly higher propagation rates for the catalysts bearing the SIMes ligand (k_p around 0.5 L mol^{-1} min^{-1}) when compared to the catalysts bearing the sterically less demanding ligand (k_p around 0.1 L mol^{-1} min^{-1}). This shows that the influence of the catalyst's electronic structure surpasses sterical aspects, contrarily to our initial rationale. Given that every polymerization step requires a "re-initiation step" of Hoveyda-Grubbs type catalysts (due to the coordination of the aromatic ether), we compared our findings with recent results of Engle *et al*. They reported a positive correlation of ln(k_i) with a downfield shift of the carbene proton in the ^{1}H-

NMR spectrum (equivalent to a weakening of the Ru-O bond).[31] In accordance with their results, catalysts **3**, **5** and **7** exhibiting the carbene signals around 15.64 and 15.72 ppm, showed slower polymerization compared to catalysts **4** and **6** (see **Figure 23**), which show signals around 16.00 and 16.09 ppm for the initiated species (in d_8-THF). Furthermore, the fact that sterical aspects are exceeded by electronic aspects might be a hint for a dissociative mechanism as the major pathway rather than an interchange or associative mechanism. The dissociative pathway suggests a bottom-bound transition state which would also imply that the steric effect imposed by the substituents on the NHC ligand has little influence. However, as the olefin approach towards the catalyst is not yet completely understood, it is still topic of ongoing studies and, thus, an affirmative statement cannot be made at this point.[31,32]

To complete the reactivity studies on isomer **2a** k_i/k_p ratios were calculated (see **Table 1**). Not surprisingly the largest ratios were obtained for catalysts **6** and **7** - 0.4128 and 4.0374 mol L^{-1}, respectively, which contain labile pyridine ligand. Furthermore, as mentioned before, initiation rates of catalysts **6** and **7** were collected at 25 °C while polymerization was carried out at 40 °C. This leads to the estimation that the actual k_i/k_p ratios are even higher than the ones reported in this paper. Catalysts **3**, **4** and **5** showed smaller k_i/k_p ratios with values of 0.0719, 0.0112 and 0.0213 mol L^{-1}, respectively. Due to the slow propagation rates, catalysts **3**, **5** and **7** suffered from a slow, yet, significant decomposition, whereas catalyst **4** and **6** showed comparably fast polymerization. Following these results, we decided to study combinations of the other isomers with catalysts **4**, **6** and **7**.

Table 1. Reaction details, initiation (k_i) and propagation rate constants (k_p) and k_i/k_p ratios for all catalyst/isomer combinations (molecular weights and PDIs of all polymers can be obtained from the supporting information **Table S1**).

Entry	Isomer	Catalyst	k_i (min^{-1})	k_p (L mol^{-1} min^{-1})	k_i/k_p (mol L^{-1})
1[b)]	2a	3	0.0063	0.0876	0.0719
2[a)]	2a	4	0.0059	0.5276	0.0112
3[a)]	2a	5	0.0022	0.1035	0.0213
4[b)]	2a	6	0.2240	0.5427	0.4128
5[b)]	2a	7	0.3670	0.0909	4.0374
6[a)]	2b	4	0.0055	0.4153	0.0132
7[b)]	2b	6	0.2461	0.4745	0.5187
8[b)]	2b	7	0.7494	0.2066	3.6273
9[c)]	2c	4	0.0004	0.1644	0.0026

[a)] T = 313 K, [b)] k_i measured at 298 K and k_p at 313 K, [c)] T = 384 K.

Isomer **2b** was expected to have a slightly higher reactivity compared to isomer **2a**. This prediction is based on the more favorable approach of the monomer to the catalyst via the side exhibiting two less sterically demanding methoxy substituents. Yet, a similar initiation rate of k_i = 0.0055 min^{-1} was found using catalyst **4** (compared to k_i = 0.0059 min^{-1} in case of isomer **2a**), whereas the propagation rate showed an even slightly lower value of k_p = 0.4153 L mol^{-1} min^{-1} compared to that of isomer **2a** (k_p = 0.5276 L mol^{-1} min^{-1}). Catalyst **6**, as expected, showed a faster initiation rate (k_i = 0.2461 min^{-1}) whereas its propagation rate (k_p = 0.4745 L mol^{-1} min^{-1}) is comparable to that of catalyst **4** (see **Figure S25**). However, the deviation in propagation rates comparing catalysts **4** and **6** is larger than for isomer **2a**. The observed deviation can be understood by comparing the ratio of propagating carbene species (coordination of methoxy or 2-ethylhexyloxy substituent). The ratio of the propagating carbene signals is very similar for catalysts **4** and **6** when using isomer **2a**, whereas the ratio proved to be very different for isomer **2b** (see **Figure S23**). In the reaction with catalyst **6** two overlapping signals with very similar chemical shifts occur. Both signals most probably originate from coordination of the methoxy substituent's oxygen, as for methoxy substituted catalysts a multiple carbene signal was reported in literature.[31,33] Furthermore, the integrals'

ratio of hydrogens attached to oxygen located next to a *trans* double bond compared to those located next to a *cis* double bond is 6:4 for the polymer obtained from isomer **2b**. Therefore, the estimated *trans* to *cis* ratio of 1:1 implies a location solely of methoxy substitutens in proximity to *trans* configurated double bonds (six hydrogens) and 2-ethyl-hexyloxy substituents in proximity to *cis* configurated double bonds (four hydrogens from O-CH_2-R) for the polymer obtained from isomer **2b** (see **Figure 25**). In contrast, when polymerizing isomer **2a** a ratio of 5:5 is obtained for the hydrogens attached to oxygen located next to a *trans* and a *cis* double bond, respectively (see **Figure 25**). This 5:5 ratio implies the same environment for each double bond (*cis* and *trans*) with a location of one methoxy and one 2-ethyl-hexyloxy substituent in proximity to each double bond.[34] Therefore, a coordination of the methoxy substituent to ruthenium during the polymerization process can be concluded.

Furthermore, as solely the methoxy substituent coordinates to the catalyst (and thus solely methoxy substituents are located in proximity to *trans* configurated double bonds) the polymerization of isomer **2b** comes along with the synthesis of (*cis*-*trans*) MEH-PPV having head-to-head configuration of the substituents, while a head-to-tail configuration is the common case (see **Figure 25**).

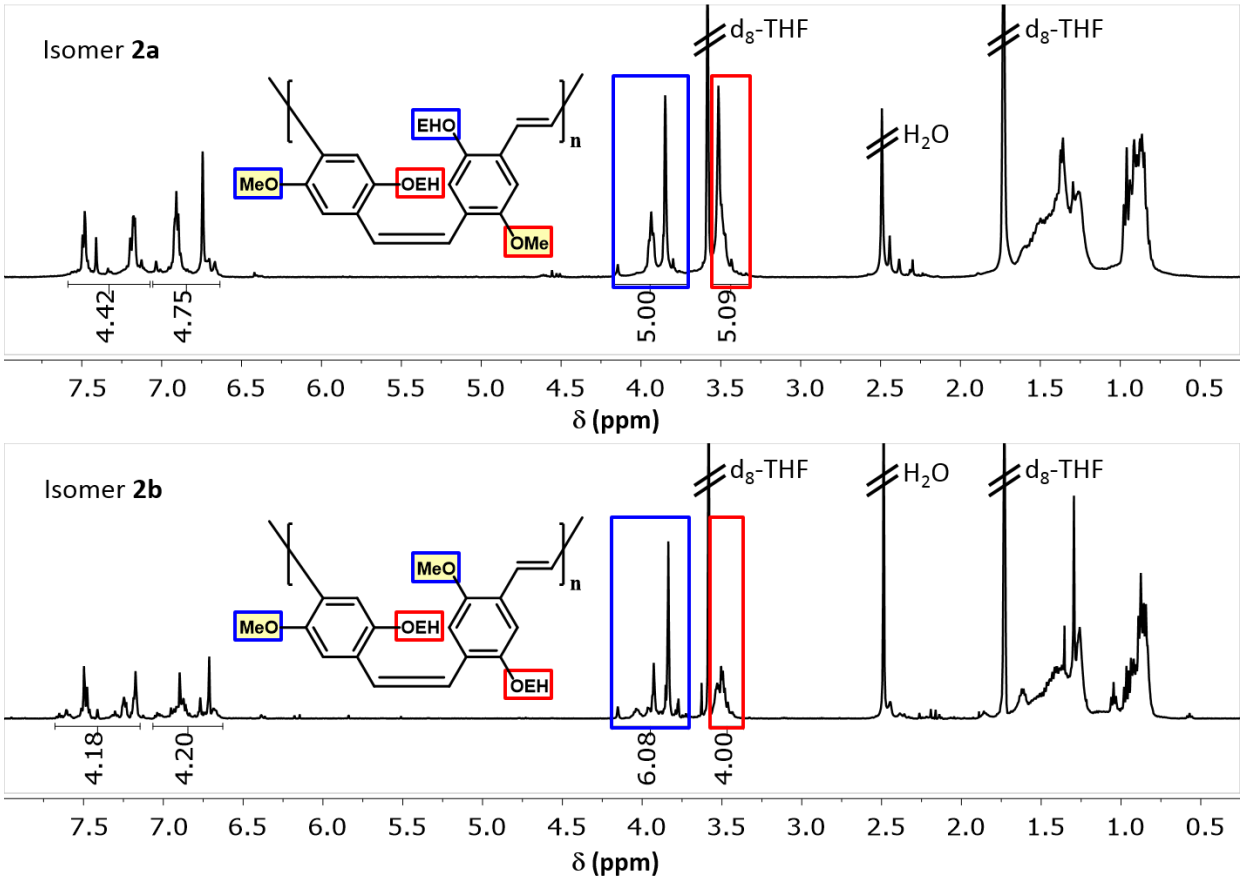

Figure 25. Representative ^{1}H-NMR spectra with highlighted comparison of O-CH_3 and O-CH_2- signals close to *trans* (≈ 3.71 – 4.18 ppm) and *cis* (≈ 3.32 – 3.56 ppm) double bonds. The ratios of 5:5 (isomer **2a**) and 6:4 (isomer **2b**) correspond to the displayed structures with either head-to-tail (isomer **2a**) or head-to-head (isomer **2b**) configuration of substituents on the aromatic rings. The integration of the aromatic and olefinic hydrogens proves that the *cis*-*trans* ratio is approximately 1:1 in both polymers.

In the reaction using catalyst **4,** an additional, upfield shifted signal occurs around 15.98 ppm, likely to originate from the coordination of the 2-ethylhexyloxy substituent (see **Figure S23**). This deviation in the ratio of carbene signals accompanies a different ratio of propagating species with coordinated oxygen of either the methoxy or the 2-ethylhexyloxy group. As the initiation rate of methoxy substituted Hoveyda-Grubbs catalysts was reported to be faster than its isopropoxy substituted counterpart, the slightly smaller propagation rate in case of catalyst **4** can be explained.[31,35] Catalyst **7** exhibited an even faster initiation rate than catalyst **6** with k_i = 0.7494 min^{-1} and, as expected, a slower propagation rate of k_p = 0.2066 L mol^{-1} min^{-1} (see **Figure S25**). In conclusion, the same trend of propagation rates comparing the catalysts (two different NHC ligands) was observed using isomer **2b** and isomer **2a**. For isomer **2b**, there is

a larger deviation in the propagation rates comparing catalyst **4** and **6**, which, however, can be understood by taking the chemical shifts and ratios of the propagating species into account. Furthermore, no clear trend comparing initiation and propagation rates of isomer **2a** and **2b** can be found. We conclude that although predicting the reactivity of both isomers is difficult, the estimation of initiation and especially propagation rates for various catalysts is working well for each isomer.

Thus far, literature reported that due to their sterics, pseudo-*ortho* isomers of tetraalkoxy-[2.2]paracyclophane-1,9-diene derivatives are not able to undergo ROMP.[11] In accordance with the literature findings, reaction of isomers **2c** and **2d** with catalysts **6** and **7** at 40 °C did not show any hints for ROMP to take place. Isomer **2d** did not polymerize even when harsh conditions with catalyst **4** in refluxing toluene were applied (**Figure 26**). By contrast, using catalyst **4** in refluxing toluene showed initiation of isomer **2c** (see **Table 1**) which was followed by a detection of the carbene signal in ^{1}H-NMR shifting from 16.59 ppm to 16.22 ppm and 16.19 ppm (in d_8-toluene). We assume that the catalyst approaches towards the smaller methoxy groups. Only this approach displays a sterical benefit when compared with an approach at any side of isomer **2d** which did not undergo ROMP (for a visualization see **Figure 26**). Therefore, after initiation of catalyst **4** coordination of the methoxy substituent would occur (see **Figure 26**) and this is supported by the splitting of the initiated carbene signal just as it is the case for isomer **2b**. In contrast to the polymerization with isomers **2a** and **2b**, the polymer obtained from isomer **2c** showed almost all *trans* configuration which is most likely caused by *in situ* isomerization due to the high reaction temperature (see **Figure S21**).

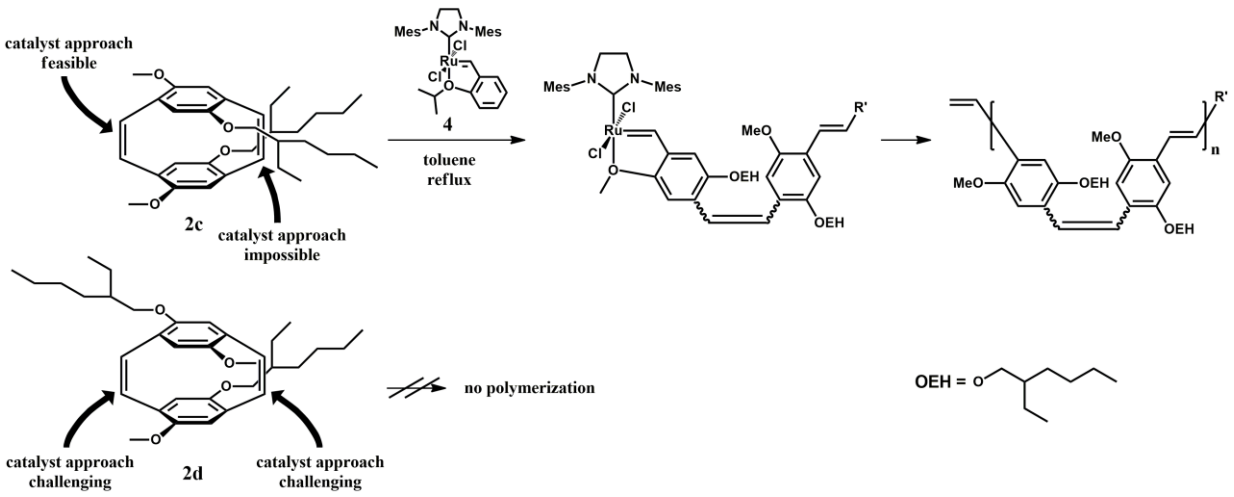

Figure 26. Polymerization of isomer **2c** illustrating the coordination of the monomer's aromatic ether to ruthenium after the first ring-opening step with the most probable coordination (methoxy) and the complete polymer structure after quenching with EVE. The arrows show the different possibilities for a catalyst approach and visualize the varying steric demands.

Summing up, 3rd Gen. Grubbs catalyst (catalyst **6**) proved to be the most suitable catalysts for polymerization of pseudo-geminal isomers. The catalyst provides fast initiation and offers a comparably high propagation rate which is why it does not suffer from slow decomposition. In addition, HG2 catalyst (**4**) proved to be a suitable catalyst. Once pseudo-*ortho* isomers shall be polymerized, harsh conditions become necessary and thus the high stability of HG2 catalyst (**4**) becomes mandatory.[36] In order to prove the quality of catalyst **6**, two polymers with higher DPs were synthesized. High molecular weight polymers are accessible only by using isomers **2a** and **2b** (only short polymers are obtained when isomer **2c** is used). Therefore, isomer **2a** was polymerized with catalyst **6** in a ratio of 20/1 and 40/1, respectively (see **Table S1**). As full conversion was reached the reaction was stopped by adding EVE. For purification the polymer was precipitated in methanol and redissolved in DCM (three times). The ^{1}H-NMR spectra of the purified polymers do not indicate any defects or any impurities such as low molecular weight side products (see **Figure S26**). In the ^{1}H-NMR spectrum of the polymer with DP ≈ 20 the vinyl end group can be detected which permits the inference that the catalyst was intact at the time of quenching (see inset **Figure S26**).

4. Conclusion

We have presented here a detailed study of the reactivity behavior regarding all structural isomers of dimethoxy-(2-ethylhexyloxy)-[2.2]paracyclophane-1,9-diene concerning ROMP. For this we investigated various metathesis catalysts and 3rd Gen. Grubbs catalyst (catalyst **6**) proved to be the most suitable catalysts for polymerization of pseudo-geminal isomers. Investigating the propagation process in detail, we observed a unique consistency of propagation rates with the catalysts' structure. Based on this we present a model of the active chain end, which is coordinated to the catalyst via the aromatic ether of the monomer repeating unit. Thus, every polymerization step requires a "re-initiation step" of Hoveyda-Grubbs type catalysts which is one aspect explaining the generally slow polymerization of alkoxy substituted [2.2]paracyclophane-1,9-dienes. A benefit of this catalyst coordinated structure (see **Figure 24**) is, however, the improvement of the catalyst stability. Therefore, the introduction of aromatic ethers should be applied especially to monomers of low reactivity to obtain a long living catalyst species and enable polymerization even under harsh conditions. Following this concept, we were able to polymerize one of the low reactive pseudo-*ortho* isomers (**2c**) in refluxing toluene which demonstrates the improved stability. On the one hand the necessity of harsh conditions for the polymerization of isomer **2c** illustrates the strong influence of sterics and the small tolerance for substituents on the side of the catalyst's approach. On the other hand only a relatively small energy barrier has to be overcome to enable ROMP. Therefore, presumably more reactive catalysts with sterically less demanding substituents as well as more stable catalysts might enable sufficient initiation using pseudo-*ortho* isomers.

Furthermore, the study at hand demonstrates the general possibility to control the configuration of asymmetric substituted PPVs via ROMP. While polymerization of isomer **2a** yields MEH-PPV with head-to-tail configuration, polymerization of isomer **2b** results in MEH-PPV exhibiting head-to-head configuration. The precise control over the polymer backbone is of great importance regarding rigidity of the polymer backbone and molecular packing. Therefore, the control over the polymer backbone is crucial in terms of film architecture and the performance of optoelectronic devices.

Overall, this study provides insights into the ring-opening metathesis polymerization of tetraalkoxy-[2.2]paracyclophane-1,9-diene derivatives which will help to optimize reaction conditions for future studies. A detailed understanding of the polymerization process is

important as aspects such as the coordination of the aromatic ether of the monomer repeating unit need to be considered. The incorporation of an aromatic ether should generally decrease the propagation rate. A decreased propagation rate might be negative, but it might also be desired, for example when two reactions are supposed to proceed one after another as in a one-shot procedure.[16c] The increased stability caused by the coordination of the aromatic ether to the catalyst can also be a desirable aspect once harsh conditions or high temperatures are needed. One example would be the synthesis of a polymer with an upper critical solution temperature (UCST) has to be respected.

ASSOCIATED CONTENT

Supporting Information

Experimental details, solid-state and solution NMR spectra as well as UV/Vis and FTIR spectra. This material is available free of charge via the Internet at http://pubs.acs.org.

AUTHOR INFORMATION

Corresponding Author

* E-mail: zentel@uni-mainz.de (R. Zentel)

E-mail: tlc@snu.ac.kr (T.-L. Choi)

ACKNOWLEDGMENT

The authors gratefully thank the Deutsche Forschungsgemeinschaft (DFG): International Research Training Group (IRTG) 1404 “Self-Organized Materials for Optoelectronics” as well as the Basic Science Research and Nano-Material Technology Development through NRF of Korea for funding.

ABBREVIATIONS

CS, chemical shift; DCM, dichloromethane; EVE, ethyl vinyl ether; FTIR, Fourier transform infrared; Mes, mesitylene; MSP, mean square plane; NMR, nuclear magnetic resonance; OEH, 2-ethylhexyloxy; MEH-PPV, poly[2-methoxy-5-(2-ethylhexyloxy)-1,4-phenylene vinylene]; MeO, methoxy; M_n, number average molar mass; PDI, polydispersity index; PPV, poly(*p*-phenylene vinylene); ROMP, ring-opening metathesis polymerization

Received: August 5, 2015; Revised: October 3, 2015; Published: October 13, 2015; DOI: 10.1021/acs.macromol.5b01737

KEYWORDS

kinetics, light-emitting diodes (LED), living polymerization, poly(p-phenylene vinylene) (PPV), ring-opening metathesis polymerization (ROMP)

References

(1) Tang, C. W.; VanSlyke, S. A. *Appl. Phys. Lett.* **1987**, *51*, 913.

(2) a) Mathias, F.; Fokina, A.; Landfester, K.; Tremel, W.; Schmid, F.; Char, K.; Zentel, R. *Macromol. Rapid Commun.* **2015**, *36*, 959–983; b) Burroughes, J. H.; Bradley, D. D. C.; Brown, A. R.; Marks, R. N.; Mackay, K.; Friend, R. H.; Burn, P. L.; Holmes, A. B. *Nature* **1990**, *347*, 539; c) Parker, I. D.; Gymer, R. W.; Harrison, M. G.; Friend, R. H.; Ahmed, H. *Appl. Phys. Lett.* **1993**, *62*, 1519; d) Koynov, K.; Bahtiar, A.; Ahn, T.; Cordeiro, R. M.; Hörhold, H.-H.; Bubeck, C. *Macromolecules* **2006**, *39*, 8692–8698.

(3) Sariciftci, N. S.; Smilowitz, L.; Heeger, A. J.; Wudl, F. *Science* **1992**, *258*, 1474–1476.

(4) Moses, D. *Appl. Phys. Lett.* **1992**, *60*, 3215.

(5) Gilch, H. G.; Wheelwright, W. L. *J. Polym. Sci. A-1 Polym. Chem.* **1966**, *4*, 1337–1349.

(6) a) Siegrist, A. E. *Helv. Chim. Acta* **1981**, *64*, 662–680; b) Kretzschmann, H.; Meier, H. *Tetrahedron Letters* **1991**, *32*, 5059–5062; c) Zur Borg, L.; Domanski, A. L.; Berger, R.; Zentel, R. *Macromol. Chem. Phys.* **2013**, *214*, 975–984; d) Zur Borg, L.; Schüll, C.; Frey, H.; Zentel, R. *Macromol. Rapid Commun.* **2013**, *34*, 1213–1219.

(7) Yu, C.-Y.; Turner, M. L. *Angew. Chem. Int. Ed.* **2006**, *45*, 7797–7800.

(8) Lidster, B. J.; Behrendt, J. M.; Turner, M. L. *Chem. Commun.* **2014**, *50*, 11867–11870.

(9) Yu, C.-Y.; Kingsley, J. W.; Lidzey, D. G.; Turner, M. L. *Macromol. Rapid Commun.* **2009**, *30*, 1889–1892.

(10) Yu, C.-Y.; Horie, M.; Spring, A. M.; Tremel, K.; Turner, M. L. *Macromolecules* **2010**, *43*, 222–232.

(11) Yu, C.-Y.; Helliwell, M.; Raftery, J.; Turner, M. L. *Chem. Eur. J.* **2011**, *17*, 6991–6997.

(12) a) Spring, A. M.; Yu, C.-Y.; Horie, M.; Turner, M. L. *Chem. Commun.* **2009**, 2676; b) Andrew Mark Spring. Preparation of Soluble Poly(phenylenevinylenes) by Ring Opening Metathesis Polymerisation. PhD Thesis, The University of Manchester, Manchester, UK, 2010; c) Mäker, D.; Bunz, U. H. F. *Macromol. Rapid Commun.* **2014**, *35*, 2096–2100; d) Horie, M.; Shen, I.-W.; Tuladhar, S. M.; Leventis, H.; Haque, S. A.; Nelson, J.; Saunders, B. R.; Turner, M. L. *Polymer* **2010**, *51*, 1541–1547.

(13) Mäker, D.; Maier, C.; Brödner, K.; Bunz, U. H. F. *ACS Macro Lett.* **2014**, *3*, 415–418.

(14) a) Wudl, F.; Allemand, P.-M.; Srdanov, G.; Ni, Z.; McBranch, D. Polymers and an Unusual Molecular Crystal with Nonlinear Optical Properties. In *Materials for Nonlinear Optics*; Marder, S. R., Sohn, J. E., Stucky, G. D., Eds.; ACS Symposium Series; American Chemical Society: Washington, DC, 1991; pp 683–686; b) *Organic light-emitting materials and devices;* Meng, H., Li, Z. R., Eds.; Optical science and engineering 111; CRC/Taylor & Francis: Boca Raton, 2007.

(15) Elacqua, E.; Weck, M. *Chem. Eur. J.* **2015**, *21*, 7151–7158.

(16) a) Lohwasser, R. H.; Thelakkat, M. *Macromolecules* **2012**, *45*, 3070–3077; b) Yoon, K.-Y.; Lee, I.-H.; Kim, K. O.; Jang, J.; Lee, E.; Choi, T.-L. *J. Am. Chem. Soc.* **2012**, *134*, 14291–14294; c) Shin, S.; Yoon, K.-Y.; Choi, T.-L. *Macromolecules* **2015**, *48*, 1390–1397; d) Mathias, F.; Tahir, M. N.; Tremel, W.; Zentel, R. *Macromol. Chem. Phys.* **2014**, *215*, 604–613; e) Palaniappan, K.; Hundt, N.; Sista, P.; Nguyen, H.; Hao, J.; Bhatt, M. P.; Han, Y.-Y.; Schmiedel, E. A.; Sheina, E. E.; Biewer, M. C.; Stefan, M. C. *J. Polym. Sci. A Polym. Chem.* **2011**, *49*, 1802–1808.

(17) Neef, C. J.; Ferraris, J. P. *Macromolecules* **2000**, *33*, 2311–2314.

(18) Mitchell, R. H.; Boekelheide, V. *J. Am. Chem. Soc.* **1974**, *96*, 1547–1557.

(19) Vehlow, K.; Maechling, S.; Blechert, S. *Organometallics* **2006**, *25*, 25–28.

(20) Sanford, M. S.; Love, J. A.; Grubbs, R. H. *Organometallics* **2001**, *20*, 5314–5318.

(21) Lichtenheldt, M.; Wang, D.; Vehlow, K.; Reinhardt, I.; Kühnel, C.; Decker, U.; Blechert, S.; Buchmeiser, M. R. *Chem. Eur. J.* **2009**, *15*, 9451–9457.

(22) a) Clark, S. J.; Segall, M. D.; Pickard, C. J.; Hasnip, P. J.; Probert, M. I. J.; Refson, K.; Payne, M. C. *Zeitschrift für Kristallographie* **2005**, *220*; b) Vanderbilt, D. *Phys. Rev. B* **1990**, *41*, 7892–7895.

(23) a) Perdew, J. P.; Burke, K.; Ernzerhof, M. *Phys. Rev. Lett.* **1996**, *77*, 3865–3868; b) Tkatchenko, A.; Scheffler, M. *Phys. Rev. Lett.* **2009**, *102*; c) Grimme, S. *J. Comput. Chem.* **2006**, *27*, 1787–1799.

(24) Dudenko, D. V.; Yates, J. R.; Harris, K. D. M.; Brown, S. P. *CrystEngComm* **2013**, *15*, 8797.

(25) a) Pickard, C. J.; Mauri, F. *Phys. Rev. B* **2001**, *63*; b) Yates, J. R.; Pickard, C. J.; Mauri, F. *Phys. Rev. B* **2007**, *76*; c) Harris, R. K.; Hodgkinson, P.; Pickard, C. J.; Yates, J. R.; Zorin, V. *Magn. Reson. Chem.* **2007**, *45*, S174-S186.

(26) Braun, D.; Heeger, A. J. *Appl. Phys. Lett.* **1991**, *58*, 1982.

(27) Stöbbe, M.; Reiser, O.; Näder, R.; Meijere, A. de. *Chem. Ber.* **1987**, *120*, 1667–1674.

(28) Hong, S. H.; Wenzel, A. G.; Salguero, T. T.; Day, M. W.; Grubbs, R. H. *J. Am. Chem. Soc.* **2007**, *129*, 7961–7968.

(29) a) Love, J. A.; Morgan, J. P.; Trnka, T. M.; Grubbs, R. H. *Angew. Chem. Int. Ed.* **2002**, *41*, 4035–4037; b) Choi, T.-L.; Grubbs, R. H. *Angew. Chem. Int. Ed.* **2003**, *42*, 1743–1746.

(30) Tanaka, K.; Böhm, V. P. W.; Chadwick, D.; Roeper, M.; Braddock, D. C. *Organometallics* **2006**, *25*, 5696–5698.

(31) Engle, K. M.; Lu, G.; Luo, S.-X.; Henling, L. M.; Takase, M. K.; Liu, P.; Houk, K. N.; Grubbs, R. H. *J. Am. Chem. Soc.* **2015**, *137*, 5782–5792.

(32) Nelson, D. J.; Manzini, S.; Urbina-Blanco, C. A.; Nolan, S. P. *Chem. Commun. (Camb.)* **2014**, *50*, 10355–10375.

(33) Kos, P.; Savka, R.; Plenio, H. *Adv. Synth. Catal.* **2013**, *355*, 439–447.

(34) Spring, A. M.; Yu, C.-Y.; Horie, M.; Turner, M. L. *Chem. Commun.* **2009**, 2676.

(35) Thiel, V.; Hendann, M.; Wannowius, K.-J.; Plenio, H. *J. Am. Chem. Soc.* **2012**, *134*, 1104–1114.

(36) Kim, K. O.; Choi, T.-L. *ACS Macro Lett.* **2012**, *1*, 445–448.

Supporting Information

Reactivity Studies of Alkoxy Substituted [2.2]Paracyclophane-1,9-dienes and Specific Coordination of the Monomer Repeating Unit during ROMP

Florian Menk, Mihail Mondeshki, Dmytro Dudenko, Suyong Shin, Dieter Schollmeyer, Oliver Ceyhun, Tae-Lim Choi*, Rudolf Zentel*

zentel@uni-mainz.de (R. Zentel)
tlc@snu.ac.kr (T.-L. Choi)

Monomer Synthesis

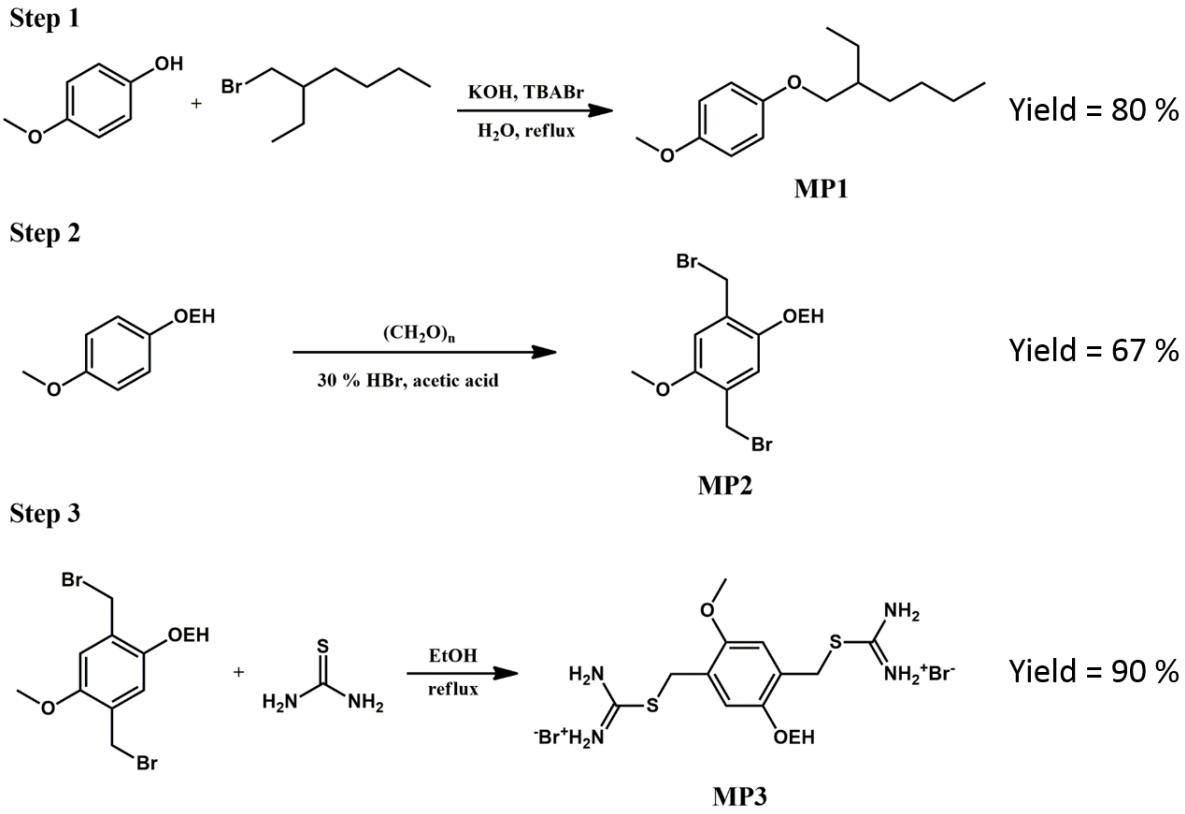

Figure S27. Synthesis of the monomer precursors **MP1** to **MP3**.

Synthesis of Monomer Precursor MP1 (Step 1). 1-((2-ethylhexyl)oxy)-4-methoxybenzene (**MP1**) was synthesized according to a modified literature procedure.[S1] 4-methoxyphenol (87.3 g, 703 mmol, 1.00 eq.), potassium hydroxide (48.5 g, 865 mmol, 1.23 eq.) and tetra-*n*-butylammonium bromide (47.6 g, 148 mmol, 0.21 eq.) were added to a round bottom flask. An argon atmosphere was established and 300 mL of water were added. After addition of 2-ethylhexyl bromide (134.4 g, 696 mmol, 0.99 eq.) the reaction mixture was refluxed for 90 h. The reaction mixture was cooled down to room temperature and extracted three times with 100 mL of diethyl ether. The organic layer was dried over $MgSO_4$, filtered and the diethyl ether was removed under reduced pressure. Further purification by distillation (bp. = 98 – 103 °C, $p \approx 1.0 \cdot 10^{-3}$ mbar) afforded the pure product in 80 % yield (130.8 g, 553 mmol).
^{1}H-NMR (400 MHz, $CDCl_3$, δ): 6.84 (s, 4H, Ar); 3.80 (d, J = 5.8 Hz, 2H, OCH_2-); 3.78 (s, 3H, OCH_3); 1.71 (hept., J = 6.0 Hz, 1H, CH); 1.31 – 1.57 (m, 8H, CH_2); 0.90 – 0.95 (m, 6H, CH_3). ^{13}C-NMR (101 MHz, $CDCl_3$, δ): 153.78; 153.71; 115.54; 114.71; 71.31; 55.86; 39.59; 30.66; 29.23; 23.98; 23.21; 14.23; 11.24.

Synthesis of Monomer Precursor MP2 (Step 2). α,α'-dibromo-2-methoxy-5-(2-ethylhexyl-oxy)-*p*-xylene (**MP2**) was synthesized via bromomethylation of **MP1** following a modified literature procedure.[S1] The reaction flask was equipped with 129.0 g (546 mmol, 1.00 eq.) of 1-((2-ethylhexyl)oxy)-4-methoxybenzene (**MP1**), 86.5 g of paraformaldehyde (2.60 mol of formaldehyde, 4.76 eq.), 260 mL of acetic acid and 260 mL of 30% HBr in acetic acid. An argon atmosphere was established and the reaction mixture was stirred at 70 °C for 4 h. Upon cooling to room temperature a colorless solid precipitated. The whole reaction mixture was dissolved in 600 mL of chloroform and a dark orange solution was obtained. The reaction mixture was washed twice with 400 mL of water and once with a solution of 28 g $NaHCO_3$ in 500 mL of water. The organic layer was dried over $MgSO_4$, filtered and the chloroform was removed under reduced pressure. After further purification by recrystallization from *n*-hexane (three times), the pure product was obtained in 67 % yield (145.1 g, 344 mmol) as a colorless solid.

^{1}H-NMR (400 MHz, $CDCl_3$, δ): 6.87 (s, 1H, CH_3O-Ar-H); 6.86 (s, 1H, EHO-Ar-H); 4.53 (s, 4H, CH_2-Br); 3.88 (d, J = 5.4 Hz, 2H, OCH_2-); 3.86 (s, 3H, OCH_3); 1.76 (hept., J = 6.3 Hz, 1H, CH); 1.30 – 1.61 (m, 8H, CH_2); 0.90 – 0.97 (m, 6H, CH_3). ^{13}C-NMR (101 MHz, $CDCl_3$, δ): 151.13; 151.09; 127.59; 127.44; 114.41; 113.89; 71.05; 56.39; 39.73; 30.77; 29.25; 28.86; 28.79; 24.16; 23.20; 14.25; 11.40.

Synthesis of Monomer Precursor MP3 (Step 3). 1,4-di(isothiouronium-methyl)-2-methoxy-5-(2-ethylhexyloxy) benzene (**MP3**) was synthesized following a modified literature procedure.[S2] Thiourea (45.0 g, 592 mmol, 2.0 eq.) was dissolved in 600 mL of hot ethanol (75 °C). 124.9 g (296 mmol, 1.0 eq.) α,α'-dibromo-2-methoxy-5-(2-ethylhexyloxy)-*p*-xylene (**MP2**) were then carefully added to the reaction mixture in small portions. After complete addition of **MP2**, the reaction mixture was heated for further 1.5 h. Then, approximately ¾ of the ethanol was removed under reduced pressure and after cooling the product was afforded in 90 % yield (153.4 g, 267 mmol) as a colorless solid.

^{1}H-NMR (400 MHz, DMSO-d_6, δ): 9.17 (bs, 4H); 9.04 (bs, 4H); 7.22 (s, 1H, CH_3O-Ar-H); 7.21 (s, 1H, EHO-Ar-H); 4.38 (s, 4H, CH_2-S-); 3.84 (d, J = 5.5 Hz, 2H, OCH_2-); 3.78 (s, 3H, OCH_3); 1.69 (hept., J = 6.0 Hz, 1H, CH); 1.27 – 1.53 (m, 8H, CH_2); 0.86 – 0.92 (m, 6H, CH_3). ^{13}C-NMR (101 MHz, DMSO-d_6, δ): 169.80; 169.58; 150.75; 150.42; 123.40; 122.95; 114.67; 114.09; 70.69; 56.25; 38.82; 30.22; 30.13; 29.99; 28.50; 23.39; 22.52; 14.00; 11.05.

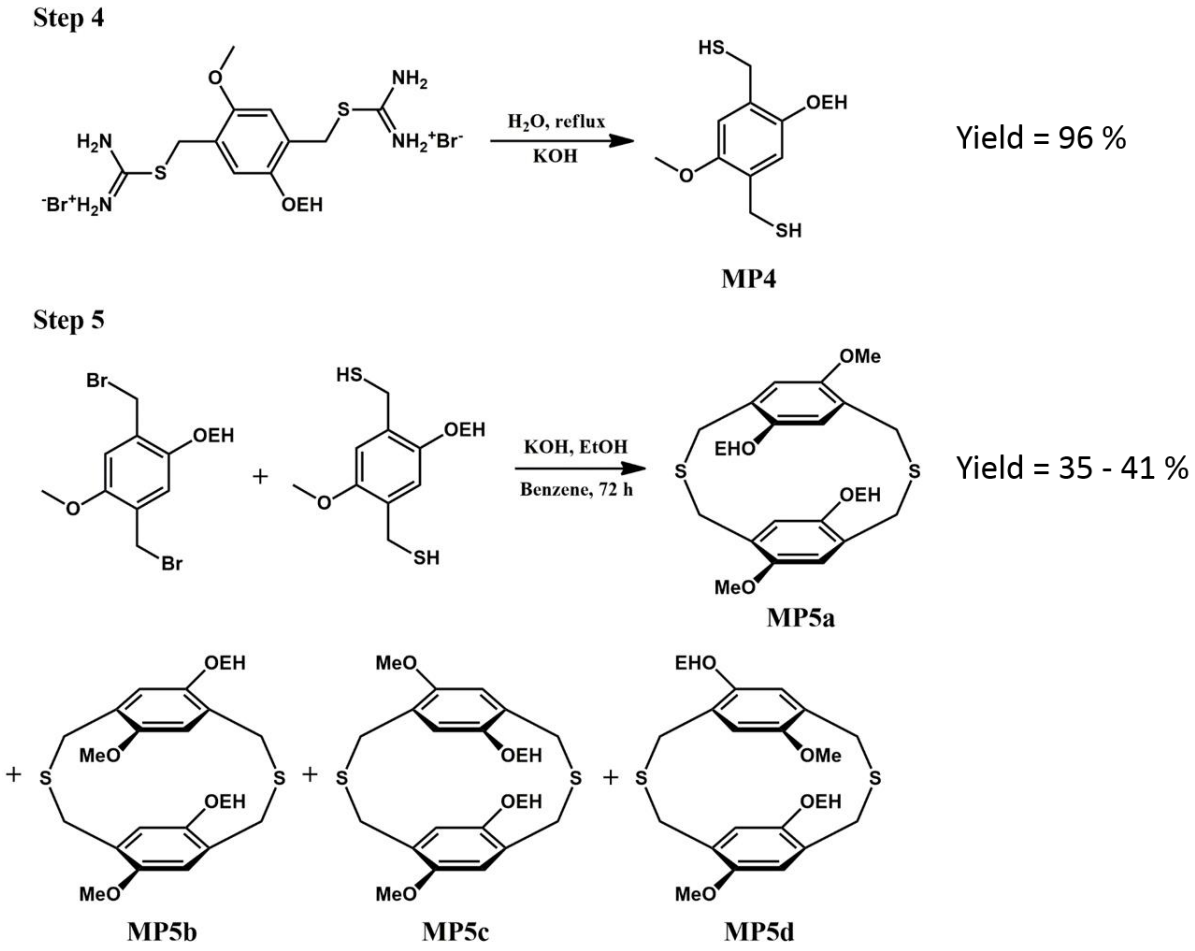

Figure S28. Synthesis of monomer precursors **MP4** and **MP5a-d**.

Synthesis of Monomer Precursor MP4 (Step 4). 1,4-di(mercaptomethyl)-2-methoxy-5-(2-ethylhexyloxy) benzene (**MP4**) was synthesized by hydrolysis of **MP3** according to a modified literature procedure.[S2] 114.0 g (198 mmol, 1 eq.) of 1,4-di(isothiouronium-methyl)-2-methoxy-5-(2-ethylhexyloxy) benzene (**MP3**) and 346.3 g (6.17 mol, 31 eq.) of potassium hydroxide were dissolved in 940 mL of water. The reaction mixture was heated to reflux for 6 h. Then, 400 mL of 9 M H_2SO_4 (aq.) were slowly added to the reaction mixture under rigorous stirring and cooling. The reaction mixture was extracted three times with ether. The combined organic phases were washed with water, dried over $MgSO_4$, filtered and the ether was removed under reduced pressure. The product was obtained as a pale yellow semi-solid in 96 % yield (62.6 g, 191 mmol).

^{1}H-NMR (400 MHz, $CDCl_3$, δ): 6.80 (s, 1H, CH_3O-Ar-H); 6.79 (s, 1H, EHO-Ar-H); 3.86 (d, J = 5.4 Hz, 2H, OCH_2-); 3.84 (s, 3H, OCH_3); 3.70 (d, J = 7.7 Hz, 4H, CH_2-SH); 1.95 (t, J = 8.0 Hz, 1H, SH); 1.94 (t, J = 7.9 Hz, 1H, SH); 1.74 (hept., J = 6.3 Hz, 1H, CH); 1.28 – 1.59 (m,

8H, CH_2); 0.89 – 0.97 (m, 6H, CH_3). ^{13}C-NMR (101 MHz, $CDCl_3$, δ): 150.60; 150.46; 129.40; 129.17; 113.11; 112.54; 70.87; 56.23; 39.81; 30.89; 29.28; 24.28; 24.18; 24.06; 23.22; 14.25; 11.41.

Synthesis of Monomer Precursor MP5 (Step 5). Coupling of compounds **MP2** and **MP4** was carried out following a modified literature procedure to obtain the mixture of isomers of the corresponding tetraalkoxy-2,11-dithia[3.3]paracyclophane.[S3] A degassed solution of 11.82 g (28.00 mmol, 1.00 eq.) of α,α'-dibromo-2-methoxy-5-(2-ethylhexyloxy)-*p*-xylene (**MP2**) and 9.20 g (28.00 mmol, 1.00 eq.) of 1,4-di(mercaptomethyl)-2-methoxy-5-(2-ethylhexyloxy) benzene (**MP4**) in 600 mL of benzene was slowly added (over a period of 90 h) to a degassed solution of 3.93 g (70.00 mmol, 2.50 eq.) of potassium hydroxide in 900 mL of ethanol. After complete addition the reaction mixture was stirred for further 6 h. The organic solvents were removed under reduced pressure and the resulting residue was dissolved in DCM. The solution was washed twice with 1.2 M HCl (aq.) and once with water, dried over $MgSO_4$, filtered and the organic solvent was removed under reduced pressure. The crude product was purified by column chromatography using a gradient eluent system of DCM/*n*-hexane, 1/3 to 2/3 – R_f (**MP5a**) ≈ 0.29 (DCM/*n*-hexane 1/3), R_f (**MP5d**) ≈ 0.51 (DCM/*n*-hexane 2/3), R_f (**MP5b**) ≈ 0.42 (DCM/*n*-hexane 2/3), R_f (**MP5c**) ≈ 0.30 (DCM/*n*-hexane 2/3).

Note: We separated all individual isomers in hope to simplify the purification of the final product. Unfortunately, we had to recognize that starting from a pure isomer of compound **MP5** leads to a mixture of two isomers of the final product. This can most probably be explained with a ring-opening during the Stevens rearrangement (step 6) which enables rotation of the aromatic rings.

Isomer MP5a. ^{1}H-NMR (400 MHz, $CDCl_3$, δ): 6.59 (s, 2H, CH_3O-Ar-H); 6.58 (s, 2H, EHO-Ar-H); 4.46 (d, J = 15.6 Hz, 2H, S-CH_2-); 4.45 (d, J = 14.6 Hz, 2H, S-CH_2-); 3.76 – 3.80 (m, 2H, OCH_2-); 3.63 (s, 6H, OCH_3); 3.51 – 3.56 (m, 2H, OCH_2-); 3.32 (d, J = 15.6 Hz, 2H, S-CH_2-); 3.23 (d, J = 14.6 Hz, 2H, S-CH_2-); 1.65 – 1.73 (m, 2H, CH); 1.32 – 1.61 (m, 16H, CH_2); 0.91 – 0.97 (m, 12H, CH_3). ^{13}C-NMR (101 MHz, $CDCl_3$, δ): 151.19; 150.82; 125.55; 125.15; 114.33; 112.52; 72.08; 71.96; 55.70; 55.68; 40.01; 39.94; 30.92; 30.85; 30.79; 30.71; 29.45; 29.23; 24.15; 24.11; 23.27; 14.28; 14.27; 11.61; 11.33.

Isomer MP5b. ^{1}H-NMR (400 MHz, $CDCl_3$, δ): 6.60 (s, 2H, CH_3O-Ar-H); 6.59 (s, 2H, EHO-Ar-H); 4.48 (d, J = 15.3 Hz, 2H, S-CH_2-); 4.43 (d, J = 15.4 Hz, 2H, S-CH_2-); 3.73 – 3.78 (m, 2H, OCH_2-); 3.68 (s, 6H, OCH_3); 3.47 – 3.52 (m, 2H, OCH_2-); 3.28 (d, J = 15.3 Hz, 2H, S-CH_2-); 3.27 (d, J = 15.4 Hz, 2H, S-CH_2-); 1.68 – 1.78 (m, 2H, CH); 1.28 – 1.60 (m, 16H, CH_2); 0.88 – 0.95 (m, 12H, CH_3). ^{13}C-NMR (101 MHz, $CDCl_3$, δ): 151.10; 151.07; 151.01;

125.61; 125.17; 114.68; 112.51; 72.56; 72.33; 55.82; 39.51; 39.49; 39.46; 39.45; 30.98; 30.76; 30.46; 30.43; 30.41; 29.38; 28.93; 23.86; 23.70; 23.68; 23.37; 23.29; 14.27; 11.41; 10.91.

Isomer MP5c. ^{1}H-NMR (400 MHz, $CDCl_3$, δ): 6.60 (s, 4H, Ar-H); 4.02 (d, J = 14.4 Hz, 2H, S-CH_2-); 4.00 (d, J = 14.7 Hz, 2H, S-CH_2-); 3.84 – 3.89 (m, 2H, OCH_2-); 3.76 (s, 6H, OCH_3); 3.62 – 3.68 (m, 2H, OCH_2-); 3.48 (d, J = 14.4 Hz, 2H, S-CH_2-); 3.45 (d, J = 14.7 Hz, 2H, S-CH_2-); 1.67 – 1.75 (m, 2H, CH); 1.33 – 1.64 (m, 16H, CH_2); 0.91 – 0.99 (m, 12H, CH_3). ^{13}C-NMR (101 MHz, $CDCl_3$, δ): 150.54; 125.23; 125.06; 115.05; 114.97; 114.96; 113.59; 113.57; 71.86; 56.17; 39.98; 32.30; 31.78; 30.85; 30.81; 29.40; 29.36; 24.26; 24.18; 23.29; 14.29; 11.56; 11.49.

Isomer MP5d. ^{1}H-NMR (400 MHz, $CDCl_3$, δ): 6.62 (s, 2H, CH_3O-Ar-H); 6.60 (s, 2H, EHO-Ar-H); 4.02 (d, J = 14.5 Hz, 2H, S-CH_2-); 4.00 (d, J = 14.5 Hz, 2H, S-CH_2-); 3.87 – 3.92 (m, 2H, OCH_2-); 3.76 (s, 6H, OCH_3); 3.59 – 3.63 (m, 2H, OCH_2-); 3.47 (d, J = 14.6 Hz, 2H, S-CH_2-); 3.46 (d, J = 14.6 Hz, 2H, S-CH_2-); 1.66 – 1.76 (m, 2H, CH); 1.32 – 1.64 (m, 16H, CH_2); 0.91 – 0.99 (m, 12H, CH_3). ^{13}C-NMR (101 MHz, $CDCl_3$, δ): 150.66; 150.51; 125.38; 124.97; 114.76; 114.04; 114.03; 71.69; 71.65; 56.33; 56.30; 40.02; 40.01; 32.11; 31.88; 30.90; 30.84; 29.38; 29.32; 24.29; 23.26; 14.29; 11.56; 11.46.

Note: Several signals depict a multiple pattern in the ^{13}C-NMR spectra due to the concomitance of diastereomers.

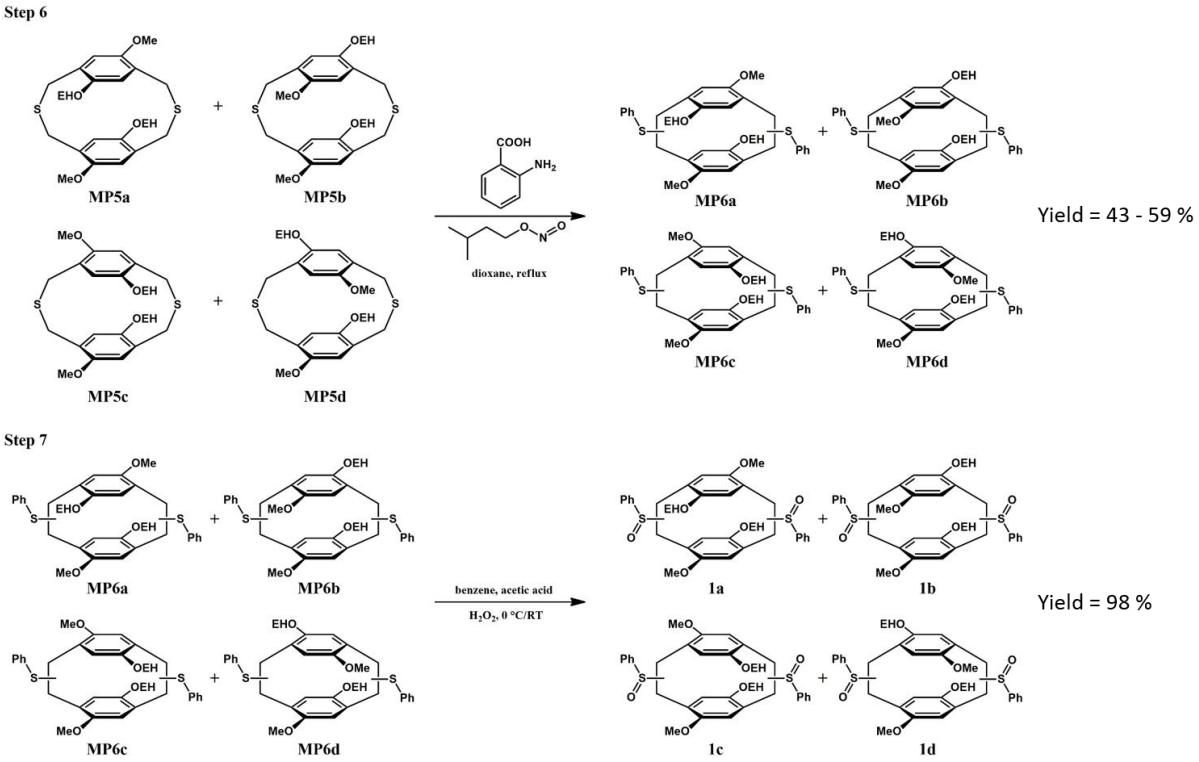

Figure S29. Synthesis of monomer precursors **MP6a-d** and **1a-d**.

Synthesis of Monomer Precursor MP6 (Step 6). Stevens rearrangement of **MP5a-d** via *in situ* formation of aryne was carried out according to a modified literature procedure.[S3] 11.3 g (19.2 mmol, 1.0 eq.) of tetraalkoxy-2,11-dithia[3.3]paracyclophane (mixture of isomers, **MP5a-d**) and 9.2 g (67.2 mmol, 3.5 eq.) of anthranilic acid were dissolved in dry dioxane and an argon atmosphere was established. The reaction mixture was heated to 95 °C and 13.5 g (15.5 mL, 115.1 mmol, 6.0 eq.) of isopentyl nitrite were added dropwise (over a period of 45 min) under the exclusion of light. After the addition was completed the reaction mixture was stirred for 3 h at 95 °C. The dioxane was removed under reduced pressure and the resulting residue was purified by column chromatography with a gradient eluent system (DCM/*n*-hexane, 1/4 – 1/2). All spots from $R_f \approx 0.28$ (DCM/*n*-hexane 1/4) to $R_f \approx 0.16$ (DCM/*n*-hexane 1/2) were collected together to give the product as a mixture of isomers. The product was obtained as a viscous, yellow oil in an overall yield of 59 % (11.3 mmol, 8.4 g).

^{1}H-NMR (400 MHz, $CDCl_3$, δ): 7.07 – 7.57 (m, Ar-S-); 5.79 – 6.79 (m, Ar); 5.05 – 5.52 (m, Ar-S-CH); 3.34 – 4.01 (m, OCH_2- + OCH_3); 3.10 – 3.30 (m, Ar-CHH); 2.28 – 2.49 (m, Ar-CHH); 1.23 – 1.84 (m, CH + CH_2); 0.86 – 1.04 (m, CH_3). ^{13}C-NMR (101 MHz, $CDCl_3$, δ): 152.4 – 153.7; 136.6 – 138.2; 125.6 – 130.6; 113.0 – 120.8; 71.4 – 73.8; 55.5 – 57.2; 42.9 – 44.8; 39.6 – 40.7; 30.6 – 31.0; 29.2 – 29.9; 24.0 – 24.4; 23.2 – 23.3; 14.2 – 14.3; 11.2 – 11.7.

Synthesis of Monomer Precursor MP7 (Step 7). Oxidation of **MP6a-d** was conducted following a modification of a literature procedure.[S3] A mixture of the isomers **MP6a-d** (7.90 g, 10.7 mmol, 1.0 eq.) was dissolved in a mixture of toluene (255 mL) and acetic acid (85 mL). The reaction mixture was degassed for 20 min. and an argon atmosphere was established. After cooling to 0 °C, 2.5 mL (24 mmol, 2.3 eq.) of hydrogen peroxide (30 wt% in water) were slowly added over a period of 20 min. The ice bath was removed and the reaction mixture was stirred for 16 h at room temperature. The reaction mixture was then diluted with 255 mL of DCM, washed twice with brine and once with water. The organic layer was dried over $MgSO_4$, filtered and the DCM removed under reduced pressure. The product was obtained in a yield of 98 % (8.13 g, 10.5 mmol) and was used without further purification.

^{1}H-NMR (400 MHz, $CDCl_3$, δ): 7.34 – 7.76 (m, Ar-SO-); 6.02 – 6.59 (m, Ar); 4.50 – 4.69 (m, Ar-SO-CH); 3.08 – 3.91 (m, OCH_2- + OCH_3); 2.47 – 3.01 (m, Ar-CHH); 1.14 – 1.77 (m, CH + CH_2); 0.77 – 1.04 (m, CH_3). ^{13}C-NMR (101 MHz, $CDCl_3$, δ): 153.0 – 154.3; 143.0 – 144.1; 127.4 – 131.0; 124.4 – 126.0; 115.2 – 118.3; 71.9 – 74.3; 62.4 – 64.1; 56.2 – 57.5; 39.5 – 40.3; 30.5 – 31.1; 28.7 – 29.8; 23.8 – 24.4; 23.1 – 23.4; 14.2 – 14.3; 11.2 – 11.7.

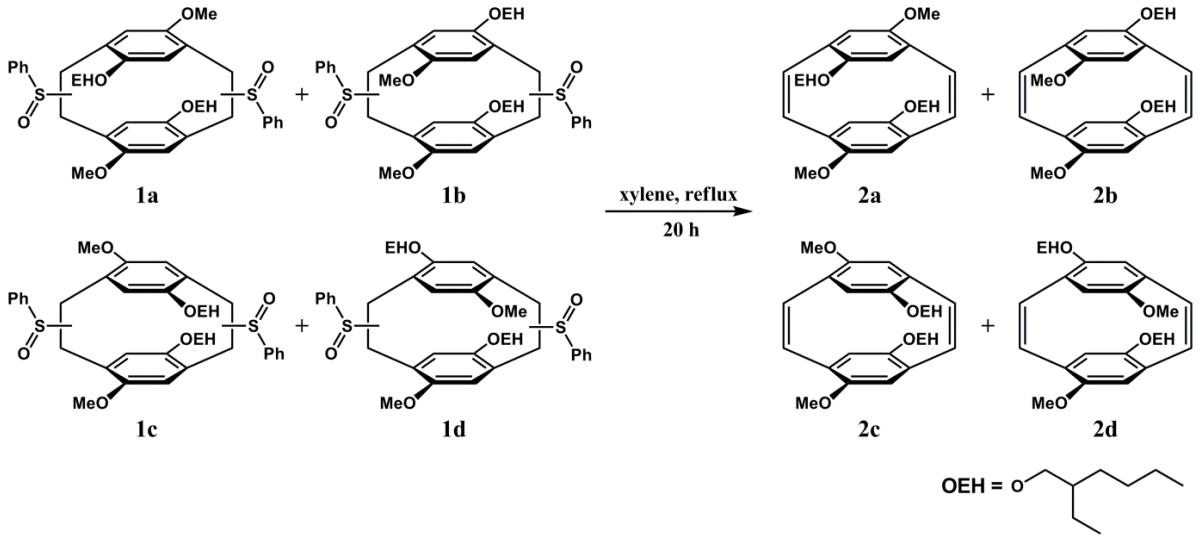

Figure S30. Synthesis of the four dimethoxy-(2-ethylhexyloxy)-[2.2]paracyclophane-1,9-diene isomers **2a-d** (yield = 48 – 60 %).

Solution NMR Spectra

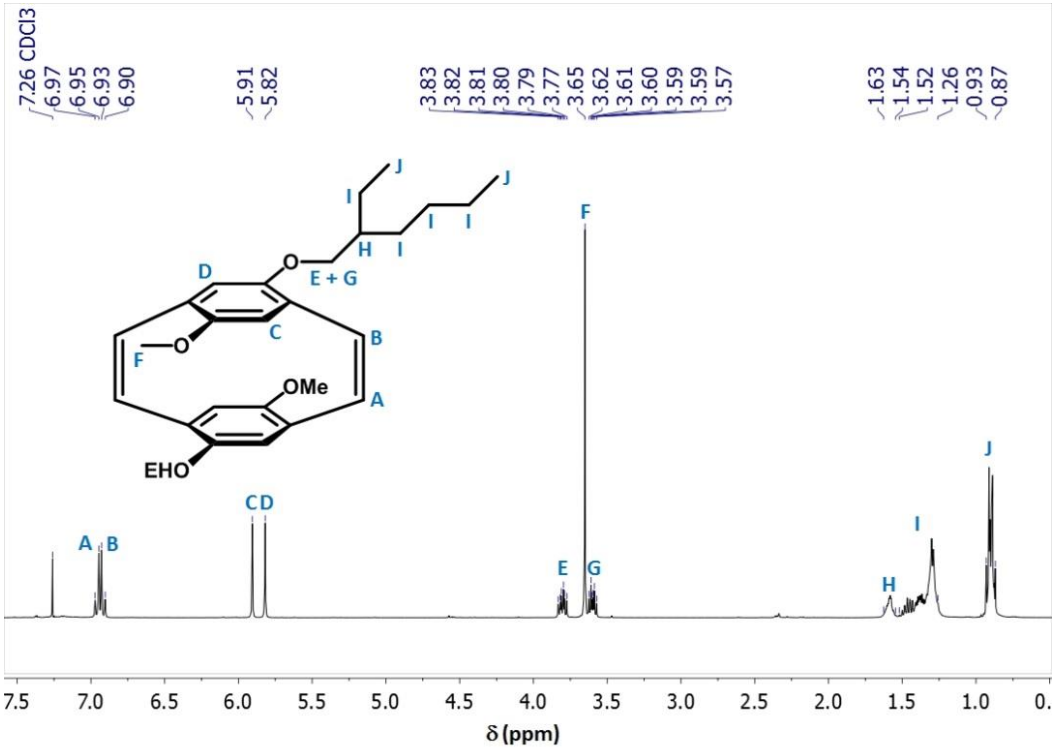

Figure S31. 400 MHz ^{1}H-NMR spectrum of isomer **2a** in $CDCl_3$.

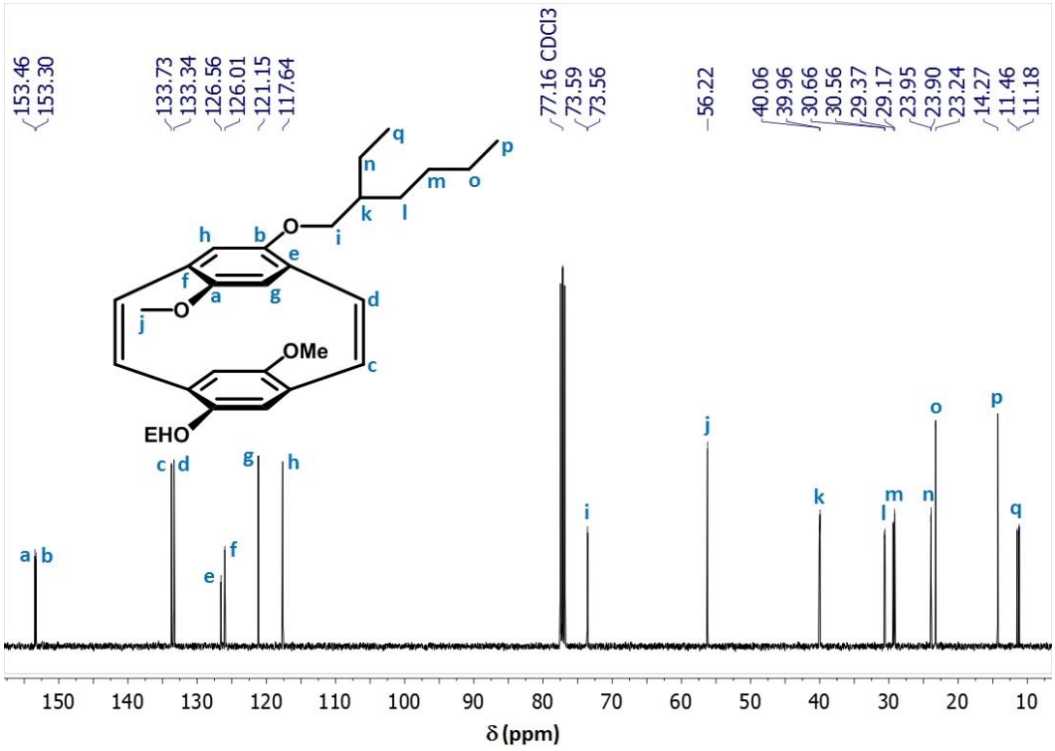

Figure S32. 101 MHz ^{13}C-NMR spectrum of isomer **2a** in $CDCl_3$. Signals i, k, l, m, n and q are doubled due to the concomitance of diastereomers.

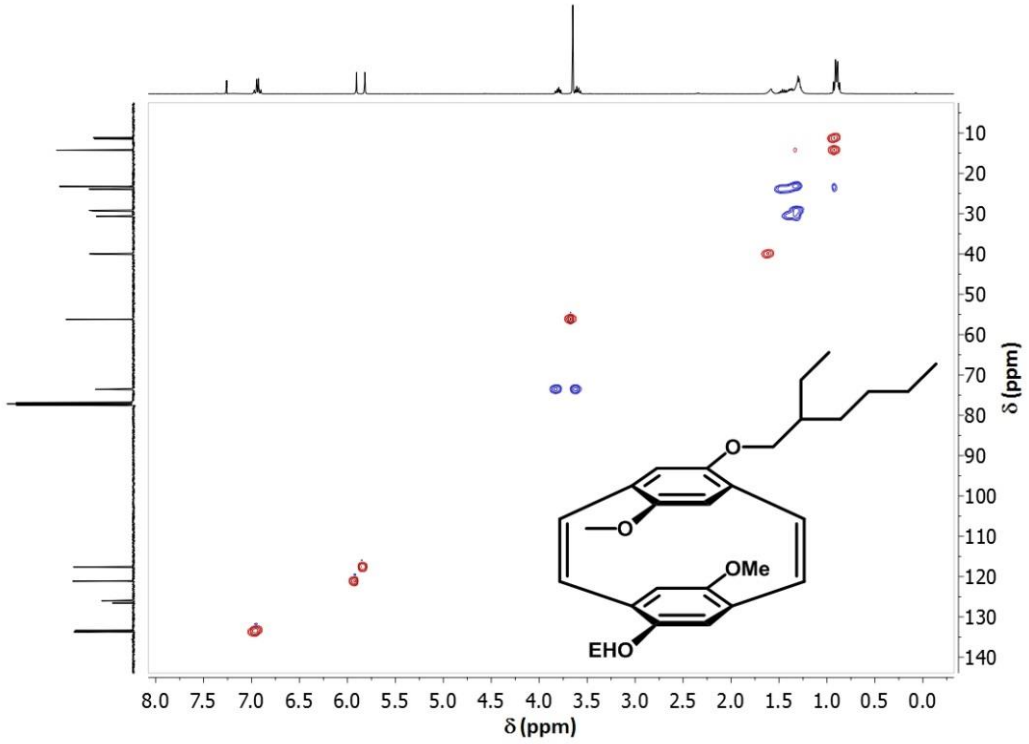

Figure S33. HSQC spectrum of isomer **2a** in $CDCl_3$.

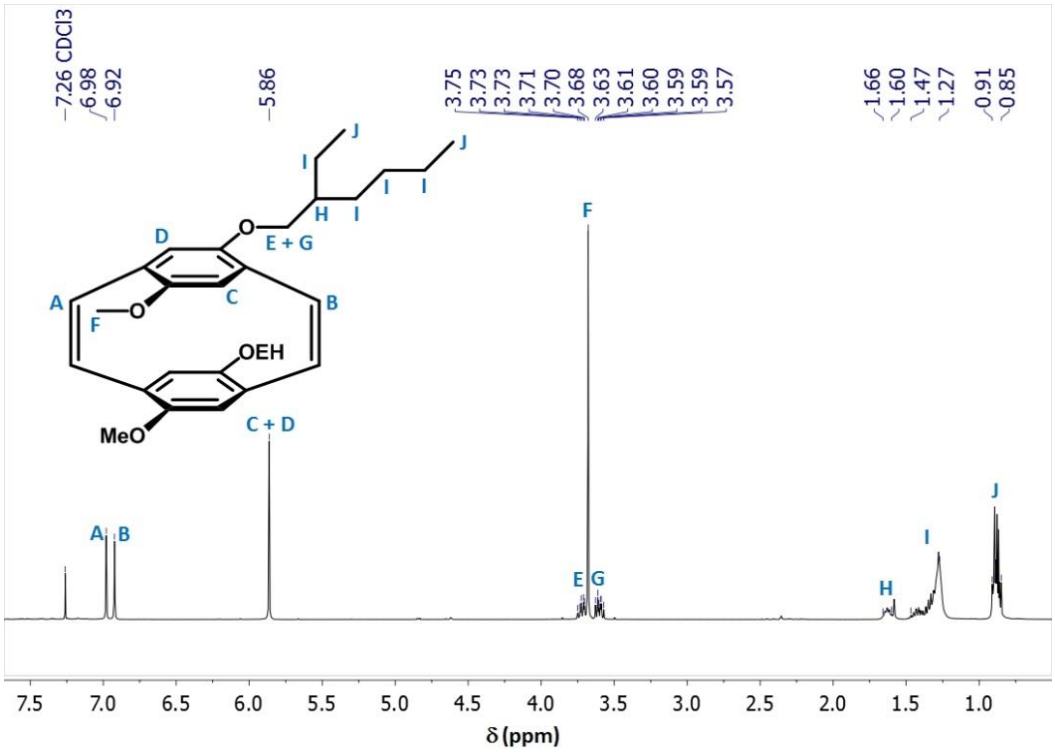

Figure S34. 400 MHz ^{1}H-NMR spectrum of isomer **2b** in $CDCl_3$.

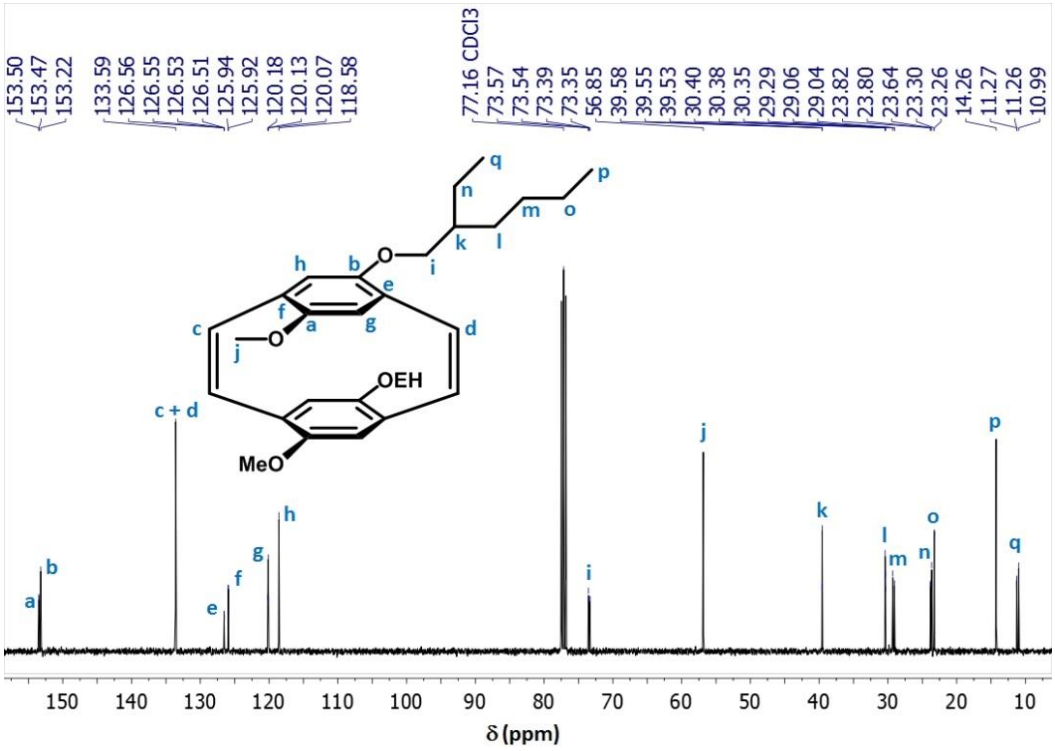

Figure S35. 101 MHz ^{13}C-NMR spectrum of isomer **2b** in $CDCl_3$. Signals a, e, f, g, i, k, l, m, n, o and q depict a multiple pattern due to the concomitance of diastereomers.

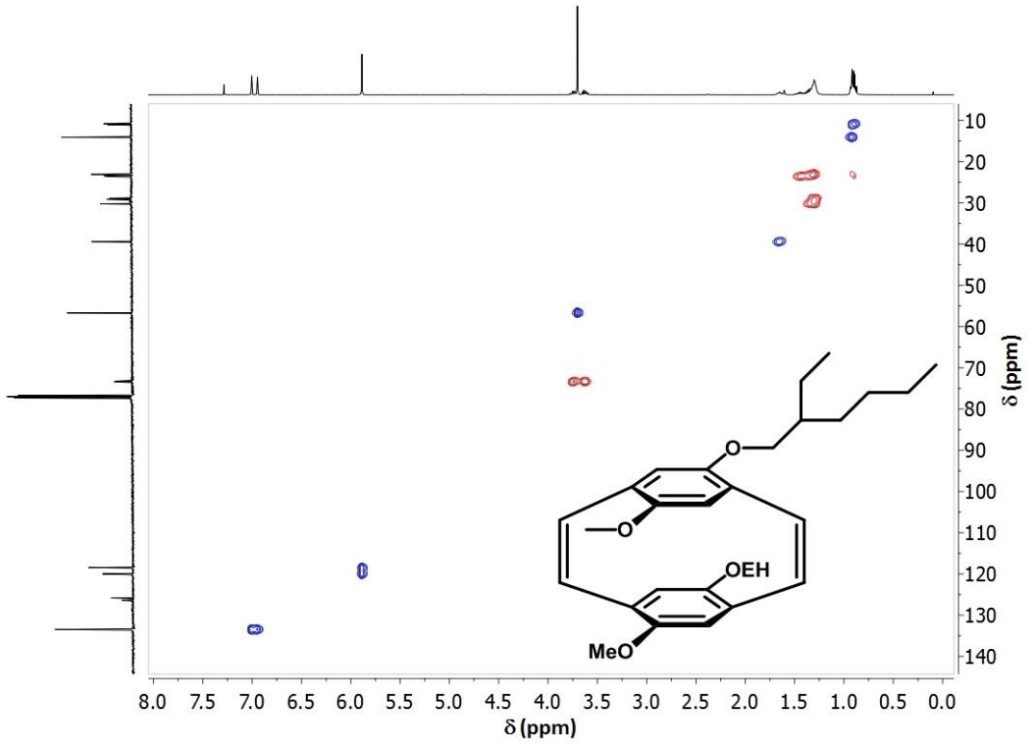

Figure S36. HSQC spectrum of isomer **2b** in $CDCl_3$.

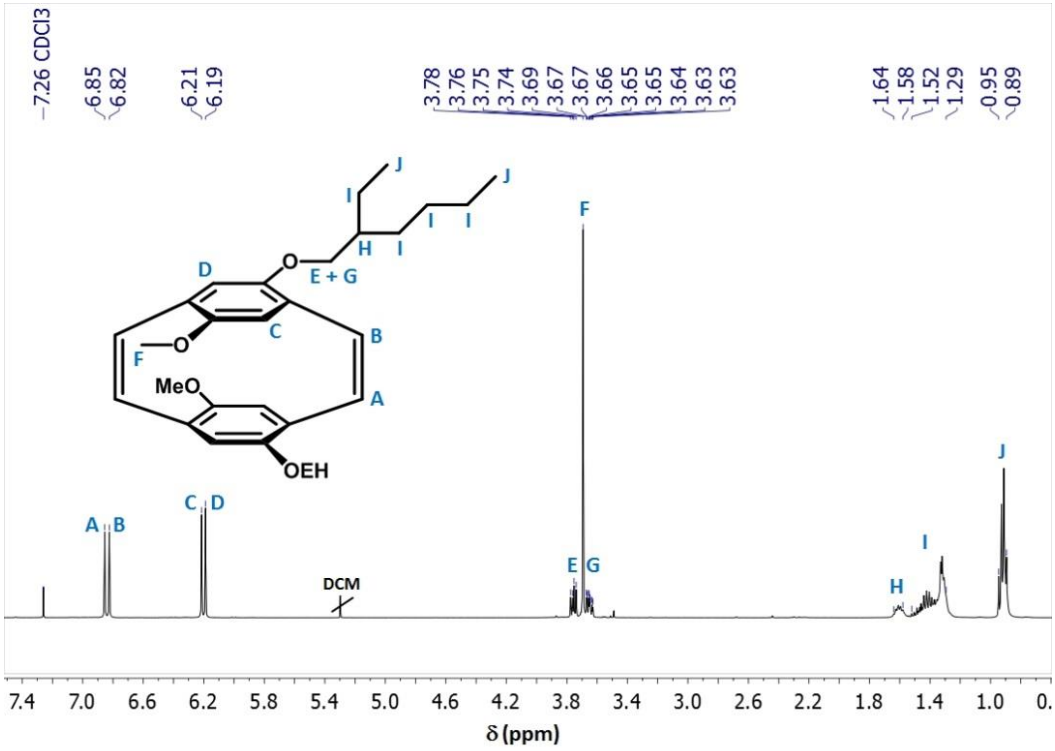

Figure S37. 400 MHz ^{1}H-NMR spectrum of isomer **2c** in $CDCl_3$.

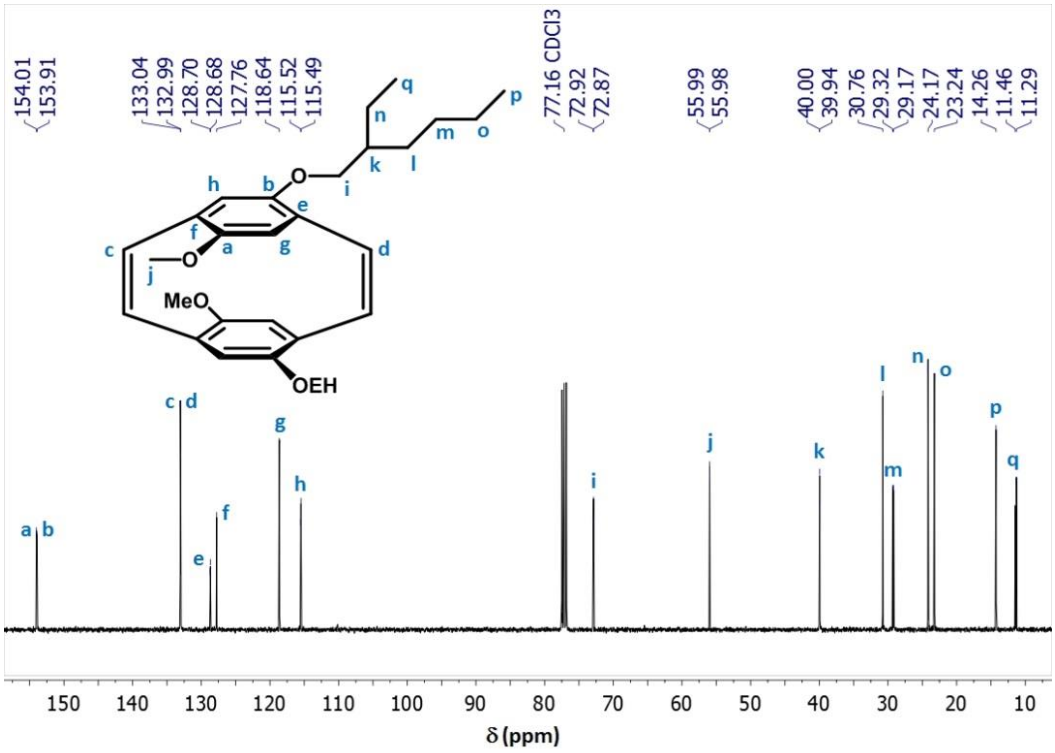

Figure S38. 101 MHz ^{13}C-NMR spectrum of isomer **2c** in $CDCl_3$. Signals e, h, i, j, k and q are doubled due to the concomitance of diastereomers.

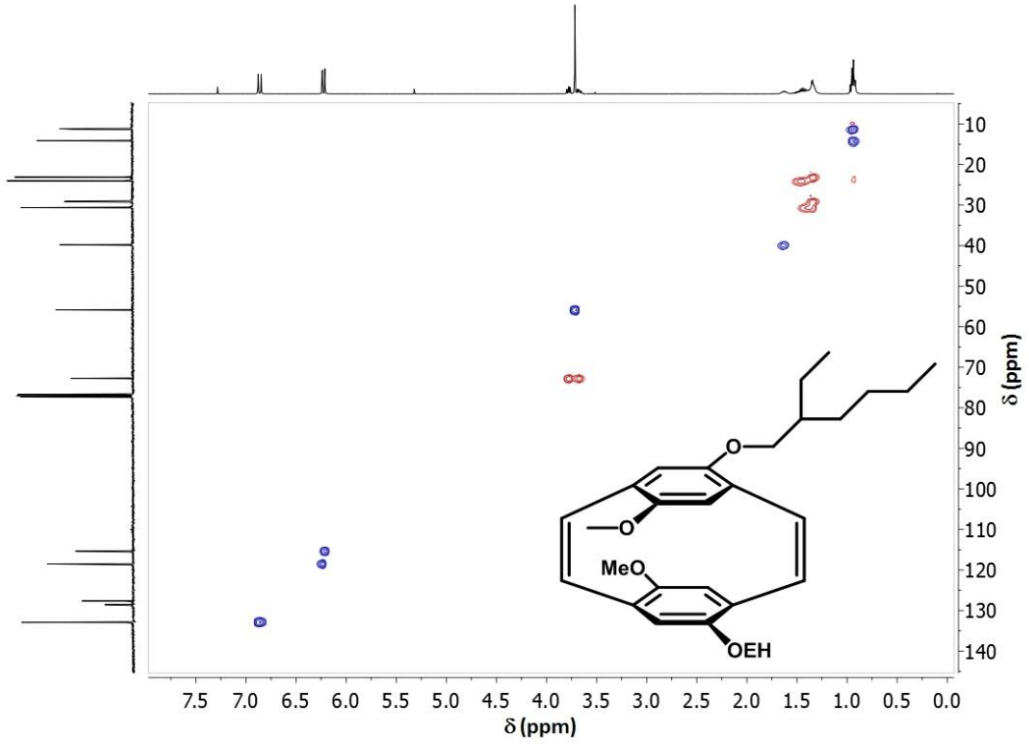

Figure S39. HSQC spectrum of isomer **2c** in $CDCl_3$.

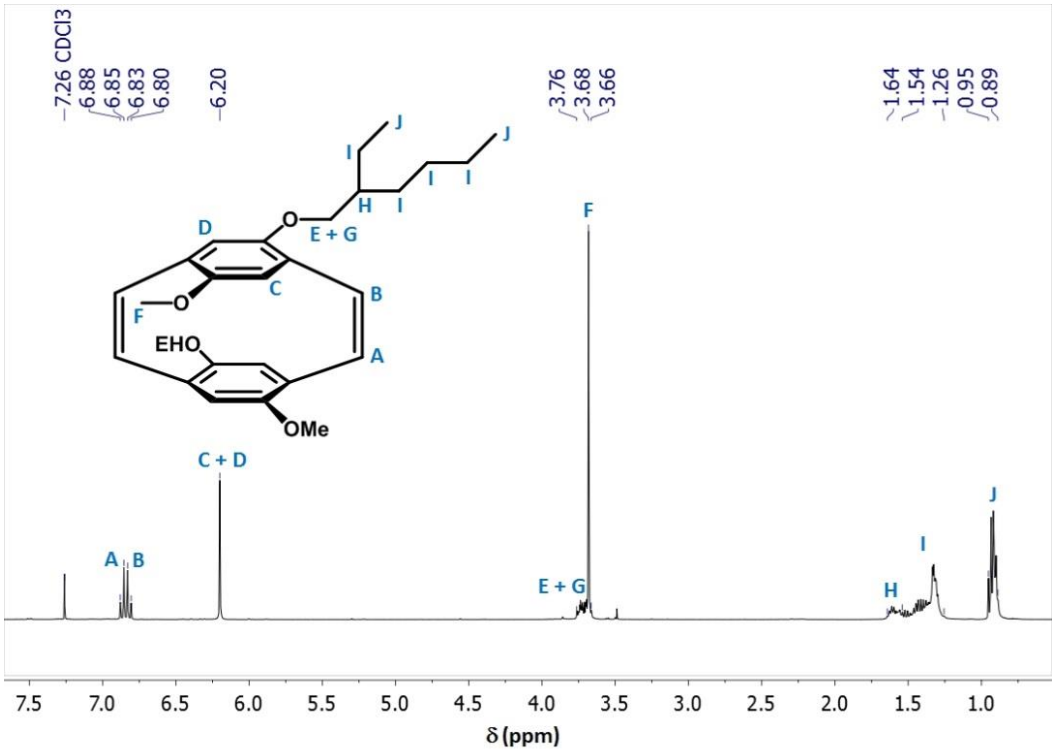

Figure S40. 400 MHz ^{1}H-NMR spectrum of isomer **2d** in $CDCl_3$.

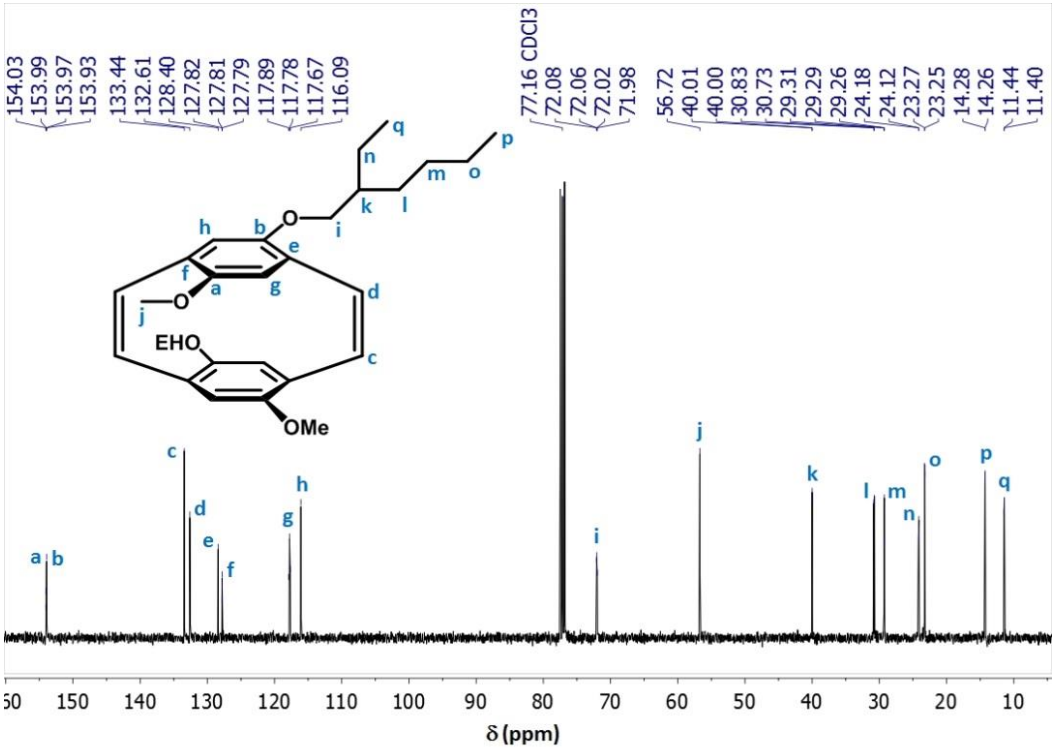

Figure S41. 101 MHz ^{13}C-NMR spectrum of isomer **2d** in $CDCl_3$. Signals a, f, g, i, k, l, m, n, o, p and q depict a multiple pattern due to the concomitance of diastereomers.

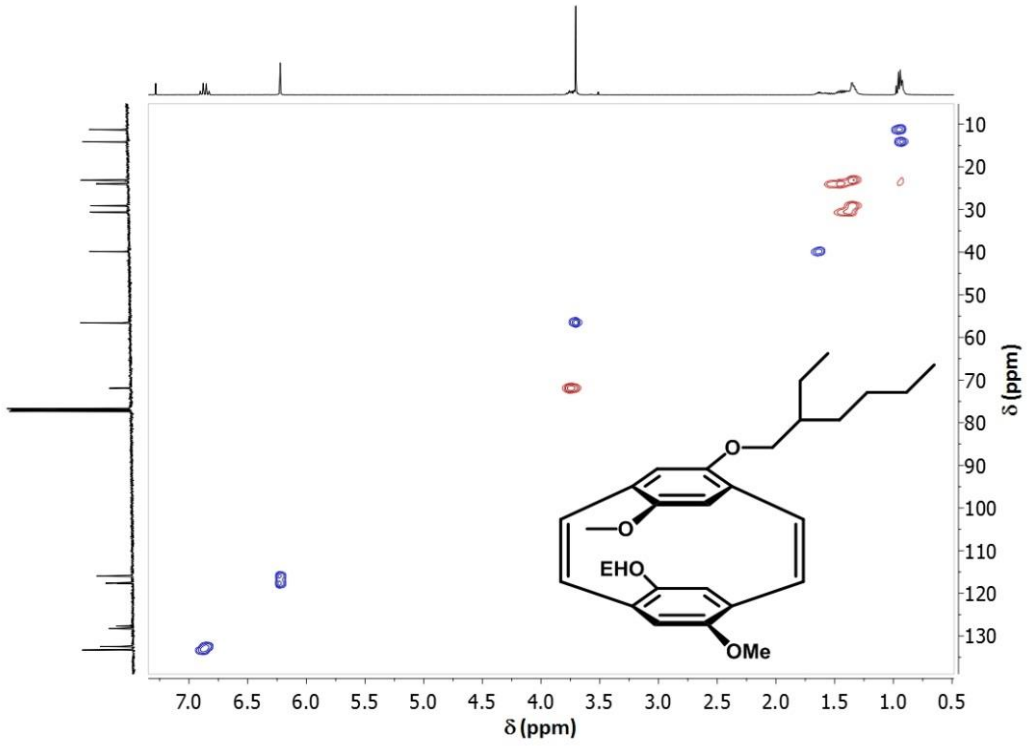

Figure S42. HSQC spectrum of isomer **2d** in $CDCl_3$.

Solid State NMR Spectra

All solid state NMR experiments were recorded on a Bruker Avance 400 DSX spectrometer at ^{1}H frequency of 399.87 and ^{13}C frequency of 100.55 MHz. A two channel commercial Bruker 2.5 mm probe head at spinning speeds of 25 kHz was used for all measurements. At those spinning frequencies additional heating effects arise due to the air friction, so the ambient sample temperature should be corrected by adding the expected 12 – 15°C. A precise temperature calibration was not carried out as no phase transitions were expected. The ^{1}H-NMR spectrum was recorded using a 30° 4 μs pulse and 5 s recycle delay averaging 32 transients. The ^{1}H Back-to-back (BaBa) NMR experiment was carried out recording 16 scans with 40, 80 and 160 μs to excite double quantum coherences. The ^{13}C single pulse (SP) direct excitation was recorded with a 30° pulse with a length of 4 μs and repetition time of 20 s acquiring 3 k transients. The ^{13}C cross-polarization (CP) NMR experiment was carried out averaging 30 k scans and using a 3 ms contact time. Both ^{13}C spectra were zero filled to 64 k points before processing and a broadening of 30 Hz was used for the CP NMR spectrum. For all ^{13}C experiments a two pulse phase modulation (TPPM) heteronuclear decoupling scheme was used. The ^{1}H and ^{13}C chemical shifts were referenced to external adamantine as a secondary standard at 1.63 ppm and 38.48 ppm, respectively.

The ^{1}H, ^{1}H BaBa and ^{13}C single pulse (SP) excitation and cross-oolarization (CP) NMR spectra of isomer **2a** were recorded at 25 kHz magic angle spinning to probe the organization and dynamics in the solid state state and correlate the result with the X-ray diffraction pattern and the theoretical calculations.

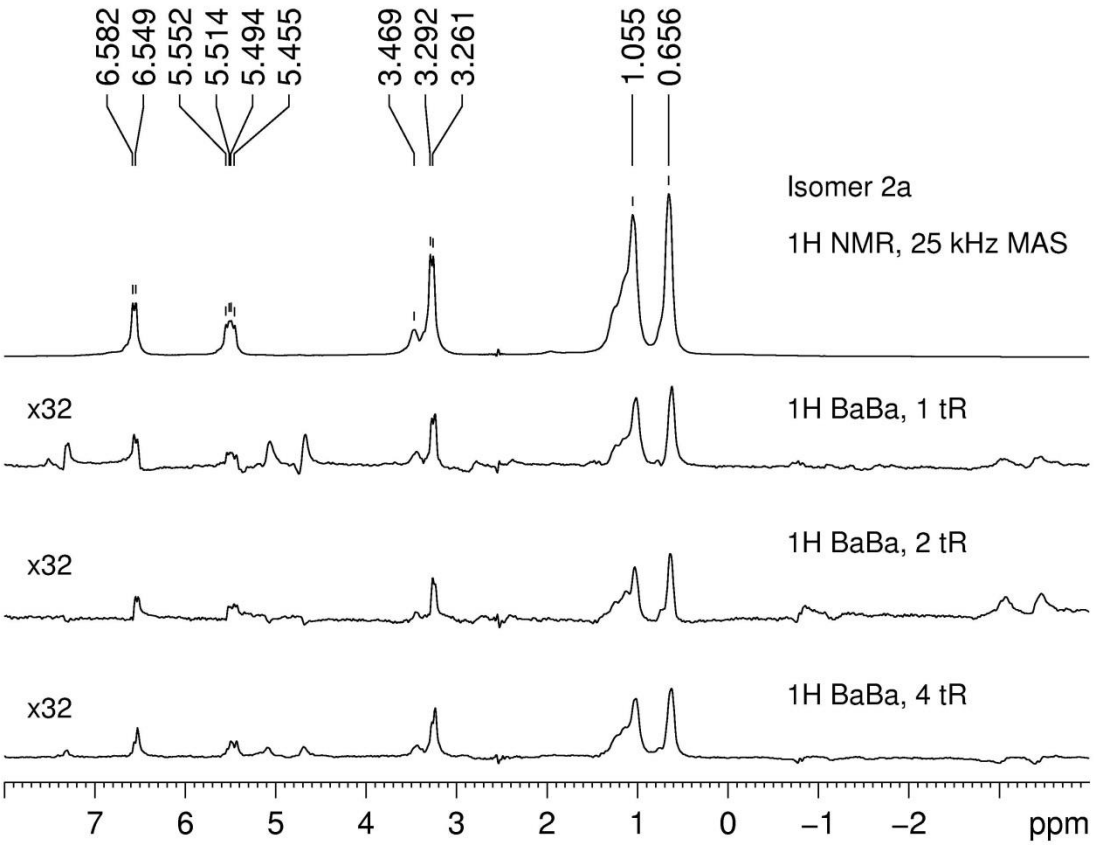

Figure S43. ^{1}H and ^{1}H Back-to-back NMR spectra of isomer **2a** recorded at 25 kHz MAS with resp. 1, 2 and 4 rotor periods (40, 80 and 160 μs) to excite double quantum coherences.

Figure S43 presents the ^{1}H and ^{1}H Back-to-back (BaBa) NMR spectra of isomer **2a**. The ^{1}H NMR spectrum of the compound in the solid state is characterized by sharp spectral lines even though the resolution in solution related with observing the splitting pattern is not achieved. This suggests a significant mobility of the sample under the conditions of the experiment. To probe further the molecular dynamics ^{1}H BaBa spectra were recorded with different excitations times at 25 kHz MAS. Provided that the ^{1}H ensembles of dipolar coupled spins were completely rigid, signal would be observed only in those spectra recorded with short excitation times, i.e. 40 and 80 μs. Furthermore, if the molecule was performing a fast motion no signal at all would be detected in these experiments. However, all BaBa spectra present peaks with almost equal intensity which is significantly lower compared to the ^{1}H single pulse excitation experiment. This leads to the conclusion that the molecule of isomer **2a** undergoes fast dynamics, however, with a broad distribution of the correlation times of the molecular motion. In the spectra the olefinic and aromatic protons resonate in the range of 5 –

7 ppm. The OCH_2 and OCH_3 signals are detected at 3.5 and 3.2 ppm, respectively, and the peaks of the alkyl chain protons are observed in the range of 0.5 – 2 ppm. Surprisingly, signals at -3.0 and -3.4 ppm are detected in all spectra. Such resonances most probably originate from protons of the alkyl chain which due to the packing experience to a large degree the ring current effect of the aromatic systems.

The ^{13}C SP and CP spectra of isomer **2a** (**Figure S44**) provide further insight into the molecular packing and dynamics. The sharp NMR transitions observed in the SP spectrum confirm fast molecular motion, which on the other hand leads to averaging out of the ^{1}H-^{13}C dipole-dipole couplings. Thus, even 30 k scans were not sufficient to record a ^{13}C CP spectrum with good signal-to-noise. In the spectrum there are three signals at 152.54, 135.68 and 57.40 ppm clearly detected, which are otherwise barely observed as small shoulders in the SP experiment. Those signals are related with a small distribution of relatively rigid molecules of the compound under investigation, which have a slightly different shift due to packing effects. This finding is consistent with the results of the ^{1}H BaBa experiments, which suggest fast molecular dynamics with a broad distribution of the correlation times.

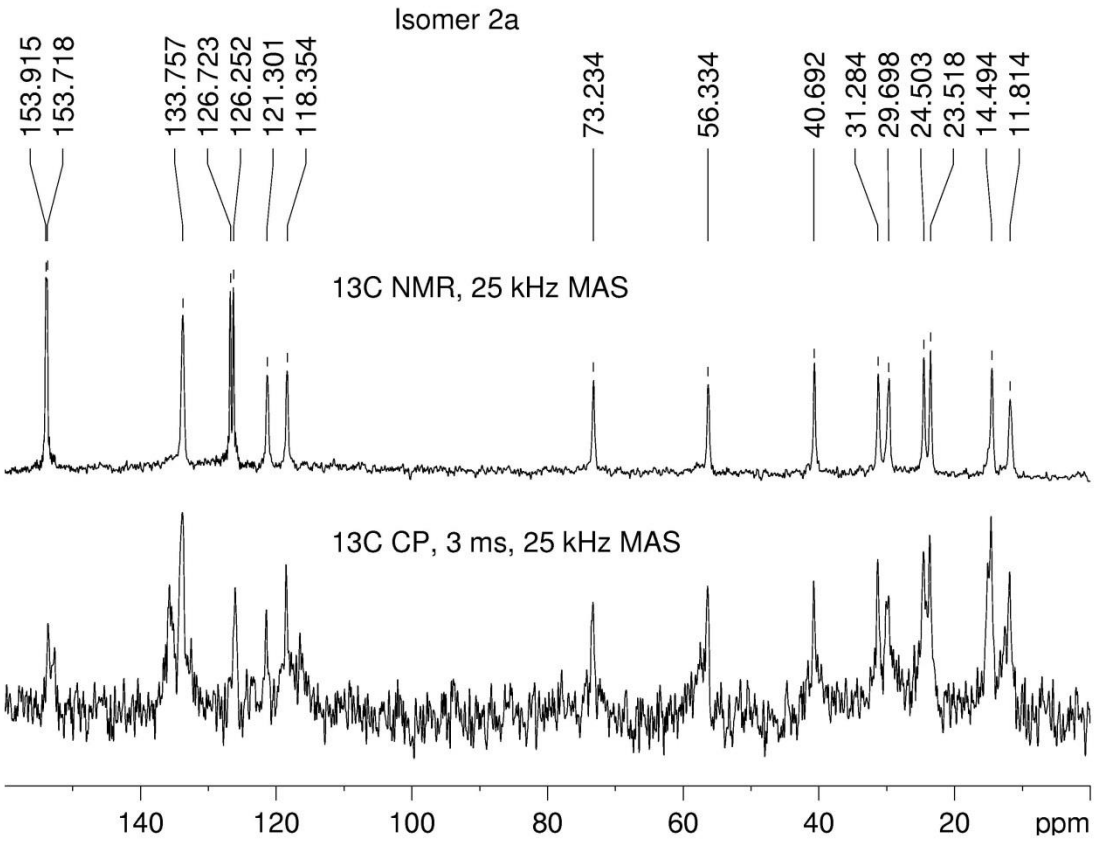

Figure S44. ^{13}C SP and ^{13}C CPNMR spectra of isomer **2a** recorded at 25 kHz MAS and resp. 3k and 30 k scans and 3 ms contact time.

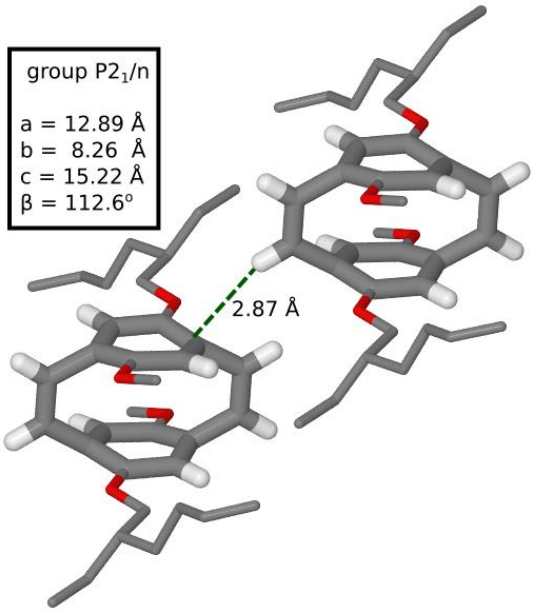

Figure S45. Zoom of the crystal packing visualizing the distance of an olefinic hydrogen above one aromatic ring of the adjacent molecule.

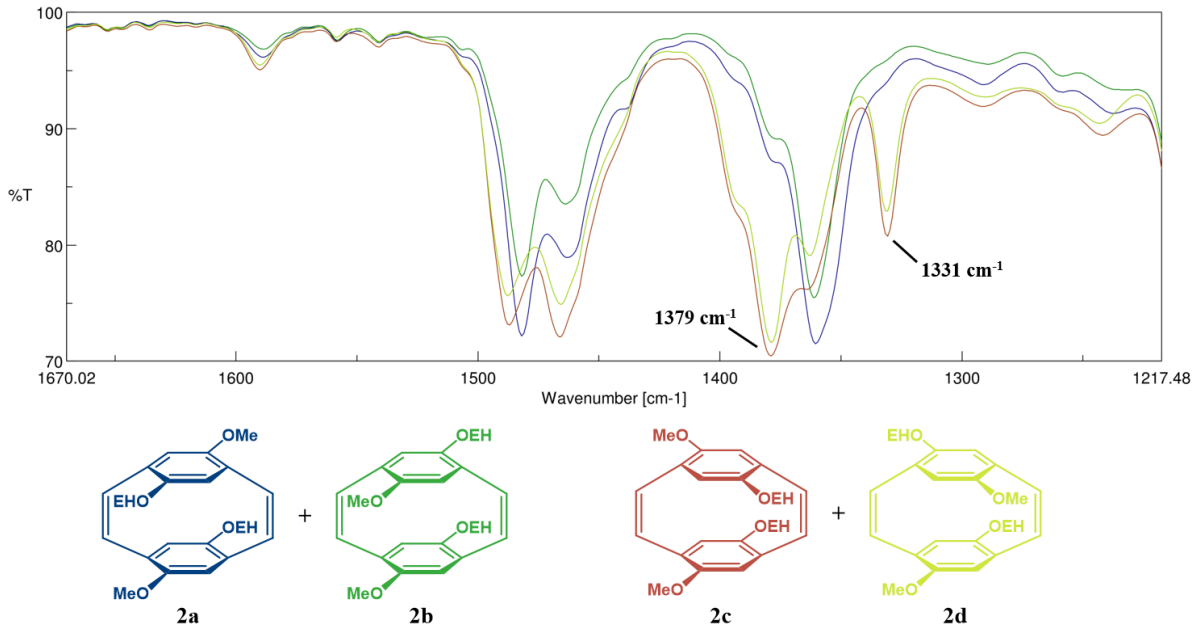

Figure S46. Overlay of the FTIR spectra of all four isomers. The shown area illustrates the two additional bands at 1379 cm^{-1} and 1331 cm^{-1} which appear solely in case of isomer **2c** and **2d**.

Polymer Characterization

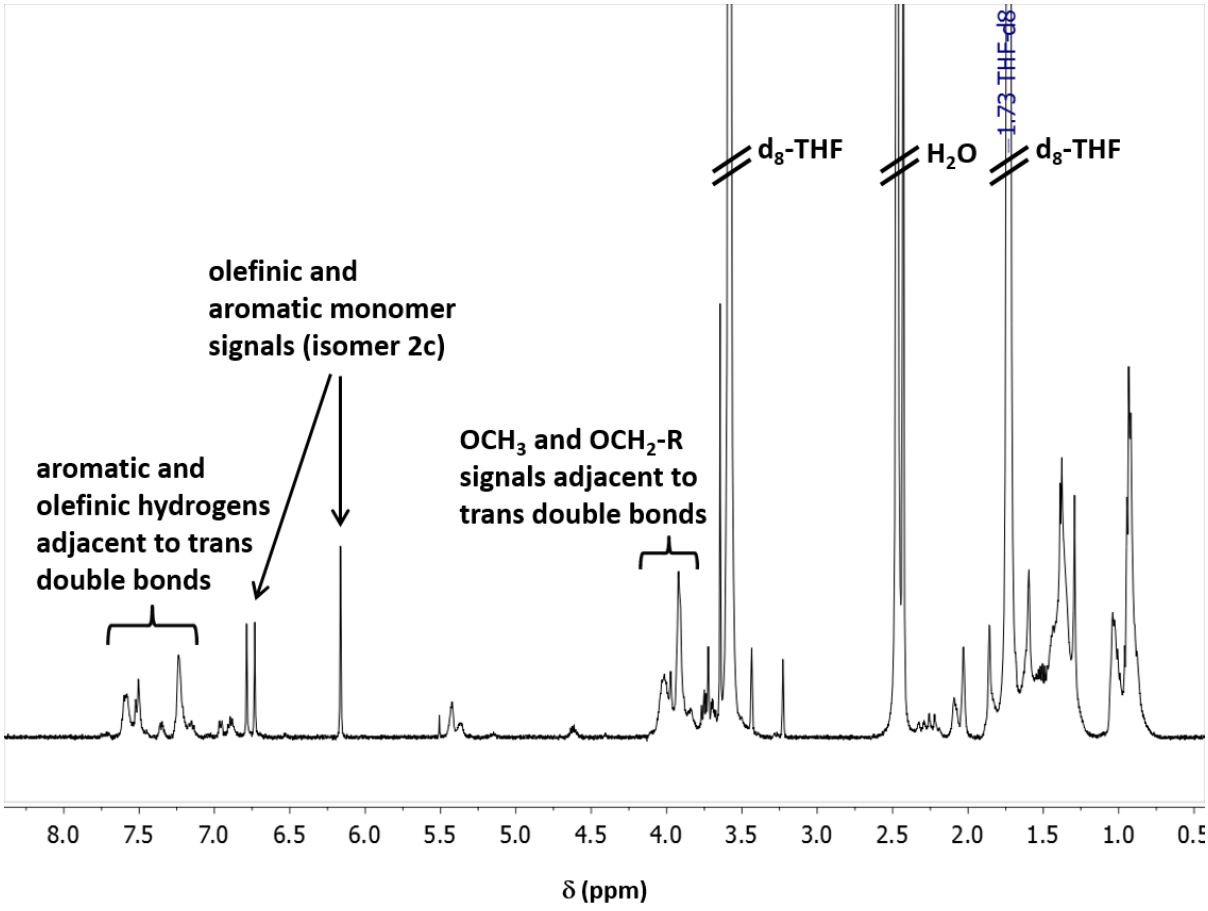

Figure S47. 500 MHz ^{1}H-NMR spectrum of MEH-PPV synthesized from isomer **2c** (in d_8-THF). The polymer exhibits an almost complete all-trans configuration. (Note: The signals of the aromatic hydrogens which resonate as two separated singlets in $CDCl_3$ (6.21 and 6.19 ppm) appear as one singlet at 6.16 ppm in d_8-THF.)

Table S1. Reaction details, molecular weights and PDIs of all polymers.

Entry	Isomer	Catalyst	M_n [d] ($g \cdot mol^{-1}$)	M_n [e] ($g \cdot mol^{-1}$)	PDI[e]
1[b]	2a	3	5311	5542	1.45
2[a]	2a	4	5369	6357	1.19
3[a]	2a	5	5369	7855	1.29
4[b]	2a	6	5311	6841	1.21
5[b]	2a	7	5311	5853	1.25
6[a]	2b	4	5369	4502	1.22
7[b]	2b	6	5311	5822	1.28
8[b]	2b	7	5311	6198	1.32
9[c]	2c	4	5369	2779	1.30
10[a]	2a	6	10519	12387	1.20
11[a]	2a	6	20934	23417	1.24

[a] T = 313 K, [b] initiation at 298 K and propagation at 313 K, [c] T = 384 K, [d] expected value from initial catalyst to monomer ratio (including end groups), [e] determined by GPC which was calibrated with polystyrene standards.

Kinetic Studies

In accordance with the literature, carrying out polymerizations in a standard reaction flask using catalyst **4** or **6** led to full conversion after 24 to 48 h (DP = 20). However, when recording the polymerization kinetics in a NMR tube, prolonged reaction times around 4 days became necessary which result most probably from a lower monomer concentration of 0.3 mol/L in the kinetic studies compared to 1.0 mol/L under standard conditions and in addition, a retarded diffusion in the reaction mixture.

The propagation rate constants were calculated from the ratio of the aromatic protons of the monomer (around 5.84 ppm in d_8-THF) to the methoxy- and O-CH_2-group of the 2-ethylhexyloxy substituents adjacent to *trans*-vinylene linkages of the polymer (from around 3.75 to 4.00 ppm in d_8-THF).

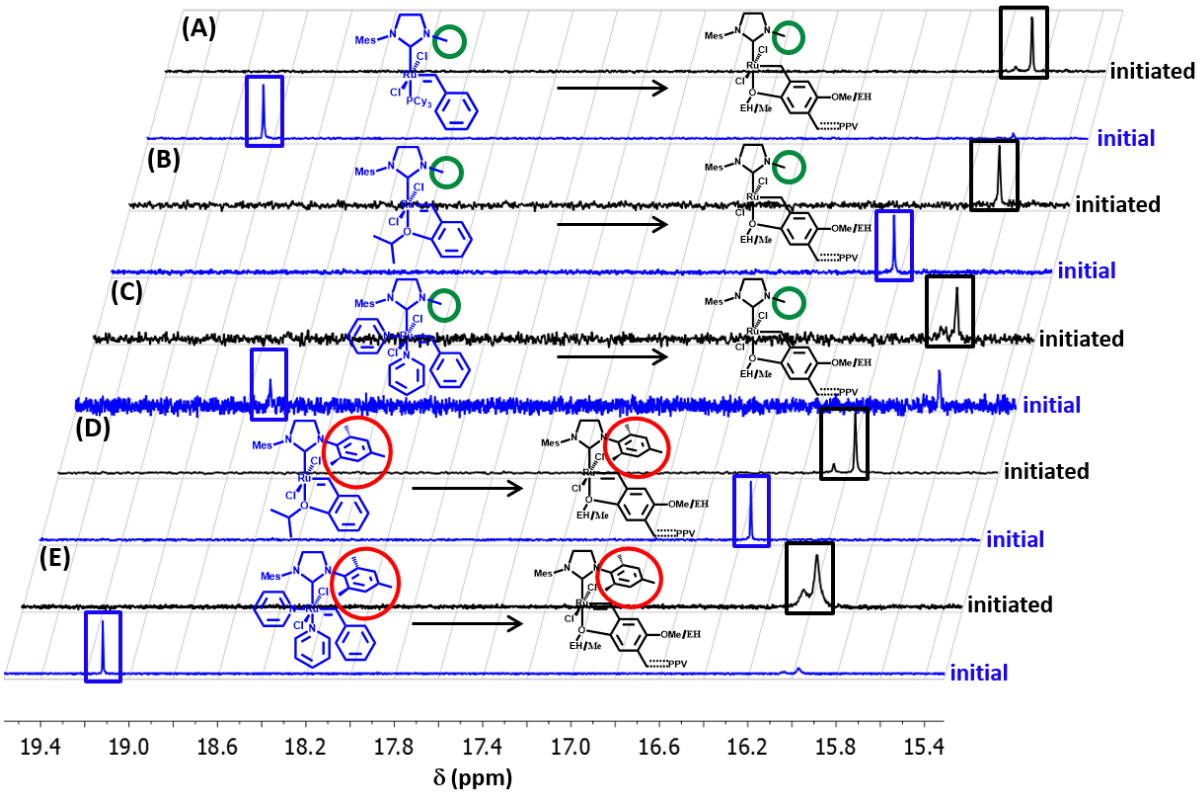

Figure S48. Representative ^{1}H-NMR spectra (in d_8-THF) monitoring the initation process via the carbene signals for isomer **2a**. The chemical shifts of the initiated species vary depending on the NHC ligand. (A), (B) and (C) with catalyst **3**, **5** and **7**, respectively, bearing the sterically less demanding NHC ligand and (D) and (E) with catalyst **4** and **6**,respectively, bearing SIMes ligand.

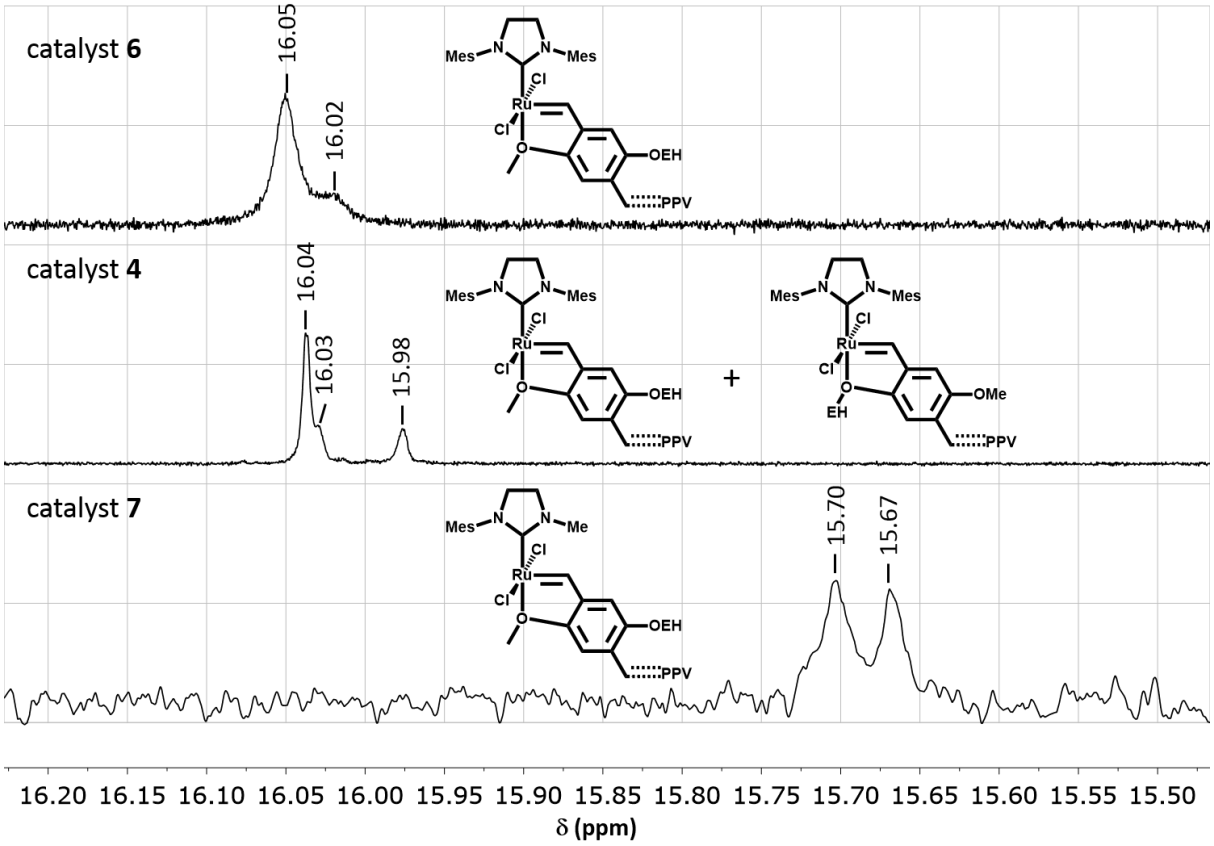

Figure S49. Magnified ^{1}H-NMR (in d_8-THF) spectra depicting the carbene signals after initiation and the structures assigned to the different peaks for isomer **2b** using catalysts **6**, **4** and **7** (top down).

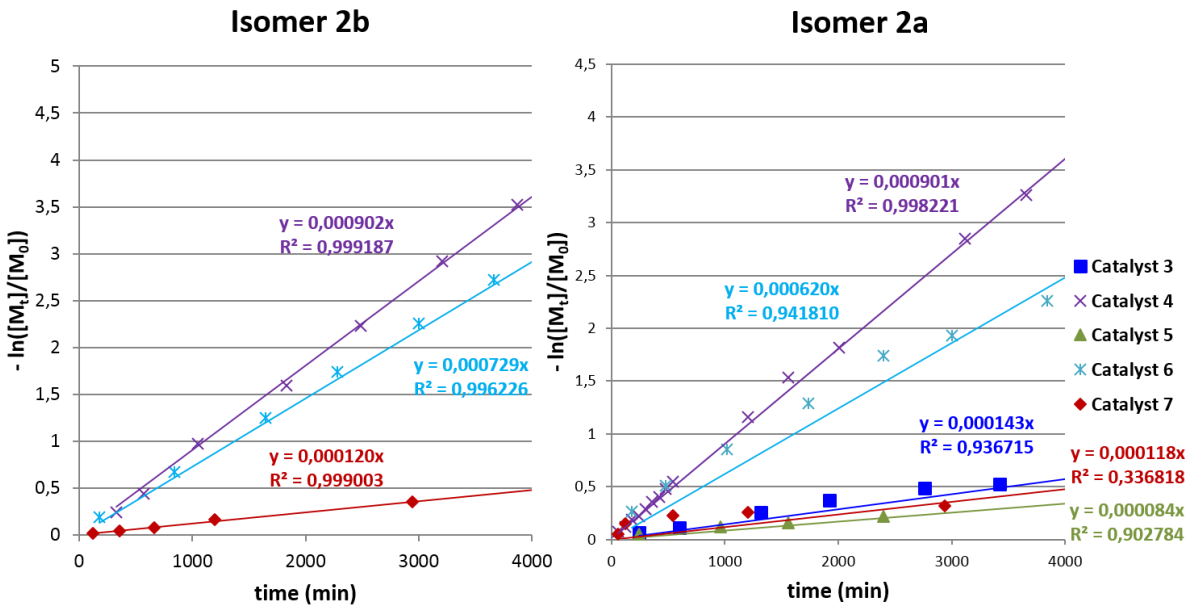

Figure S50. Propagation kinetics of isomer **2b** (left) and **2a** (right) with a constant catalyst concentration in combination with catalysts **4**, **6** and **7** for isomer **2b** and catalysts **3** – **7** for isomer **2a** (all propagations were conducted at 40 °C).

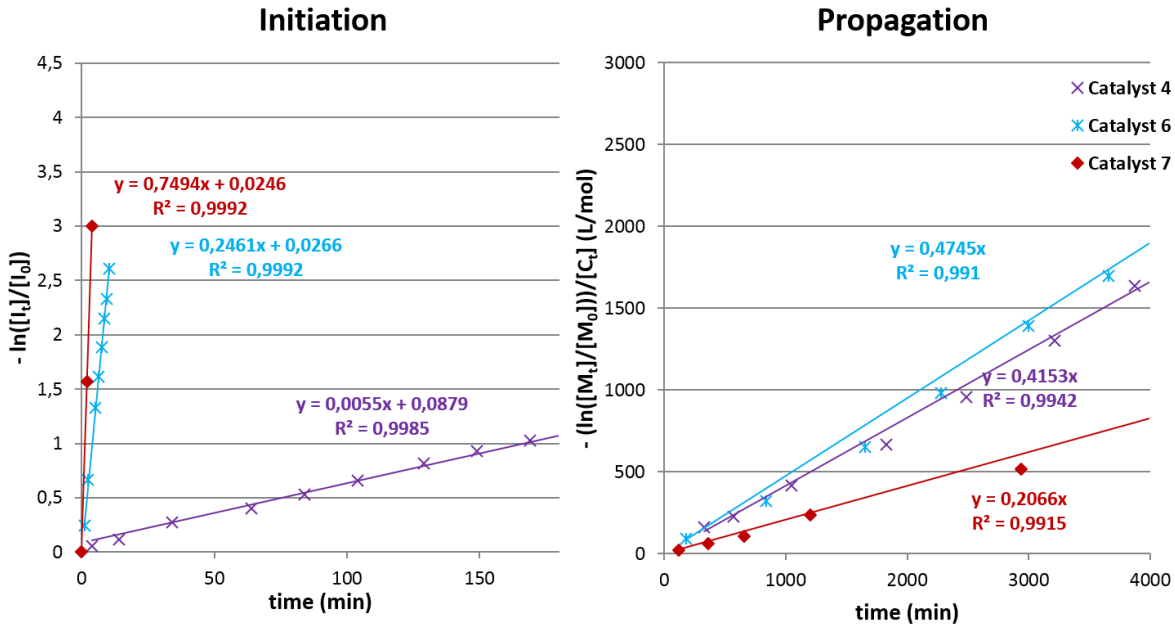

Figure S51. Initiation (left) and propagation (right) kinetics of isomer **2b** in combination with catalysts **4**, **6** and **7** (all propagations were conducted at 40 °C; initiations were conducted: **6**, **7** at 25 °C, **4** at 40 °C).

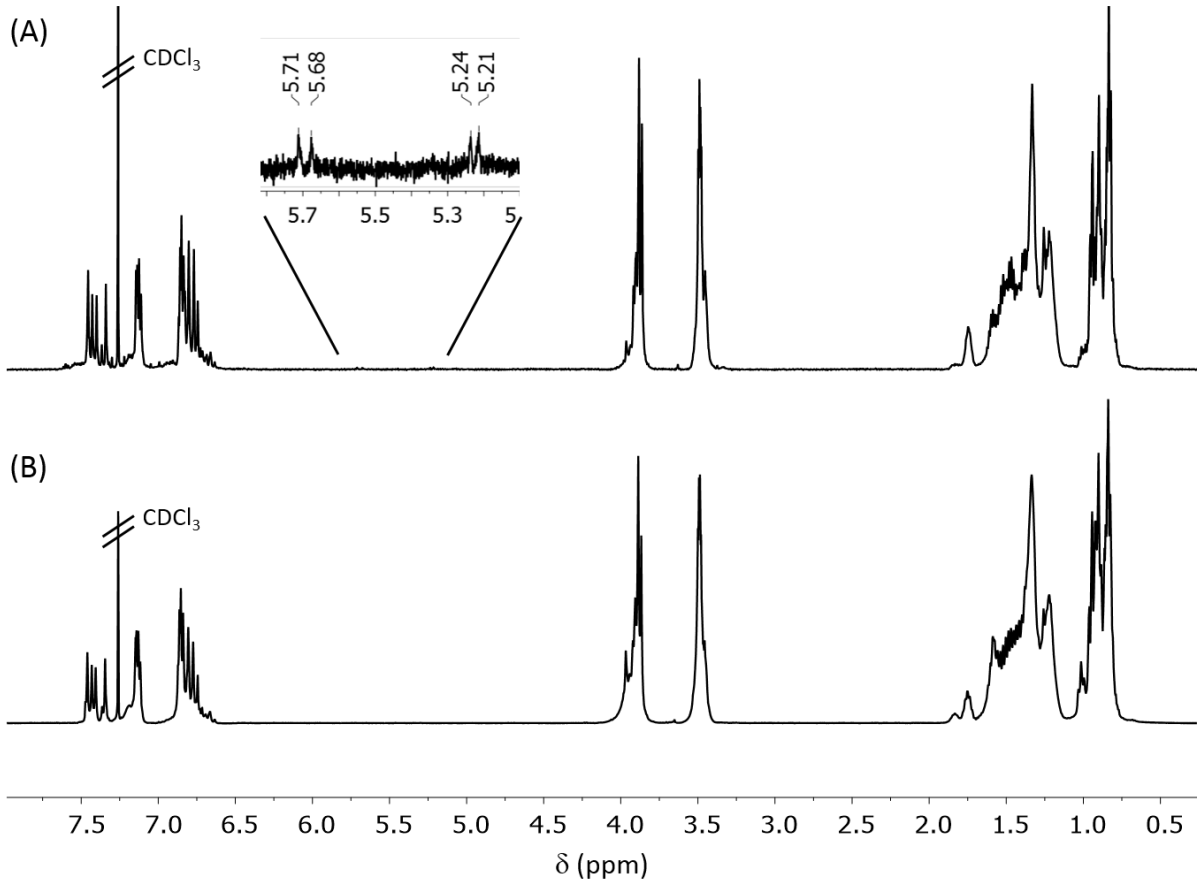

Figure S52. MEH-PPV obtained from the polymerization of isomer **2a** with catalyst **6** using a monomer/catalyst ratio of (A) 20/1 and (B) 40/1. In the polymer with DP ≈ 20 small signals of the vinyl end group can be observed (^{1}H-NMR (400 MHz, CDCl3, δ): 5.69 (d, J = 17.6 Hz); 5.22 (d, J = 11.1 Hz)). The third signal of the end group is covered by signals of the repeating unit.

References

(S1) Neef, C. J.; Ferraris, J. P. *Macromolecules* **2000**, *33*, 2311–2314.

(S2) Mitchell, R. H.; Boekelheide, V. *J. Am. Chem. Soc.* **1974**, *96*, 1547–1557.

(S3) Yu, C.-Y.; Helliwell, M.; Raftery, J.; Turner, M. L. *Chem. Eur. J.* **2011**, *17*, 6991–6997.

4.1.2.2 Manuscript to be Submitted

Synthesis of Functional Block Copolymers Carrying One Poly(para-phenylene vinylene) and One Non-Conjugated Block in a Facile One-Pot Procedure

Florian Menk, Suyong Shin, Kyung-Oh Kim, Martin Scherer, Dominik Gehrig, Frédéric Laquai, Tae-Lim Choi*, Rudolf Zentel*

Abstract

Block copolymers composed of a conjugated and a non-conjugated block are interesting materials as they enable directional self-assembly into ordered structures. In contrast to conventional synthetic routes, we synthesized such block copolymers in a facile one-pot procedure exploiting the living nature of ROMP. Therefore, polymers composed of a conjugated MEH-PPV block and a functional polynorbornene block were synthesized. Thus, amphiphilic block copolymers were obtained via incorporation of oxanorbornene carrying a PEG side chain as well as post-polymerization modification of a reactive ester carrying norbornene derivative with methoxypolyethylene glycol amine. The amphiphilic block copolymers can be self-assembled into micelles of different sizes, morphologies and optical properties depending on the polymer composition and the micellization procedure. Furthermore, the reactive ester carrying block copolymer enabled the introduction of anchor groups via primary amines. Consequently, nanocomposites with CdSe@ZnS QDs were fabricated via ligand exchange and studied using time-resolved photoluminescence measurements. The tailoring of optical and morphological properties is an important aspect in the context of optoelectronic devices and emphasizes the relevance of the study at hand. Moreover, the presented approach enables the synthesis of numerous block copolymers combining a conjugated with a non-conjugated block in a facile one-pot procedure.

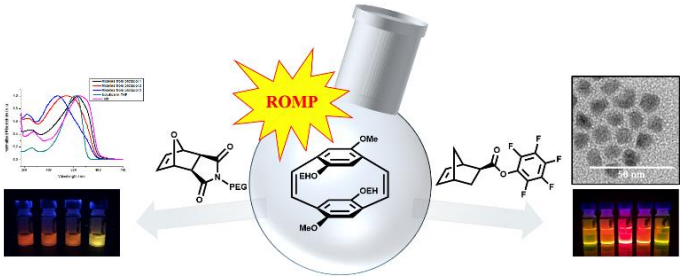

1. Introduction

The synthesis of block copolymers, in general, is a versatile approach to introduce different functionalities into one single polymer. The combination of blocks with orthogonal properties, for example in terms of solubility, enables the formation of aggregates such as micelles, vesicles or elongated structures.[1,2] Approaches for the synthesis of block copolymers can be classified into two general synthetic methods – namely the grafting-onto and the grafting-from approach.[3] In the case of the grafting-onto approach, two polymers carrying reactive counterparts at the polymers' chain end (e.g. azide and alkyne) are coupled.[4] However, polymer end group reactions often suffer from incomplete conversion and purification. The grafting-from approach applies homopolymers exhibiting a functional end group as macro-initiators for the polymerization of the second block. Ideally, block copolymers can be synthesized via a single living polymerization technique such as atom transfer radical polymerization (ATRP), reversible addition-fragmentation chain transfer (RAFT) polymerization or anionic polymerization without involving end group modifications. Unfortunately, as soon as a conjugated backbone is desired, the choice of living polymerization techniques is confined to only three techniques – Grignard metathesis (GRIM) polymerization, cyclopolymerization and ring-opening metathesis polymerization (ROMP). These conjugated polymers are frequently used materials in electronic devices such as light-emitting diodes, solar cells and lasers due to their favorable optoelectronic properties.[5,6,7]

One way to tailor the properties of conjugated polymers is the exploitation of the self-assembly behavior of block copolymers. Therefore, various block copolymers containing P3ATs (poly(3-alkylthiophene)s) as the conjugated block have been synthesized and self-assembled structures such as micelles have been reported.[8,9] The assembly into micelles allows – to some extend – the manipulation of optical properties which means that the optical properties of one single compound can be adjusted for different applications.[4,10] For the synthesis of block copolymers composed of a conjugated and a non-conjugated block, complex synthetic methods involving a combination of different polymerization techniques or polymer end group reactions are usually required. The synthesis via a single polymerization technique is, unfortunately, not trivial. For example, GRIM polymerization is an inappropriate method for the facile block copolymerization of such block copolymers as it is usually limited to conjugated monomers. Therefore, additional synthetic steps, often involving multiple end group reactions, become necessary. Yet, as discussed above, these are undesirable.[8] By contrast, cyclopolymerization is capable of synthesizing both, conjugated as well as non-conjugated backbones.[11] Unfortunately, the conjugated backbone is restricted to

poly(acetylene) derivatives, generally suffering from low stabilities. In addition, ROMP is a suitable technique for the synthesis of the two types of polymers (conjugated and non-conjugated).[2,12] Conjugated polymers applicable via ROMP are poly(acetylene)s, poly(thienylene vinylene)s and, known for their favorable optoelectronic properties, poly(*p*-phenylene vinylene)s (PPVs).[13,14]

The first report of soluble poly(dialkoxy-*p*-phenylenevinylene)s synthesized via ROMP was published in 2006 by Turner and Yu.[14] Their approach for the synthesis of soluble PPVs via ROMP exhibits narrow polydispersity indices (PDIs), allows controlling molecular weights (M_n), enables the incorporation of a distinct end group and the possibility of block copolymerization. The incorporation of a controlled end group was exploited to synthesize a macro initiator for ATRP and for the introduction of supramolecular motifs to facilitate directional self-assembly.[15] Furthermore, fully conjugated block copolymers composed of different conjugated blocks such as poly(2,5-dialkoxy-1,4-phenylene vinylene)s, poly(1,4-phenylene vinylene-2,5-dialkoxy-1,4-phenylene vinylene)s and poly(1,3-phenylene vinylene-2,5-dialkoxy-1,4-phenylene vinylene)s have been synthesized.[16]

Our group recently carried out a study on the varying reactivity of the four individual isomers of dimethoxy-(2-ethylhexyloxy)-[2.2]paracyclophane-1,9-diene to undergo ROMP.[17] The individual isomers were polymerized using various metathesis catalysts and a specific coordination of the aromatic ether substituent on the monomer repeating unit was revealed. Optimized polymerization conditions based on the experiences of the reactivity study enabled controlled living polymerization. Consequently, facile one-pot block copolymerization as shown in **Figure 53Figure 19** became possible.

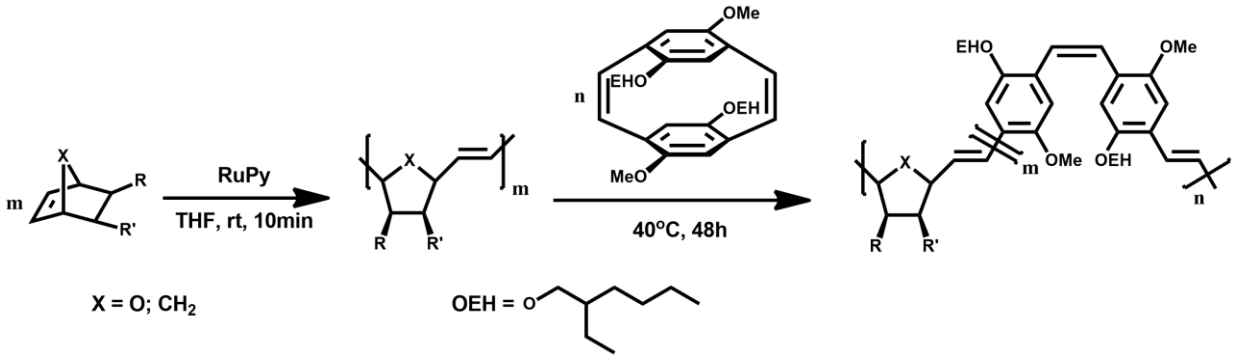

Figure 53. General reaction scheme for the one-pot synthesis of functional block copolymers via ROMP.

In the study at hand we present the synthesis of block copolymers composed of a MEH-PPV block and a second non-conjugated functional block. Notably, as a consequence of the polymerization mechanism, the double bonds of the MEH-PPV block exhibit a cis/trans ratio of approximately 1/1. The non-conjugated block enabled the introduction of different properties and functionalities. Thus, amphiphilic block copolymers synthesized by the introduction of PEG (poly(ethylene glycol)) side chains were assembled into micelles. This enabled a manipulation of the optical properties. In addition, the introduction of a reactive ester containing block permitted the incorporation of amines. Consequently, anchor groups facilitating an effective binding to inorganic nanocrystals and amphiphilic side chains were incorporated via post-polymerization modification. Generally, the possibility to incorporate reactive esters enables the introduction of a broad variety of different functionalities.[18,19] Therefore, the combination of poly(*p*-phenylene vinylene)s with a non-conjugated block via ROMP permits facile incorporation of various functionalities which simplifies modifications for a specific application.

2. Experimental Section

Materials and Characterization. All commercially available chemicals were purchased from Alfa Aesar, Acros Organics, Fluka, Sigma-Aldrich, Tokyo Chemical Industry or Rapp Polymere and used without further purification unless otherwise noted. Anhydrous THF was freshly distilled from sodium under a dry argon atmosphere. All reactions were carried out under dry argon atmospheres using standard Schlenkline techniques. All polymerizations, post-polymerization modifications as well as micellization procedures were carried out in the dark to prevent photoisomerization and photooxidation of the PPV backbone from happening. Exo-7-oxabicyclo[2.2.1]hept-5-ene-2,3-dicarboximide and 4,12-dimethoxy-7,15-di(2'-ethylhexyl-oxy)-[2.2]paracyclophane-1,9-diene (**2**) were synthesized according to the literature.[17,20] ^{1}H-NMR, ^{19}F-NMR and ^{13}C-NMR spectra were acquired on a Bruker ARX 400 at a Lamor frequency of 400 MHz, 400 MHz and 101 MHz, respectively, or by Varian/Oxford As-500 (500 MHz for ^{1}H/125 MHz for ^{13}C) spectrometer. FTIR spectra were performed on a Vector 22 ATR-FTIR-spectrometer made by Bruker. UV/Vis spectra were obtained using Jasco Inc. UV/Vis-Spectrometer V-630. Transmission electron microscopy (TEM) images of the polymer/QD nanocomposites were recorded with JEOL ARM 200 F operating at 20 kV. TEM images of the micelles were collected using a JEOL JEM-2100 operating at 120 kV. TEM samples were prepared by drop casting a dispersion of the QDs in

chloroform or a dispersion of the micelles in water on a standard carbon-coated copper grid. Molecular weights determined by gel permeation chromatography (GPC) were determined using concentrations of approximately 1.2 mg/mL in THF with polystyrene as external and toluene as internal standard. Time-resolved photoluminescence was measured with a Streak Camera System (Hamamatsu C4742, C5680) on a nanosecond timescale. The excitation wavelength was 510 nm with ~6 ps pulse duration, using the output of an ultrafast fiber laser (Fianium SC-400-2-PP). Description of the dynamic light scattering (DLS) experiments can be found in the Supporting Information.

Synthesis of exo-*N*-PEG-7-oxabicyclo[2.2.1]hept-5-ene-2,3-dicarboximide (PEG-ONB, 1). Compound **1** was synthesized following a modified literature procedure.[21] A 250 mL round bottom flask was charged with exo-7-oxabicyclo[2.2.1]hept-5-ene-2,3-dicarboximide (0.650 mg, 3.936 mmol, 6 eq.), Ph_3P (1.032 mg, 3.936 mmol, 6 eq.) and PEG-OH ($M_n \approx 350$ g/mol, 0.230 mg, 0.656 mmol, 1 eq.) while an argon atmosphere was applied. 60 mL of dry THF were added and the reaction mixture was cooled to 0 °C. After dropwise addition of DIAD (0.796 mg, 3.936 mmol, 6 eq.) the reaction mixture was stirred for 72 h at room temperature. The solvent was removed under reduced pressure and the crude product purified by column chromatography on silica gel using a gradient eluent system (1. DCM, 2. MeOH/DiEt 4/96 – 10/90). The product was obtained as an almost colorless oil in a yield of 64 % (210 mg, 0.423 mmol, $M_n \approx 497$ g/mol).
^{1}H-NMR (400 MHz, $CDCl_3$, δ): 6.50 (t, J = 0.9 Hz, 2H, =CH-), 5.24 (t, J = 0.9 Hz, 2H, -CH-), 3.58 – 3.68 (m, 30H, O-CH_2-), 3.52 – 3.54 (m, 2H, N-CH_2-), 3.36 (s, 3H, OCH_3) 2.84 (s, 2H, O=C-CH-); ^{13}C-NMR (101 MHz, $CDCl_3$, δ): 176.24, 136.79, 136.51, 81.17, 80.81, 72.23, 72.03, 71.83, 70.84 – 70.48, 70.16, 69.97, 69.58, 69.47, 69.39, 67.41, 67.22, 67.04, 59.25, 59.02, 47.73, 47.44, 38.28; IR: ν (cm^{-1}) = 2870, 1698, 1096.

Synthesis of pentafluorophenyl bicyclo[2.2.1]hept-5-ene-exo,endo- 2-carboxylate (PFP-NB, 2). Bicyclo[2.2.1]hept-5-ene-exo,endo-2-carboxylic acid (5.00 g, 36.19 mmol, 1 eq.), *N*,*N*'-Dicyclohexylcarbodiimide (7.47 g, 36.19 mmol, 1 eq.) and pentafluorophenol (7.33 g, 39.81 mmol, 1.1 eq.) were dissolved in dichloromethane (100 mL) at 0 °C. Then 4-dimethylaminopyridine (0.22 g, 1.81 mmol, 0.05 eq.) was added. The reaction was monitored by TLC and stirred until all the starting materials were consumed. The urea by-product was filtered off and the mixture was purified by column chromatography (diethyl ether/hexane = 3/7). Concentration of the solvent afforded the product as a colorless oil (yield: 96%).

^{1}H-NMR (400 MHz, $CDCl_3$, δ): 6.27-6.29 (*endo*, m, 1H, olefin), 6.17-6.24 (*exo*, m, 2H, olefin), 6.05-6.07 (*endo*, m, 1H, olefin), 3.42 (*endo*, s, 1H, COORCHCH), 3.29-3.33 (*endo*, m, 1 H, -CH_2CH), 3.27 (*exo*, s, COORCHCH), 3.01 (*exo*/*endo*, s, 1H, COORCH), 2.57-2.61 (*exo*, m, -CH_2CH), 2.01 – 2.10 (*exo*/*endo*, m, 1 H, COORCHCH_2), 1.37 – 1.58 (*exo*/*endo*, m, 3 H, bridge+COORCHCH_2); ^{13}C-NMR (101 MHz, $CDCl_3$, δ): 172.54, 170.86, 141.31 (d, J_{HF} = 260 Hz), 139.43 (d, J_{HF} = 253 Hz), 138.67, 138.65, 137.97 (d, J_{HF} = 254 Hz), 135.46, 131.98, 125.41, 49.94, 47.16, 46.55, 46.43, 43.04, 42.87, 42.75, 41.95, 30.89, 29.47; ^{19}F-NMR (400 MHz, $CDCl_3$, δ): - 154.37 – - 154.05 (m, 2F), - 159.75 – - 159.54 (m, 1F), - 163.90 – - 163.64 (m, 2F); IR: ν (cm^{-1}) = 2981, 1781, 1516, 1090, 995.

Synthesis of poly(PEG-ONB-*b*-MEH-PPV). In a flame-dried vial, PEG-ONB (7.40 mg, 14.89 μmol, 40 eq.) was dissolved in 120 μL of degassed, dry THF. RuPy (0.54 mg, 0.74 μmol, 2 eq.) was separately dissolved in 58 μL of degassed, dry THF. Then, 29 μL of the catalyst's solution (0.37 μmol, 1 eq.) were added to the monomer solution. After ten minutes, a solution of 4,12-dimethoxy-7,15-di(2'-ethylhexyloxy)-[2.2]paracyclophane-1,9-diene (1.74 mg, 3.35 μmol, 9 eq.) in 74 μL of degassed, dry THF was added. The reaction mixture was then stirred for 72 h at 40 °C. The reaction was stopped adding EVE and purified through dialysis against THF. The product was collected as a red semi-solid in quantitative yield (M_n = 16.9 kg/mol, PDI = 1.29).

^{1}H-NMR (400 MHz, $CDCl_3$, δ): 7.30 – 7.52 (m, Ar-H *trans*), 7.09 – 7.21 (m, Ar-CH=CH *trans*), 6.65 – 6.87 (m, Ar-H + Ar-CH=CH *cis*), 6.04 – 6.11 (br, CH=CH *trans*), 5.70 – 5.84 (br, CH=CH *cis*) 4.89 – 5.11 (br, ROCH *cis*), 4.37 – 4.50 (br, ROCH *trans*), 3.83 – 3.99 (m, OCH_3 + OCH_2R *trans*), 3.42 – 3.80 (br, OCH_3 + OCH_2R *cis* + PEG-CH_2), 3.37 (s, PEG-OCH_3), 3.26 – 3.37 (br, O=C-CH), 1.15 – 1.65 (m, OCH_2CH + CH_2), 0.77 – 1.03 (m, OCH_3).

General procedure for the synthesis of poly(PFP-NB-*b*-MEH-PPV). In a flame-dried vial, PFP-NB (5.84 mg, 19.21 μmol, 10 eq.) was dissolved in 150 μL of degassed, dry THF. RuPy (2.79 mg, 3.84 μmol, 2 eq.) was separately dissolved in 84 μL of degassed, dry THF. Then, 42 μL of the catalyst's solution (1.92 μmol, 1 eq.) was added to the monomer solution. After ten minutes, a solution of 4,12-dimethoxy-7,15-di(2'-ethylhexyloxy)-[2.2]paracyclophane-1,9-diene (20.01 mg, 38.42 μmol, 20 eq.) in 192 μL of degassed, dry THF was added. The reaction mixture was then stirred for 48 h at 40 °C. The reaction was stopped adding EVE and purified via precipitation in methanol. The product was collected as a red solid in quantitative yield (M_n = 23.2 kg/mol, PDI = 1.25).

^{1}H-NMR (400 MHz, $CDCl_3$, δ): 7.32 – 7.51 (m, Ar-H *trans*), 7.10 – 7.23 (m, Ar-CH=CH *trans*), 6.63 – 6.90 (m, Ar-H + Ar-CH=CH *cis*), 5.24 – 5.69 (br, CH=CH *cis*/*trans*), 3.80 – 4.04 (m, OCH_3 + OCH_2R *trans*), 3.39 – 3.55 (m, OCH_3 + OCH_2R *cis*), 3.22 – 3.37 (br, COORCHCH + CH_2CH), 2.86 – 3.09 (br, COORCH), 2.15 – 2.38 (br, $COORCHCH_2$), 1.79 – 2.11 (br, $COORCHCH_2$ + $CHCH_2$), 1.13 – 1.79 (m, $CHCH_2$ + OCH_2CH + CH_2), 0.76 – 1.06 (m, OCH_3); ^{19}F-NMR (400 MHz, $CDCl_3$, δ): - 153.26 – - 152.27 (br, *ortho*), - 154.82 – - 153.85 (br, *ortho*), - 159.73 – - 158.86 (br, *para*), - 164.20 – - 163.22 (br, *meta*).

General procedure for post-polymerization modifications. In a vial wrapped with aluminum foil, poly(PFP-NB-*b*-MEH-PPV) (0.156 µmol, 1 eq.) was dissolved in 1 mL of dry THF under an argon atmosphere. The respective primary amine (9.37 µmol, 60 eq.) and triethylamine (9.37 µmol, 60 eq.) were added and the reaction mixture was stirred at 30 °C for 48 – 72 h. Purification was achieved either by precipitation in methanol or dialysis against purified water.

P3: ^{1}H-NMR (400 MHz, $CDCl_3$, δ): 7.31 – 7.50 (m, Ar-H *trans*), 7.08 – 7.21 (m, Ar-CH=CH *trans*), 6.64 – 6.86 (m, Ar-H + Ar-CH=CH *cis*), 3.83 – 4.00 (m, OCH_3 + OCH_2R *trans*), 3.43- 3.81 (br, OCH_3 + OCH_2R *cis* + PEG-CH_2), 3.36 (s, PEG-OCH_3), 1.10 – 1.75 (m, OCH_2CH + CH_2), 0.76 – 1.07 (m, OCH_3). Note: Due to the strong signals of the PEG side chain the signals of the norbornene backbone cannot clearly be distinguished from the background. ^{19}F-NMR (400 MHz, $CDCl_3$, δ): no signals.

P4: ^{1}H-NMR (400 MHz, $CDCl_3$, δ): 7.31 – 7.49 (m, Ar-H *trans*), 7.09 – 7.23 (m, Ar-CH=CH *trans*), 6.66 – 6.91 (m, Ar-H + Ar-CH=CH *cis*), 5.17 – 5.57 (br, CH=CH *cis*/*trans*), 3.79 – 4.06 (m, OCH_3 + OCH_2R *trans*), 3.38 – 3.57 (m, OCH_3 + OCH_2R *cis* + $NHCH_2$ + O=C-CH), 2.62 – 2.89 (br, O=C-CHCH + CH_2CH + SCH_2), 2.36 – 2.47 (br, SCH_3), 1.13 – 2.10 (m, OCH_2CH + CH_2 + O=C-$CHCH_2$ + $CHCH_2$), 0.75 – 1.05 (m, OCH_3); ^{19}F-NMR (400 MHz, $CDCl_3$, δ): no signals.

P5: ^{1}H-NMR (400 MHz, $CDCl_3$, δ): 7.32 – 7.48 (m, Ar-H *trans*), 7.09 – 7.22 (m, Ar-CH=CH *trans*), 6.63 – 6.89 (m, Ar-H + Ar-CH=CH *cis*), 5.16 – 5.55 (br, CH=CH *cis*/*trans*), 3.80 – 4.04 (m, OCH_3 + OCH_2R *trans*), 3.39 – 3.55 (m, OCH_3 + OCH_2R *cis*), 3.18 – 3.37 (br, $NHCH_2$ + O=C-CH), 2.60 – 2.88 (br, O=C-CHCH + CH_2CH), 2.28 – 2.51 (br, NR_2CH_2 + O=C-$CHCH_2$), 2.12 – 2.28 (br, $N(CH_3)_2$), 1.12 – 2.05 (m, OCH_2CH + CH_2 + $CHCH_2$), 0.76 – 1.04 (m, OCH_3); ^{19}F-NMR (400 MHz, $CDCl_3$, δ): no signals.

Micellization. In a vial wrapped with aluminum foil, 1.5 mg of the amphiphilic block copolymer were dissolved either in 0.5 mL of THF (protocol 1) or acetone (protocol 2). The solution was stirred and 3.0 mL of purified water were added via a syringe pump over a period of 17.5 h. The obtained dispersions were kept at 30 °C for 24 h to remove the organic solvent. For protocol 3, 1.5 mg of the amphiphilic block copolymer were directly dispersed in 3.0 mL of purified water.

General procedure for the functionalization of QDs. In a vial wrapped with aluminum foil, 1.35 mg of the respective polymer were dissolved in chloroform and an argon atmosphere was established. The polymer solution was placed in an ultrasonic bath and 1.35 mg CdSe@ZnS QDs (22.5 µL, c = 60 mg/mL) dispersed in toluene were added. The dispersion was placed in an oil bath and stirred over night at 30 °C. For purification, the dispersion was precipitated in *n*-hexane and centrifuged. The overlaying solution was removed before the functionalized QDs were redispersed in chloroform. This procedure was repeated three times.

3. Results and Discussion

Block copolymers containing one PPV block and one non-conjugated block create the possibility of directional self-assembly into microphase separated structures. Especially amphiphilic block copolymers can be assembled into micelles with different dimensions depending on the polymer composition.[22] Despite their interesting properties, only a few examples of amphiphilic block copolymers were reported which involve a conjugated PPV block exhibiting more than ten repeating units.[22,23] By contrast, due to its favorable optoelectronic properties, MEH-PPV homopolymers were applied to various applications (e.g. light-emitting diodes, solar cells and lasers) which underlines the high relevance of facile modification techniques in terms of functionalities and optoelectronic properties regarding MEH-PPV.[6,7,24] In a recent study we investigated the reactivity behavior of the four isomers of dimethoxy-(2-ethylhexyloxy)-[2.2]paracyclophane-1,9-diene which, in principle, can be used for the synthesis of MEH-PPV via ROMP. Following the results from this study, we optimized the polymerization process which enables the one-pot synthesis of functional block copolymers.

In a first approach, the amphiphilic block copolymer was synthesized by a one-pot procedure polymerizing firstly the hydrophilic block and secondly the hydrophobic block. Therefore, as first block, an oxanorbornene which was modified with a short PEG side chain (PEG-ONB, **1**)

was polymerized. The short length of the PEG side chain was chosen to simplify complete functionalization of the oxanorbornene precursor, enable successful purification via column chromatography and, thus, guarantee the absence of free PEG bearing a hydroxy end group. After approximately ten minutes full conversion was reached and the second monomer (**2**), 4,12-dimethoxy-7,15-di(2'-ethylhexyloxy)-[2.2]paracyclophane-1,9-diene, was added in order to obtain the conjugated MEH-PPV block (see **Figure 54**). The synthesized MEH-PPV block exhibits an approximate 1/1 ratio of cis and trans double bonds as verified via ^{1}H-NMR spectroscopy (see **Figure S6**). The backbone can be isomerized to an all trans configuration via illumination at 365 nm for 36 hours (c = 2 mg/mL).[25] For the investigations performed in the present study, isomerization was prevented by conducting the reactions and storing the block copolymers in the dark and limiting their exposure to sunlight to only some minutes.

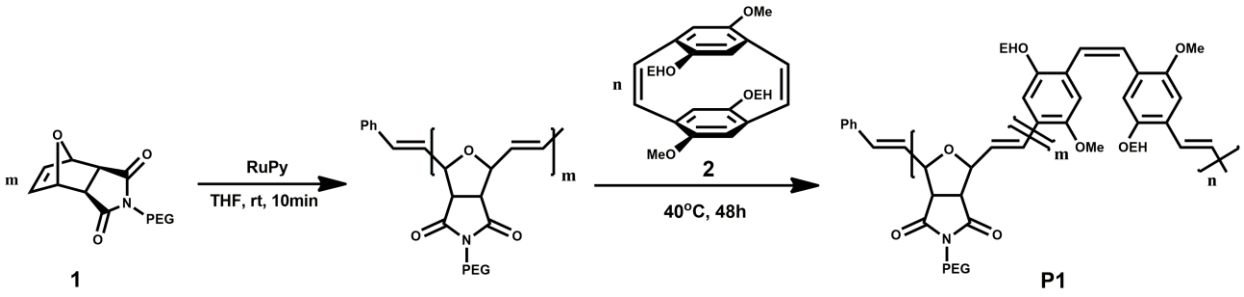

Figure 54. Reaction scheme illustrating the one-pot synthesis of the amphiphilic block copolymer **P1** composed of PEG modified oxanorbornene (**1**) as first block and MEH-PPV as second block.

To the best of our knowledge, this approach presents the first route for a one-pot synthesis of an amphiphilic block copolymer containing a PPV block or, in general, a backbone conjugated block. The simplicity of this approach prevents impurities such as homo polymers which would be difficult to separate from the desired block copolymer. The absence of polymeric or low molecular weight impurities is assured by the monomodal GPC trace and the ^{1}H-DOSY spectrum (see **Figure S7**). To achieve a suitable composition for micelle formation, the length of the first hydrophilic block was adjusted to a DP ≈ 40 and the second hydrophobic block to a DP ≈ 9 which results in a weight ratio of 81 to 19. The obtained polymer (**P1**) was used for the formation of micelles following different micellization protocols. Depending on the procedure, the average size and the morphology of the micelles were varied which allowed for a manipulation of the optical properties (see **Table 2**). The micelle formation will be discussed at a later point in this section together with the results of polymer **P3**. Although the PDI of the resulting polymer was relatively narrow (PDI = 1.29,

M_n(GPC) = 17 kg/mol), due to purification issues of the oxanorbornene monomer this approach was not assumed to be very promising with regards to the incorporation of long PEG side chains. Therefore, a second approach was applied which involved the introduction of a reactive ester block. In this procedure, as first block, the reactive ester functionalized norbornene (monomer **3**) was polymerized. After full conversion was achieved (around ten minutes), the second monomer (**2**) was added for the synthesis of the MEH-PPV block. The composition of the block copolymer was well controllable and moderate PDIs were obtained (see **Table 1**). The successful synthesis of well-defined block copolymers is evidenced by the monomodal GPC traces and diffusion NMR spectroscopy (see **Figure S8**). As reported in the literature, reactive esters are tolerant of many functional groups such as alcohols and thiols while being reactive towards various amines.[19,26] To achieve modified optical properties of the MEH-PPV block (compared to **P1**), polymer **P2c** exhibiting a long conjugated block with DP ≈ 40 and a short norbornene block with DP ≈ 10 was chosen for further studies.

Table 1. Polymer composition, molecular weights and PDIs of all polymers.

Polymer	First Block (A)	Second Block (B)	Block Ratio (A:B)	M_n [a)] (kg · mol^{-1})	M_n [b)] (kg · mol^{-1})	PDI[b)]
P1	PEG-ONB	MEH-PPV	40:9	24.7	16.9	1.29
P2a	PFP-NB	MEH-PPV	10:10	8.4	6.9	1.17
P2b	PFP-NB	MEH-PPV	10:20	13.6	23.2	1.25
P2c	PFP-NB	MEH-PPV	10:40	24.0	36.2	1.30
P3	PEG-NB	MEH-PPV	10:40	122.9	83.5	1.49
P4	SSMe-NB	MEH-PPV	10:40	23.4	41.4	1.36
P5	$N(Me)_2$-NB	MEH-PPV	10:40	23.0	28.9	1.32

[a)] expected value from initial catalyst to monomer ratio (including end groups), [b)] determined by GPC which was calibrated with polystyrene standards.

In order to obtain a suitable ratio of the hydrophobic to the hydrophilic block, polymer **P2c** was reacted with commercially available CH_3O-PEG-NH_2 (M_n = 10000 g/mol). The resulting amphiphilic block copolymer has a theoretical weight ratio of the hydrophilic to the hydrophobic block of 83 to 17. Purification of the product was achieved by dialysis against water. Successful incorporation of the PEG side chain was verified by ^{1}H-NMR spectroscopy.

While all signals of the MEH-PPV backbone remained, signals from the PEG repeating unit were detected at 3.44 – 3.81 ppm. Furthermore, the ratio of the methoxy end group of the PEG side chains (3.36 ppm, s, 3H) to the signals from the aromatic and olefinic protons in proximity to cis double bonds of the MEH-PPV block (6.64 – 6.89 ppm, m, 4H) is 0.76 to 4.00 (see **Figure 55**). This corresponds to a block ratio of the PEG functionalized norbornene block to the MEH-PPV block of 10 to 40. Full conversion of the post-polymerization modification was evidenced by the absence of any signals in the ^{19}F-NMR spectrum after purification (see **Figure S9**).

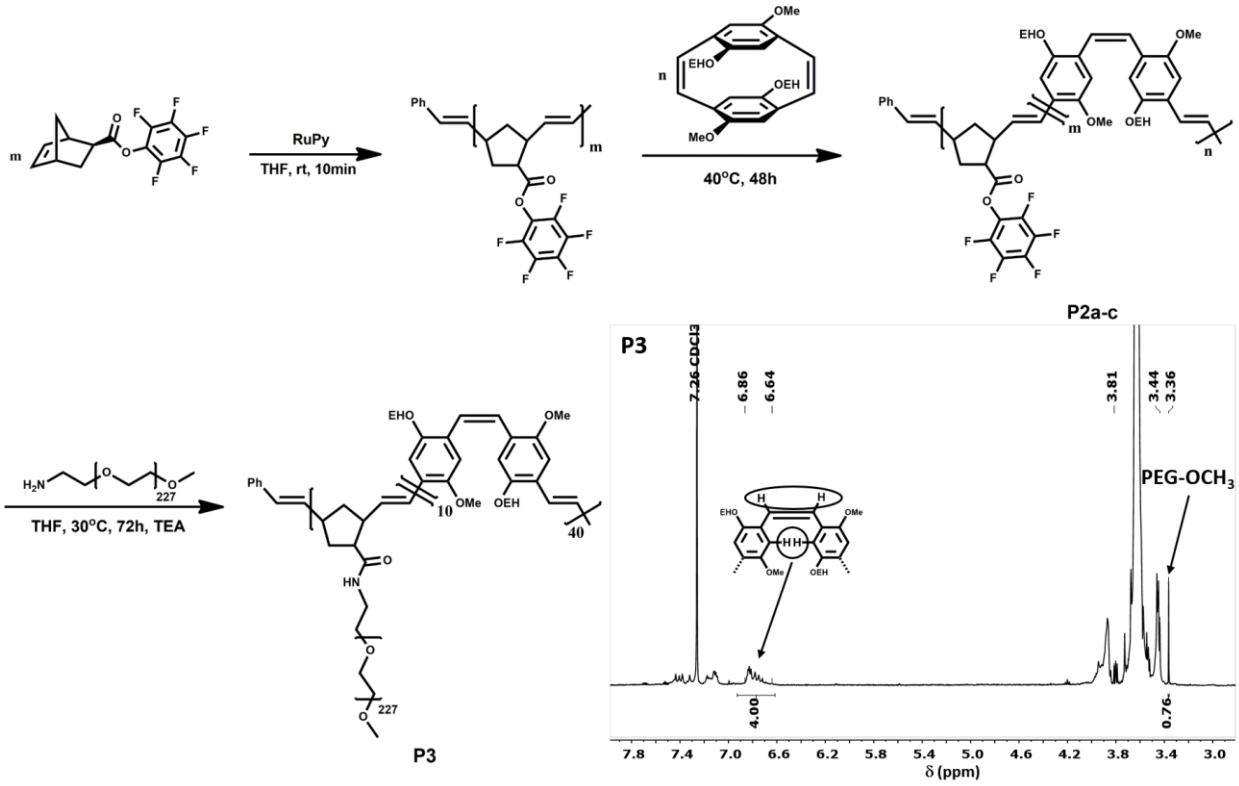

Figure 55. Reaction scheme and ^{1}H-NMR spectrum (in $CDCl_3$) of the synthesis of the amphiphilic block copolymer **P3** via post-polymerization modification of precursor polymer **P2**.

Both amphiphilic block copolymers **P1** and **P3** were used for the fabrication of micelles. The self-assembly of both polymers was achieved applying three different micellization procedures. In the first procedure, the polymer was dissolved in warm THF (≈ 40 °C) which is a good solvent for both blocks and the self-assembly was induced by slow addition of water. In the second procedure, before self-assembly was induced by slow addition of water, the polymer was dissolved in acetone which is a moderate solvent for both blocks. In the third procedure, the undissolved polymer was directly dispersed in water. The different approaches

were applied in order to vary the sizes and morphologies of the micelles. In all cases, the micelle formation was carried out at a polymer concentration of c = 0.5 mg/mL in the resulting dispersion (after removal of the organic solvent). The average size, the morphologies and the optical properties of the micelles could by varied depending on the micellization procedure (see **Table 2**).

Table 2. Properties of the amphiphilic block copolymers and micelles obtained from different micellization protocols.

			Absorption		
Protocol	**Polymer**	**R_h / nm[d)]**	**λ_{max} / nm**	**λ_{onset} / nm**	**λ_{PL} / nm**
-	P1	-	469	549	561
1[a)]	P1	58.8	489	621	599
2[b)]	P1	64.9	467	607	599
3[c)]	P1	78.2	445	616	594
-	P3	-	508	553	565
1[a)]	P3	78.2	516	595	595
2[b)]	P3	92.6	469	587	593
3[c)]	P3	93.5	435	580	592

[a)] Micellization via addition of water into THF solution, [b)] Micellization via addition of water into acetone solution, [c)] Micellization via dispersion in water [d)] Hydrodynamic radius determined by DLS.

As shown in **Table 2**, the size of the nanoparticles determined via DLS increased from micellization protocol 1 to 3 (autocorrelation functions for the measurements of micelles obtained from **P3** are displayed in **Figure S18**). Moreover, the micelles' morphologies depended on the micellization protocol. Self-assembly of polymer **P3** following protocol 1 resulted in the formation of regular micelles as displayed in **Figure 56a**. Due to dissolution in a good solvent (THF) prior to the addition of water, the self-assembly occurred in a controlled manner leading to regular micelles. Following protocol 2, the block copolymer (**P3**) assembled into short chain-like aggregates (see **Figure 56b**). As acetone is a moderate solvent for both blocks, preaggregation occurred resulting in the formation of partially fused micelles upon the addition of water. The self-assembly into micelles applying protocol 3 also led to the

formation of fused aggregates. Caused by the instantaneous self-assembly from the undissolved state, the fusion of the micelles was less controlled leading to the micelle clusters depicted in **Figure 56c**. The increasing size and accumulation of the micelles result from the rising degree of preaggregation of the polymer from protocol 1 to 3. Similar results were observed for polymer **P1** (see **Figure S10**). Comparing the UV/Vis spectra of polymers **P1** and **P3** in THF, in acetone and in film confirms the rising degree of aggregation prior to self-assembly induced via the addition of water as displayed in **Figure S11**. Notably, the higher solubility of **P1** in acetone led to the coexistence of regular micelles and caterpillar-like aggregates when applying protocol 2 (see **Figure S10**). Nevertheless, all dispersions exhibited colloidal stability over several weeks (stored under dark conditions).

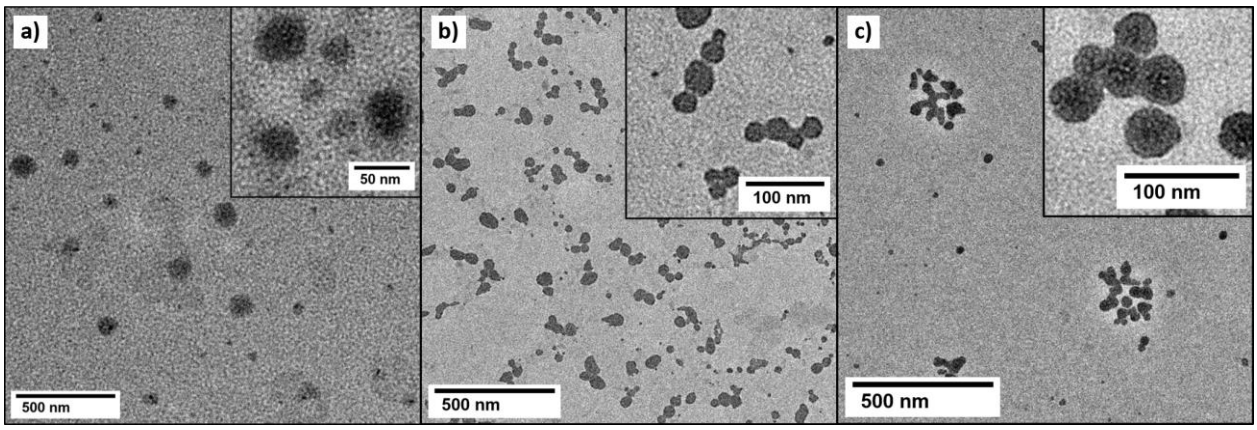

Figure 56. TEM images of micelles obtained from the self-assembly of polymer **P3** following protocols 1 – 3 (from left to right). a) Regular micelles are obtained applying protocol 1. b) Partially fused micelles in the shape of caterpillars are formed following protocol 2. c) Further merging of micelles leads to larger aggregates (protocol 3).

Interestingly, micelle formation had an influence on the optoelectronic properties. In order to investigate this influence, the emission and absorption spectra of the micelles and the polymers dissolved in THF were compared. The emission spectra (**Figure S12**) of the micelles display a bathochromic shift of approximately 30 nm compared to the non-aggregated polymer. However, the spectra reveal only a slight dependence on the micelles' size (see **Table 2** and **Figure S12**). In **Figure 57a**, a photograph comparing the emission of the micellar dispersions with a solution of **P3** in THF is shown. In agreement with the photoluminescence spectra, the appearance of the dispersions is hardly affected by the micellization procedure.

By contrast, the absorption responsible for the optical appearance of the micellar dispersions and the solution of **P3** (no UV irradiation) reveals differences for all samples (see **Figure 57b**). Therefore, the absorption properties were investigated in more detail.

While the size of micelles is increasing from protocol 1 to 3, the absorption maximum is decreasing and is shifted from 489 to 445 nm in the case of **P1** and 516 to 435 nm in the case of **P3**, respectively. This corresponds to a shift of the absorption maximum of 44 nm (**P1**) and 81 nm (**P3**), respectively, which allows for an adjustment of the absorption properties to match the requirements for a specific application.

When comparing the optical properties of the micelles with the properties of the non-aggregated polymer dissolved in THF, a general broadening of the spectra in the case of micelles is observed (see **Figure 57c** and **Figure S13a**). This "inhomogeneous broadening" is caused by a larger deviation of the microenvironment in the case of nanoparticles compared with non-aggregated polymers.[27] Furthermore, the onset of the absorption is strongly red shifted (approximately 30 to 70 nm depending on the micellization procedure) which is resulting from areas in which the conjugated backbone is highly ordered. Therefore, the absorption's onset is at a similar wavelength as compared to the film spectra (see **Figure 57c** and **Figure S13a**).

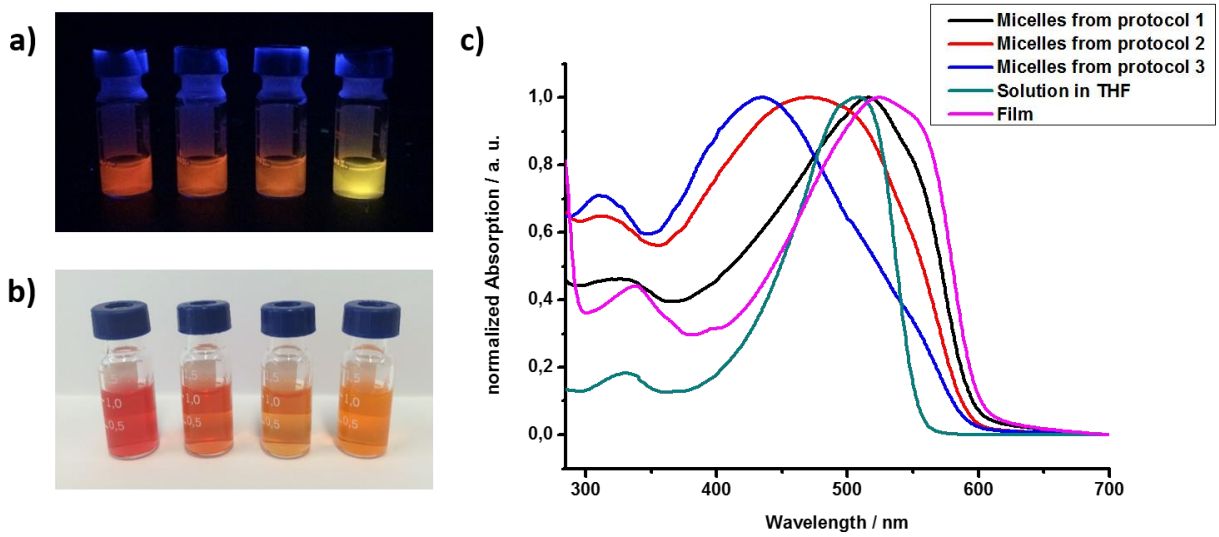

Figure 57. a) Photographs with and b) without UV irradiation @ 365 nm (from left to right: micelles from protocol 1, 2, 3 and solution in THF, respectively). c) Absorption spectra of micelles from polymer **P3** in water fabricated following micellization protocols 1 – 3, spectrum of solution in THF and film spectrum. Spectra and photographs obtained from polymer **P1** can be found in the Supporting Information (**Figure S13**).

For a deeper understanding of the micellization procedure's influence on the optical properties it is important to take several aspects into account. On the one hand the stacking of the conjugated chains in the micelles leads to an increase of the conjugation and, therefore, causes a red shift of the absorption (i.e., micelles obtained from protocol 1). In addition, a vibronic shoulder indicating a partial crystallization of the conjugated core can be observed which is comparable to the film spectra (see **Figure 57c** and **Figure S13a**).[4] On the other hand the interaction of the MEH-PPV with water has to be considered. Solvatochromism was described for amphiphilic oligomers composed of hydrophobic alkoxy substituted oligo(phenylene vinylene)s and a hydrophilic PEG unit.[28,29] The absorption showed hypsochromic shifts in the range of 45 nm when comparing micelles with the non-aggregated polymer.[29] This is similar to the maximum hypsochromic shift observed in the study at hand of approximately 25 (**P1**) and 70 nm (**P3**) with respect to the particular polymer.

Taking a look at the non-normalized absorption spectra (c = 0.5 mg/mL) the increasing influence of water, associated with a progressive blue shift, is supported. An intensity decrease from the non-aggregated polymer over the micelles obtained from protocol 1 to the micelles obtained from protocol 2 and 3 is observed (see **Figure S14**).

To demonstrate the versatile possibilities resulting from the incorporation of the reactive ester, two further primary amines were incorporated via post-polymerization modification. One of the amines possessed a disulfide (**P4**) and the other one a tertiary amine (**P5**) as a second functional group (see **Figure 58a**). Both groups are known to support an effective binding towards inorganic nanocrystals such as CdSe@ZnS quantum dots (QDs).[30] Hence, the incorporation of these amines underlines the wide applicability of the approach involving the reactive ester.

The success of the reactions was verified using ^{19}F- and ^{1}H-NMR spectroscopy. The absence of any signals in the ^{19}F-NMR spectrum evidences full conversion of the pentafluorophenyl ester. Furthermore, in the ^{1}H-NMR spectrum signals from the incorporated amines are detected (see **Figure 58b**+**c**). For polymer **P4** a singlet resonates at 2.41 ppm and a broad signal occurs at 2.78 ppm (in $CDCl_3$) which can be assigned to the methyl and methylene group, respectively, attached to the disulfide. In the spectrum of polymer **P5**, a singlet at 2.20 ppm and a broad signal at 2.36 ppm are detected. The first can be assigned to the methyl groups attached to the tertiary amine and the second signal originates from the methylene group adjacent to the tertiary amine. The third signal resonates at approximately 3.30 ppm and overlaps with a signal of the cyclopentane unit. Furthermore, in the IR spectra the signal of

the pentafluorophenyl ring (1519 cm^{-1}) disappears after the reaction with the amines.[26,31] The C=O band shifts from 1780 cm^{-1} in the ester to 1646 cm^{-1} (**P4**) and 1649 cm^{-1} (**P5**) in the amides (see **Figure S15**). Moreover, in **P4** two C-S bands are detected at 732 and 756 cm^{-1}.

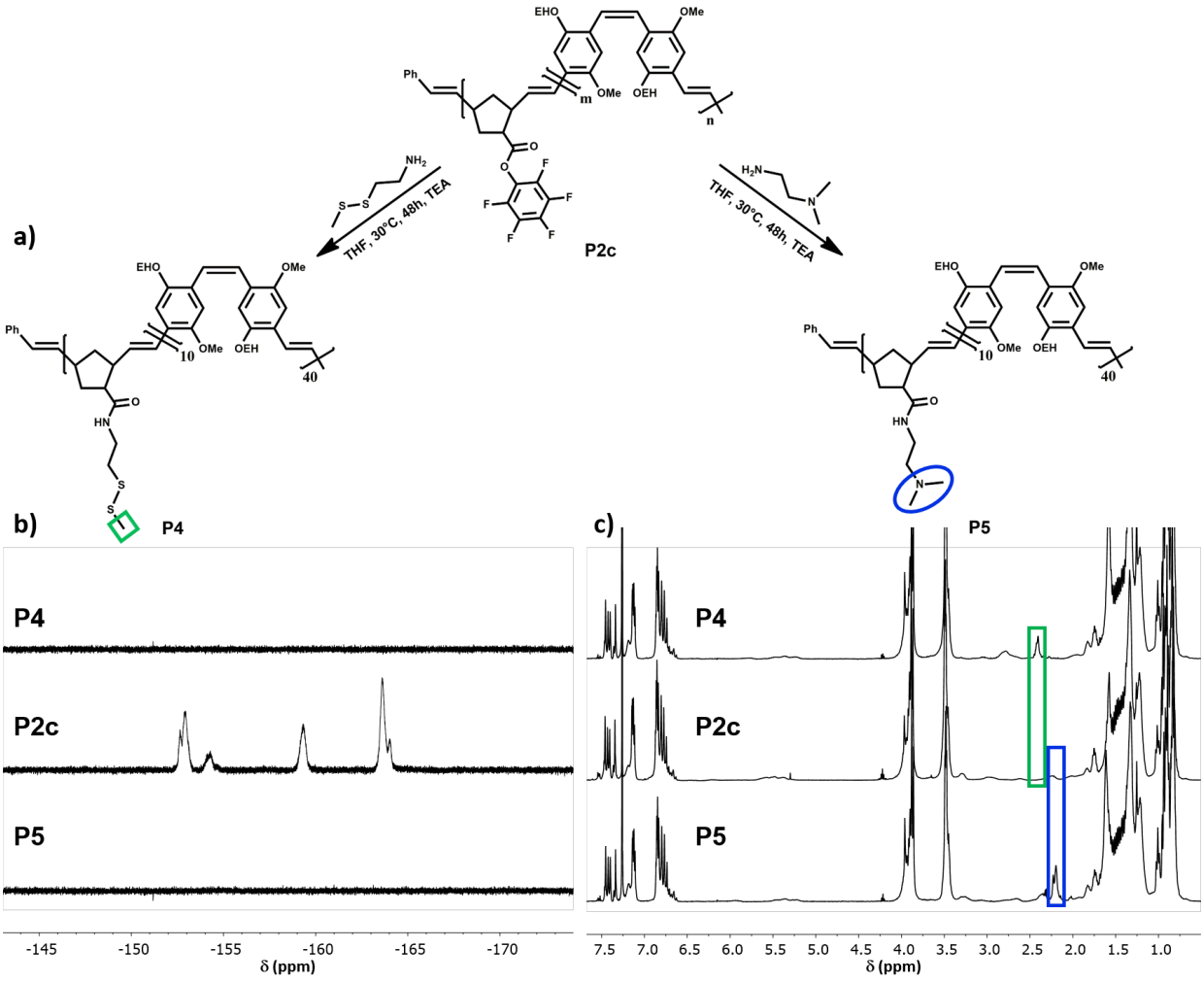

Figure 58. a) Incorporation of anchor groups via post-polymerization modification for the synthesis of polymers **P4** and **P5**; b) ^{19}F-NMR and c) ^{1}H-NMR spectra (in $CDCl_3$) of precursor polymer **P2c** (middle), polymer **P4** (top) and polymer **P5** (bottom). The ^{19}F-NMR spectra prove full conversion of the aminolysis and in the ^{1}H-NMR spectra new signals of the anchor groups are detected (see indication).

Both polymers (**P4** and **P5**) were used for the functionalization of CdSe@ZnS quantum dots via ligand exchange and hybrids **H4** and **H5**, respectively, were fabricated. While the pristine QDs (functionalized with oleic acid) form a stable dispersion in *n*-hexane, the polymer-coated

quantum dots precipitate in *n*-hexane. Therefore, unfunctionalized QDs can easily be separated from the polymer-coated QDs. Under irradiation with UV light (365 nm), the precipitated hybrids show emission in the color of the QDs which confirms the presence of QDs in the hybrid materials (see **Figure 59c**). Furthermore, the IR spectra of the hybrids **H4** and **H5** exhibit all bands of the polymer surfactant as well as a band at approximately 1540 cm^{-1} which originates from the zinc sulfide shell of the QDs (and not from oleic acid). In addition, in the case of hybrid **H4** both C-S bands which are detectable in the spectrum of polymer **P4** (732 and 756 cm^{-1}) vanished due to the interaction with the QD surface (see **Figure 59a**). Consequently, the hybrids form stable dispersions which are composed of well-dispersed QDs as observed by the help of transmission electron microscopy (TEM) (see **Figure 59b** and **Figure S16**).

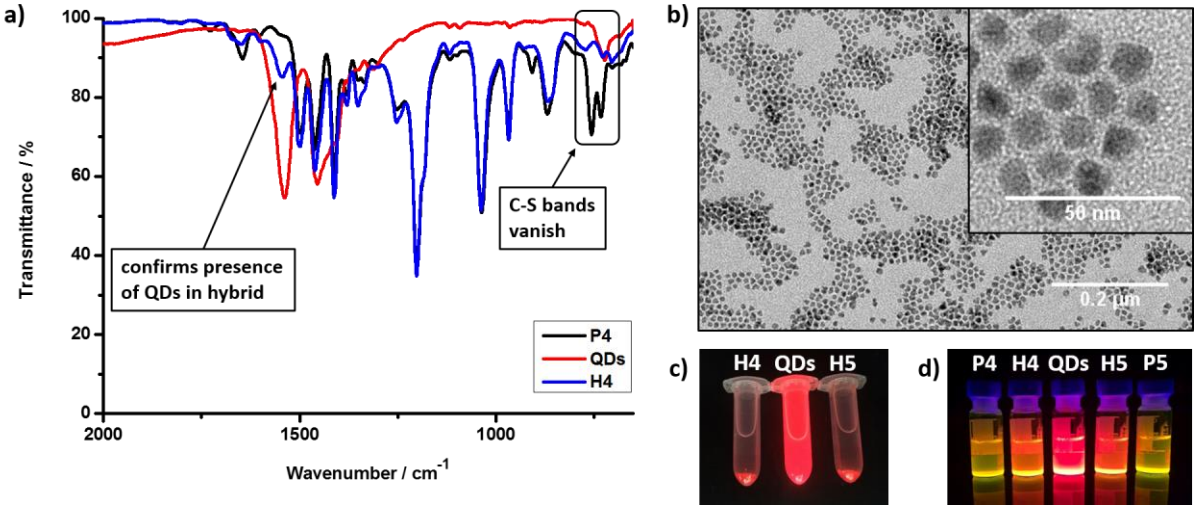

Figure 59. a) FTIR spectra monitoring the successful functionalization of the CdSe@ZnS QDs with polymer **P4**, b) TEM images of **H4** exhibiting well-dispersed QDs, c) precipitated hybrids **H4** and **H5** and stable dispersion of QDs in *n*-hexane under UV irradiation @ 365 nm, d) chloroform solutions of polymers **P4**, **P5**, hybrids **H4**, **H5** and the unfunctionalized QDs under irradiation with UV light (365 nm). The FTIR spectra monitoring the functionalization of the QDs with **P5** and TEM images of **H5** can be found in the Supporting Information (**Figure S16**).

The close contact of the QDs with the polymer coating results in the interaction of both materials. Under UV irradiation at 365 nm both, the unfunctionalized QDs as well as the hybrids, exhibit emission characteristic for the QDs (**Figure 59d**). To achieve further evidence for the interaction of the QDs with the polymer coating, time-resolved photoluminescence measurements were performed. Firstly, the pure polymers and QDs were

investigated. The decay of **P4** and **P5** could be described with a monoexponential decay function resulting in inverse decay rates of 0.41 and 0.42 ns, respectively (**Figure S17**). Interestingly, the lifetime of the polymer excited states were not affected when linked to the QDs. Also the decay of the QDs showed a monoexponential decay behavior with a larger inverse decay rate of 24.8 ns. When the QDs were mixed with the precursor polymer **P2c** (no bonding/hybrid formation) a biexponential decay was detected which consists of the parallel decay of polymer and QD emission. The inverse decay rate of the QD emission remained similar with an inverse decay rate of 21.5 ns which accounted for a relative amplitude of 12 % of the overall decay tracked in a wavelength range of 625–645 nm, *i.e.* the emission maximum of QD emission (**Figure 60**). The decay is, however, accelerated when the polymers are attached to the QDs via disulfide or tertiary amine functionalities (**H4** and **H5**). In fact, the inverse decay rates are reduced to 12.6 ns and 19.5 ns, respectively, accounting for 4 % and 6 % of the overall decay in the range from 625–645 nm (**Figure 60b**). The faster decay in the case of **H4** compared to **H5** can be understood as the disulfide anchor group (**H4**) interacts more strongly with the CdSe@ZnS QDs than the tertiary amine (**H5**). The reduced lifetime, as well as the smaller relative amplitude of the QD emission clearly indicate an interaction between polymers carrying anchor groups and QDs.

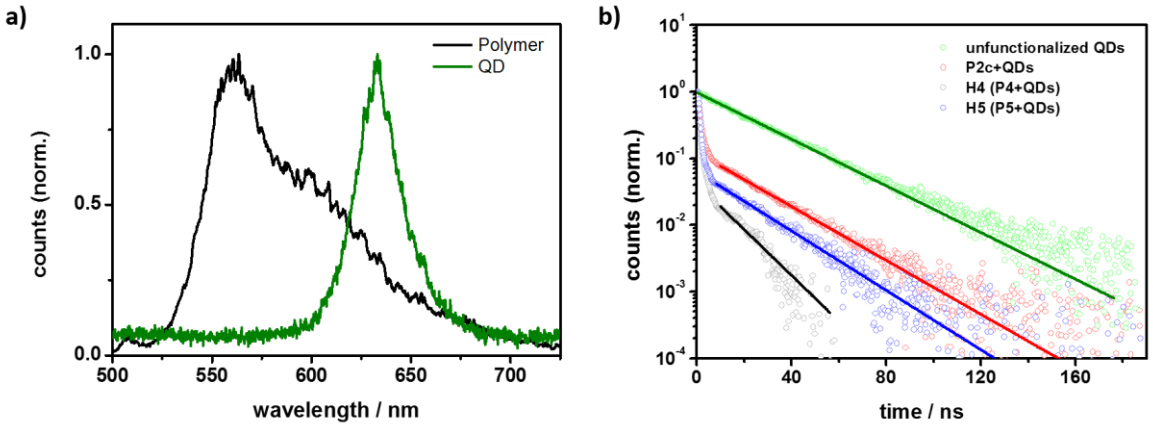

Figure 60. a) PL spectra of **P2c** (black solid line) and QDs (green solid) line. b) PL decay of QDs (green symbols), mixture of QDs and non-adsorbing polymer **P2c** (red symbols), **H4** (black symbols), and **H5** (blue symbols) with the respective monoexponential fits of the long decay component (solid lines).

4. Conclusion

With the present study we demonstrate that block copolymers composed of a conjugated and a non-conjugated block can be synthesized in a facile one-pot reaction. ROMP is capable of synthesizing both conjugated and non-conjugated polymers. Furthermore, under appropriate circumstances ROMP exhibits living nature which allows for the facile synthesis of block copolymers. Therefore, the living nature of ROMP enables the synthesis of block copolymers exhibiting one conjugated and one non-conjugated block in a facile one-pot procedure. As no end group modifications had to be applied, this approach displays a straightforward approach for the synthesis of various block copolymers. Consequently, we synthesized two different amphiphilic block copolymers. In the first route we directly synthesized the amphiphilic block copolymer using 4,12-dimethoxy-7,15-di(2'-ethylhexyloxy)-[2.2]paracyclophane-1,9-diene and an oxanorbornene equipped with a PEG side chain as monomers. In the second route the oxanorbornene block was substituted by a norbornene carrying a reactive ester which was used to incorporate a PEG side chain via post-polymerization modification. Both amphiphilic block copolymers were used for the fabrication of micelles. The size and, thereby, the optical properties of the polymers could be controlled depending on the micellization procedure. Thus, the optical properties of a single compound can be tailored to some extend in order to match the requirements for different applications. The route including a reactive ester further proves the versatility of the approach presented in the study at hand. When exploiting the reactive ester, numerous primary amines can be incorporated as both, the polymer backbone as well as the reactive ester, are tolerant of many functional groups. Hence, two primary amines carrying functional groups which allow for an effective interaction with inorganic nanocrystals (anchor groups) were incorporated. The anchor groups enabled functionalization of CdSe@ZnS QDs via ligand exchange as evidenced via time-resolved photoluminescence measurements which further supports the applicability for optoelectronic devices.

The huge advantage of the approach presented in this paper is the simplicity of synthesizing a variety of block polymers with controllable properties such as variations in the length of both blocks. For each block ratio only one single polymerization is necessary. By contrast, in a procedure involving several end group reactions this would mean a tremendous synthetic effort.

Overall, the routes presented in the study at hand can be exploited for the synthesis of a great variety of block copolymers combining a conjugated and a non-conjugated block. Thereby, numerous functional groups can be incorporated into the block copolymers which usually have to be incorporated following long, complicated synthetic protocols. Thus, the block copolymers can be modified to match the requirements for a specific application such as optoelectronic devices as demonstrated in the study at hand.

ASSOCIATED CONTENT

Supporting Information.

Experimental details, ^{1}H-, ^{19}F- and ^{13}C- solution NMR spectra of the monomers. This material is available from the author.

AUTHOR INFORMATION

Corresponding Author

* E-mail: zentel@uni-mainz.de (R. Zentel)

E-mail: tlc@snu.ac.kr (T.-L. Choi)

ACKNOWLEDGMENT

The authors gratefully thank the Deutsche Forschungsgemeinschaft (DFG): International Research Training Group (IRTG) 1404 “Self-Organized Materials for Optoelectronics” as well as the Basic Science Research and Nano-Material Technology Development through NRF of Korea for funding. In addition, the authors would like to thank the group of Prof. Kookheon Char from Seoul National University for providing the CdSe@ZnS QDs.

ABBREVIATIONS

DCM, dichloromethane; DIAD, diisopropyl azodicarboxylate; DiEt, diethyl ether; DOSY, diffusion ordered spectroscopy; DP, degree of polymerization; EVE, ethyl vinyl ether; FTIR, Fourier transform infrared; NMR, nuclear magnetic resonance; OEH, 2-ethylhexyloxy; MEH-PPV, poly[2-methoxy-5-(2-ethylhexyloxy)-1,4-phenylenevinylene]; MeO, methoxy; M_n, number average molar mass; PDI, polydispersity index; PEG, poly(ethylene glycol); PFP, pentafluorophenyl; PPV, poly(*p*-phenylene vinylene); R_h, hydrodynamic radius; ROMP, ring-opening metathesis polymerization; RuPy, $(IMesH_2)(Cl)_2(C_5H_5N)_2Ru{=}CHPh$ with $IMesH_2$ = 1,3-dimesityl-4,5-dihydroimidazol-2-ylidene; TLC, thin layer chromatography

KEYWORDS

amphiphiles, block copolymers, living polymerization, poly(*p*-phenylene vinylene) (PPV), ring-opening metathesis polymerization (ROMP)

References

(1) a) Riess, G. *Progress in Polymer Science* **2003**, *28*, 1107–1170; b) Discher, D. E. *Science* **2002**, *297*, 967–973.

(2) Shin, S.; Yoon, K.-Y.; Choi, T.-L. *Macromolecules* **2015**, *48*, 1390–1397.

(3) Liu, C.-L.; Lin, C.-H.; Kuo, C.-C.; Lin, S.-T.; Chen, W.-C. *Progress in Polymer Science* **2011**, *36*, 603–637.

(4) Kempf, C. N.; Smith, K. A.; Pesek, S. L.; Li, X.; Verduzco, R. *Polym. Chem.* **2013**, *4*, 2158.

(5) a) Burroughes, J. H.; Bradley, D. D. C.; Brown, A. R.; Marks, R. N.; Mackay, K.; Friend, R. H.; Burn, P. L.; Holmes, A. B. *Nature* **1990**, *347*, 539; b) Mathias, F.; Fokina, A.; Landfester, K.; Tremel, W.; Schmid, F.; Char, K.; Zentel, R. *Macromol. Rapid Commun.* **2015**, *36*, 959–983.

(6) Sariciftci, N. S.; Smilowitz, L.; Heeger, A. J.; Wudl, F. *Science* **1992**, *258*, 1474–1476.

(7) Moses, D. *Appl. Phys. Lett.* **1992**, *60*, 3215.

(8) Iovu, M. C.; Jeffries-EL, M.; Sheina, E. E.; Cooper, J. R.; McCullough, R. D. *Polymer* **2005**, *46*, 8582–8586.

(9) a) Moon, H. C.; Anthonysamy, A.; Lee, Y.; Kim, J. K. *Macromolecules* **2010**, *43*, 1747–1752; b) Li, Z.; Ono, R. J.; Wu, Z.-Q.; Bielawski, C. W. *Chem. Commun.* **2011**, *47*, 197–199.

(10) Li, W.; He, Y.-G.; Shi, S.-Y.; Liu, N.; Zhu, Y.-Y.; Ding, Y.-S.; Yin, J.; Wu, Z.-Q. *Polym. Chem.* **2015**, *6*, 2348–2355.

(11) a) Kang, E.-H.; Lee, I. S.; Choi, T.-L. *J. Am. Chem. Soc.* **2011**, *133*, 11904–11907; b) Uemura, T.; Nakanishi, R.; Kaseda, T.; Uchida, N.; Kitagawa, S. *Macromolecules* **2014**, *47*, 7321–7326.

(12) Yoon, K.-Y.; Shin, S.; Kim, Y.-J.; Kim, I.; Lee, E.; Choi, T.-L. *Macromol. Rapid Commun.* **2015**, *36*, 1069–1074.

(13) a) Gorman, C. B.; Ginsburg, E. J.; Grubbs, R. H. *J. Am. Chem. Soc.* **1993**, *115*, 1397–1409; b) Horie, M.; Shen, I.-W.; Tuladhar, S. M.; Leventis, H.; Haque, S. A.; Nelson, J.; Saunders, B. R.; Turner, M. L. *Polymer* **2010**, *51*, 1541–1547.

(14) Yu, C.-Y.; Turner, M. L. *Angew. Chem. Int. Ed.* **2006**, *45*, 7797–7800.

(15) a) Lidster, B. J.; Behrendt, J. M.; Turner, M. L. *Chem. Commun.* **2014**, *50*, 11867–11870; b) Elacqua, E.; Weck, M. *Chem. Eur. J.* **2015**, *21*, 7151–7158.

(16) a) Yu, C.-Y.; Kingsley, J. W.; Lidzey, D. G.; Turner, M. L. *Macromol. Rapid Commun.* **2009**, *30*, 1889–1892; b) Yu, C.-Y.; Horie, M.; Spring, A. M.; Tremel, K.; Turner, M. L. *Macromolecules* **2010**, *43*, 222–232.

(17) Menk, F.; Mondeshki, M.; Dudenko, D.; Shin, S.; Schollmeyer, D.; Ceyhun, O.; Choi, T.-L.; Zentel, R. *Macromolecules* **2015**, *48*, 7435–7445.

(18) Eberhardt, M.; Mruk, R.; Zentel, R.; Théato, P. *European Polymer Journal* **2005**, *41*, 1569–1575.

(19) Tahir, M. N.; Eberhardt, M.; Theato, P.; Faiss, S.; Janshoff, A.; Gorelik, T.; Kolb, U.; Tremel, W. *Angew. Chem. Int. Ed.* **2006**, *45*, 908–912.

(20) a) Villemin, E.; Herent, M.-F.; Marchand-Brynaert, J. *Eur. J. Org. Chem.* **2012**, *2012*, 6165–6178; b) Neef, C. J.; Ferraris, J. P. *Macromolecules* **2000**, *33*, 2311–2314; c) Mitchell, R. H.; Boekelheide, V. *J. Am. Chem. Soc.* **1974**, *96*, 1547–1557; d) Yu, C.-Y.; Helliwell, M.; Raftery, J.; Turner, M. L. *Chem. Eur. J.* **2011**, *17*, 6991–6997.

(21) Alfred, S. F.; Al-Badri, Z. M.; Madkour, A. E.; Lienkamp, K.; Tew, G. N. *J. Polym. Sci. A Polym. Chem.* **2008**, *46*, 2640–2648.

(22) Zur Borg, L.; Schüll, C.; Frey, H.; Zentel, R. *Macromol. Rapid Commun.* **2013**, *34*, 1213–1219.

(23) a) Wang, H.; Wang, H. H.; Urban, V. S.; Littrell, K. C.; Thiyagarajan, P.; Yu, L. *J. Am. Chem. Soc.* **2000**, *122*, 6855–6861; b) Cosemans, I.; Vandenbergh, J.; D'Olieslaeger, L.; Ethirajan, A.; Lutsen, L.; Vanderzande, D.; Junkers, T. *European Polymer Journal* **2014**, *55*, 114–122.

(24) Braun, D.; Heeger, A. J. *Appl. Phys. Lett.* **1991**, *58*, 1982.

(25) Spring, A. M.; Yu, C.-Y.; Horie, M.; Turner, M. L. *Chem. Commun.* **2009**, 2676.

(26) Roth, P. J.; Wiss, K. T.; Zentel, R.; Theato, P. *Macromolecules* **2008**, *41*, 8513–8519.

(27) *Practical fluorescence;* Guilbault, G. G., Ed., 2. ed., rev. and expanded.; Modern monographs in analytical chemistry 3; Dekker: New York, 1990.

(28) Hoeben, F. J. M.; Shklyarevskiy, I. O.; Pouderoijen, M. J.; Engelkamp, H.; Schenning, Albertus P H J; Christianen, P. C. M.; Maan, J. C.; Meijer, E. W. *Angew. Chem. Int. Ed.* **2006**, *45*, 1232–1236.

(29) Feng, C.; Gonzalez-Alvarez, M. J.; Song, Y.; Li, I.; Zhao, G.; Molev, G.; Guerin, G.; Walker, G.; Scholes, G. D.; Manners, I.; Winnik, M. A. *Soft matter* **2014**, *10*, 8875–8887.

(30) a) Wang, M.; Dykstra, T. E.; Lou, X.; Salvador, M. R.; Scholes, G. D.; Winnik, M. A. *Angew. Chem. Int. Ed.* **2006**, *45*, 2221–2224; b) Zur Borg, L.; Lee, D.; Lim, J.; Bae, W. K.; Park, M.; Lee, S.; Lee, C.; Char, K.; Zentel, R. *J. Mater. Chem. C* **2013**, *1*, 1722.

(31) Jochum, F. D.; Theato, P. *Macromolecules* **2009**, *42*, 5941–5945.

Supporting Information

Synthesis of Functional Block Copolymers Carrying One Poly(para-phenylene vinylene) and One Non-Conjugated Block in a Facile One-Pot Procedure

Florian Menk, Suyong Shin, Kyung-Oh Kim, Martin Scherer, Dominik Gehrig, Frédéric Laquai, Tae-Lim Choi*, Rudolf Zentel*

zentel@uni-mainz.de (R. Zentel)

tlc@snu.ac.kr (T.-L. Choi)

Characterization

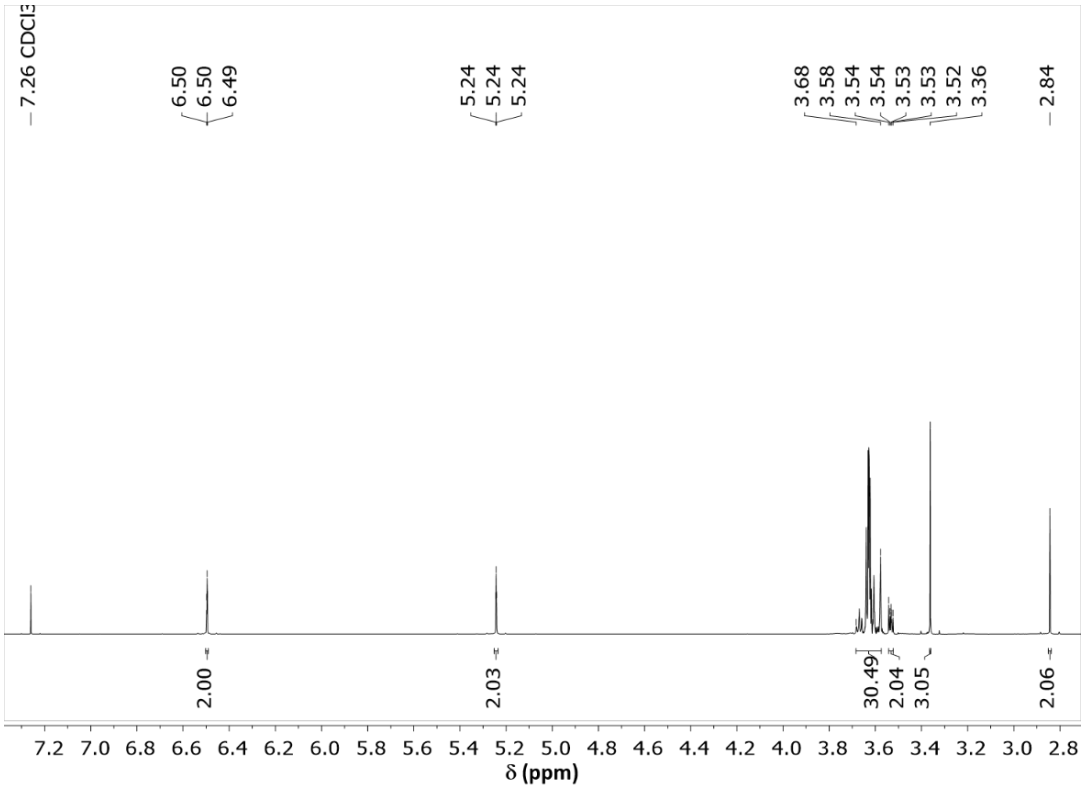

Figure S61. 500 MHz ^{1}H-NMR spectrum of compound **1** (PEG-ONB) in $CDCl_3$.

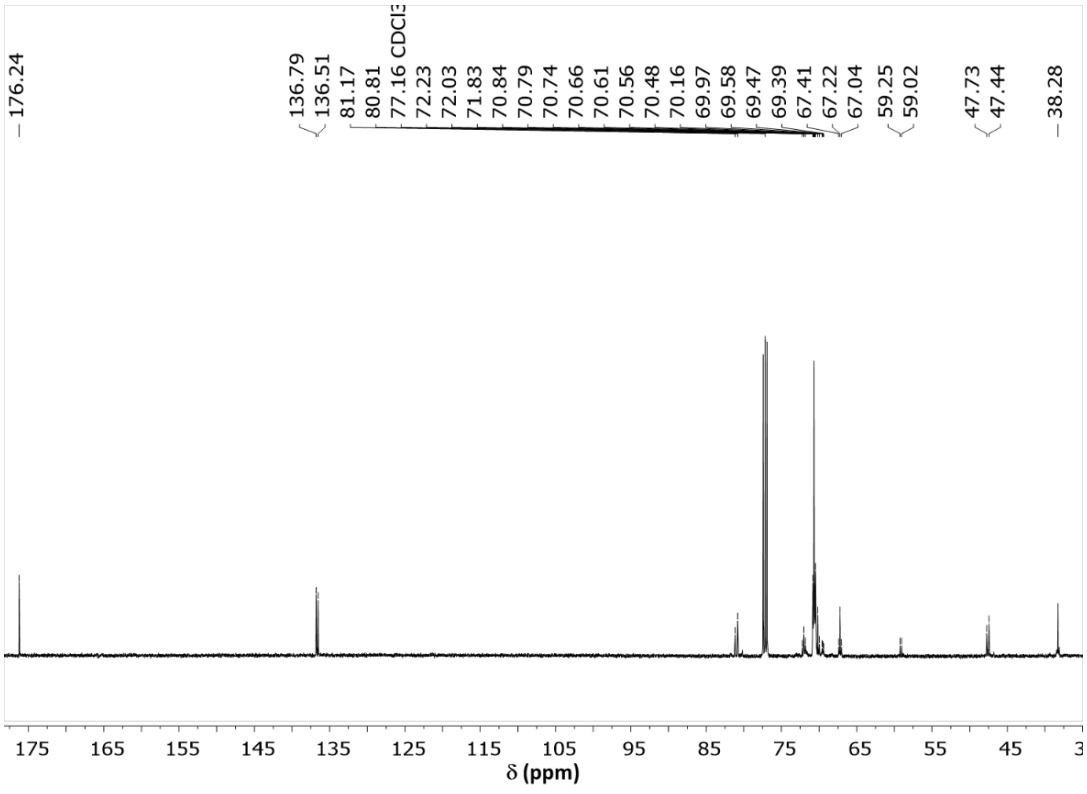

Figure S62. 125 MHz ^{13}C-NMR spectrum of compound **1** (PEG-ONB) in $CDCl_3$.

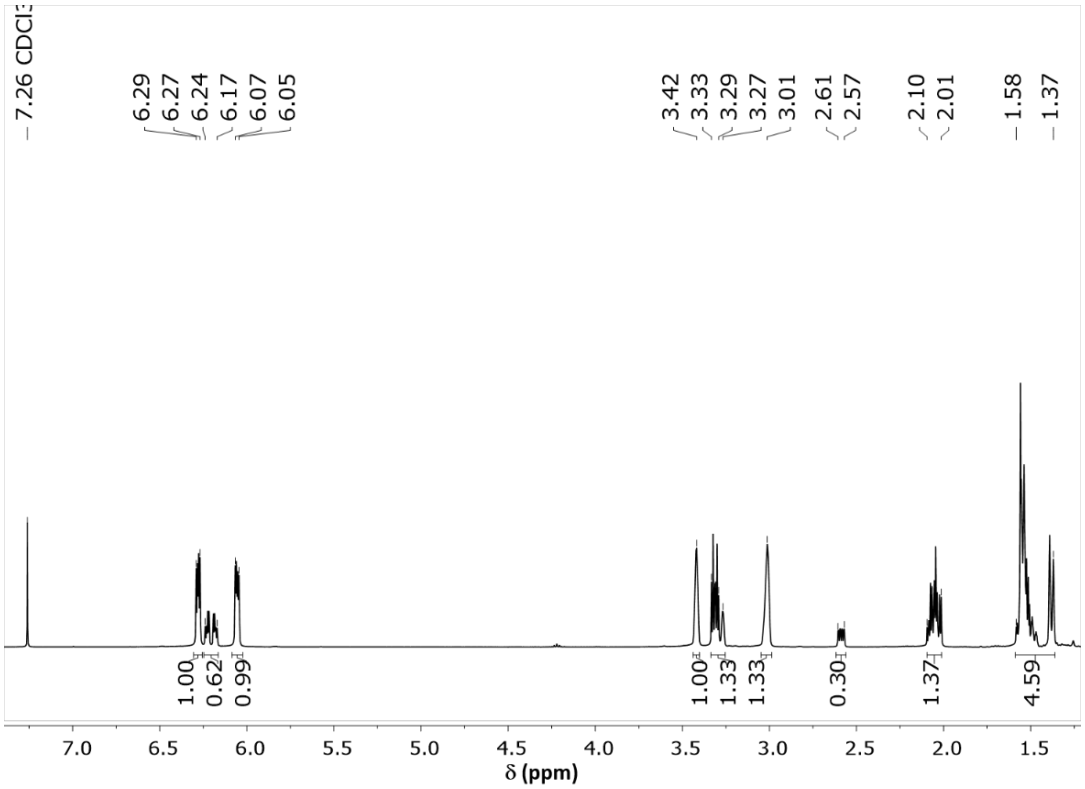

Figure S63. 400 MHz ^{1}H-NMR spectrum of compound **2** (PFP-NB) in $CDCl_3$.

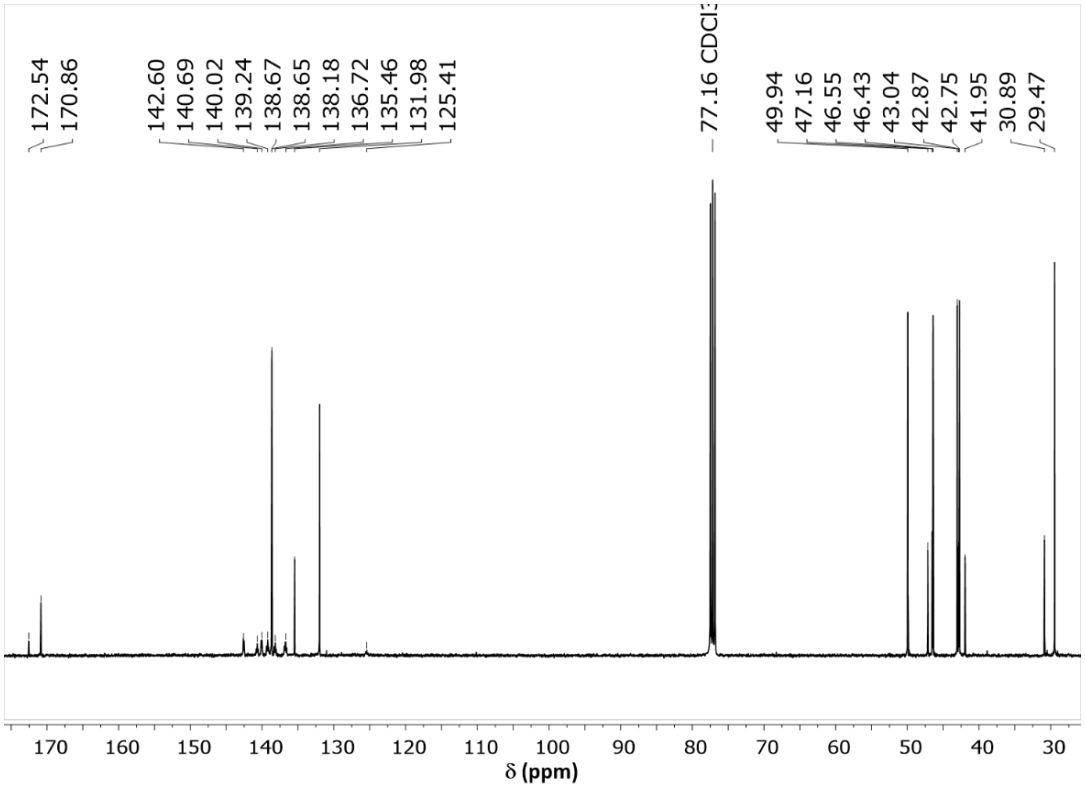

Figure S64. 75 MHz ^{13}C-NMR spectrum of compound **2** (PFP-NB) in $CDCl_3$.

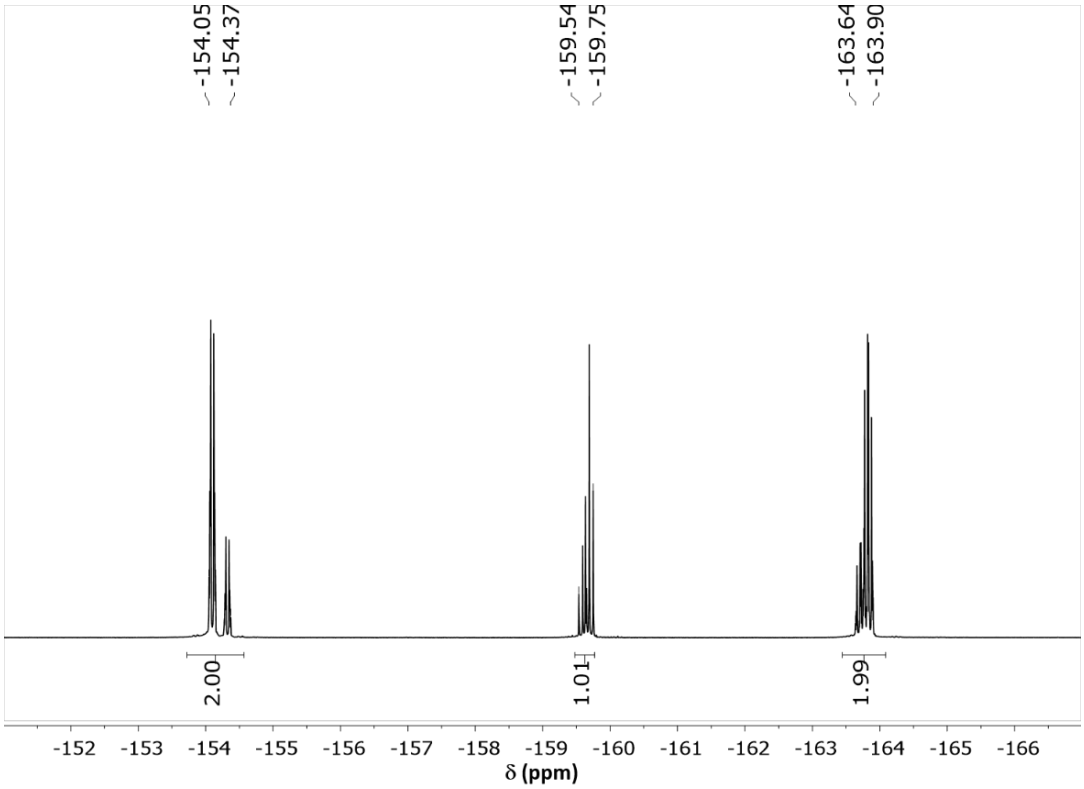

Figure S65. 400 MHz ^{19}F-NMR spectrum of compound **2** (PFP-NB) in $CDCl_3$.

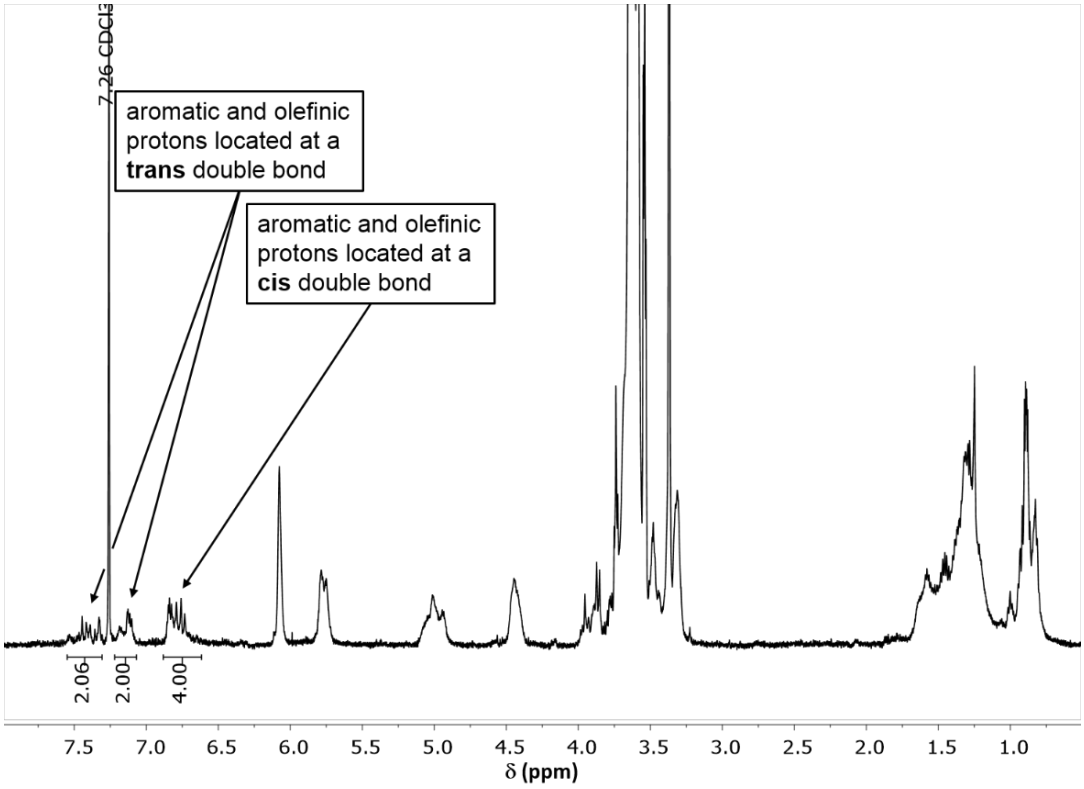

Figure S66. ^{1}H-NMR spectrum of **P1** verifying the approximate 1/1 ratio of cis/trans double bonds in the MEH-PPV backbone.

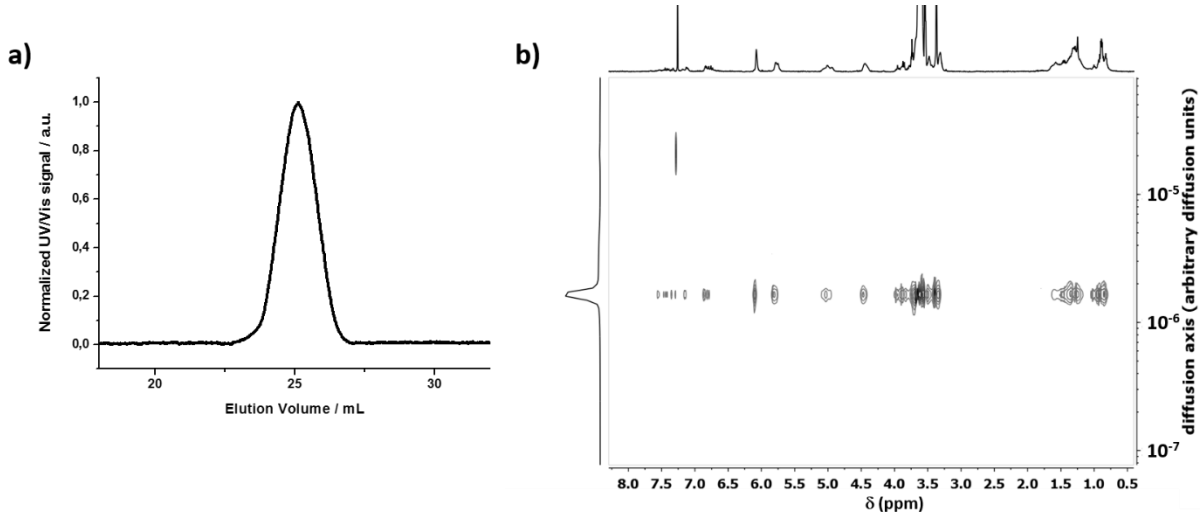

Figure S67. a) GPC trace of the amphiphilic block copolymer **P1** exhibiting a monomodal distribution; b) ^{1}H-DOSY spectrum of **P1** (in $CDCl_3$) – the signals of both blocks are detected at the same diffusion coefficient.

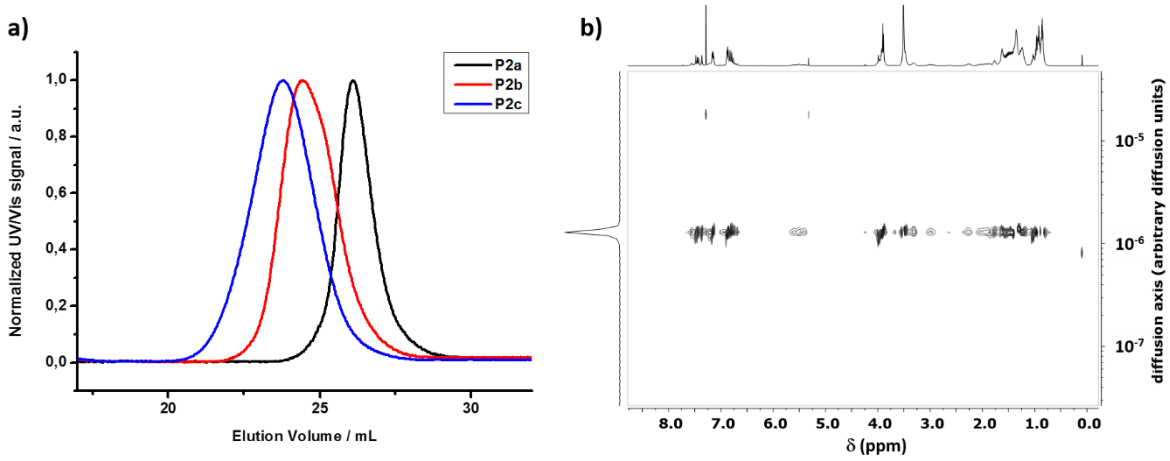

Figure S68. a) GPC traces of block copolymers **P2a-c** exhibiting a monomodal distribution; b) ^{1}H-DOSY spectrum of **P2b** (in CDCl3) – the signals of both blocks are detected at the same diffusion coefficient.

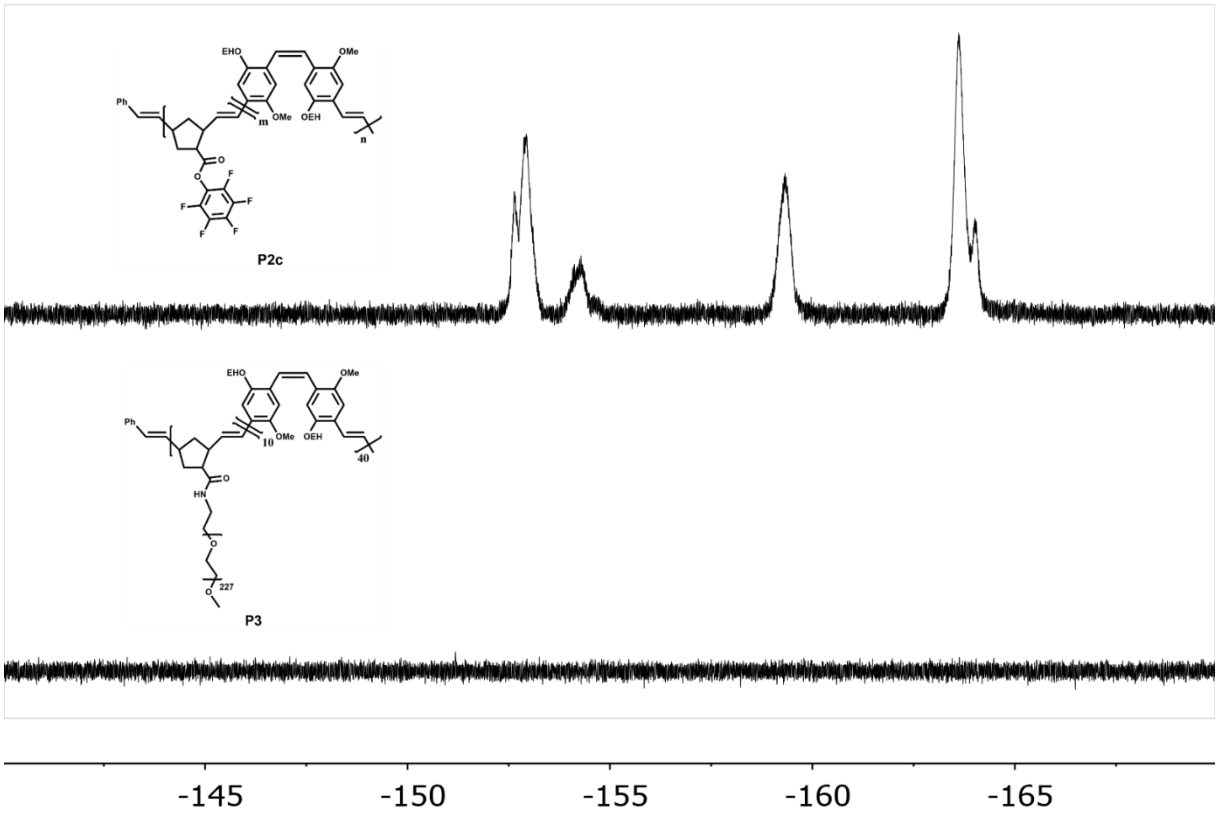

Figure S69. ^{19}F-NMR spectra (in $CDCl_3$) of **P2c** and **P3** giving evidence for the full conversion of the post polymerization modification.

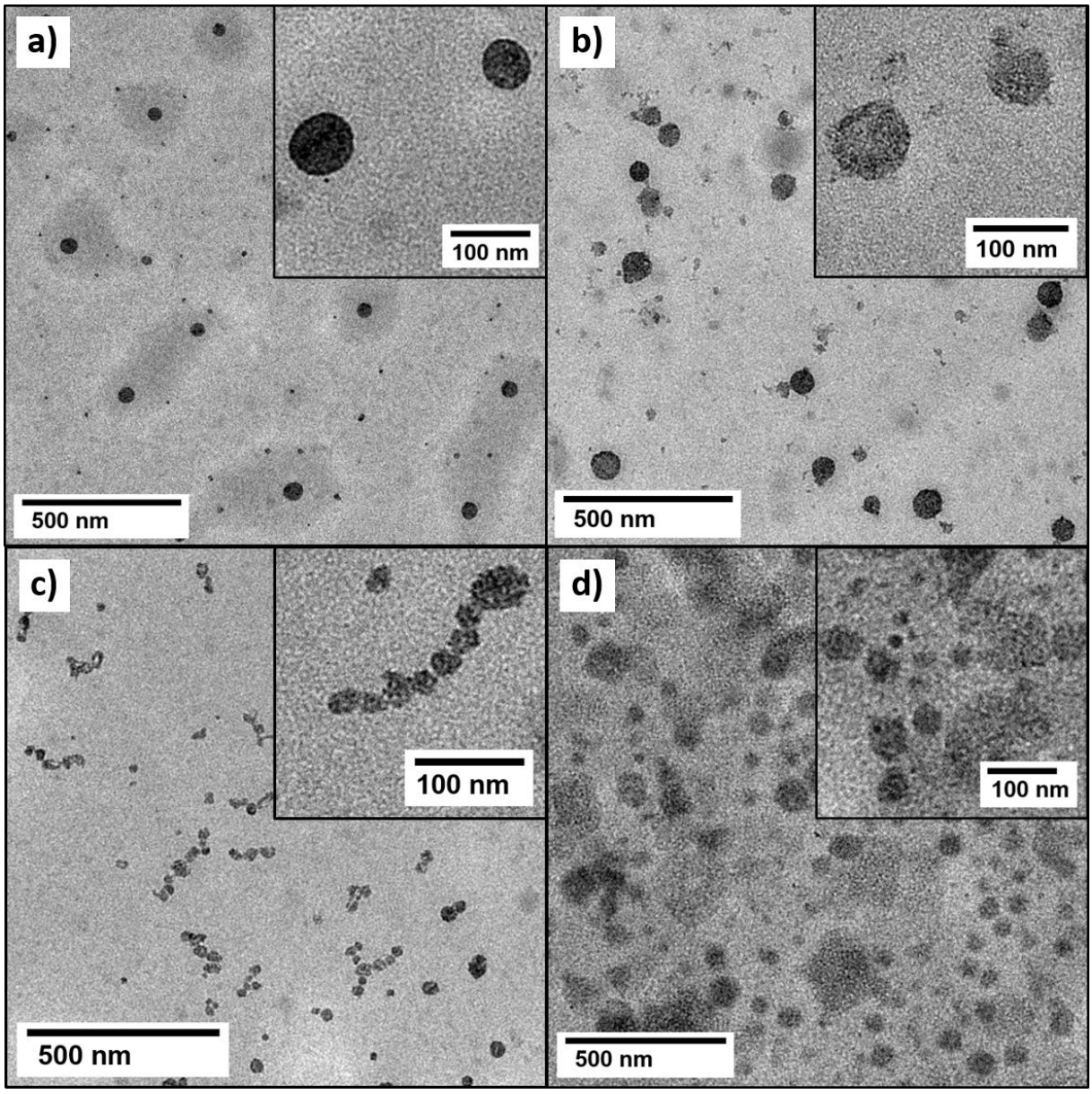

Figure S70. TEM images of micelles obtained from the self-assembly of polymer **P1** following protocols 1 – 3. a) Regular micelles are obtained applying protocol 1. b) + c) Regular micelles and partially fused of micelles in the shape of caterpillars are coexisting (protocol 2). d) A mixture of regular micelles and merged micelles in the shape of larger aggregates are obtained following protocol 3.

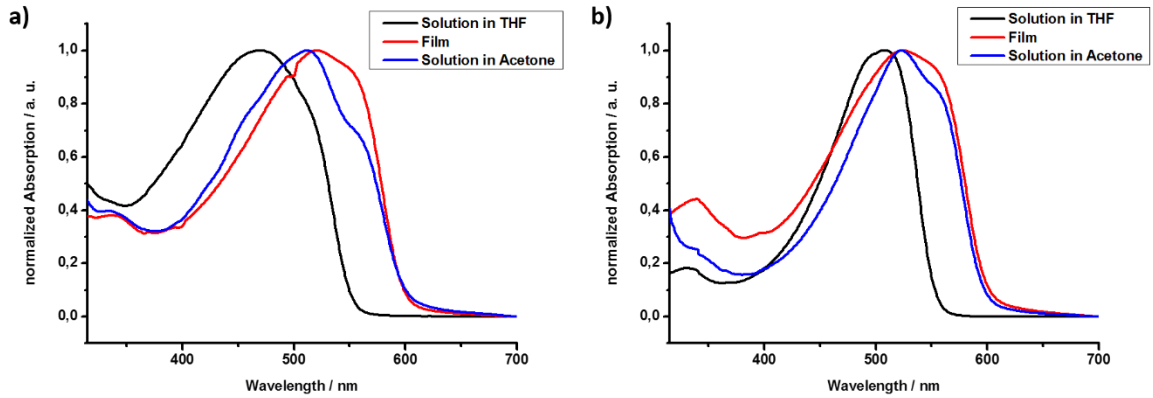

Figure S71. Comparison of the UV/Vis spectra of: a) **P1** and b) **P3** in THF, acetone and in film. The spectra of **P1** and **P3** dissolved in THF are strongly blue shifted confirming that the polymers are molecularly dissolved. Although the intensity of the vibronic shoulder is less compared to the film spectra, the spectra in acetone reveal a high degree of aggregation. **P1** is a little less aggregate in acetone as compared to **P3** due to the higher solubility caused by the shorter PEG side chains and the shorter MEH-PPV block.

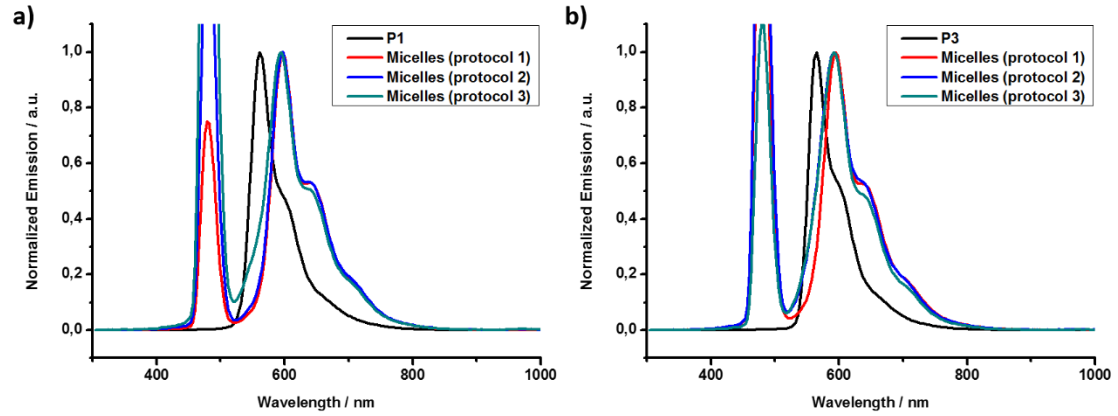

Figure S72. Photoluminescence spectra of a) polymer **P1**, b) polymer **P3** (in THF) and the respective micelles (in water) obtained from the different micellization protocols. When comparing the polymer solutions with the micelles a strong bathochromic shift of a) 23-28 nm and b) 27-30 nm is observed.

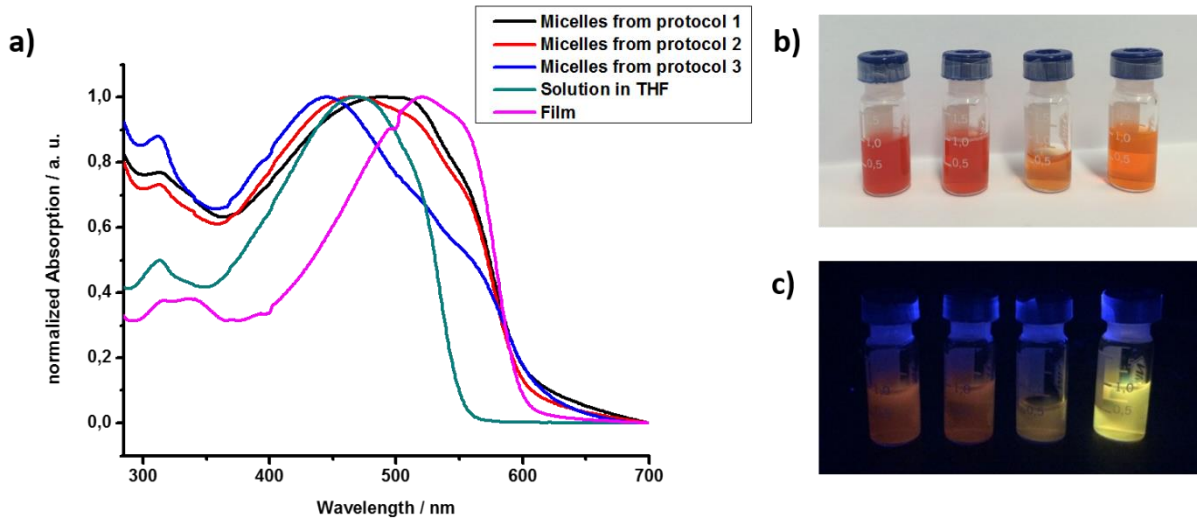

Figure S73. a) Absorption spectra of micelles from polymer **P1** in water fabricated following micellization protocols 1 – 3, spectrum of solution in THF and film spectrum; b) Photographs without and c) with UV irradiation @ 365 nm (from left to right: micelles from protocol 1, 2, 3 and solution in THF, respectively).

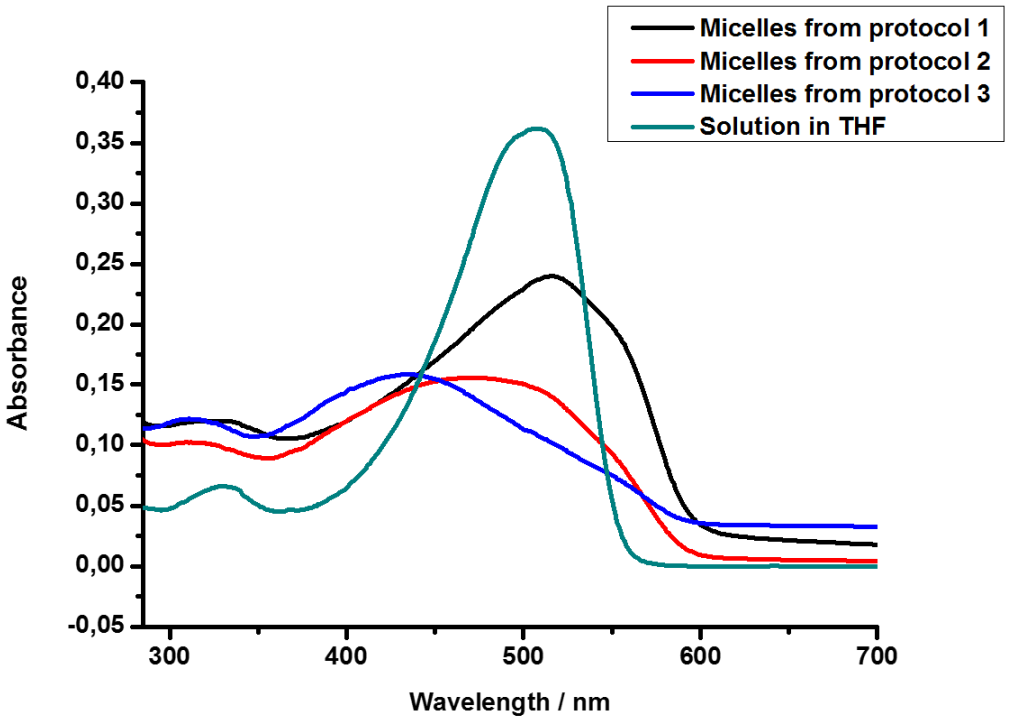

Figure S74. Non-normalized absorption spectra of micelles from polymer **P3** in water fabricated following micellization protocols 1 – 3. All spectra were collected at a concentration of c = 0.5 mg/mL.

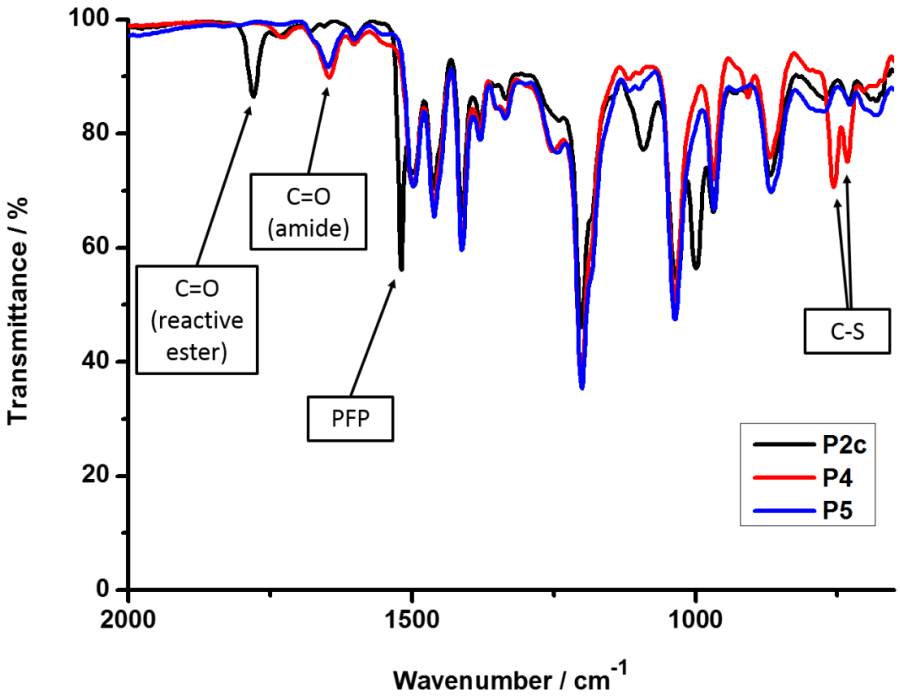

Figure S75. FTIR spectra monitoring the incorporation of the two anchor groups via post-polymerization modification. After the reaction the signal of the pentafluorophenyl ring (1519 cm^{-1}) is vanished. The C=O band shifts from 1780 cm^{-1} in the reactive ester (**P2c**) to 1646 cm^{-1} (**P4**) and 1649 cm^{-1} (**P5**), respectively, in the amides. Furthermore, in **P4** two C-S bands are detected at 732 and 756 cm^{-1}.

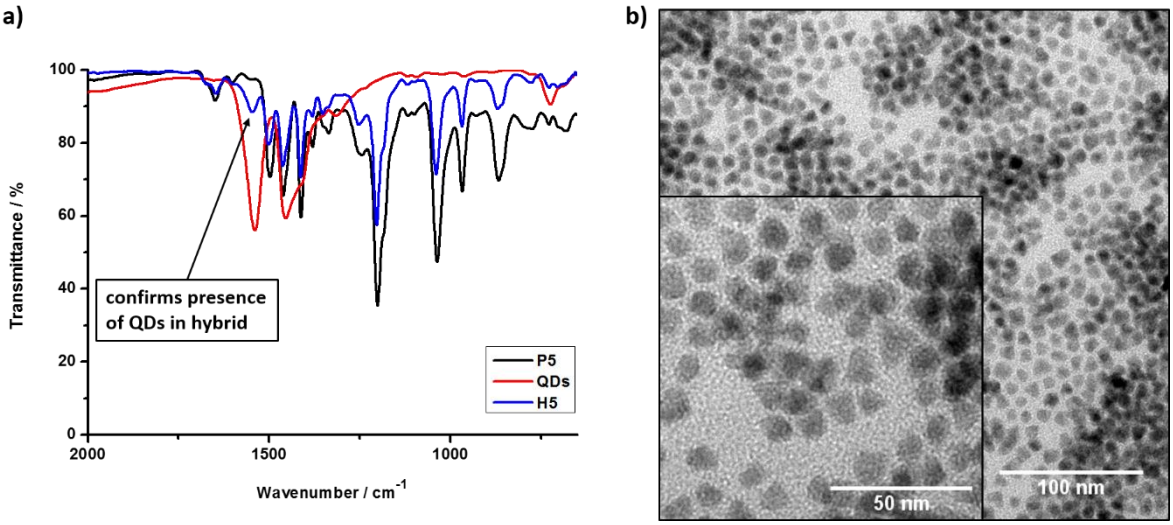

Figure S76. a) FTIR spectrum monitoring the successful functionalization of the CdSe@ZnS QDs with polymer **P5**, b) TEM images of **H5** exhibiting well-dispersed QDs.

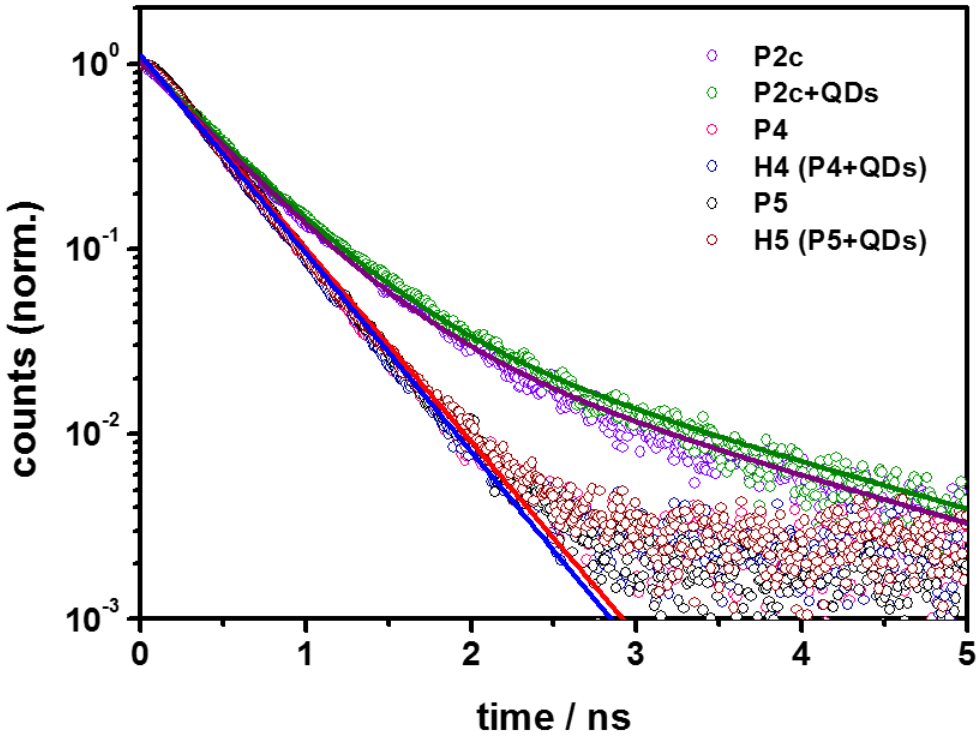

Figure S77. Photoluminescence decay of **P2c**, **P2c** with CdSe@ZnS QD, **P4**, **H4**, **P5**, and **H5** tracked from 555–575 nm (symbols) i.e. the emission maximum of the polymere where no QD emission is observed. Solid lines represent monoexponential or biexponential fits to the data.

Table S2. Fitting results of the polymer emission as shown in **Figure S77**.

	τ_1 / ns	A_1	τ_2 / ns	A_2
P2c	0.4	0.94	1.7	0.06
P2c + QDs	0.4	0.94	1.7	0.06
P4	0.4	1	---	---
H4 (P4 + QDs)	0.4	1	---	---
P5	0.4	1	---	---
H4 (P5 + QDs)	0.4	1	---	---

Table S3. Fitting results of the PL decay tracked from 625–645 nm where QD emission is at its maximum and overlaps with the polymer emission.

	τ_1 / ns	A_1
QD	24.8	1
P2c + QD	21.5	0.12
H4	12.6	0.04
H5	19.5	0.06

Dynamic light scattering experiments

For light scattering experiments, colloidal dispersions in MilliQ water were prepared and filtered into dust free cylindrical scattering cells (Suprasil, 20 mm diameter, Hellma, Mühlheim, Germany) in a dust free flow box using Millex GHP 0.45µm filters.

DLS measurements were performed using a Uniphase He/Ne Laser (λ = 632.8 nm, 25 mW), a ALV-SP125 goniometer, a ALV/High QE APD Avalanche photo diode with fibre optical detection, a ALV 5000/E/PCI correlator and a Lauda RC-6 thermostat unit at 20 °C. Angular dependent measurements were carried out in the range of 30°-150° at steps of 15°. Experimental intensity correlation functions were transformed into amplitude correlation functions applying the Siegert relation extended to include negative values after baseline subtraction by calculation $g_1(t) = SIGN(G_2(t)) \cdot SQRT(ABS(G_2(t)-A)/A)$ with A the measured baseline and G2(t) the experimental intensity correlation function . The field correlation functions were fitted by a sum of two exponentials $g_1(t) = a \cdot exp(-t/b) + c \cdot exp(-t/d)$ to take polydispersity into account. Average apparent diffusion coefficients D_{app} were obtained by applying $q^2 \cdot D_{app} = (a \cdot b^{-1} + c \cdot d^{-1})/(a+c)$ resulting in an angular-dependent diffusion coefficient or reciprocal hydrodynamic radius $<1/R_h>_{app}$. The z-average hydrodynamic radii R_h were obtained by extrapolation of $<1/R_h>_{app}$ to q = 0. The normalized second cumulant µ2 was calculated using a cumulant fit at 90°.

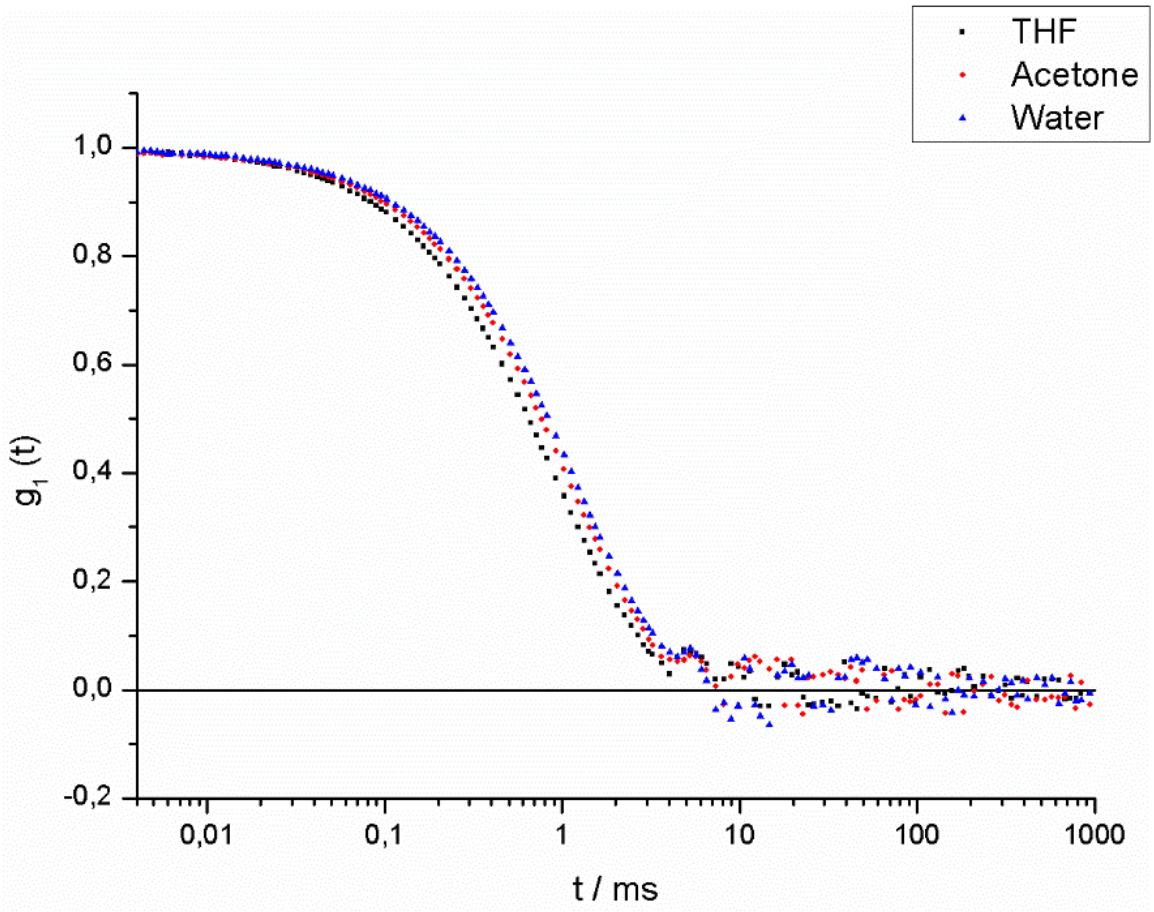

Figure S78. Aggregate Size examination by DLS: Autocorrelation functions (ACF) obtained from aqueous dispersions of aggregates prepared from tetrahydrofuran (black), acetone (red) and water (blue); Scattering angle 90°.

4.2 Approaches for the Incorporation of Anchor Groups into Conjugated Polymers

The interface of the organic and the inorganic material has been identified to be one of the most critical factors influencing the performance of hybrid optoelectronic devices. The surface of the inorganic nanocrystals is usually coated with ligands (small molecules or polymer ligands) which prevent the aggregation of nanocrystals. Consequently, the interaction between the inorganic acceptor and the organic donor is dominated by the ligands separating both materials. Therefore, various ligand modification procedures have been described in literature substituting the initial ligands by ligands which lead to an improved interaction between donor and acceptor and, thereby, improve device performance. Most approaches aim at decreasing the distance between donor and acceptor using small ligands for the ligand exchange.

As the ligands influence several parameters beside the distance such as the conductivity, energy levels, stability and the morphology of casted films, however, predicting the effect of a specific ligand is very difficult. For example, thiols have been reported to create charge traps in the nanocrystals which should affect the device efficiency. Nevertheless, ligand exchange procedures using thiols have resulted in improved performances of hybrid solar cells in many examples. As the ligands influence the film morphology, which by itself influences the device performance, the effect of ligands ought to be studied first in solution before involving morphological aspects. Therefore, an intimate contact between the inorganic nanocrystals and the organic compound is required. This requirement can be satisfied via block copolymers composed of the donor material and a short anchor block which leads to a stable coating of the nanocrystals.

To investigate the influence originating exclusively from different anchor groups, approaches which enable the modification of the polymers with various anchor groups while keeping other properties of the polymer constant have to be developed.

In this section, three approaches which fulfill the above-mentioned requirement will be presented and applied to investigate the influence on the optical and material properties of CdSe nanoplatelets.

4.2.1 Incorporation of Anchor Groups into PPV Containing Block Copolymers and their Influence on the Properties of Polymer/Nanoplatelet Composites

In the following publication, rod-coil block copolymers composed of a conjugated block and a non-conjugated block were synthesized using a combination of Siegrist polycondensation and RAFT polymerization. In the first step, the conjugated polymer poly(*p*-(2,5-di(2'-ethylhexyloxy)phenylene vinylene) (DEH-PPV) was synthesized. The defined imine end group resulting from the mechanism of the Siegrist polycondensation was selectively converted into an aldehyde end group during the aqueous work-up. The aldehyde was further exploited for the incorporation of a trithiocarbonate converting the polymer into a macro-CTA. In a subsequent step, the macro-CTA was applied in a RAFT polymerization of PFPA to attach a short reactive ester block to the DEH-PPV. Consequently, the obtained block copolymer was equipped with different anchor groups varying in size and functional group via post-polymerization modification.

Following this approach, composites consisting of CdSe nanoplatelets and block copolymers which solely differ in the attached anchor groups were fabricated. The anchor groups assured a stable coating of the nanoplatelets and an intimate contact with the conjugated polymers. Thus, the optical properties of the nanocomposites could be studied depending on the different anchor groups without the interfering effects of varying morphologies.

Burak Guzelturk contributed to the following publication, supported by Murat Olutas and Yusuf Kelestemur, by conducting and interpreting all optical measurements as well as recording the TEM images. The synthesis and characterization of the block copolymers was done by the author of this dissertation and, under his supervision, Kai Phillips.

4.2.1.1 Manuscript to be submitted

Colloidal Nanoplatelet/Conducting Polymer Hybrids: Excitonic and Material Properties

Burak Guzelturk*,#, Florian Menk#, Kai Philipps, Murat Olutas, Yusuf Kelestemur, Rudolf Zentel, Hilmi Volkan Demir*

# These authors contributed equally to this work.

Abstract

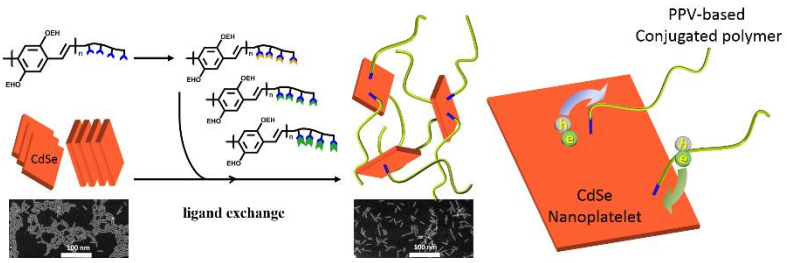

Here, we present the first account of conductive polymer/colloidal nanoplatelet hybrids. For this, we develop DEH-PPV based polymers with two different anchor groups (i.e. sulfide and amine) acting as surfactants for CdSe nanoplatelets, which are atomically flat semiconductor nanocrystals. Hybridization of polymers and nanoplatelets in solution-phase is observed to cause strong photoluminescence quenching in both of the materials. Through steady state photoluminescence and excitation spectrum measurements, the photoluminescence quenching is shown to be due to dominant exciton dissociation and charge transfer at the polymer/nanoplatelet interfaces that possess a staggered (i.e. Type II) band alignment. Furthermore, we observe that sulfide based anchor group enables a stronger emission quenching than amine based ones suggesting that sulfide anchors exhibit more efficient binding to the nanoplatelet surfaces. Also, shorter surfactants are also found to be more effective for exciton dissociation as compared to the longer ones. In addition, we show homogenously distributed nanoplatelets in the hybrid solid films owing to the use functional polymers. These nanocomposites can be used as building blocks for new hybrid optoelectronic devices such as solar cells.

1. Introduction

Organic-inorganic hybrids comprising organic semiconductors and colloidal nanocrystals are attractive materials for optoelectronic devices such as solar cells[1–5] and light-emitting diodes.[5–11] Interest in hybrid materials is caused, in particular, by their solution processability, which permits the fabrication of devices via low-cost printing and patterning techniques on arbitrary substrates at large scale. There has been an ever growing interest for this type of hybrid systems since the breakthrough achievement of Alivisatos' group, who reported a hybrid solar cell composed of CdSe nanorods and poly(3-hexylthiophene) (P3HT) conjugated polymers.[1] Recent reports show that the power conversion efficiencies in the hybrid solar cells can attain more than 5%.[12,13] Also, based on theoretical calculations, hybrid solar cells are predicted to achieve efficiencies that could exceed 10% by employing optimized hybrid structures offering enhanced free carrier generation and charge transport.[14,15]

In a hybrid solar cell, exciton dissociation, charge transport and charge extraction are the essential processes. Efficient free carrier generation via exciton dissociation requires assistance of exciton diffusion since excitons should reach the exciton dissociating interfaces before they would recombine.[16] Unfortunately, exciton diffusion in the colloidal nanocrystals and organic semiconductors is generally limited to short distances (< 20 nm).[5] As a result of this limitation, it is commonly desired to realize nanoscale morphologies having very small domains on the order of exciton diffusion length so that free carrier generation could be maximized. In addition to nanoscale morphology, extrinsic and intrinsic properties of the inorganic nanocrystals, including their ligands, size and geometry also play a significant role in the free carrier generation efficiency and, thus, the overall solar cell efficiency in hybrid systems.[5,17]

Long alkyl chain-based insulating ligands of the nanocrystals restrict charge separation and transport in their solid films. In an early report, Geenham *et al*. described ligand modification of CdSe quantum dots (QDs) that were primarily coated with insulating tri-*n*-octylphosphine oxide (TOPO) ligands by the treatment with an excess of pyridine.[16] Since then, various ligand modification procedures have been developed either using short organic or inorganic ligands.[10,15,18,19] However, ligand exchange does not simply change the QD/QD and QD/polymer distances, it also affects the conductivity, energy levels, stability and the morphology of casted films.[20–22] Furthermore, some functional groups such as thiols are known to create charge traps in the nanocrystals and quench their photoluminescence.[23,24] Therefore, predicting the influence of a specific ligand on the optical properties of the hybrids

is difficult and complex. Consequently, studies that separately investigate the influence on the individual aspects depending on both the size and the functional group of the ligands are required.

Morphology of the nanocrystals (i.e. size, shape and dimensionality) is another important feature determining the performance of the organic-inorganic hybrids. To date, CdSe and CdS nanorods have shown favorable performance as compared to that of the colloidal QDs thanks to their large surface area and high aspect ratio, which considerably increases the overall free carrier generation efficiency at the organic-inorganic interfaces.[4,17,25] High aspect ratio organic materials such as conjugated polymer nanowires have been also proposed and shown to enhance the power conversion efficiencies through creating a nanoscale morphology favorable for charge separation and transport.[26] Recently, a new type of colloidal semiconductors has been introduced, which is called colloidal nanoplatelet (NPL).[27] The NPLs are atomically flat nanocrystals that exhibit unique optical and material properties, including extremely large linear and nonlinear absorption cross-sections with large oscillator strength and narrow emission linewdith.[28,29] Thanks to these favorable properties, recent reports have shown that the NPLs are highly promising for light-emitting diodes[30], lasers[31,32], photo-detectors[33,34] and photocatalysis.[35] Moreover, ultra-efficient exciton transfer has been show to prevail in the close-packed solid films of the NPLs,[36,37] which could facilitate long exciton diffusion lengths (> 100 nm) in their solid films.[38] These long exciton diffusion lengths would clearly manifest the high potential of NPLs in light-harvesting applications. In addition, their high aspect-ratio, large surface area and anisotropic shape also make the NPLs interesting candidates for organic-inorganic hybrid systems. However, to date, there has not been any systematic study or demonstration of organic-inorganic nanocomposites of the NPLs.

In this work, we develop polymer/colloidal nanoplatelet composites based on conjugated polymers having different anchor groups to hybridize with CdSe NPLs. To this end, we propose and develop DEH-PPV based co-block polymers having two different ligands with varying size and anchor groups. Through investigation of steady state optical properties of the hybrids in solution-phase, we reveal strong photoluminescence quenching in both polymers and nanoplatelets. We explain the quenching of the emission via exciton dissociation at the polymer/nanoplatelet interfaces, which are shown to have a staggered band alignment. Among different anchors, sulfides show the strongest quenching as attributed to their higher tendency to attach to the NPL surfaces. Also, shorter ligand size of the same anchor group is shown to cause a larger photoluminescence quenching as compared to the ligands with a

larger size. Furthermore, we observe that hybridization helps to form well-dispersed NPL films as revealed by transmission electron microscopy, whereas the NPLs alone tend to form aggregated assemblies in absence of the functional polymers. These hybrid composites with exciton dissociating interfaces and homogenous NPL distribution are expected to be promising for hybrid solar cells.

2. Experimental Section

Materials and Characterization. All commercially available chemicals were purchased from Alfa Aesar, Acros Organics, Fluka, Sigma-Aldrich or Tokyo Chemical Industry and used without further purification unless otherwise noted. Anhydrous THF was freshly distilled from sodium under a dry argon atmosphere. All reactions were carried out under dry argon atmospheres using standard Schlenkline techniques unless otherwise noted. 2',5'-di(2''-ethylhexyloxy)-4'-methyl-*N*-benzylideneaniline (**1**) and the reactive ester block copolymer **P1** were synthesized according to a modified literature procedure.[1] ^{1}H-NMR and ^{19}F-NMR spectra were acquired on a Bruker ARX 400 at a Lamor frequency of 400 MHz. FTIR spectra were performed on a Vector 22 ATR-FTIR-spectrometer made by Bruker. Molecular weights of all synthesized polymers were determined by gel permeation chromatography (GPC) with a concentration of 1.2 mg/mL in THF with polystyrene as external and toluene as internal standard.

Cyclic voltammetry measurements were carried out on a drop-cast film at room temperature in a nitrogen glove box. Platinum electrodes were used as working and counter electrodes. The reference electrode was an Ag/Ag^{+} electrode and the measurements were conducted in a 0.1 M solution of tetrabutylammonium hexafluorophosphate ($TBAPF_6$) as supporting electrolyte in anhydrous acetonitrile. Ferrocene was used as an internal standard and the energy levels were calculated from the onsets of the oxidation and reduction potential, respectively, with an assumed level of the Fc/Fc+ redox couple of -5.1 eV versus the vacuum.

General procedure for post-polymerization modifications. The precursor polymer **P1** (0.032 mmol, 1 eq.) was dissolved in 2.5 mL of dry THF under an argon atmosphere. The respective primary amine (0.476 mmol, 15 eq.) and triethylamine (0.476 mmol, 15 eq.) were added and the reaction mixture was stirred at 30 °C for 48 h. Purification was achieved by precipitation in methanol and redissolving in DCM for three times.

P2a: ^{1}H-NMR (400 MHz, $CDCl_3$, δ): 7.38 – 7.60 (m, 36H, Ar), 7.02 – 7.26 (m, 36H, CH=CH), 3.68 – 4.06 (m, 80H, O-CH_2), 2.60 (br, 8H, S-CH_2), 2.13 (br, 12H, S-CH_3), 1.17 – 1.86 (m, 336H, CH + CH_2), 0.82 – 1.05 (m, 222H, CH_3); ^{19}F-NMR (400 MHz, $CDCl_3$, δ): no signals; FTIR: v = 1676 cm^{-1}.

P2b: ^{1}H-NMR (400 MHz, $CDCl_3$, δ): 7.38 – 7.56 (m, 36H, Ar), 7.02 – 7.24 (m, 36H, CH=CH), 3.65 – 4.02 (m, 80H, O-CH_2), 2.87 (br, 8H, N-CH_2), 2.23 (br, 24H, N-CH_3), 1.17 – 1.86 (m, 336H, CH + CH_2), 0.83 – 1.04 (m, 222H, CH_3); ^{19}F-NMR (400 MHz, $CDCl_3$, δ): no signals; FTIR: v = 1672 cm^{-1}.

P2c: ^{1}H-NMR (400 MHz, $CDCl_3$, δ): 7.38 – 7.56 (m, 36H, Ar), 7.02 – 7.24 (m, 36H, CH=CH), 3.65 – 4.01 (m, 80H, O-CH_2), 2.84 (br, 8H, N-CH_2), 2.25 (br, 24H, N-CH_3), 1.17 – 1.86 (m, 352H, CH + CH_2), 0.83 – 1.03 (m, 222H, CH_3); ^{19}F-NMR (400 MHz, $CDCl_3$, δ): no signals; FTIR: v = 1668 cm^{-1}.

Synthesis of four monolayer thick CdSe NPLs. We used a synthesis recipe for the four monolayer CdSe nanoplatelets based on our previous report.[38] Consequently, CdSe NPLs having vertical thickness of four monolayers (1.2 nm) are synthesized together with other quantum dot populations as side products. To purify the NPLs and separate them from the quantum dots, we clean them via ultracentrifugation with the addition of acetone/ethanol mixture. The cleaning step is repeated few times and the precipitate (i.e. purified NPLs) is then dissolved in toluene. The purity of the nanoplatelets is evidenced by the pure absorbance and photoluminescence spectra.

3. Results and Discussion

Surfactants have a strong influence on the properties of organic-inorganic nanocomposites with regard to their optoelectronic applications. As both, the size and the functional group of a surfactant affect the properties, here we studied the influence of the two aspects separately. The required interaction of the inorganic nanocrystals and the conjugated polymer was accomplished by the incorporation of anchor groups into the polymer. These anchor groups were composed of a functional group targeted to enable an effective binding to the inorganic nanocrystals and a spacer which determined the distance between polymers and nanocrystals. Due to its favorable optoelectronic properties, the poly(*p*-phenylene vinylene) derivative DEH-PPV was selected as conjugated block. DEH-PPV can be synthesized via Siegrist

polycondensation, which offers a defined functional end group. This end group was further exploited for the incorporation of a second block, which is non-conjugated, composed of a reactive ester repeating unit via RAFT polymerization,[39] which allows for the incorporation of different anchor groups (see **Figure 79**). To guarantee that the observed differences in the properties originate from the varying anchor groups, all polymers employed in the study were synthesized from a single precursor polymer as illustrated in **Figure 79**. By exploiting only the same block copolymer architecture, influence of the anchor groups on the torsion and, thereby, photophysical properties of the conjugated backbone was also avoided. The precursor polymer that does not have any anchor group is hereafter named as the reference polymer **P1**. The functional polymers with anchors based on sulfide is called **P2a** and the ones based on amino are called **P2b** and **P2c**. The ligand size is the same in **P2a** and **P2b** polymers, while the spacer is longer in **P2c** (see **Figure 79**).

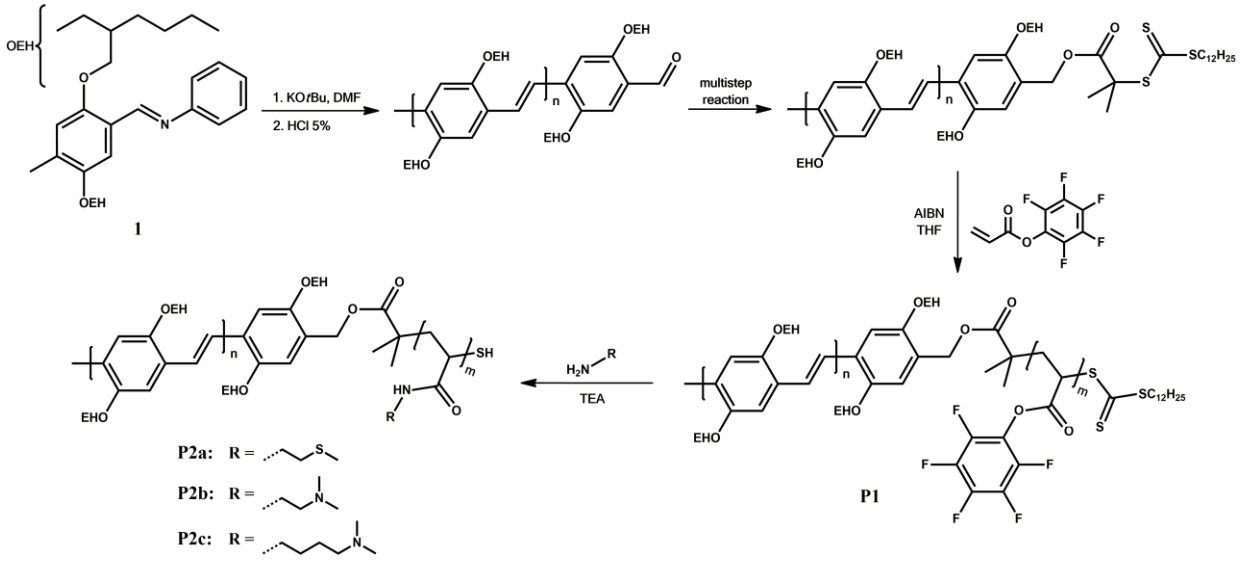

Figure 79. General reaction scheme for the incorporation of anchor groups into the block copolymer containing a conjugated DEH-PPV block and assignment of the polymers **P1** and **P2a-c**.

When incorporating anchor groups into a conjugated polymer, several aspects have to be taken into account. The incorporation of anchor groups as side chains into the conjugated polymer backbone or as end groups is usually relatively simple. Unfortunately, both approaches come along with disadvantages. The incorporation of anchor groups as side chains disturbs the polymer's regioregularity, causes a torsion of the backbone and decreases the planarity of the conjugated backbone.[3,40] Also, with an increasing chain length of the polymer

the possibility of a single functional end group to be in a suitable position for interacting with the nanocrystal surface is significantly decreased. In this latter case, only very strong anchor groups such as enediols in the case of TiO_2 nanoparticles could form stable coatings.[41,42] Therefore, use of block copolymers, which we employ here, is highly desired since they both allow for multiple anchor groups and, thereby, enable the formation of a stable coating without sacrificing the original optoelectronic properties of the conjugated polymer owing to the separation of the conjugated block from the anchor groups. Therefore, torsion of the conjugated backbone does not occur. Since the combination of a conjugated PPV block and a non-conjugated block via one-pot block copolymerization can be solely achieved by applying ring-opening metathesis polymerization (ROMP), which involves complicated monomer synthesis, a synthetic route exploiting the defined end group installed via Siegrist polycondensation was applied in the study at hand.[39,43]

Successful incorporation of the anchor groups via post-polymerization modification is evidenced via FTIR spectroscopy. Upon incorporation of the anchor groups, the band originating from the pentafluorophenyl ring at 1519 cm^{-1} disappears. Moreover, the C=O band shifts from 1783 cm^{-1} in the reactive ester to approximately 1670 cm^{-1} in the amides (see **Figure 80a** and **S2, S4** and **S6**). Full conversion of the post-polymerization modification is verified by the absence of any signals in the ^{19}F-NMR spectra of the amides. In addition, the successful incorporation of the anchor groups is verified via ^{1}H-NMR spectroscopy. After post-polymerization modification, the spectra of the polymers exhibit signals, which can be assigned to the respective anchor group (see **Figure S3**, **S5** and **S7**).

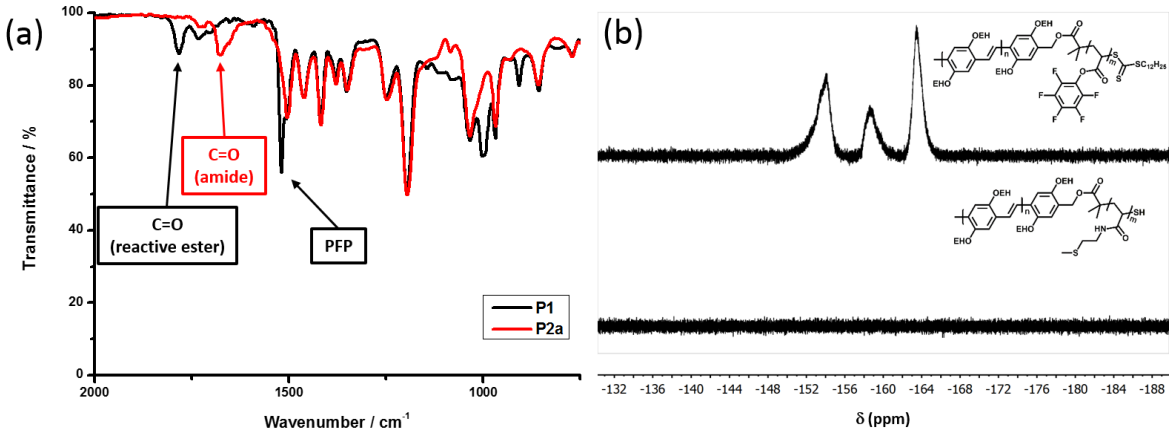

Figure 80. (a) FTIR spectra verifying the success of the post-polymerization modification and (b) ^{19}F-NMR spectra of polymers **P1** and **P2a**. While signals of the reactive ester occur in the ^{19}F-NMR spectrum of precursor polymer **P1**, full conversion of the post-polymerization modification is evidenced by the absence of any signals in the spectrum of polymer **P2a**. (Spectra verifying the successful synthesis of polymers **P2b** and **P2c** can be obtained from the Supporting Information – **Figures S4** and **S6**.)

As the inorganic nanocrystals, we employ atomically flat CdSe NPLs having four monolayer (4 ML) vertical thickness (~1.2 nm). We chose 4 ML CdSe NPLs because of their well-established synthesis and increased stability. In **Figure 81a**, absorbance and photoluminescence (PL) spectra of the NPLs are shown (in solution-phase). The absorbance of the NPLs exhibit two peaks that are at 480 and 512 nm arising from electron/light-hole and electron/heavy-hole transitions. The PL peak arises from the recombination of the excitons at the electron/heavy-hole transition (~513 nm). The emission linewidth in the NPLs is as narrow as ~8 nm due to absence of inhomogenous broadening.[44] The inset in **Figure 81a** shows a high-angle annular dark-field scanning transmission electron microscopy (HAADF-STEM) image of the NPLs. In the STEM image, most of the NPLs can be seen lying flat on the TEM grid, while some of them can be observed to form stack-like assemblies, which lie perpendicular to the TEM grid. The stacking of the NPLs is commonly observed in their solid-films since the NPLs tend to assemble together due to strong van der Walls forces between their large and flat surfaces.[45] The absorbance and PL spectra of the conjugated polymers are also presented in **Figure 81b**. The PL peak of the polymers are at ~550 nm and their absorption peaks are at approximately at 460 nm. We observe very slight shifts between the absorbance and emission spectra of different polymers used here, which may arise from use of different ligands.

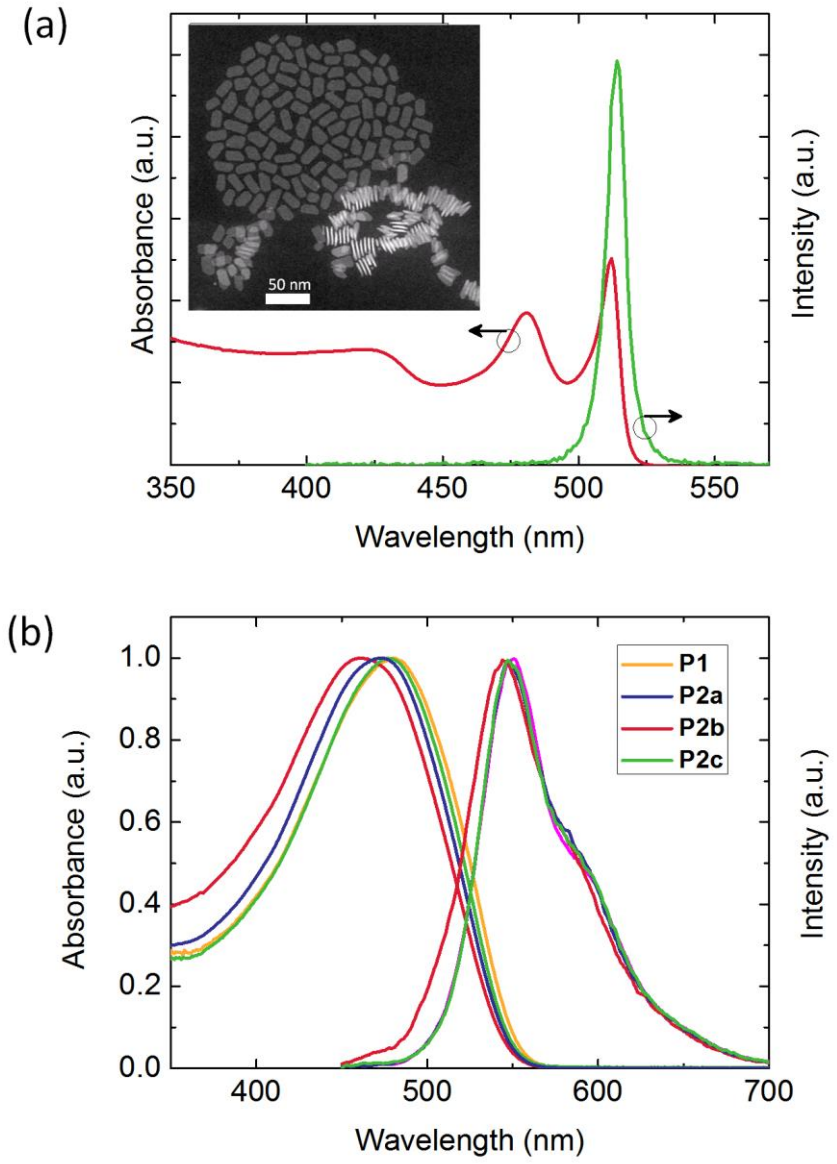

Figure 81. Absorbance and photoluminescence of (a) 4 monolayer thick CdSe nanoplatelets, and (b) conjugated polymers **P1** and **P2a-c**. Inset in (a) shows the HAADF-STEM image of the CdSe nanoplatelets, the scale bar is 50 nm.

We investigate the steady state PL of the NPLs and the polymers when they are mixed together in solution-phase. For this, first, we prepare a dilute nanoplatelet solution in toluene. The absorbance of the initial NPL solution is very low (~0.1 at the first exciton peak 512 nm) to prevent reabsorption and concentration based energy transfer effects. The concentration of the NPLs is calculated to be 12.3 nM (in 3 mL toluene) by using their reported absorption cross-section.[44] Polymer solutions are prepared separately using toluene as the solvent with a concentration of 2 mg/mL. Then, step-by-step we add small amounts of a polymer into the

NPL solution. Each step corresponds to addition of 5 µL polymer solution into the NPL solution. Also, each step corresponds to ~1.4 nmol for **P2a** and **P2b** polymers and ~1.3 nmol for **P1** as calculated by their molecular weight (see Supporting Information).

As the polymer **P2a** (polymer with sulfide anchor) is added to the NPL solution, we observe that the NPL emission starts to immediately decrease (see **Figure 82a**) when the samples are excited at 375 nm. In the case of polymer **P2b,** which carries an amine anchor with the same ligand size as in **P2a**, the decrease in the NPL emission is also evident (see **Figure 82b**). As more polymer is added step-by-step, the NPL emission is observed to further decrease (see **Figure 82a, b)**. The insets in the **Figure 82a, b** also show the evolution of the NPL emission after spectral profile of the polymer emission has been mathematically subtracted for each case. The precursor polymer (**P1**), which does not carry any specific anchor group but the same conjugated block, is also investigated as the negative control group (see **Figure 82c**). Addition **P1** is observed to cause a decrease in the NPL emission but it is observed to be less than that observed with **P2a** and **P2b**. **Figure 82d** summarizes the change in the NPL emission as a function of increasing polymer amounts. In the case of reference polymer **P1**, the quenching of the NPL is found to be up to 2-folds. This decrease in the NPL emission can be well explained due to absorption of the NPL emission by the polymer since there is a non-zero absorbance of polymers at the emission peak of the NPLs (see **Figure 81b** for the absorbance of the polymers). We have measured the absorbance of the polymer **P1** as ~0.3 at 512 nm, when 5.2 nmol **P1** has been added to the solution. The absorbance of **P2a** and **P2b** is also measured ~0.32 when 5.6 nmol of these polymers have been added to the solution. According to the following relation; $\phi^{transmitted} = \phi^{incident} 10^{-A}$, where ϕ is the light intensity and A is the measured absorbance. For A = 0.3, one could simply calculate a 2-fold decrease (i.e. 50% change) in the NPL emission due to the absorption by the polymer. Therefore, this explains the decreased NPL emission with the addition of polymer **P1**.

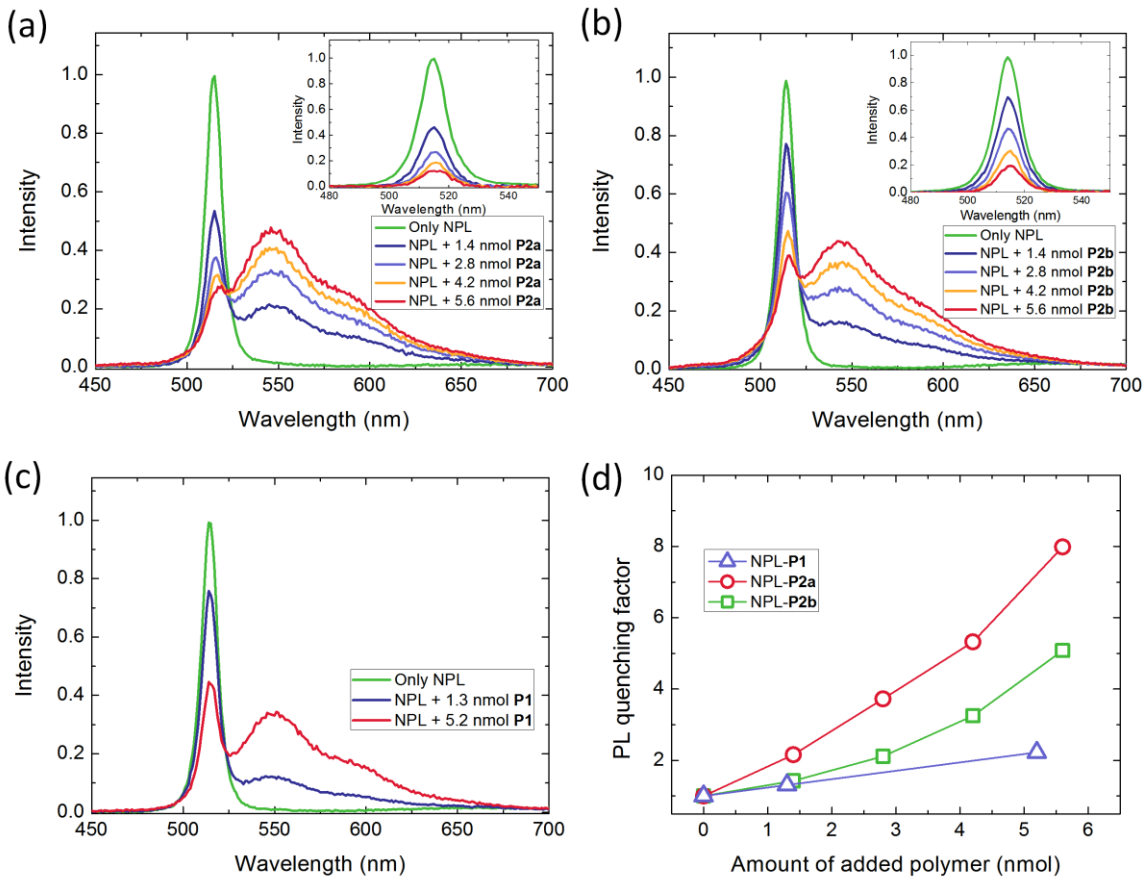

Figure 82. Steady state photoluminescence spectra of the hybrids as polymer is added step-by-step for (a) NPL-P2a, (b) NPL-P2b and (c) NPL-P1 samples. The excitation wavelength for all cases is 375 nm. The insets in (a) and (b) show the NPL emission after spectral shape of the polymer emission has been subtracted. (d) Evolution of the NPL emission as a function of added polymer amount for three different cases.

In the case of polymers with anchor groups, the PL quenching is found to be much stronger than that caused by **P1**. With polymer **P2b** (having amine anchor), we observe that the quenching of the NPL emission is up to 5-folds (80% decrease in the NPL emission). Moreover, polymer **P2a** carrying the sulfide anchor shows the largest quenching in the NPL emission, a factor larger than 8 (~90% decrease in the NPL emission). Therefore, strong quenching of the NPL emission in the presence of functional polymers (**P2a and P2b**) strongly suggests that an additional process exists in addition to just absorption of the polymers.

There exists a spectral overlap between the NPL emission and the polymer absorbance. Thus, Förster resonance energy transfer (FRET) may be possible in these hybrids and FRET might the underlying process that can explain the emission quenching in the NPLs. To check this

hypothesis with FRET, we investigate and analyze steady state PL emission of the polymers. In FRET process, the emission of the donor is decreased while the emission of the acceptor is concomitantly increased due to exciton transfer from the donor to the acceptor.[46–48] Therefore, we look a sign of an increased polymer emission due to FRET. **Figure 83a** shows the emission spectra of polymer **P2a** emission in the absence (dotted line) and presence (solid line) of the NPLs when excited at 375 nm. The only **P2a** emission is larger than the polymer emission in NPL-**P2a** samples for two different polymer amounts. This simply rules out FRET as the dominant process behind the PL quenching in the NPLs. Also, **Figure 83b** illustrates the overall change of the emission intensity in the functional polymers **P2a** and **P2b** as a function of the added polymer amount (calculated from the emission spectra measured under excitation of 375 nm). Both polymers exhibit a decreased emission when mixed with the NPLs. The decrease in the polymer emission is larger for **P2a** than that of **P2b** (see **Figure 83b**). We also observed a larger quenching in the NPL emission for the case of **P2a** polymer.

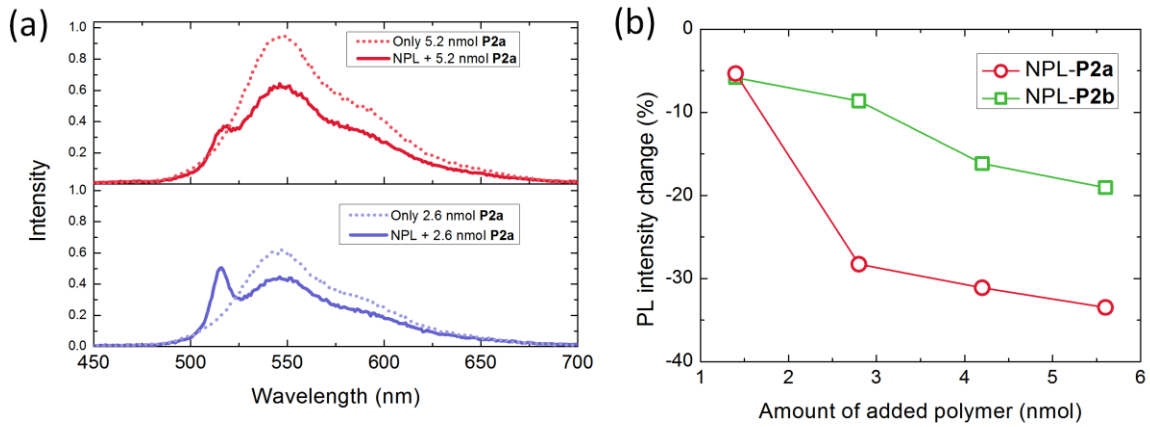

Figure 83. (a) Emission of the only polymer **P2a** and NPL + **P2a** for 5.2 nmol (top) and 2.6 nmol (bottom) polymer amounts. The excitation wavelength for all cases is 375 nm. (b) Emission intensity change in the polymers **P2a** and **P2b** in the presence of the NPLs as compared to bare polymer emission.

To explain the emission quenching of both the NPLs and the polymers, we consider another hypothesis, which is the exciton dissociation at the NPL-polymer interface. Exciton dissociation is expected to decrease radiative emission since free carriers are generated instead of exciton recombination. Previously, DEH-PPV based polymers have been shown to be effective electron donors through exciton dissociation at the organic-organic interfaces with C60 molecules.[49] To check exciton dissociation in polymer/NPL hybrids, we look into

the excitation spectra of the NPLs and the polymers. **Figure 84a** shows the excitation spectra of the NPL peak emission at 513 nm for three different cases: Only NPL, NPL + 1.4 nmol **P2a** and NPL + 2.8 nmol **P2a** samples. The excitation spectra of the NPLs show a broadband quenching as the polymer amount is increased in the hybrid. This indicates that excitons formed in the NPLs are quenched independent of the excitation wavelength. This may suggest the possibility of a photoinduced charge transfer from the NPL into the polymer through exciton dissociation at the interface. In **Figure 84b,** we also plot the excitation spectra of the polymer **P2a** emission measured for its peak emission wavelength at 545 nm in two different cases: only 5.6 nmol **P2a** and NPL + 5.6 nmol **P2a**. We also observe a broadband decrease in the excitation spectrum of the polymer, when the polymer is mixed with the NPLs.

To analyze the decrease in the excitation spectra of the **P2a** emission, first we consider the absorption of the excitation light by the NPLs. Using the measured absorbance spectrum of the NPLs, we calculate the decreased excitation light intensity by the following relation: $\phi^{transmitted} = \phi^{incident} 10^{-A}$. Then, we estimate the decrease in the polymer's excitation spectra due to NPL absorption as plotted by the black solid curve in **Figure 84b**. We see dips in the polymer's excitation spectrum at 512 and 480 nm, where the NPL has strong absorption. However, experimentally measured excitation spectra of the **P2a** emission in the presence of the NPLs (red solid curve) is still much lower than the estimated excitation spectra (black solid curve). Moreover, for excitation wavelengths longer than 520 nm, where there is no NPL absorbance, the excitation spectrum of the **P2a** shows decreased intensity in the hybrid sample as compared to estimated excitation. These observations strongly suggest that the excitons in the polymer **P2a** are also dissociated at the polymer/NPL interface, possibly due to photoinduced electron transfer from the polymer.

As a negative control sample, we also test the excitation spectra of the polymer **P1** before and after mixed with the NPLs. **Figure 84c** shows the excitation spectra of only 5.2 nmol **P1** and NPL + 5.2 nmol **P1** samples. Here, we observed that the black curve (calculated excitation spectrum by considering the absorption of the excitation light by the NPLs) and the orange curve (measured excitation spectrum of the polymer in the presence of the NPLs) shows a very good agreement as shown in **Figure 84c**. Therefore, this strongly supports our view that the change in the excitation of the **P1** polymer just arises from the NPL absorption since there is no near-field interaction between the species in solution-phase. However, in the case of **P2a**, there has to be near-field interactions (i.e. exciton dissociation) between the species to explain the observed changes.

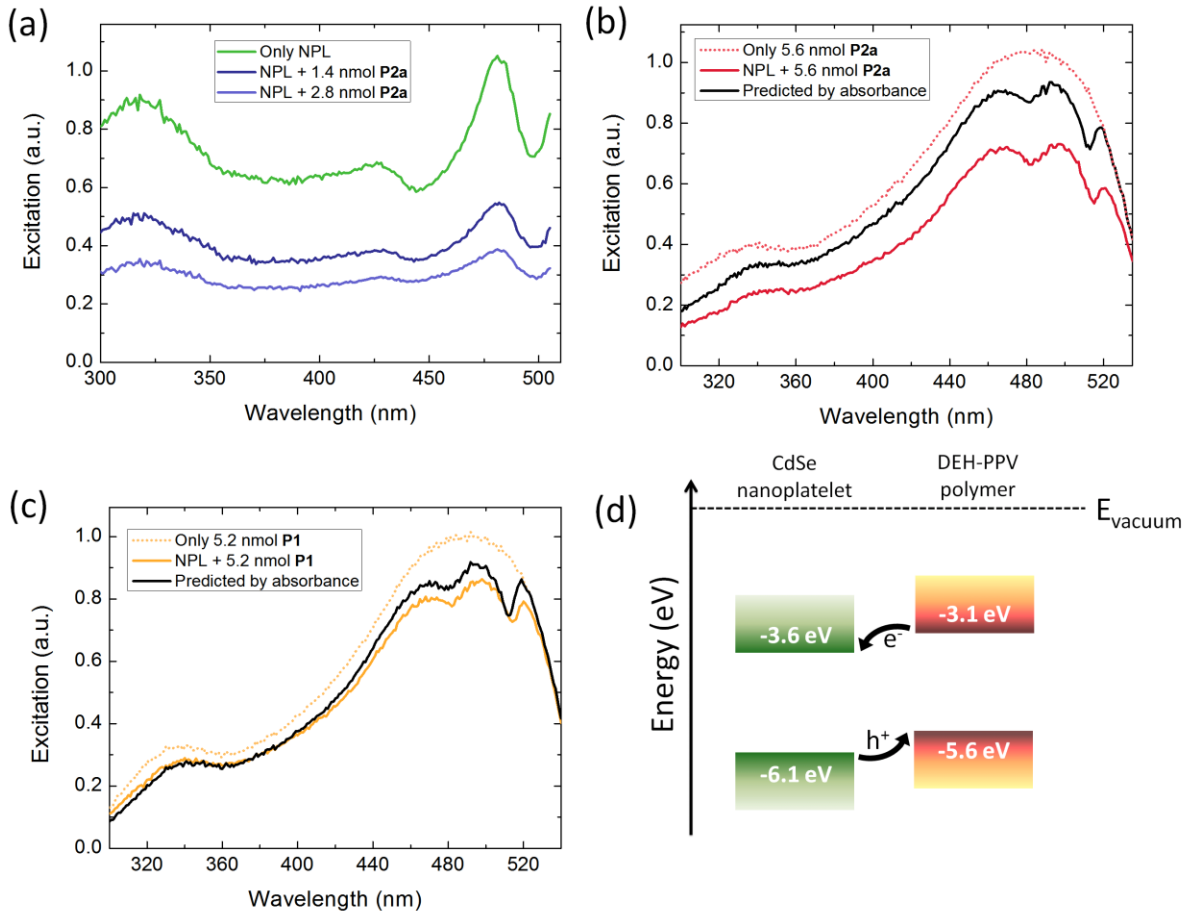

Figure 84. (a) Excitation spectra of the NPL emission for three different samples: Only NPL (green), NPL + 1.4 nmol **P2a** (dark blue) and NPL + 2.8 nmol **P2a** (light blue). (b) Excitation spectra of the **P2a** for only 5.6 nmol **P2a** (red dotted curve) and NPL + 5.6 nmol **P2a** (red solid curve) samples. Also, excitation of the **P2a** emission is estimated by considering the absorption of the excitation light by the NPLs (black solid curve). (c) Excitation spectra of the **P1** for only 5.2 nmol **P1** (orange dotted curve) and NPL + 5.2 nmol **P1** (orange solid curve) samples. Also, excitation of the **P1** emission is estimated by considering the absorption of the excitation light by the NPLs (black solid curve). (d) Energy bands of the NPLs and polymers exhibiting a staggered (Type II) band alignment favoring exciton dissociation.

To further support exciton dissociation at the NPL-polymer interfaces, we investigate the energy band alignment between the NPLs and polymers. For this, we apply cyclic voltammetry (CV) to determine the energy levels of the polymers. From the CV data, the onset potentials for oxidation and reduction are found to be E^{Ox} = 0.5 V and E^{Red} = -2.0 V vs Fc/Fc^{+}. Thus, with an assumed level of the Fc/Fc+ redox couple of -5.1 eV versus the vacuum, the HOMO and LUMO energy levels are calculated to be -5.6 eV and -3.1 eV,

respectively (see **Figure S1**).[50] Previously, the conduction and valence band levels have been measured via ultraviolet photoelectron spectroscopy (UPS) in 4 ML thick CdSe NPLs as -3.6 and -6.1 eV, respectively.[51] The resulting bands alignment at the polymer-NPL hybrids is illustrated in **Figure 84d**, which exhibits a staggered (i.e. Type-II) band alignment. Therefore, exciton dissociation in the NPLs and the polymers is expected to be favored via hole transfer from the NPLs and electron transfer from the polymers (see **Figure 84d)**. Based on these observations, we can propose that exciton dissociation in the NPL-polymer hybrids is the dominant process.

Considering **Figure 82a**, which summarizes the emission quenching in the NPLs as a function of polymer addition for different polymers, **P2a** (functional polymer with the sulfide anchor) is observed to cause a larger quenching in the NPL emission than **P2b** (functional polymer with the amine anchor) while the ligand lengths are the same. This may suggest that **P2a** has a higher tendency to bind to the NPL surfaces than **P2b**. Thus, the emission of more NPLs could be quenched in solution-phase with more attached **P2a** due to exciton dissociation. Another possibility for the stronger quenching might be that sulfide anchors could create surface traps in the NPLs leading to nonradiative decay of the excitons. Such emission quenching arising from ligands in the nanocrystals have been shown previously.[15,24] Generally, thiol-based ligands were shown to create surface trap states within the bandgap of the quantum dots causing charge trapping and quenching.[15] However, we also observed a larger quenching of the polymer **P2a** emission as compared to **P2b** as shown in **Figure 83b**. Thus, this opposes the possibility that the sulfide anchor might act as quencher, but most likely it acts as a stronger agent for hybridization with the NPLs than amine based anchors. Moreover, enhanced interaction of **P2a** with the CdSe NPLs would explain the stronger PL quenching on both side of the hybrid via exciton dissociating Type-II interfaces.

In addition to different anchor types, we also investigate the effect of the size of the ligand to the optical properties of the hybrids. For this, we developed **P2b** and **P2c** polymers both having amine based anchor but with different sizes. **P2c** has a large size than **P2b** polymer as shown in **Figure 79**. **Figure 85** shows the emission spectra of the NPL + 9 nmol **P2b** and NPL + 9 nmol **P2c** samples. As shown in the inset of **Figure 85**, after the spectral shape of the polymer emission is subtracted, we observe that the quenching of the NPL emission is larger in **P2b**. The quenching factor of the NPL emission is calculated to be 11.3 and 6.8 for **P2b** and **P2c**, respectively. This also suggests that shorter ligands are more efficient for exciton

dissociation. The charge transfer process, which generally occurs for distances less than 1 nm, is highly distance sensitive. Therefore, slight increase in the ligand size (as in the case of **P2c** polymer) can decrease the exciton dissociation efficiencies.

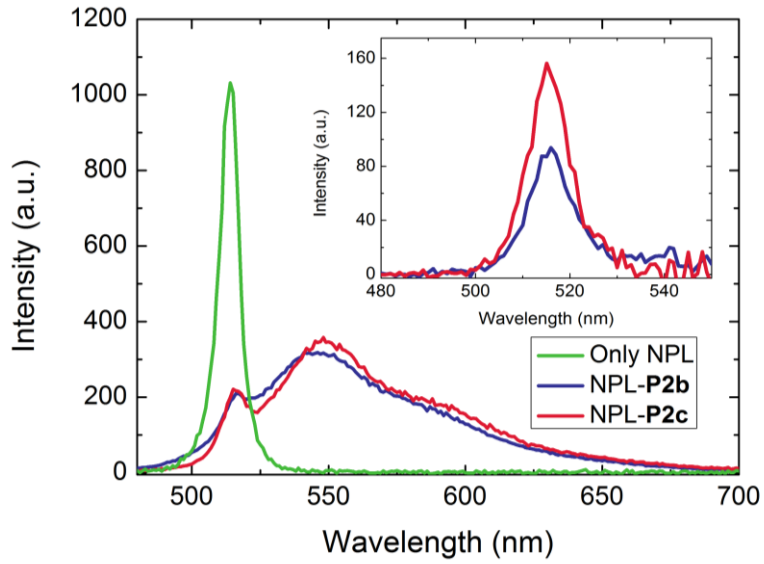

Figure 85. Emission spectra of the only NPL, NPL + 9 nmol **P2b** and NPL + 9 nmol **P2c** samples. The inset shows the NPL emission after spectral shape of the polymer emission has been subtracted. The emission quenching is larger for **P2b** than **P2c** since **P2b** has a shorter anchor ligand.

Finally, we study the solid-film morphology of the hybrids. For this, we prepare solutions with only NPL and NPL/**P2a** samples. **Figure 86a** shows HAADF-STEM images of the NPLs before they are mixed with the functional polymers. The NPLs tend to exhibit a degree of aggregation during the drying process of the solvent. This also leads to stacking of the NPLs when used with higher concentrations. In the case of the hybrid, **Figure 86b** shows highly uniform distribution of the NPLs without any considerable aggregation although the same amount of NPLs have been employed. This also suggests that the functional polymers bind to the NPL surfaces and help creating an increased separation between the NPLs so that NPL-to-NPL interactions could significantly be reduced. Such hybrids could be utilized for hybrid optoelectronic applications. The homogenous distribution of the NPLs would be useful for efficient exciton dissociation in solar cells or exciton injection in light-emitting diodes.

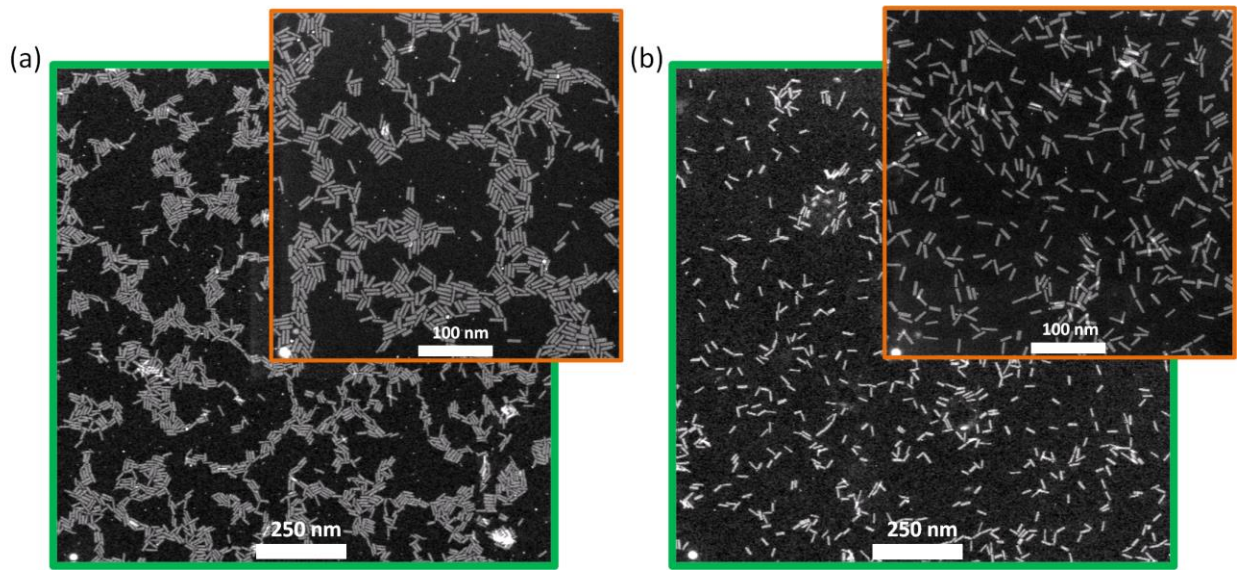

Figure 86. HAADF-STEM images of (a) only NPLs and (b) NPL-**P2a** hybrids. The insets show zoomed-in images with scale bar of 100 nm.

4. Conclusion

Here, we introduced a hybrid conjugated polymer/nanoplatelet system for the first time, which exhibited strong photoluminescence quenching in their dilute solutions. The quenching has been well explained with exciton dissociation at Type-II band aligned organic-inorganic interfaces rather than dipole-dipole coupling. We investigated the effect of the anchor type on the hybridization efficiency and showed that sulfide based anchors lead to a stronger binding to the NPL surfaces as compared to amine based anchors. Furthermore, shorter ligands in the polymer have been shown to increase exciton dissociation at the interfaces due to their intimately close integration to the NPL surfaces. These organic-inorganic hybrids also exhibited uniform NPL coatings in their solid thin-films as revealed by TEM imaging. The polymer-NPL nanocomposites are expected to be promising for hybrid optoelectronics, particularly in solar cells.

ASSOCIATED CONTENT

Supporting Information.

AUTHOR INFORMATION

# BG and FM contributed equally to this work.

Corresponding Author

* E-mail: guzelturk@gmail.com, volkan@bilkent.edu.tr, hvdemir@ntu.edu.sg

ACKNOWLEDGMENT

The authors gratefully thank the Deutsche Forschungsgemeinschaft (DFG): International Research Training Group (IRTG) 1404 "Self-Organized Materials for Optoelectronics" for funding. The authors also would like to thank the following funding agencies for financial support: EU-FP7 Nanophotonics4Energy NoE, and TUBITAK EEEAG 109E002, 109E004, 110E010, 110E217, ESF-EURYI, TUBA-GEBIP and in part from NRF-RF-2009-09, NRF-CRP-6-2010-02, A*STAR of Singapore and EPSRC (EP/I029141). H.V.D. acknowledges support from ESF-EURYI and TUBA-GEBIP.

ABBREVIATIONS

DCM, dichloromethane; DEH-PPV, poly[2,5-di(2'-ethylhexyloxy)-1,4-phenylene vinylene]; FTIR, Fourier transform infrared; NMR, nuclear magnetic resonance; OEH, 2-ethylhexyloxy; M_n, number average molar mass; PDI, polydispersity index; PPV, poly(*p*-phenylene vinylene); ROMP, ring-opening metathesis polymerization.

KEYWORDS

Colloidal nanoplatelets, CdSe, poly(*p*-phenylene vinylene) (PPV), nanocomposite, hybrid, exciton dissociation, charge transfer, photoluminescence quenching, solar cell.

References

(1) Huynh, W. U.; Dittmer, J. J.; Alivisatos, A. P. Hybrid Nanorod-Polymer Solar Cells. *Science* **2002**, *295* (5564), 2425–2427.

(2) He, M.; Qiu, F.; Lin, Z. Toward High-Performance Organic–Inorganic Hybrid Solar Cells: Bringing Conjugated Polymers and Inorganic Nanocrystals in Close Contact. *J. Phys. Chem. Lett.* **2013**, *4* (11), 1788–1796.

(3) Reiss, P.; Couderc, E.; De Girolamo, J.; Pron, A. Conjugated Polymers/semiconductor Nanocrystals Hybrid Materials--Preparation, Electrical Transport Properties and Applications. *Nanoscale* **2011**, *3* (2), 446–489.

(4) Wright, M.; Uddin, A. Organic—inorganic Hybrid Solar Cells: A Comparative Review. *Sol. Energy Mater. Sol. Cells* **2012**, *107*, 87–111.

(5) Guzelturk, B.; Demir, H. V. Organic-Inorganic Composites of Semiconductor Nanocrystals For Efficient Excitonics. *J. Phys. Chem. Lett.* **2015**, 150528082340007.

(6) Guzelturk, B.; Hernandez Martinez, P. L.; Sharma, V. K.; Coskun, Y.; Ibrahimova, V.; Tuncel, D.; Govorov, A. O.; Sun, X. W.; Xiong, Q.; Demir, H. V.; et al. Study of Exciton Transfer in Dense Quantum Dot Nanocomposites. *Nanoscale* **2014**, *6* (19), 11387–11394.

(7) Kwak, J.; Bae, W. K.; Zorn, M.; Woo, H.; Yoon, H.; Lim, J.; Kang, S. W.; Weber, S.; Butt, H.-J. H.-J.; Zentel, R.; et al. Characterization of Quantum Dot/conducting Polymer Hybrid Films and Their Application to Light-Emitting Diodes. *Adv. Mater.* **2009**, *21* (48), 5022–5026.

(8) Zorn, M.; Bae, W. K.; Kwak, J.; Lee, H.; Lee, C.; Zentel, R.; Char, K. Quantum Dot-Block Copolymer Hybrids with Improved Properties and Their Application to Quantum Dot Light-Emitting Devices. *ACS Nano* **2009**, *3* (5), 1063–1068.

(9) Chin, P. T. K.; Hikmet, R. A. M.; Janssen, R. A. J. Energy Transfer in Hybrid Quantum Dot Light-Emitting Diodes. *J. Appl. Phys.* **2008**, *104* (1), 013108.

(10) Holder, E.; Tessler, N.; Rogach, A. L. Hybrid Nanocomposite Materials with Organic and Inorganic Components for Opto-Electronic Devices. *J. Mater. Chem.* **2008**, *18* (10), 1064.

(11) Mutlugun, E.; Guzelturk, B.; Abiyasa, A. P.; Gao, Y.; Sun, X. W.; Demir, H. V. Colloidal Quantum Dot Light-Emitting Diodes Employing Phosphorescent Small Organic Molecules as Efficient Exciton Harvesters. *J. Phys. Chem. Lett.* **2014**, *5* (16), 2802–2807.

(12) Zhou, R.; Stalder, R.; Xie, D.; Cao, W.; Zheng, Y.; Yang, Y.; Plaisant, M.; Holloway, P. H.; Schanze, K. S.; Reynolds, J. R.; et al. Enhancing the Efficiency of Solution-Processed Polymer:Colloidal Nanocrystal Hybrid Photovoltaic Cells Using Ethanedithiol Treatment. *ACS Nano* **2013**, *7* (6), 4846–4854.

(13) Liu, Z.; Sun, Y.; Yuan, J.; Wei, H.; Huang, X.; Han, L.; Wang, W.; Wang, H.; Ma, W. High-Efficiency Hybrid Solar Cells Based on polymer/PbSx Se1-X Nanocrystals Benefiting from Vertical Phase Segregation. *Adv. Mater.* **2013**, *25* (40), 5772–5778.

(14) Scharber, M. C.; Mühlbacher, D.; Koppe, M.; Denk, P.; Waldauf, C.; Heeger, A. J.; Brabec, C. J. Design Rules for Donors in Bulk-Heterojunction Solar Cells—Towards 10 % Energy-Conversion Efficiency. *Adv. Mater.* **2006**, *18* (6), 789–794.

(15) Greaney, M. J.; Brutchey, R. L. Ligand Engineering in Hybrid Polymer:nanocrystal Solar Cells. *Mater. Today* **2015**, *18* (1), 31–38.

(16) Greenham, N.; Peng, X.; Alivisatos, A. Charge Separation and Transport in Conjugated-Polymer/semiconductor-Nanocrystal Composites Studied by Photoluminescence Quenching and Photoconductivity. *Phys. Rev. B* **1996**, *54* (24), 17628–17637.

(17) Martínez-Ferrero, E.; Albero, J.; Palomares, E. Materials, Nanomorphology, and Interfacial Charge Transfer Reactions in Quantum Dot/Polymer Solar Cell Devices. *J. Phys. Chem. Lett.* **2010**, *1* (20), 3039–3045.

(18) Tang, J.; Kemp, K. W.; Hoogland, S.; Jeong, K. S.; Liu, H.; Levina, L.; Furukawa, M.; Wang, X.; Debnath, R.; Cha, D.; et al. Colloidal-Quantum-Dot Photovoltaics Using Atomic-Ligand Passivation. *Nat. Mater.* **2011**, *10* (10), 765–771.

(19) Tomczak, N.; Jańczewski, D.; Han, M.; Vancso, G. J. Designer Polymer–quantum Dot Architectures. *Prog. Polym. Sci.* **2009**, *34* (5), 393–430.

(20) Soreni-Harari, M.; Yaacobi-Gross, N.; Steiner, D.; Aharoni, A.; Banin, U.; Millo, O.; Tessler, N. Tuning Energetic Levels in Nanocrystal Quantum Dots through Surface Manipulations. *Nano Lett.* **2008**, *8* (2), 678–684.

(21) Munro, A. M.; Zacher, B.; Graham, A.; Armstrong, N. R. Photoemission Spectroscopy of Tethered CdSe Nanocrystals: Shifts in Ionization Potential and Local Vacuum Level as a Function of Nanocrystal Capping Ligand. *ACS Appl. Mater. Interfaces* **2010**, *2* (3), 863–869.

(22) Mathias, F.; Fokina, A.; Landfester, K.; Tremel, W.; Schmid, F.; Char, K.; Zentel, R. Morphology Control in Biphasic Hybrid Systems of Semiconducting Materials. *Macromol. Rapid Commun.* **2015**, *36* (11), 959–983.

(23) Munro, A. M.; Jen-LaPlante, I.; Ng, M. S.; Ginger, D. S. Quantitative Study of the Effects of Surface Ligand Concentration on CdSe Nanocrystal Photoluminescence. *J. Phys. Chem. C* **2007**, *111* (17), 6220–6227.

(24) Knowles, K. E.; Tice, D. B.; McArthur, E. A.; Solomon, G. C.; Weiss, E. A. Chemical Control of the Photoluminescence of CdSe Quantum Dot−Organic Complexes with a Series of Para-Substituted Aniline Ligands. *J. Am. Chem. Soc.* **2010**, *132* (3), 1041–1050.

(25) Günes, S.; Neugebauer, H.; Sariciftci, N. S. Conjugated Polymer-Based Organic Solar Cells. *Chem. Rev.* **2007**, *107* (4), 1324–1338.

(26) Ren, S.; Chang, L.-Y.; Lim, S.-K.; Zhao, J.; Smith, M.; Zhao, N.; Bulović, V.; Bawendi, M.; Gradecak, S. Inorganic-Organic Hybrid Solar Cell: Bridging Quantum Dots to Conjugated Polymer Nanowires. *Nano Lett.* **2011**, *11* (9), 3998–4002.

(27) Lhuillier, E.; Pedetti, S.; Ithurria, S.; Nadal, B.; Heuclin, H.; Dubertret, B. Two-Dimensional Colloidal Metal Chalcogenides Semiconductors: Synthesis, Spectroscopy, and Applications. *Acc. Chem. Res.* **2015**, *48* (1), 22–30.

(28) Ithurria, S.; Tessier, M. D.; Mahler, B.; Lobo, R. P. S. M.; Dubertret, B.; Efros, A. L. Colloidal Nanoplatelets with Two-Dimensional Electronic Structure. *Nat. Mater.* **2011**, *10* (12), 936–941.

(29) Olutas, M.; Guzelturk, B.; Kelestemur, Y.; Yeltik, A.; Delikanli, S.; Demir, H. V. Lateral Size-Dependent Spontaneous and Stimulated Emission Properties in Colloidal CdSe Nanoplatelets. *ACS Nano* **2015**, *9* (5), 5041–5050.

(30) Chen, Z.; Nadal, B.; Mahler, B.; Aubin, H.; Dubertret, B. Quasi-2D Colloidal Semiconductor Nanoplatelets for Narrow Electroluminescence. *Adv. Funct. Mater.* **2014**, *24* (3), 295–302.

(31) Guzelturk, B.; Kelestemur, Y.; Olutas, M.; Delikanli, S.; Demir, H. V. Amplified Spontaneous Emission and Lasing in Colloidal Nanoplatelets. *ACS Nano* **2014**, *8* (7), 6599–6605.

(32) Grim, J. Q.; Christodoulou, S.; Di Stasio, F.; Krahne, R.; Cingolani, R.; Manna, L.; Moreels, I. Continuous-Wave Biexciton Lasing at Room Temperature Using Solution-Processed Quantum Wells. *Nat. Nanotechnol.* **2014**, *9* (11), 891–895.

(33) Lhuillier, E.; Dayen, J.-F.; Thomas, D. O.; Robin, A.; Doudin, B.; Dubertret, B. Nanoplatelets Bridging a Nanotrench: A New Architecture for Photodetectors with Increased Sensitivity. *Nano Lett.* **2015**, *15* (3), 1736–1742.

(34) Lhuillier, E.; Robin, A.; Ithurria, S.; Aubin, H.; Dubertret, B. Electrolyte-Gated Colloidal Nanoplatelets-Based Phototransistor and Its Use for Bicolor Detection. *Nano Lett.* **2014**, *14*, 2715–2719.

(35) Wu, K.; Li, Q.; Du, Y.; Chen, Z.; Lian, T. Ultrafast Exciton Quenching by Energy and Electron Transfer in Colloidal CdSe nanosheet–Pt Heterostructures. *Chem. Sci.* **2015**, *6* (2), 1049–1054.

(36) Guzelturk, B.; Olutas, M.; Delikanli, S.; Kelestemur, Y.; Erden, O.; Demir, H. V. Nonradiative Energy Transfer in Colloidal CdSe Nanoplatelet Films. *Nanoscale* **2015**, *7* (6), 2545–2551.

(37) Rowland, C. E.; Fedin, I.; Zhang, H.; Gray, S. K.; Govorov, A. O.; Talapin, D. V.; Schaller, R. D. Picosecond Energy Transfer and Multiexciton Transfer Outpaces Auger Recombination in Binary CdSe Nanoplatelet Solids. *Nat. Mater.* **2015**, *14*, 484–489.

(38) Guzelturk, B.; Erdem, O.; Olutas, M.; Kelestemur, Y.; Demir, H. V. Stacking in Colloidal Nanoplatelets: Tuning Excitonic Properties. *ACS Nano* **2014**, *8* (12), 12524–12533.

(39) zur Borg, L.; Domanski, A. L.; Berger, R.; Zentel, R. Photoinduced Charge Separation of Self-Organized Semiconducting Superstructures Composed of a Functional Polymer-TiO 2 Hybrid. *Macromol. Chem. Phys.* **2013**, *214* (9), 975–984.

(40) Sirringhaus, H.; Brown, P. J.; Friend, R. H.; Nielsen, M. M.; Bechgaard, K.; Langeveld-Voss, B. M. W.; Spiering, A. J. H.; Janssen, R. A. J.; Meijer, E. W.; Herwig, P.; et al. Two-Dimensional Charge Transport in Self-Organized, High-Mobility Conjugated Polymers. *Nature* **1999**, *401* (6754), 685–688.

(41) Rajh, T.; Chen, L. X.; Lukas, K.; Liu, T.; Thurnauer, M. C.; Tiede, D. M. Surface Restructuring of Nanoparticles: An Efficient Route for Ligand−Metal Oxide Crosstalk. *J. Phys. Chem. B* **2002**, *106* (41), 10543–10552.

(42) Mathias, F.; Tahir, M. N.; Tremel, W.; Zentel, R. Functionalization of TiO 2 Nanoparticles with Semiconducting Polymers Containing a Photocleavable Anchor Group and Separation via Irradiation Afterward. *Macromol. Chem. Phys.* **2014**, *215* (7), 604–613.

(43) Menk, F.; Mondeshki, M.; Dudenko, D.; Shin, S.; Schollmeyer, D.; Ceyhun, O.; Choi, T.-L.; Zentel, R. Reactivity Studies of Alkoxy-Substituted [2.2]Paracyclophane-1,9-Dienes and Specific Coordination of the Monomer Repeating Unit during ROMP. *Macromolecules* **2015**, *48* (20), 7435–7445.

(44) She, C.; Fedin, I.; Dolzhnikov, D. S.; Demortière, A.; Schaller, R. D.; Pelton, M.; Talapin, D. V; Richard, D. Low-Threshold Stimulated Emission Using Colloidal Quantum Wells. *Nano Lett.* **2014**, *14* (5), 2772–2777.

(45) Abécassis, B.; Tessier, M. D.; Davidson, P.; Dubertret, B. Self-Assembly of CdSe Nanoplatelets into Giant Micrometer-Scale Needles Emitting Polarized Light. *Nano Lett.* **2014**, *14* (2), 710–715.

(46) Guzelturk, B.; Martinez, P. L. H.; Zhang, Q.; Xiong, Q.; Sun, H.; Sun, X. W.; Govorov, A. O.; Demir, H. V. Excitonics of Semiconductor Quantum Dots and Wires for Lighting and Displays. *Laser Photon. Rev.* **2014**, *8* (1), 73–93.

(47) Guzelturk, B.; Hernandez Martinez, P. L.; Zhao, D.; Sun, X. W.; Demir, H. V. Singlet and Triplet Exciton Harvesting in the Thin Films of Colloidal Quantum Dots Interfacing Phosphorescent Small Organic Molecules. *J. Phys. Chem. C* **2014**, *118* (45), 25964–25969.

(48) Lakowicz, J. R. *Principles of Fluorescence Spectroscopy*; Springer: Berlin, 2006.

(49) van der Veen, M. H.; de Boer, B.; Stalmach, U.; van de Wetering, K. I.; Hadziioannou, G. Donor−Acceptor Diblock Copolymers Based on PPV and C 60 : Synthesis, Thermal Properties, and Morphology. *Macromolecules* **2004**, *37* (10), 3673–3684.

(50) Thompson, B. C.; Kim, Y.-G.; McCarley, T. D.; Reynolds, J. R. Soluble Narrow Band Gap and Blue Propylenedioxythiophene-Cyanovinylene Polymers as Multifunctional Materials for Photovoltaic and Electrochromic Applications. *J. Am. Chem. Soc.* **2006**, *128* (39), 12714–12725.

(51) Fan, F.; Kanjanaboos, P.; Saravanapavanantham, M.; Beauregard, E.; Ingram, G.; Yassitepe, E.; Adachi, M. M.; Voznyy, O.; Johnston, A. K.; Walters, G.; et al. Colloidal CdSe(1-x)S(x) Nanoplatelets with Narrow and Continuously-Tunable Electroluminescence. Nano Lett. 2015, 15 (7), 4611–4615.

Supporting Information

Colloidal Nanoplatelet/Conducting Polymer Hybrids: Excitonic and Material Properties

Burak Guzelturk*[#], Florian Menk[#], Kai Philipps, Yusuf Kelestemur, Murat Olutas, Rudolf Zentel, Hilmi Volkan Demir*

[#] These authors contributed equally to this work.

guzelturk@gmail.com (B. Guzelturk)

volkan@bilkent.edu.tr, hvdemir@ntu.edu.sg (H. V. Demir)

Polymer Characterization

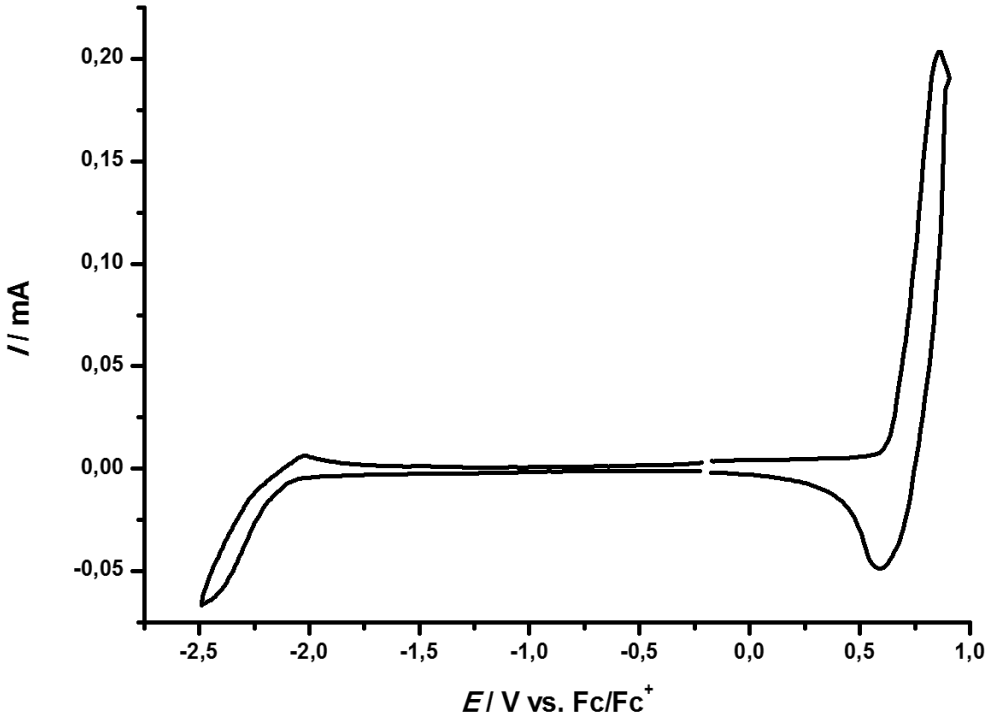

Figure S1. Cyclic voltammetry of precursor polymer **P1** measured in a 0.1 M solution of TBAPF6 in anhydrous acetonitrile versus Fc/Fc+.

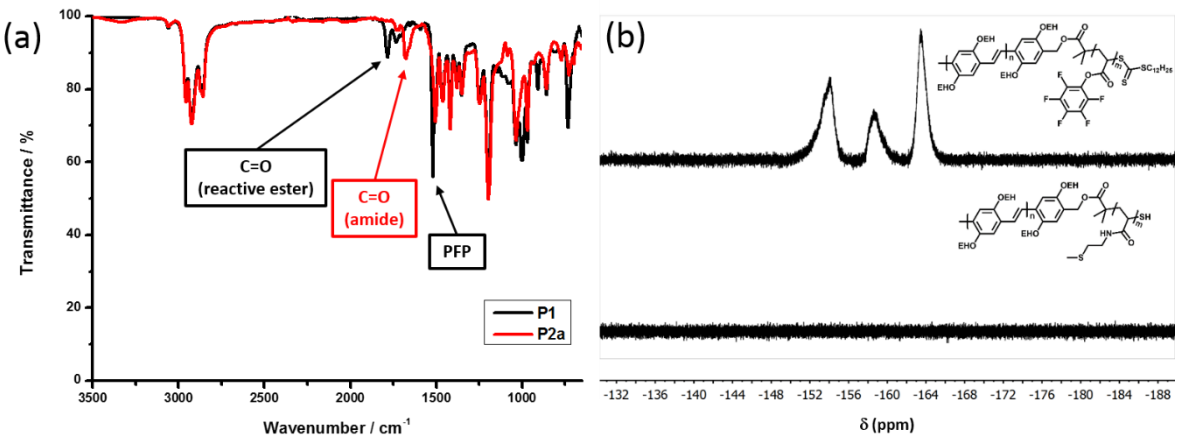

Figure S2. (a) FTIR spectra verifying the successful post-polymerization modification (transferring **P1** to **P2a**) and (b) ^{19}F-NMR spectra of polymers **P1** and **P2a**. While signals of the reactive ester occur in the ^{19}F-NMR spectrum of precursor polymer **P1**, no signals occur in the spectrum of **P2a** which verify full conversion of the post-polymerization modification.

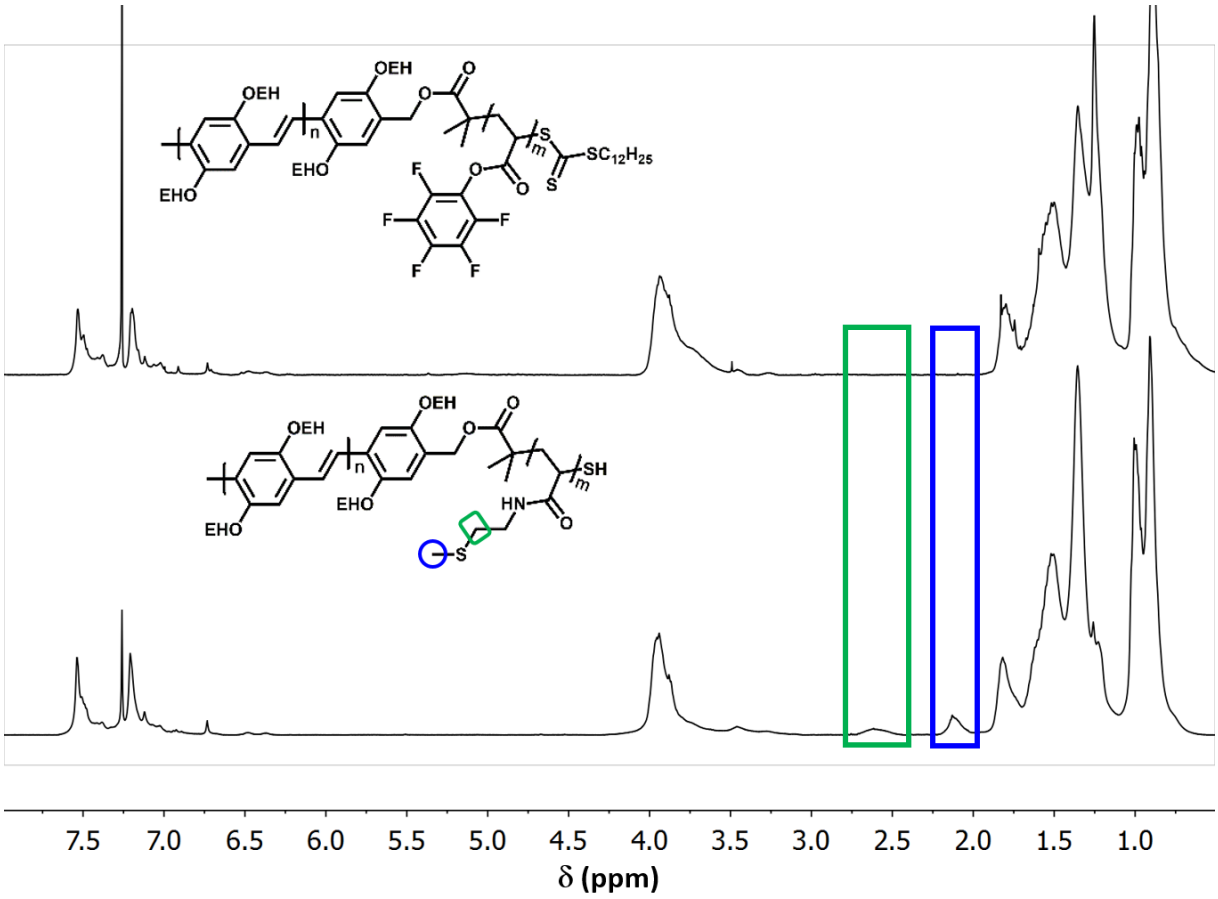

Figure S3. 400 MHz ^{1}H-NMR spectra of the precursor polymer **P1** and polymer **P2a** carrying a sulfide anchor group (in $CDCl_3$). After post-polymerization modification signals of the anchor group are detected in the spectrum.

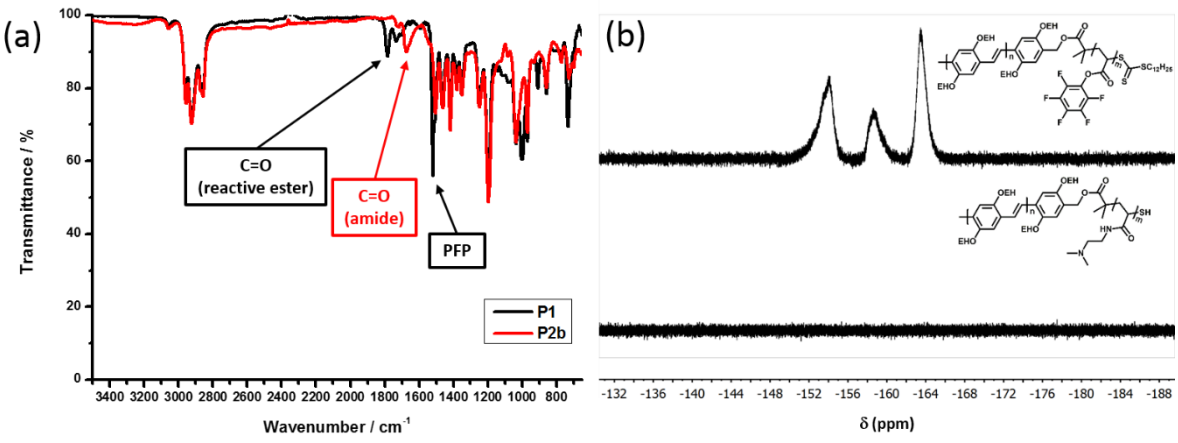

Figure S4. (a) FTIR spectra verifying the success of the post-polymerization modification and (b) ^{19}F-NMR spectra of polymers **P1** and **P2b**. While signals of the reactive ester occur in the ^{19}F-NMR spectrum of precursor polymer **P1**, full conversion of the post-polymerization modification is evidenced by the absence of any signals in the spectrum of polymer **P2b**.

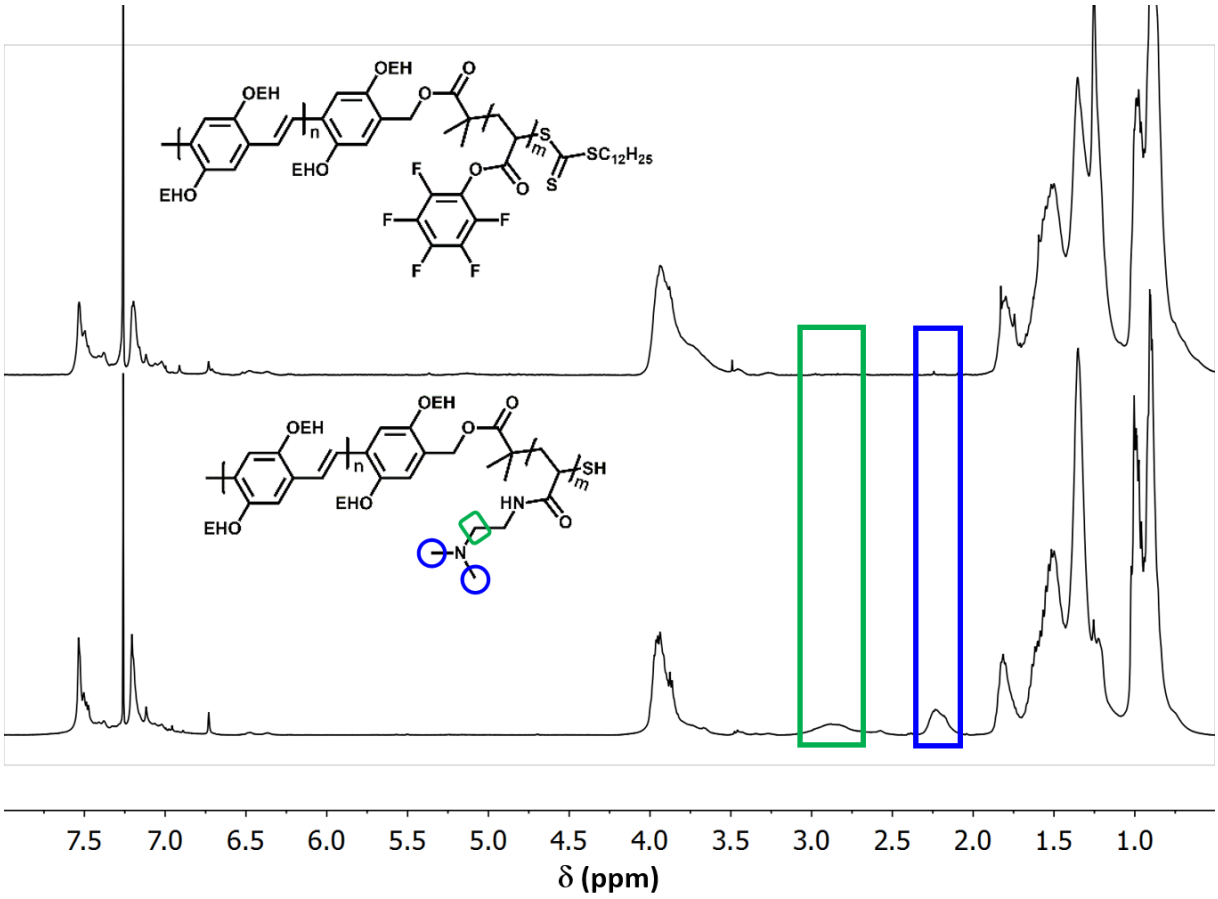

Figure S5. 400 MHz ^{1}H-NMR spectra of the precursor polymer **P1** and polymer **P2b** carrying an amino anchor group (in $CDCl_3$). After post-polymerization modification signals of the anchor group are detected in the spectrum.

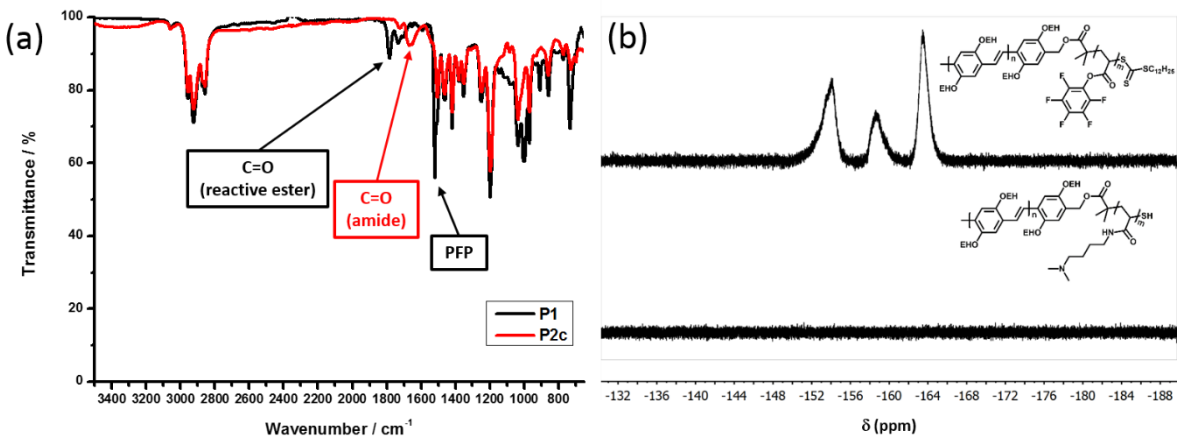

Figure S6. (a) FTIR spectra verifying the successful post-polymerization modification (transferring **P1** to **P2c**) and (b) ^{19}F-NMR spectra of polymers **P1** and **P2c**. While signals of the reactive ester occur in the ^{19}F-NMR spectrum of precursor polymer **P1**, no signals occur in the spectrum of **P2c** which verify full conversion of the post-polymerization modification.

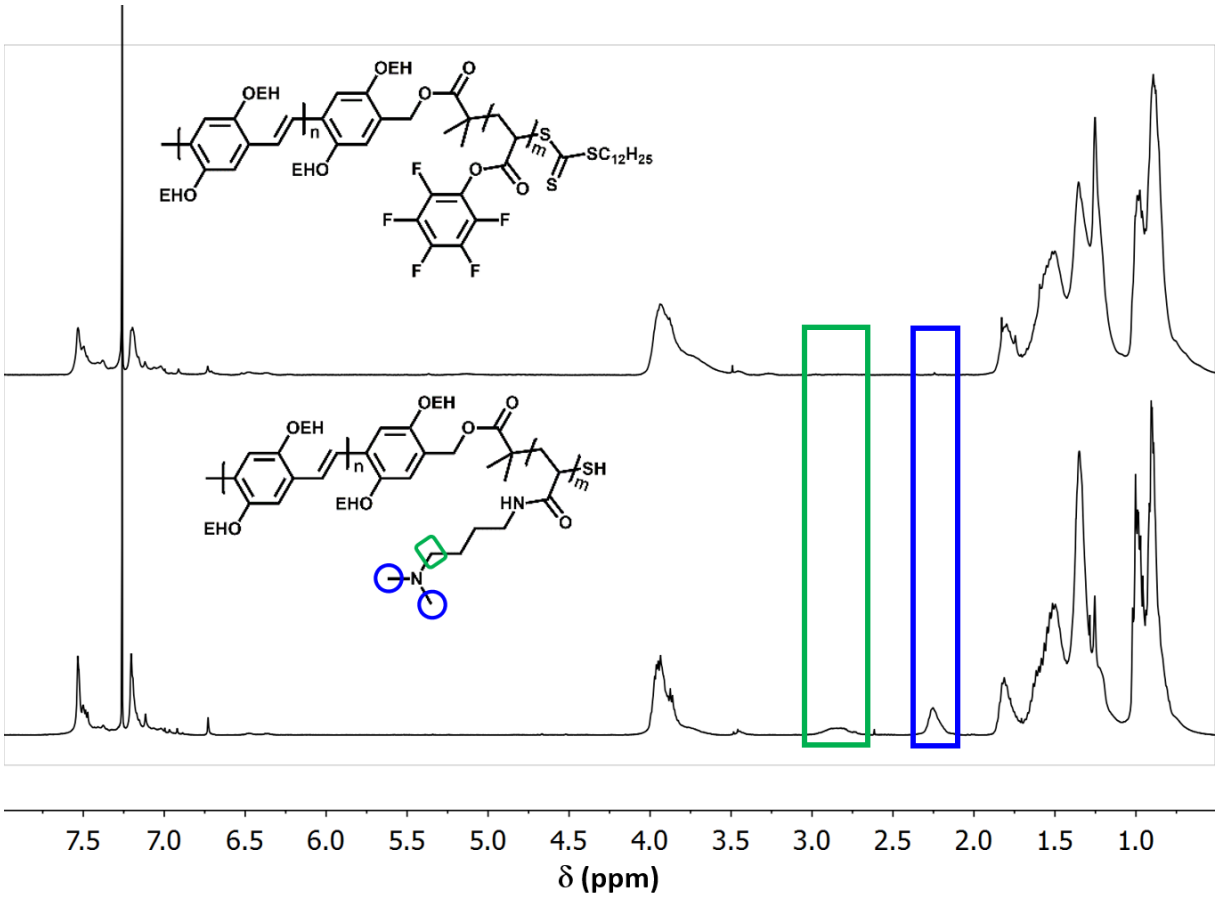

Figure S7. 400 MHz ^{1}H-NMR spectra of the precursor polymer **P1** and polymer **P2c** carrying an amino anchor group (in $CDCl_3$). After post-polymerization modification signals of the anchor group are detected in the spectrum.

Table S1. Molecular weights and PDIs of all polymers.

Polymer	**Block Ratio [a] (PPV:Acrylate)**	***M*n [b] (g · mol^{-1})**	***M*n [c] (g · mol^{-1})**	**PDI[b]**
P1	(≈ 18:4)[d]	9538	≈ 7700	1.31
P2a	≈ 18:4	10319	≈ 7200	1.33
P2b	≈ 18:4	8566	≈ 7200	1.28
P2c	≈ 18:4	8731	≈ 7300	1.30

[a] calculated from the ^{1}H-NMR spectra, [b] determined by GPC which was calibrated with polystyrene standards, [c] calculated from block ratio (including end groups), [d] estimated value from polymers **P2a-c**.

4.2.2 Equipping P3HT with Anchor Groups via End Group Modification

As one of the most applied conjugated polymers, P3HT or, in general, P3ATs denote very important representatives of conjugates polymers. Therefore, the development of new approaches for the modification of P3ATs are of enormous significance.

In the following publication we investigated two approaches which enable the incorporation of various anchor end groups on the example of P3HT. The approaches demonstrated to be capable of incorporating three different types of anchor groups which permit the functionalization of the most common classes of inorganic nanocrystals. As representatives of hard, intermediate and soft bases in the context of the "hard soft acids and bases" (HSAB) theory, in each case, a catechol anchor group, an amine and lipoic acid anchor groups were incorporated. Thus, following the presented approaches, stable coatings of hard, intermediate and soft acids such as TiO_2, ZnO and CdSe@ZnS nanocrystals, respectively, with P3HT became accessible. Consequently, the obtained polymers were applied to achieve stable coatings of CdSe@ZnS QDs and TiO_2 nanocrystals. Furthermore, efficient electron transfer from the conjugated polymer to the functionalized TiO_2 nanocrystals was observed under irradiation via KPFM.

Yannick Nyquist, supervised by Bernd Oschmann and the author of this dissertation, Lydia Braun and Tobias A. Bauer, supervised by Ana Fokina and the author, synthesized and characterized the polymers used in the context of this study. TEM images and TGA measurements were recorded by Bernd Oschmann. MALDI-TOF mass spectra were recorded by the author together with Stephan Türk from the Max Planck Institute for Polymer Research. Preparation of the KPFM samples was accomplished by the author and Victor W. Bergmann conducted and interpreted the KPFM measurements.

4.2.2.1 Manuscript to be Submitted

Functionalization of P3HT with Various Mono- and Multidentate Anchor Groups

Florian Menk‡, Ana Fokina‡, Bernd Oschmann‡, Victor W. Bergmann, Tobias A. Bauer, Yannick Nyquist, Jonathan Kiehl, Stefan Weber, Rudolf Zentel*

‡ These authors contributed equally to this work.

Abstract

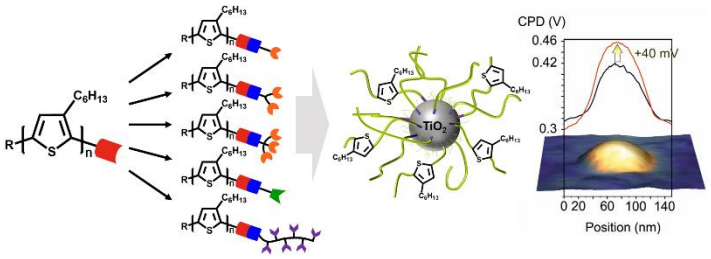

Due to its favorable optoelectronic properties and the accessibility via Grignard metathesis (GRIM) polymerization, poly(3-hexylthiophene) (P3HT) is one of the most applied conjugated polymers. The living nature of GRIM polymerization enables modification of the polymer to install desired properties. In the present study, two versatile approaches for the synthesis of a library of anchor group-functionalized P3HT have been developed. The different anchor groups enable the adsorption onto various types of inorganic nanoparticles. Depending on the polymerization conditions, P3HT consisting of mono- and bifunctional ethynyl-terminated polymer chains or of solely monofunctionalized aldehyde terminated polymer chains was synthesized. Subsequently, the quantitative introduction of amine, mono- and multidentate disulfide and catechol anchor groups was performed via copper-catalyzed 1,3-dipolar cycloaddition and via imine formation reactions. The influence of the polymeric ligand structure on the functionalization of nanoparticles was then investigated. Finally, the charge separation between the inorganic core and the semiconducting polymer corona was studied via Kelvin probe force microscopy using individually dispersed TiO_2 nanoparticles functionalized with catechol terminated P3HT.

1. Introduction

Conjugated polymers have been the subject of research for several decades due to their favorable optoelectronic properties. Consequently, they have been studied for the application in optoelectronic devices such as organic solar cells, light-emitting diodes, optical waveguides and lasers.[1] In 1993 McCullough *et al*. first reported the so-called GRIM (Grignard metathesis) polymerization.[2] GRIM polymerization is, besides ROMP and cyclopolymerization, one of the few living polymerization techniques capable of synthesizing conjugated polymers.[3] Moreover, it enables the facile synthesis of conjugated polymers such as regioregular poly(3-alklythiophenes) (P3ATs). Caused by the living nature, the synthesis of block copolymers and the incorporation of defined polymer end groups is facilitated.[4,5] Favorable optoelectronic properties resulting from the high regioregularity achieved via GRIM polymerization and the possibility to incorporate desired functionalities via end groups have made P3ATs one of the most applied conjugated polymers.

Concerning hybrid optoelectronic devices, the incorporation of functional end groups facilitating an effective interaction of the conjugated polymer with inorganic nanoparticles (so-called anchor groups) is very desirable. The beneficial effect of anchor groups due to a closer contact between donor (polymer) and acceptor material (inorganic nanoparticles) on the performance of hybrid solar cells was first demonstrated by Liu *et al*.[6] They studied hybrid solar cells composed of poly(3-hexylthiophene) (P3HT)/CdSe QDs and achieved an improved device performance upon the incorporation of an amino anchor group at the P3HT chain end.[6] Moreover, recent advances in the field of hybrid solar cells emphasize the importance of ligand exchange steps to substitute the initial, insulating surfactants on the QD surface. The application of appropriate ligand exchange procedures, generally, leads to improved efficiencies and, thus, enables the fabrication of hybrid solar cells exhibiting efficiencies of 4.5 to 5.5 %.[7] Furthermore, several studies have been carried out with the aim to investigate the influence of various ligands on different aspects such as the film morphology and the charge separation at the organic/inorganic interface.[8] As the incorporation of different and multidentate anchoring end groups is difficult in the case of conjugated polymers, most studies, so far, focused on ligand exchange using small molecules such as pyridine or 1,2-ethanedithiol.[9] Literature demonstrates, however, that the incorporation of anchor groups at the polymer chain end can lead to enhanced efficiencies.[6,10] Moreover, the influence of anchor groups at the polymer chain end might differ from the effects of small molecules exhibiting the same functional groups. Therefore, techniques which facilitate the incorporation of various anchor groups at the chain end of conjugated polymers such as P3HT are required.

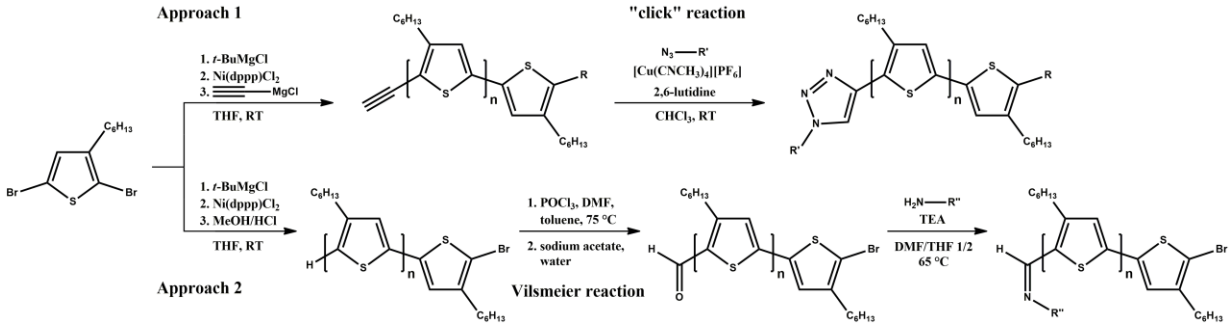

Figure 87. General reaction scheme illustrating the two approaches exploited in the present study.

In the study at hand we describe the exploitation of two approaches which enable the incorporation of various mono- and multidentate anchor groups at the polymer chain end of P3HT (see **Figure 87**). Furthermore, approach 1 in **Figure 87** leads not solely to monofunctional polymer chains, but also, in parts, to bifunctional polymers which exhibit the functional group at both chain ends. The bifunctional polymers should, therefore, have the possibility to adsorb simultaneously to two nanoparticles. Thus, some polymer chains should act as "crosslinkers" resulting in a partially percolated morphology of polymer/nanoparticle composite films. Such a partially percolated morphology is expected to be desirable with regards to hybrid solar cells as it leads to an improved electron transport. On the contrary, following approach 2 in **Figure 87** solely monofunctional polymer chains are obtained. The monofunctional polymers result in a film morphology exhibiting individually distributed nanoparticles which enabled the investigation of the optoelectronic properties of a single nanoparticle.

In addition, the morphology of nanocomposite films depends on the stability of the polymer coating at the nanoparticle surface. The stability of the coating can be influenced by the number of binding sites and the affinity of the functional group toward the respective inorganic compound.[11] Therefore, we incorporated both, mono- as well as multidentate anchor groups and, furthermore, various functional groups (i.e., catechol, lipoic acid, amine and trithiocarbonate). As the device performance strongly depends on the functional group interacting with the inorganic nanoparticles, the possibility to incorporate different functional groups following the same approach is of special interest regarding studies with the aim to investigate the influence of various functional groups on the device performance.

Consequently, inorganic TiO_2 nanoparticles were functionalized with P3HT carrying catechol anchor groups obtained following the two approaches 1 and 2. The film morphology observed using transmission electron microscopy (TEM) varied depending on the presence or absence

of bifunctional polymer “crosslinkers”. Moreover, the intimate contact of the polymer coating with the nanoparticle surface led to an electron transfer from the polymer to the inorganic nanoparticles as evidenced via Kelvin probe force microscopy (KPFM).

2. Experimental Section

Materials and Characterization. All commercially available chemicals were purchased from Alfa Aesar, Acros Organics, Fluka, Sigma-Aldrich, or Tokyo Chemical Industry and used without further purification unless otherwise noted. Anhydrous THF was freshly distilled from sodium under a dry argon atmosphere. All reactions were carried out under dry nitrogen or argon atmospheres using standard Schlenkline techniques. Molecular weights of all synthesized polymers were determined by gel permeation chromatography (GPC) with a concentration of approximately 1.2 mg/mL in THF with polystyrene as external and toluene as internal standard. Azides **1-5** – an illustration of compounds **1-5** can be found in the Supporting Information (**Figure S1**) – and pentafluorophenyl 4-vinylbenzoate (PFP4VB) (**6**) were synthesized according to literature procedures.[12,13] Syntheses of ethynyl-terminated and aldehyde-terminated P3HT were conducted following modifications of established literature procedures.[14,15] ^{1}H-NMR, ^{19}F-NMR and ^{13}C-NMR spectra were acquired on a Bruker ARX 400 spectrometer at a Lamor frequency of 400 MHz, 400 MHz and 101 MHz, respectively. FTIR spectra were performed on a Vector 22 ATR-FTIR-spectrometer made by Bruker. UV/Vis spectra were obtained by Jasco Inc. UV/vis-Spectrometer V-630. Transmission electron microscopy (TEM) images of P3HT coated CdSe@ZnS QDs were recorded with JEOL ARM 200 F operating at 20 kV or. P3HT coated TiO_2 particles were characterized by TEM using a Philips EM 420. TEM samples were prepared by drop casting a dispersion of the QDs in chloroform on a standard carbon-coated copper grid. Kelvin probe force microscopy measurements were performed using an Asylum Research MFP3D setup in a glovebox under nitrogen atmosphere with low humidity (<0.1%) and low oxygen (<0,01%) conditions. For single pass double sideband frequency modulation KPFM we used an external Zurich Instruments HF2LI-MOD lock-In amplifier to control the cantilever excitation and the potential feedback.[16] We used PPP-EFM cantilevers with a nominal resonance frequency of ~70 kHz. For sample illumination a diode laser (Point Source) with a wavelength of 488 nm, power of 13.3 mW, and intensity on the sample of ~10 W/cm² was directed on the sample

from underneath. KPFM samples were prepared by spin-coating a dispersion of the nanocomposite in chloroform (c ≈ 0.01 mg/mL) – ITO substrate PGO, CEC020S. (MALDI-TOF MS) were recorded using a Bruker-reflex-TOF (FM-0405) and a nitrogen laser (Laser Science, Inc., VSL-337ND-S, wavelength = 337 nm). The spectra were collected in reflector mode, calibration was done against C60/C70 and 2,2':5,2''-terthiophene was used as matrix for all samples.

General Procedure for End Group Modifications via 1,3-Dipolar Cycloaddition. Azides were installed as polymer end groups according to a modified literature procedure.[17] Under a dry nitrogen atmosphere ethynyl-terminated P3HT (150 mg, 0.029 mmol, M_n(GPC) ≈ 5200 g/mol, 1 eq.) was dissolved in 20 mL of dry chloroform. Subsequently, the respective azide (0.288 mmol, 10 eq.), 2,6-lutidine (309 mg, 0.34 mL, 2.88 mmol, 100 eq.) and $[Cu(NCCH_3)_4][PF_6]$ (54 mg, 0.144 mmol, 5 eq.) were added. The reaction mixture was stirred at room temperature for 64 h. The reaction mixture was concentrated under reduced pressure and P3HT was precipitated in methanol. After redissolving the P3HT in DCM and precipitation in methanol three times, the product was collected as a violet solid.

P2a: ^{1}H-NMR (400 MHz, $CDCl_3$, δ/ppm): 7.73 (s, 1H, triazole), 6.81 – 7.03 (m, 20H, Ar), 5.77 (t, J = 6.2 Hz, 1H, NH), 4.49 (t, J = 6.5 Hz, 2H, triazole-CH_2), 3.52 – 3.59 (m, 1H, S-CH), 3.33 (q, J = 6.2 Hz, 2H, NH-CH_2), 3.07 – 3.19 (m, 2H, S-CHH), 2.53 – 2.82 (m, 40H, Ar-CH_2), 2.40 – 2.48 (m, 1H, S-CH_2-CHH), 2.14 – 2.21 (m, 4H, CH_2), 1.85 – 1.93 (m, 1H, S-CH_2-CHH), 1.26 – 1.74 (m, 166H, CH_2), 0.87 – 0.94 (m, 60H, CH_3).

P2b: ^{1}H-NMR (400 MHz, $CDCl_3$, δ/ppm): 7.64 (s, 1H, triazole), 6.81 – 7.02 (m, 20H, Ar), 6.52 (t, J = 6.3 Hz, 2H, NH), 4.80 – 4.85 (m, 1H, O-CH), 4.44 (t, J = 6.8 Hz, 2H, triazole-CH_2), 3.51 – 3.58 (m, 2H, S-CH), 3.28 – 3.34 (m, 4H, NH-CH_2), 3.06 – 3.19 (m, 4H, S-CHH), 2.52 – 2.82 (m, 40H, Ar-CH_2), 2.40 – 2.48 (m, 2H, S-CH_2-CHH), 2.33 (t, J = 7.2 Hz, 2H, O=C-CH_2), 2.26 (t, J = 7.5 Hz, 4H, O=C-CH_2), 2.00 (p, J = 7.2 Hz, 2H, triazole-CH_2-CH_2), 1.85 – 1.93 (m, 2H, S-CH_2-CHH), 1.22 – 1.74 (m, 176H, CH_2), 0.84 – 0.95 (m, 60H, CH_3).

P2c: ^{1}H-NMR (400 MHz, $CDCl_3$, δ/ppm): 7.64 (s, 1H, triazole), 6.81 – 7.01 (m, 20H, Ar), 6.49 (br, 1H, NH), 4.38 – 4.47 (m, 8H, O-CH_2 + triazole-CH_2), 3.52 – 3.57 (m, 3H, S-CH), 3.06 – 3.21 (m, 6H, S-CHH), 2.54 – 2.82 (m, 40H, Ar-CH_2), 2.42 – 2.50 (m, 3H, S-CH_2-CHH), 2.36 (t, J = 7.3 Hz, 6H, O=C-CH_2), 2.16 – 2.28 (m, 4H, O=C-CH_2 + CH_2), 1.98 – 2.03 (m, 2H, triazole-CH_2-CH_2), 1.87 – 1.95 (m, 3H, S-CH_2-CHH), 1.22 – 1.74 (m, 180H, CH_2), 0.85 – 0.95 (m, 60H, CH_3).

P2d: ^{1}H-NMR (400 MHz, $CDCl_3$, δ/ppm): 7.77 (s, 1H, triazole), 6.81 – 7.01 (m, 17H, Ar), 4.76 (br, 1H, NH), 4.49 (t, J = 6.7 Hz, 2H, triazole-CH_2), 3.20 (q, J = 6.4 Hz, 2H, NH-CH_2), 2.51 – 2.83 (m, 34H, Ar-CH_2), 2.14 (p, J = 6.4 Hz, 2H, CH_2), 1.25 – 1.74 + 1.45 (m + s, 145H, CH_2 + *t*-Bu), 0.83 – 0.93 (m, 51H, CH_3). Note: Polymer **P2d** was synthesized from ethynyl-terminated P3HT with DP ≈ 17 (**P1b**).
P2e: ^{1}H-NMR (400 MHz, $CDCl_3$, δ/ppm): 7.67 (s, 1H, triazole), 6.80-7.03 (m, 21H, Ar), 4.46 (t, 2H, triazole-CH_2), 4.19 (t, 2H, COO-CH_2), 3.28 (m, 2H, CTA-CH_2), 2.50-2.85 (m, 42H, Ar-CH_2), 2.32 (t, 2H, CH_2), 1.05-1.75 (m, 168, CH_2), 0.88-0.93 (m, 63H, CH_3).

Deprotection of Polymer P2d (Synthesis of Polymer P3). Polymer **P2d** (250 mg, 0.063 mmol, M_n(GPC) ≈ 4000 g/mol, 1 eq.) was dissolved in 6.5 mL of DCM. Trifluoroacetic acid (1.6 mL) was added and the reaction mixture was stirred at room temperature for one hour. Then, the pH was adjusted to a value of 12 using 10% aqueous sodium carbonate solution and the reaction mixture was extracted three times with chloroform. The combined organic extracts were dried over MgSO4, filtered and the solvent was removed under reduced pressure. The residue was purified by redissolving in a small amount of chloroform and precipitation in methanol for three times. Further purification was achieved via column chromatography using an 8/1 eluent system of chloroform/*n*-hexane. The product was afforded as a violet solid in 40% yield.
^{1}H-NMR (400 MHz, $CDCl_3$, δ): 7.70 (s, 1H, triazole), 6.82 – 7.03 (m, 17H, Ar), 5.35 (br, 2H, NH_2), 4.52 (t, J = 6.4 Hz, 2H, triazole-CH_2), 3.45 (q, J = 6.4 Hz, 2H, NH-CH_2), 2.53 – 2.84 (m, 34H, Ar-CH_2), 2.32 – 2.39 (m, 2H, CH_2), 1.23 – 1.74 (m, 136H, CH_2), 0.83 – 0.93 (m, 51H, CH_3). Note: Polymer **P3** was synthesized from ethynyl-terminated P3HT with DP ≈ 17 (**P2d**).

Synthesis of P4b. PFP4VB (231,4 mg, 0.42 mmol, 25 eq.), the macro-CTA (**P2e**) (75.0 mg, 0.017 mmol, M_n(NMR) ≈ 4400 g/mol 1eq.), and AIBN (0.28 mg, 0.0017 mmol, 0.2 eq.) were dissolved in 2 ml o-dichlorobenzene followed by three freeze-pump-thaw cycles. The reaction mixture was stirred for 48 hours at 70 °C. The reaction was stopped by quenching in methanol and the product **P4a** was further purified by solving and precipitating two more times. The yield was about 85%.
^{1}H-NMR (400 MHz, $CDCl_3$, δ/ppm): 7.70-8.25 (m, 10H, Ar of PFP4VB,); 7.60 (s, 1H, triazole), 6.60-7.20 (m, 30H, Ar of P3HT and PFP4VP); 4.39 (m, 2H, triazole-CH_2); 3.77 (m, 2H, COO-CH_2), 3.27 (m, 2H, CTA-CH_2), 2.50-2.85 (m, 40H, Ar-CH_2), 2.13 (m, 2H, CH_2),

1.05-1.5 (m, 160, CH_2), 0.88-0.93 (m, 60H, CH_3); ^{19}F-NMR (400 MHz, $CDCl_3$, δ/ppm): -154.3 (m, 2F, ortho-F); -157.9 (m, 1F, para-F); -163.3 (m, 2F, meta-F); IR (FTIR): ν = 2925 (CH), 1760 (C=O), 1519 (Ar-F), 1240, 1044 (aromatic band), 1013, 819 cm^{-1}.

P(3HT-b-PFP4VB) (27 mg, 0.0034 mmol, 1 eq.) was dissolved in 1.4 ml THF and a solution of dopamine hydrochloride (12.7 mg, 0.068 mmol, 20 eq.) in 0.6 ml DMF was added. Triethylamine (2.4 ml, 0.068 mmol, 20 eq.) was added as well. The reaction mixture was stirred at room temperature overnight.
^{1}H-NMR (400 MHz, $CDCl_3$, δ/ppm): 7.67 (s, triazole); 6.68-7.28 (m, Ar of P3HT, PFP4VB and dopamine); 4.32 (m, triazole-CH_2); 4.19 (m, COO-CH_2); 3.72(m, CTA-CH_2); 2.80 (m, Ar-CH_2); 1.5-1.0 (m, CH_2); 0.92-0.88 (b, CH_3). Note: Integration is due to the overlap of several aromatic hydrogens not reasonable. IR (FTIR): ν = 3248 (O-H), 1734 (C=O) cm^{-1}.

Synthesis of dopamine-P3HT (P5c). The formylation of hydrogen terminated P3HT (**P5a**) (120 mg, 0.022 mmol, M_n(GPC) ≈ 5400 g/mol, 1eq.) was conducted following a reported method by a Vilsmeier reaction.[15] Briefly, P3HT was dissolved in toluene (30 ml) under an argon atmosphere. DMF (0.36 ml, 4.66 mmol, 212 eq.) and $POCl_3$ (0.25 ml, 2.7 mmol, 122 eq.,) were added. The reaction mixture was stirred for 50 h at 75 °C. After the completion of the reaction saturated aqueous sodium acetate solution was added and stirred for further 30 min. Thereafter, the reaction mixture was precipitated in methanol and dried under reduced pressure. The product (**P5b)** was dissolved in chloroform and precipitated two more times in methanol. The yield was about 87%.
^{1}H-NMR (400 MHz, $CDCl_3$, δ/ppm): 10.02 (s, 1H, aldehyde-H), 6.91-7.09 (m, 26H, Ar), 2.95 (t, 2H, Ar-CH_2 in *ortho*-position to aldehyde group) 2.60-3.05 (m, 52H, Ar-CH_2), 1.15-1.80 (m, 208H, CH_2), 0.84-0.96 (m, 78H, CH_3); IR (FTIR): ν = 2924 (w, CH), 1649 (s, C=O), 1443 (w, aromatic ring), 820 (w) cm^{-1}.

Dopamine was introduced via aminolysis of the carbonyl group. Therefore, **P5b** (38 mg, 9 mmol, M_n(NMR) ≈ 4200 g/mol, 1 eq.) was dissolved in dried THF (1 ml) and a solution of dopamine hydrochloride (25.7 mg, 135 mmol, 15 eq.), triethylamine (17 µl, 135 mmol, 15 eq.) in DMF (1 ml) was added. The reaction mixture was stirred at 65 °C overnight. The final product, polymer **P5c**, was purified by precipitation in methanol. The yield was 76 %.
^{1}H-NMR (400 MHz, $CDCl_3$, δ/ppm): 8.22 (s, 1H, imine H), 6.91-7.09 (m, 31H, Ar), 6.50-6.85 (m, 3H, Ar of dopamine), 2.90-2,70 (m, 62H, Ar-CH_2), 1.15-1.80 (m, 248H, CH_2), 0.84-0.96 (m, 93H, CH_3); IR (FTIR): ν = 2924 (CH), 1654 (C=C), 1617 (C=N), 1453 (aromatic ring), 820 cm^{-1}.

Functionalization of inorganic particles.

10 mg of CdSe@Zns nanoparticles were dispersed in 1 mL of chloroform and an argon atmosphere was applied. While the dispersion was ultrasonicated 10 mg of the respective polymer dissolved in 1 mL of chloroform were added. The mixture was then stirred at 40 °C overnight. Unfunctionalized QDs were removed via precipitation in *n*-hexane and redispersion in chloroform (two times).

TiO_2 particles were synthesized following a previous method.[18] TiO_2 particles were dispersed in chloroform with a concentration of 10 mg/mL. Polymer **P4b** or **P5c** respectively were dissolved in chloroform with a final polymer concentration of 5 mg/mL. The polymer solution was added to the particle dispersion and ultrasonicated under argon for 30 min. Afterwards the mixture was stirred at 40 °C overnight. Unbound polymer was removed by three centrifugation and redispersion steps.

3. Results and Discussion

In the first approach, ethynyl-terminated P3HT was synthesized via GRIM polymerization and quenching with ethynylmagnesium bromide which led to 85 % mono- and 15% bifunctional P3HT according to the literature.[14] The synthesis of partially bifunctional polymer chains was desired to enable an interaction of some polymers (after incorporation of anchor groups) with two inorganic nanoparticles. Consequently, polymers interacting with two nanoparticles should act as crosslinkers and facilitate the formation of a partially percolated morphology in the film state. The coexistence of mono- and bifunctional ethynyl-terminated P3HT was verified using matrix-assisted laser desorption ionization time-of-flight mass spectrometry (MALDI-TOF MS, see **Figure S2**). The ethynyl end group was exploited for the incorporation of various azides via copper catalyzed azide-alkyne Huisgen cycloaddition (“click” reaction) as illustrated in **Figure 88**.

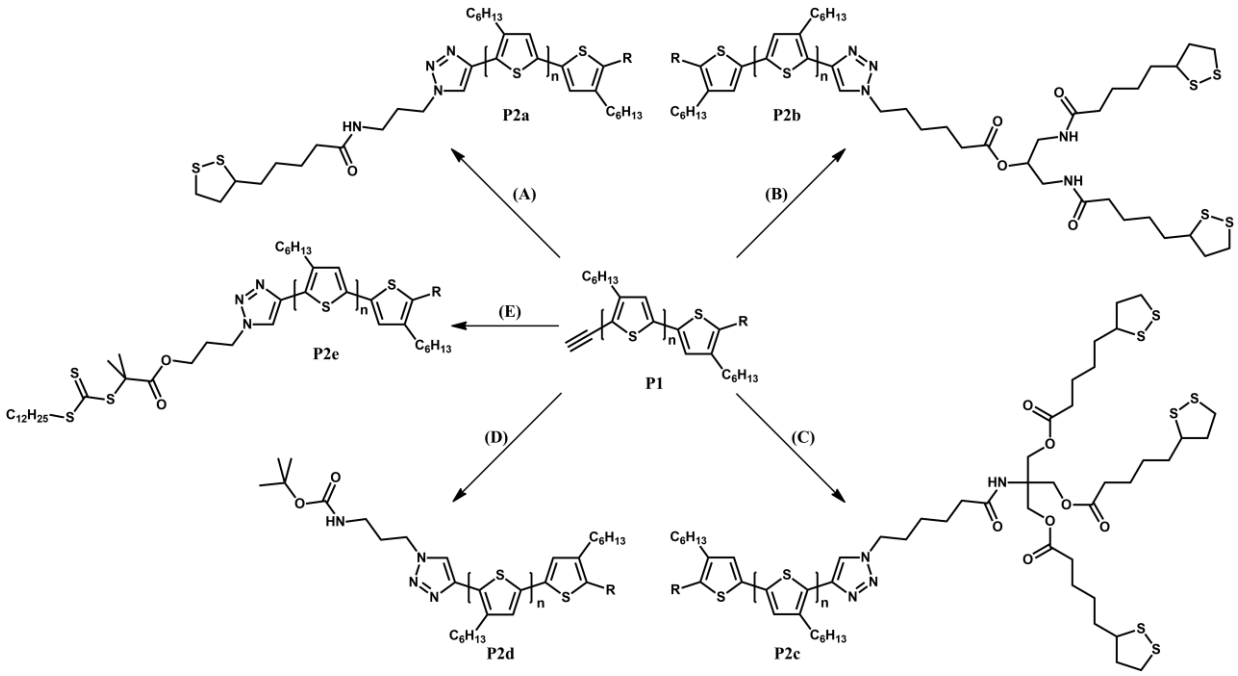

Figure 88. Incorporation of functional end groups via copper catalyzed azide-alkyne Huisgen cycloaddition with $[Cu(NCCH_3)_4][PF_6]$, 2,6-lutidine and azides carrying (A) monolipoic acid (**1**), (B) dilipoic acid (**2**), (C) trilipoic acid (**3**), (D) Boc-protected amine (**4**) and (E) trithiocarbonate (**5**). The structures of azides **1-5** are illustrated in **Figure S1**.

To demonstrate the versatility of the approaches presented in the study at hand, the incorporation of different anchor groups was required in order to enable effective functionalization of the most applied inorganic nanoparticles (e.g. CdSe@ZnS and TiO_2). Therefore, lipoic acid which is known to facilitate ligand exchange with for example CdSe@ZnS nanoparticles was incorporated as the anchoring end group.[19] In a one-step procedure, the lipoic acid was installed via copper-catalyzed 1,3-dipolar cycloaddition of ethynyl-terminated P3HT (**P1**) and the lipoic acid carrying azide **1** (**Figure S1** illustrating the structure of all azides used in the present study can be found in the Supporting Information). The successful end group modification was verified using ^{1}H-NMR spectroscopy and MALDI-TOF MS (see **Figure 89**). During the reaction the singlet of the alkyne proton (3.53 ppm) disappeared and a singlet of the triazole ring resonated at 7.73 ppm (in $CDCl_3$). Moreover, after end group modification, characteristic signals appeared in the NMR spectrum which could be assigned to the lipoic acid carrying end group. For example, the triplet of the methylene group attached to the azide shifted from 3.37 ppm to 4.49 ppm (in $CDCl_3$) upon the formation of the triazole ring (**P2a**, see **Figure 89A**).

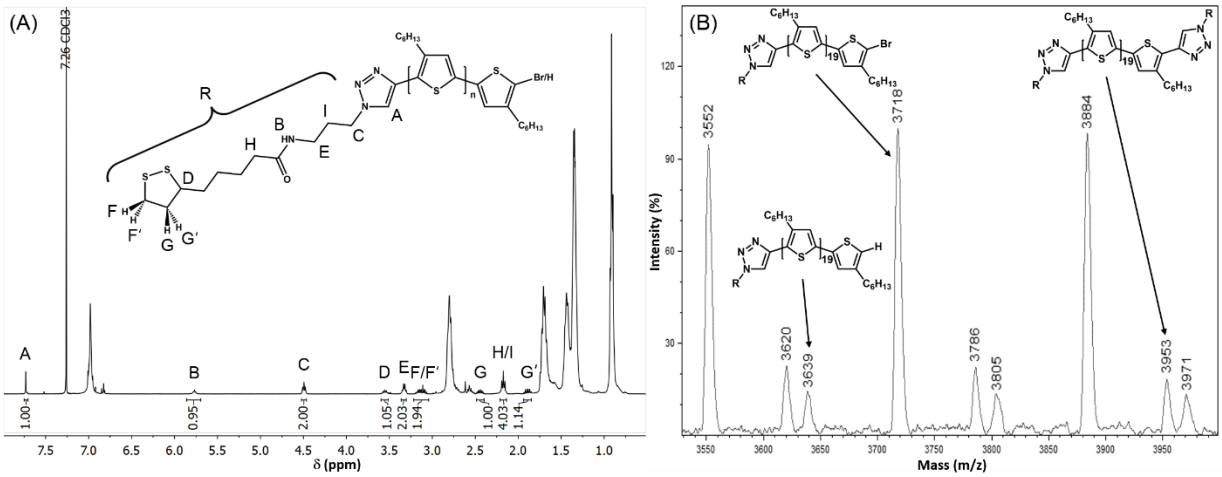

Figure 89. (A) ^{1}H-NMR spectrum of polymer **P2a** (in $CDCl_3$) proving the successful incorporation of the lipoic acid end group. (B) MALDI-TOF mass spectrum exhibiting the three possible end group combinations – H/triazole, Br/triazole and triazole/triazole. (For a magnified NMR spectrum and the complete MALDI-TOF mass spectrum see **Figures S3** and **S4**.)

In addition, three coexisting species were to be determined via MALDI-TOF MS. These three species can be assigned to the three possible end group combinations as shown in **Figure 89B**. The concomitance of monofunctional P3HT (carrying a proton or bromine at the alpha end) and bifunctional P3HT originates from the coexistence of mono- and bifunctional polymer chains in the precursor polymer **P1** (see **Figure S2**).[14]

Although lipoic acid, a bidentate ligand, has been exploited to achieve coatings of CdSe@ZnS QDs via ligand exchange, the application of multidentate anchor groups is often desirable to realize a more complete ligand exchange and facilitate stable coating. Therefore, we conducted 1,3-dipolar cycloaddition with azides **2** and **3** which carry two and three lipoic acid groups, respectively. The successful incorporation of the respective end group was verified via ^{1}H-NMR spectroscopy and MALDI-TOF MS (see **Figures S5** to **S8**). Consequently, as lipoic acid is already a bidentate ligand, the resulting polymers **P2b** and **P2c** were equipped with tetradentate and hexadentate anchor groups, respectively. The incorporation of the multidentate anchor groups should simplify ligand exchange compared to polymer **P2a**. However, stable dispersions of CdSe@ZnS QDs were achieved upon ligand exchange using either **P2a**, **P2b** or **P2c**. In addition, the characterization of the nanocomposites via TEM revealed individually dispersed QDs in all cases (see **Figure S12**). IR spectroscopy gave further evidence for the successful ligand exchange. The spectrum of the nanocomposite

displayed characteristic bands of the QDs as well as the P3HT such as the band at approximately 1545 cm^{-1} originating from the zinc sulfide shell of the QDs and the aromatic C=C band at 1653 cm^{-1} from P3HT (see **Figure S13**).

To expand the scope of incorporable anchor groups, we aimed at installing primary amines as the polymer end group. Primary amines are popular anchor groups which have been applied successfully to achieve ligand exchange in many cases and their incorporation underlines the versatility of the approach presented in the study at hand. In a first step, a Boc-protected amine carrying azide (**4**) was installed at the polymer chain end (**P2d**). In the following step, the desired primary amine was obtained via deprotection with trifluoroacetic acid (**P3**). The polymer end group reactions were monitored using ^{1}H-NMR spectroscopy and the successful incorporation of the primary amine as the polymer end group was evidenced via MALDI-TOF MS (see **Figure 90**). Upon the incorporation of compound **4** via 1,3-dipolar cycloaddition, the singlet of the alkyne proton (3.53 ppm) disappeared and a new singlet resonated at 7.77 ppm (in $CDCl_3$) which can be assigned to the proton located at the triazole ring. Deprotection of the amine in the following step was evidenced by the disappearance of the strong singlet at 1.45 ppm (in $CDCl_3$) which originates from the *tert*-butyloxycarbonate (see **Figure 90A**). Moreover, the MALDI-TOF mass spectrum exhibited three concomitant molecular weight distributions which were assigned to the three possible end group combinations as displayed in **Figure 90B**.

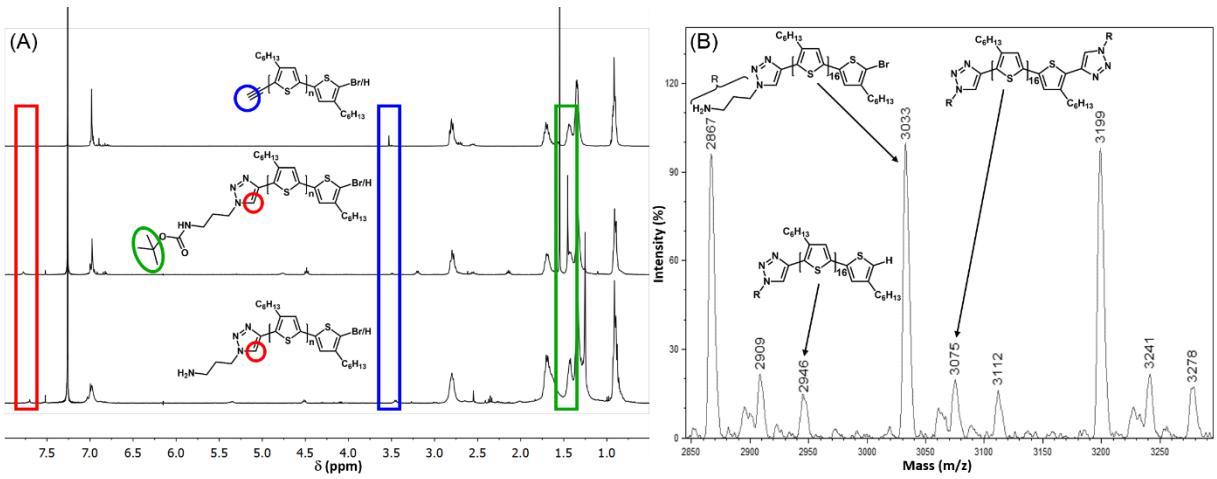

Figure 90. (A) ^{1}H-NMR spectra monitoring the incorporation of the azide via 1,3-dipolar cycloaddition (**P2d**) and synthesis of polymer **P3** via deprotection of the amine (in $CDCl_3$). (B) MALDI-TOF mass spectrum of **P3** (DP ≈ 17) with assignment of the three possible end group combinations. (For magnified NMR spectra of **P2d** and **P3** and the complete MALDI-TOF mass spectrum of **P3** see **Figures S9** to **S11**.)

To further cover the scope of commonly used nanoparticles, catechol which is a well-known anchor group for metal oxides such as TiO_2 or Fe_2O_3 should be installed as polymer end group.[20] In the case of TiO_2, for example, a single catechol unit located at the polymer chain end should be sufficient to achieve a stable coating.[21] Caused by the interaction with unsaturated metal centers at the nanoparticle surface, the catechol forms a coordination complex with a beneficial five-membered ring geometry which leads to a very stable functionalization of the TiO_2 nanoparticles.[22] Unfortunately, the incorporation of a catechol carrying azide via 1,3-dipolar cycloaddition was not successful. Therefore, azide **5** was incorporated carrying a trithiocarbonate group as shown in **Figure 91** (^{1}H-NMR see **Figure S14**). The resulting polymer **P2e** was used as macro-CTA in the RAFT polymerization of pentafluorophenyl 4-vinylbenzoate (**6**). The incorporated reactive ester block is well known to be reactive toward various aliphatic and aromatic amines. Crucial for the reaction with dopamine is, moreover, the selective reactivity of the pentafluorophenyl-based reactive ester with amine groups and its tolerance toward other functional groups such as alcohols and thiols.[13,20] The successful synthesis of block copolymer **P4a** was verified by ^{1}H- and ^{19}F-NMR spectroscopy (see **Figure S15** and **S16**), where the incorporation of the reactive ester monomer were observed via the typical broadened monomer peaks. ^{1}H-NMR spectroscopy allowed for a rough estimation of the number of repeating units of the reactive ester block, which was approximately five repeating units per polymer (see **Figure S15**). The shift in the GPC elugram (see **Figure 92A**) to lower elution volumes, i.e. higher hydrodynamic radii of the polymer, clearly demonstrates that the block copolymer **P4a** was formed. Indicated by the rather low PDI of 1.31 the controllable character of this polymerization was evidenced.

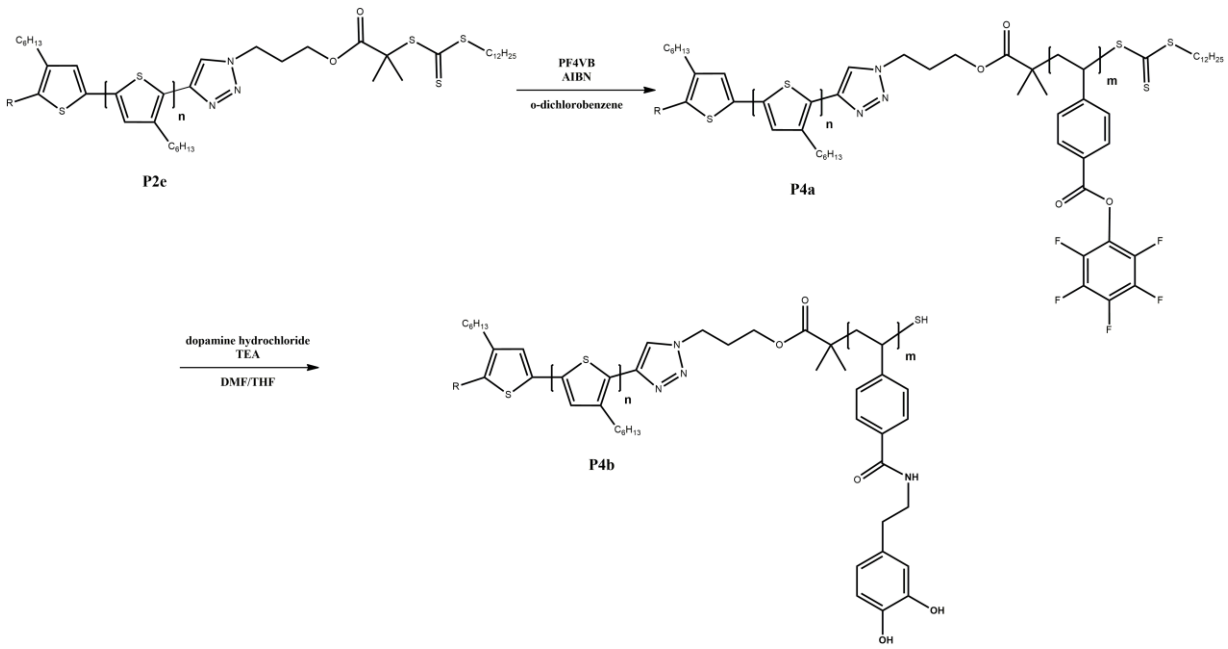

Figure 91. Synthesis scheme of P3HT containing a dopamine anchor block via a reactive ester approach.

The reaction of **P4a** with dopamine in the presence of triethylamine led to the formation of the block copolymer **P4b**. In the present study, dopamine was chosen as the amine component for post-polymerization modification. Reason for this was the aim to coordinate the polymer onto TiO_2 nanoparticles. However, the reactive ester approach enables the incorporation of a broad variety of anchor groups bearing amine functionalities.[20]

Verifying full conversion, the peaks of the reactive ester disappeared in the ^{19}F-NMR spectrum (see **Figure S16**) upon the aminolysis. Additionally, IR spectroscopy proves the successful incorporation of dopamine as significant signals of the reactive ester (C=O and C-F band) disappeared and a C=O band appeared at a wavenumber typical for amides (see **Figure 92B**).

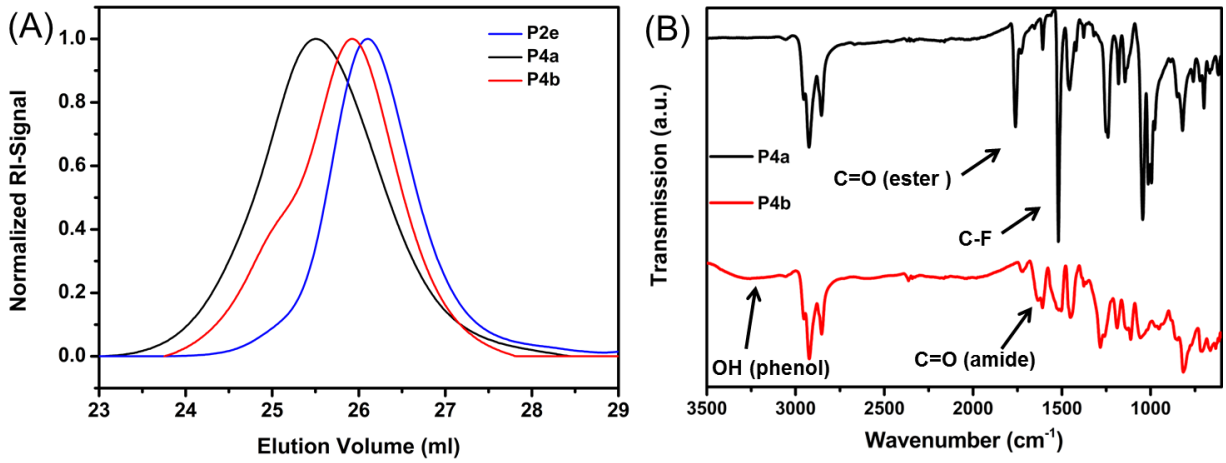

Figure 92. (A) IR spectra of **P4a** (black) and **P4b** (red) proving the successful aminolysis with dopamine. (B) GPC data of **P2e** (blue), **P4a** (black) and **P4b** (red).

Again a shift in the GPC is observable as displayed in **Figure 92A**, whereby the curve shifts to higher elution volumes, which might be explained by the lower solubility of the incorporated dopamine moiety in THF.

The introduction of dopamine allows the polymer to coordinate onto inorganic metal oxide nanoparticles, as demonstrated herein for TiO_2 nanoparticles. The functionalization of the particles resulted in dispersions which are stable for weeks. However, partial aggregation was observed as shown the TEM image in **Figure S17A**, which can most probably be attributed to the bifunctional polymer chains bearing anchoring units on both ends. The bifunctional polymers result from the P3HT precursor which is partially functionalized with two alkyne groups, both being reactive toward the CTA-azide.

Consequently, an alternative approach for the incorporation of dopamine in P3HT was developed. This approach (Approach 2 in **Figure 87**) permits selective incorporation of dopamine as the ω end group as shown in **Figure 93A**.

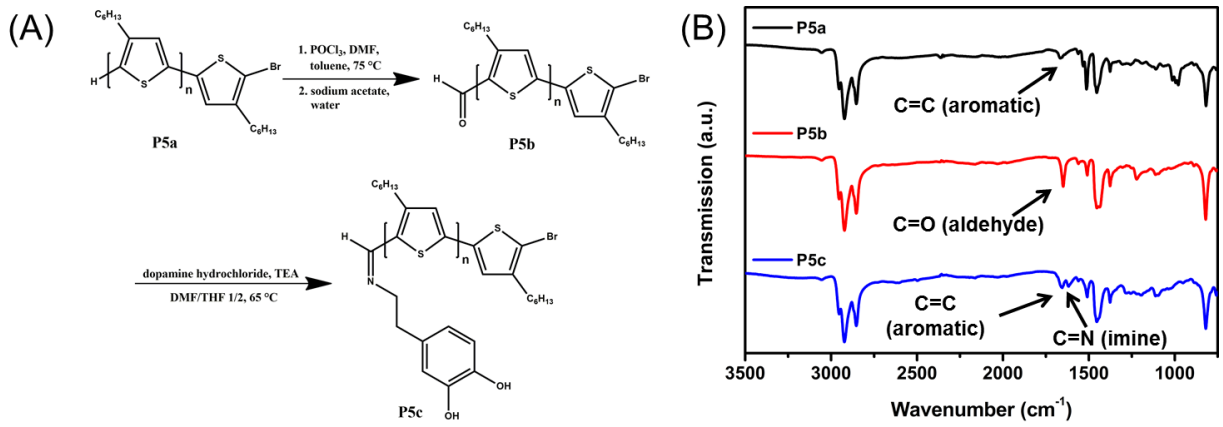

Figure 93. (A) Synthesis route for dopamine end-group functionalized P3HT and (B) IR spectra of **P5a** (black), **P5b** (red) and **P5c** (blue).

Therefore, α-Br-ω-H-P3HT (**P5a**) was synthesized via GRIM polymerization quenched with hydrochloric acid in methanol. The resulting polymer is known to have a high end group fidelity with H/Br terminated polymers.[5]

The ω end group was, subsequently, transformed into an aldehyde applying Vilsmeier reaction (see **Figure 93A**) resulting in polymer **P5b**. The success of the end group modification was verified using ^{1}H-NMR and IR spectroscopy displaying the typical aldehyde peak (δ = 10.02 ppm in $CDCl_3$) and band (ν (C=O) = 1649 cm^{-1}), respectively (**Figure S18** and **Figure 93B**). In the final step, dopamine was introduced by the formation of an imine. Evidence of the successful reaction is given by IR spectroscopy as shown in **Figure 93B** (disappearance of the C=O band and appearance of C=N band at 1617 cm^{-1}) and ^{1}H-NMR spectroscopy (imine proton at 8.22 ppm in $CDCl_3$, see **Figure S19**). The dopamine end group carrying P3HT (**P5c**) was used for the functionalization of TiO_2 nanoparticles via ligand exchange. The successful ligand exchange was evidenced via IR spectroscopy. After the hybridization step typical bands of the polymer were observed in the IR spectrum of the nanocomposite such as the aromatic C=C (1654 cm^{-1}) and the aromatic ring vibration (1453 cm^{-1}) bands (see **Figure S20**). The TEM image of the respective nanocomposite, presented in **Figure S17B**, displays well dispersed particles and, in contrast to particles coated with **P4b**, no aggregates were formed. Thus, the incorporation of dopamine as single anchoring end group led to individually dispersed TiO_2 nanoparticles avoiding the formation of aggregates which was observed for particles functionalized with P3HT obtained from approach 1 (see **Figure 87**).

Figure S21 shows thermogravimetric data of both **P4b** and **P5c** functionalized TiO_2 nanoparticles. The weight loss detected for the block copolymer is higher (28 wt.%) compared to the end-group functionalized P3HT **P5c** (12.5 wt.%) indicating that the block copolymer binds more efficiently to the TiO_2 nanoparticles.

For a more detailed investigation of the internal charge separation process between the donor corona and the acceptor core, frequency modulation Kelvin probe force microscopy (KPFM) on a single nanoparticle was performed. KPFM is a surface sensitive technique which detects changes in the surface potential with a high lateral resolution (<50 nm).[23] In order to compare the surface potential response between dark and illuminated conditions, the dispersed particles were deposited on a conductive, transparent indium tin oxide (ITO) substrate (**Figure 94a**). By scanning a single particle in dark and under illumination, the difference in potential resulting from the charge separation process could be measured. **Figure 94b** shows two line profiles with (red line profile) and without (black line profile) illumination for the same scanline across one separated nanoparticle. With the light-induced charge separation without charge extraction, holes are left in the polymer corona of the nanoparticle, resulting in a positive shift of 40 mV in the KPFM measurement (yellow arrow). Thereby, the high spatial resolution of the frequency modulation KPFM technique gets more electrostatic interaction from the positive charges on the polymer corona than from the electrons in the core. With the positive shift in surface potential, when changing to illuminated conditions, the existence of a photo-potential can be confirmed. Such photo-potential confirms the charge separation process, which takes place at the internal pn-junction of the conjugated polymer corona with the TiO_2 nanoparticle core.

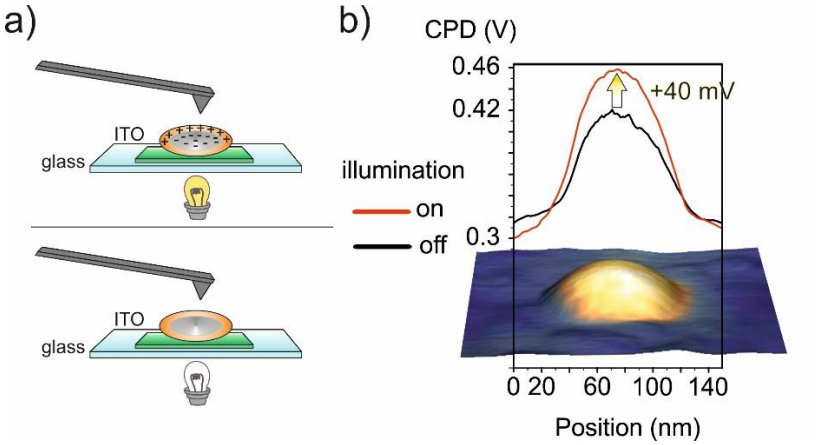

Figure 94. (a) Sketch of the experimental setup for KPFM measurements under illumination (top) and in dark (bottom). The tip detects a change in the electrostatic force because of the separation of charges from the conjugated polymer corona to the TiO_2 nanoparticle. (b) Potential line profiles for the illuminated (red) and dark (black) case with a peak potential difference of 40 mV (yellow arrow). The image underneath the profiles shows the 3D mapping of the topography with the illuminated potential as the color overlay.

4. Conclusion

In the study at hand, the synthesis of P3HT equipped with a diversity of anchor groups for the functionalization of inorganic nanoparticles has been presented. Mono- and bifunctionalized ethynyl-terminated P3HT with a narrow molecular weight distribution was synthesized via GRIM polymerization and quenching with ethynylmagnesium bromide. Consequently, quantitative copper-catalyzed 1,3-dipolar cycloaddition of the ethynyl end groups and functional azides led to the formation of P3HT equipped with amine, mono- and multidentate disulfide and catechol anchor groups. The cycloaddition approach enabled the incorporation of different anchor groups into the same batch of ethynyl-terminated P3HT leading to polymers with the same optoelectronic but different anchoring properties.

The modification of bifunctional P3HT yielded polymer chains with anchor groups on both ends. These bifunctional chains act as crosslinker ligands and connect individual nanoparticles. Thus, the attachment of multiple nanoparticles to a single polymer chain can lead to partial aggregation of nanoparticles as demonstrated in the example of TiO_2 nanoparticles. Such aggregation is attractive once the formation of organic/inorganic films with a percolated morphology is desired. Contrarily, for the case that aggregation has to be avoided, a synthetic route to achieve solely monofunctionalized aldehyde terminated P3HT

was developed. The resulting P3HT was equipped with a catechol anchor group and P3HT/TiO_2 nanocomposites were fabricated. Finally, the optoelectronic functionality of the particles was demonstrated via Kelvin probe force microscopy. Thereby, charge separation between the inorganic core and the semiconducting polymer corona on individually dispersed TiO_2 nanoparticles was observed.

Depending on the future application of nanoparticles functionalized with semiconducting polymers, different anchoring abilities of the polymer are desired. The synthetic routes presented in this study enable the versatile functionalization of P3HT and its further use in multifarious applications. Moreover, the incorporation of different anchor groups into the same electroactive backbone enables investigating the selective influence of anchor groups on the performance of hybrid optoelectronic devices.

ASSOCIATED CONTENT

Supporting Information.

NMR spectra, MALDI-TOF mass spectra, TEM images, TGA data as well as a table summarizing the Polymers used in this study. This material is available from the author.

AUTHOR INFORMATION

Corresponding Author

* E-mail: zentel@uni-mainz.de (R. Zentel)

ACKNOWLEDGMENT

The authors gratefully thank the Deutsche Forschungsgemeinschaft (DFG): International Research Training Group (IRTG) 1404 “Self-Organized Materials for Optoelectronics” for funding. A.F. and B.O. would like to thank the graduate school MAINZ and are recipients of the fellowship through the Excellence Initiative (DFG/GSC 266). Furthermore, the authors want to thank Muhammad Nawaz Tahir from Johannes Gutenberg University and group of Prof. Kookheon Char from the Seoul National University for providing the inorganic nanoparticles.

ABBREVIATIONS

Boc, *tert*-butyloxycarbonyl; CTA, chain transfer agent; DCM, dichloromethane; FTIR, Fourier transform infrared; GRIM, Grignard metathesis; MALDI-TOF MS, matrix-assisted laser desorption ionization time-of-flight mass spectrometry; M_n, number average molar mass; NMR, nuclear magnetic resonance; PDI, polydispersity index; QD, quantum dot; RAFT, reversible addition-fragmentation chain transfer; ROMP, ring-opening metathesis polymerization.

References

(1) a) Sariciftci, N. S.; Smilowitz, L.; Heeger, A. J.; Wudl, F. *Science* **1992**, *258*, 1474–1476; b) Burroughes, J. H.; Bradley, D. D. C.; Brown, A. R.; Marks, R. N.; Mackay, K.; Friend, R. H.; Burn, P. L.; Holmes, A. B. *Nature* **1990**, *347*, 539; c) Koynov, K.; Bahtiar, A.; Ahn, T.; Cordeiro, R. M.; Hörhold, H.-H.; Bubeck, C. *Macromolecules* **2006**, *39*, 8692–8698; d) Moses, D. *Appl. Phys. Lett.* **1992**, *60*, 3215.

(2) McCullough, R. D.; Lowe, R. D.; Jayaraman, M.; Anderson, D. L. *J. Org. Chem.* **1993**, *58*, 904–912.

(3) a) Yu, C.-Y.; Turner, M. L. *Angew. Chem. Int. Ed.* **2006**, *45*, 7797–7800; b) Menk, F.; Mondeshki, M.; Dudenko, D.; Shin, S.; Schollmeyer, D.; Ceyhun, O.; Choi, T.-L.; Zentel, R. *Macromolecules* **2015**, *48*, 7435–7445; c) Kang, E.-H.; Lee, I. S.; Choi, T.-L. *J. Am. Chem. Soc.* **2011**, *133*, 11904–11907.

(4) a) Jeffries-EL, M.; Sauvé, G.; McCullough, R. D. *Adv. Mater.* **2004**, *16*, 1017–1019; b) Handa, N. V.; Serrano, A. V.; Robb, M. J.; Hawker, C. J. *J. Polym. Sci. Part A: Polym. Chem.* **2015**, *53*, 831–841.

(5) Iovu, M. C.; Sheina, E. E.; Gil, R. R.; McCullough, R. D. *Macromolecules* **2005**, *38*, 8649–8656.

(6) Liu, J.; Tanaka, T.; Sivula, K.; Alivisatos, A. P.; Fréchet, J. M. J. *J. Am. Chem. Soc.* **2004**, *126*, 6550–6551.

(7) a) Zhou, R.; Stalder, R.; Xie, D.; Cao, W.; Zheng, Y.; Yang, Y.; Plaisant, M.; Holloway, P. H.; Schanze, K. S.; Reynolds, J. R.; Xue, J. *ACS nano* **2013**, *7*, 4846–4854; b) Liu, Z.; Sun, Y.; Yuan, J.; Wei, H.; Huang, X.; Han, L.; Wang, W.; Wang, H.; Ma, W. *Adv. Mater.* **2013**, *25*, 5772–5778.

(8) a) Soreni-Harari, M.; Yaacobi-Gross, N.; Steiner, D.; Aharoni, A.; Banin, U.; Millo, O.; Tessler, N. *Nano letters* **2008**, *8*, 678–684; b) Knowles, K. E.; Tice, D. B.; McArthur, E. A.; Solomon, G. C.; Weiss, E. A. *J. Am. Chem. Soc.* **2010**, *132*, 1041–1050; c) Olson, J. D.; Gray, G. P.; Carter, S. A. *Solar Energy Materials and Solar Cells* **2009**, *93*, 519–523.

(9) a) Greenham, N. C.; Peng, X.; Alivisatos, A. P. *Phys. Rev. B* **1996**, *54*, 17628–17637; b) Greaney, M. J.; Brutchey, R. L. *Materials Today* **2015**, *18*, 31–38.

(10) Chen, H.-C.; Lai, C.-W.; Wu, I.-C.; Pan, H.-R.; Chen, I.-W. P.; Peng, Y.-K.; Liu, C.-L.; Chen, C.-h.; Chou, P.-T. *Adv. Mater.* **2011**, *23*, 5451–5455.

(11) a) Ehlert, S.; Taheri, S. M.; Pirner, D.; Drechsler, M.; Schmidt, H.-W.; Förster, S. *ACS nano* **2014**, *8*, 6114–6122; b) Mathias, F.; Fokina, A.; Landfester, K.; Tremel, W.; Schmid, F.; Char, K.; Zentel, R. *Macromol. Rapid Commun.* **2015**, *36*, 959–983.

(12) a) Carboni, B.; Benalil, A.; Vaultier, M. *J. Org. Chem.* **1993**, *58*, 3736–3741; b) Xiao, S.; Fu, N.; Peckham, K.; Smith, B. D. *Organic letters* **2010**, *12*, 140–143; c) Gondi, S. R.; Vogt, A. P.; Sumerlin, B. S. *Macromolecules* **2007**, *40*, 474–481; d) Fokina, A.; Klinker, K.; Jeong, B. G.; Bae, W. K.; Barz, M.; Zentel, R. *in Preparation*.

(13) Nilles, K.; Theato, P. *European Polymer Journal* **2007**, *43*, 2901–2912.

(14) Jeffries-EL, M.; Sauvé, G.; McCullough, R. D. *Macromolecules* **2005**, *38*, 10346–10352.

(15) Surin, M.; Coulembier, O.; Tran, K.; Winter, J. de; Leclère, P.; Gerbaux, P.; Lazzaroni, R.; Dubois, P. *Organic Electronics* **2010**, *11*, 767–774.

(16) a) Zerweck, U.; Loppacher, C.; Otto, T.; Grafström, S.; Eng, L. M. *Phys. Rev. B* **2005**, *71*; b) Bergmann, V. W.; Weber, S. A. L.; Javier Ramos, F.; Nazeeruddin, M. K.; Grätzel, M.; Li, D.; Domanski, A. L.; Lieberwirth, I.; Ahmad, S.; Berger, R. *Nature communications* **2014**, *5*, 5001.

(17) Weymiens, W.; Hartl, F.; Lutz, M.; Slootweg, J. C.; Ehlers, A. W.; Mulder, J. R.; Lammertsma, K. *Eur. J. Org. Chem.* **2012**, *2012*, 6711–6721.

(18) Oschmann, B.; Bresser, D.; Tahir, M. N.; Fischer, K.; Tremel, W.; Passerini, S.; Zentel, R. *Macromol. Rapid Commun.* **2013**, *34*, 1693–1700.

(19) Mattoussi, H.; Mauro, J. M.; Goldman, E. R.; Anderson, G. P.; Sundar, V. C.; Mikulec, F. V.; Bawendi, M. G. *J. Am. Chem. Soc.* **2000**, *122*, 12142–12150.

(20) Zorn, M.; Meuer, S.; Tahir, M. N.; Khalavka, Y.; Sönnichsen, C.; Tremel, W.; Zentel, R. *J. Mater. Chem.* **2008**, *18*, 3050.

(21) Mathias, F.; Tahir, M. N.; Tremel, W.; Zentel, R. *Macromol. Chem. Phys.* **2014**, *215*, 604–613.

(22) Rajh, T.; Chen, L. X.; Lukas, K.; Liu, T.; Thurnauer, M. C.; Tiede, D. M. *J. Phys. Chem. B* **2002**, *106*, 10543–10552.

(23) Berger, R.; Domanski, A. L.; Weber, S. A. *European Polymer Journal* **2013**, *49*, 1907–1915.

Supporting Information

Functionalization of P3HT with Various Mono- and Multidentate Anchor Groups

Florian Menk‡, Ana Fokina‡, Bernd Oschmann‡, Victor W. Bergmann, Tobias A. Bauer, Yannick Nyquist, Lydia Braun, Jonathan Kiehl, Stefan A. L. Weber, Rudolf Zentel*

‡ These authors contributed equally to this work.

zentel@uni-mainz.de (R. Zentel)

Structure Illustrations

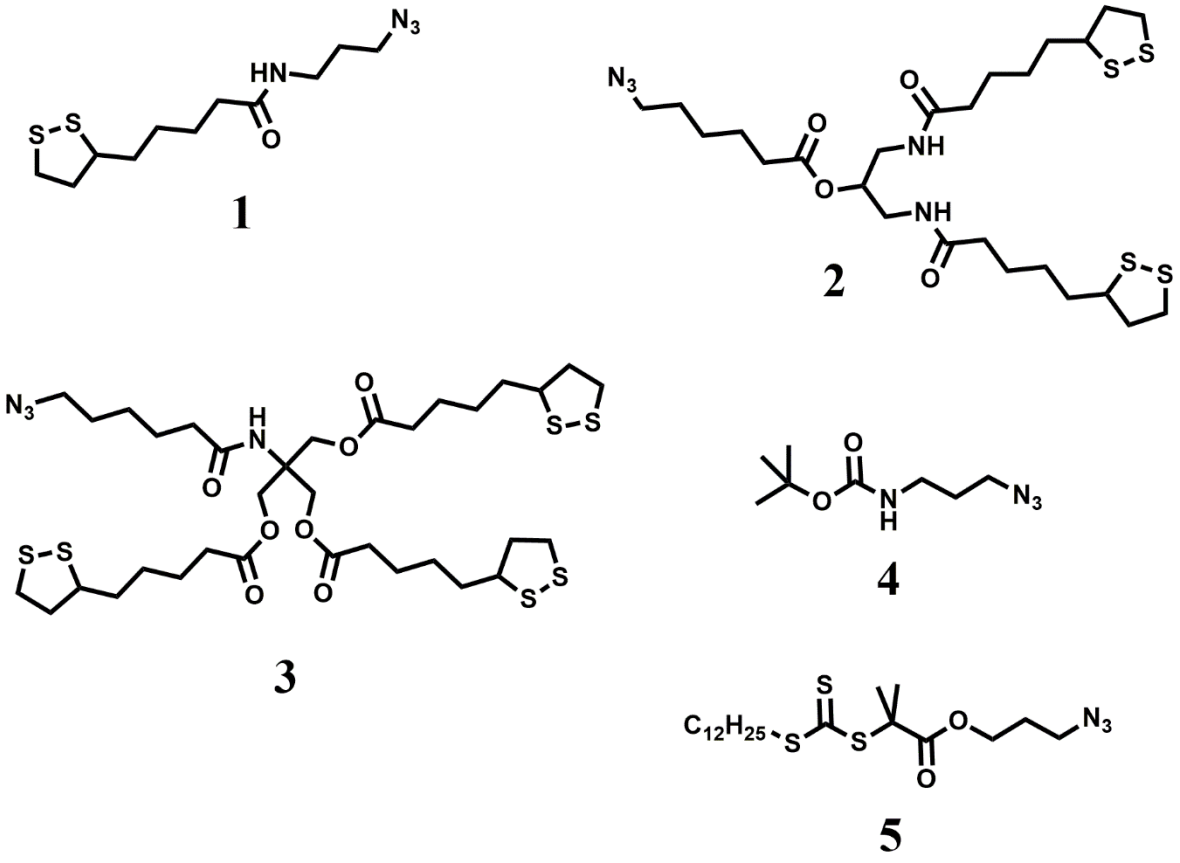

Figure S8. Illustration of all azides used in the study at hand. The azides are equipped with various functional groups – i.e., monolipoic acid (**1**), dilipoic acid (**2**), trilipoic acid (**3**), Boc-protected amine (**4**) and trithiocarbonate (**5**).

Characterization

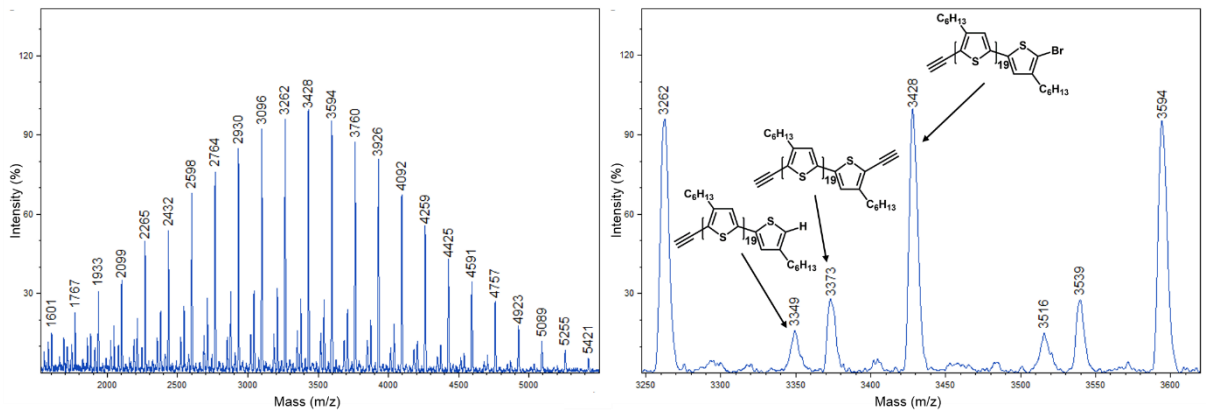

Figure S9. MALDI-TOF mass spectra of ethynyl-terminated P3HT (**P1**) with DP ≈ 20. Three different species are present over the whole molecular weight distribution (left) and can be assigned to the three possible end group combinations (right).

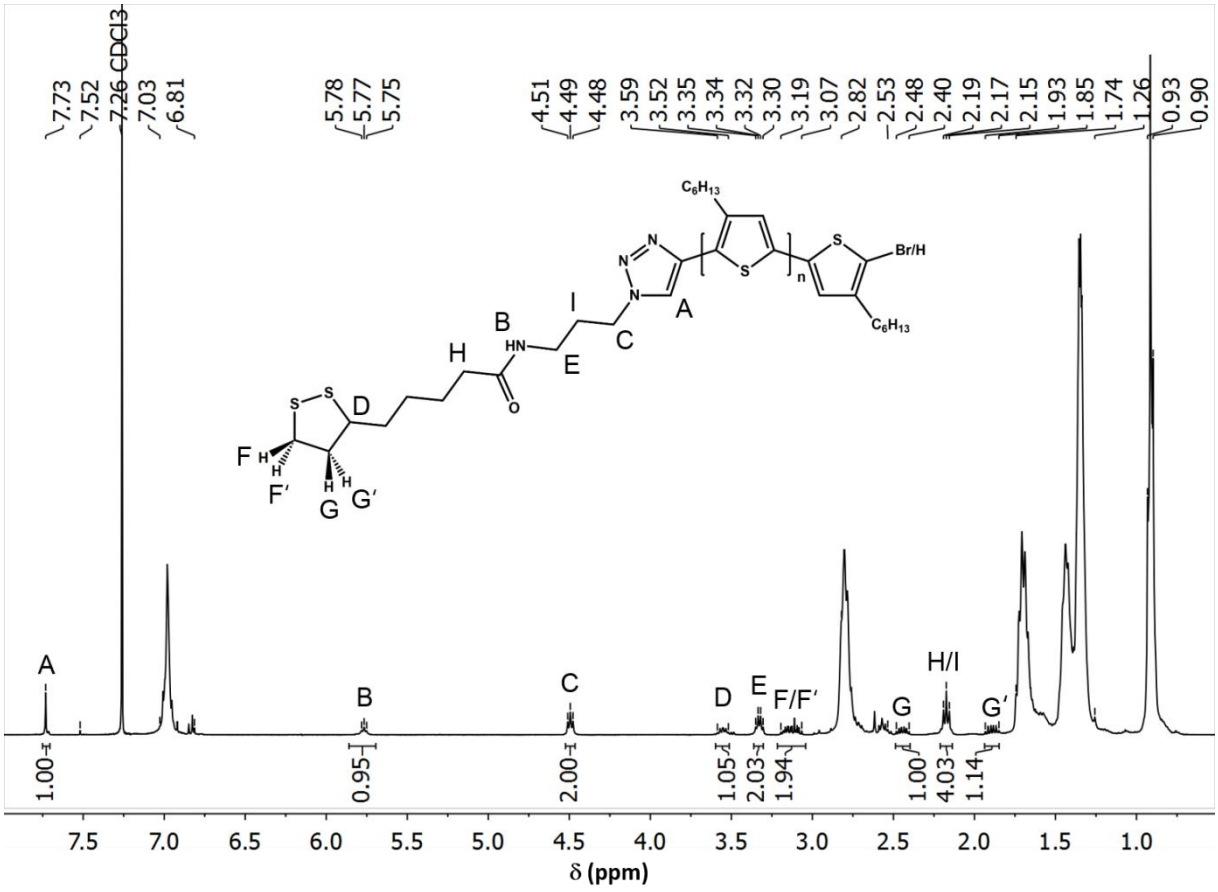

Figure S10. 400 MHz ^{1}H-NMR spectrum (in $CDCl_3$) of polymer **P2a** exhibiting the triazole proton as a singlet at 7.73 ppm and several signals of the lipoic acid carrying end group.

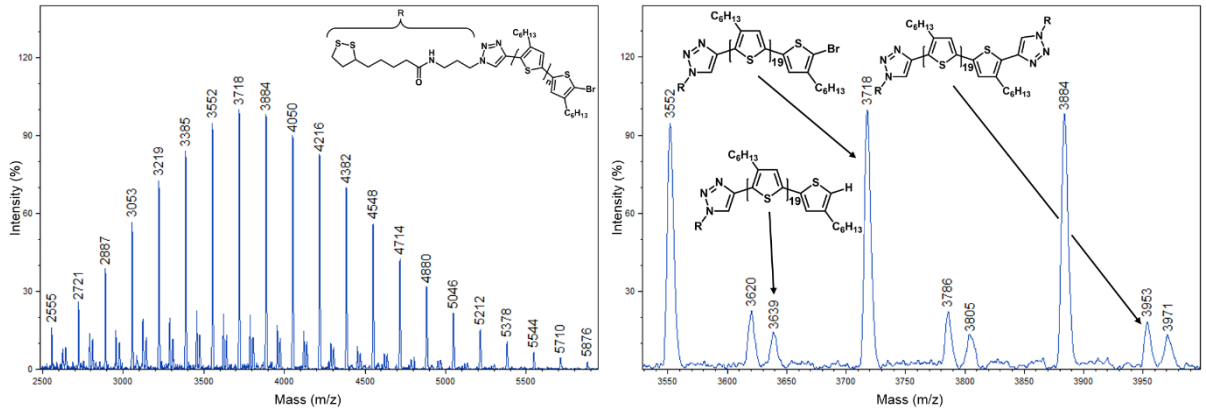

Figure S11. MALDI-TOF mass spectra of polymer **P2a** with DP ≈ 20. Three different species are present over the whole molecular weight distribution (left) and can be assigned to the three possible end group combinations (right).

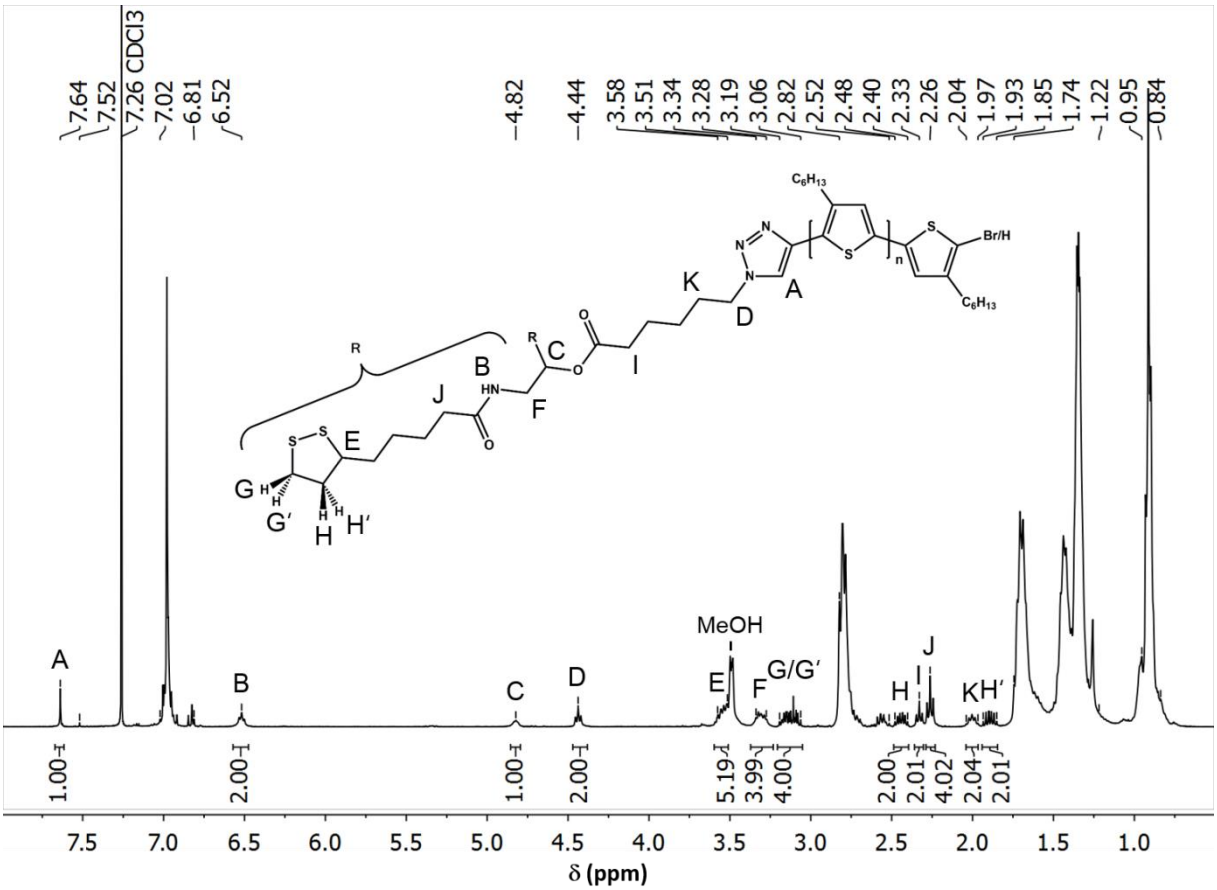

Figure S12. 400 MHz ^{1}H-NMR spectrum (in $CDCl_3$) of polymer **P2b** displaying the triazole proton as a singlet at 7.64 ppm and several signals of the lipoic acid carrying end group.

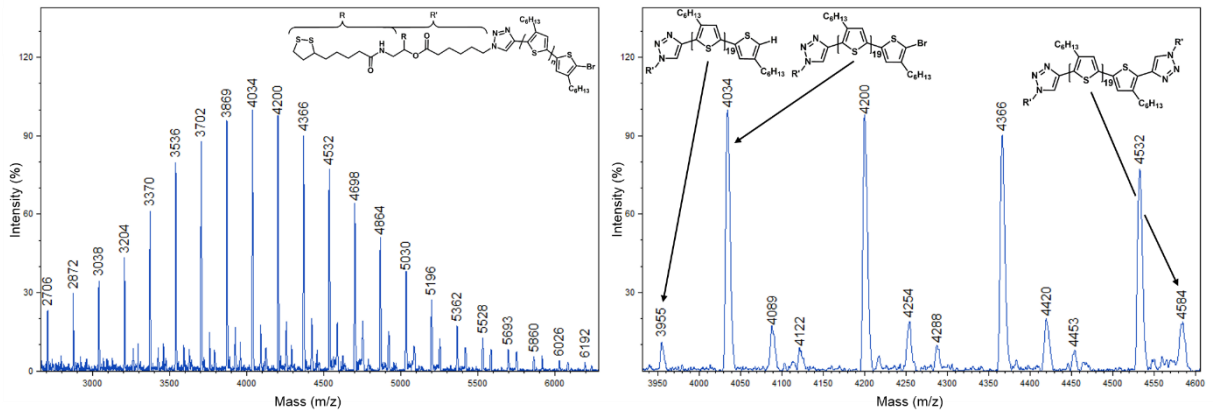

Figure S13. MALDI-TOF mass spectra of polymer **P2b** with DP ≈ 20. Three different species are present over the whole molecular weight distribution (left) and can be assigned to the three possible end group combinations (right).

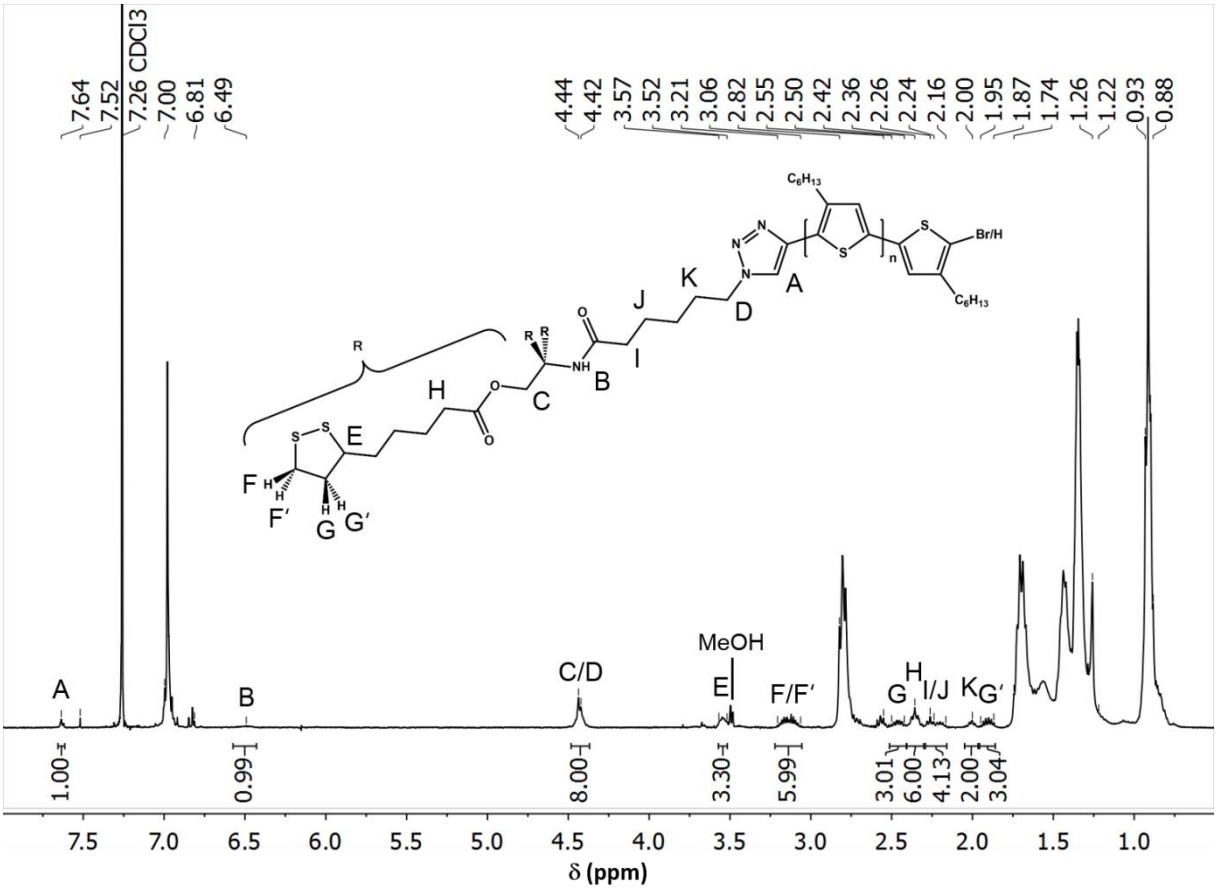

Figure S14. 400 MHz ^{1}H-NMR spectrum (in $CDCl_3$) of polymer **P2c** depicting the triazole proton at 7.64 ppm and several signals of the lipoic acid carrying end group.

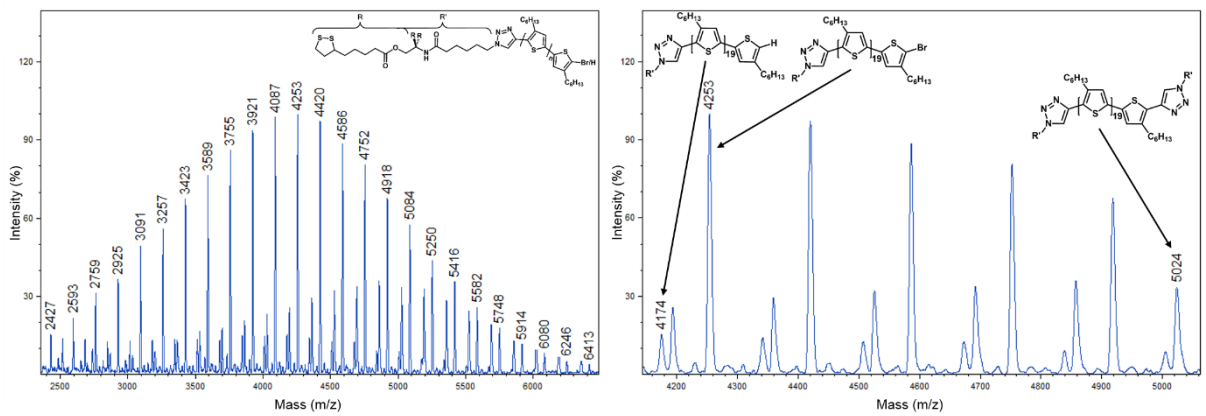

Figure S15. MALDI-TOF mass spectra of polymer **P2c** with DP ≈ 20. Three different species are present over the whole molecular weight distribution (left) and can be assigned to the three possible end group combinations (right).

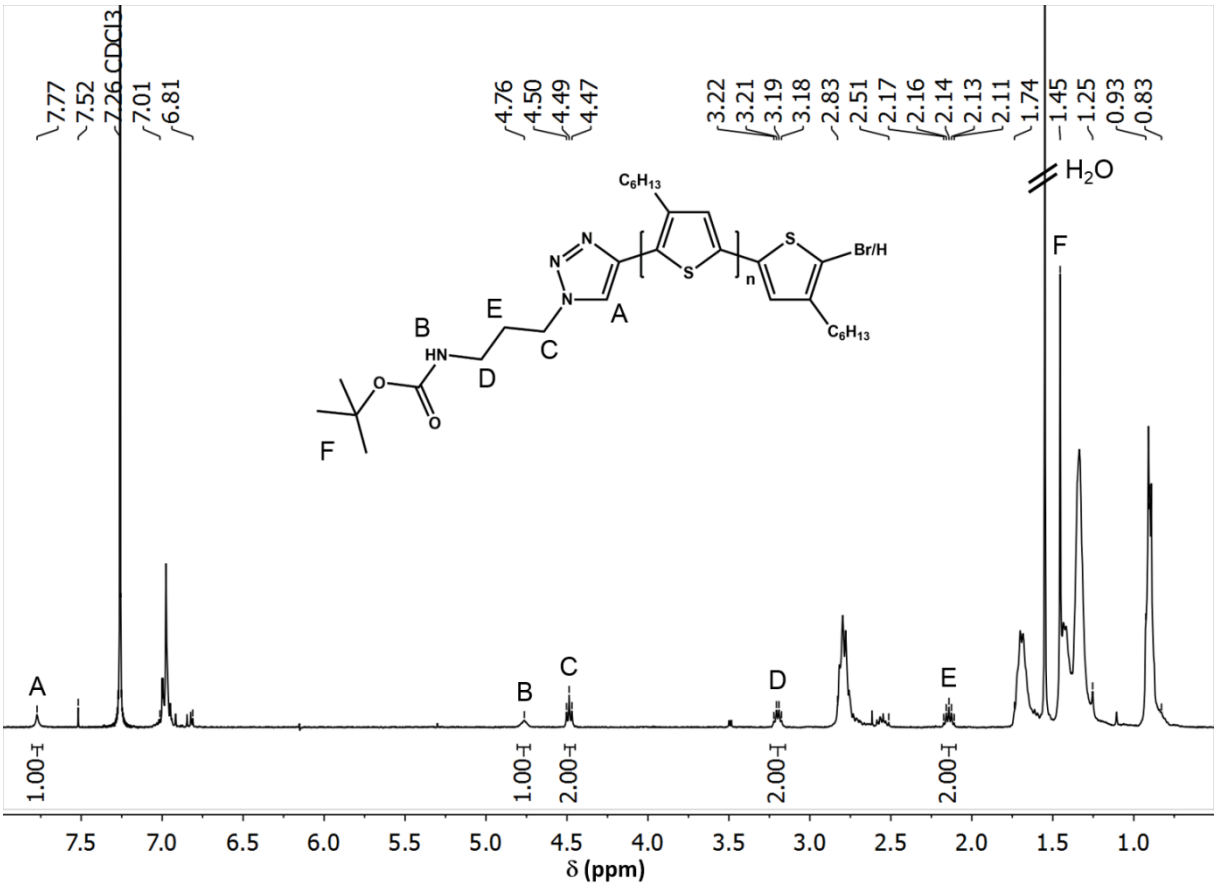

Figure S16. 400 MHz ^{1}H-NMR spectrum (in $CDCl_3$) of polymer **P2d** exhibiting the triazole proton as a singlet at 7.77 ppm and all signals of the end group.

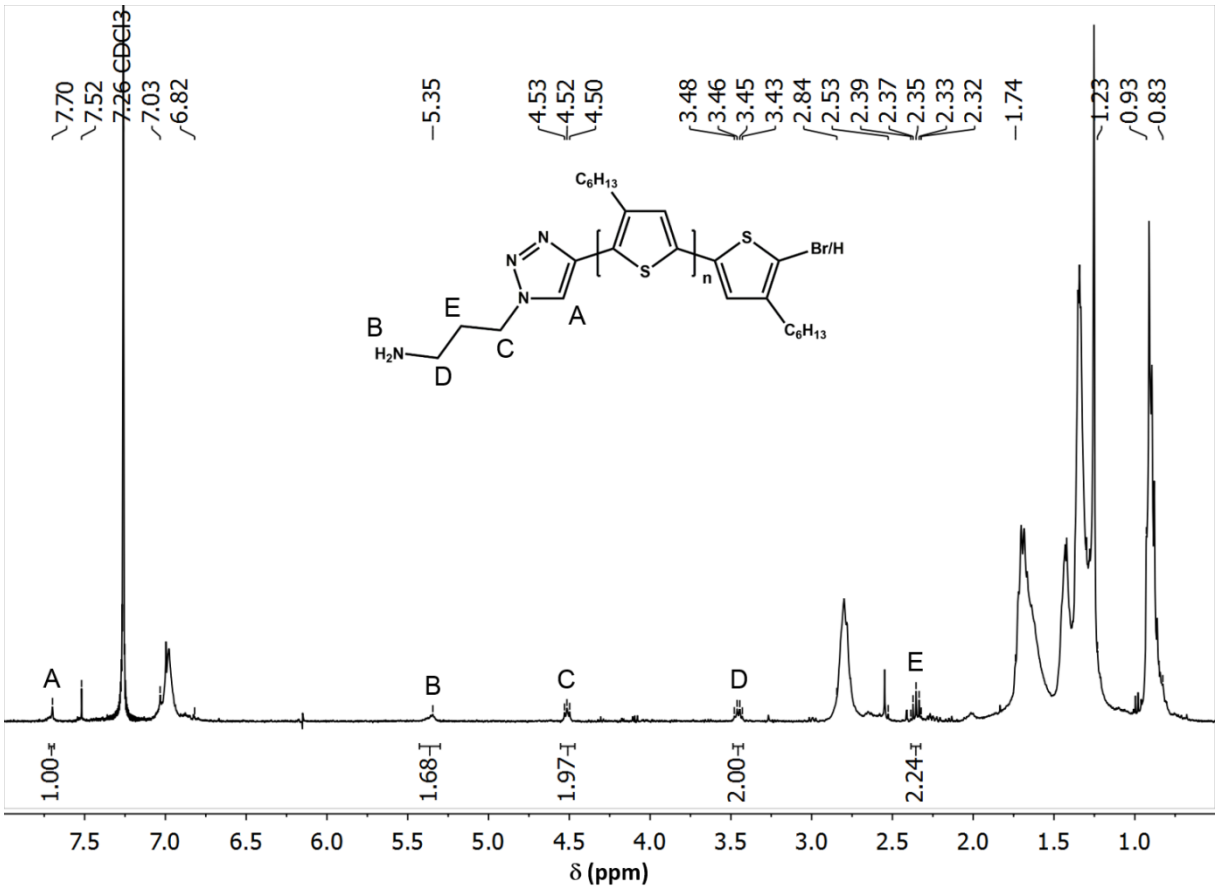

Figure S17. 400 MHz ^{1}H-NMR spectrum (in $CDCl_3$) of polymer **P3** displaying the triazole proton as a singlet at 7.70 ppm and all signals of the end group.

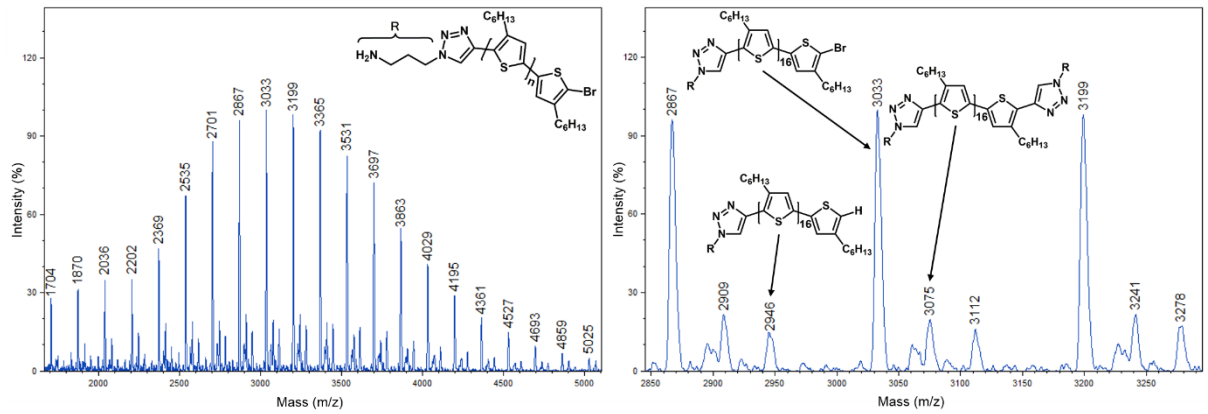

Figure S18. MALDI-TOF mass spectra of polymer **P3** with DP ≈ 17. Three different species are present over the whole molecular weight distribution (left) and can be assigned to the three possible end group combinations (right).

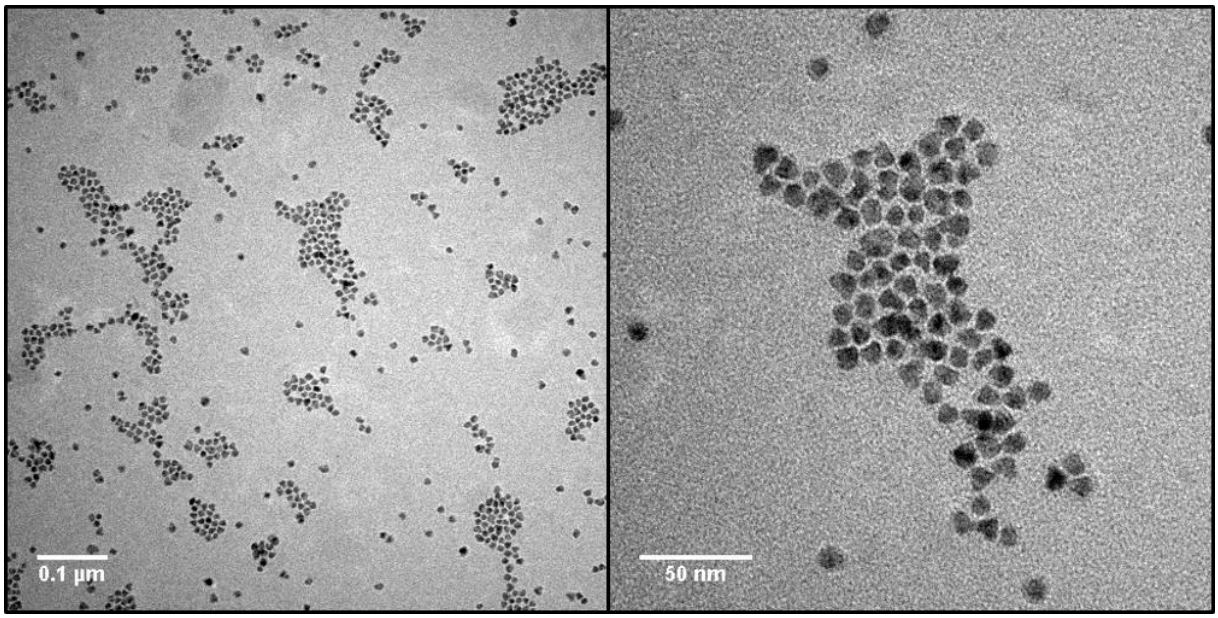

Figure S19. Representative TEM images of CdSe@ZnS QD/polymer nanocomposites showing individually dispersed QDs. The depicted nanocomposite is composed of CdSe@ZnS QDs with an average size of 8 nm and polymer **P2a** carrying lipoic acid anchor group.

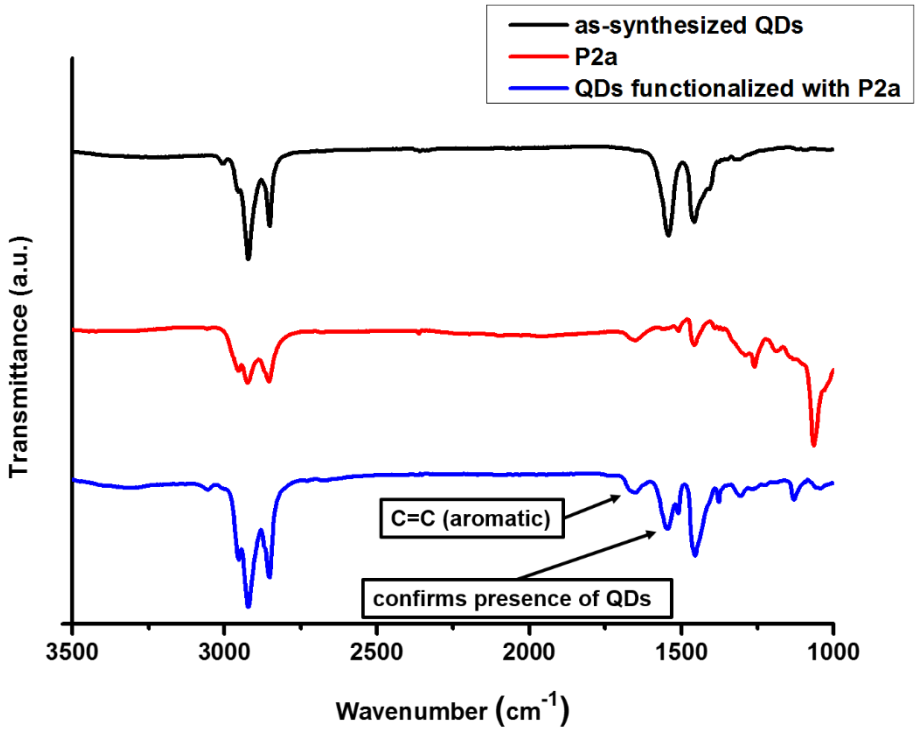

Figure S20. IR spectra of as-synthesized CdSe@ZnS QDs (black) passivated with oleic acid, **P2a** (red) and CdSe@ZnS QDs functionalized with **P2a** (blue).

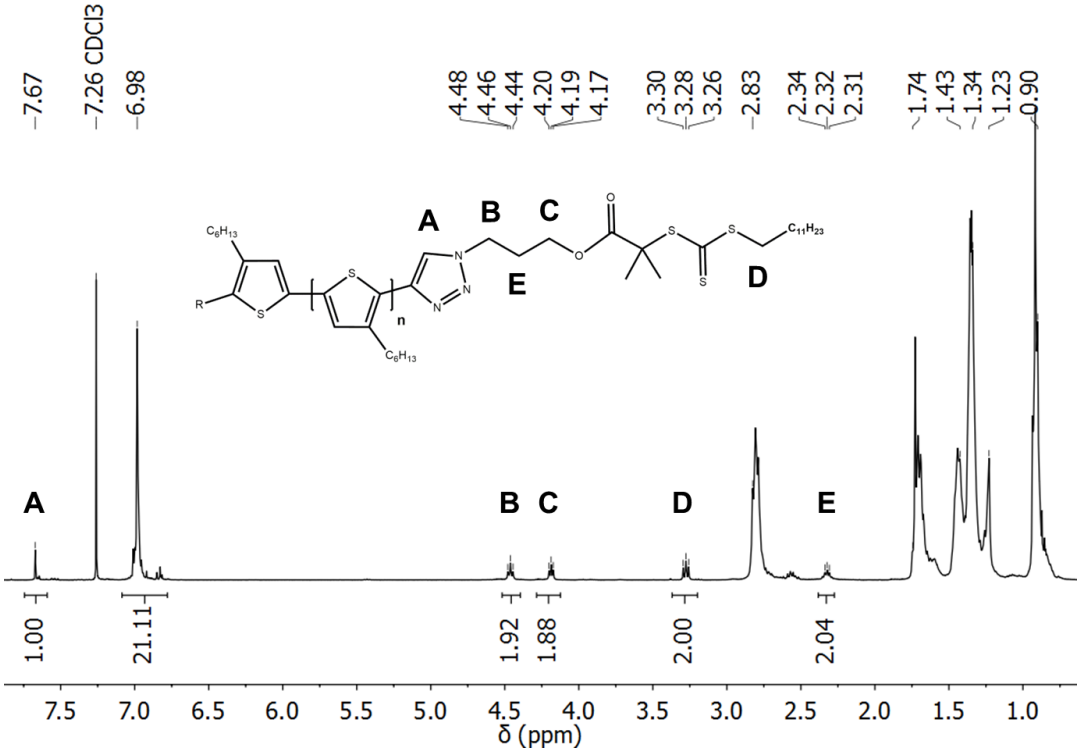

Figure S21. 400 MHz ^{1}H-NMR spectrum (in $CDCl_3$) of polymer **P2e** displaying the triazole proton as a singlet at 7.67 ppm and several signals of the end group.

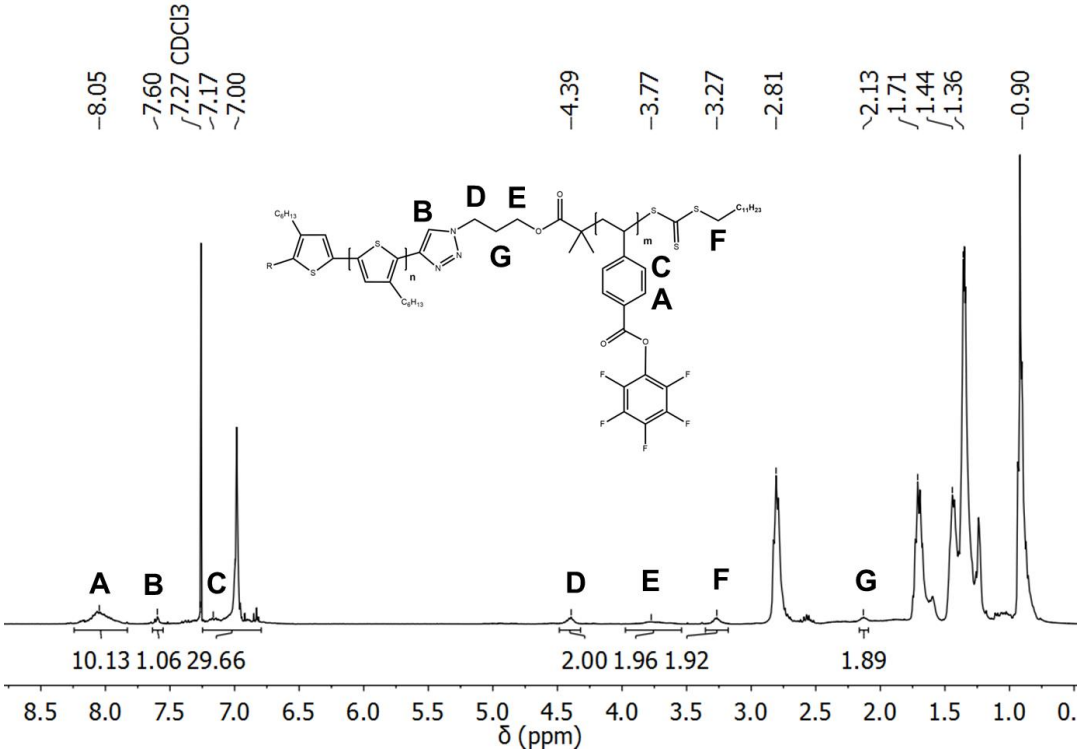

Figure S22. 400 MHz ^{1}H-NMR spectrum (in $CDCl_3$) of polymer **P4a** displaying the typical peaks of the reactive ester monomer incorporated in the block copolymer.

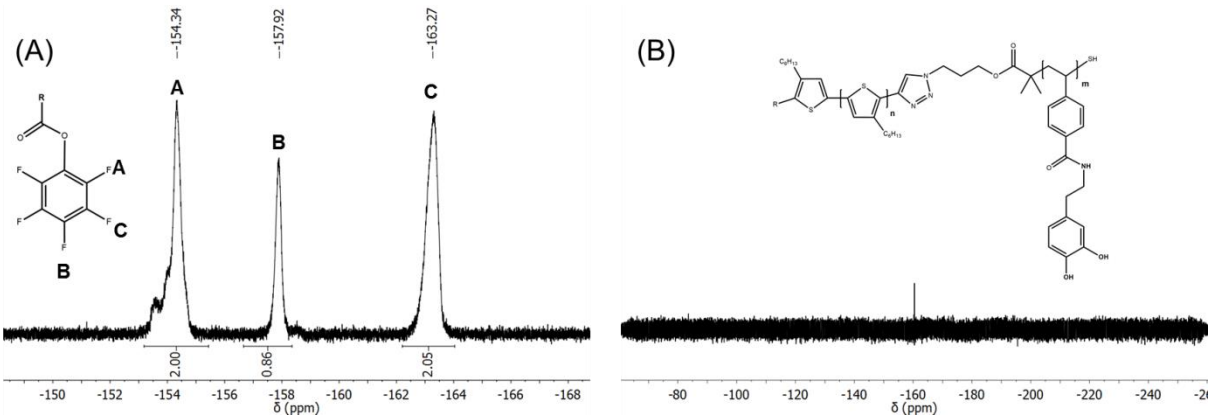

Figure S23. ^{19}F-NMR spectrum of **P4a** (A) showing the peaks of the fluorinated reactive ester. (B) shows the ^{19}F-NMR spectrum of **P4b** (B) with no peaks detectable.

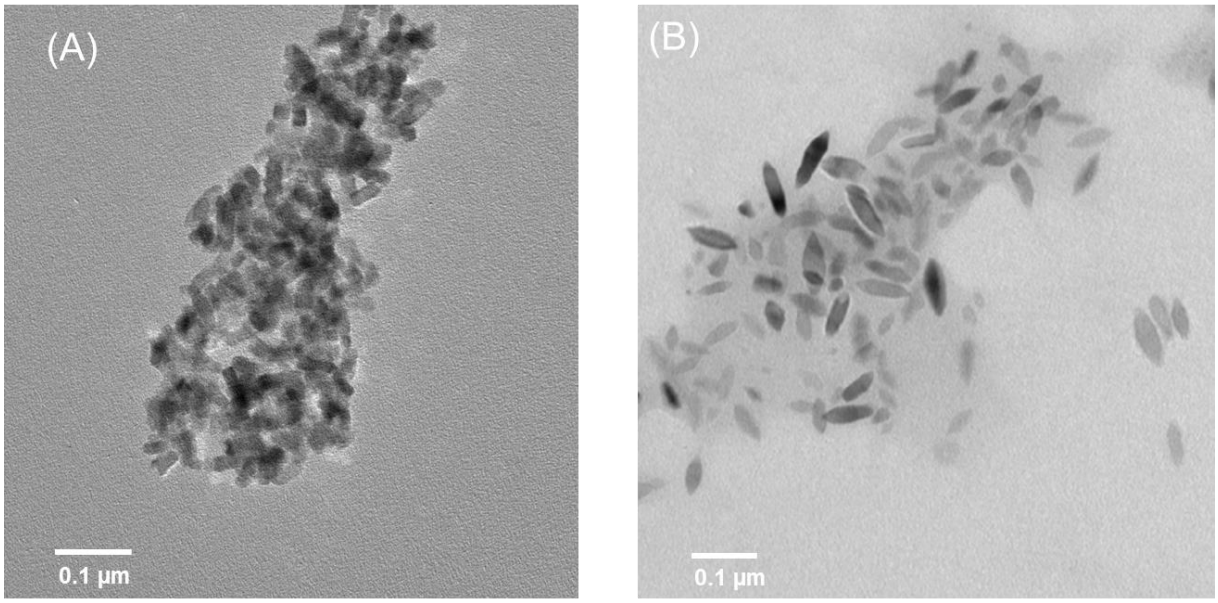

Figure S24. TEM images of TiO_2 nanoparticles coated with **P4b** (A) and **P5c** (B). While the nanoparticles coated with **P4b** are partially aggregated, the nanoparticles coated with **P5c** show no aggregation.

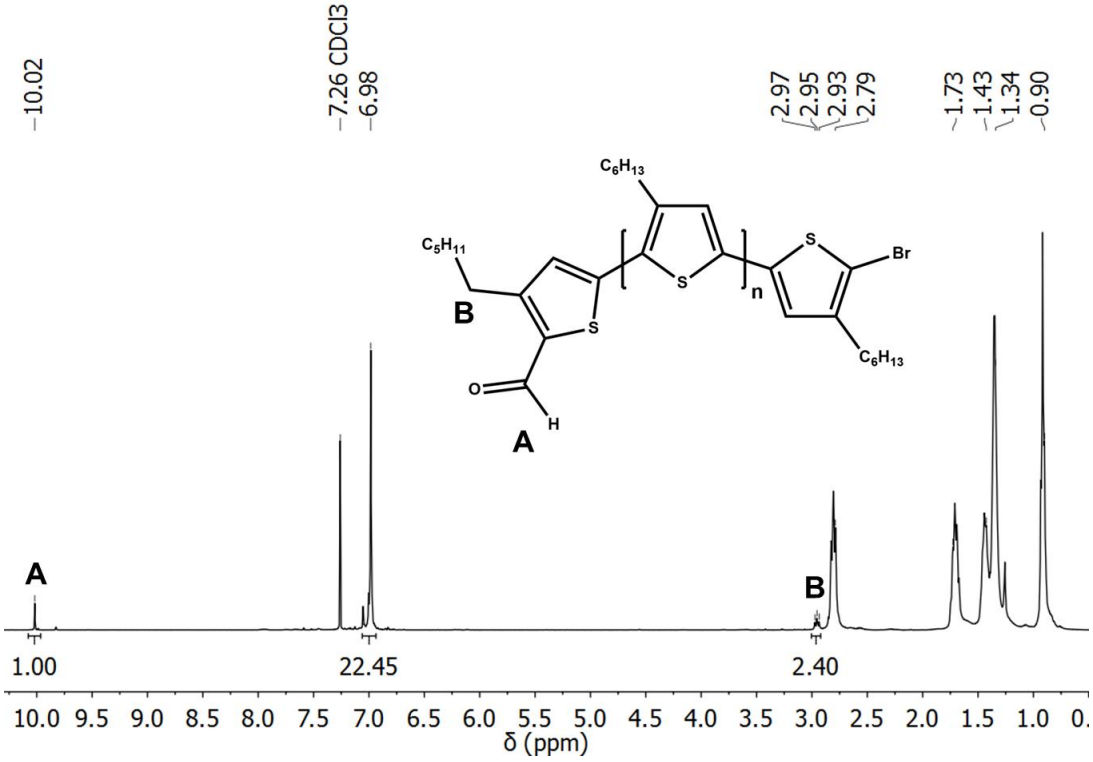

Figure S25. 400 MHz ^{1}H-NMR spectrum (in $CDCl_3$) of polymer **P5b** displaying the aldehyde peak at 10.02 ppm of the end-group.

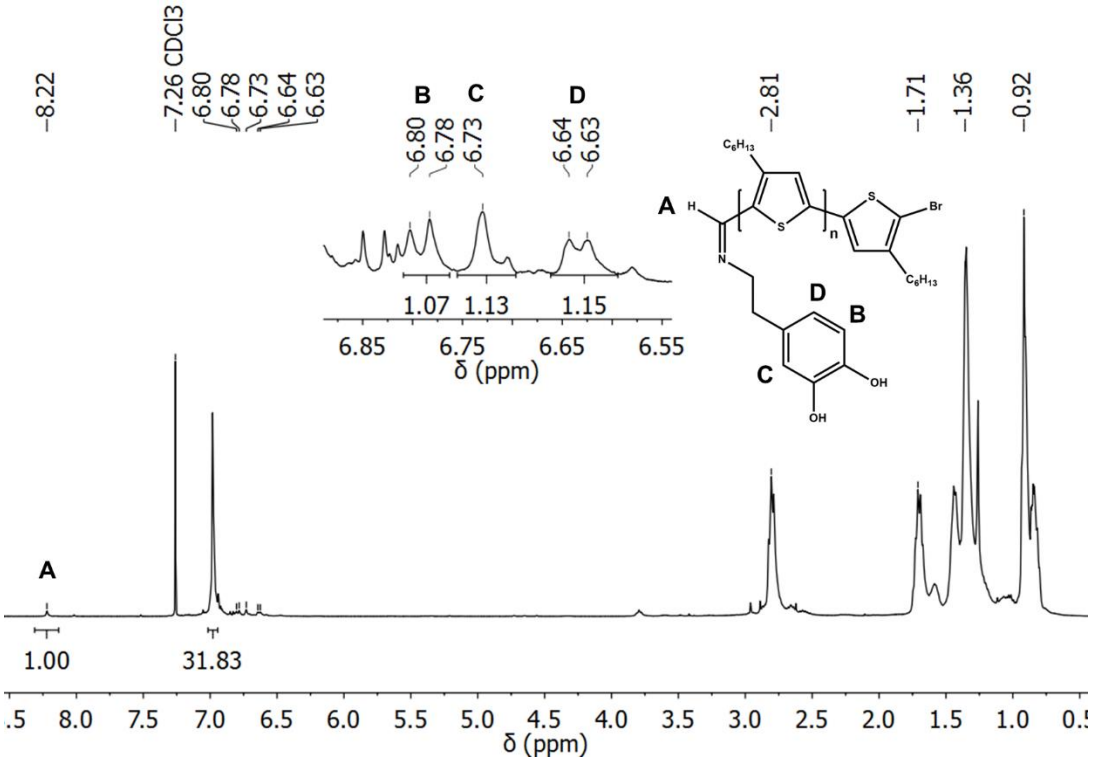

Figure S26. 400 MHz ^{1}H-NMR spectrum (in $CDCl_3$) of polymer **P5c** displaying the imine peak at 8.22 of the end-group as well as typical dopamine peaks in the inset.

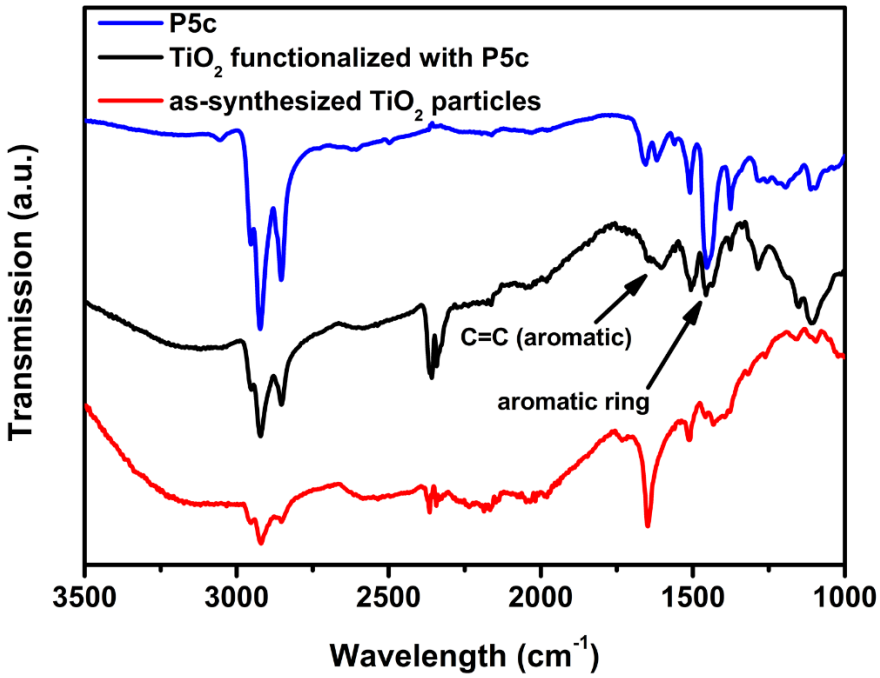

Figure S27. IR spectra of as-synthesized TiO_2 nanoparticles (red) passivated with oleic acid, **P5c** (blue) and TiO_2 particles functionalized with **P5c** (black).

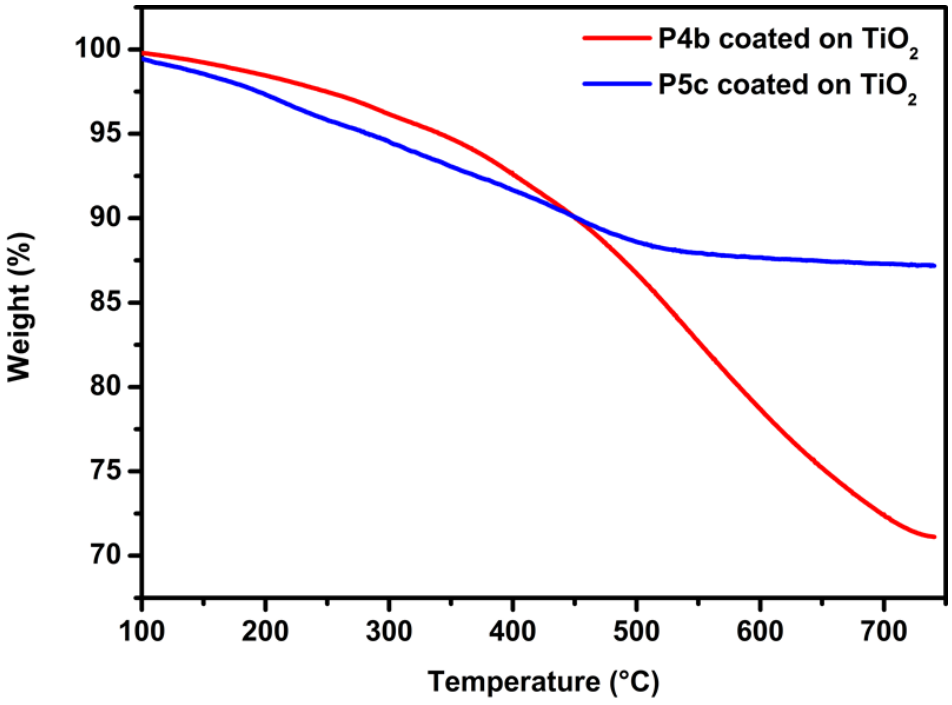

Figure S28. Thermogravimetric analysis of TiO_2 particles coated with **P4b** (red) and **P5c** (blue).

Table S1. Molecular weights, determined via GPC and NMR, and PDIs of all polymers.

Polymer	M_n [a] (kg · mol^{-1})	M_n [b] (kg · mol^{-1})	DP[c]	PDI[a]
P1	6.7	4.6	20	1.19
P1b	6.2	4.2	17	1.11
P2a	5.2	4.0	20	1.23
P2b	5.6	4.5	20	1.21
P2c	5.5	5.6	20	1.24
P2d	3.5	2.5	–	1.21
P2e	5.1	4.0	-	1.26
P3	6.2	4.6	17	1.35
P4a	6.2	4.9	–	1.31
P4b	5.4	~4.8	–	1.45
P5a	5.8	-	–	1.14
P5b	5.7	3.8	–	1.12
P5c	5.6	~3.9	–	1.14

[a] determined via GPC which was calibrated with polystyrene standards, [b] determined using ^{1}H-NMR spectroscopy (including the most probable end group combination), [c] determined via MALDI-TOF MS.

5. Summary and Conclusion

Summing up the research conducted in the context of this dissertation, new approaches in view of the morphology control of conducting materials, on the one hand, and approaches regarding the incorporation of various anchor groups into conjugated polymers, on the other hand, were developed. Within the scope of this dissertation, the morphology control of hybrid as well as all-organic systems was investigated. The results of this research, therefore, offer strategies applicable for both, organic and hybrid optoelectronic devices. As morphology plays an important role in the context of optoelectronic devices' efficiency, the approaches presented in this dissertation will support further optimization of organic and hybrid optoelectronic devices. Given the low efficiencies of organic and hybrid optoelectronic devices (particularly solar cells) compared to inorganic devices, their application is still limited. The importance of the research presented here is, therefore, even further emphasized. Looking at hybrid optoelectronic devices, the interface of the organic and the inorganic compounds has been identified to be one of the most critical factors limiting the device performance. Therefore, several approaches which allow for modifications of conjugated polymers with various anchor groups have been developed in the context of this dissertation. Consequently, these approaches permit systematic studies on the influence of various anchor groups with respect to the organic/inorganic interface.

In the first approach, a procedure for the controlled assembly of organic/inorganic nanocomposites upon an external stimulus (i.e, UV light) was developed. To demonstrate the applicability for optoelectronic devices, a semiconducting polymer composed of a triphenylamine repeating unit was synthesized via RAFT polymerization. Exploiting a functional CTA, the polymer was equipped with a reactive ester end group. Subsequently, an amine carrying a photocleavable anchor group was incorporated via end group modification. The obtained polymer was applied to achieve a stable functionalization of TiO_2 nanorods via ligand exchange. While the obtained nanocomposites were composed of individually dispersed nanorods, assembly of the nanocomposites into spherical aggregates occurred upon UV irradiation.

The second project presented in the present dissertation developed a controlled assembly of conjugated polymers into micelles. Thus, amphiphilic block copolymers composed of a MEH-PPV block and a second polynorbornene block carrying PEG side chains were synthesized. In contrast to approaches previously described in literature, the block copolymers

were synthesized in a facile one-pot procedure via ROMP. Two synthetic routes were developed to obtain block copolymers with amphiphilic properties. In the first route, a hydrophilic oxanorbornene functionalized with a PEG side chain was polymerized as first block followed by polymerization of 4,12-dimethoxy-7,15-di(2'-ethylhexyloxy)-[2.2]paracyclophane-1,9-diene to build the conjugated MEH-PPV block. In the second route, an intermediate block copolymer carrying a reactive ester block was synthesized first and, subsequently, converted into the amphiphilic block copolymer via post-polymerization modification with methoxypolyethylene glycol amine. The resulting block copolymers were assembled into micelles with varying sizes and varying optical properties depending on the block copolymer composition and the micellization procedure.
In the context of this study, a detailed investigation on the dependence of reactivity behavior and polymerization of the four isomers of dimethoxy-(2-ethylhexyloxy)-[2.2]para-cyclophane-1,9-diene regarding ROMP was conducted. Optimization of the polymerization conditions according to the reactivity study enabled the synthesis of block copolymers as described above.

Furthermore, the polymers carrying a reactive ester block were exploited for the incorporation of different anchor groups enabling the functionalization of CdSe@ZnS QDs via ligand exchange. The incorporation of anchor groups into conjugated polymers was further investigated in the second part of this dissertation.

With the aim to equip different conjugated polymers with anchor groups, three approaches were developed enabling the incorporation of various anchor groups into the two most applied classes of conjugated polymers – P3ATs and PPVs.
In the first approach, DEH-PPV was synthesized via Siegrist polycondensation and equipped with a defined aldehyde end group. The aldehyde was exploited for the incorporation of a trithiocarbonate converting the polymer into a macro-CTA. Subsequently, the obtained macro-CTA was applied in RAFT polymerization of PFPA attaching a reactive ester block to the conjugated backbone. Therefore, the obtained block copolymer was equipped with different anchor groups via post-polymerization modification. Consequently, the block copolymers were applied for the functionalization of CdSe nanoplatelets via ligand exchange. As the anchor groups varied either in their size or in the functional group interacting with the inorganic nanoplatelets, a study of the anchor groups' influence regarding the organic/inorganic interface was conducted.

In the second approach, two synthetic routes were developed permitting the incorporation of various anchoring end group into P3ATs. On the one hand, copper catalyzed azide-alkyne Huisgen cycloaddition was applied. On the other hand, Vilsmeier reaction was used to induce an aldehyde end group. The aldehyde was, subsequently, reacted with amines carrying the desired anchor group.

Thus, P3HT was equipped with anchor groups for the most common classes of inorganic nanocrystals, such as TiO_2, ZnO and CdSe@ZnS. Consequently, effective functionalization of CdSe@ZnS QDs and TiO_2 nanocrystals using appropriate anchor groups led to stable dispersions. Furthermore, electron transfer from the polymer to TiO_2 nanocrystals was observed under irradiation via KPFM demonstrating the intimate contact of both materials.

In general, the approaches for the incorporation of various anchor groups into conjugated polymers presented in this dissertation represent tools for future studies on the effects of anchor groups in hybrid optoelectronic devices. Analyzing the dependence of different properties (e.g. charge separation and energy levels) on the anchor groups shall lead to a deeper understanding on the role of anchor groups. Consequently, being able to tailor the organic/inorganic interface shall lead to improved device performances.

6. List of Abbreviations

AFM	atomic force microscopy
AIBN	azobisisobutyronitrile
ATR	attenuated total reflection
ATRP	atom transfer radical polymerization
CTA	chain transfer agent
CV	cyclic voltammetry
DCM	dichloromethane
δ	chemical shift
DEH-PPV	poly[2,5-di(2'-ethylhexyloxy)-1,4-phenylene vinylene]
DIAD	diisopropyl azodicarboxylate
DiEt	diethylether
DMF	*N*,*N*'-dimethyl formamide
DMSO	dimethylsulfoxide
DOSY	diffusion ordered spectroscopy
DP	degree of polymerization
eq.	equivalent
EVE	ethyl vinyl ether
GPC	gel permeation chromatography
GRIM	Grignard metathesis
HOMO	highest occupied molecular orbital
FTIR	Fourier transform infrared
ITO	indium tin oxide
KPFM	Kelvin probe force microscopy
OLED	organic light emitting diode
LUMO	lowest unoccupied molecular orbital
MALDI-TOF	matrix-assisted laser desorption/ionization time of flight
MEH-PPV	poly[2-methoxy-5-(2-ethylhexyloxy)-1,4-phenylene vinylene]
Me	methyl
MeO	methoxy
Mes	mesityl or 2,4,6-trimethylphenyl
M_n	molecular weight, number average

M_w	molecular weight, weight average
MS	mass spectroscopy
MSP	mean square plane
NMP	nitroxide mediated polymerization
NMR	nuclear magnetic resonance
OEH	2-ethylhexyloxy
OLED	organic light emitting diode
OPV	organic photovoltaic
P3AT	poly(3-alkylthiophene-2,5-diyl) or poly(3-alkylthiophene)
P3HT	poly(3-hexylthiophene-2,5-diyl) or poly(3-hexylthiophene)
PDI	polydispersity index
PFPA	pentafluorophenyl acrylate
PPV	poly(*p*-phenylene vinylene)
PFP4VB	pentafluorophenyl 4-vinylbenzoate
QD	quantum dot
RAFT	reversible addition-fragmentation chain transfer
RI	refractive index
R_f	retention factor
ROMP	ring-opening metathesis polymerization
RuPy	$(IMesH_2)(Cl)_2(C_5H_5N)_2Ru=CHPh$ with $IMesH_2$ = 1,3-dimesityl-4,5-dihydroimidazol-2-ylidene
SEC	size exclusion chromatography
SEM	scanning electron microscope
TEM	transmission electron microscopy
TGA	thermogravimetric analysis
THF	tetrahydrofuran
TLC	thin layer chromatography
UV-Vis	ultraviolet-visible
wt%	weight per cent
XRD	x-ray diffraction